

1. REPORT NUMBER CA15-2264	2. GOVERNMENT ASSOCIATION NUMBER	3. RECIPIENT'S CATALOG NUMBER
4. TITLE AND SUBTITLE Understanding the Confined Concrete Behavior on the Response of Hollow Bridge Columns		5. REPORT DATE January 2015
		6. PERFORMING ORGANIZATION CODE
7. AUTHOR Xiao Liang, Ryan Beck and Sri Sritharan		8. PERFORMING ORGANIZATION REPORT NO.
9. PERFORMING ORGANIZATION NAME AND ADDRESS Department of Civil, Construction and Environmental Engineering Iowa State University		10. WORK UNIT NUMBER
		11. CONTRACT OR GRANT NUMBER 65A0412
12. SPONSORING AGENCY AND ADDRESS California Department of Transportation Division of Engineering Services 1801 30th Street, MS #9-2/5i Sacramento, CA 95816		13. TYPE OF REPORT AND PERIOD COVERED Final Report June, 2012 – January, 2015
		14. SPONSORING AGENCY CODE
15. SUPPLEMENTARY NOTES Prepared in cooperation with the State of California Department of Transportation		
16. ABSTRACT In seismic design practice, hollow concrete columns offer an efficient alternative especially for tall bridge columns. The confinement in critical regions of these columns is not well understood and the confinement models developed for solid concrete sections are used to characterize these columns. This report identifies several shortcomings in current practice associated with hollow column design. Using experimental and analytical means, it is shown that the confined concrete behavior in hollow concrete columns is different from that established for solid sections. Recommendations to improve analysis and design of hollow columns are presented with experimental verification. Modification to alter the confinement models developed for solid sections and a design example are also provided.		
17. KEY WORDS Seismic; bridge; hollow; concrete; column; confinement; analysis; FE model; testing	18. DISTRIBUTION STATEMENT No restriction. This document is available to the public through the National Technical Information Service, Springfield, Virginia 22161	
19. SECURITY CLASSIFICATION (of this report) Unclassified	20. NUMBER OF PAGES 336	21. COST OF REPORT CHARGED

DISCLAIMER STATEMENT

This document is disseminated in the interest of information exchange. The contents of this report reflect the views of the authors who are responsible for the facts and accuracy of the data presented herein. The contents do not necessarily reflect the official views or policies of the State of California or the Federal Highway Administration. This publication does not constitute a standard, specification or regulation. This report does not constitute an endorsement by the Department of any product described herein.

For individuals with sensory disabilities, this document is available in alternate formats. For information, call (916) 654-8899, TTY 711, or write to California Department of Transportation, Division of Research, Innovation and System Information, MS-83, P.O. Box 942873, Sacramento, CA 94273-0001.

X. Liang, R. Beck, S. Sritharan

**Understanding the Confined Concrete Behavior on the
Response of Hollow Bridge Columns**

**Submitted to the
California Department of Transportation
Caltrans Project Contract: 65A0412**

JANUARY 2015

Final

REPORT

IOWA STATE UNIVERSITY

OF SCIENCE AND TECHNOLOGY

**Department of Civil, Construction
and Environmental Engineering**

Understanding the Confined Concrete Behavior on the Response of Hollow Bridge Columns

by

Xiao Liang

Graduate Research Assistant, Iowa State University

Ryan Beck

Graduate Research Assistant, Iowa State University

Sri Sritharan

Wilson Engineering Professor, Iowa State University

Caltrans Project Contract: 65A0412

A Final Report to the California Department of Transportation

**Department of Civil, Construction and Environmental Engineering
Iowa State University
Ames, IA 50011**

January 2015

ACKNOWLEDGMENTS

The research team thanks the following individuals for their support and assistance in the completion of the research presented in this report. Without their help, support and advice, much of this research would not have been possible:

- Caltrans for sponsoring this research project under Agreement #65A0412 and Charlie Sikorsky for serving as the project manager; and
- Michael Keever, Tom Ostrom, Mark Mahan and Tariq Masroor for their advice and assistance.

ABSTRACT

In seismic design practice, hollow concrete columns offer unique advantages especially for tall bridges by reducing the seismic mass, to attain greater strength-to-mass and stiffness-to-mass ratios when compared to solid concrete bridge columns. However, the behavior of confined concrete in hollow concrete is not well understood, providing what appears to be conflicting findings in the literature. Furthermore, the hollow concrete has been designed with either single outer layer or two layers of confinement reinforcement. With two layers, one layer is provided near the outside face and the second layer is placed near the inside face of the column with cross-ties linking the two layers. The size and spacing of the transverse reinforcing bar for the two reinforcement layers are typically kept constant. Furthermore, confinement models developed for solid sections are used to model confined concrete in hollow columns.

A systematic investigation is presented in this report using analytical and experimental investigations to understand the confinement effects in hollow concrete columns. Also, how they should be designed and analyzed to obtain realistic lateral displacement and force resistant capacities is presented. It is shown that the column designed with two layers of confinement reinforcement and cross ties are the most effective, but the required quantity near the inside surface should be much smaller than that required on the outer surface. This is because the tension demand developed in the inner reinforcement is effectively transferred to the outer reinforcement with the help of the cross ties. However, this specific detail is cumbersome and difficult to construct and therefore an in depth investigation was completed on hollow columns with single a layer reinforcement. It is shown that hollow circular and square columns can be designed to achieve a minimum displacement capacity. In these columns, the effectiveness of confinement reinforcement is less than that expected for solid columns with the same outer section. Therefore, the confinement models developed for solid columns should be appropriately modified. Suitable modifications are presented for a confinement model frequently used in design practice. With these modifications, the hollow columns can be adequately designed and their monotonic response can be accurately predicted.

TABLE OF CONTENTS

TECHNICAL REPORT DOCUMENTATION PAGE	i
DISCLAIMER	iii
ACKNOWLEDGMENTS	iv
ABSTRACT	v
TABLE OF CONTENTS	vi
LIST OF FIGURES	ix
LIST OF TABLES	xix
LIST OF NOTATIONS	xxi
CHAPTER 1 INTRODUCTION	1
1.1 Overview	1
1.2 Background	2
1.3 Research scope and objectives	4
1.4 Report layout	5
CHAPTER 2 LITERATURE REVIEW	6
2.1 Introduction	6
2.2 Experimental study on hollow column behavior	6
2.2.1 Lateral load tests	6
2.2.2 Axial load tests	25
2.2.3 Summary	26
2.3 Analytical study of hollow column behaviors	27
2.4 Confined concrete models	33
2.4.1 Overview	33
2.4.2 Mander et al. model (1988)	34
2.4.3 Other confined concrete models	40

2.4.4	Summary	49
CHAPTER 3	ANALYTICAL INVESTIGATION	51
3.1	Introduction	51
3.1.1	Definition of key variables	51
3.2	Concentric axial load.....	52
3.2.1	Overview.....	52
3.2.2	Material properties.....	53
3.2.3	FE modelling.....	57
3.2.4	Analysis matrix	58
3.2.5	FE model validation.....	64
3.2.6	Analysis results	71
3.3	Flexure behavior.....	111
3.3.1	Fiber-based beam elements analysis.....	111
3.3.2	3D finite element analysis.....	136
CHAPTER 4	EXPERIMENTAL INVESTIGATION	142
4.1	Overview	142
4.2	Test specimen.....	142
4.3	Material properties.....	145
4.3.1	Concrete quality	146
4.4	Test setup.....	147
4.5	Test Instrumentation.....	150
4.6	Loading protocol.....	154
CHAPTER 5	EXPERIMENTAL AND ANALYTICAL RESULTS	157
5.1	Fiber-based modelling method.....	157
5.1.1	Hollow column section layout	158
5.2	Finite element modelling method.....	159
5.2.1	Introduction.....	159
5.2.2	Material model.....	160
5.2.3	Boundary conditions	161
5.2.4	FEM results.....	161

5.3	Comparisons between analyses results and experimental results	169
5.3.1	Circular section	169
5.3.2	Square section	212
5.4	Analytical accuracy	255
5.5	Ideal specimens	259
5.6	Alternative analysis method	263
CHAPTER 6 CONCLUSIONS AND RECOMMENDATIONS		271
6.1	Conclusions	271
6.1.1	Confinement effect in hollow columns.....	271
6.1.2	Experimental study of hollow columns	272
6.1.3	Analytical analyses of hollow columns	273
6.2	Design recommendations	275
6.2.1	Applicability of Mander’s model to hollow sections.....	275
6.2.2	Design parameters.....	276
6.2.3	Confinement configurations applicability for different wall thicknesses	276
6.2.4	Recommended hollow column design procedure with one layer of transverse reinforcement	277
6.3	Design example	278
6.4	Future research	289
REFERENCE.....		290
APPENDIX.....		293
Appendix A: Concentric Axial Load FEM Analysis Input Material Properties		293
Appendix B: Model Validation – HF1 FEM Analysis Input Material Properties		295
Appendix C: FEM Analyses of Test Hollow Columns Input Material Properties.....		297
Appendix D: Radial behavior of two-inch wall hollow section at given concrete layer		299
Appendix E: Radial behavior of one-inch wall hollow section at given concrete layer		303
Appendix F: Concrete dilation		306

LIST OF FIGURES

Figure 1-1: Hollow bridge columns of the high-speed rail project in Taiwan (Mo et al. 2003).....	2
Figure 2-1: Dimensions of test units by Zahn et al. (1990), (1mm = 0.0394 inch)	8
Figure 2-2: Lateral force vs. displacement response and neutral axis position of column unit 2 with $t/D = 0.235$ (Zahn et al. 1990)	9
Figure 2-3: Lateral force vs. displacement response and neutral axis position of column unit 3 with $t/D = 0.185$ (Zahn et al. 1990)	9
Figure 2-4: Lateral force vs. displacement response and neutral axis position of column unit 5 with $t/D = 0.135$ (Zahn et al. 1990)	10
Figure 2-5: Cross sectional dimensions (in mm) of columns tested by Hoshikuma and Priestley (2000), (1 mm = 0.0394 inches)	11
Figure 2-6: Lateral force vs. displacement response of specimen HF1 tested by Hoshikuma and Priestley (2000), (1 mm = 0.0394 inches, 1 KN = 0.225 kips).....	12
Figure 2-7: Lateral force vs. displacement response of specimen HF2 tested by Hoshikuma and Priestley (2000), (1 mm = 0.0394 inches, 1 KN = 0.225 kips).....	13
Figure 2-8: Cross sectional dimensions (in mm) of column tested by Ranzo and Priestley (2001), (1 mm = 0.0394 inches)	14
Figure 2-9: Lateral force vs. displacement response of specimen HS1 tested by Ranzo and Priestley (2001), (1 mm = 0.039 inches, 1 KN = 0.225 kips).....	15
Figure 2-10: Cross sectional dimensions (in mm) of columns tested by Yeh et al. (2002),.....	17
Figure 2-11: Lateral force vs. displacement response of specimen PS1 tested by Yeh et al. (2002), (1 mm = 0.039 inches, 1 KN = 0.225 kips)	18
Figure 2-12: Lateral force vs. displacement response of specimen PI1 tested by Yeh et al. (2002), (1 mm = 0.039 inches, 1 KN = 0.225 kips)	18
Figure 2-13: Lateral reinforcement configurations used for test specimens (in mm) by Mo et al. (2003), (1mm = 0.0374 inch).....	20
Figure 2-14: Effect of spacing of confinement reinforcement on the moment-curvature curves for normal strength concrete and high strength concrete by Mo et al. (2003)	21
Figure 2-15: Comparison of experimental results with moment-curvature curves based on the modified Muguruma et al. model of Specimen HB4 by Mo et al. (2003).....	22
Figure 2-16: Stress-strain relationship of modified Muguruma et al. (2003) model	26
Figure 2-17: Symbols and boundary conditions (Lignola et al., 2008)	28
Figure 2-18: Radial displacement contributions of concrete tube and FRP Jacket (Lignola et al., 2008)	29
Figure 2-19: The axial stress vs. axial and radial strain relationship of confined concrete developed by Lignola et al., 2008 [1MPa = 145 psi].....	31
Figure 2-20: The axial stress vs. dilation ratio of confined concrete developed by Lignola et al., 2008 [1MPa = 145 psi]	31

Figure 2-21: Effectively Confined Core for Circular and Rectangular Sections [(Mander et al., 1988)].....	36
Figure 2-22: Comparison of Reinforcement Effects between Predicted and Measured Results (Mander et al., 1988) (1 MPa = 145 psi)	39
Figure 2-23: Confined concrete models comparisons for circular section	48
Figure 2-24: Confined concrete models comparisons for square section	49
Figure 2-25: Confinement effectiveness for different section geometry and confinement configurations	50
Figure 3-1: Comparisons between input unconfined concrete behavior and results expected for the confined concrete behavior based on Mander’s model (Mander et al., 1988).....	56
Figure 3-2: The tension stiffening model for concrete in ABAQUS (Abaqus Analysis User’s Manual 6.12, 2012).....	57
Figure 3-3: The boundary and loading conditions of a modeled two-inch-wall hollow section under concentric axial load	59
Figure 3-4: Comparison of the derived analytical axial stress vs. strain relationship of concrete and the Mander’s model predictions.....	65
Figure 3-5: FEM model and boundary conditions of HF1 model	67
Figure 3-6: FEM mesh of HF1 model.....	68
Figure 3-7: Lateral force vs. lateral displacement response comparisons among FEM, moment curvature analyses and measured experimental results	69
Figure 3-8: Inside concrete face crushing (a) FEM, (b) Experimental	70
Figure 3-9: Longitudinal reinforcement strain profiles comparisons between experimental test and FEM at ductility 4	71
Figure 3-10: Axial concrete behavior comparisons among different confinement configurations for the two-inch wall hollow sections.....	73
Figure 3-11: Deformed shape of the two-inch wall hollow section with one layer of confinement	74
Figure 3-12: Axial concrete compressive stress contour for the two-inch wall hollow section with two layers of confinement but no cross ties.....	74
Figure 3-13: Radial concrete stress with respect to each concrete layer for the two-inch wall hollow section with one layer of confinement only.....	76
Figure 3-14: Radial concrete stress with respect to each concrete layer for the two-inch wall hollow section with two layers of confinement but no cross ties	76
Figure 3-15: Radial concrete stress with respect to each concrete layer for the two-inch wall hollow section with two layers of confinement connected with cross ties.....	77
Figure 3-16: Axial concrete behavior comparisons among different confinement configurations for the one-inch wall hollow sections	78
Figure 3-17: Radial concrete stress with respect to each concrete layer for the one-inch wall hollow section only with an outer layer of confinement.....	79
Figure 3-18: Radial concrete stress with respect to each concrete layer for the one-inch wall hollow section with two layers of confinement but no cross ties	80

Figure 3-19: Radial concrete stress with respect to each concrete layer for the one-inch wall hollow section with two layers of confinement connected with cross ties	80
Figure 3-20: The axial stress vs. axial strain behavior corresponding to different wall thickness to diameter ratios for the circular section.....	83
Figure 3-21: The axial stress vs. axial strain behavior corresponding to different wall thickness to diameter ratios for the square section	83
Figure 3-22: The resulting relationship between the axial stress and axial strain for circular hollow sections that have one layer of confinement.....	86
Figure 3-23: The resulting relationship between the axial stress and axial strain for square hollow sections that have one layer of confinement	86
Figure 3-24: The concrete outward dilation of the outermost layer for circular hollow sections with one layer of confinement	89
Figure 3-25: The selected 1.8-inch-wall hollow section to study the concrete dilation	90
Figure 3-26: Concrete dilation for both solid and 1.8-inch-wall hollow sections at 0.01 in/in and 0.02 in/in axial concrete strain.....	91
Figure 3-27: Axial stress vs. axial strain behavior comparisons for different wall thicknesses with different ratios of inner to outer confinement amount.....	94
Figure 3-28: Confinement of concrete for solid section	96
Figure 3-29: Confinement of concrete for hollow sections with a single layer of confinement ..	97
Figure 3-30: Confinement of concrete for hollow sections having two layers of confinement without cross ties.....	99
Figure 3-31: Confinement of concrete for hollow sections having two layers of confinement connected with cross ties, if the capacity of the cross ties is greater than that of the inner layer of confinement	101
Figure 3-32: Confinement of concrete for hollow sections having two layers of confinement connected with cross ties, if the capacity of the cross ties is lower than that of the inner layer of confinement	102
Figure 3-33: Confinement of concrete for hollow sections having two layers of confinement connected with cross ties, if the capacity of the cross ties is equal to that of the inner layer of confinement	103
Figure 3-34: The confinement effectiveness coefficient vs. β relationship comparisons of circular hollow columns between the FE analyses and the Mander's predictions.....	109
Figure 3-35: The confinement effectiveness coefficient vs. β relationship comparisons of square hollow columns between the FE analyses and the Mander's predictions.....	110
Figure 3-36: The relationship between the multiplier and t/D ratio for circular hollow columns	110
Figure 3-37: The relationship between the multiplier and t/D ratio for square hollow columns	111
Figure 3-38: Circumferential stress distribution of solid and hollow circular columns	115
Figure 3-39: Approximated stress distributions in hollow circular sections with one layer of transverse reinforcement.....	115
Figure 3-40: Regions for unconfined and confined concrete for circular hollow columns with one layer of transverse reinforcement.....	118

Figure 3-41: Regions for unconfined and confined concrete in rectangular hollow columns with one layer of transverse reinforcement.....	120
Figure 3-42: Possible transverse reinforcement arrangements in solid rectangular columns.....	121
Figure 3-43: Confined concrete strength from lateral confining stress [Mander et al. (1988)]..	122
Figure 3-44: Hollow rectangular section confined with overlapping hoops and separation into individual wall section	123
Figure 3-45: Cross-section dimensions (in mm) of the hollow column tested by Hoshikuma and Priestley (2000), (1mm = 0.0394 inch).....	125
Figure 3-46: Test setup of Hoshikuma and Priestley (2000) and corresponding model configuration (Dimensions in mm), (1 mm = 0.0394 inch).....	126
Figure 3-47: Comparison between analytical analysis and experimental results of Specimens HF1 and HF2 tested by Hoshikuma and Priestley (2000)	127
Figure 3-48: Cross-section dimensions and reinforcement layout of square hollow columns with one layer of transverse reinforcement tested by Calvi et al. (2005), (1 mm = 0.0394 inch)	129
Figure 3-49: Force-displacement response comparisons between Test Unit S250 by Calvi et al. (2005) and analytical results	130
Figure 3-50: Cross-section dimensions and lateral reinforcement details of hollow columns tested by Yeh et al. (2001), (Dimensions in mm, 1mm = 0.0394 inch).....	131
Figure 3-51: Comparison between analytical results and experimental results of Specimen PS1 tested by Yeh et al. (2001)	132
Figure 3-52: Cross-section dimensions of Specimen PS1 tested by Yeh et al. (2002) (Dimensions in mm), (1 mm = 0.0394 inch).....	134
Figure 3-53: Cross-section dimensions of Specimen PI1 tested by Yeh et al. (2002) (Dimensions in mm), (1 mm = 0.0394 inch).....	134
Figure 3-54: Comparison between analytical results and experimental results for hollow square specimens with two layers of transverse reinforcement by Yeh et al. (2002)	135
Figure 3-55: The loading and boundary conditions of the hollow columns modelled with a combined axial and flexure loadings	137
Figure 3-56: Force - displacement response comparisons with different longitudinal reinforcement ratios and axial load ratios for one-inch-wall hollow columns with a single layer of transverse reinforcement.....	138
Figure 3-57: Force vs. displacement response comparisons for two-inch-wall hollow columns with three different confinement configurations.....	140
Figure 3-58: Force vs. displacement response comparisons for two-inch-wall hollow columns with three different confinement configurations under the same longitudinal reinforcement ratio	141
Figure 4-1: Cross-sections of circular hollow columns	143
Figure 4-2: Cross-sections of square hollow columns.....	145
Figure 4-3: Overall test frame.....	148
Figure 4-4: Frame cutaway showing test specimen setup	149
Figure 4-5: Picture of experimental testing setup.....	149

Figure 4-6: Transverse reinforcement spacing for both circular and square columns.....	150
Figure 4-7: Strain gauge layout of circular section.....	151
Figure 4-8: Strain gauge layout of square section	152
Figure 4-9: LVDT locations.....	152
Figure 4-10: General LED layout	153
Figure 4-11: Loading history selected for testing	156
Figure 5-1: Schematic of the OpenSees model representing the test units.....	157
Figure 5-2: General section model for tested hollow circular specimens.....	158
Figure 5-3: General section model for tested hollow square specimens	159
Figure 5-4: Analyses steps in ABAQUS	161
Figure 5-5: FEM results comparisons between circular solid columns under 22.6 kips axial load and 45.2 kips axial load	162
Figure 5-6: FEM results comparisons between two-inch wall circular hollow columns under 22.6 kips axial load and 45.2 kips axial load	163
Figure 5-7: FEM results comparisons between one-inch wall circular hollow columns under 22.6 kips axial load and 45.2 kips axial load	164
Figure 5-8: The axial compressive plastic concrete strain contour of one-inch wall circular hollow column under 45.2 kips axial load	165
Figure 5-9: The axial compressive plastic concrete strain contour of two-inch wall circular hollow column under 45.2 kips axial load	165
Figure 5-10: The deformed shape of one-inch wall circular hollow column under 45.2 kips axial load.....	166
Figure 5-11: The deformed shape of two-inch wall circular hollow column under 45.2 kips axial load.....	166
Figure 5-12: FEM results comparisons between square solid columns under 22.6 kips axial load and 45.2 kips axial load	167
Figure 5-13: FEM results comparisons between two-inch wall square hollow columns under 22.6 kips axial load and 45.2 kips axial load	168
Figure 5-14: FEM results comparisons between one-inch wall square hollow columns under 22.6 kips axial load and 45.2 kips axial load	169
Figure 5-15: Specimen SC1-M shear cracking at peak displacement	171
Figure 5-16: Large flexural crack in Specimen SC1-M at end of test.....	171
Figure 5-17: Specimen SC2-C after flexural failure.....	172
Figure 5-18: Close-up view of large flexural crack in Specimen SC2-C	173
Figure 5-19 - Specimen H2C1-M after tension steel failure.....	174
Figure 5-20: Inside face at the compression face in the constant moment region of Specimne H2C1-M before and after testing	174
Figure 5-21: Specimen H2C2-C after failure.....	175
Figure 5-22: Close-up view of flexural cracks in Specimen H2C2-C after failure	176
Figure 5-23: Inside face of Specimen H2C2-C in constant moment region under compression	176
Figure 5-24: Close-up view of flexural cracks in Specimen H2C3-C after failure	177
Figure 5-25: Specimen H1C1-M shear/local failure at west point of load application	178

Figure 5-26: Specimen H1C2-C wooden braces located at load points and support to avoid punching failure	179
Figure 5-27: Specimen H1C2-C after shear failure	180
Figure 5-28: Specimen H1C2-C shear failure region	180
Figure 5-29: Specimen H1C3-C local failure near loading point	181
Figure 5-30: Close-up of local failure on LED side in Specimen H1C3-C after clearing damaged concrete	182
Figure 5-31: Force-displacement response of Test Unit SC1-M	183
Figure 5-32: Force-displacement response of Test Unit SC2-C	184
Figure 5-33: Force-displacement response of Test Unit H2C1-M	184
Figure 5-34: Force-displacement response of Test Unit H2C2-C	185
Figure 5-35: Force-displacement response of Test Unit H2C3-C	185
Figure 5-36: Force-displacement response of Test Unit H1C1-M	186
Figure 5-37: Force-displacement response of Test Unit H1C2-C	186
Figure 5-38: Force-displacement response of Test Unit H1C3-C	187
Figure 5-39: Force-displacement response comparisons for solid, two-inch wall, and one-inch wall hollow circular columns under 22.6 kips axial load	188
Figure 5-40: Force-displacement response comparisons of two-inch wall hollow columns under monotonic and cyclic loadings.....	189
Figure 5-41: Force-displacement relationship of Specimen H2C1-M with and without shear deformation	191
Figure 5-42: Force vs. shear displacement relationship of Specimen H2C1-M	191
Figure 5-43: Force-displacement relationship of Specimen H2C2-C with and without shear deformation	192
Figure 5-44: Force vs. shear displacement relationship of Specimen H2C2-C	193
Figure 5-45: Force-displacement relationship of Specimen H2C3-C with and without shear deformation	193
Figure 5-46: Force-displacement relationship of Specimen H1C1-M with and without shear deformation	194
Figure 5-47: Force-displacement relationship of Specimen H1C2-C with and without shear deformation	195
Figure 5-48: Force-displacement relationship of Specimen H1C3-C with and without shear deformation	195
Figure 5-49: Measured force-displacement response of Specimen SC1-M compared to analytical envelope response	197
Figure 5-50: Experimental and analytical axial load vs. applied load relationship for the Specimen SC1-M	197
Figure 5-51 Measured force-displacement response of Specimen SC2-C compared to analytical envelope response	198
Figure 5-52: Measured force-displacement response of Specimen H2C1-M with shear deformation removed compared to analytical envelope response	199
Figure 5-53: Measured force-displacement response of Specimen H2C2-C with shear deformation removed compared to analytical envelope response	200

Figure 5-54: Measured force-displacement response of Specimen H2C3-C with shear deformation removed compared to analytical envelope response	200
Figure 5-55: Measured force-displacement response of Specimen H1C1-M with shear deformation removed compared to analytical envelope response	201
Figure 5-56: Measured force-displacement response of Specimen H1C2-C with shear deformation removed compared to analytical envelope response	201
Figure 5-57: Measured force-displacement response of Specimen H1C3-C with shear deformation removed compared to analytical envelope response	202
Figure 5-58: Circular section strain gauge locations	203
Figure 5-59: Specimen SC2-C longitudinal strain near longitudinal bar 1 vs. applied load	204
Figure 5-60: Specimen H2C2-C longitudinal strain near longitudinal bar 1 vs. applied load....	204
Figure 5-61: Specimen H2C3-C longitudinal strain near longitudinal bar 1 vs. applied load....	205
Figure 5-62: Specimen H1C2-C longitudinal strain near longitudinal bar 1 vs. applied load....	206
Figure 5-63: Specimen H1C3-C longitudinal strain near longitudinal bar 11 vs. applied load..	206
Figure 5-64: LED Layout with Highlighted Strain Locations	208
Figure 5-65: Attached LED concrete strain measured during testing and analytical steel strain vs. applied lateral load for Specimen SC2-C.....	208
Figure 5-66: Attached LED concrete strain measured during testing and analytical steel strain vs. applied lateral load for Specimen H2C2-C	209
Figure 5-67: Attached LED concrete strain measured during testing and analytical steel strain vs. applied lateral load for Specimen H2C3-C	209
Figure 5-68: Attached LED concrete strain measured during testing and analytical strain vs. applied lateral load for Specimen H1C2-C	210
Figure 5-69: Hoop strains near longitudinal bar 1 vs. applied load in Specimen SC2-C.....	211
Figure 5-70: Hoop strains near longitudinal bar 11 vs. applied load for Specimen SC2-C	212
Figure 5-71: Specimen SS1-M prior to failure	213
Figure 5-72: Close-up view of large flexural crack after failure for Specimen SS1-M	214
Figure 5-73: Crack pattern of Specimen SS2-C at displacement ductility three prior to failure	215
Figure 5-74: Large flexural crack in constant moment region of Specimen SS2-C after failure	215
Figure 5-75: Local crushing and spalling of cover concrete in Specimen H2S1-M at displacement ductility one	217
Figure 5-76: Compression face prior to failure and inward failure of the compression face concrete in the wall of Specimen H2S1-M	217
Figure 5-77: Longitudinal reinforcement buckling after failure in Specimen H2S1-M.....	218
Figure 5-78: Crack pattern of Specimen H2S2-C in the cycle at $0.75F_y$	219
Figure 5-79: Shear failure in the linear moment region in Specimen H2S2-C.....	219
Figure 5-80: Large shear crack in the linear moment region on LED side of Specimen H2S2-C after failure.....	220
Figure 5-81: Local spalling and crack pattern in the first part of cycle at F_y in Specimen H2S3-C	221
Figure 5-82: Close-up view of local cover crushing at load point while unloaded prior to the second part of the cycle at F_y in Specimen H2S3-C	221
Figure 5-83: Shear failure in the linear moment region in Specimen H2S3-C.....	222

Figure 5-84: LED side after failure in Specimen H2S3-C.....	222
Figure 5-85: Shear failure in the linear moment region in Specimen H1.25S1-M.....	223
Figure 5-86: LED side of damaged linear moment region after failure in Specimen H1.25S1-M	224
Figure 5-87: Specimen H1.25S2-C support after failure	225
Figure 5-88: Specimen H1.25S3-C end support after failure	226
Figure 5-89: Force-displacement response of Test Unit SS1-M	227
Figure 5-90: Force-displacement response of Test Unit SS2-C	227
Figure 5-91: Force-displacement response of Test Unit H2S1-M.....	228
Figure 5-92: Force-displacement response of Test Unit H2S2-C.....	228
Figure 5-93: Force-displacement response of Test Unit H2S3-C.....	229
Figure 5-94: Force-displacement response of Test Unit H1.25S1-M.....	229
Figure 5-95: Force-displacement response of Test Unit H1.25S2-C.....	230
Figure 5-96: Force-displacement response of Test Unit H1.25S3-C.....	230
Figure 5-97: Force-displacement response comparisons for solid, two-inch wall, and 1.25-inch wall hollow columns under 22.6 kips axial load.....	232
Figure 5-98: Force-displacement of Specimen SS1-M with and without shear deformation.....	233
Figure 5-99: Force vs. shear displacement response for Specimen SS1-M.....	234
Figure 5-100: Force-displacement response of Specimen SS2-C with and without shear deformation	235
Figure 5-101: Force vs. shear displacement of Specimen SS2-C.....	235
Figure 5-102: Force-displacement response of Specimen H2S1-M with and without shear deformation	236
Figure 5-103: Force vs. shear displacement response of Specimen H2S1-M	237
Figure 5-104: Force-displacement response of Specimen H2S2-C with and without shear deformation	238
Figure 5-105: Force-displacement response of Specimen H2S3-C with and without shear deformation	238
Figure 5-106: Force-displacement response of Specimen H1.25S1-M with and without shear deformation	239
Figure 5-107: Force-displacement response of Specimen H1.25S2-C with and without shear deformation	239
Figure 5-108: Force-Displacement of Specimen H1.25S3-C with and without Shear Deformation	240
Figure 5-109: Measured force-displacement response of Specimen SS1-M with shear deformation removed compared to analytical envelope response	241
Figure 5-110: Measured force-displacement response of Specimen SS2-C with shear deformation removed compared to analytical envelope response.....	242
Figure 5-111: Measured force-displacement response of Specimen H2S1-M with shear deformation removed compared to analytical envelope response	242
Figure 5-112: Measured force-displacement response of Specimen H2S2-C with shear deformation removed compared to analytical envelope response	243

Figure 5-113: Measured force-displacement response of Specimen H2S3-C with shear deformation removed compared to analytical envelope response	243
Figure 5-114: Measured force-displacement response of Specimen H1.25S1-M with shear deformation removed compared to analytical envelope response	244
Figure 5-115: Measured force-displacement response of Specimen H1.25S2-C with shear deformation removed compared to analytical envelope response	244
Figure 5-116: Measured force-displacement response of Specimen H1.25S3-C with shear deformation removed compared to analytical envelope response	245
Figure 5-117: Square section strain gauge locations	246
Figure 5-118: Longitudinal strain near longitudinal bar 1 vs. applied load of Specimen	247
Figure 5-119: Longitudinal strain near longitudinal bar 1 vs. applied load of Specimen H2S2-C	247
Figure 5-120: Longitudinal strain near longitudinal bar 12 vs. applied load of Specimen H2S3-C	248
Figure 5-121: Longitudinal strain near longitudinal bar 1 vs. applied load of Specimen H1.25S2-C	248
Figure 5-122: Longitudinal strain near longitudinal bar 1 vs. applied load of Specimen H1.25S3-C	249
Figure 5-123: LED layout with highlighted strain locations	250
Figure 5-124: Attached LED concrete strain measured during testing and analytical steel strain vs. applied load for Specimen SS2-C	251
Figure 5-125: Attached LED concrete strain measured during testing and analytical steel strain vs. applied load for Specimen H2S2-C	252
Figure 5-126: Attached LED concrete strain measured during testing and analytical steel strain vs. applied load for Specimen H1.25S2-C	252
Figure 5-127: Hoop strain near longitudinal bar 1 vs. applied load for Specimen SS2-C	254
Figure 5-128: Hoop strain near longitudinal bar 12 vs. applied load for Specimen SS2-C	254
Figure 5-129: Hoop strain at side of section vs. applied load for Specimen SS2-C	255
Figure 5-130: Measured and analytical strain vs. displacement relationship for Specimen H2C1-M	256
Figure 5-131: Strain profile at first yield (measured steel strain of 3300 microstrain) for Specimen H2C1-M	257
Figure 5-132: Strain profile between yield and ultimate for Specimen H2C1-M	258
Figure 5-133: Strain profile at ultimate (tension strain 20,000 microstrain) for Specimen H2C1-M	259
Figure 5-134: Analytical force vs. displacement response of ideal solid specimen under 22.6 kips axial load	261
Figure 5-135: Analytical force vs. displacement response of ideal hollow two-inch thick specimen under 22.6 kips axial load	262
Figure 5-136: Analytical force vs. displacement response of ideal solid specimen under 45.2 kips axial load	262
Figure 5-137: Analytical force vs. displacement response of ideal hollow two-inch thick specimen under 45.2 kips axial load	263

Figure 5-138: The ratio between the circumferential stress in hollow concrete columns and that in solid concrete columns against the confinement reinforcement volumetric ratio	265
Figure 5-139: The confinement effectiveness coefficient comparisons between the refined analytical method and the finite element analysis	265
Figure 5-140: Comparison between original and refined analysis and experimental results of Specimens HF1 and HF2 tested by Hoshikuma and Priestley (2000)	267
Figure 5-141: Comparison between original and refined analysis for ideal two-inch wall specimen under 22.6 kips axial load	269
Figure 5-142: Comparison between original and refined analysis for ideal two-inch wall specimen under 45.2 kips axial load	269
Figure 6-1: Pushover analysis of example column as hollow and solid	283
Figure 6-2: Pushover analysis of 10 foot diameter circular columns	286
Figure 6-3: Pushover analysis of 3.5 foot diameter circular columns	287
Figure 6-4: Pushover analysis of 5 foot diameter square columns	288

LIST OF TABLES

Table 2-1: Test parameters and failure mode of column tested by Zahn et al. (1990)	8
Table 2-2: Test parameters and failure mode of column tested by Hoshikuma and Priestley (2000)	12
Table 2-3: Test parameters and failure mode of columns tested by Ranzo and Priestley (2001). 15	
Table 2-4: Test parameters and failure mode of column tested by Yeh et al. (2002).....	17
Table 2-5: Test parameters and failure modes of columns tested by Mo et al. (2003), (1mm = 0.0394 inch)	20
Table 2-6: Summary of previous experimental studies on hollow reinforced concrete columns. 23	
Table 2-7: Summary of experimentally observed failure modes of tests listed in Table 2-6	24
Table 2-8: Design recommendations proposed by previous researchers on hollow reinforced columns based on their investigations	24
Table 2-9: Comparisons of two types of confinement configurations.....	27
Table 2-10: Summary of parameters accounted by different confined concrete models	43
Table 2-11: Test specimen details used in developing confined concrete models	44
Table 2-12: Summary of various confined concrete models proposed in the literature	45
Table 2-13: Summary of expressions to calculate the peak stress and the corresponding strain based on different confined concrete models.....	46
Table 2-14: Influence of different parameters on confined concrete behavior.....	47
Table 3-1: Analysis matrix of confinement configurations	60
Table 3-2: Analysis matrix of wall thickness	62
Table 3-3: Analysis matrix of proportion between inner and outer confinement amount.....	63
Table 3-4: Deformed shape of circular hollow sections having one layer of confinement placed at the outside concrete wall under the same amount of confinement	87
Table 3-5: Deformed shape of square hollow sections having one layer of confinement placed at the outside concrete wall under the same amount of confinement	88
Table 3-6: Confined concrete states for each confinement configuration	104
Table 3-7: Recommendations of confinement for different wall thickness hollow sections.....	106
Table 3-8: Analyses matrix for hollow columns confined with a single layer of confinement reinforcement	107
Table 3-9: The confinement effectiveness coefficient of circular hollow columns for both the FE analyses and the Mander's model	108
Table 3-10: The confinement effectiveness coefficient of square hollow columns for both the FE analyses and the Mander's model	109
Table 3-11: The modelling matrix for one-inch-wall hollow columns with a single layer of transverse reinforcement (1 inch = 25.4 mm, 1 kips = 4.45 KN)	138
Table 3-12: The modelling matrix for the two-inch-wall hollow columns confined with three types of confinement configurations.....	140

Table 4-1: Measured steel reinforcement properties	145
Table 4-2: Measured concrete strength on day of testing	146
Table 4-3: Summary of the test of circular specimens	154
Table 4-4: Summary of the test of square specimens	155
Table 6-1: Properties of example columns	285

LIST OF NOTATIONS

A_s	bar area of lateral reinforcement
A_{s1}	bar area of outer layer of lateral reinforcement
A_{s2}	bar area of inner layer of lateral reinforcement
A_{tr}	area of cross ties in hollow columns with two layers of confinement connected with cross ties
b_c	width of the concrete core measured to the outside of the peripheral hoop of square column
d	outer diameter of circular hollow column, same as D
d'	inner diameter of circular hollow column, same as D'
d''	nominal diameter of lateral steel tie
E_c	initial stiffness of concrete
E_{des}	slope of falling branch or softening rate of confined concrete models
f_c	compressive strength of concrete
f'_{c0}	compressive strength of unconfined concrete, same as f_{c0}
f'_{cc}	compressive strength of confined concrete
f_{cr}	circumferential stress
f_r	lateral confining stress, same as f_l
f_{r1}	lateral confining stress applied by the outer layer of lateral reinforcement
f_{r2}	lateral confining stress applied by the inner layer of lateral reinforcement
$f_{r,max}$	maximum confining pressure experienced by each individual layer of hollow columns in FE analysis

f_s	tensile strength of lateral reinforcement
f_{s1}	tensile strength of outer layer of lateral reinforcement
f_{s2}	tensile strength of inner layer of lateral reinforcement
f_{tr}	tensile strength of cross ties in hollow columns with two layers of confinement connected with cross ties
f_{yh}	yield strength of lateral reinforcement
h''	inside length of side of rectangular ties
k_e	confinement effectiveness coefficient
K_s	ratio of the confined concrete strength to unconfined concrete strength
n	number of cross ties in hollow columns with two layers of confinement connected with cross ties
r/f	abbreviation of reinforcement
s	longitudinal spacing of lateral reinforcement
u	displacement in the x direction for FE modelling in ABAQUS
v	displacement in the y direction for FE modelling in ABAQUS
w	displacement in the z direction for FE modelling in ABAQUS
β	wall thickness to section diameter ratio (t/D)
ε_0	strain at peak stress for unconfined concrete
ε_c	compression strain in concrete
ε_{cc}	strain at peak stress for confined concrete
ε_{cu}	ultimate compression strain in concrete

- ϵ_{s1} minimum strain at peak stress for confined concrete models
- ϵ_{s2} maximum strain at peak stress for confined concrete models
- ϵ_{sxx} strain corresponding to xx% of the maximum stress on the descending branch of confined concrete models
- ρ_l area ratio of longitudinal reinforcement based on the gross concrete area
- ρ_{sh} volumetric ratio of lateral reinforcement to concrete core, same as ρ_s

CHAPTER 1 INTRODUCTION

1.1 Overview

In seismic regions, bridge columns are required to be designed for significant lateral loads, which produce large shear forces in the columns and large bending moments at the column ends. To design these columns efficiently and to enable them to respond in a ductile manner, they are designed with preselected inelastic regions. These regions, known as the plastic hinges, will experience inelastic strains when they are subjected to moderate to severe earthquake excitations. While helping to dissipate the energy imparted to the structure by the earthquake, these hinge regions will also experience structural damage.

Since bridge columns are usually designed for a low axial load ratio and high flexural moment, the solid column section is not always efficient. The central portion of the column sections provides little moment resistance, but helps to reduce the axial stress due to the gravity loads. In order to increase the efficiency of the materials and reduce the seismic mass, hollow reinforced concrete columns are becoming a preferred choice, especially for tall bridge columns in seismic regions. Figure 1-1 provides a picture of the high-speed rail project in Taiwan using a hollow section for the column and the corresponding configuration of the lateral reinforcement used. The reduction in seismic mass associated with the use of hollow columns can improve the overall structural behavior due to the reduction in inertia forces generated during an earthquake. The reduced inertia force not only makes the column design efficient, but also reduces the design force in the superstructures and foundations, reducing the overall structural cost.

To ensure dependable seismic performance of columns, their plastic hinge regions must be provided with sufficient transverse reinforcement, to ensure adequate concrete confinement as well as to prevent column shear failure and the longitudinal reinforcement from experiencing buckling. Therefore, satisfactory ductility for columns (a structural ductility of four to five is typically required for bridge columns) could be attained. This reinforcement is typically provided in the form of hoop and spiral reinforcement. Due to the Poisson's effect, concrete will dilate as it experiences increased axial compression until it ultimately fails. This failure results from either crushing of the concrete or fracture of the transverse reinforcement. In the design process, an

adequate amount of transverse reinforcement is provided for the concrete in the plastic hinge regions, so that the columns will achieve the desired level of ductility, and will not experience any undesired failure mode that can cause a brittle failure of the column and collapse of the structure.



Figure 1-1: Hollow bridge columns of the high-speed rail project in Taiwan (Mo et al. 2003)

1.2 Background

It has been widely accepted that well-confined concrete members could sustain large axial concrete strains without significant loss of concrete strength (e.g.; Hines, 2002). The confinement in critical regions of concrete columns is typically designed using the models developed primarily for solid concrete sections, such as the model proposed by Mander et al. (1988). The stress-strain model of confined concrete members proposed by Mander et al. (1988) was originally calibrated based on solid sections. This model has been studied and utilized widely in seismic design of reinforced concrete bridges (Caltrans 2013; AASHTO 2012; AASHTO 2013 and AASHTO 2014). Experimental studies conducted by previous researchers indicated that the stress-strain model of confined concrete, proposed by Mander et al., could accurately predict the flexural behavior of reinforced concrete columns or bridge piers under a lateral load, such as an earthquake. Besides Mander's model, there are several other confined

concrete models that also describe the increased strength and ductility of concrete due to the transverse confinement, such as the models proposed by Park et al. (1982), Saatcioglu and Razvi (1992), Hoshikuma et al. (1997) etc. These models were also developed based on experimental testing of cylinders under pure axial compression. However, these confined concrete models may not be applicable to hollow sections. This concern is due to complexity arising from the void in the middle of the column section and its negative influence on the effectiveness of confinement. The applicability of the confined concrete models developed for solid sections to hollow sections has not been studied extensively, requiring a detailed investigation.

Designing the amount and spacing of confinement reinforcement for seismic bridge columns with solid sections is fairly well established. However, significant inconsistencies in the required amount and variations in quantifying some of the key parameters (e.g.; ultimate compression strains) continue to exist (Shelman and Sritharan, 2014). The confinement topic has created more inconsistencies in the design of hollow reinforced concrete columns due to a lack of fundamental understanding of concrete dilation when subjected to axial compression with a void in the middle of the section. Although limited research exists, the previous research has mostly focused on investigating flexural and shear strength of hollow reinforced concrete columns by conducting experimental tests on large-scale hollow bridge column models. Some tested columns with one layer of transverse reinforcement that was placed near the outside surface of the concrete wall (e.g.; Zahn et al., 1990; Hoshikuma and Priestley, 2000; Ranzo and Priestley, 2001). They found that limited ductile behavior could be achieved for these columns if the axial load ratio, wall thickness-to-section diameter ratio, longitudinal reinforcement ratio, as well as transverse reinforcement amount and spacing are all designed properly to guarantee that the neutral axis would be located within the concrete wall thickness (Zahn et al., 1990). This would eliminate the possibility of the inside concrete wall from experiencing high compressive strains, hence allowing the section to experience limited ductile behavior.

Some other researchers (e.g.; Yeh et al., 2001 and 2002) tested specimens with two layers of transverse reinforcement, distributed equally close to both the inside and outside concrete wall surfaces with cross ties. They stated that this type of confinement configuration was effective for hollow sections because they believed that the inside concrete wall had to be confined to reach a higher axial concrete strain in the inner region. The inner layer of transverse reinforcement is to

prevent concrete crushing at the inside concrete wall surface and to allow the member to reach a higher ductility level, if the inner layer of transverse reinforcement was tied to the outer layer of transverse reinforcement effectively (see more details in Section 2.2.1). Their test results confirmed that this type of confinement configuration was more effective when compared to the configuration with one layer of transverse reinforcement placed near the outside concrete wall surface. This is because the column failure in this case was dominated by longitudinal reinforcement rupture instead of inside concrete wall crushing. A higher ductility (in the range of eight to ten) was experienced by the test specimens with two layers of transverse reinforcement connected with cross ties. However, it should be noted that the primary role of the cross ties in two layers of confinement reinforcement configurations is to transfer the demand from the inner layer of transverse reinforcement to the outer layer of transverse reinforcement. Therefore, it is not conducive to place an equal amount of transverse reinforcement near both the inside and outside concrete wall surfaces, because the demand for these two layers of reinforcement was different. The demand for the outer layer of transverse reinforcement was significantly greater than the inner layer of transverse reinforcement. Placing two layers of transverse reinforcement connected with cross ties also creates significant construction challenges, as it requires more labor and construction time, compared to placing one layer of transverse reinforcement closer to the outside concrete wall surface only. With two layers of confinement reinforcement, some additional longitudinal reinforcing bars will also be needed closer to the inner surface of the concrete wall for construction purposes.

1.3 Research scope and objectives

Given the lack of understanding on the confinement of hollow concrete columns and their seismic behavior, the overall scope of this research project was to understand the confinement effects in hollow concrete columns. This research project also shows how these columns should be designed and analyzed with due consideration realistic confinement effects with one and two layers of transverse reinforcement. The project scope is fulfilled by achieving the following objectives:

- Investigate the confinement effect in hollow bridge columns with the amount of transverse reinforcement, confinement configurations and wall thickness as main variables

- Examine the applicability of commonly-used confined concrete models in seismic design practice (i.e., Mander's model) for hollow bridge columns and identify areas where improvements are needed
- Study the flexural behavior of small-scale hollow rectangular and circular reinforced concrete bridge columns confined with single layer of confinement reinforcement experimentally
- Propose a set of preliminary guidelines for seismic design of hollow columns.

The above objectives were achieved by using a combination of analytical and experimental studies. The analytical study was completed using 3D finite element models developed in ABAQUS and fiber-based pushover analyses using the Open System for Earthquake Engineering Simulation (OpenSees). The experimental study used a total 16 small-scale columns subjected to a combination of axial and lateral loads, with the section shape, wall thickness, axial load ratio and loading type as the main variables.

1.4 Report layout

Following the introduction presented in this chapter, a literature review summarizing previous research on hollow columns and confined concrete models are provided in Chapter 2. Chapter 3 illustrates the confinement effect in hollow columns using 3D finite element modelling method and presents the suggested modelling method used to predict the flexure behavior of hollow columns in OpenSees. Chapter 4 gives an overview of the design, instrumentation and loading protocols for the test columns. Chapter 5 discusses the predictions of test hollow column analyses and presents the comparisons between the experimental and the analysis results. Finally, Chapter 6 gives a set of conclusions and design recommendations for design of hollow columns based on the research findings.

CHAPTER 2 LITERATURE REVIEW

2.1 Introduction

In tall seismic bridge columns, it has been noted that it is economical to use hollow concrete members due to high strength-to-mass and stiffness-to-mass ratios as well as low inertia force. However, the structural performance of hollow columns under lateral loads, such as those induced by an earthquake, is still not fully understood although several experimental and analytical works have been conducted by previous researchers. To better understand the current state of knowledge on the flexural behavior of hollow reinforced concrete columns, a review of literature on related topics is summarized in the following sections.

2.2 Experimental study on hollow column behavior

2.2.1 Lateral load tests

The behavior of hollow reinforced concrete columns under cyclic lateral loading has attracted a lot of researchers' attention since the hollow columns were first investigated. Many efforts have focused on the flexural ductility and shear strength of hollow reinforced concrete columns and developing design approaches. Previous researchers suggested that the following design parameters would control the structural response of hollow concrete columns:

1. Wall thickness-to-section diameter/width ratio
2. Confinement configurations: one layer or two layers with cross tie
3. Axial load ratio
4. Longitudinal reinforcement ratio
5. Transverse reinforcement amount and spacing

The test specimens conducted in the previous research typically consisted of two different confinement configurations: one layer of confinement reinforcement placed near the outside concrete wall surface and two layers of confinement reinforcement placed near both the inside and outside concrete wall surfaces, connected with cross ties. For the test specimens that had two layers of confinement reinforcement, the inner layer of reinforcement, which had the same

diameter with the same spacing as the outer reinforcement, was usually tied to the outer layer of reinforcement. This is because previous studies showed that the inner layer of reinforcement confined only the inner concrete cover of the section if it was not tied to the outer layer of reinforcement, leaving the region around the inner layer of reinforcement unconfined. This indicated that the inner layer of reinforcement was not effective in confining the concrete, unless it was tied to the outer layer of reinforcement for circular hollow sections (Papanikolaou & Kappos, 2009).

2.2.1.1 Single layer of confinement

Several studies demonstrated that a limited ductile behavior could be achieved in hollow concrete columns with only one layer of transverse reinforcement as long as the columns have a low axial load ratio, small longitudinal steel ratio, and a relatively thicker wall. The transverse reinforcement was usually placed near the outside concrete wall surface, that is, in the typical location of transverse reinforcement for solid sections.

Zahn et al. (1990)

Zahn et al. tested six circular hollow reinforced concrete columns without confinement reinforcement on the inside concrete wall face. Wall thickness-to-section diameter ratio, axial load ratio and longitudinal reinforcement ratio were three primary variables studied in this research. A less ductile behavior was observed for hollow sections, due to the concrete that crushed on the inside face of the concrete wall. The longitudinal reinforcement ratio was 2.56% for all the column units based on the gross section, which ranged from 3.67% to 5.4% based on the net section. Three different wall thickness-to-section diameter ratios were selected for the six test specimens with each two column units having the same t/D ratio. The two column units that had the same t/D ratio were subjected to different axial load ratios. The test parameters and corresponding results are summarized in Table 2-1 for the three selected column units (column units 2, 3 and 5). The results of these three column units were representative of the performance for all the column units that were tested in this study. Figure 2-2 to Figure 2-4 present the hysteretic loops of column unit 2, 3 and 5. It was found that the ductility of hollow concrete columns with one layer of transverse reinforcement placed near the outside concrete face was primarily determined by the location of the neutral axis. If the neutral axis was located inside the

concrete wall, a limited ductile behavior could have been expected. Otherwise, if the neutral axis was located away from the concrete wall toward the centroid of the section, a very brittle failure would have been exhibited. Zahn et al. suggested that the concrete that crushed on the inside face was at 0.008 longitudinal compressive strains, which could be used to define the ultimate limit state. In addition, a limited ductile behavior could be expected by using low axial load ratio, moderate longitudinal reinforcement ratio and a wall thickness-to-section diameter ratio equal to, or greater than 0.15. The key to experiencing ductile behavior for hollow columns as described by Zahn et al. (1990) was that the neutral axis of the section should move into the column wall.

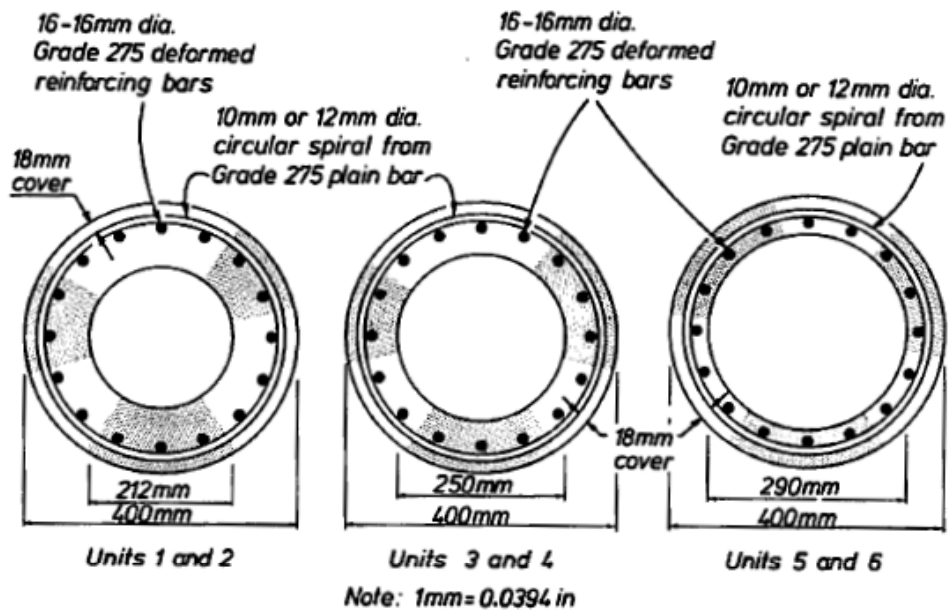


Figure 2-1: Dimensions of test units by Zahn et al. (1990), (1mm = 0.0394 inch)

Table 2-1: Test parameters and failure mode of column tested by Zahn et al. (1990)

Unit	Ductility level	t/D	Longitudinal reinforcement ratio, gross (net)	Axial load ratio, gross (net)	Failure
2	2.0	0.235	2.56% (3.67%)	28% (40%)	Brittle failure
3	5.8	0.185	2.56% (4.2%)	6% (10%)	Ductile failure
5	3.2	0.135	2.56% (5.4%)	5.6% (12%)	Limit ductile failure

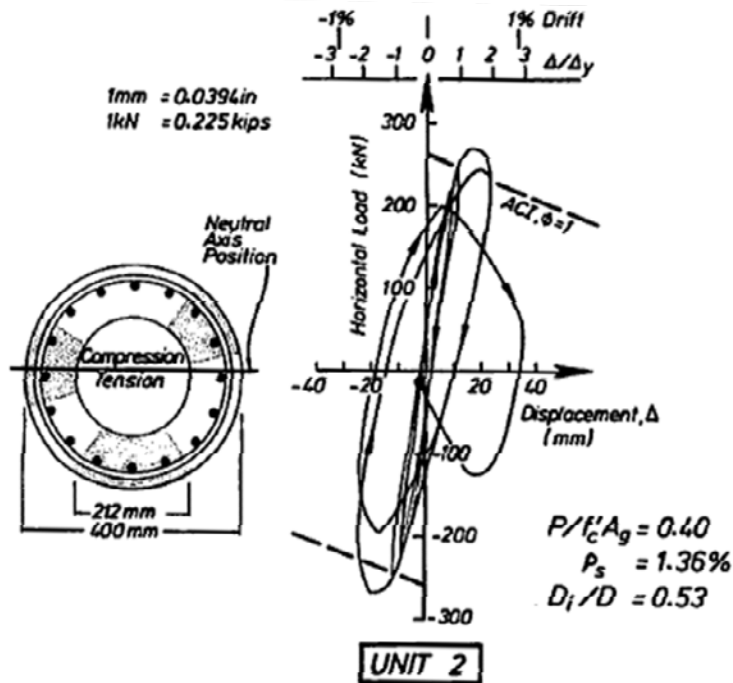


Figure 2-2: Lateral force vs. displacement response and neutral axis position of column unit 2 with $t/D = 0.235$ (Zahn et al. 1990)

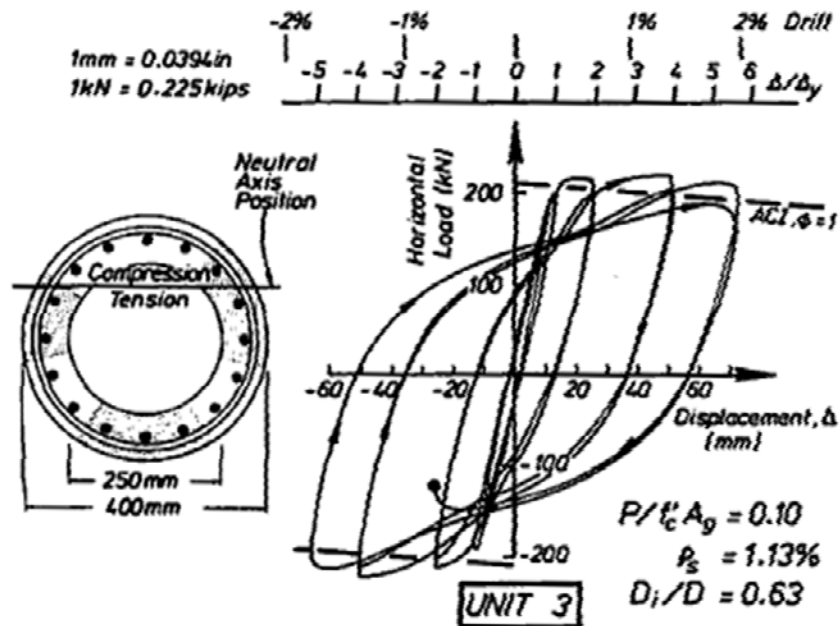


Figure 2-3: Lateral force vs. displacement response and neutral axis position of column unit 3 with $t/D = 0.185$ (Zahn et al. 1990)

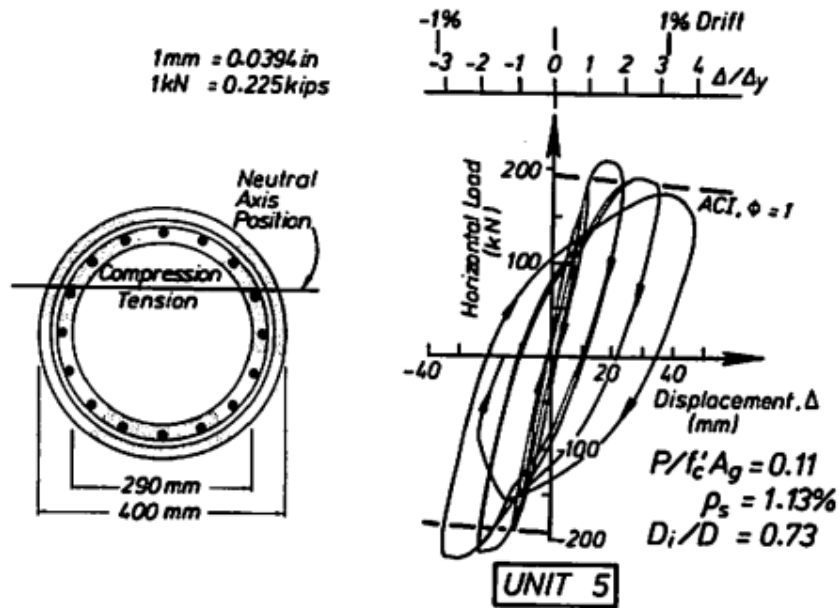


Figure 2-4: Lateral force vs. displacement response and neutral axis position of column unit 5 with $t/D = 0.135$ (Zahn et al. 1990)

Kawashima et al. (1992)

In 1992, Kawashima et al. tested two pairs of circular hollow reinforced concrete columns with two different longitudinal reinforcement ratios (1.35% and 2.19% based on the net section, which corresponded to 0.8% and 1.3% based on the gross section). They found that the crushing of concrete at the inside concrete face dominated the behavior, which was much more obvious for higher longitudinal reinforcement ratios. They confirmed that a limited ductile behavior could be expected from specimens with a low longitudinal reinforcement ratio for hollow columns. They also found that the confinement effect, in terms of both increased strength and ductility, was weakened due to concrete crushing at the inside face for the hollow columns.

Hoshikuma and Priestley (2000)

Due to a lack of knowledge about the ductility capacity and shear strength of hollow bridge columns designed in California, two thin-walled circular hollow columns with one layer of confinement reinforcement placed near the outside face of the concrete wall were tested by Hoshikuma and Priestley (2000). In this study, the researchers primarily focused on the flexural

performance. The shear strength of hollow circular columns was studied by Ranzo and Priestley, which will be discussed in the next section. The wall thickness-to-section diameter ratio of the specimens in this study was much smaller (0.092) than those tested by previous researchers, i.e., Zahn et al. (0.14-0.24) and Kawashima et al. (0.18). The structural responses of these two specimens were dominated by flexural failure and the primary test variable was the longitudinal reinforcement ratio. The test parameters and corresponding results are summarized in Table 2-2. Similar to the test results presented by Zahn et al. (1990) and Kawashima et al. (1992), the failure of both specimens in this study was also controlled by the concrete crushing at the inside face of concrete wall. It was reported that the concrete crushed on the inside face at a longitudinal compressive strain of 0.005. From Figure 2-6 and Figure 2-7, the specimen with the lower amount of longitudinal reinforcement (i.e., Specimen HF1) reached a higher ductility of 3.3. When this observation is complemented with the previous findings drawn by Zahn et al. (1990) and Kawashima et al. (1992), it follows that a larger longitudinal reinforcement ratio would reduce the ductility of the hollow columns (also true for solid columns). Also, the transverse reinforcement did not reach yield strain when the column failure was observed, which indicated that the one layer of confinement reinforcement placed near the outside concrete wall could not confine the concrete core as well as solid sections. Therefore, the confinement effectiveness for hollow sections with one layer of confinement reinforcement was less compared to solid sections, reducing the ductility of hollow bridge columns.

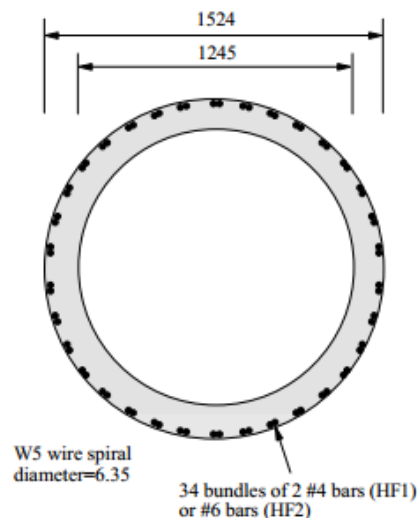


Figure 2-5: Cross sectional dimensions (in mm) of columns tested by Hoshikuma and Priestley (2000), (1 mm = 0.0394 inches)

Table 2-2: Test parameters and failure mode of column tested by Hoshikuma and Priestley (2000)

Unit	Ductility level	Wall thickness-to-section diameter ratio	Longitudinal reinforcement ratio, gross (net)	Axial load ratio, gross (net)	Failure
HF1	3.3	0.092	0.48% (1.45%)	4.3% (13%)	Brittle failure
HF2	1.8	0.092	1.06% (3.18%)	4.3% (13%)	Brittle failure

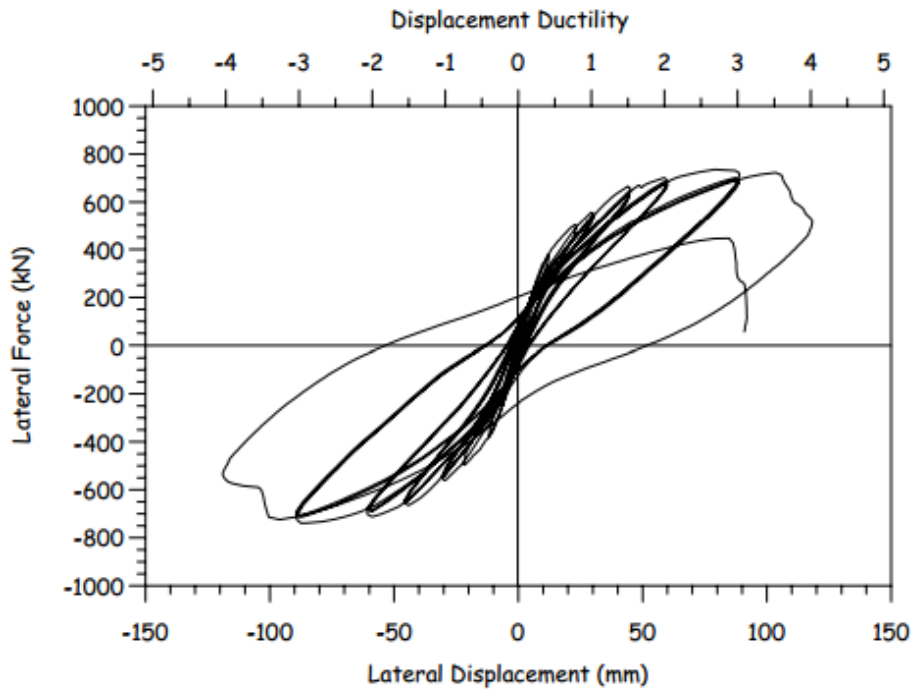


Figure 2-6: Lateral force vs. displacement response of specimen HF1 tested by Hoshikuma and Priestley (2000), (1 mm = 0.0394 inches, 1 kN = 0.225 kips)

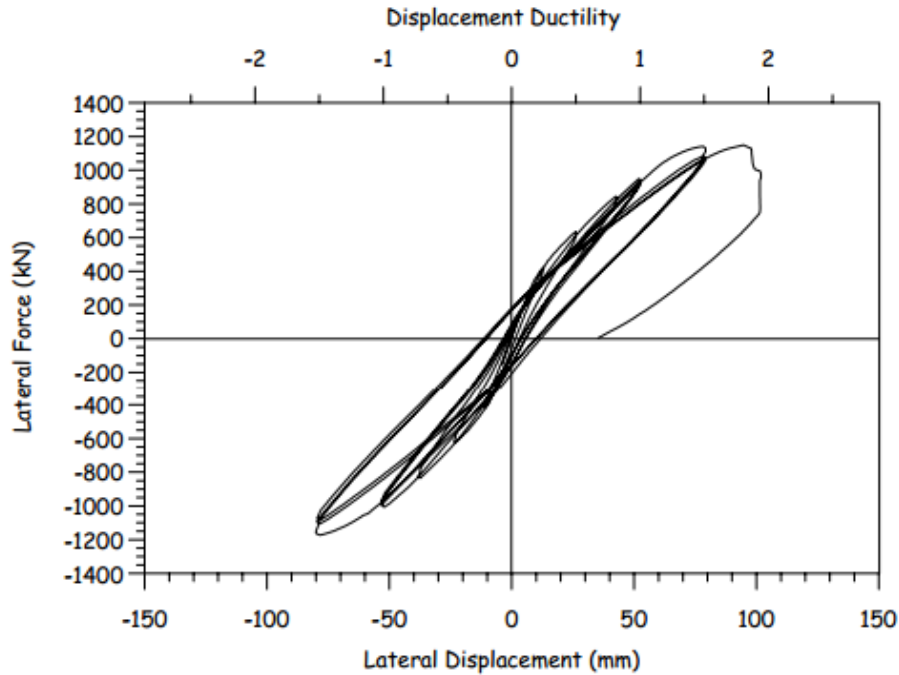


Figure 2-7: Lateral force vs. displacement response of specimen HF2 tested by Hoshikuma and Priestley (2000), (1 mm = 0.0394 inches, 1 kN = 0.225 kips)

Ranzo and Priestley (2001)

The purpose of the study conducted by Ranzo and Priestley was to investigate the shear strength of thin-walled circular hollow columns with one layer of lateral reinforcement placed near the outside face of concrete wall. This is a follow-up study of the research conducted by Hoshikuma and Priestley (2000). Although this topic is outside the scope of research presented in this report, it is included here due to some column responses being dominated by the flexure performance. Three specimens were tested under a constant axial load and a cyclically varying lateral load. Two failure types were observed: flexural failure and shear failure. The shear strength of circular hollow columns was predicted using three different models: UCSD model, ATC 32 model and Caltrans Memo 20-4 model. The test variables were the longitudinal reinforcement ratio and the axial load ratio. The test specimen is shown in Figure 2-8, while the test parameters and corresponding results for the three test specimens are summarized in Table 2-3.

Limited ductile behavior could have been expected from specimens with low level of axial load and low longitudinal reinforcement ratio if sufficient transverse reinforcement was

provided. The measured lateral force vs. displacement response as well as the analytical prediction for the first specimen (i.e., Specimen HS1) is shown in Figure 2-9. The predicted failure was longitudinal reinforcement rupture at a tension steel strain of 0.06. However, the actual failure experienced by this test specimen was due to the concrete crushing at the inside concrete wall in compression at about 300 mm (11.8 inch) from the base, which occurred during the third cycle in the push direction. This indicated that the analytical model was not able to capture the failure experienced by the test specimen, although the overall behavior was predicted fairly accurately.

By comparing the experimental results to the analytical models, it was found that the UCSD model had the ability to be fairly accurate when predicting the shear strength of hollow columns. The shear strength improvement due to axial load seemed to be less significant compared to solid sections. Therefore, the shear strength due to axial load could be ignored for the design purpose of hollow columns. In addition, a minimum ratio of 0.1 between wall thickness and section diameter was suggested.

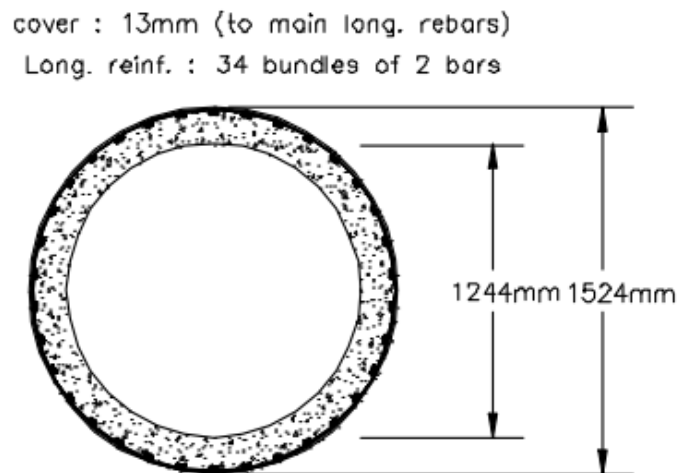


Figure 2-8: Cross sectional dimensions (in mm) of column tested by Ranzo and Priestley (2001), (1 mm = 0.0394 inches)

Table 2-3: Test parameters and failure mode of columns tested by Ranzo and Priestley (2001)

Ductility level	Wall thickness-to-section diameter ratio	Longitudinal reinforcement ratio, gross (net)	Axial load ratio, gross (net)	Failure
6.0	0.097	0.49% (1.4%)	1.75% (5%)	Flexural failure
3.0	0.091	0.8% (2.3%)	1.75% (5%)	Brittle flexural/Shear failure
2.0	0.091	0.8% (2.3%)	5.25% (15%)	Shear failure

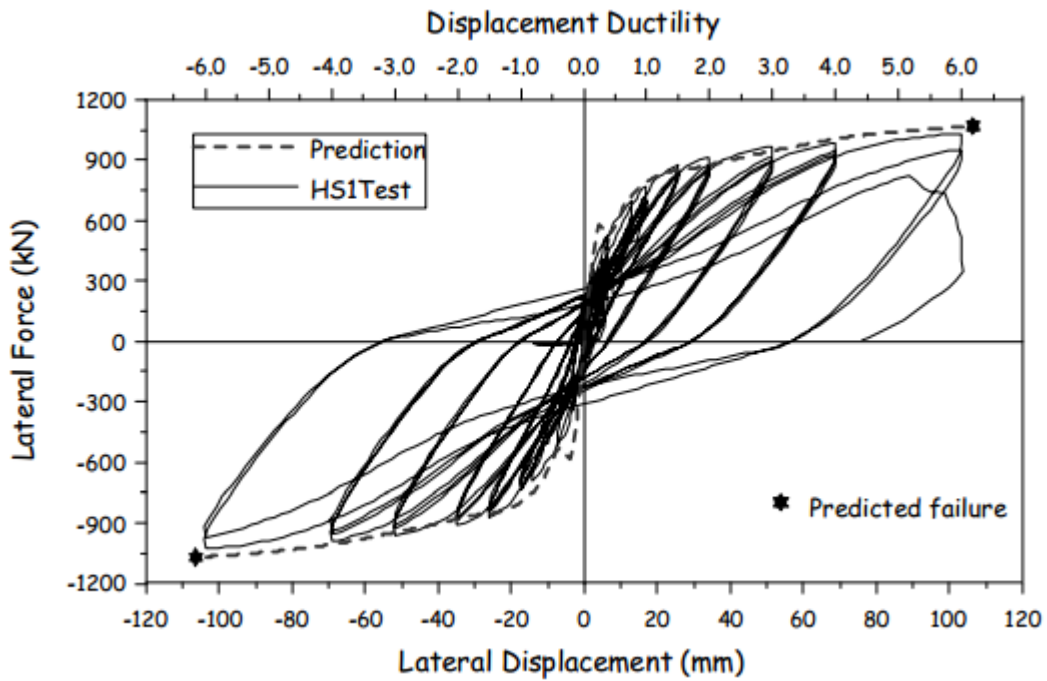


Figure 2-9: Lateral force vs. displacement response of specimen HS1 tested by Ranzo and Priestley (2001), (1 mm = 0.039 inches, 1 kN = 0.225 kips)

2.2.1.2 Two layers of confinement

The most commonly used section for hollow concrete columns are confined with two layers of transverse reinforcement. One layer of transverse reinforcement was provided near the outside concrete wall surface (in the typical transverse reinforcement location of solid columns), and the other layer of transverse reinforcement, which had the same diameter with the same spacing as the outer reinforcement, was provided near the inside face to confine the inside concrete wall and prevent brittle failure that resulted from the inside concrete wall crushing. The inner layer of transverse reinforcement was usually tied to the outer layer of transverse reinforcement to effectively confine the concrete core. There have been several studies related to the flexural behavior of hollow concrete columns that were confined with two layers of transverse reinforcement.

Yeh et al. (2002)

In order to study the seismic behavior of rectangular hollow bridge piers in Taiwan, three prototype rectangular bridge columns were tested under a constant axial load and a cyclically reversed horizontal load. The effect of lateral reinforcement amount was analyzed in this study. Two failures types were observed: flexural failure and shear failure. The flexural failure was characterized by rupture of tension longitudinal steel at the bottom of the piers, while the shear failure was characterized by lateral reinforcement failure. Since the focus of the research presented in this report is the flexure behavior, the specimen which failed by shear was not included here. The test specimens which failed by flexure are shown in Figure 2-10 with two different amounts of lateral reinforcement, and the corresponding test results are tabulated in Table 2-4. The lateral force vs. displacement responses for specimen PS1 and PI1 are shown in Figure 2-11 and Figure 2-12, respectively. The specimen with a larger amount of lateral reinforcement (HS1) reached a higher ductility (10.3). It was concluded that the greater the amount of lateral reinforcement provided, the greater ductility was achieved. The effect of confinement provided by the lateral reinforcement was clearly represented through the test results regarding increased ductility. In addition, compared to the ACI code (1995), the equation proposed by Priestley et al. (1996) was more accurate when designing the required lateral reinforcement.

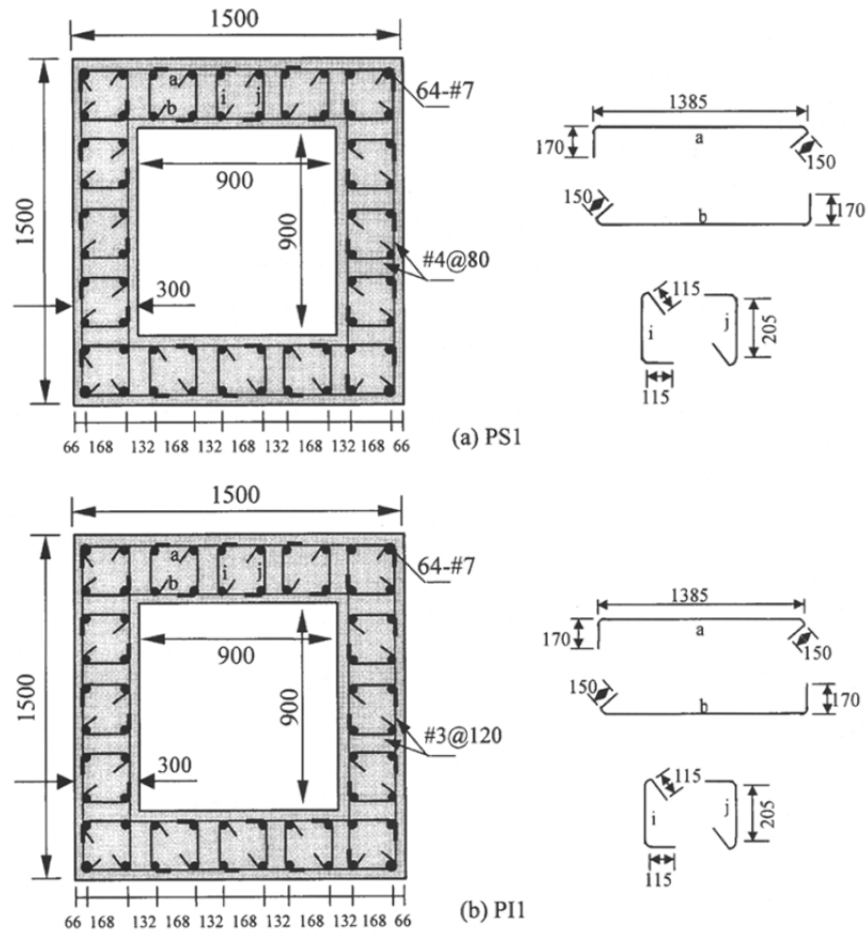


Figure 2-10: Cross sectional dimensions (in mm) of columns tested by Yeh et al. (2002),
(1 mm = 0.0394 inches)

Table 2-4: Test parameters and failure mode of column tested by Yeh et al. (2002)

Unit	Ductility level	Wall thickness-to-section diameter ratio	Longitudinal reinforcement ratio, gross (net)	Axial load ratio, gross (net)	Shear reinforcement	Failure
PS1	10.3	0.2	1.1% (1.7%)	5.2% (8.2%)	>100% ACI code*	Flexural failure
PI1	8.7	0.2	1.1% (1.7%)	5.2% (8.2%)	50% ACI code*	Flexural failure

*ACI code: ACI seismic provisions (ACI Committee 318: 1995, Building code requirement for reinforced concrete, ACI, Detroit)

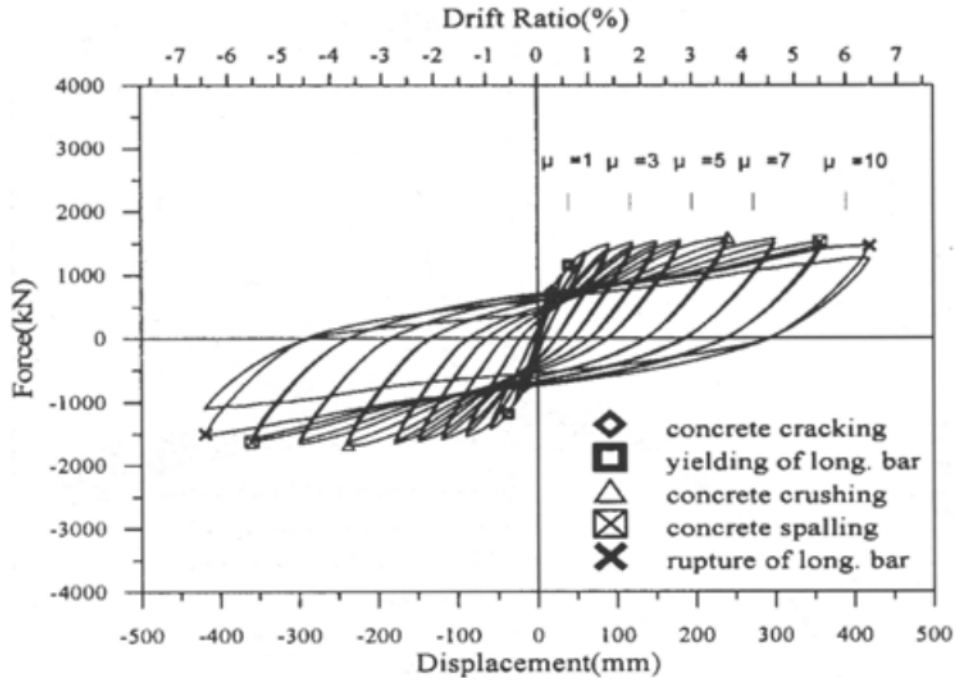


Figure 2-11: Lateral force vs. displacement response of specimen PS1 tested by Yeh et al. (2002), (1 mm = 0.039 inches, 1 kN = 0.225 kips)

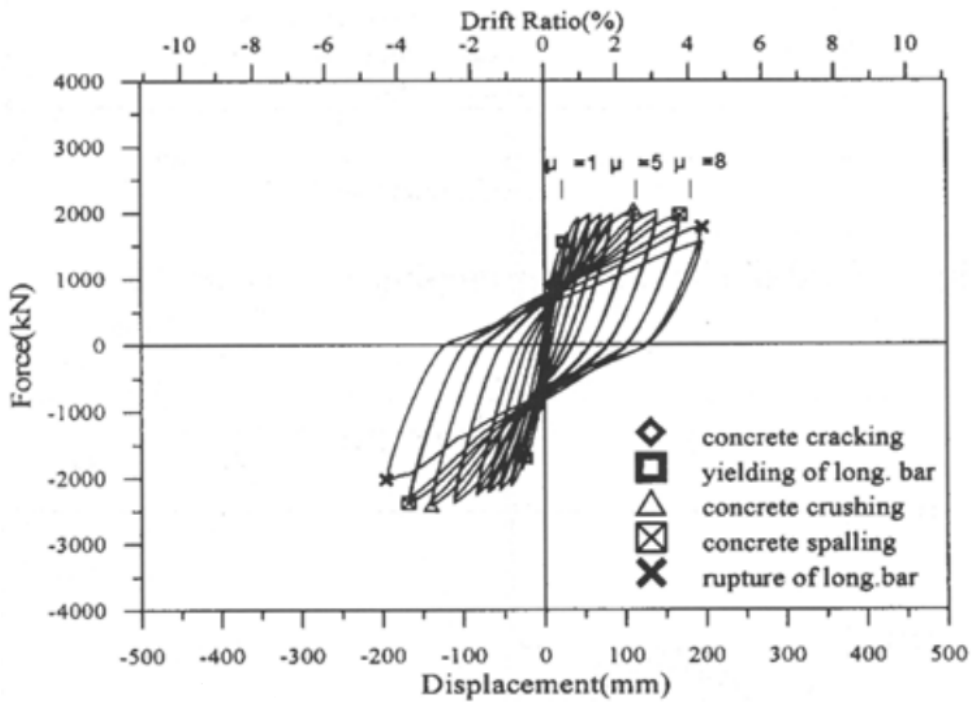


Figure 2-12: Lateral force vs. displacement response of specimen PI1 tested by Yeh et al. (2002), (1 mm = 0.039 inches, 1 kN = 0.225 kips)

Mo et al. (2003)

The seismic performance of eight scaled hollow columns under cyclically reversed horizontal load was investigated in an experimental program by Mo et al. (2003). The effects of concrete compressive strength (normal and high), confinement configurations (type A and type B shown in Figure 2-13) and lateral reinforcement spacing (40 mm and 80 mm) were investigated both experimentally and analytically in this study. Two types of failure modes were observed during the tests, which were shear failure caused by longitudinal reinforcement buckling and tension longitudinal reinforcement rupture at the base of the columns. In this study, ductility was defined as the ratio of displacement corresponding to 80% maximum horizontal force in the descending portion to the displacement corresponding to first yield of longitudinal reinforcement. By examining the moment curvature diagrams developed from the measured horizontal force as well as the readings of LVDTs located at both the right and left concrete surfaces in the plastic hinge regions, the following observations were reported.

1. For normal strength concrete with a given confinement configuration, the specimens with greater lateral reinforcement spacing presented a larger strength deterioration rate after the peak moment, which was not the case for high-strength concrete specimens as shown in Figure 2-14 .
2. The ductility for the hollow section was smaller compared to the solid section, which was suspected by the researchers to be due to the following aspects: the confined area for the hollow section was smaller than for the solid section, and the concrete behavior was likely degraded due to the void in the middle for hollow section.
3. As the axial ratio increased from 11% to 19%, the failure modes changed from reinforcing bar rupture to reinforcing bar buckling.
4. The moment-curvature analyses based on the modified Murguruma et al. (1980) confined concrete model could adequately predict the lateral force vs. displacement response of hollow reinforced concrete columns with two layers of confinement (Figure 2-15).

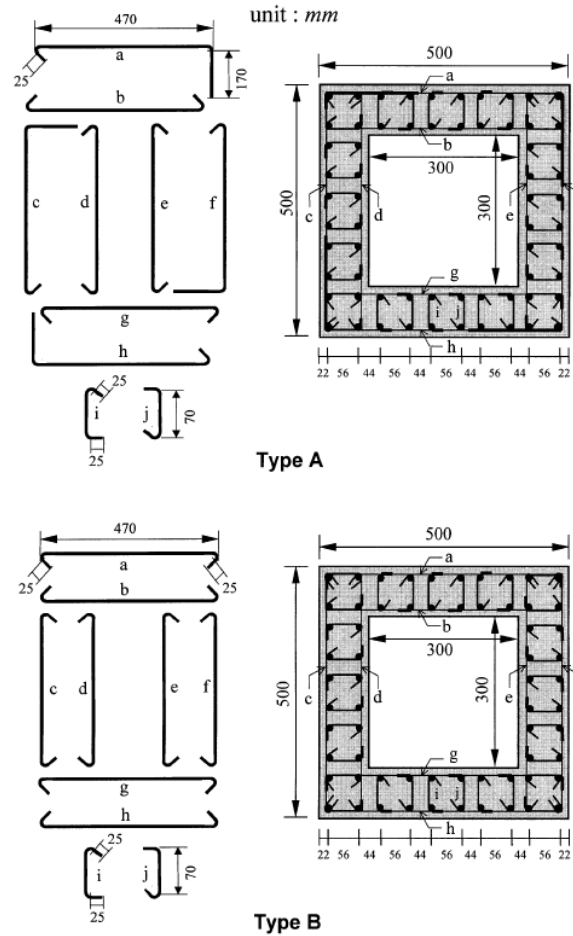


Figure 2-13: Lateral reinforcement configurations used for test specimens (in mm) by Mo et al. (2003), (1mm = 0.0374 inch)

Table 2-5: Test parameters and failure modes of columns tested by Mo et al. (2003), (1mm = 0.0394 inch)

Ductility level	Wall thickness-to-section diameter ratio	Longitudinal reinforcement ratio, gross (net)	Axial load ratio, gross (net)	Lateral reinforcement spacing	Failure
3.7	0.2	0.7% (1.1%)	12% (19%)	40 mm	Shear failure
6.3	0.2	0.7% (1.1%)	5.8% (9%)	40 mm	Flexural failure
6.6	0.2	0.7% (1.1%)	7% (11%)	80 mm	Flexural failure
6.3	0.2	0.7% (1.1%)	7% (11%)	80 mm	Flexural failure

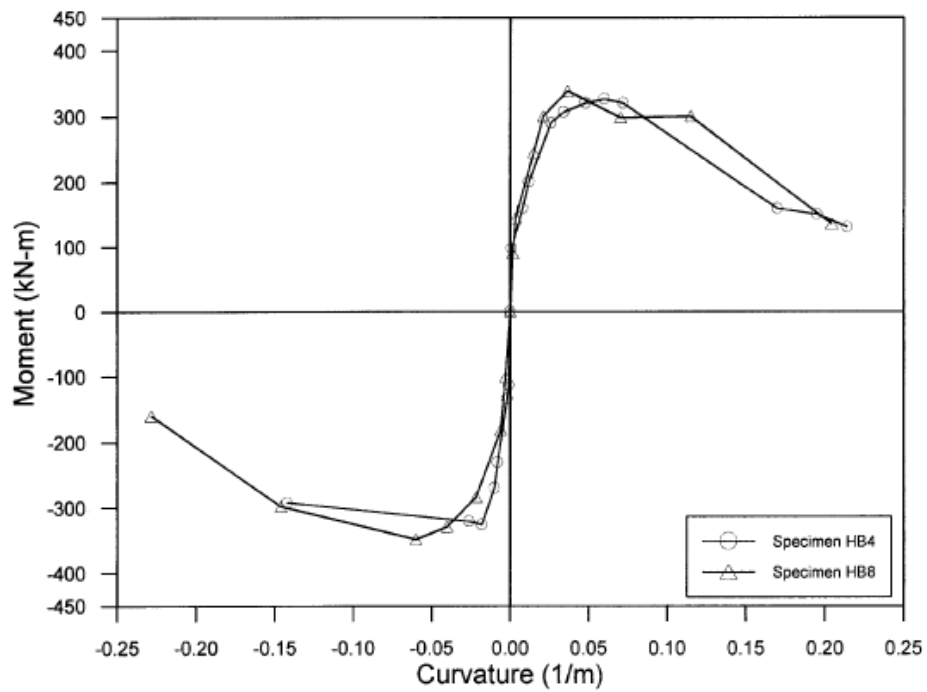
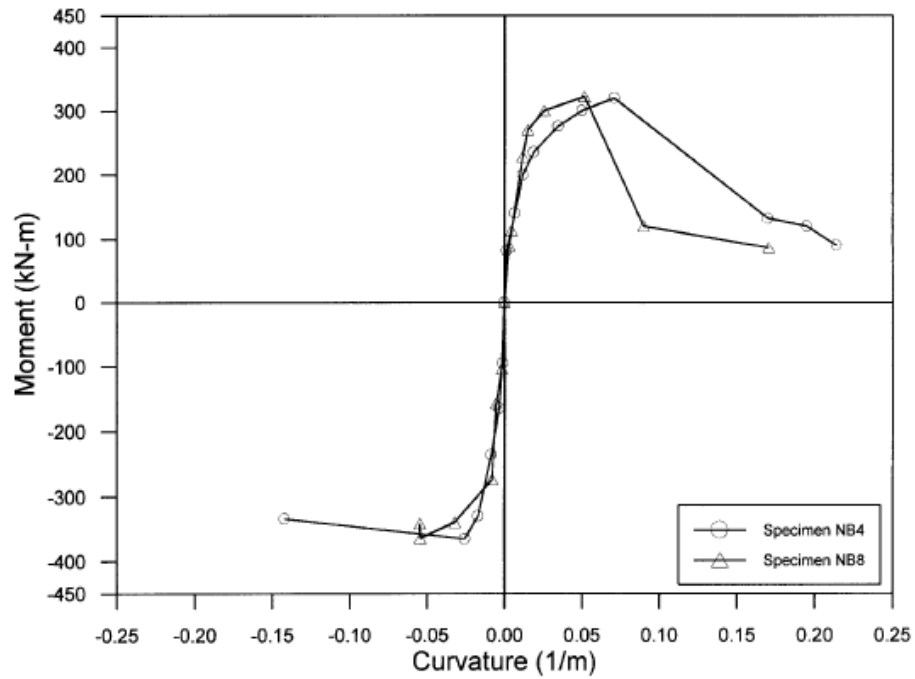


Figure 2-14: Effect of spacing of confinement reinforcement on the moment-curvature curves for normal strength concrete and high strength concrete by Mo et al. (2003)

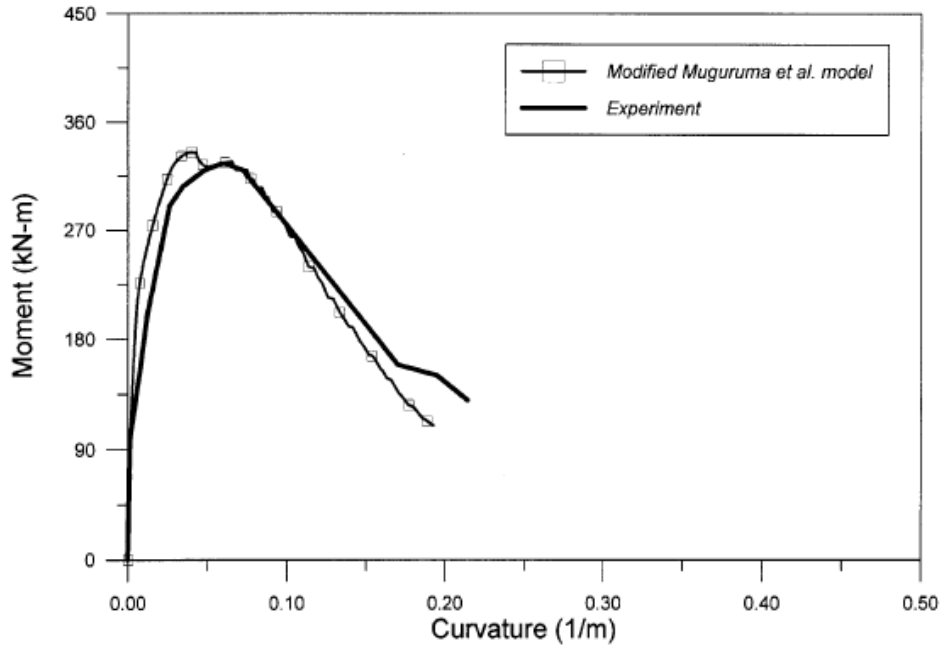


Figure 2-15: Comparison of experimental results with moment-curvature curves based on the modified Muguruma et al. model of Specimen HB4 by Mo et al. (2003)

Table 2-6 summarizes the previous studies on the hollow reinforced concrete columns discussed thus far, and compares the test unit details used in these past experiments. Corresponding design recommendations are tabulated in Table 2-8. It is seen that, the wall thickness-to-section diameter/length ratio used for one layer of confinement reinforcement is generally smaller than that used for two layers of confinement connected with cross ties, especially for the specimens tested by Hoshikuma and Priestley (2000) as well as Ranzo and Priestley (2001). The axial load ratio, longitudinal reinforcement ratio and the transverse reinforcement also varied significantly among the test specimens.

Table 2-6: Summary of previous experimental studies on hollow reinforced concrete columns

Researchers	Section type	Wall thickness-to-section diameter/width ratio	Axial load ratio, gross	Aspect ratio	Longitudinal reinforcement ratio, gross	Transverse reinforcement amount (Volumetric ratio, gross)	Confinement configurations
Zahn et al. (1990)	Circular	0.14-0.24	0.05-0.28	4.5	2.56%	10-12 mm dia. @ 75-90 mm (1.13%-1.36%)	One layer
Kawashima et al. (1992)	Circular	0.18	0	3.1	0.8% and 1.3%	9 mm dia. @ 200 mm (0.18%)	One layer
Hoshikuma and Priestley (2000)	Circular	0.092	0.04	4.3	0.48% and 1.06%	6.35 mm dia. @ 35 mm (0.22%)	One layer
Ranzo and Priestley (2001)	Circular	0.097 0.091	0.02 0.05	2.5	0.49% 0.8%	6.35 mm dia. @ 70 mm (0.12%)	One layer
Yeh et al. (2002)	Square	0.2	0.05	4.3 3.0	1.1%	13 mm dia. @ 80 mm 10 mm dia. @ 120 mm (0.56%-1.52%)	Two layers with cross ties
Mo et al. (2003)	Square	0.2	0.12 0.06 0.07	4.0	0.7%	4 mm dia. @ 40 mm 4 mm dia. @ 80 mm (0.45%-0.9%)	Two layers with cross ties

Table 2-7: Summary of experimentally observed failure modes of tests listed in Table 2-6

Researchers	Section type	Ductility level	Wall thickness-to-section diameter ratio	Longitudinal reinforcement ratio, gross	Axial load ratio, gross	Failure type	Confinement configurations
Zahn et al. (1990)	Circular	2.0	0.235	2.56%	28%	Brittle failure	One layer
		3.2	0.135	2.56%	6%	Limit ductile failure	
		5.8	0.185	2.56%	5.6%	Ductile failure	
Brittle failure was caused by high axial load ratio							
Hoshikuma and Priestley (2000)	Circular	3.3	0.092	0.48%	4.3%	Brittle failure	One layer
		1.8	0.092	1.06%	4.3%	Brittle failure	
Shear failure was caused by high axial load ratio and/or high longitudinal reinforcement ratio							
Yeh et al. (2002)	Square	10.3	0.2	1.1%	5.2%	Flexural failure	Two layers with cross ties
		8.7	0.2	1.1%	5.2%	Flexural failure	
Shear failure was caused by high axial load ratio and/or high longitudinal reinforcement ratio							
Mo et al. (2003)	Square	3.7	0.2	0.7%	12%	<i>Shear failure</i>	Two layers with cross ties
		6.3	0.2	0.7%	5.8%	Flexural failure	
		6.6	0.2	0.7%	7%	Flexural failure	
		6.3	0.2	0.7%	7%	Flexural failure	
Shear failure was caused by high axial load ratio							

Table 2-8: Design recommendations proposed by previous researchers on hollow reinforced columns based on their investigations

Variables	Zahn et al. (1990)	Hoshikuma and Priestley (2000)	Ranzo and Priestley (2001)	Yeh et al. (2002)	Mo et al. (2003)
Wall thickness-to-section diameter/width ratio	≥15% with one layer of reinforcement		≥10% with one layer of reinforcement		
Transverse reinforcement spacing and size	Relatively minor effect			ACI code (1995)	Equation proposed by Priestley et al. (1996)
Axial load ratio	Low (5.6%, gross section)		Low (1.75%, gross section)		<7%, gross section
Longitudinal reinforcement ratio	Small (2.56%, gross section)	Small (0.48%, gross section)	Small (0.5%, gross section)		
Ductility	Longitudinal concrete compressive strain at 0.008	Longitudinal concrete compressive strain at 0.0035			

2.2.2 Axial load tests

Mo et al. (2003)

Mo et al. (2003) tested twenty-eight concrete panels subjected to axial compression load to determine the complete stress-strain behavior of confined concrete in hollow bridge columns. In the compression tests, three types of concrete failures were observed. These failures were concrete splitting (plain concrete), concrete crushing (most specimens) and longitudinal reinforcing bar buckling (specimens having high strength concrete and greater lateral confinement spacing). By examining the experimental stress-strain curves, the following was reported:

1. The confined specimens with normal strength concrete presented greater ductility compared to those with high strength concrete.
2. For normal strength concrete with given confinement configuration, smaller lateral reinforcement spacing led to greater strength and ductility. However, no obvious difference was observed for specimens with high strength concrete in terms of ductility.
3. The lateral reinforcement spacing required by the ACI code (2002) was not sufficient to prevent longitudinal reinforcement buckling. However, the equation suggested by Priestley et al. (1996) was fairly satisfactory.

The test results were then compared to the analytical models available in the literature and it was found that the axial stress-strain relationship for confined concrete in square hollow sections could be predicted by the confined concrete model proposed by Murguruma et al. (1978) with a modification. The modified Murguruma et al. model is shown in Figure 2-16 and the mathematical equations are proposed as follows:

$$\text{Region AB: } f_c = E_c \varepsilon + \frac{f'_c - E_c \varepsilon_c}{\varepsilon_c^2} \times \varepsilon^2, \text{ where } E_c = 4730 \sqrt{f'_c} \text{ in } N/mm^2$$

$$\text{Region BC: } f_c = \frac{f'_c - f_{cc}}{(\varepsilon_c - \varepsilon_{cc})^2} (\varepsilon_c - \varepsilon_{cc})^2 + f'_{cc} \quad \text{(Equation 2-1)}$$

$$\text{Region CD: } f_c = \frac{f_{cu} - f_{cc}}{(\varepsilon_{cu} - \varepsilon_{cc})} (\varepsilon_c - \varepsilon_{cc})^2 + f'_{cc}$$

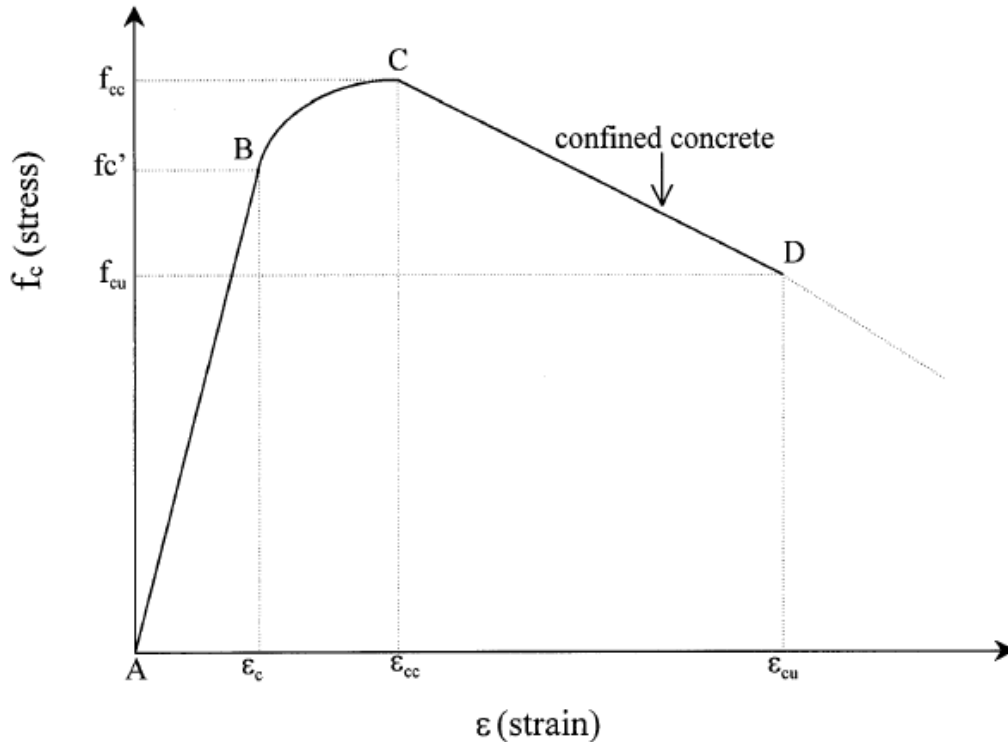


Figure 2-16: Stress-strain relationship of modified Muguruma et al. (2003) model

2.2.3 Summary

Based on the experimental research conducted by previous researchers, the hollow reinforced concrete columns with one layer of confinement reinforcement placed near the outside face of the section would fail as soon as the inside face of the concrete wall experienced crushing. Such columns can experience sudden failure (brittle failure) if not designed properly. The inside face of hollow concrete sections would control the failure of such columns although sufficient transverse reinforcement was placed near the outside face of the concrete wall. A limited ductile behavior could be expected from specimens with a relatively low axial load ratio, a low amount of longitudinal reinforcement ratio and a relatively thicker wall. The confinement effect induced in such columns was significantly less than in the solid section because of the reduced effectively confined concrete area.

The previous research indicated that hollow reinforced concrete columns with two layers of confinement reinforcement placed near both the inside and outside faces, as well as cross ties through the wall thickness, can produce adequate ductile behavior. The failure of such columns

was primarily dominated by the longitudinal reinforcement rupture. Table 2-9 summarizes the comparisons between these two commonly studied confinement configurations.

Table 2-9: Comparisons of two types of confinement configurations

Confinement configurations	Advantages	Disadvantages
One layer	Convenient Simple construction	The inside concrete face is unconfined and brittle failure may occur; the confinement effect is significantly reduced.
Two layers with cross ties	Ductile behavior	Significant construction effort and cost; interaction between the two reinforcement layers is not well understood

2.3 Analytical study of hollow column behaviors

In addition to experimental testing conducted on hollow reinforced concrete columns as discussed in the Section 2.2, several analytical studies were also performed to better understand the confinement effect in hollow columns.

Lignola et al. 2008

Lignola et al. (2008) performed a study, which provided a unified theory for the confinement of circular solid and hollow column sections. The study resulted in an adjusted confining pressure, which was intended for the use of columns confined with fiber reinforced polymer (FRP). However, the confinement model could be adjusted for application to other forms of confinement as well. The proposed concrete model is based on the Mander et al. model (1988), and provides the adjusted confining pressure based on the concept of equilibrium conditions and radial displacement compatibility between the concrete and the confining device (i.e., FRP). The equilibrium conditions and the radial displacement compatibility are illustrated in Figure 2-17 and Figure 2-18, respectively.

As shown in Figure 2-17, the inward confining pressure exerted by the FRP, q_e , should be equal to the outward pressure, q_i , acting inside the confined concrete cylinder, based on the

equilibrium conditions. According to Figure 2-18, a concrete cylinder would have a radial displacement of s_{cc} under axial concrete strain ϵ_c for free dilation. This radial displacement s_{cc} depended on the outer diameter of the concrete cylinder and Poisson's ratio of concrete, which would be the same for both solid and hollow concrete sections that have the same outer diameter. For the concrete cylinder confined with confinement, a confining pressure provided by the confinement would apply to the concrete and resist the concrete dilation. This confining pressure would cause an inward concrete displacement s_{cq} under the assumption of plane strain conditions. This inward displacement s_{cq} depended on the elastic modulus of the concrete (E_c), the Poisson's ratio of concrete, and both the outer and inner diameters of the concrete section. It was shown that the thinner the concrete wall, the higher is the inward displacement under the given pressure q . Therefore, the hollow concrete section with a thinner wall would have a smaller outward dilation ($s_{cc} + s_{cq}$). At the same time, an outward FRP jacket dilation, s_{fq} , resulting from the pressure q acting inside the FRP thin cylinder would be induced, which depended on the Poisson's ratio and elastic modulus of the confining device (i.e., FRP). Based on the radial displacement compatibility, the outward concrete dilation, $s_{cc} + s_{cq}$, should be equal to the FRP jacket outward dilation, s_{fq} .

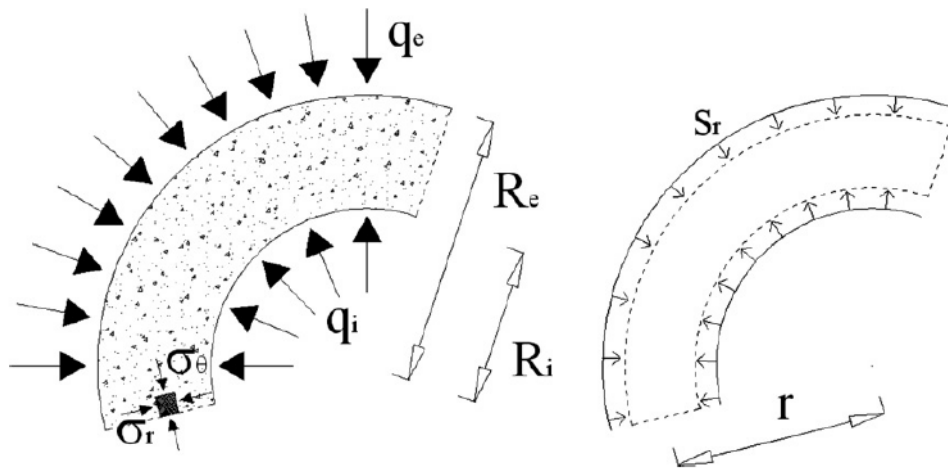


Figure 2-17: Symbols and boundary conditions (Lignola et al., 2008)

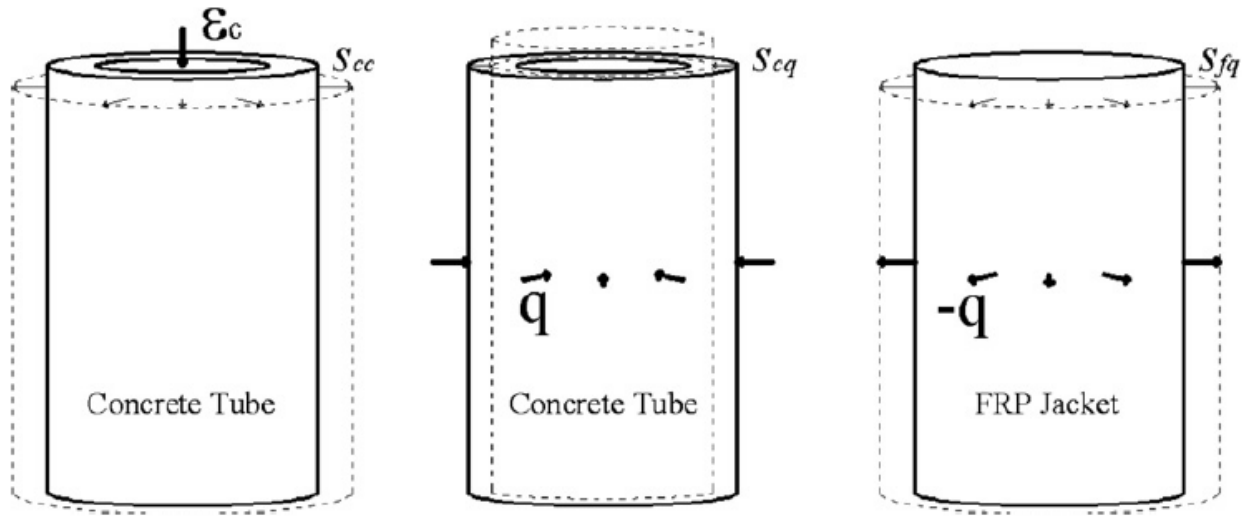


Figure 2-18: Radial displacement contributions of concrete tube and FRP Jacket (Lignola et al., 2008)

Using radial displacement compatibility between the confined concrete and the confining device (i.e., FRP jacket), combined with the equilibrium conditions of confined concrete, the researchers were able to develop an equation to calculate the pressure applied to the concrete by the confinement, q .

$$q = \frac{\gamma_c - \gamma_f}{\frac{R_e}{E_f t}(1 - \gamma_f) + \frac{1 + \gamma_c}{E_c} \frac{R_e^2}{R_e^2 - R_i^2} [(1 - 2\gamma_c) + (\frac{R_i}{R_e})^2]} \epsilon_c \quad \text{(Equation 2-2)}$$

The variables influencing this pressure are the Poisson's ratios of concrete and confinement (γ_c and γ_f), the elastic modulus of concrete and confinement (E_c and E_f), and the external and internal radius of the column section (R_e and R_i). For a solid column, the internal radius would be taken as zero. Using this confining pressure, the radial stress and circumferential stresses in the concrete can be calculated based on the equilibrium equations of confined concrete. An equivalent confining pressure (f'_l), which took account of equal contribution from the radial and circumferential stresses in the concrete, can be calculated as:

$$f'_l = \frac{\sigma_r + \sigma_\theta}{2} \rightarrow f'_l = \frac{q R_e^2}{R_e^2 - R_i^2} \quad \text{(Equation 2-3)}$$

This equivalent confining pressure is equal to the confining pressure multiplied by a factor based on the internal and external radius of a column. For a solid column, the equivalent confining pressure is simply equal to the confining pressure. This equivalent confining pressure is then used with Mander's model. To account for the nonlinear behavior of concrete, an iteration flow chart was developed to evaluate the stress-strain relationship for concrete confined with FRP.

An important concept discussed by this paper is that hollow columns have increased lateral deformability compared to solid columns. It suggested that the radial outward displacement of the concrete column is the same, regardless of whether the columns are solid or hollow. However, the hollow columns' radial displacement requires less external pressure to restrain. Therefore, for the same axial strain applied to a solid and a hollow column, the hollow column would require less pressure to be restrained radially. Since less pressure is required, there would be less strain induced in the confinement. Their work suggested that the higher the internal radius of the specimen (the larger the void), the more deformable the specimen is and therefore, the less pressure will be required to restrain radial displacement.

A parametric study was performed to study the effect of the hole size on the overall relationship between axial stress and axial strain of confined concrete. The derived axial stress vs. axial strain relationship of confined concrete for different external and internal radius ratios under the same relative confinement stiffness (i.e., same value of $\frac{E_f t}{R_e - R_i}$) was shown in Figure 2-19. It shows that as the hole size increases, the confinement effect is reduced and therefore the enhancement of concrete strength is reduced. Figure 2-20 shows the axial stress vs. dilation ratio relationships of confined concrete for different external and internal radius ratios under the same relative confinement stiffness. Based on this figure, the concrete dilation ratio is relatively constant for both the confined solid and hollow sections before the axial concrete stress reached the peak stress for unconfined concrete. After that, the hollow sections have a smaller enhancement of axial concrete stress compared to solid section under the same dilation ratio. This is due to the increased lateral deformability of hollow sections as described previously, which is more significant for a thinner wall, that is corresponding to a bigger hole size.

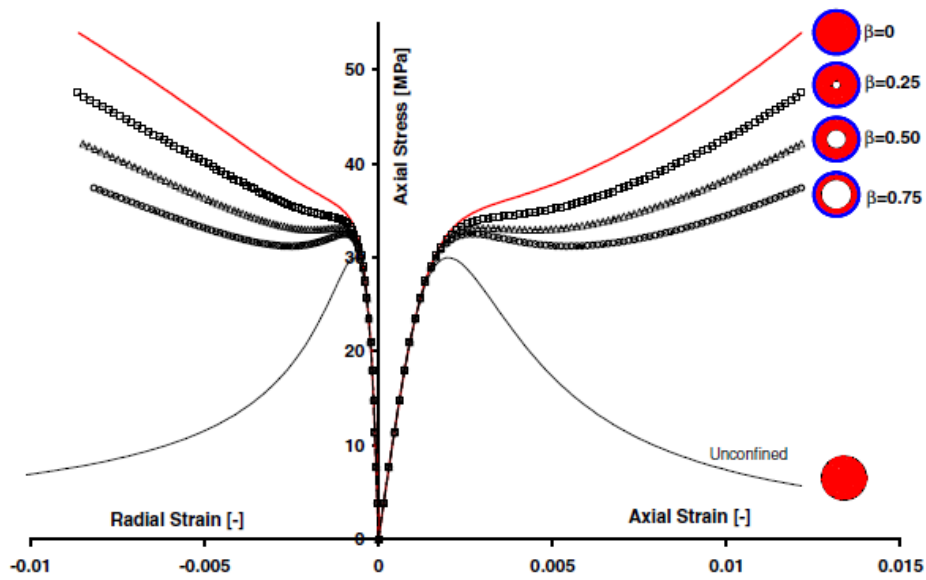


Figure 2-19: The axial stress vs. axial and radial strain relationship of confined concrete developed by Lignola et al., 2008 [1MPa = 145 psi]

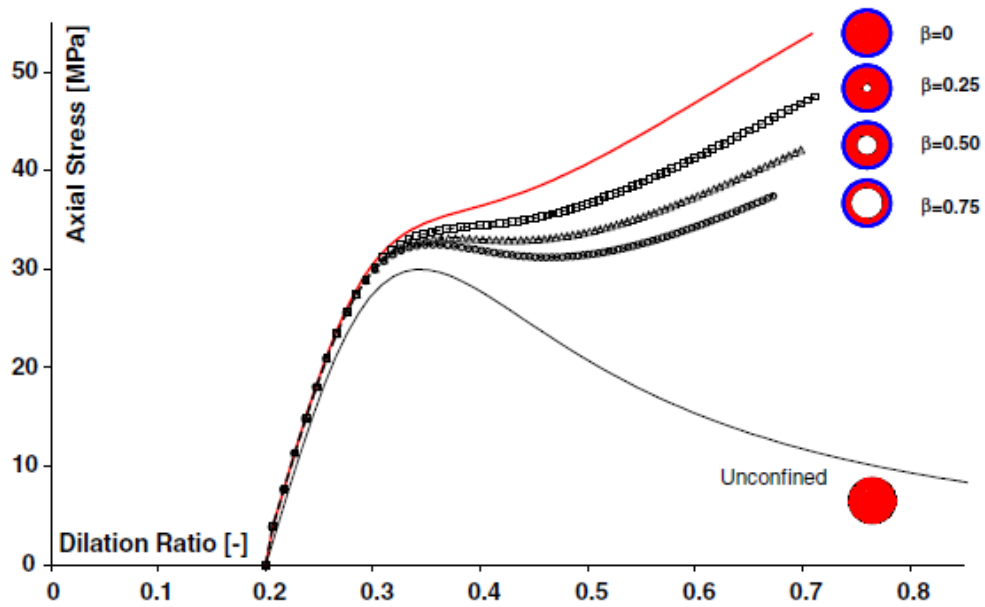


Figure 2-20: The axial stress vs. dilation ratio of confined concrete developed by Lignola et al., 2008 [1MPa = 145 psi]

Papanikolaou and Kappos (2009)

This pair of companion papers performed a parametric analysis of a series of approximately 180 columns (circular, square, solid, and hollow) using three-dimensional finite element analysis. The analysis was verified by comparing experimental results to the analytical results, and found an acceptable agreement. The parametric analysis subjected the columns to pure increasing axial compression, while the specimens had various arrangements and quantities of transverse reinforcement. The goal of the study was to determine the most efficient and effective ways to confine concrete columns. It was noted that the finite element analysis was capable of modeling longitudinal and transverse steel as well as producing accurate behavior of confined concrete, with the help of a user-defined model for triaxial confined state. The user-defined model was calibrated based on researchers' previous experimental results.

This research drew several important conclusions. One such conclusion was that for circular columns, providing an inner layer of transverse reinforcement without cross ties to the outer layer of transverse reinforcement does not provide useful benefits. For certain sections, use of this detail can actually be detrimental due to that the inner layer of transverse reinforcement tried to confine the inner concrete cover only, leaving the region around the inner layer of transverse reinforcement unfavorably unconfined. However, when outer and inner spirals are effectively tied together with cross ties, the strength and ductility of circular columns are increased. This is due to the confining action of the inner spiral being transferred to the outer spiral, through the cross ties. A simple economic analysis, based on quantity of reinforcing steel compared to strength and ductility gain, found that the provision of an inner layer with cross ties was justified.

Other conclusions reported in the study included the following:

- Providing smaller confinement spacing improved the strength and ductility of concrete, although the economic indicator showed that it is often not worth the extra reinforcement based on the marginal gains made.
- Heavier confinement configurations caused the first yield of the transverse reinforcement to occur before the section achieved the peak strength. This is contrary to the assumption made by several confinement models that the yield of transverse reinforcement occurs simultaneously with the peak compressive strength.

- The behavior of specimen, which used high-strength concrete and normal strength concrete, were compared and found that high-strength concrete experiences a smaller strength and ductility increase due to confinement effects compared to normal strength concrete. The smaller gains experienced by high-strength concrete are due to the more brittle nature of the unconfined high-strength concrete when compared to unconfined normal strength concrete.
- The analysis of rectangular column sections also had similar results, with an additional finding: providing overlapping hoops as opposed to cross ties only had a small effect on strength, while achieving a large increase in ductility. Rectangular hollow columns with only an outer layer of confinement reinforcement did not appear to be analyzed.

2.4 Confined concrete models

2.4.1 Overview

It is well known that concrete has large compression resistance, but it is fairly weak in tension. For this reason, concrete is typically reinforced with steel, which facilitates a concrete member to experience a ductile response. In seismic regions, this reinforcing steel becomes especially important, since the behavior of the members in the non-linear range is critical to prevent sudden failure of the concrete member, such as compression zone failure. Therefore, the plastic hinge regions of columns are required to be designed to sustain large inelastic strains without significant strength degradation.

Even though concrete failure can occur in axial compression or due to dilatational tension, the latter is a more common failure type for concrete. This dilation takes place in the direction perpendicular to the loading axis. This phenomenon is known as the Poisson's effect. Previous researchers found that applying lateral pressure around the perimeter of concrete cylinder could restrain this dilation and cause an increase in the strength and ductility of the concrete. It was found that this lateral pressure could be achieved by providing transverse reinforcement in the form of spiral or hoop reinforcement. For concrete, which was confined with adequate transverse reinforcement, subjected to axial compression, the ultimate failure was considered as the first transverse reinforcement rupture occurred.

Over the past decades, various studies have investigated the confinement effects of transverse reinforcement in columns, because the accuracy of confined concrete stress-strain relationships in model simulations determined that the prediction of reinforced concrete columns under flexure could be improved. Several models have been presented by past researchers to define the stress-strain behavior of concrete confined with transverse reinforcement. These models were generally developed based on the equilibrium between force in the transverse reinforcement and force generated by dilatational pressure induced by concrete in solid sections, and verified using confined solid sections subjected to pure axial compression. The confined concrete model presented by Mander et al. (1988) is one such model, and is one of the most widely-used and well-accepted models in current practice. The Caltrans Seismic Design Criteria (2013) and the AASHTO LRFD Seismic Bridge Design Specifications (2011; 2012; 2014) have endorsed this model for bridge design practice. This model has been shown to provide satisfactory response for bridge columns when the confined concrete is modeled accordingly. Besides Mander's model, there are several other confined concrete models that also describe the increased strength and ductility of concrete due to the confinement reinforcement. They include the models proposed by Park (1982), Saatcioglu and Razvi (1992), and Hoshikuma (1997). These models were developed based on experimental testing on solid circular and square specimens under pure axial compression. Due to the widespread use of Mander's model, it has been given emphasis in the current study as there are no significant advantages seen in using other confined concrete models.

2.4.2 Mander et al. model (1988)

An overview of companion papers by Mander is provided in this section, which describe the confined concrete model as well as the testing which verified the model.

2.4.2.1 Theory

Much of the strength and ductility of confined concrete depends on how effectively it is confined. The effectiveness of the confinement depends on a number of factors. Previous researchers determined the factors that have the largest effect on confinement effectiveness. These factors were summarized by Mander et al. (1988) as follows:

- Transverse reinforcement spacing

- Distribution of longitudinal bars
- Volumetric ratio of transverse steel to concrete core (ρ_s)
- Yield strength of transverse reinforcement
- Presence of additional supplementary overlapping hoops or cross ties
- Type of transverse steel (spirals, circular hoops, or rectangular hoops with cross-ties)

The transverse reinforcement spacing is important because the more uniform the confining pressure is throughout the height of confined concrete, the more effective the confinement would be. If the transverse reinforcement spacing is large, the reinforcement will not effectively resist the pressure resulting from the concrete dilation. This concept is illustrated in Figure 2-21, which shows the arching action along the member height assumed by Mander et al. (1988). Additionally, Figure 2-21 shows the effective confined region for rectangular sections. As seen, the arching action was also assumed to occur between the longitudinal steel in these sections. The arching action between the longitudinal steel shows the importance of a good distribution of longitudinal steel. Uneven distribution can cause large areas of ineffectively confined concrete. The study used this arching action to determine the area of the effectively confined concrete core. Based on this arching action, a confinement effectiveness coefficient was then defined. This represents the ratio between the effectively confined core area and the area of the entire concrete reinforced by the transverse reinforcement. The confinement effectiveness coefficient is essentially used as a reduction factor to account for the longitudinal steel distribution and the spacing of the transverse reinforcement.

As previously noted, Mander et al. (1988) used force equilibrium between the tension force developed in the transverse steel at yield and the dilatational pressure induced by the concrete dilation to determine the maximum confining pressure. It was found that the confining pressure depends entirely upon the ratio of the volume of the transverse confinement to the volume of the confined concrete core, as well as the yield stress of the transverse steel. Supplemental cross-ties and overlapping hoops greatly impact the confinement effect, since providing this reinforcement

will increase the volumetric ratio of transverse steel to the confined core and minimize the arching action.

The model uses the aforementioned factors to calculate the confining pressure and the confinement effectiveness factor. These values are then used to calculate the effective confining pressure, which is essentially the confining pressure multiplied by the confinement effectiveness factor. The model then calculates the confined concrete compressive strength of the concrete using the unconfined concrete compressive strength and the effective confining pressure. The calculation of the confined concrete compressive strength is based upon a model, which was originally used to predict triaxial test results. In this case, the effective confining pressure is used as the lateral pressure in the triaxial equation. The model is also capable of predicting behavior at various strain rates as well as predicting unloading and reloading at slow strain rates. Additionally, the model predicts the ultimate compressive strain of concrete. This strain is considered as the strain at which the first hoop fracture occurs, since the column can experience sudden failure or significant strength loss after the first hoop fracture.

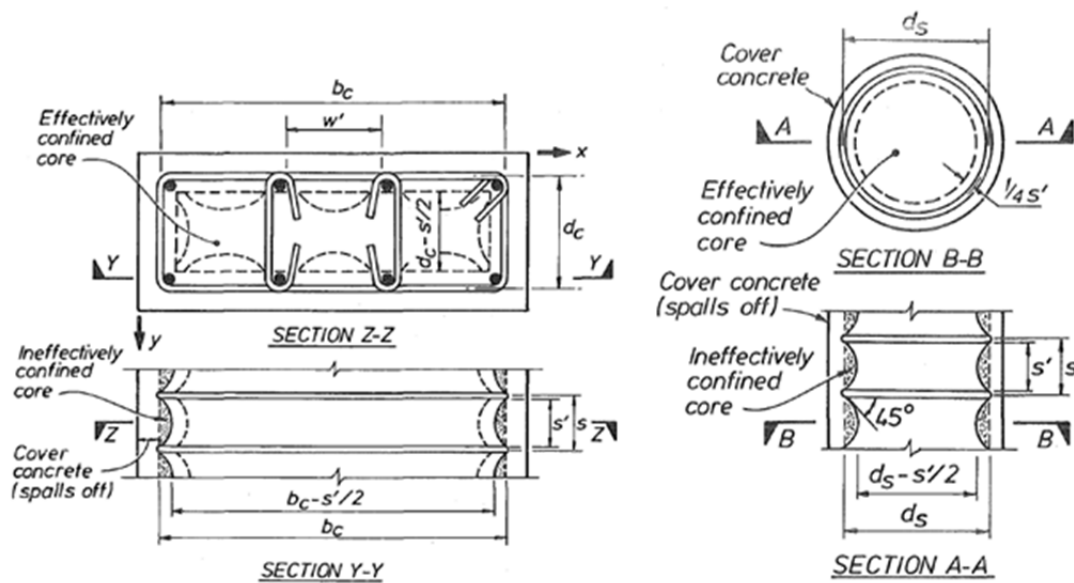


Figure 2-21: Effectively Confined Core for Circular and Rectangular Sections [(Mander et al., 1988)]

2.4.2.2 Testing

Mander also performed testing of thirty-one nearly full-size concrete columns with varying cross-sections including circular and square columns as well as rectangular walls (Mander et al. 1988). The circular columns had an aspect ratio of three, and the square columns had an aspect ratio of 2.67. The columns had varying amounts of transverse and longitudinal reinforcement and were loaded concentrically in increasing axial compression with different strain rates. The tested circular specimens used spiral reinforcement for the confining steel, and the square and rectangular specimens used transverse hoops. The results of the tests were compared to the results predicted by the confined concrete model that they proposed in order to determine the accuracy of the model. All the columns were tested at a fast strain rate (0.0167/s) in order to simulate seismic effects. Each series of column sections had an unreinforced column cast as well, in order to compare the unconfined behavior to the confined behavior.

The columns had a variety of reinforcement arrangements in order to determine the accuracy of the model for an assortment of situations, and to see the effects of changing some of these values. The first series reported is the circular column series. For these columns, there were two main sets tested with seven columns in each set. The first set contained six columns with the same amount of longitudinal steel, but with different transverse reinforcement spacing. One of the seven columns was unreinforced. The second series contained six columns with constant transverse reinforcement spacing but with varying amounts of longitudinal steel. This series also contained an unreinforced column. For both series, the confinement effectiveness coefficient was in the range of 0.89 to 1.002 (the confinement effectiveness coefficient may exceed 1.0 when the longitudinal reinforcement is high, as noted by Mander et al.). The concrete strength for each series was approximately between 4,000 and 5,000 psi. The square and circular specimens were all tested monotonically.

The results of the test were compared with the predicted results using the model, and good agreement was generally found. It was found that for even the lightly confined columns, there was a significant increase in compressive strength and greatly improved ductility. The results showed that providing more confinement enhances this behavior, also providing increased compressive strength and an even more ductile response. Increasing the volume of confinement also resulted in an increase in the strain at which the hoop fracture occurred. The results showed

that the predicted and actual stress-strain behaviors were very close. The peak stress and strain at peak stress were also very close to those predicted, with the experimental peak strength exceeding the predicted strength by 1.7% on average. The experimental measured strain at peak strength was about 1.3% on average less than predicted. The predicted strain at the hoop fracture also seemed to agree with the experimental results, although it seemed the prediction was somewhat conservative by about 9.5% in most cases.

Mander et al. (1988) also found several important trends, which furthered the understanding of confined concrete behavior. One important finding was that the amount of longitudinal bars had minimal effects on the concrete stress-strain behavior. The second series, which varied the amount of longitudinal steel but kept the confining steel volume constant, found very little variation in the stress-strain behavior. Additionally, the research found that the volumetric ratio of the confining steel was the most influential factor on the stress-strain behavior. Two cylinders, which had a very similar volumetric ratio of confinement but had different arrangements, were compared. One of these cylinders had a larger spiral spacing than the other, but had a larger confining steel diameter, resulting in approximately the same volumetric ratio. The results showed that the behavior was very similar. The cylinder with smaller spacing experienced a slightly more favorable descending branch. This suggests that the volumetric ratio was the more important factor, as long as the spacing of the confinement was reasonable and was close enough to effectively confine the concrete. These trends and results are visualized in Figure 2-22, which also lists the volumetric ratios of the cylinders shown.

The grade of steel used for the confining steel affects the confinement pressure as well. When using a higher grade of transverse steel, the yield stress is higher which causes a higher confinement pressure to be experienced. Although the yield stress is higher for higher steel grades, the ultimate strain of the steel is typically lower, which can cause premature fracture of the steel. Although Mander et al. (1988) did not test specimens with different confining steel strengths, this had been previously tested by Zahn et al. (1990). It was found that using a higher grade of transverse steel allowed the reduction of the volumetric ratio of transverse steel while still achieving a similar confined concrete compressive strength. It was also found that due to the lower ultimate strain of the confinement, the ductility would slightly decrease, although the ductility was still high.

Additional tests were performed on square columns and rectangular wall sections. The model was able to predict the response of these columns fairly accurately. The square columns also tested the influence of the age of concrete on the confinement behavior. Specimens with ages between 60 and 80 days were compared to specimens with ages greater than 940 days. It was found that age of each specimen did not have much influence on the response of the specimens.

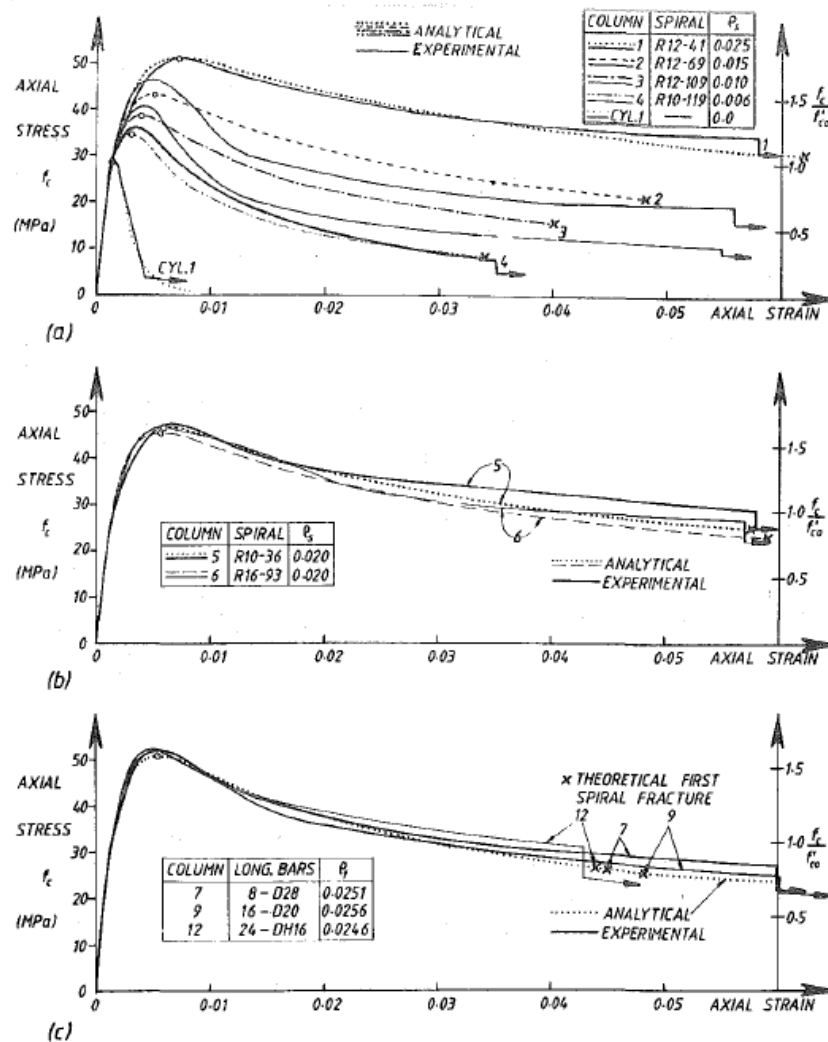


Figure 2-22: Comparison of Reinforcement Effects between Predicted and Measured Results (Mander et al., 1988) (1 MPa = 145 psi)

2.4.3 Other confined concrete models

Several other confined concrete models have also been proposed, which take account of various parameters such as confinement spacing, confinement configuration, confinement amount, cross-section shape and unconfined concrete compressive strength. Table 2-10 summarizes the parameters accounted by different confined concrete models.

As with the model proposed by Mander et al. (1988) almost all confined concrete models were developed primarily based on test data or by observations obtained from previous experimental studies. Table 2-11 lists the test specimen details used by previous researchers when developing the confined concrete models. Most models were similar to each other in form. Unlike Mander's model, where both the ascending branch and the descending branch of the stress-strain curve were represented by using a fractional expression, these models usually consist of three parts: an ascending branch, a linear falling branch and a sustaining branch reflecting the residual stress.

Kent and Park (1971) proposed a stress-strain model for concrete confined by rectilinear ties, which consisted of an ascending branch (same as the plain concrete), a linear falling branch and a sustaining branch corresponding to 20% peak stress. The peak concrete stress and the strain corresponding to the peak stress were conservatively assumed to be the same as unconfined concrete. The confinement effect began to take place after the stress passed the peak stress. In this model, the confinement effect was represented by the slope of the descending branch only.

The stress-strain relationship proposed by **Vallenas et al. (1977)** was similar to the Kent and Park's model. One major difference between these two models was Vallenas et al.'s model considered the confinement effect on concrete peak stress. Vallenas et al. (1977) concluded the concrete peak stress enhancement was a function of the volumetric ratio of transverse reinforcement.

Sheikh and Uzumeri (1980)'s confined concrete model consisted of three parts: a second order parabola ascending branch, a descending straight line, and a horizontal straight line. In this model, the distribution of longitudinal reinforcement and the resulting tie configurations were considered. It was concluded that the amount of longitudinal reinforcement did not affect the confined concrete behavior significantly. The idea of effectively confined concrete area is first

proposed, which represented the reduced confinement effectiveness of concrete members confined by rectangular hoops than closely spaced circular hoops or spirals. The effectively confined concrete area is smaller than the concrete area embraced by the confinement due to the arching effect. The longitudinal reinforcement distribution and the resulting confinement configuration significantly affected the magnitude of the confinement effectiveness coefficient.

Saatcioglu and Razvi (1992)'s model was derived by computing equivalent uniform confinement pressure for different confinement configurations. They showed that the falling branch was a function of the strain that corresponded to 85% of the peak stress.

Hoshikuma et al. (1997) proposed a stress-strain relationship for confined concrete consisting of three parts: a high-order ascending branch, a linear descending branch, and a sustaining branch. This model was developed based on four boundary conditions and was validated through test data. The effect of confinement configuration (therefore, the confinement effectiveness coefficient) was not considered in their model. This may have been one possible reason that the model experienced less stiffness in the ascending branch compared to other models. It was found that both the peak stress and also the strain at peak stress increased as the volumetric ratio of transverse reinforcement increased. This model proposed a higher (50% peak stress) residual stress compared to other models (20% or 30% peak stress). The peak stress enhancement was proportional to the volumetric ratio of transverse reinforcement and the spacing of hoop reinforcement significantly affected the deterioration after the peak stress.

Similar to most of the established models, the model proposed by Bousalem (2006) also consisted of three parts. The peak stress enhancement, the strain corresponding to the peak stress enhancement and the softening rate were considered as the three most important parameters that controlled the model. All of these parameters were dependent on the same variables, i.e., the volumetric ratio of transverse reinforcement, the yield strength of confinement, the concrete strength, and the confinement effectiveness coefficient.

The model proposed by Samani and Attard (2012) was applicable for both normal strength and high strength concrete. This model also addressed the limitations presented by models proposed

by Attard and Setunge, as well as Binici. No limitations on confinement type (reinforcing steel or FRP sheets) were presented.

Shelman and Sritharan (2014) conducted a detailed examination of the current approaches to calculate the amount of confinement reinforcement in the plastic hinge of concrete bridge columns, when subjected to seismic situations. It was found significant different amounts of confinement reinforcement were proposed by different approaches. The ultimate strain capacity is not well established due to effects of multiple factors.

Most of the confined concrete models, which were proposed after Mander (1988), extended the confinement to other types of confinement reinforcement (i.e. FRP sheets), beside the transverse reinforcement. These researchers did not seem to compare their models to the model proposed by Mander (1988).

A summary of mathematical expressions for each of the confined concrete models are shown in Table 2-12. A summary of concrete peak stress and the strain at peak stress for each confined concrete model are presented in Table 2-13. According to the literature review presented above, it was concluded that the most important four parameters that had significant effects on the confined concrete behavior were: unconfined concrete strength, yield strength of confinement, volumetric ratio of confinement to concrete core and confinement configuration. The effect of each individual parameter on the confined concrete behavior is summarized in Table 2-14.

Table 2-10: Summary of parameters accounted by different confined concrete models

Parameters	Kent and Park, 1972	Vallenas et al., 1977	Sheikh and Uzumeri, 1980	Mander et al., 1988	Saatcioglu and Razvi, 1992	Hoshikuma et al., 1997
Volumetric ratio of lateral steel to concrete core	✓	✓	✓	✓	✓	✓
Confinement spacing	✓	✓	✓	✓	✓	✓
Confinement diameter	✓	✓	✓	✓	✓	✓
Confinement yield strength		✓	✓	✓	✓	✓
Area of longitudinal reinforcement to area of core section ratio		✓		✓		
Lateral steel configuration (spiral, circular hoops and cross ties)	✓	✓	✓	✓	✓	
Section geometry				✓	✓	✓
Unconfined concrete compressive strength	✓	✓		✓	✓	✓
Strain rate				✓		

Note: ✓ - indicates the use of parameter in specified confined concrete model

Table 2-11: Test specimen details used in developing confined concrete models

Reference	Section shape	Section (inch ²)	Parameters			
			ρ_l %	f'_{c0} (psi)	ρ_{sh} %	f_{yh} (ksi)
Sheikh and Uzumeri, 1980	Square	12×12	2.2-4.8	3916-5076	0.76-2.4	38-116
Mander et al., 1988	Circular	20 dia.	1.23-3.69	4060-4786	0.6-2.5	45-49
	Square	17.7×17.7	1.08-3.06	4060-5947	1.62-7.87	45-52
Saatcioglu and Razvi, 1989	Square	6.3×6.3	1.56-3.13	4206-5656	1.34-2.78	54
Hoshikuma et al., 1997	Circular	8 dia.	0	2680	0.39-4.66	34
		20 dia.	1.01	4177	0.19-0.58	43
	Square	8×8	0	3365	0.39-4.66	34
		20×20	0.95	3525	1.73-4.1	43
		13.8×27.6	0.97	3525	1.72	43
		11.8×35.4	1.03	3525	1.74	43
		9.8×39.4	0.95	3525	1.77-2.45	43

* ρ_l % is the longitudinal reinforcement ratio based on gross section, f'_{c0} is the unconfined concrete compressive strength at time of testing, ρ_{sh} % is the transverse steel ratio based on core area and f_{yh} is the yield strength of transverse steel.

Table 2-12: Summary of various confined concrete models proposed in the literature

Researchers	Stress-Strain Model for Confined Concrete				Applicable Cross-Sectional Shape
	Ascending Branch	Descending Branch	Softening rate	Residual Stress	
Kent and Park, 1971	$f_c = Kf_{c0} [2 \times (\frac{\epsilon_c}{0.002K}) - (\frac{\epsilon_c}{0.002K})^2]$ K = 1.0	$f_c = Kf_{c0} [1 - Z(\epsilon_c - 0.002K)]$ K = 1.0	$Z = \frac{\tan \theta}{f_{c0}}$	$0.2f_{cc}$	Square
Vallenas et al., 1977	$f_c = f_{c0} \frac{\frac{E_c \epsilon_{cc}}{f_{c0}} (\frac{\epsilon_c}{\epsilon_{cc}}) - k \times (\frac{\epsilon_c}{\epsilon_{cc}})^2}{1 + [\frac{E_c \epsilon_{cc}}{k_3 f_{c0}} - 2] \times (\frac{\epsilon_c}{\epsilon_{cc}})}$	$f_c = Kf_{c0} [1 - Z(\epsilon_c - \epsilon_{cc})]$	$Z = \frac{0.5}{\frac{3}{4} \rho_s \sqrt{\frac{h''}{s}} + \frac{3 + 0.002f_{c0}}{f_{c0} - 1000} - 0.002}$	$0.3f_{cc}$	Square
Sheikh and Uzumeri, 1980	$f_c = Kf_{c0} [2 \times (\frac{\epsilon_c}{\epsilon_{cc}}) - (\frac{\epsilon_c}{\epsilon_{cc}})^2]$	$f_c = f_{cc} [1 - Z(\epsilon_c - \epsilon_{cc})]$	$Z = \frac{0.5}{\frac{3}{4} \rho_s \sqrt{\frac{B}{s}}}$	$0.3f_{cc}$	Square
Park et al., 1982	$f_c = f_{cc} [2 \times (\frac{\epsilon_c}{\epsilon_{cc}}) - (\frac{\epsilon_c}{\epsilon_{cc}})^2]$	$f_c = f_{cc} [1 - Z_m(\epsilon_c - \epsilon_{cc})]$ $\geq 0.02f_{cc}$	$Z_m = \frac{0.5}{(\frac{3 + 0.29f_{c0}}{145f_{c0} - 1000}) + \frac{3}{4} \rho_s \sqrt{\frac{b_c}{s}} - \epsilon_{cc}}$	-	Square
Mander et al., 1988	$f_c = \frac{f_{cc} x^r}{r - 1 + x^r}$	$f_c = \frac{f_{cc} x^r}{r - 1 + x^r}$	-	-	Circle Square Wall-type
Saatcioglu and Razvi, 1992	$f_c = f'_{cc} [2 \times (\frac{\epsilon_c}{\epsilon_{cc}}) - (\frac{\epsilon_c}{\epsilon_{cc}})^2]^{1/(1+2K)}$	$f_c = f_{cc} - \frac{0.15f_{cc}}{\epsilon_{85} - \epsilon_{cc}} (\epsilon - \epsilon_{cc})$	$Z = \frac{0.15f_{cc}}{\epsilon_{85} - \epsilon_{cc}}$	$0.2f_{cc}$	Circle Square Wall-type
Hoshikuma et al., 1997	$f_c = E_c \epsilon [1 - \frac{1}{n} (\frac{\epsilon}{\epsilon_{cc}})^{n-1}]$	$f_c = f_{cc} - E_{des} (\epsilon - \epsilon_{cc})$	$E_{des} = \frac{11.2f_{c0}^2}{\rho_{sh} f_{yh}}$	$0.5f_{cc}$	Circle Square
Bousalem and Chikh, 2006	$f_c = \frac{f_{cc} x^n}{n - 1 + x^n}$	$f_c = f_{cc} - E_{soft} (\epsilon_c - \epsilon_{cc})$	$E_{soft} = \frac{4f_{c0}^2}{k_e \rho_s f_{yh}}$	$0.3f_{cc}$	Square

Table 2-13: Summary of expressions to calculate the peak stress and the corresponding strain based on different confined concrete models

Researchers	Stress-Strain Model for Confined Concrete	
	f_{cc}	ε_{cc}
Kent and Park, 1971	f_{c0}	0.002
Vallenas et al., 1977	$f_{cc} = f_{c0} \times (1 + 0.0091 \times (1 - 0.245 \frac{s}{h''}) \frac{(\rho_s + \frac{d''}{d} \rho_s) f_{yh}}{\sqrt{f_{c0}}})$	$\varepsilon_{cc} = 0.0024 + 0.005 \times (1 - \frac{0.734s}{h''}) \frac{\rho_s f_{yh}}{\sqrt{f_{c0}}}$
Sheikh and Uzumeri, 1980	$f_{cc} = f_{c0} \times (1 + \frac{b_c^2}{140 P_{occ}} [(1 - \frac{nC^2}{5.5b_c^2})(1 - \frac{s}{2b_c})^2] \times \sqrt{\rho_s f_{yh}}$	$\varepsilon_{cc} = \varepsilon_{c0} \times (1 + \frac{248}{C} [1 - 5.0 \times (\frac{s}{B})^2] \frac{\rho_s f_{yh}}{\sqrt{f_{c0}}})$
Park et al., 1982	$f_{cc} = f_{c0} + \rho_s f_{yh}$	$\varepsilon_{cc} = \varepsilon_{c0} \times (1 + \rho_s f_{yh} / f_{c0})$
Mander et al., 1988	$f'_{cc} = f_{c0} (-1.254 + 2.254 \sqrt{1 + \frac{7.94 f_{le}}{f_{c0}} - 2 \frac{f_{le}}{f_{c0}}})$	$\varepsilon_{cc} = \varepsilon_{c0} [1 + 5 \times (\frac{f'_{cc}}{f_{c0}} - 1)]$
Saatcioglu and Razvi, 1992	$f_{cc} = f_{c0} + k_1 f_{le}$ $k_1 = 6.7 (f_{le})^{-0.17}$ $f_{le} = k_2 f_l$	$\varepsilon_{cc} = \varepsilon_{c0} (1 + 5K)$ $K = \frac{k_1 f_{le}}{f'_{c0}}$
Hoshikuma et al., 1997	$f_{cc} = f_{c0} + 3.8 \alpha \rho_s f_{yh}$	$\varepsilon_{cc} = 0.002 + 0.033 \beta \rho_s f_{yh} / f_{c0}$
Bousalem and Chikh, 2006	$f_{cc} = f_{c0} + 0.4 k_e \rho_{sh} f_{yh} \sqrt{f_{c0}}$	$\varepsilon_{cc} = \varepsilon_{c0} \times [1 + 2.7 \frac{k_e \rho_{sh} f_{yh}}{\sqrt{f_{c0}}}]$

* α, β are modification factors depending on cross sectional shape for the Hoshikuma et al.'s model; d is the nominal diameter of longitudinal reinforcing bar and d'' is the nominal diameter of lateral steel tie.

Table 2-14: Influence of different parameters on confined concrete behavior

Parameters	Effect on confined concrete behavior
Concrete compressive strength	Peak stress
Volumetric ratio of transverse steel to concrete core (Transverse reinforcement spacing) (Transverse reinforcement diameter)	Significant effect Peak stress Strain at peak stress Slope of descending branch Longitudinal reinforcement buckling
Yield strength of transverse steel	Ductility Peak stress
Configuration of transverse steel (Spiral/Circular hoop) (Tie configuration and the resulting longitudinal reinforcement distribution)	Significant effect on ductility improvement Little effect on strength enhancement (ductility)
Amount of longitudinal reinforcement	Negligible effect
Section type	Significant variable affecting the confinement effectiveness or the uniformity of confining pressure applied to the concrete core

To better compare the confined concrete models for circular and square sections, a 4 ft diameter/width circular/square column with a longitudinal reinforcement ratio of 2% and an axial load ratio of 5%, which are typically used in high seismic regions, was selected. The concrete compressive strength was assumed to be 4500 psi. Both transverse and longitudinal reinforcement have yield strengths of 60 ksi. The concrete cover to the main longitudinal

reinforcing bars was selected to be 3 inch. The circular/square column was reinforced with 46 or 58 #8 reinforcing bars (1 in. diameter and 0.79 in² cross sectional area), corresponding to 2% longitudinal reinforcement ratio. The transverse reinforcement for both columns used #5 reinforcing bar (0.625 inch diameter and 0.31 in² cross sectional area) with 1.5 inch spacing, corresponding to 2% transverse reinforcement ratio. The confined concrete models comparisons for both circular and square sections are shown in Figure 2-23 and Figure 2-24. Compared to circular sections, more researches have been devoted to study the confined concrete behavior in square sections. This is because there are more variations for the confinement configurations in square sections.

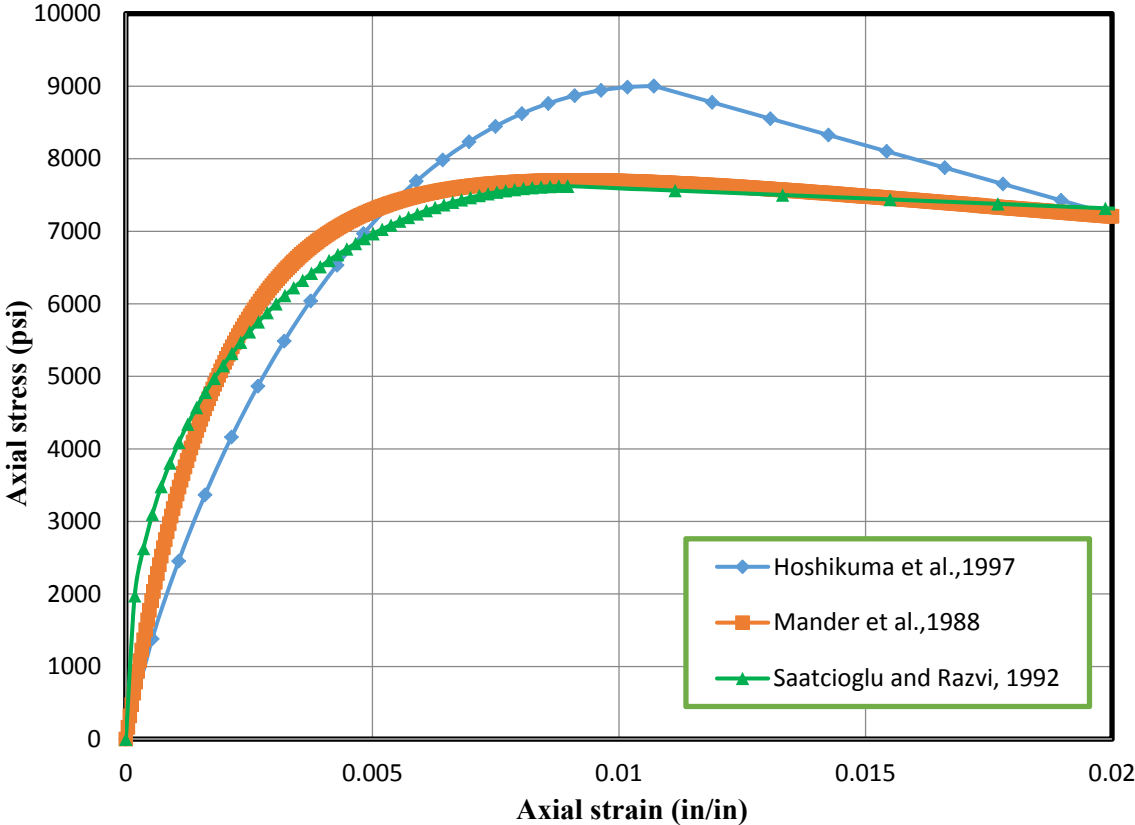


Figure 2-23: Confined concrete models comparisons for circular section

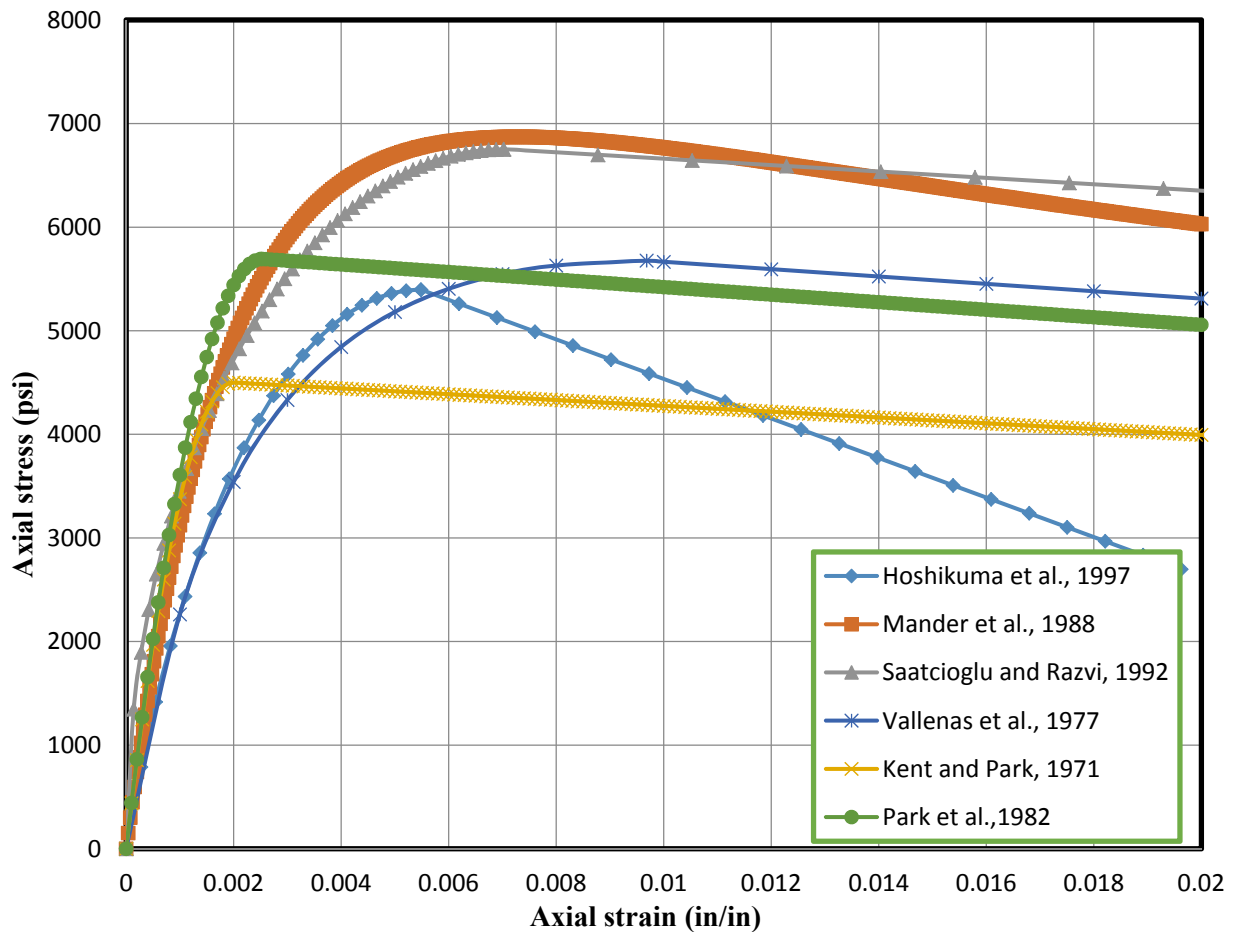


Figure 2-24: Confined concrete models comparisons for square section

2.4.4 Summary

Based on the literature presented in the previous sections, the following summaries are made:

1. The confined concrete behavior is directly related to the effective lateral confining stress.
2. Strength enhancement of confined concrete is proportional to the volumetric ratio of lateral reinforcement and the concrete compressive strength.
3. The amount of longitudinal reinforcement does not affect the confined concrete behavior significantly.
4. For square or rectangular sections, the effective lateral confining stress depends greatly on the longitudinal reinforcement distribution and the resulting confinement configurations, which can be reflected by the confinement effectiveness coefficient.

- The confinement provided by the rectangular hoops and ties is not as effective as the circular hoops or spirals; therefore, the confinement effectiveness coefficient for circular section (0.9-1.0) is greater than the rectangular section (0.4-0.7), which is clearly represented by Figure 2-25.

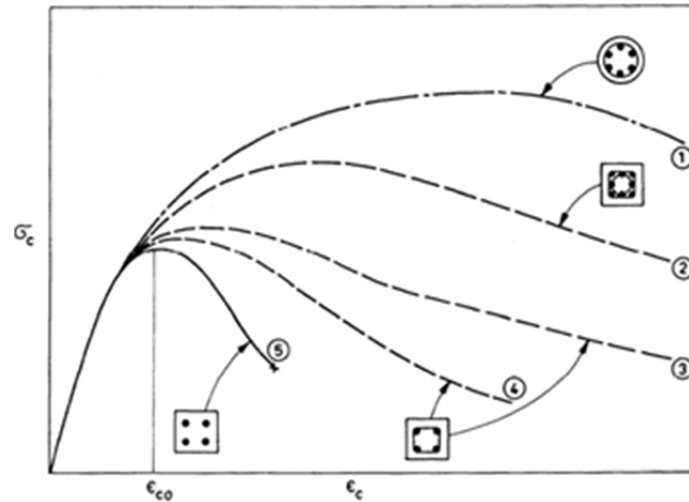


Figure 2-25: Confinement effectiveness for different section geometry and confinement configurations

- The initial stress-strain relationship does not depend on the confinement level and confinement mechanism is activated after the concrete strain reaches a considerable value (0.002 in/in).

CHAPTER 3 ANALYTICAL INVESTIGATION

3.1 Introduction

In order to further study the behavior of confined concrete and its application to hollow sections, a series of detailed analyses was performed on concrete specimens. Two types of analysis were performed, including OpenSees fiber based analysis and finite element analysis (FEA) using readily available software ABAQUS (CAE 6.12, 2012). The FEA was able to give a detailed response and shows the interaction among specimen components. The fiber based analysis is more simplistic and based upon the definition of a two-dimensional section of the member. The finite element method can provide insight into detailed behavior but is more time consuming to perform, while the fiber based OpenSees analysis is similar to the type of analysis performed in design practice. It can determine if typical design software will be able to achieve simple modeling techniques with accurate results.

3.1.1 Definition of key variables

Before discussing the details of the analyses, it is important to define how the section properties will be referred. In the past, there has been some confusion and disagreement regarding a consistent way to define and describe parameters, such as axial load ratio and reinforcing steel ratios. The main source of confusion was whether to define these ratios while ignoring the void (assuming that the void is filled and the column is solid) or including the void (using the net area of present concrete). The axial load ratio and reinforcing steel ratios may significantly increase if hollow sections are used for bridge columns based on net concrete area. Therefore, it is important to establish a standard to reduce confusion and to provide an appropriate way to compare hollow column behavior with that of solid columns.

As discussed in Chapter 1, hollow columns provide several benefits when compared to solid columns. These benefits are typically in the form of reduced mass and materials. In order for this to truly be a benefit, the hollow column must be approximately the same diameter as the solid column, or any reductions in mass and materials, due to the void, will be lost with the increase in mass and materials associated with increasing the diameter. For example, an axial load ratio of five percent is fairly typical for solid columns. If the axial load ratio for a hollow column is

based on the net section, or the actual area of present concrete, then a five percent axial load ratio for a hollow column with a similar outside diameter to the solid column would mean that the axial load is significantly reduced for the hollow column. To hold the axial load of one column, it would be required to provide several hollow columns, and the reduction of mass would be negated. For this reason, it has been considered appropriate to define the section properties as if the hollow column was actually solid, in order to better compare between solid and hollow columns. The following terminology and variable definitions will be used throughout this report.

Gross section =	Area of section based on the outer diameter (as if section were solid)
Net section =	Area of present concrete (gross section area with area of void subtracted)
$\rho_s = \frac{V_h}{V_{cg}} = \frac{4A_h}{d_s s} =$	Ratio of the volume of transverse reinforcement to the gross volume of concrete within transverse reinforcement.
$\rho_l = \frac{A_l}{A_g} =$	Ratio of area of longitudinal reinforcement to gross area of section
$\frac{P}{f'_c A_g} =$	Axial load ratio, the ratio of the axial load to the capacity of the section if it were solid

Defining the above variables in this manner will enable an easy comparison to the solid section in order to determine whether the hollow section can provide similar results. If desired, the above values can also be calculated to the net section in order to determine the ratio of axial load to the present concrete area. This can give a good idea of how much of the compressive strength of the concrete is being utilized by the axial load. However, using the gross section will enable easier comparison and determination of the viability of hollow columns relative to solid columns.

3.2 Concentric axial load

3.2.1 Overview

Although there were several advantages that hollow reinforced concrete columns would provide compared to the solid sections (especially for tall structures subjected to seismic activities) as described in Chapter 1, it was not fully understood how to confine the concrete core effectively to ensure satisfactory ductility levels. In other words, the confinement effect was not fully

understood from a fundamental point of view. In addition, the confinement in critical regions of these columns is typically designed using the confined concrete models that were developed primarily for solid concrete sections. The extension of these confined concrete models toward hollow sections needs further investigation. In order to examine the applicability of these models and identify areas where improvements are needed, a detailed analytical study on the confinement effect in hollow reinforced concrete columns was necessary and is presented below.

As discussed in Chapter 1, until now, there have been disagreements among researchers on how to confine hollow concrete sections. Previous researchers tested specimens with different confinement configurations, wall thicknesses, and different ranges of longitudinal reinforcement ratio, as well as volumetric ratio of lateral reinforcement. Therefore, significantly different design guidelines were proposed for the design of hollow columns. In order to better understand the effect of each of the parameters on the confinement effectiveness of hollow concrete sections, the analysis variables in this study included confinement configurations (one layer of confinement placed near the outside concrete face and two layers of confinement placed near both the outside and the inside face of concrete), wall thickness, and proportion of inner to outer confinement amount if two layers of confinement were utilized.

A finite element method (FEM) was utilized in this project to model hollow concrete columns under concentric axial compression. This aimed at loading the specimen beyond its ultimate strength and establishing the complete relationship between axial load and axial deformation including softening that occurs beyond the peak strength. The hollow reinforced concrete columns with different confinement configurations, wall thicknesses and proportions of inner to outer confinement amount were systematically analyzed using the 3D nonlinear finite element software ABAQUS (CAE 6.12, 2012). The following sections present this study in detail for circular sections, which include both hollow and solid sections. The model development for square columns followed similar method as circular columns and will not be discussed here due to limited space.

3.2.2 Material properties

The concrete material model was of great importance during the model development process. In ABAQUS, there are three different models that can be used for defining concrete material

behavior: brittle cracking, smeared cracking, and damaged plasticity. Each model has been developed for a distinct purpose with many differences among them. The brittle cracking model assumes that the concrete compressive response remains linearly elastic while the tensile cracking dominates failure. The smeared cracking model was developed for use during loading in a monotonic manner, with a low confining stress. This allows the concrete to experience either compressive crushing or tensile cracking. The damaged plasticity model is the most complex among the three models, which incorporates two damage variables, one for compression and one for tension. This is to model the stiffness degradation during the inelastic action of concrete. Tensile cracking and compressive crushing are two main mechanisms of the concrete failure in the concrete damage plasticity model. Therefore, the concrete stiffness can be modeled during inelastic action to a greater level of accuracy, if calibrated properly.

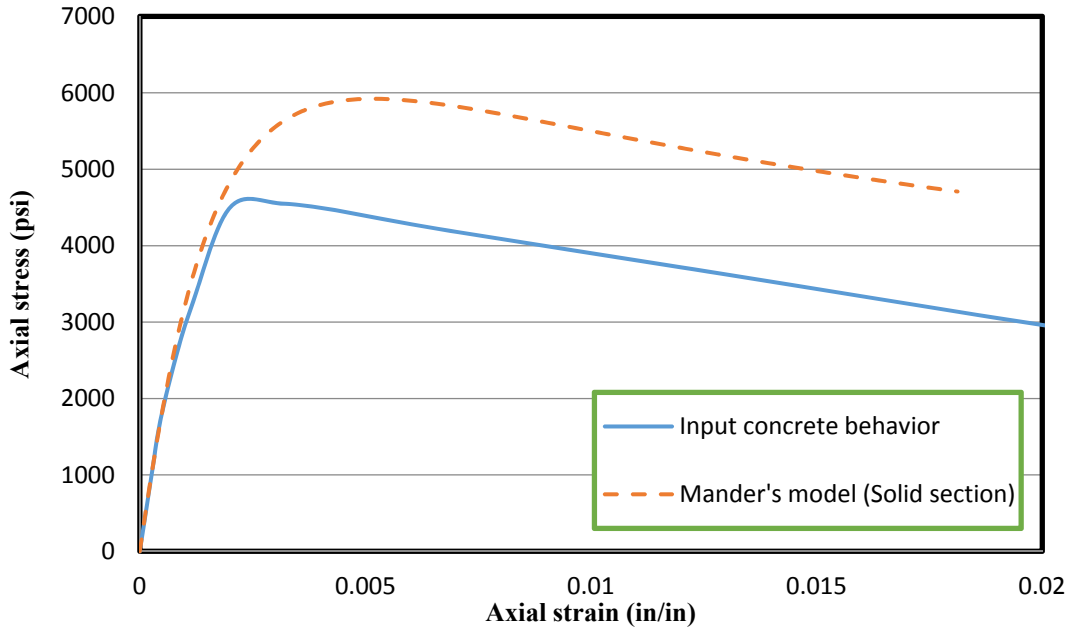
For the analysis conducted in this project, the concrete damaged plasticity model was chosen. The concrete damaged plasticity model is based on the Lubliner et al. (1989) studies and modifications made by Lee and Fenves (1998). Concrete stress-strain behavior under uniaxial compression after the elastic range was defined in terms of yield stress versus inelastic strain (crushing strain) as shown in Appendix A. The input concrete stress-strain behavior under uniaxial compression after the elastic range was defined parallel to the Mander's model (1988) as successfully done in Snyder et al. (2011). This is because the concrete damaged plasticity model is a pressure-dependent model, which means the stress versus strain relationship for each individual concrete element depends on the pressure it experiences. The purpose of defining the descending branch of the input concrete behavior parallel to the Mander's model is not only to avoid convergence problem, but also to match the descending branch of the confined concrete behavior with the increased confining pressure provided by the transverse reinforcement. This pressure-dependent characteristic is same for both hollow and solid columns. The comparisons between the input concrete behavior as well as the Mander's model corresponding to two different sizes of confinement reinforcement for circular solid sections are shown in Figure 3-1. The input concrete material model was validated by comparing the derived average axial stress versus strain relationship to Mander's model for solid concrete columns, which will be discussed in detail in Section 3.2.5.1. This validated input concrete material model, instead of Mander's model, was used to model the unconfined concrete behavior in hollow columns. The confining

effect provided by the transverse reinforcement was automatically taken into account by the finite element analysis program.

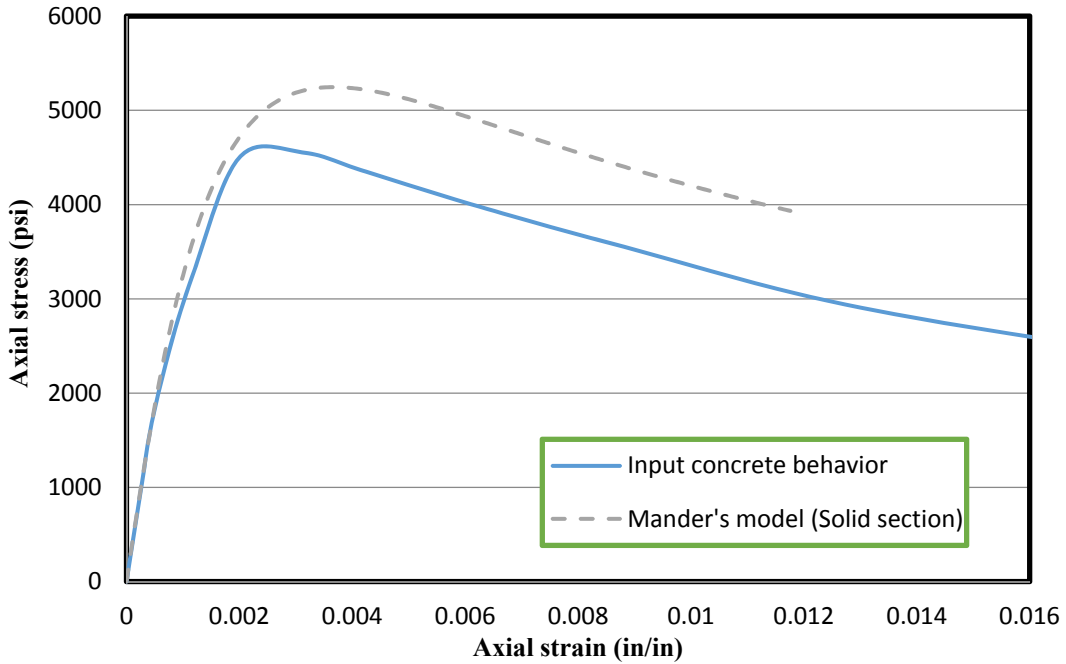
Concrete behavior under uniaxial tension was assumed to be linear until forming the initial macroscopic cracks at the peak stress (failure stress), which was assumed to be $7.5\sqrt{f'_c}$. Post failure behavior was defined in terms of stress versus cracking strain. This behavior allowed defining the effects of the reinforcement interaction with concrete by introducing some tension stiffening to the softening branch. A typical tension stiffening model is shown in Figure 3-2. It was important to select appropriate tension stiffening parameters to obtain numerical solutions, and also to avoid local cracking failure in the concrete that introduced temporarily unstable behavior in the overall response of the model. The tension stiffening in numerical simulation could have been represented either by modifying the stiffness of reinforcing bars, or by modifying the stiffness of concrete so that the concrete could carry the tensile force after it cracked. The tensile behavior of concrete defined in this set of analyses is shown in Appendix A (tensile behavior).

Additional inputs such as dilation angle, eccentricity, uniaxial to biaxial stress ratio, stress variant, and viscosity parameters were required to completely define the damage plasticity model of concrete. The suggested default values from ABAQUS were used as tabulated in Appendix A (Plasticity).

Longitudinal and transverse reinforcement behavior was defined as an elastic-plastic material using a bilinear curve. Slope of the plastic range was assumed to be about 1.3 % of the steel modulus of elasticity. The steel stress-strain behavior after elastic range was defined in terms of yield stress versus plastic strain as tabulated in Appendix A (Reinforcing steel - Plastic).



(a) 0.177 inch dia. Circular hoop



(b) 0.125 inch dia. Circular hoop

Figure 3-1: Comparisons between input unconfined concrete behavior and results expected for the confined concrete behavior based on Mander's model (Mander et al., 1988)

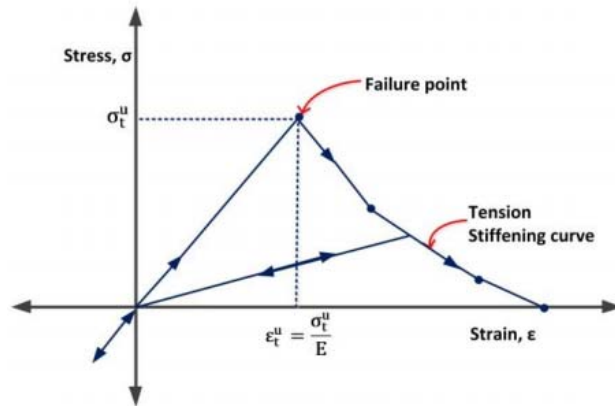


Figure 3-2: The tension stiffening model for concrete in ABAQUS (Abaqus Analysis User’s Manual 6.12, 2012)

3.2.3 FE modelling

The modeled hollow circular concrete cylinder was 12 inches outer diameter and the inner diameter was calculated based on a series of pre-selected β values, where β represented the ratio of wall thickness to outer diameter. The height was 48 inches, which led to an aspect ratio of 1:4. The element size was selected to be 0.5 inches, which was small enough to capture the stress/strain variations across the wall thickness. The circular hoop was spaced at one inch along the entire height of the cylinder and was placed as close as possible to the outside concrete face (one layer of confinement) or both to the outside and inside concrete face (two layers of confinement), which led to zero concrete cover in the analysis. This option was preferred to avoid any numerical instability resulting from crushing of cover concrete.

Two element types were primarily used in the development of all FE models: C3D8R and T3D2. The C3D8R element is a continuum three dimensional 8-noded solid element with three translational degrees of freedom at each node, commonly known as the “brick” element. This type of element was used to model concrete elements. The other element, T3D2, is a three-dimensional 2-noded truss element (only resists forces in the axial direction), which was used to model embedded longitudinal and transverse reinforcement bars. This element has two nodes with three translational degrees of freedom at each node.

The embedded region constraint option was used for connecting reinforcement elements to the surrounding concrete. This option could constrain translational degrees of freedom of the embedded element nodes (steel reinforcement) to the degrees of freedom of the surrounding element nodes called the host elements (concrete).

Due to triple symmetry, only 1/8 of the hollow section was modeled to reduce the computational time. Symmetric boundary conditions were enforced on the symmetric planes, which were $u = 0$ on the plane normal to the x-axis, $v = 0$ on the plane normal to the y-axis and $w = 0$ on the bottom surface normal to the z-axis. The top and bottom horizontal planes were unrestrained and allowed displacement to take place in the z direction. This was made to capture the confinement behavior of an arbitrary block along the height of the column that is undisturbed from any local boundary conditions (e.g.; foundations, connection to the deck, etc.), under compressive axial loading. Uniform compressive displacement in the z direction was applied to the top surface. Figure 3-3 shows the boundary and loading conditions of a modeled two-inch wall hollow section under concentric axial load.

3.2.4 Analysis matrix

The test matrix for each investigated parameter was carefully chosen, which is shown in Table 3-1 through Table 3-3.

3.2.4.1 Confinement configurations

Two series of analyses with two different wall thicknesses were performed to study the influence of confinement configurations (one layer of confinement placed near the outside concrete face, two layers of confinement placed both near the inside and outside concrete faces without cross ties and two layers of confinement placed both near the inside and outside concrete faces with cross ties connecting these two layers) on the confined concrete behavior for hollow columns.

3.2.4.2 Wall thickness

Two series of analyses were performed to study the influence of wall thickness on the confined concrete behavior for hollow columns, corresponding to same transverse reinforcement amount. This will lead to the same volumetric ratio of transverse reinforcement based on the gross section (i.e., ignoring the void in the middle for the hollow columns).

3.2.4.3 Proportion of inner to outer confinement ratio

A series of analyses were performed to study the influence of different proportions between the inner and outer confinement amount within the same spacing on the confined concrete behavior for hollow columns.

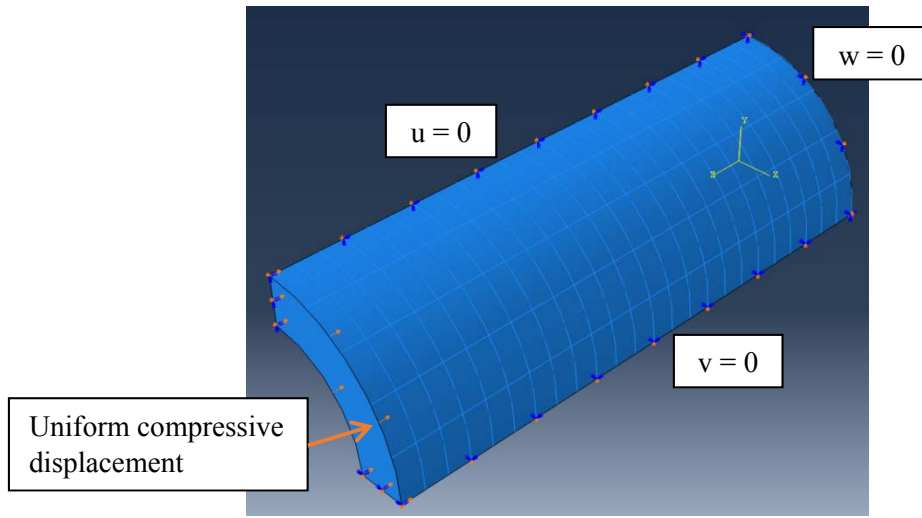
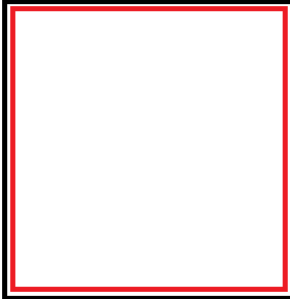
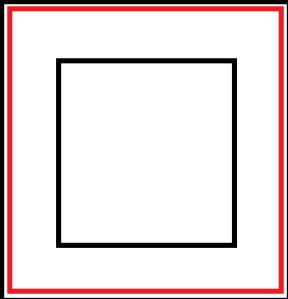
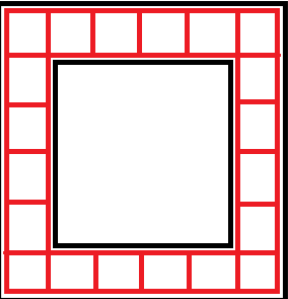


Figure 3-3: The boundary and loading conditions of a modeled two-inch-wall hollow section under concentric axial load

Table 3-1: Analysis matrix of confinement configurations

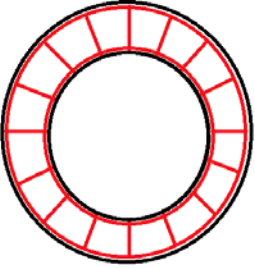
Section	Solid	1 inch wall thickness			2 inch wall thickness		
	<i>One layer of confinement</i>	<i>Two layers of confinement</i>		<i>One layer of confinement</i>	<i>Two layers of confinement</i>		<i>One layer of confinement</i>
		With cross ties	Without cross ties		With cross ties	Without cross ties	
Inner layer of transverse reinforcement dia. (inch)	-	0.125	0.125	-	0.177	0.177	-
Outer layer of transverse reinforcement dia. (inch)	0.177 0.125	0.125	0.125	0.125	0.177	0.177	0.177
Cross ties dia. (inch)	-	0.177	-	-	0.177	-	-
Transverse reinforcement volumetric ratio, gross (net concrete area)	0.41% 0.82%	0.75%* (2.46%)	0.75% (2.46%)	0.41% (1.34%)	1.37%* (2.46%)	1.37% (2.46%)	0.82% (1.48%)
Lateral reinforcement configuration							

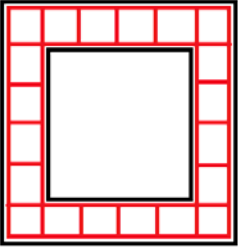
Section	Solid	1.2 inch wall thickness		2 inch wall thickness	
	<i>One layer of confinement</i>	<i>Two layers of confinement with cross ties</i>	<i>One layer of confinement</i>	<i>Two layers of confinement with cross ties</i>	<i>One layer of confinement</i>
Inner layer of transverse reinforcement dia. (inch)	-	0.125	-	0.177	-
Outer layer of transverse reinforcement dia. (inch)	0.177 0.125	0.125	0.125	0.177	0.177
Cross ties dia. (inch)	-	0.177	-	0.177	-
Transverse reinforcement volumetric ratio, gross (net concrete area)	0.4% 0.8%	0.74% * (2.05%)	0.4% (1.14%)	1.37% * (2.46%)	0.8% (1.48%)
Lateral reinforcement configuration					

*: exclude the area of cross-ties

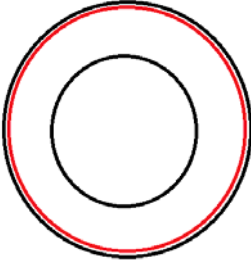
Table 3-2: Analysis matrix of wall thickness

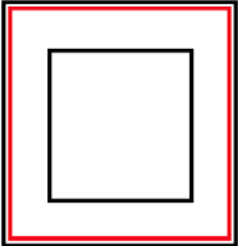
(a) Two layers of confinement connected with cross-ties

Lateral reinforcement configuration	d' (inch)	d (inch)	t (inch)	t/d	Lateral reinforcement cross-sectional areas (inch ²)
	9.6	12	1.2	0.1	0.0246
	9	12	1.5	0.125	0.0246
	8.4	12	1.8	0.15	0.0246
	8	12	2	0.167	0.0246
	7.8	12	2.1	0.175	0.0246
	7.2	12	2.4	0.2	0.0246

Lateral reinforcement configuration	b' (inch)	b (inch)	t (inch)	t/b	Lateral reinforcement cross-sectional areas (inch ²)
	9.6	12	1.2	0.1	0.017
	9	12	1.5	0.125	0.017
	8.4	12	1.8	0.15	0.017
	8	12	2	0.167	0.017
	7.8	12	2.1	0.175	0.017
	7.2	12	2.4	0.2	0.017

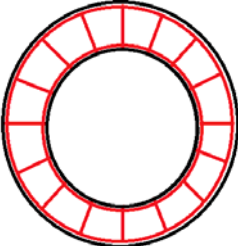
(b) Outer layer of confinement only

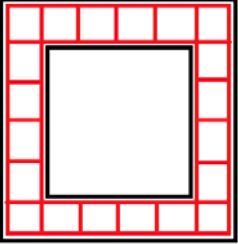
Lateral reinforcement configuration	d' (inch)	d (inch)	t (inch)	t/d	Lateral reinforcement cross-sectional areas (inch ²)
	9.6	12	1.2	0.1	0.034
	9	12	1.5	0.125	0.034
	8.4	12	1.8	0.15	0.034
	8	12	2	0.167	0.034
	7.8	12	2.1	0.175	0.034
	7.2	12	2.4	0.2	0.034

Lateral reinforcement configuration	b' (inch)	b (inch)	t (inch)	t/b	Lateral reinforcement cross-sectional areas (inch ²)
	9.6	12	1.2	0.1	0.034
	9	12	1.5	0.125	0.034
	8.4	12	1.8	0.15	0.034
	8	12	2	0.167	0.034
	7.8	12	2.1	0.175	0.034
	7.2	12	2.4	0.2	0.034

* d' / b' is the inner diameter/width of hollow sections, d / b is the outer diameter/width of hollow sections and t represents the wall thickness

Table 3-3: Analysis matrix of proportion between inner and outer confinement amount

Lateral reinforcement configuration	Proportion of outer lateral reinforcement to inner lateral reinforcement amount	Outer lateral reinforcement cross-sectional areas (inch ²)	Inner lateral reinforcement cross-sectional areas (inch ²)
	5:5	0.0246	0.0246
	6:4	0.03	0.02
	7:3	0.034	0.015
	8:2	0.039	0.0098
	9:1	0.044	0.0049
	10:0	0.049	0

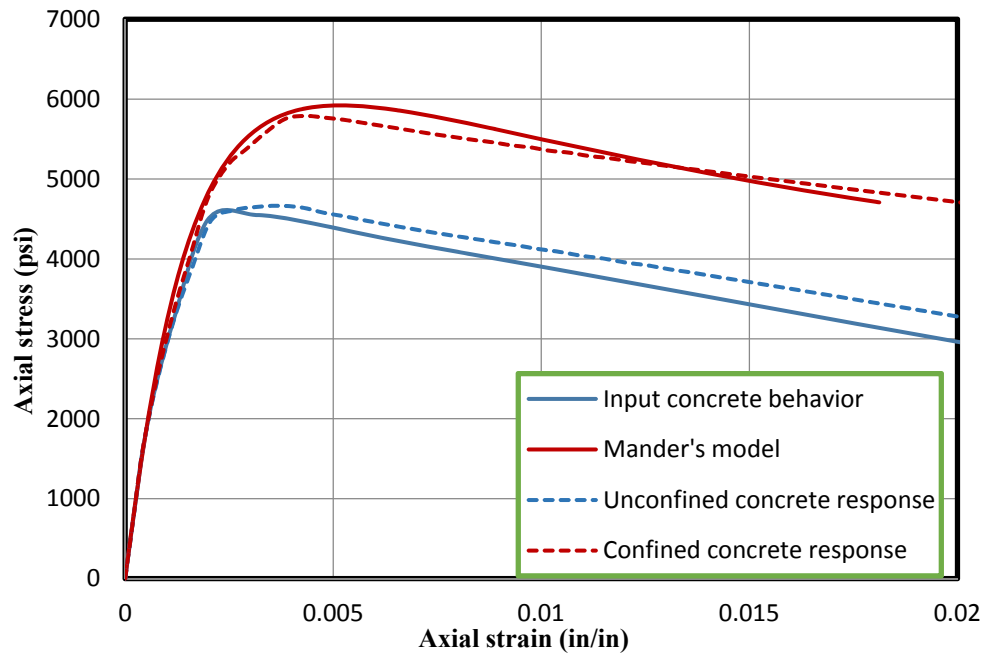
Lateral reinforcement configuration	Proportion of outer lateral reinforcement to inner lateral reinforcement amount	Outer lateral reinforcement cross-sectional areas (inch ²)	Inner lateral reinforcement cross-sectional areas (inch ²)
	5:5	0.017	0.017
	6:4	0.02	0.014
	7:3	0.024	0.01
	8:2	0.027	0.007
	9:1	0.03	0.004
	10:0	0.034	0

3.2.5 FE model validation

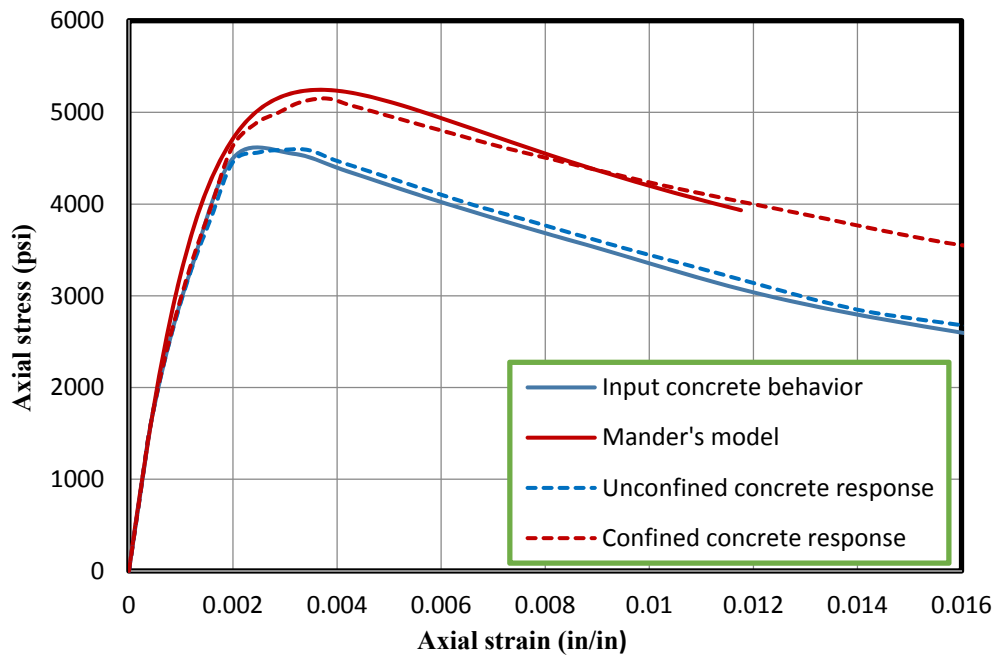
3.2.5.1 Solid section

In order to validate the simulation model, a solid section with the same geometry that was subjected to the same boundary as well as loading conditions (as the hollow sections discussed in previous sections) was modeled in ABAQUS. The derived stress vs. strain relationship of concrete in the loading direction was compared to the input concrete behavior as well as the Mander's prediction for two different cases.

A preliminary analysis on the solid reinforced concrete section showed that the employed material model could adequately describe the confinement effect in terms of enhanced strength and ductility characteristics of confined concrete members. The derived axial stress vs. strain relationship of concrete matched with the Mander's prediction favorably (Figure 3-4). The same material models were applied to hollow sections in order to compare the behavior between solid and hollow sections.



(a) 0.177 inch dia. confinement



(b) 0.125 inch dia. confinement

Figure 3-4: Comparison of the derived analytical axial stress vs. strain relationship of concrete and the Mander's model predictions

3.2.5.2 *Hollow Column HF1*

The accuracy of the simulation model was also evaluated for the displacement of a hollow bridge system (HF1) subjected to a static increasing lateral load. The ability of the simulation model to accurately represent the local behavior (in terms of failure mode and damage region) of the hollow bridge system was also discussed.

A three-dimensional finite element model of specimen HF1 tested by Hoshikuma and Priestley (2000) was developed using ABAQUS. A concrete damaged plasticity model was utilized in the FE analysis to define the uniaxial compressive and tensile concrete material properties of the bridge column. Concrete in the foundation block was modeled as a linear-elastic material because the foundation structural elements had a much larger capacity than the column and the foundation experienced no observable damage during the test. The stress-strain curve in compression for the bridge column was defined using the Mander's unified stress-strain model under monotonic loading at slow strain rates (confinement dependent uniaxial concrete model).

As discussed in Section 3.2.2, the tensile behavior of concrete within the concrete damage plasticity model could be defined to take into account the ability of the concrete to have a tension stiffening effect. This represents the interaction between the reinforcement and surrounding concrete. To simulate the materials of the test specimen realistically, $3.5\sqrt{f'_c}$ was used to define the failure tensile strength, and 0.008 in/in cracking strain was found to be satisfactory to define the tension stiffening parameter that ensured the best convergence. The angle of cracking was assumed to be 45 degrees to obtain smooth decreases in the tensile stresses after cracking.

A uniaxial bilinear steel model with isotropic kinematic hardening properties was used to simulate the behavior of the longitudinal steel and transverse steel. The input material properties are tabulated in Appendix B.

The circular hollow column and the footing were modeled using 3D continuum 8-node brick elements (C3D8R), whereas longitudinal reinforcement and transverse steel hoops were defined using the 1D 2-node linear truss element (T3D2). The longitudinal steel had a cross-sectional area of 0.2 in² and the transverse hoops had 0.05 in² cross-sectional area. The top of the hollow columns were covered with a steel base plate and a rigid steel tube (beam element) was

connected to the base plate. Lateral displacement was applied at the top of the steel tube. A tie constraint was selected to model the contact surface between the column and foundation as well as the contact surface between the steel base plate and the top of the hollow column. Coupling constraint was used to connect the steel tube to the top center of the base plate in order to distribute the load coming from the top of steel tube to the hollow column uniformly. The FE model and boundary conditions of HF1 are shown in Figure 3-5.

The FE mesh of the solid elements was generated, considering the location of the longitudinal reinforcement. Truss elements were linked to the edge of the solid elements using an embedded constraint option. A mesh size of 0.5 inches along the top and bottom plastic hinge regions of the column, and 2 inches outside the hinge regions, were used in the analysis (Figure 3-6). A coarser mesh (4 inches) was used for the footing because it was modeled with elastic material properties. The FE model was analyzed under displacement control.

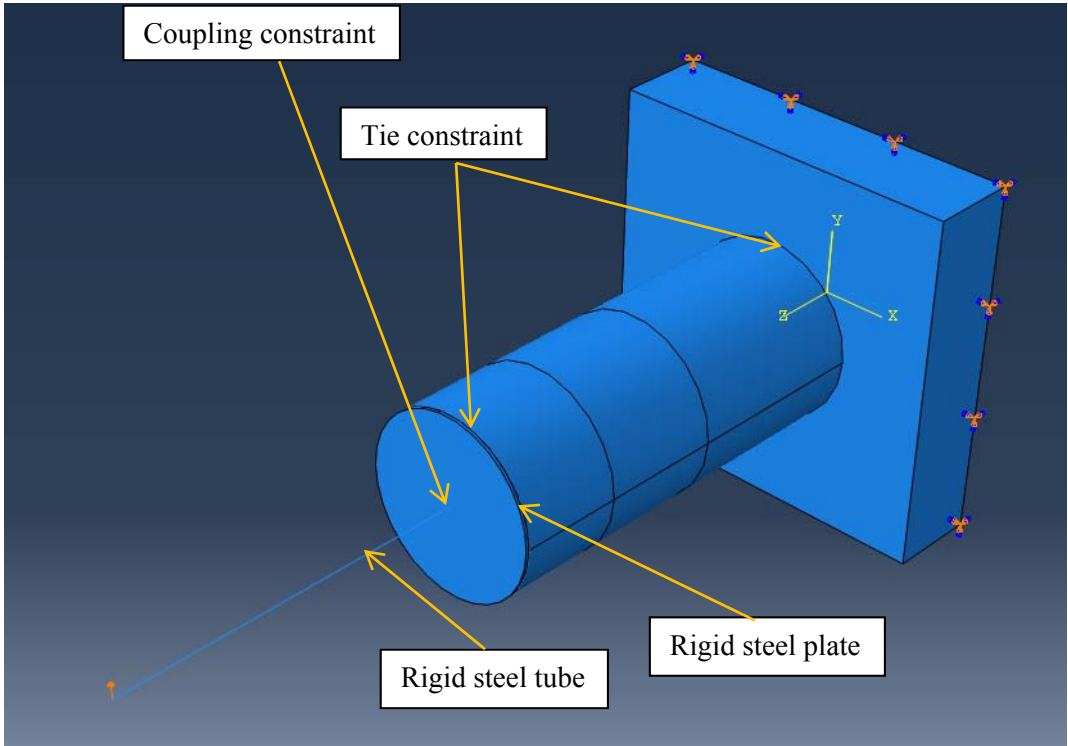


Figure 3-5: FEM model and boundary conditions of HF1 model

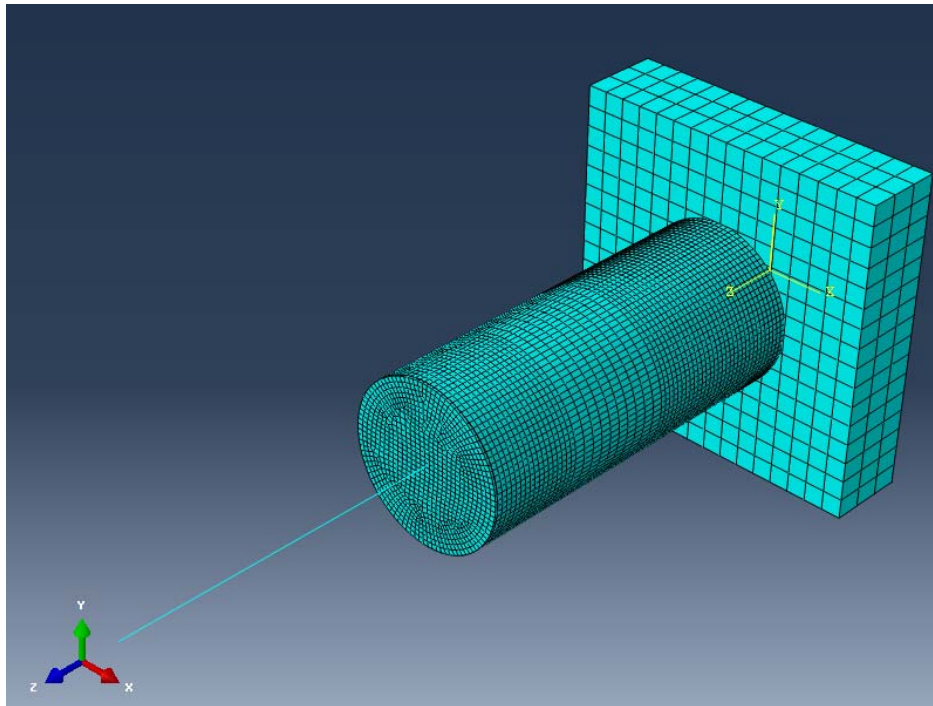


Figure 3-6: FEM mesh of HF1 model

The results of the FE model of the HF1 were obtained and compared with the measured experimental results. The overall load-displacement curve of the finite element model and the envelope of the hysteretic load-displacement response of the experimental test are compared in Figure 3-7. The FEM response curve shows a 7.8% lower ultimate load than the experimental one, but matches the overall force displacement trend and the moment curvature analyses based on Hoshikuma and Priestley's study pretty well. The predicted lateral displacement when the inside face concrete crushed is about 88 mm (3.5 inches), which is 2.3% higher than the measured displacement corresponding to the inside face concrete crushing (86 mm, 3.4 inches). These indicate accepted accuracy for the FEM results.

In addition to the overall force vs. displacement response comparisons between the FE model and the experimental results, some local comparisons were also made to represent that the FE model could simulate the test specimen favorably. According to the test results, the original specimen failed in the first push cycle to ductility 4.0 by the inside face concrete crushing over a height of 300 mm (11.8 inches) to 600 mm (23.6 inches) from the column base as shown in

Figure 3-8 (b). N300 in Figure 3-8 (b) represents 300 mm (11.8 inches) measured from the column base. The comparison of the damage zone demonstrated in Figure 3-8 shows good accuracy between the damaged elements of the FEM and the experimental specimen.

The longitudinal reinforcement strain profiles comparison between the experimental test and FEM is present in Figure 3-9. According to this figure, the measured longitudinal strains are lower than those derived from the FEM near the column base, while the measured longitudinal strains are greater than those derived from the FEM away from the base. This difference could be expected as the strain penetration effect was not fully accounted for in the FEM as this is an inherent problem with FE modeling (Sritharan et al., 2000).

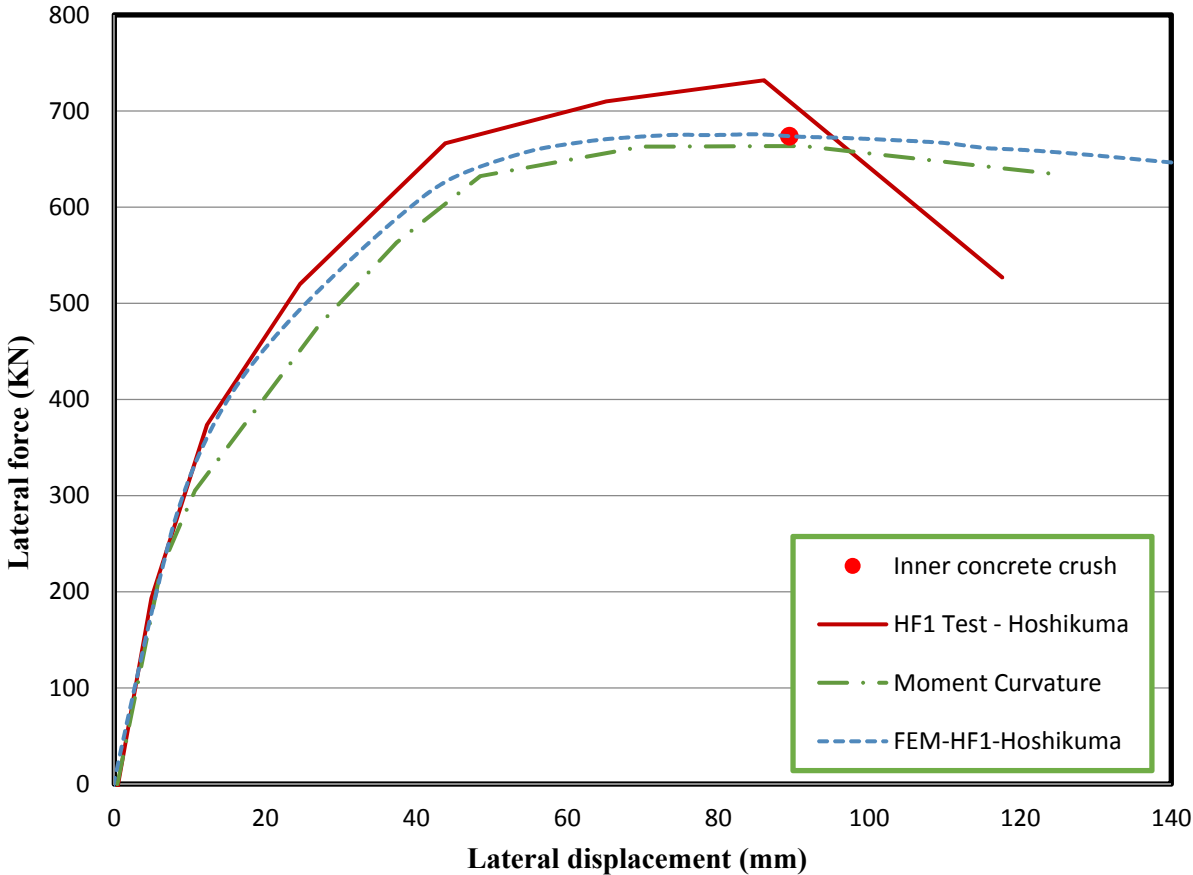
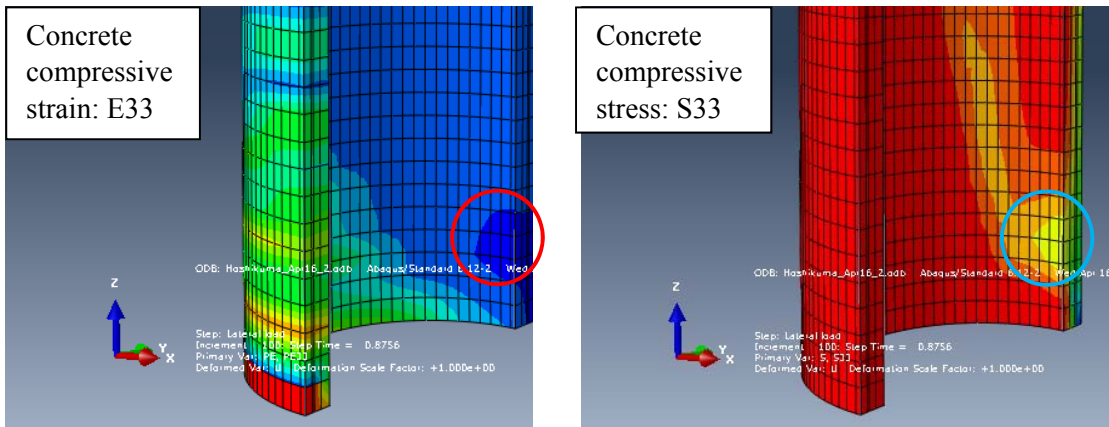
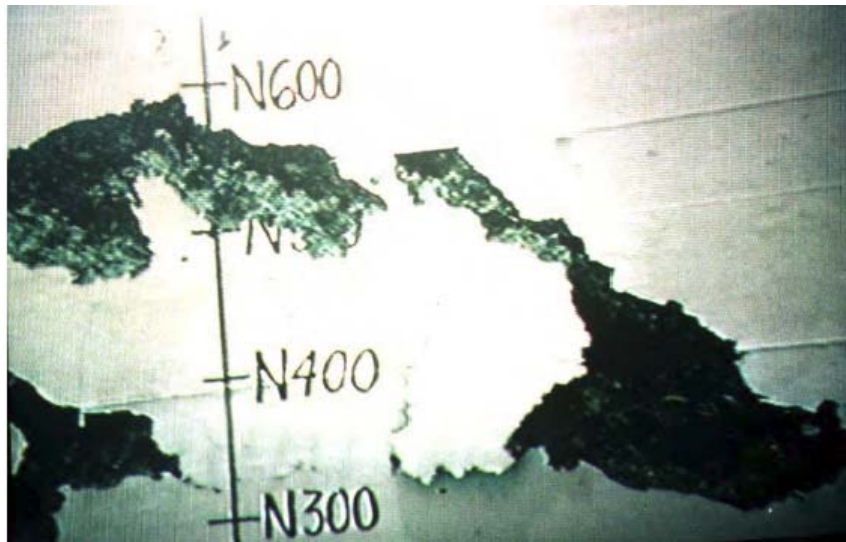


Figure 3-7: Lateral force vs. lateral displacement response comparisons among FEM, moment curvature analyses and measured experimental results



(a) FEM



(b) Experimental

Figure 3-8: Inside concrete face crushing (a) FEM, (b) Experimental

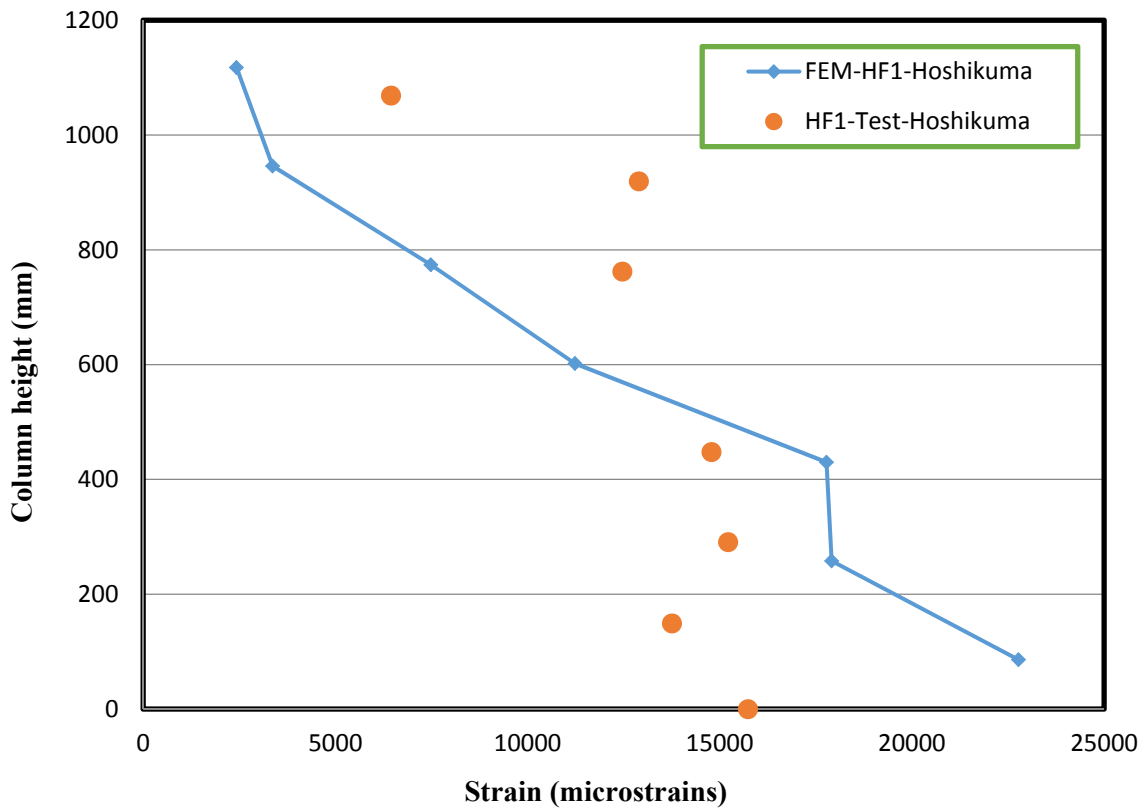


Figure 3-9: Longitudinal reinforcement strain profiles comparisons between experimental test and FEM at ductility 4

3.2.6 Analysis results

3.2.6.1 Confinement configurations

Two different wall thicknesses (one inch and two inch), corresponding to three types of confinement configurations, were analyzed for hollow sections. The circular hoop for the one-inch wall thickness was 0.125 inches in diameter and was 0.177 inches in diameter for the two-inch wall thickness. The resulting transverse reinforcement volumetric ratios for these two wall thicknesses with respect to different confinement configurations are tabulated in Table 3-1.

3.2.6.1.1 Two-inch wall thickness circular section

Based on the axial behavior comparisons among the three types of confinement configurations (Figure 3-10), the section that had two layers of transverse reinforcement without cross ties

behaved the worst, while the section with two layers of transverse reinforcement connected with effective cross ties behaved the best. There was no significant difference in the axial stress vs. axial strain relationship between the sections with an outer layer of confinement only, and that with two layers of confinement connected with effective cross ties, in the ascending branch. The difference started to occur after the axial stress passed the peak stress. The deterioration rate in the descending branch for the section with single layer of confinement was greater than that with two layers of confinement connected with effective cross ties. As discussed in Section 2.4, the deterioration rate in the descending branch of the confined concrete behavior depended greatly on the volumetric ratio of transverse reinforcement. The hollow section with two layers of confinement had a volumetric ratio of transverse reinforcement (1.37%) greater than that with one layer of confinement only (0.82%). The observation derived from the ABAQUS analysis was complied with those findings in the literature that the deterioration rate in the descending branch of the confined concrete behavior for hollow sections also depended on the volumetric ratio of transverse reinforcement.

For the two-inch wall thickness, the inner layer of transverse reinforcement was not strained to the yield strain for the hollow section that had two layers of transverse reinforcement without cross ties. This observation indicated that the inner layer of transverse reinforcement was not effective in confining concrete for such hollow sections. For the hollow section with two layers of transverse reinforcement connected with cross ties, the outer layer of transverse reinforcement reached the yield strain earlier than the inner layer of transverse reinforcement. This implied that the outer layer of transverse reinforcement was activated prior to the inner layer of transverse reinforcement, and that the tension demand developed in the inner layer of transverse reinforcement was effectively transferred to the outer layer of transverse reinforcement with the help of the cross ties.

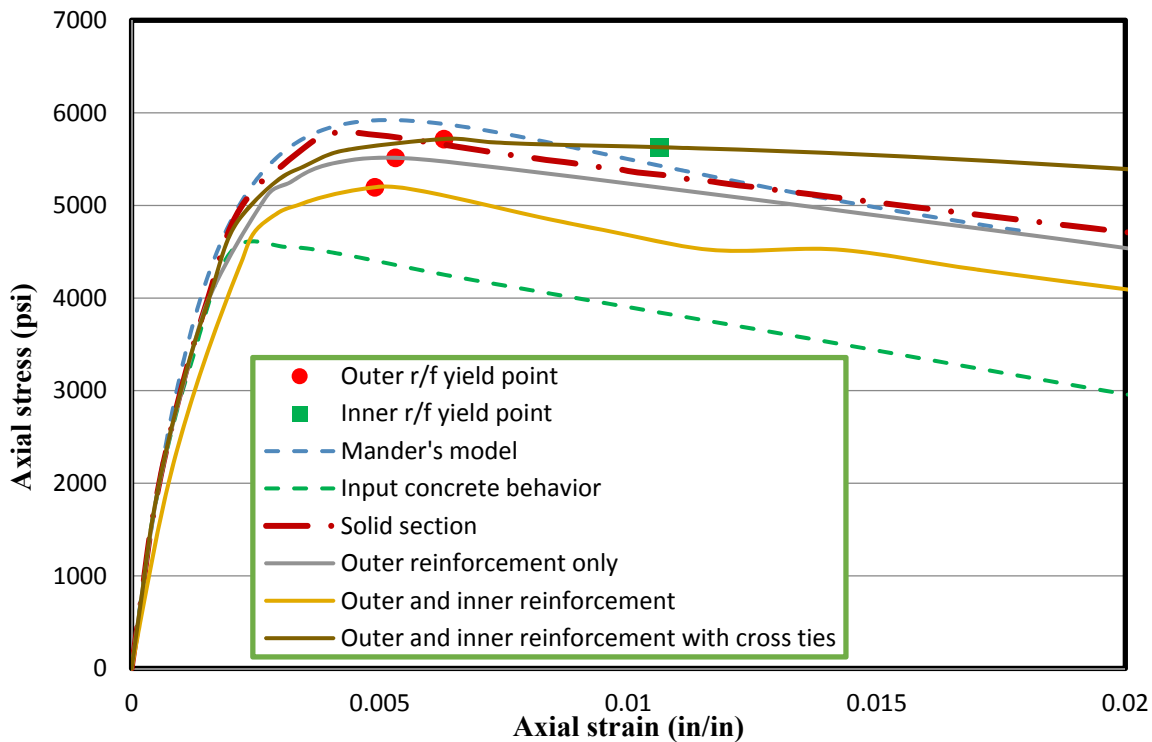


Figure 3-10: Axial concrete behavior comparisons among different confinement configurations for the two-inch wall hollow sections

The reasons why the hollow section with two layers of confinement connected with effective cross ties behaved best, while the section with two layers of reinforcement but no cross ties behaved even worse than that with outer layer of confinement only, could be demonstrated in the following aspects. Figure 3-11 shows the deformed shape of the two-inch wall hollow section with one layer of confinement (0.0246 cross-sectional bar area) placed near the outside concrete wall compared to the undeformed shape at the ultimate concrete strain (0.0135 in/in) suggested by Mander et al. (1988). The ultimate concrete strain proposed by Mander et al. (1988) based on the gross section is

$$\varepsilon_{cu} = 0.004 + \frac{1.4\rho_s f_{yh} \varepsilon_{su}}{f'_{cc}} = 0.004 + \frac{1.4 \times 0.0082 \times 60 \times 0.08}{5.8} = 0.0135 \quad \text{(Equation 3-1)}$$

The entire member of the modeled hollow column moved outward as the axial load increased before the axial strain reached 0.0135 inches/inches. Therefore, the presence of the inner layer of confinement only tried to confine the inner concrete cover, if the inner layer of confinement was

not connected to the outer layer of confinement effectively. This may also partly due to ABAQUS strengthened the inner layer of concrete artificially. This condition would lead to an unconfined ring-shaped region around the inner confinement, which could be illustrated clearly by the axial stress contour for the hollow section with two layers of confinement but without cross ties (Figure 3-12). As a result, the inside concrete cover tended to crack and spall off at high levels of axial strain and the behavior of such columns was controlled primarily by the weakest concrete portion around the inner confinement instead of the inside concrete face.

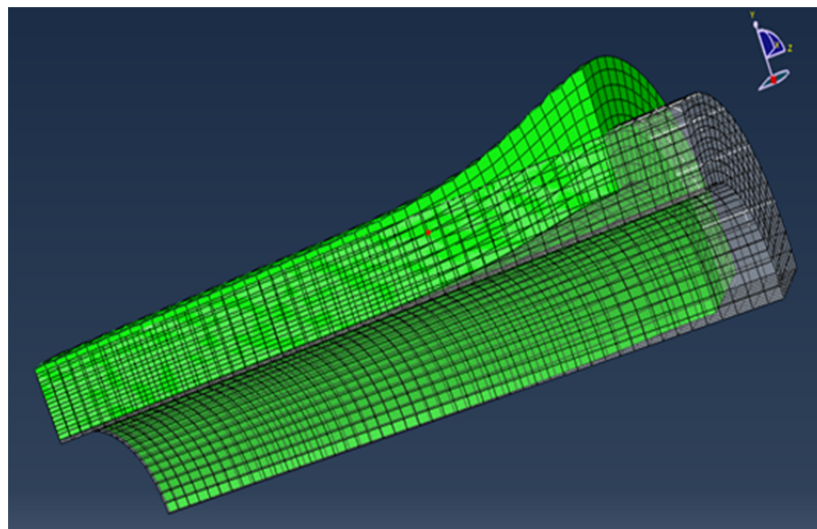


Figure 3-11: Deformed shape of the two-inch wall hollow section with one layer of confinement

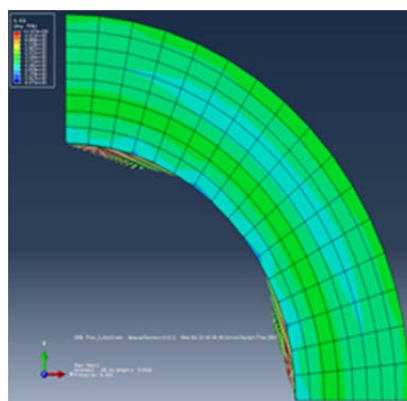


Figure 3-12: Axial concrete compressive stress contour for the two-inch wall hollow section with two layers of confinement but no cross ties

This phenomenon could also be more obviously illustrated by plotting the relationship between the radial stresses that caused the confining pressure and the axial strain of concrete. Based on the coordinate system used in ABAQUS, the negative radial stress indicated that the concrete experienced positive confining pressure, while the positive radial stress indicated that the concrete experienced negative confining pressure. The larger the magnitude of negative radial stress, the more the concrete was confined and therefore, the better the concrete would behave. The following figures (Figure 3-13, Figure 3-14, and Figure 3-15) show the radial behavior regarding the sections with three types of confinement configurations for the two inch wall thickness. The concrete wall was divided into 8 layers and 1 to 8 represented the layer counted from the inside concrete face to the outside concrete face. For the hollow section with two layers of reinforcement but no cross ties, the inner concrete section (layer 1 to layer 3) was not confined at all (Figure 3-14). These three layers experienced positive radial stress (i.e., negative confining pressure), which could also explain the reduced strength of hollow sections with two layers of confinement but no cross ties. Compared to the hollow section with one layer of confinement, the hollow section with two layers of reinforcement connected with cross ties experienced higher negative confining pressure in the outer-most concrete layer. The magnitude of the radial stress for the hollow section with two layers of reinforcement connected with cross ties was greater than that with one layer of reinforcement. The magnitude of the radial stress for the hollow section with two layers of reinforcement but no cross ties was the smallest. Therefore, two layers of reinforcement connected with cross ties provided the most efficient confining pressure to the concrete core of the hollow sections, followed by one layer of reinforcement placed near the outside concrete wall. Two layers of reinforcement without cross ties was the least efficient confinement configurations among the three types. The relationship between the radial concrete stress and the axial concrete strain with respect to each confinement configuration at the given concrete layer, are presented in Appendix D.

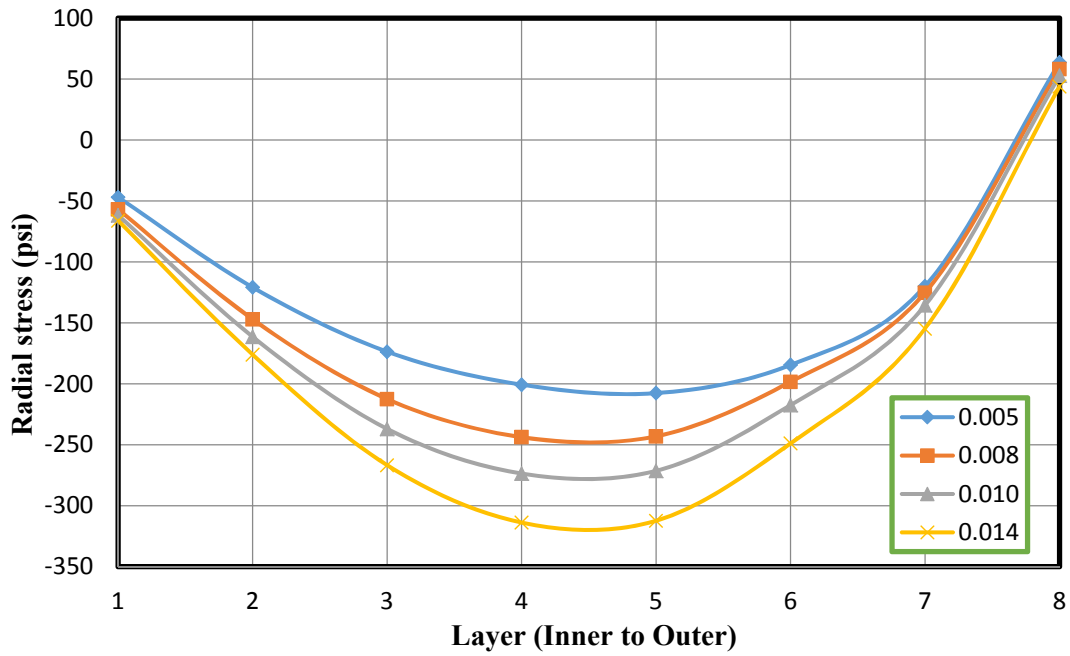


Figure 3-13: Radial concrete stress with respect to each concrete layer for the two-inch wall hollow section with one layer of confinement only

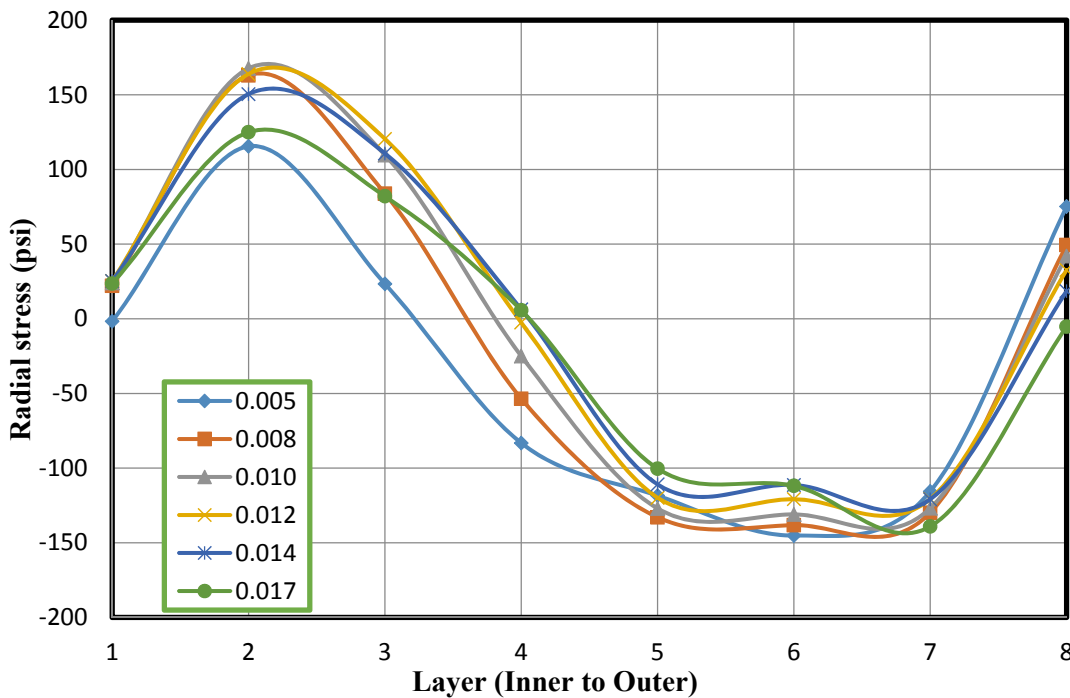


Figure 3-14: Radial concrete stress with respect to each concrete layer for the two-inch wall hollow section with two layers of confinement but no cross ties

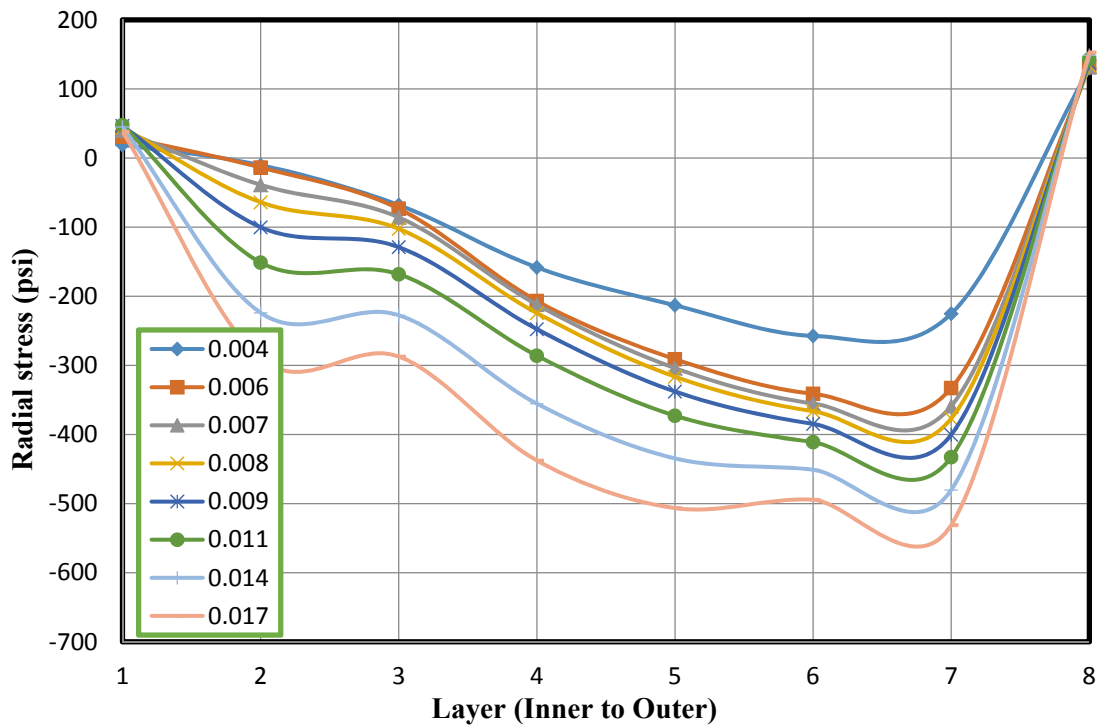


Figure 3-15: Radial concrete stress with respect to each concrete layer for the two-inch wall hollow section with two layers of confinement connected with cross ties

3.2.6.1.2 One-inch wall thickness circular section

Similar to the two-inch wall thickness, the hollow section with two layers of confinement connected with effective cross ties behaved the best among the three types of confinement configurations for the one-inch wall thickness (Figure 3-16). It was interesting to notice that there was no significant difference between the behavior for the section with two layers of reinforcement without cross ties, and the section with one layer of reinforcement only. The presence of the inner layer of reinforcement did not help to improve the concrete behavior unless the inner layer of reinforcement was tied to the outer layer of confinement with cross ties. For the hollow sections with two layers of reinforcement connected with cross ties, both the inner and the outer reinforcements yielded at the same time.

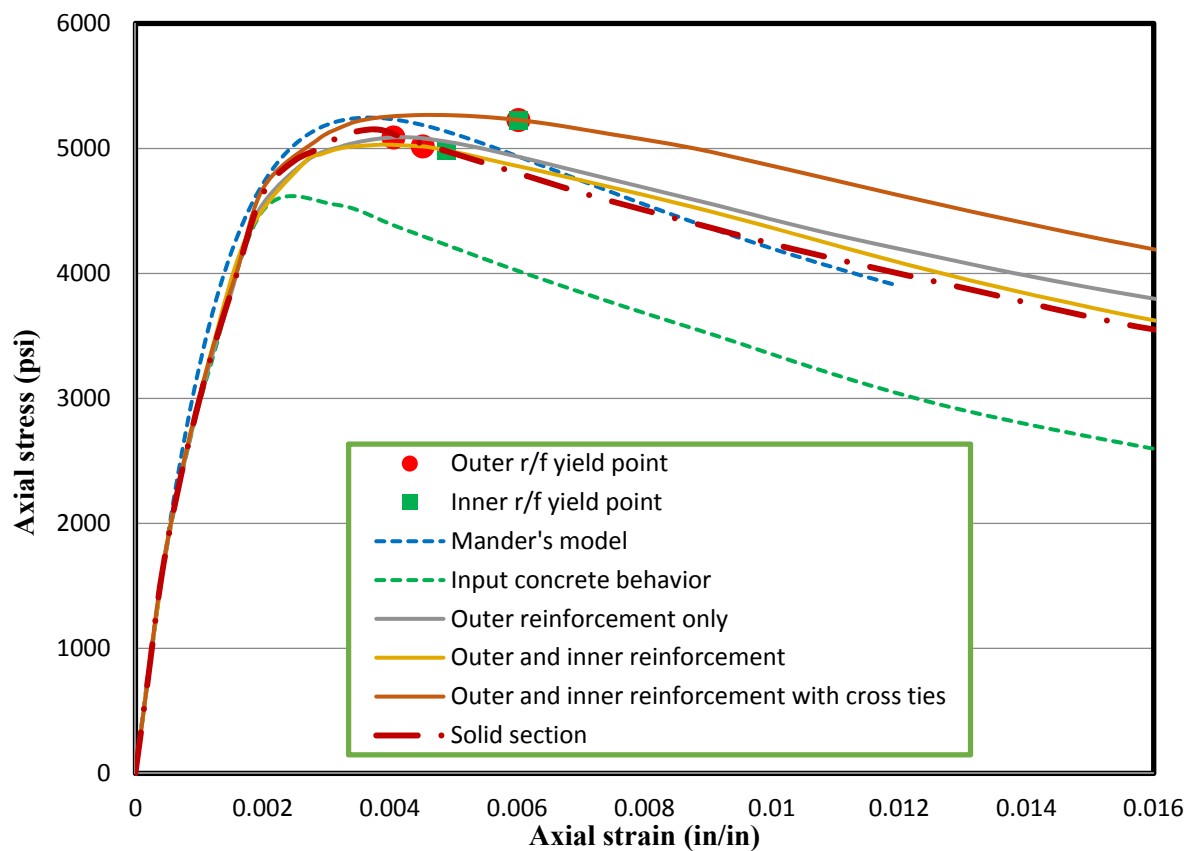


Figure 3-16: Axial concrete behavior comparisons among different confinement configurations for the one-inch wall hollow sections

For the hollow section with two layers of confinement but no cross ties, both the inner and the outer layer of confinement reached the yielding strain, which was different than the two-inch wall hollow section where the inner layer of confinement did not reach the yielding strain before the axial strain arrived at 0.02 in/in.

Due to the Poisson's effect, as the axial load was applied in the z direction, the concrete tended to expand in the directions perpendicular to the loading direction, i.e., the x and y directions. Outward dilation is easier to be restrained for hollow sections with thinner walls, so the one-inch wall hollow section did not move outward as much as the two-inch wall hollow section. This meant that the one-inch wall hollow section did not pull away from the inner confinement as much as the two-inch wall hollow section, if the inner layer of confinement was not tied to the outer layer of confinement.

Similar to the two-inch wall hollow section, the radial behavior of the one-inch wall hollow sections with respect to three different confinement configurations are shown in Figure 3-17 to Figure 3-19. For the one-inch wall hollow section with two layers of confinement but no cross ties (Figure 3-18), the inner concrete layer experienced small positive confining pressure, which indicated that the inner concrete layer was relatively confined. This observation was different from the two-inch wall hollow section where the inner concrete layer experienced negative confining pressure and was not confined. In addition, the second layer counted from the inner wall experienced negative confining pressure as the axial concrete strain was small, while it began to experience positive confining pressure as the axial concrete strain was greater than 0.009 in/in. This observation was also different from the two-inch wall hollow section, where the inner concrete wall section (the first three layers counted from the inner wall) experienced negative confining pressure, regardless of the concrete strain in the axial direction. Compared to the one-inch wall hollow section with one layer of confinement, the increase of the magnitude of the radial stress for the section with two layers of confinement connected with cross ties was not as significant as the two-inch wall hollow section. This implied that two layers of confinement connected with cross ties for the one-inch wall hollow section did not help confine the concrete as much as the same confinement configuration in a two-inch wall hollow section.

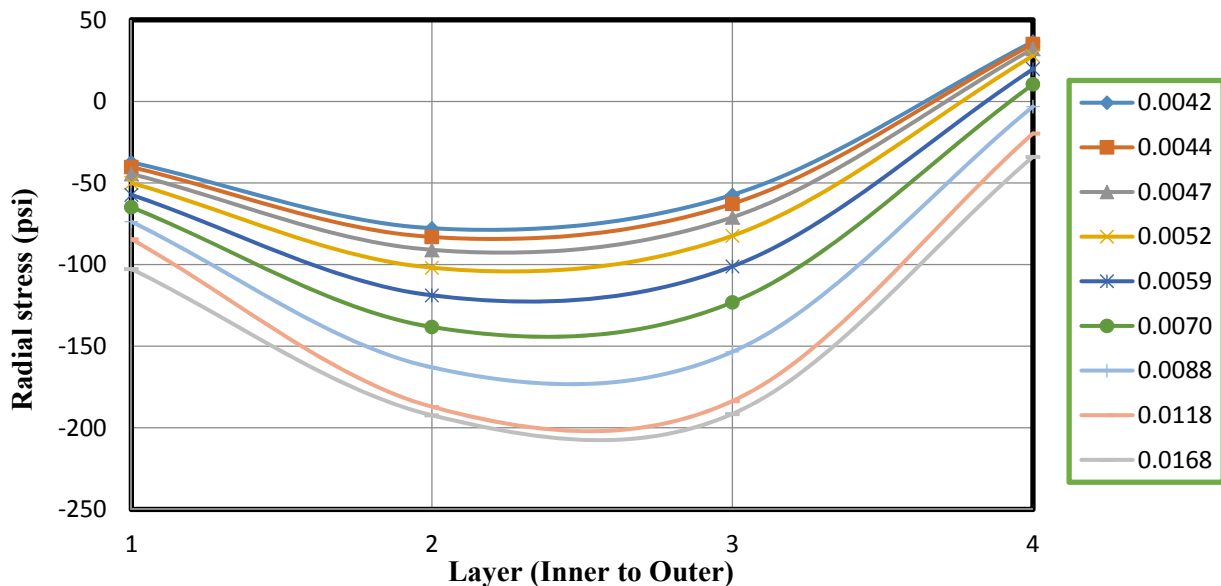


Figure 3-17: Radial concrete stress with respect to each concrete layer for the one-inch wall hollow section only with an outer layer of confinement

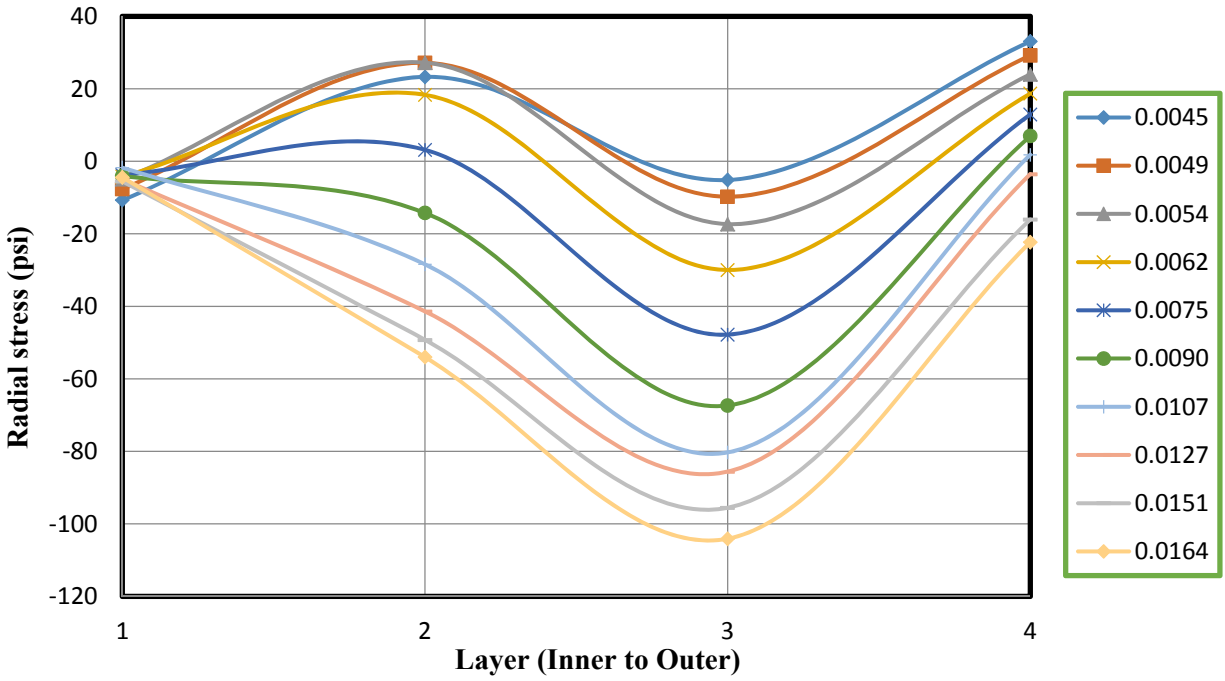


Figure 3-18: Radial concrete stress with respect to each concrete layer for the one-inch wall hollow section with two layers of confinement but no cross ties

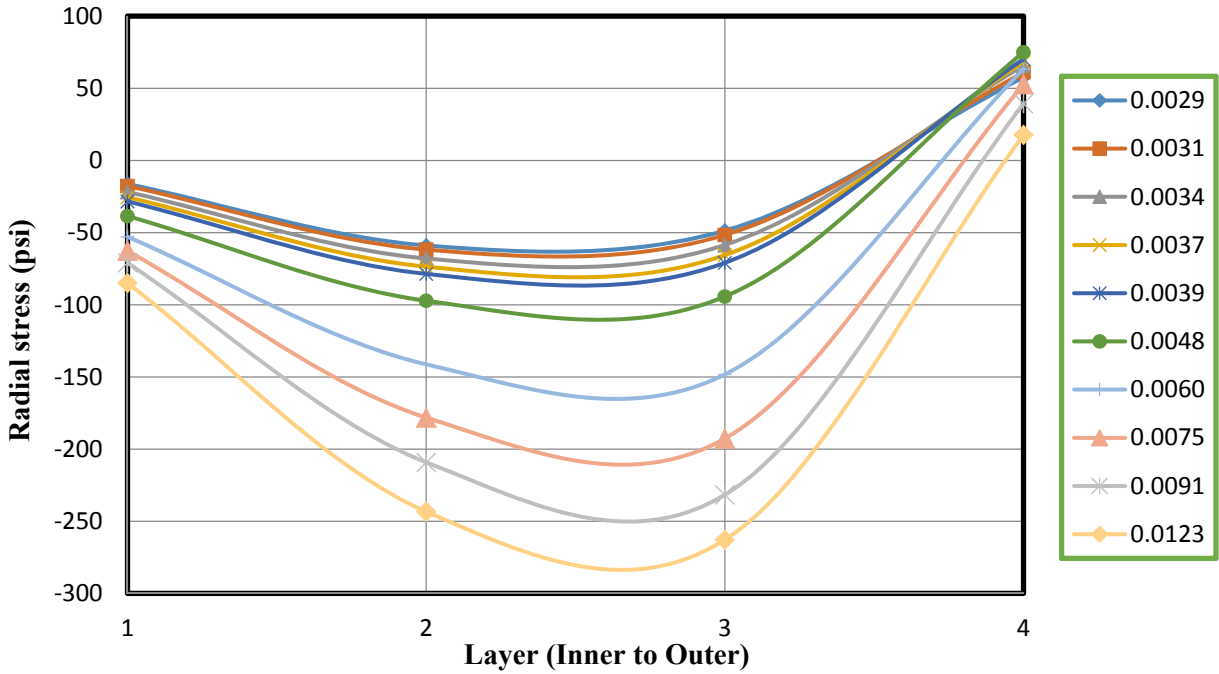


Figure 3-19: Radial concrete stress with respect to each concrete layer for the one-inch wall hollow section with two layers of confinement connected with cross ties

3.2.6.2 *Wall thickness*

3.2.6.2.1 **Two layers of confinement connected with cross ties**

Based on the analysis conducted on the confinement configurations, it was found that the hollow sections confined with two layers of confinement and cross ties generally behaved the best among the three types of confinement configurations. By examining the analysis results for the one-inch and two-inch wall thicknesses, the peak stress enhancement that came from the two layers of confinement connected with effective cross ties was more significant for thicker walls. In this section, a set of analyses was presented which examined the effect of wall thickness on the confined concrete behavior. A series of analyses for hollow sections that were confined with same amount of transverse reinforcement (0.0246 in^2 cross-sectional areas) placed at both the inside and the outside concrete face, were performed. Sufficient cross ties were provided to connect these two layers of confinement effectively. This would lead to the same volumetric ratio of transverse reinforcement based on the gross section (0.82%) as defined in Section 3.2.1. Different wall thicknesses corresponding to different ratios between the wall thickness and the outer diameter are tabulated in Table 3-2. These ratios generally covered all the ratios that had been tested or analyzed by previous researchers as summarized in Section 2.2.1.

The derived axial stress vs. axial strain relationship corresponding to different wall thickness to section diameter ratios are presented in Figure 3-20 for the circular hollow sections. From this figure, the 2.4-inch-wall hollow column behaves better than all the other wall thicknesses. There is no obvious difference among the other ratios in the ascending branch up to the peak stress. The difference starts to occur after the axial stress passed the peak stress. In all of these cases, the outer layer of lateral reinforcement reached the yield strain prior to the inner layer, and both layers of lateral reinforcement reached the yield strain before the axial strain arrived at 0.02 in/in. This indicated that both the inner and the outer layer of confinement were effective in confining the concrete core. For the hollow section with a wall thickness ratio of 0.2 (2.4-inch wall), it was observed from Figure 3-20 that the inner layer of confinement reached the yield strain right after the outer layer of confinement, which was a lot earlier than the other wall thickness ratios. This is because the hollow section with a thicker wall will experience a greater

outward dilation under the same amount of transverse reinforcement. The concrete dilation will be discussed in detail in Section 3.2.6.2.2. Therefore, more tension demand needed to be transferred from the inner reinforcement to the outer reinforcement through the cross ties to resist the larger concrete outward dilation. This would drive the inner reinforcement to reach the yield strain earlier. The deterioration rate in the descending branch was generally low, which implied that the strength degradation after the peak stress was small for the hollow sections confined with two layers of confinement connected with cross ties. Therefore, the hollow columns confined with two layers of confinement connected with cross ties would potentially experience a higher ductility under flexure loading.

The derived axial stress vs. axial strain relationships corresponding to different wall thickness ratios for square sections is presented in Figure 3-21. The confined concrete behavior of hollow square sections that have two layers of transverse reinforcement connected with cross ties is very comparable to the Mander's prediction based on the solid square sections, especially for thicker wall thickness. This observation is different from circular sections, where the confined concrete behavior for solid sections is better than hollow sections. Unlike the circular sections, where the outer reinforcement reached the yield strain prior to the inner reinforcement, the inner reinforcement reached the yield strain earlier than the outer reinforcement for square sections. For the 1.2-inch-wall hollow square section, the outer reinforcement did not reach the yield strain before the axial strain reached to 0.02 in/in. This observation implied that the concrete dilation mechanism for square hollow sections is different from the circular hollow sections.

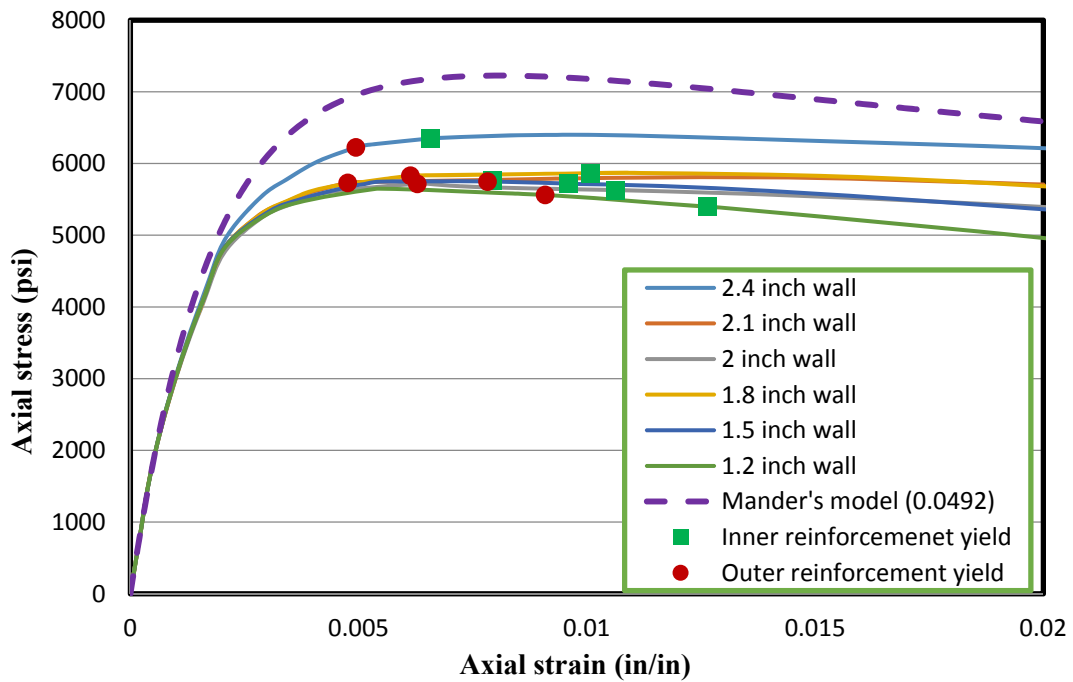


Figure 3-20: The axial stress vs. axial strain behavior corresponding to different wall thickness to diameter ratios for the circular section

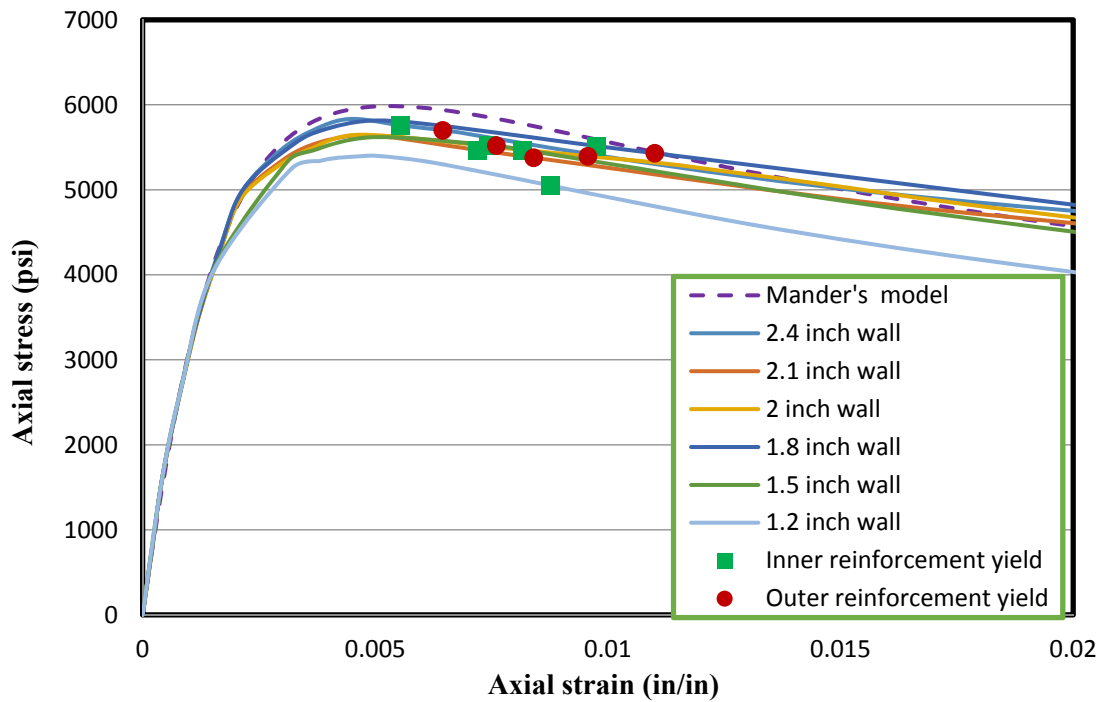


Figure 3-21: The axial stress vs. axial strain behavior corresponding to different wall thickness to diameter ratios for the square section

3.2.6.2.2 One layer of confinement

In order to better understand the concrete dilation from a fundamental point of view and also provide further information about the confined concrete behavior for hollow sections confined with one layer of reinforcement (same as test specimens), another series of analyses were conducted for the hollow section with one layer of lateral reinforcement placed near the outside concrete face under the same volumetric ratio of confinement.

Table 3-2 presents the analyses matrix. Different wall thicknesses corresponding to different wall thickness-to-section diameter ratios were analyzed and the resulting relationship between the axial stress and axial strain relationship for circular sections is shown in Figure 3-22. For better comparisons, the Mander's prediction and the derived concrete behavior for solid section were also included. According to this figure, the confinement effectiveness for hollow sections is reduced compared to solid section. For the hollow sections with different wall thicknesses, the confined concrete behavior is very similar to each other with slightly increase of peak stress and peak strain (concrete strain corresponding to the peak stress) for thinner walls. The confinement reached the yield strain at different stages for different wall thicknesses. As the wall thickness increases, the axial concrete strain corresponding to the yielding of confinement decreases. This indicated that as the wall thickness increased, more confining pressure was required to restrain the outward concrete dilation, at given axial compressive strain. Therefore, a thicker wall would drive the confinement to yield earlier than a thinner wall. For the circular hollow section, the peak concrete stress typically occurred as the confinement reached the yielding stress.

Same type of analyses was also performed for square hollow sections and the resulting relationship between the axial stress and axial strain for different wall thicknesses is shown in Figure 3-23. Compared to the Mander's prediction, the confinement effectiveness for square hollow sections is further reduced. Same as circular hollow sections, the confined concrete behavior is also very similar to each other for different wall thickness with slightly increase of the peak stress for thinner walls. However, it seemed that the strain corresponding to the peak stress was approximately the same for different wall thickness, which was different from the circular hollow sections. In addition, the confinement behavior is also different from the circular sections. For circular sections, the yielding of confinement typically corresponded to the peak

stress of confined concrete behavior. However, the yielding of confinement occurs in the descending branch of the confined concrete behavior for square sections.

Besides the axial behavior comparisons, the derived relationships between the radial displacements (concrete dilation) and the axial concrete strains were also compared and are shown in Appendix F for circular sections with different wall thickness. In this set of figures, 1 to 9 represents the concrete layer counted from the inside concrete wall to outside concrete wall. The corresponding deformed shape is present in Table 3-4. According to this table, it was found that the entire concrete wall dilated outward for all the wall thicknesses before the axial concrete compressive strain reached 0.02 in/in, which implied that the inside concrete wall layer would also experience positive confining pressure under the uniaxial compression. Similarly, the deformed shape for square sections is shown in Table 3-5. Unlike the circular hollow sections, where the entire concrete wall dilated outward, the inner concrete wall dilated inward while the outer concrete wall dilated outward for square hollow sections, before the axial concrete strain reached to 0.02 in/in. Therefore, the inside concrete wall may experience premature failure if square hollow columns were confined with one layer of lateral reinforcement only.

The concrete outward dilation of the outermost layer for circular hollow sections with each wall thickness and also the solid section with the same outer diameter is compared in Figure 3-24. Based on this figure, as the wall thickness increased, the outward dilation of the outermost concrete layer also increased. This increase of the outward concrete dilation becomes negligible as the wall thickness increased from 2 inches to 2.4 inches. This indicated that the confinement reinforcement placed near the outside concrete face could more easily restrain the concrete dilation of the hollow section with a thinner wall. Therefore, one layer of lateral reinforcement was more efficient in confining the thinner wall hollow sections. Referring to Figure 3-13 and Figure 3-17, the radial stress (positive confining pressure) experienced by the inside concrete face layer for the one-inch wall hollow section (100 psi) is greater than the two-inch wall hollow section (50 psi). This observation confirmed that the one layer of lateral reinforcement was more efficient for the thinner wall hollow sections. Compared to the outward dilation of the outermost layer for solid sections, the hollow section with a wall thickness of 1.5 inches experienced a very similar outward dilation. For the hollow section that has a wall thickness greater than 1.5 inches,

the outward dilation of the outermost layer is greater than the solid section, while is smaller for the hollow section that has a wall thickness smaller than 1.5 inches.

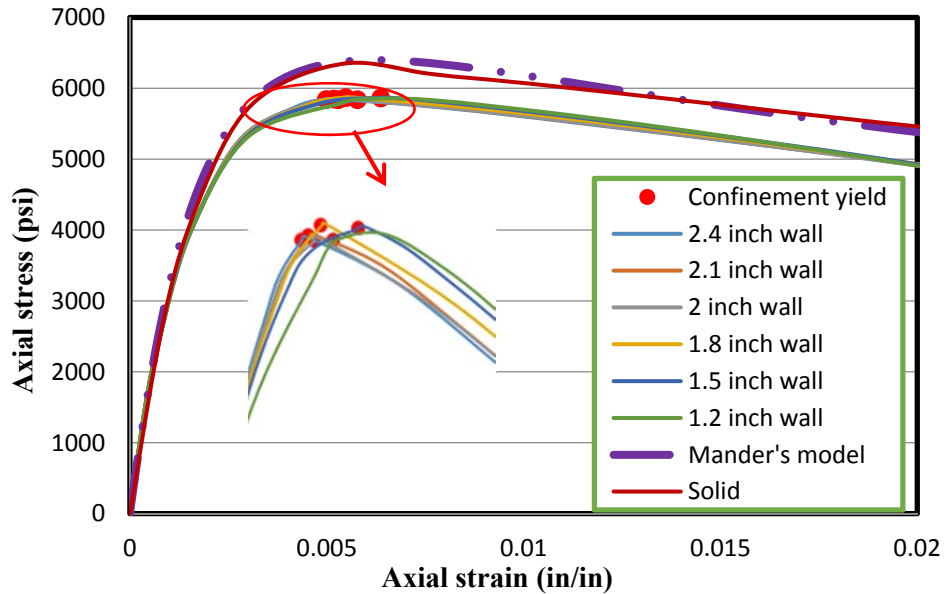


Figure 3-22: The resulting relationship between the axial stress and axial strain for circular hollow sections that have one layer of confinement

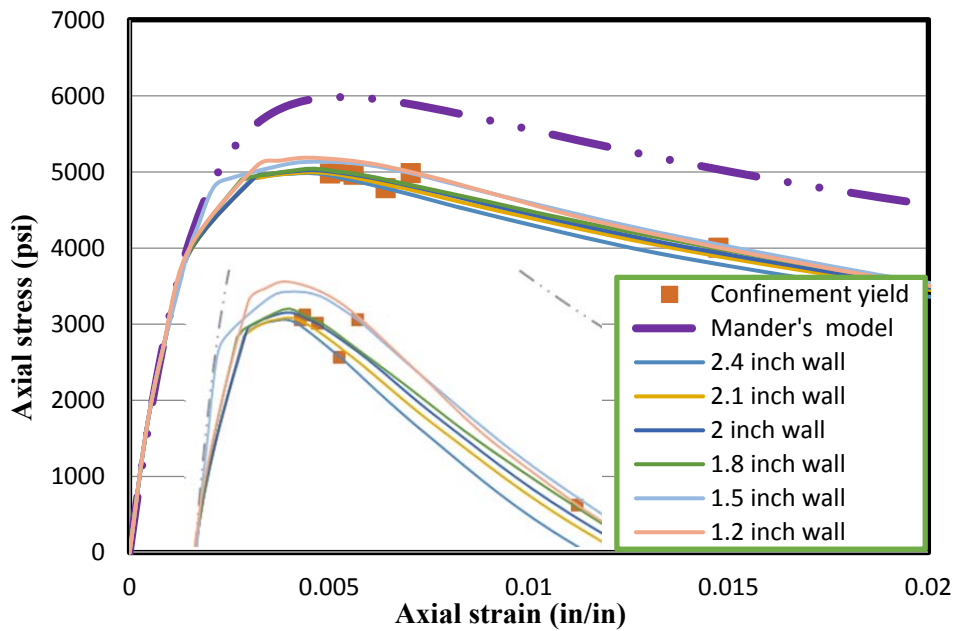


Figure 3-23: The resulting relationship between the axial stress and axial strain for square hollow sections that have one layer of confinement

Table 3-4: Deformed shape of circular hollow sections having one layer of confinement placed at the outside concrete wall under the same amount of confinement

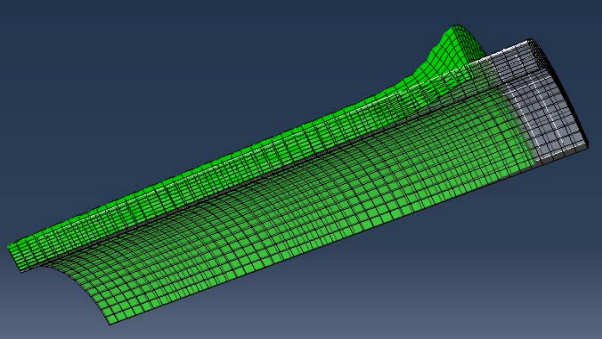
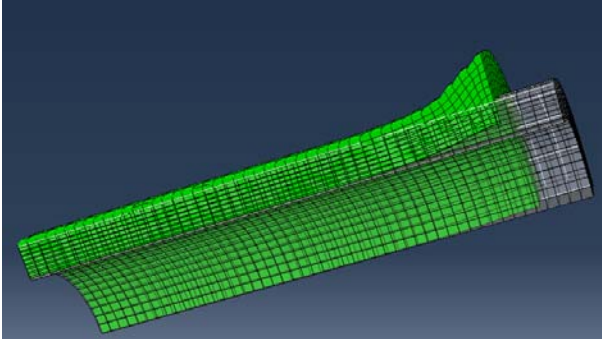
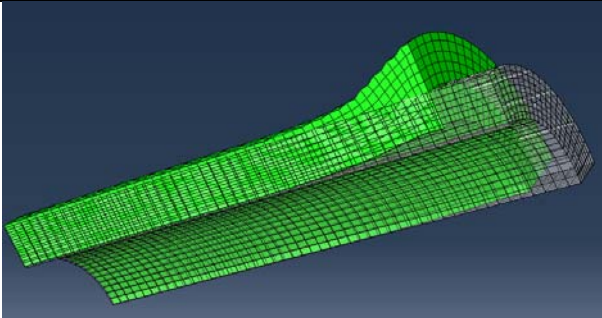
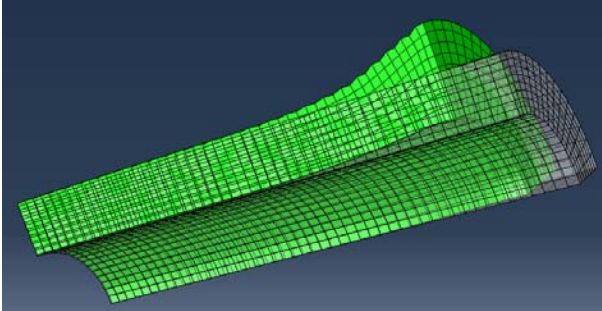
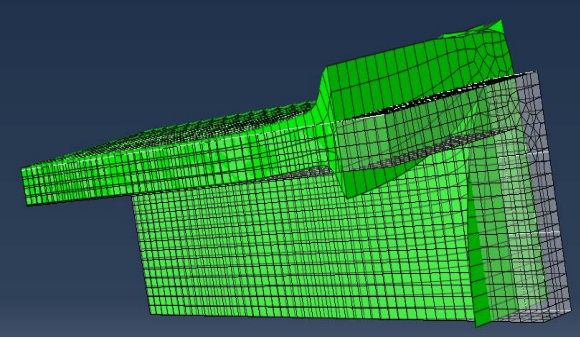
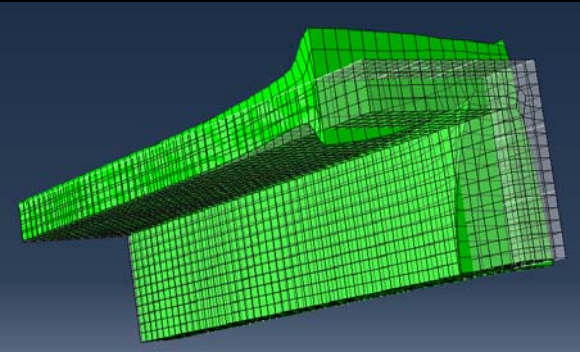
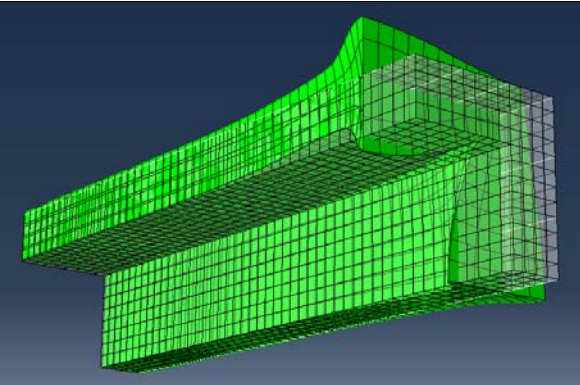
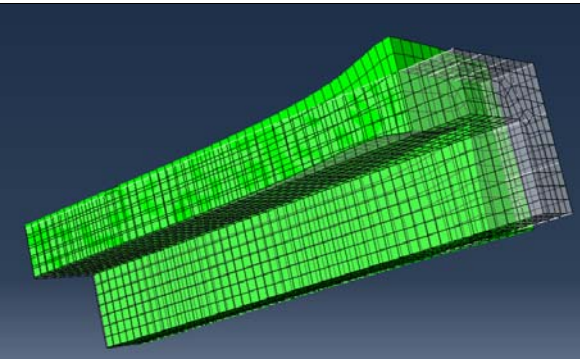
Wall thickness (inch)	Deformed shape of circular sections
1.2	
1.5	
2	
2.4	

Table 3-5: Deformed shape of square hollow sections having one layer of confinement placed at the outside concrete wall under the same amount of confinement

Wall thickness	Deformed shape of square sections
1.2	
1.5	
2	
2.4	

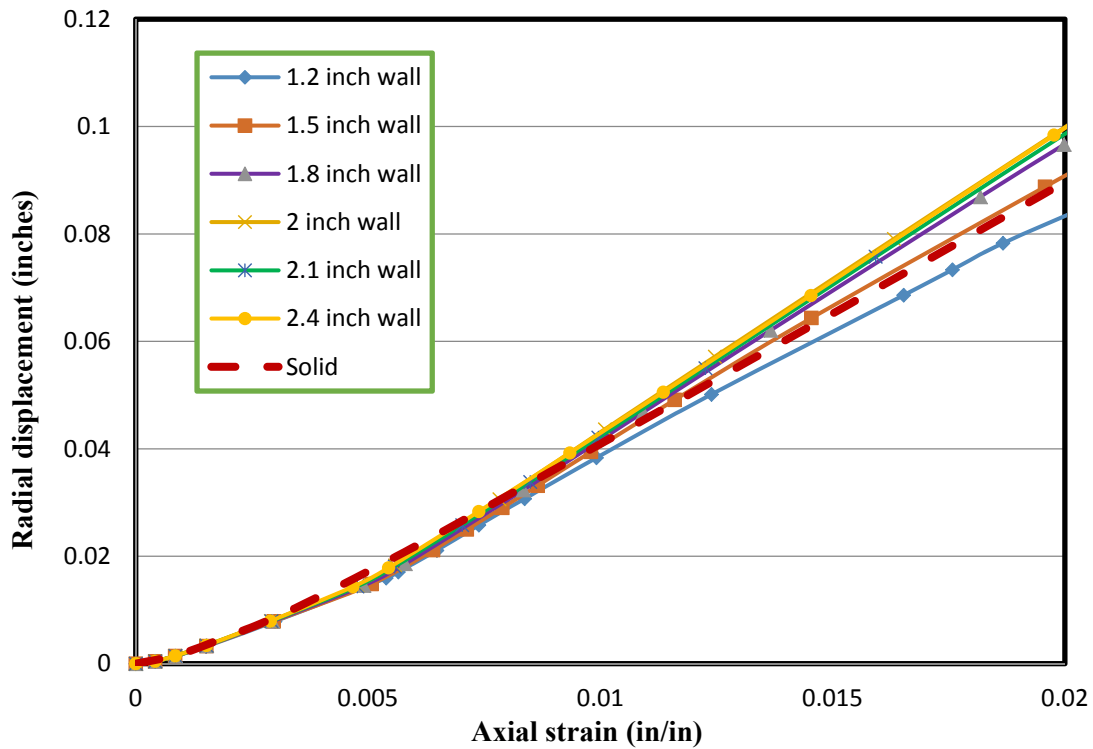


Figure 3-24: The concrete outward dilation of the outermost layer for circular hollow sections with one layer of confinement

The confined concrete dilation could be expressed as a combination of Poisson’s effect for plain concrete cylinder and the confining effect exerted by the confinement. A plain concrete cylinder is free to dilate outward under the axial compressive concrete strain due to the Poisson’s effect. This outward concrete dilation is associated with the axial compressive concrete strain, Poisson’s ratio and outer diameter of the concrete cylinder, which does not depend on the wall thickness for hollow sections. Therefore, both hollow and solid sections that have the same outer diameter (12 inches) would experience the same amount of concrete outward dilation based on the Poisson’s effect. For the confined concrete members, the concrete is not free to dilate, since the transverse reinforcement would try to restrain this concrete dilation by providing confining pressure. By providing same amount of confinement near the outside concrete wall for both hollow and solid sections, the confinement would be more efficient to restrain the concrete dilation of hollow columns with thinner walls. Therefore, the hollow sections that have a thicker wall would experience a greater concrete outward dilation.

To illustrate the concrete dilation for both hollow and solid sections clearly, a 1.8-inch wall hollow section, which had the same number of concrete layers as the solid section over the 1.8 inch portion, was selected for the analysis (Figure 3-25). The resulting concrete dilation is shown in Figure 3-26. Compared to the solid section, the 1.8-inch wall hollow section experienced a greater concrete dilation in both inward and outward directions. This figure clearly represents that the concrete element in hollow sections is not confined as well as in solid sections and the confinement effectiveness in hollow sections is reduced.

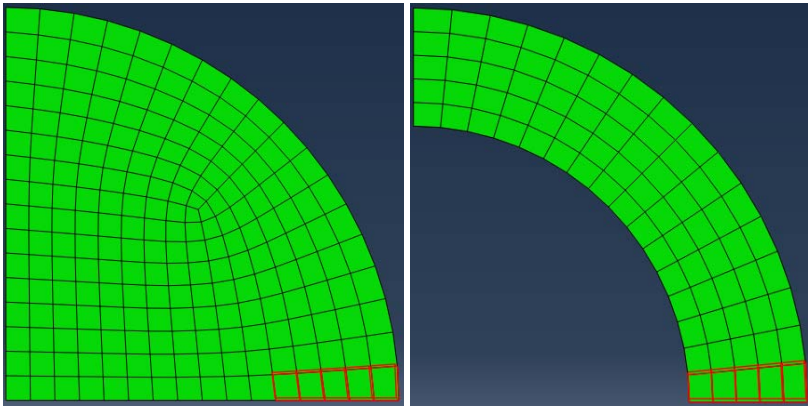
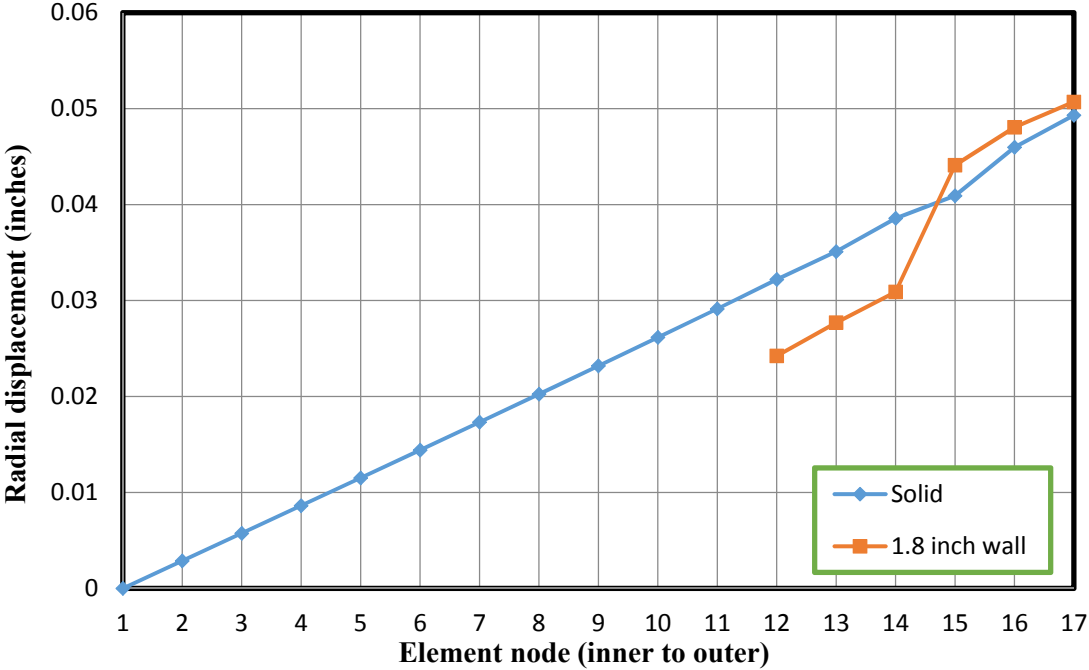
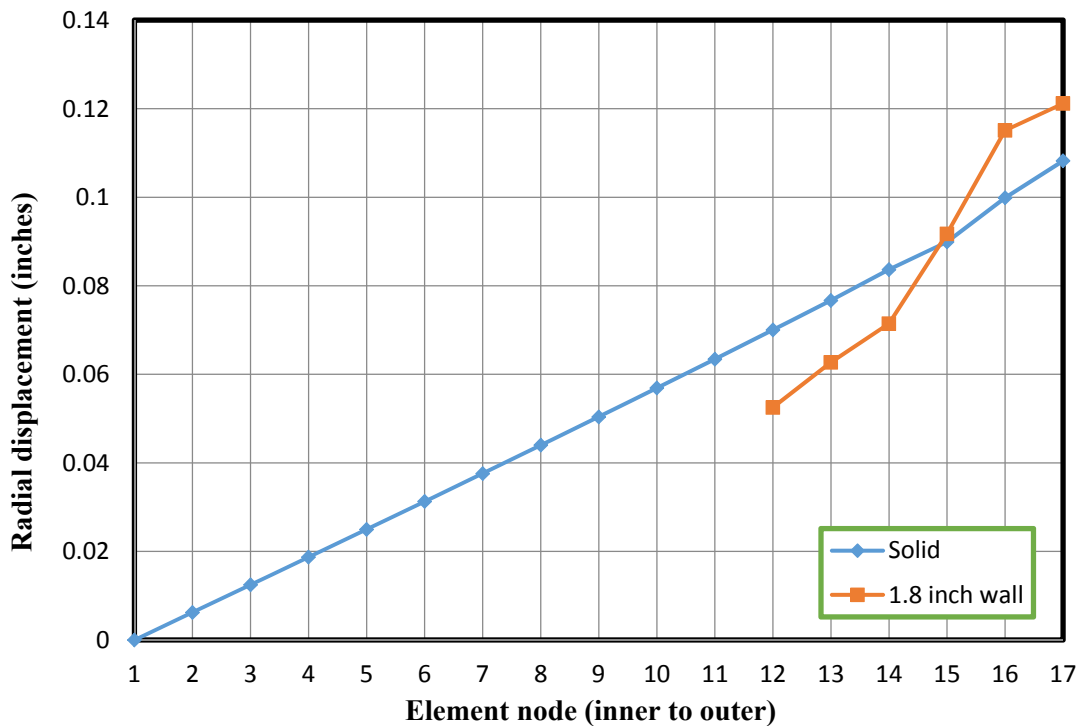


Figure 3-25: The selected 1.8-inch-wall hollow section to study the concrete dilation



(a) At 0.01 in/in axial strain



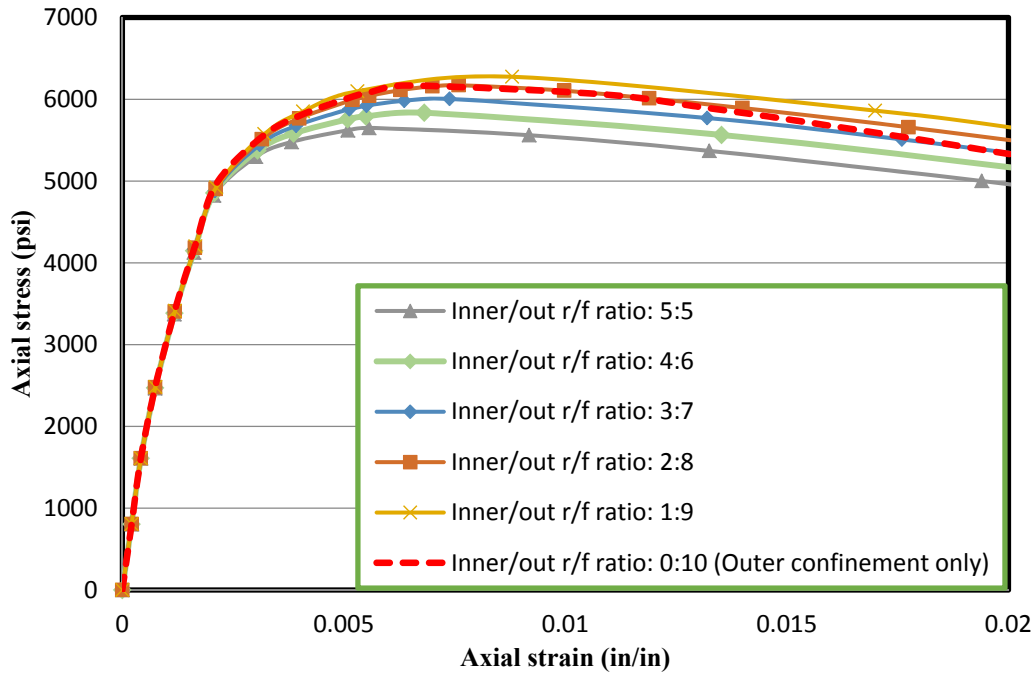
(b) At 0.02 in/in axial strain

Figure 3-26: Concrete dilation for both solid and 1.8-inch-wall hollow sections at 0.01 in/in and 0.02 in/in axial concrete strain

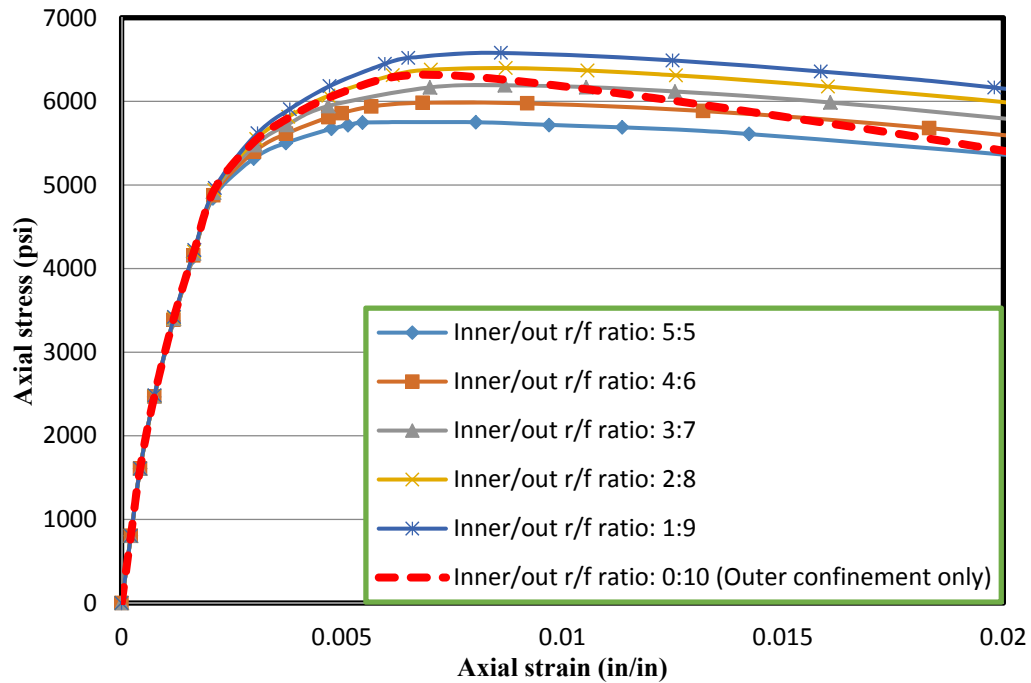
3.2.6.3 Inner layer of confinement to outer layer of confinement ratios

It was clear that two layers of confinement connected with cross ties was the most effective confinement configuration in hollow sections, especially for larger wall thickness based on the analysis conducted on confinement configurations as discussed previously. However, the difference between the inner and outer layers of confinement arriving to the yielding point might come from applying the same amount of the inner and outer confinement in the analysis. The best proportion between these two layers of confinement therefore needs to be investigated. Previous researchers used an equal amount of reinforcement for both layers and there was not any available information regarding this proportion. In order to further improve the material effectiveness, hollow sections with different proportions of outer to inner confinement amount were analyzed. The resulting inner to outer reinforcement cross-sectional areas are tabulated in Table 3-3. For each wall thickness-to-section diameter ratio, the same

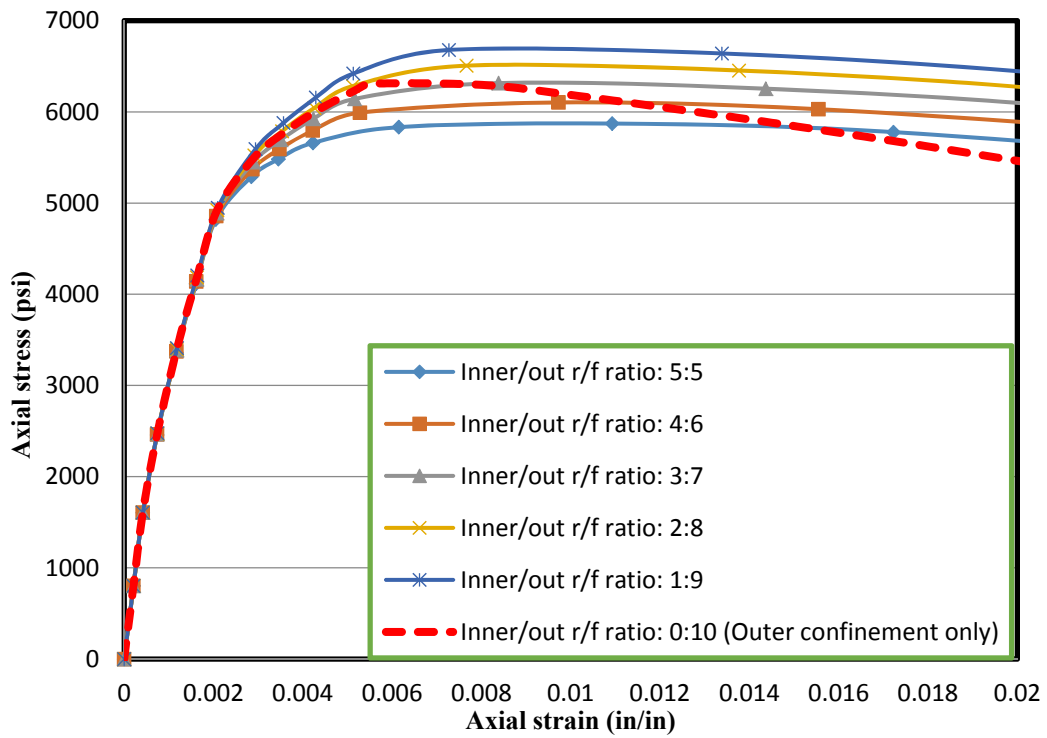
volumetric ratio of transverse reinforcement was used in this set of analyses. The axial stress vs. axial strain relationship comparisons for each wall thickness ratio is presented in Figure 3-27.



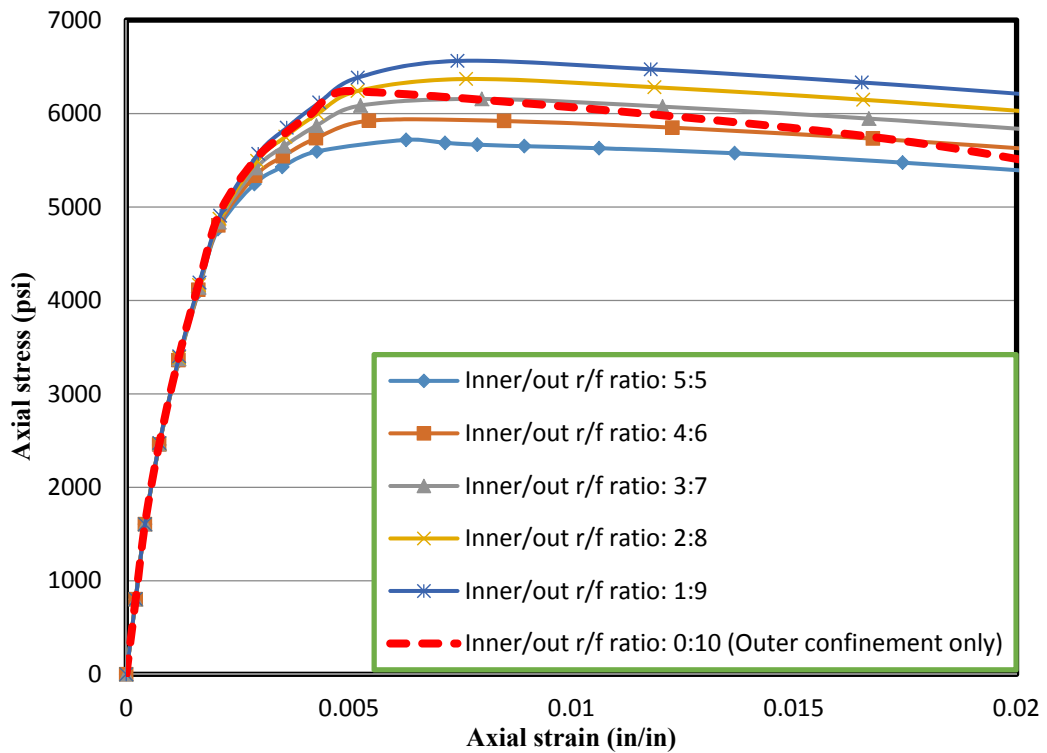
(a) $t/D = 0.1$



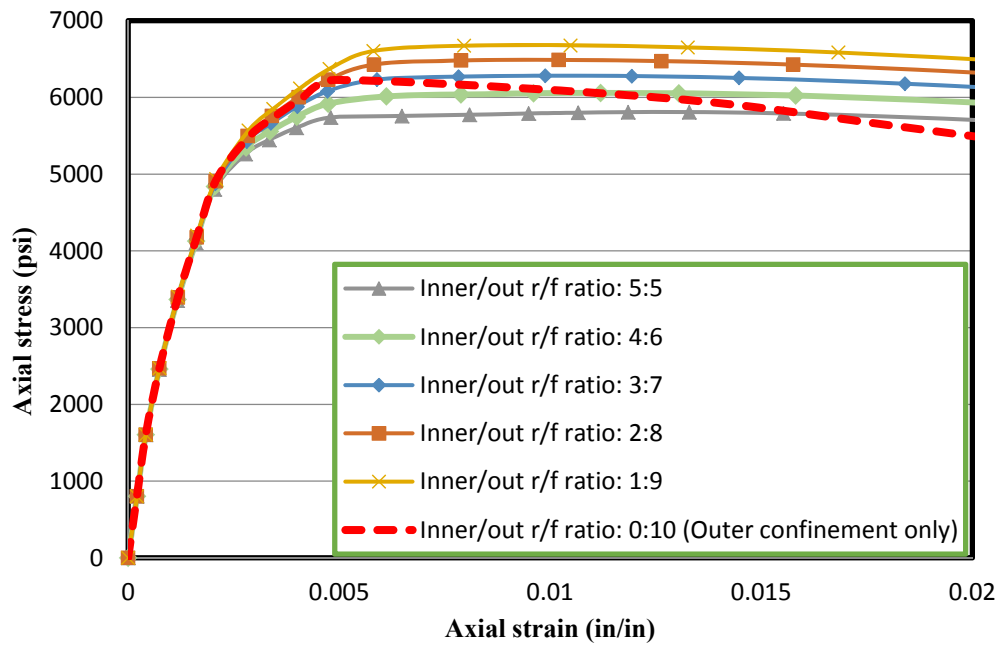
(b) $t/D = 0.125$



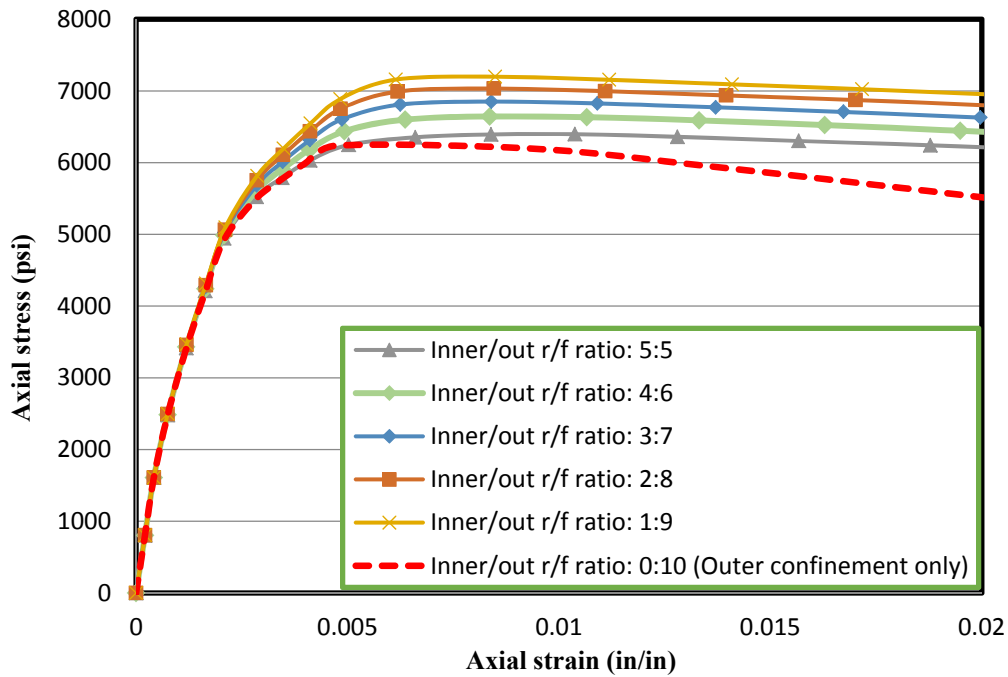
(c) $t/D = 0.15$



(d) $t/D = 0.167$



(e) $t/D = 0.175$



(f) $t/D = 0.2$

*r/f is the abbreviation of reinforcement

Figure 3-27: Axial stress vs. axial strain behavior comparisons for different wall thicknesses with different ratios of inner to outer confinement amount

As the wall thickness to outer diameter ratio t/D increased, the peak stress enhancement due to the two layers of confinement connected with cross ties became more significant when compared to the outer layer of confinement only. For a 0.1 wall thickness-to-diameter ratio, the hollow section with the outer layer of confinement only, performed very similarly to that with a 2:8 inner-to-outer confinement ratio connected with cross ties. Therefore, it would be not necessary to place two layers of confinement for thin wall hollow sections as found previously. On the other hand, the peak stress improved by the two layers of confinement connected with cross ties was much higher for the larger wall thickness. Therefore, a critical value associated with wall thickness-to-section diameter ratio exists and is identified below.

For all the wall thickness-to-diameter ratios analyzed in this study, the axial stress vs. axial strain behavior of concrete closely follows a similar initial ascending branch. The behavior started to deviate after the confinement effect was activated. For each wall thickness-to-section diameter ratio, the peak stress increased as the inner to outer layer confinement ratio changed from 5:5 to 1:9. This indicated that the peak stress of confined concrete was positively related to the outer layer of confinement amount under the same volumetric ratio of transverse reinforcement, if two layers of confinement connected with effective cross ties were utilized.

For a different inner to outer reinforcement ratio, the axial stress vs. axial strain behavior followed the same deterioration rate in the descending branch. This observation complies with the conclusions derived by previous researchers that the deterioration rate of the descending branch in the axially loaded behavior of confined concrete is proportional to the transverse reinforcement volumetric ratio. However, as the wall thickness increased, the axial stress corresponding to the descending branch deteriorated faster for hollow sections with an outer layer of confinement than those with two layers of confinement with cross ties.

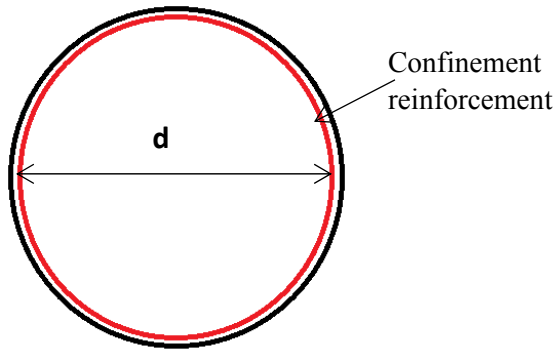
3.2.6.4 Summary

3.2.6.4.1 Concrete core confined states

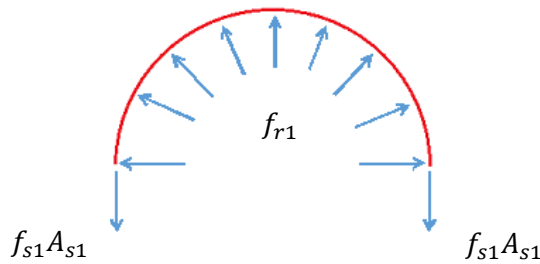
Based on the analyses conducted and discussions of results presented thus far, the concrete core confined states for hollow sections with each confinement configuration could be clearly illustrated by drawing the free body diagrams for both the confined concrete core and the

confinement, and developing equilibrium of the internal forces resulting from an axial load. The solid section is also included for better comparisons.

Solid section



(a) Solid section

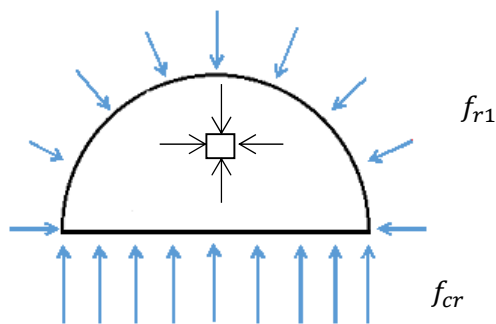


(b) Forces acting on one-half spiral or circular hoop

For outer reinforcement:

$$2f_{s1}A_{s1} = f_{r1} \times d \times s$$

$$f_{r1} = \frac{2f_{s1}A_{s1}}{d \times s}$$



(c) Forces acting on one-half confined concrete core

For confined concrete:

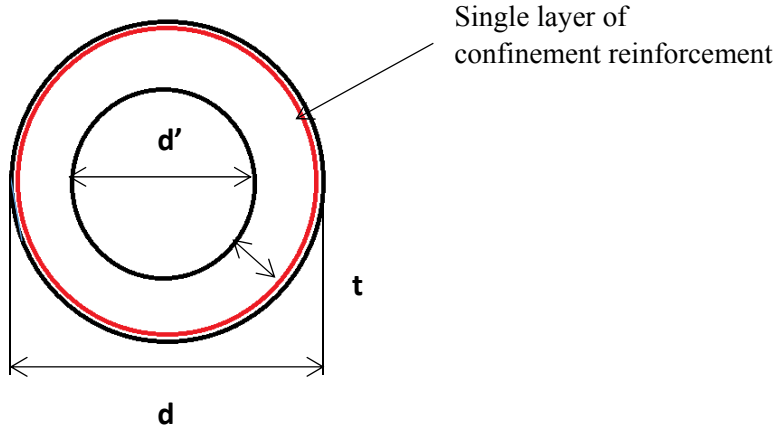
$$f_{r1} \times d \times s = f_{cr} \times d \times s$$

$$f_{cr} = f_{r1} = \frac{2f_{s1}A_{s1}}{d \times s}$$

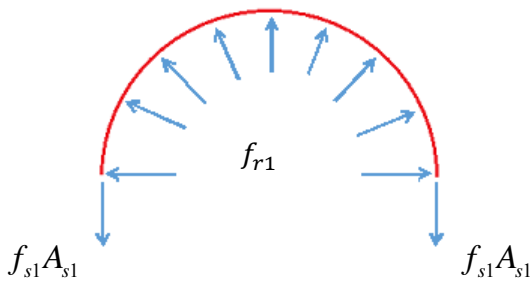
Figure 3-28: Confinement of concrete for solid section

According to Figure 3-28, the concrete element is in a triaxially confined state and the circumferential stress f_{cr} is equal to the radial stress f_{r1} .

Hollow section with a single layer of confinement



(a) Hollow section with outer layer of confinement only

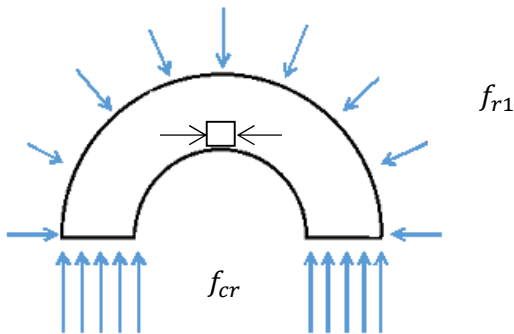


For outer reinforcement:

$$2f_{s1}A_{s1} = f_{r1} \times d \times s$$

$$f_{r1} = \frac{2f_{s1}A_{s1}}{d \times s}$$

(b) Forces acting on one-half spiral or circular hoop



For confined concrete:

$$f_{r1} \times d \times s = 2f_{cr} \times t \times s$$

$$2t = d - d'$$

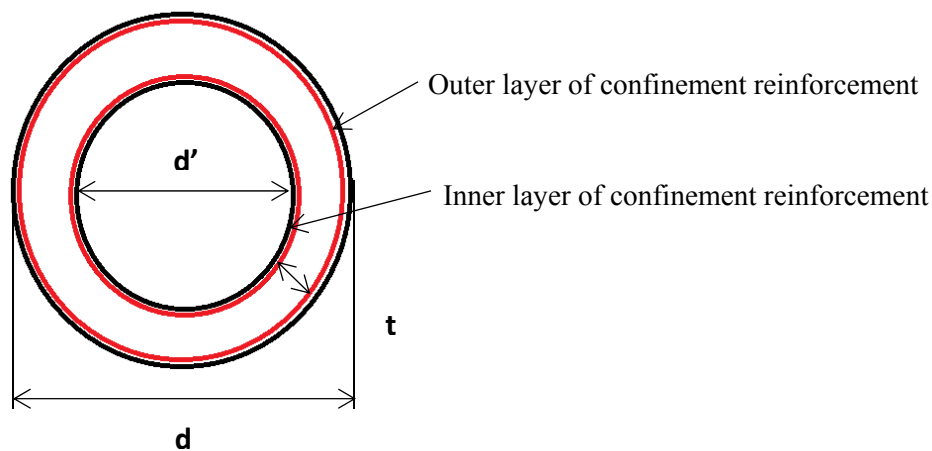
$$f_{cr} = \frac{f_{r1} \times d \times s}{2t \times s} = \frac{2f_{s1}A_{s1}}{2t \times s} = \frac{2f_{s1}A_{s1}}{(d - d') \times s}$$

(c) Forces acting on one-half confined concrete core

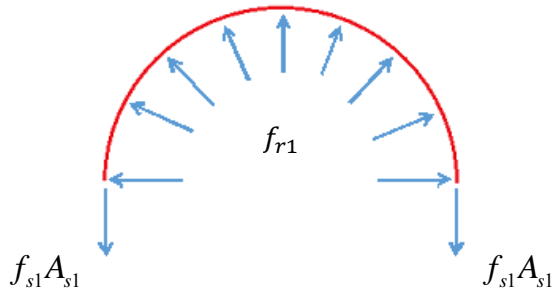
Figure 3-29: Confinement of concrete for hollow sections with a single layer of confinement

As shown in Figure 3-29, compared to the solid section, the circumferential stress experienced by the hollow section (f_{cr}) was greater when the transverse reinforcement was stressed to the same tensile stress. The thinner the wall, the more circumferential stress was generated. However, the radial stress was reduced since the inside concrete wall was relatively not confined, therefore, the concrete element located near the inside concrete wall is under biaxially confined state instead of triaxially confined state. According to the FEA results as well as the previous study conducted by Lignola et al. (2008), the transverse reinforcement for hollow sections was not fully activated as much as the solid sections. This indicated that under the same axial concrete strain, the outer layer of confinement applied smaller confining pressure to the hollow concrete core than the solid concrete core. Therefore, the inside concrete wall was essentially in a biaxially confined state and the outside concrete wall was in a triaxially confined state, with a smaller radial stress compared to the solid section. This leads to inside concrete face crushing controlling the behavior of such hollow sections.

Hollow section with two layers of confinement without cross ties



(a) Hollow sections that have two layers of confinement without cross ties

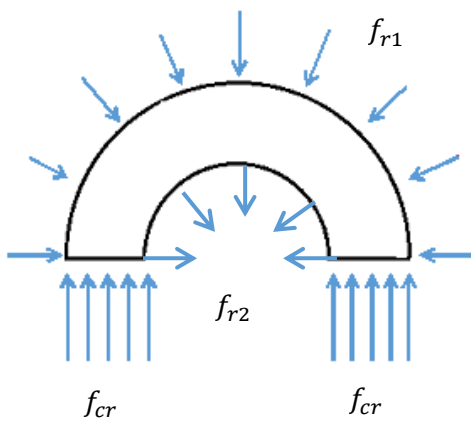


(b) Forces acting on one-half outer layer of confinement

For outer reinforcement:

$$2f_{s1}A_{s1} = f_{r1} \times d \times s$$

$$f_{r1} = \frac{2f_{s1}A_{s1}}{d \times s}$$



(c) Forces acting on one-half confined concrete core

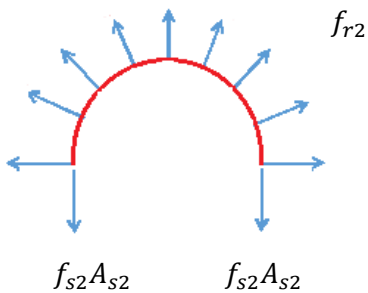
For confined concrete:

$$f_{r1} \times d \times s + f_{r2} \times d' \times s = 2f_{cr} \times t \times s$$

$$2t = d - d'$$

$$f_{cr} = \frac{f_{r1} \times d \times s + f_{r2} \times d' \times s}{2t \times s}$$

$$= \frac{2(f_{s1}A_{s1} + f_{s2}A_{s2})}{2t \times s}$$



(d) Forces acting on one-half inner layer of confinement

For inner reinforcement:

$$2f_{s2}A_{s2} = f_{r2} \times d' \times s$$

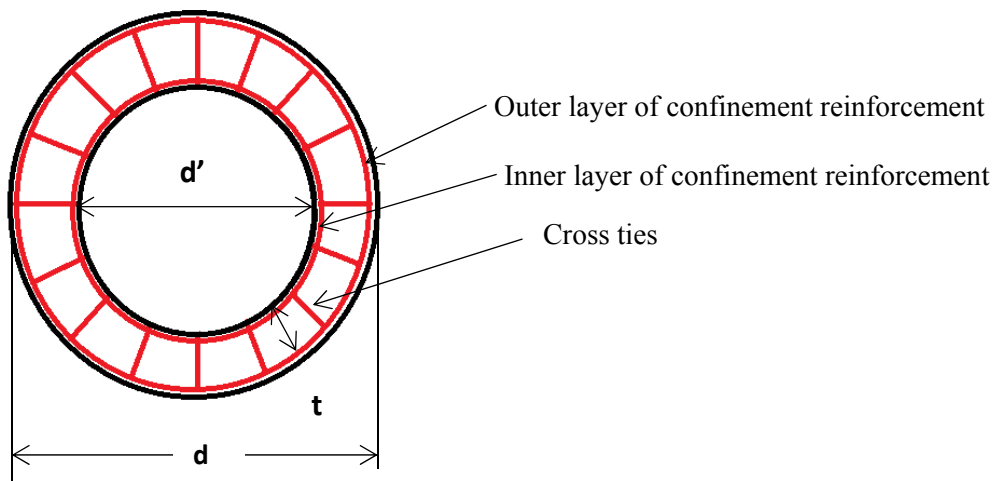
$$f_{r2} = \frac{2f_{s2}A_{s2}}{d' \times s}$$

Figure 3-30: Confinement of concrete for hollow sections having two layers of confinement without cross ties

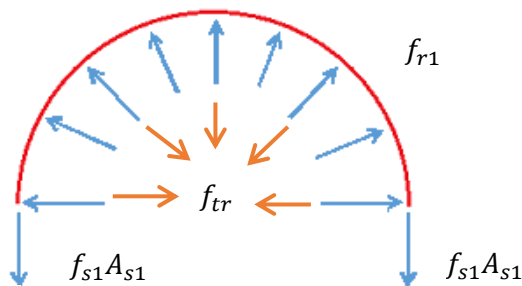
For the circular hollow sections, the inside concrete wall moved outward based on the finite element analysis. Therefore, the inner concrete face experienced a negative confining effect as

shown in Figure 3-30 (c). The inner layer of confinement tended to pull through the inner concrete cover, and the resulting confining pressure applied to the inside face of the concrete wall was negative. Based on this observation, sufficient cross links were required to ensure adequate radial confinement. The inner layer is likely to be detrimental rather than beneficial for hollow sections that had two layers of confinement without cross ties connecting these two layers of confinement.

Hollow section with two layers of confinement with cross ties



(a) Hollow section that have two layers of confinement connected with cross ties



For outer reinforcement:

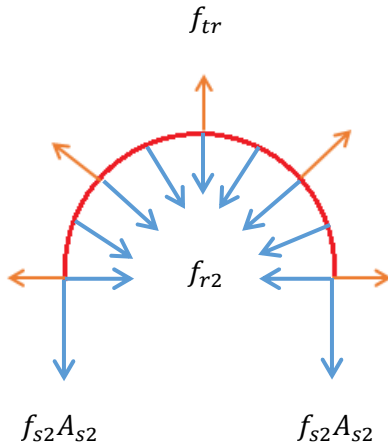
$$2f_{s1}A_{s1} + f_{tr} \times n \times A_{tr} = f_{r1} \times d \times s$$

$$f_{r1} = \frac{2f_{s1}A_{s1} + f_{tr} \times n \times A_{tr}}{d \times s}$$

(b) Forces acting on one-half outer layer of confinement

Based on the capacity of cross ties as well as the inner layer of confinement, three different sub-cases would be expected.

$$1. \quad 2f_{s2}A_{s2} < f_{tr} \cdot n \cdot A_{tr}$$

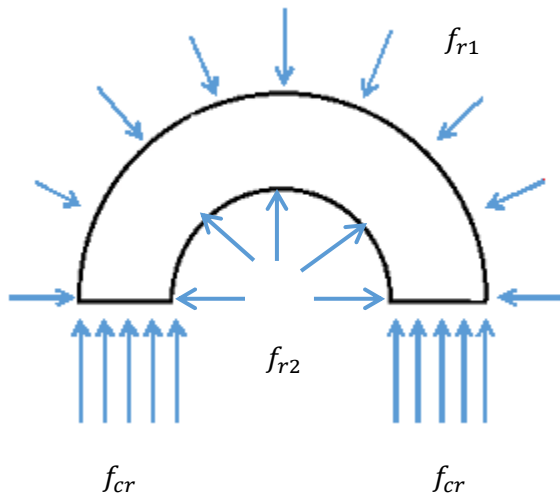


For inner reinforcement:

$$2f_{s2}A_{s2} + f_{r2} \times d' \times s = f_{tr} \times n \times A_{tr}$$

$$f_{r2} = \frac{f_{tr} \times n \times A_{tr} - 2f_{s2}A_{s2}}{d' \times s}$$

(c) Forces acting on one-half inner layer of confinement, if $2f_{s2}A_{s2} < f_{tr} \cdot n \cdot A_{tr}$



For confined concrete:

$$f_{r1} \times d \times s = f_{r2} \times d' \times s + 2f_{cr} \times t \times s$$

$$2t = d - d'$$

$$f_{cr} = \frac{f_{r1} \times d \times s - f_{r2} \times d' \times s}{2t \times s}$$

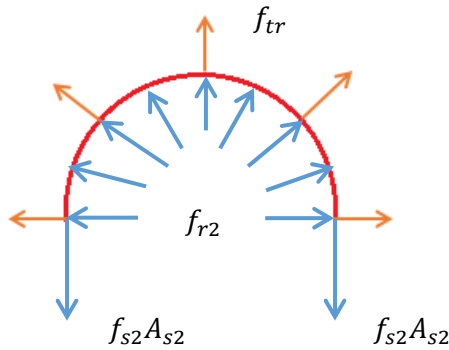
$$= \frac{2f_{s1}A_{s1} + 2f_{s2}A_{s2}}{2t \times s}$$

(d) Forces acting on one-half confined concrete core, if $2f_{s2}A_{s2} < f_{tr} \cdot n \cdot A_{tr}$

Figure 3-31: Confinement of concrete for hollow sections having two layers of confinement connected with cross ties, if the capacity of the cross ties is greater than that of the inner layer of confinement

According to Figure 3-31, both the inside and outside concrete faces experienced positive confining pressure. Compared to the solid section, both the radial stress and the circumferential stress were greater and the entire section was effectively confined.

$$2. \quad 2f_{s2}A_{s2} > f_{tr} \cdot n \cdot A_{tr}$$

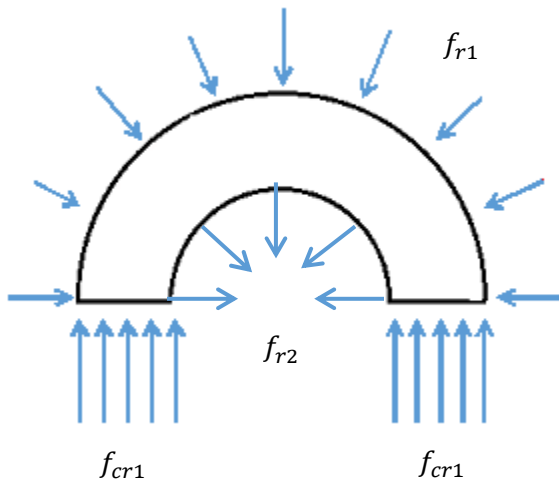


For inner reinforcement:

$$2f_{s2}A_{s2} = f_{r2} \times d' \times s + f_{tr} \times n \times A_{tr}$$

$$f_{r2} = \frac{2f_{s2}A_{s2} - f_{tr} \times n \times A_{tr}}{d' \times s}$$

(c) Forces acting on one-half inner layer of confinement, if $2f_{s2}A_{s2} > f_{tr} \cdot n \cdot A_{tr}$



For confined concrete:

$$f_{r1} \times d \times s + f_{r2} \times d' \times s = 2f_{cr1} \times t \times s$$

$$2t = d - d'$$

$$f_{cr1} = \frac{f_{r1} \times d \times s + f_{r2} \times d' \times s}{2t \times s}$$

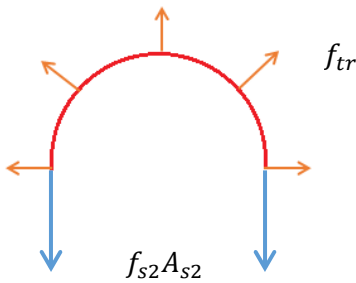
$$= \frac{2f_{s1}A_{s1} + 2f_{s2}A_{s2}}{2t \times s}$$

(d) Forces acting on one-half confined concrete core, if $2f_{s2}A_{s2} > f_{tr} \cdot n \cdot A_{tr}$

Figure 3-32: Confinement of concrete for hollow sections having two layers of confinement connected with cross ties, if the capacity of the cross ties is lower than that of the inner layer of confinement

Based on Figure 3-32, this confined state is similar to the two layers of confinement without cross ties.

$$3. \quad 2f_{s2}A_{s2} = f_{tr} \cdot n \cdot A_{tr}$$

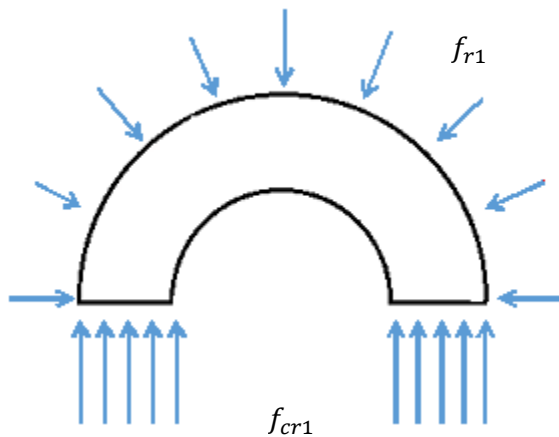


For inner reinforcement:

$$2f_{s2}A_{s2} = f_{tr} \times n \times A_{tr}$$

$$f_{r2} = 0$$

(c) Forces acting on one-half inner layer of confinement, if $2f_{s2}A_{s2} = f_{tr} \cdot n \cdot A_{tr}$



For confined concrete:

$$f_{r1} \times d \times s = 2f_{cr1} \times t \times s$$

$$2t = d - d'$$

$$\begin{aligned} f_{cr1} &= \frac{f_{r1} \times d \times s}{2t \times s} \\ &= \frac{2f_{s1}A_{s1} + 2f_{s2}A_{s2}}{2t \times s} \end{aligned}$$

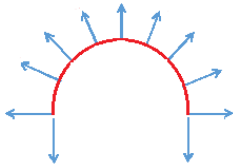
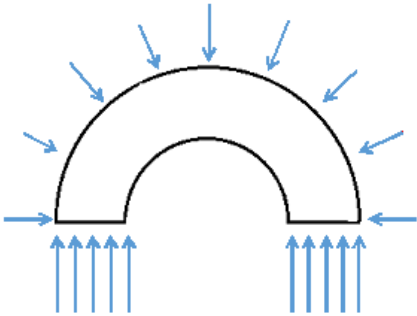
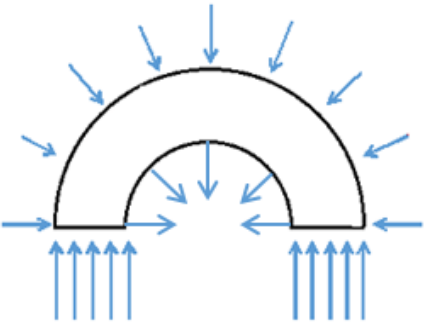
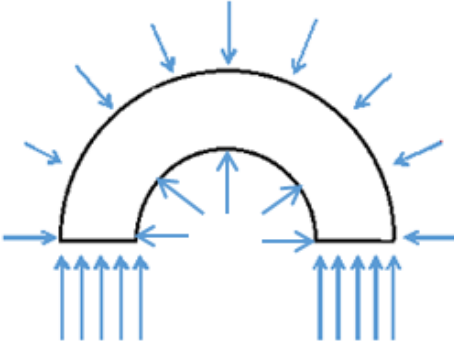
(d) Forces acting on one-half confined concrete core, if $2f_{s2}A_{s2} = f_{tr} \cdot n \cdot A_{tr}$

Figure 3-33: Confinement of concrete for hollow sections having two layers of confinement connected with cross ties, if the capacity of the cross ties is equal to that of the inner layer of confinement

Based on Figure 3-33, this confined state is similar to that with outer layer of confinement only.

Most researchers agreed that the confined concrete strength was proportional to the effective confining pressure that was applied to the concrete core. This meant that the greater the effective confining pressure experienced by the concrete core, the more the concrete was confined. Therefore, the better the confined concrete would behave. Table 3-6 summarizes the confined concrete states for each confinement configuration as discussed above.

Table 3-6: Confined concrete states for each confinement configuration

Outer layer of confinement only	Two layers of confinement	Two layers of confinement with cross ties
<p><u><i>Triaxially confined state</i></u> <u><i>(outer concrete section)</i></u> <u><i>Biaxially confined state</i></u> <u><i>(Near the inside face)</i></u></p>	<p><u><i>Triaxially confined state</i></u> <u><i>Inside layer of confinement was detrimental</i></u></p>	<p><u><i>Triaxially confined state</i></u></p>
		
		
<p>Inside face concrete crushing controlled the behavior of such hollow columns.</p>	<p>Inner layer of confinement provided negative confining pressure if it was not connected to outer layer of confinement effectively.</p>	<p>Both inner and outer layer of confinement provided positive confining pressure if they were connected effectively.</p>

Based on the confinement analyses discussed previously, the peak stress of the confined concrete behavior was positively proportional to the outer layer confinement amount, under the same volumetric ratio of transverse reinforcement, while the slope of the descending branch was associated with transverse reinforcement volumetric ratio.

For hollow sections with two layers of confinement connected with effective cross ties, the entire section moved outward as a unit. The smaller the amount of inner confinement that was placed near the inside concrete face, the more demand was exerted to the outer layer of confinement. Therefore, the outer layer of confinement would reach the yield strain at an early stage, which would lead to more confining pressure that was applied to the concrete core and the concrete behavior would be improved.

For hollow sections with a wall thickness-to-section diameter ratio that is equal to or less than 0.125, placing one layer of confinement reinforcement near the outside concrete wall surface is sufficient to provide satisfactory confined concrete behavior. Placing two layers of confinement reinforcement does not improve the confined concrete behavior significantly, but may cause reinforcement congestion and also impose challenges to cast concrete in such a smaller wall thickness. However, this is not the case for thicker walls. For hollow sections that have a wall thickness-to-section diameter ratio that is in the range of 0.125 to 0.2, two layers of confinement reinforcement connected with cross ties are the most effective, but the required quantity near the inside concrete wall surface should be much smaller than that required near the outside concrete wall surface. This is because the tension demand developed in the inner transverse reinforcement is effectively transferred to the outer layer of transverse reinforcement with the help of cross ties. For a given volumetric ratio of transverse reinforcement, the confinement for different wall thicknesses was recommended as shown in Table 3-7.

Table 3-7: Recommendations of confinement for different wall thickness hollow sections

Section type	Wall thickness-to-section diameter ratio (β)	One layer of lateral reinforcement	Two layers of lateral reinforcement with cross ties
Hollow	0.1	✓	
Hollow	0.125	✓	
Hollow	0.15		✓ The best ratio 1:9
Hollow	0.1667		✓ The best ratio 1:9
Hollow	0.175		✓ The best ratio 1:9
Hollow	0.2		✓ The best ratio 1:9
Solid		✓	

3.2.6.4.2 Applicability of Mander’s model for hollow columns confined with a single layer of confinement reinforcement

Based on the discussion presented in Section 3.2.6.4.1, in the hollow concrete columns confined with a single layer of confinement reinforcement, the inside concrete wall is relatively not confined, while the concrete near the outside face experiences reduced confining pressure from the outer layer of reinforcement compared to that in solid columns. Therefore, the confinement effectiveness in hollow concrete columns confined with a single layer of confinement reinforcement should not be assumed to be the same as that has been established for solid columns.

In order to better understand the behavior of hollow columns confined with a single layer of confinement reinforcement placed near the outside concrete wall (same as test specimens), and also examine the areas where improvements are needed to make Mander’s model applicable for hollow sections, a series of analyses were performed on hollow circular/square columns with different wall thickness. The analysis matrix is presented in Table 3-8. The wall of hollow columns was divided into eight layers for the FE analyses. The same amount of lateral

reinforcement and longitudinal reinforcement was placed for hollow sections with different wall thickness, which allowed for the same volumetric ratio of lateral reinforcement as well as same longitudinal reinforcement ratio based on the gross section.

Table 3-8: Analyses matrix for hollow columns confined with a single layer of confinement reinforcement

Section	Outer (inch)	Inner (inch)	t/D	t (inch)	f'_{c0} (psi)	Lateral reinforcement (inch ²)	Longitudinal reinforcement (inch ²)
Hollow (Circular/Square)	12	10	0.083	1	4500	0.034	0.05
		9.6	0.100	1.2			
		9	0.125	1.5			
		8.4	0.150	1.8			
		8	0.167	2			
		7.8	0.175	2.1			
		7.2	0.200	2.4			

The maximum confining pressure experienced by each individual layer of circular hollow columns ($f_{r,max}$) was obtained from the FE analyses and was listed in Table 3-9 for each wall thickness as well as the solid section. As wall thickness increased, the maximum confining pressure experienced by each individual layer of hollow circular columns ($f_{r,max}$) also increased. According to Table 3-9, the maximum confining pressure experienced by each individual layer of circular hollow sections ($f_{r,max}$) is smaller than the maximum effective confining pressure experienced by the solid section (381.75 psi), which indicates that one layer of confinement reinforcement was not as effective in confining the concrete for circular hollow sections as for solid sections. This observation is more significant for square hollow sections (Table 3-10), which indicates that the confinement effectiveness for square hollow sections is further reduced compared to the circular hollow sections. Therefore, a multiplier to the maximum effective lateral pressure for solid sections was expected to be introduced to account for the reduction of confinement effectiveness for hollow columns. Table 3-9 shows the confinement effectiveness coefficient (i.e., the ratio between the confined concrete strength to the unconfined concrete strength) of circular hollow columns for both the FE analyses and the Mander's prediction using

the maximum confining pressure experienced by each individual layer of hollow columns ($f_{r,max}$). It was found that using $f_{r,max}$ in the Mander's equation instead of f'_l could obtain satisfactory peak stress compared to the FE analyses (Figure 3-34). The same observations were also obtained for square hollow columns (Figure 3-35). Therefore, the multiplier could be expressed as the ratio between $f_{r,max}$ and $f_{r,solid}$, and it was reasonable to conclude that the confined concrete strength of hollow columns with one layer of confinement reinforcement could be obtained by applying the multiplier ($f_{r,max} / f_{r,solid}$) to the maximum effective confining pressure calculated from the solid section to the Mander's model. By plotting the multiplier ($f_{r,max} / f_{r,solid}$) against the t/D ratio for circular hollow columns, it was clear that a positive linear relationship could represent this relationship pretty well. Therefore, it was conservative to assume the multiplier as the summation of t/D and 0.45 (Figure 3-36). However, the relationship between the $f_{r,max} / f_{r,solid}$ ratio and the t/D ratio for square hollow sections was not as clear as circular ones (Figure 3-37). It seemed that the wall thickness had little effect on the maximum confining pressure and a constant multiplier of 0.28 was seemed to be a good fit except for very thin wall thickness (t/D = 0.1). The confinement effect for hollow square sections with one layer of confinement reinforcement placed near the outside concrete wall was not as well understood as circular ones, and therefore needs further study.

Table 3-9: The confinement effectiveness coefficient of circular hollow columns for both the FE analyses and the Mander's model

t (inch)	$f_{r,max}$	$f_{r,max} / f'_{c0}$	ABAQUS		Mander's model	
			f'_{cc}	f'_{cc} / f'_{c0}	f'_{cc}	f'_{cc} / f'_{c0}
1	210.2944	0.0467	5784.4925	1.2854	5813.049	1.2918
1.2	219.1223	0.0487	5856.1525	1.3014	5862.667	1.3028
1.5	227.7689	0.0506	5870.9513	1.3047	5910.901	1.3135
1.8	235.4674	0.0523	5876.2850	1.3058	5953.547	1.3230
2.0	231.8215	0.0515	5852.9150	1.3006	5933.385	1.3185
2.1	254.3438	0.0565	5856.0613	1.3013	6056.944	1.3460
2.4	258.5845	0.0575	5852.0413	1.3005	6079.949	1.3511
Solid	381.7517	0.0848	6357.5247	1.4128	6715.182	1.4923

Table 3-10: The confinement effectiveness coefficient of square hollow columns for both the FE analyses and the Mander's model

t (inch)	$f_{r,max}$	$f_{r,max}/f'_{c0}$	ABAQUS		Mander's model	
			f'_{cc}	f'_{cc}/f'_{c0}	f'_{cc}	f'_{cc}/f'_{c0}
1.2	191.551	0.0426	5267.738	1.1706	5706.421	1.2681
1.5	84.841	0.0189	5185.975	1.1524	5063.043	1.1251
1.8	77.766	0.0173	5119.638	1.1377	5017.984	1.1151
2.0	45.140	0.0100	5022.368	1.1161	4805.910	1.0680
2.1	59.489	0.0132	5037.595	1.1195	4900.074	1.0889
2.4	92.334	0.0205	5011.850	1.1137	5110.413	1.1356
Solid	270.774	0.0602	5533.003	1.2296	6145.629	1.3657

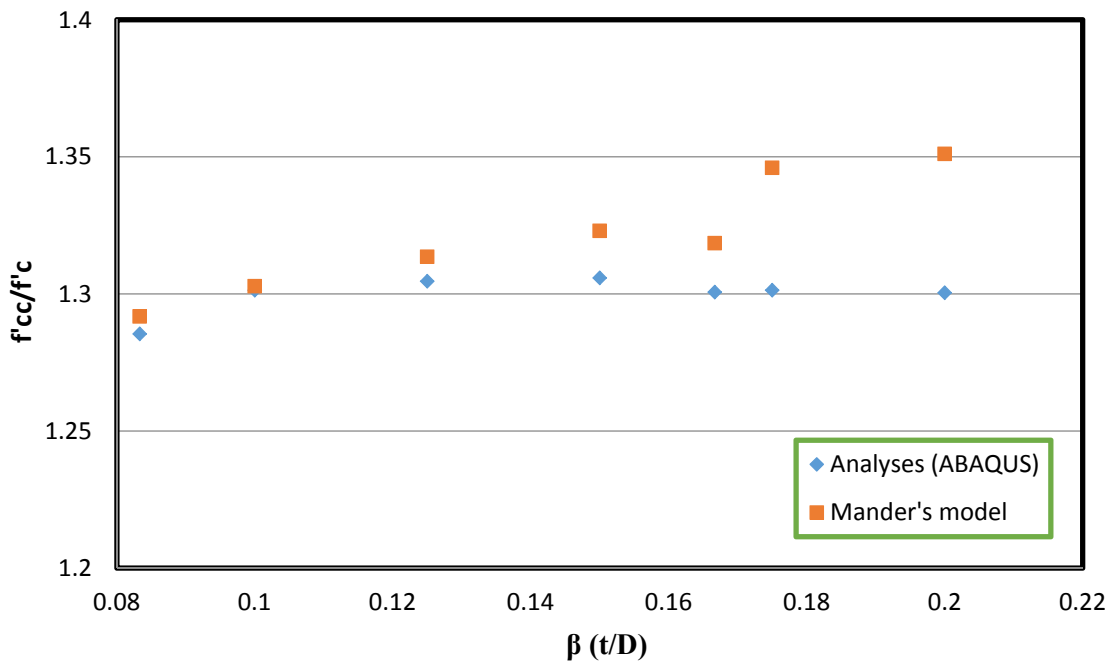


Figure 3-34: The confinement effectiveness coefficient vs. β relationship comparisons of circular hollow columns between the FE analyses and the Mander's predictions

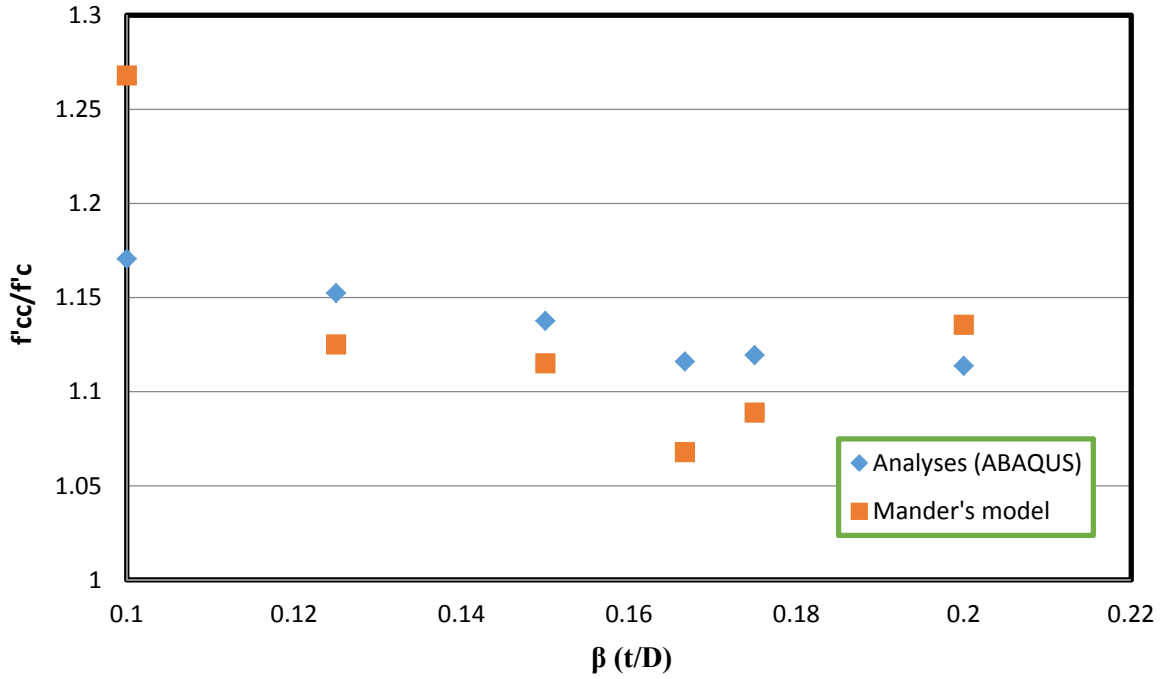


Figure 3-35: The confinement effectiveness coefficient vs. β relationship comparisons of square hollow columns between the FE analyses and the Mander's predictions

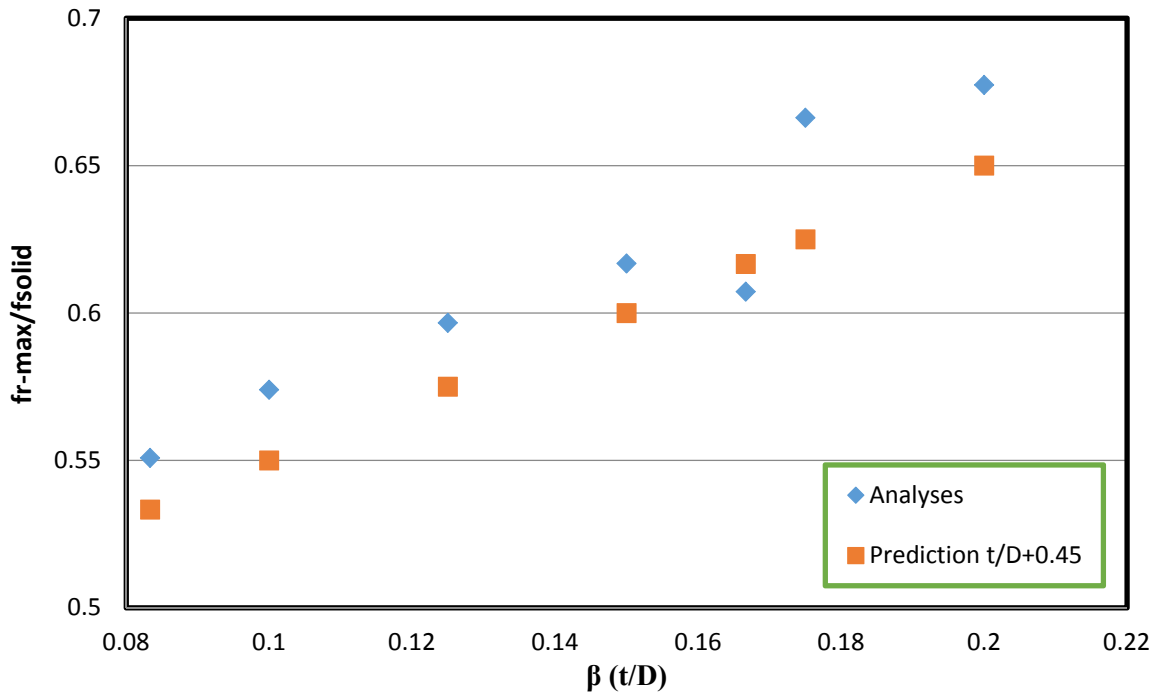


Figure 3-36: The relationship between the multiplier and t/D ratio for circular hollow columns

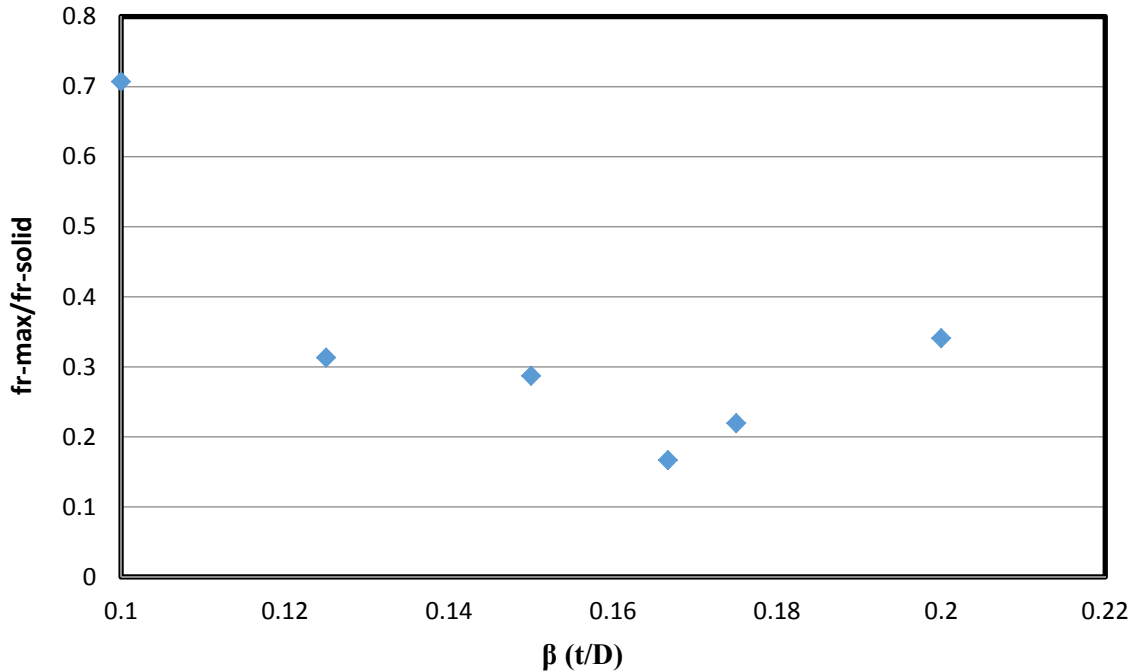


Figure 3-37: The relationship between the multiplier and t/D ratio for square hollow columns

3.3 Flexure behavior

3.3.1 Fiber-based beam elements analysis

The 3D finite element analysis is very capable of providing detailed results, which incorporates 3D effects as well as interaction between various materials. This type of analysis is ideal for determining the detailed behavior of various components. However, it is time-consuming and resource intensive. For the design work performed by engineers, an analysis method is necessary, which is less time-consuming but can still provide an accurate model of the behavior of structural systems. For this reason a fiber-based analysis has been performed in addition to the 3D finite element analysis. The Open System for Earthquake Engineering Simulation (OpenSees) was used for this type of analysis. OpenSees is a software framework developed by Pacific Earthquake Engineering Research Center (PEER), which is capable of modeling and analysis through the use of beam-column and other elements as well as uniaxial materials and section models. These modeling capabilities are combined with a wide range of algorithms and solution methods, which are capable of nonlinear analysis.

OpenSees is capable of performing both a fiber-based moment-curvature analysis as well as two and three-dimensional analysis using beam elements. For this research a two dimensional beam element analysis was chosen since this analysis is still based on a defined fiber section and since it directly calculates the force-displacement response. This was more useful for modeling the results of the past research as well as the current experimental testing. Since the analysis is still based on a defined fiber-section, it will be comparable to the section analysis methods employed by practicing engineers.

The analysis was performed by creating the model geometry and defining a section or set of sections. The sections are made up of patched areas of uniaxial materials. Various material models are available within OpenSees, which represent different stress-strain models for materials such as concrete and steel. A section is patched with these uniaxial materials and the sections are then applied to the elements. The program then uses the section definition to apply stiffness and to determine the force-displacement response. It is able to analyze non-linear behavior by performing an iterative process between element deformation and the stress and strain behavior of the various section materials.

Since the program uses a 2D section to define the elements, this means it is able to model concrete and longitudinal steel, but is unable to model transverse reinforcement. Instead, the confined concrete material properties have to be applied directly. To achieve accurate results, the confined concrete model must be as realistic as possible. The stress state in the hollow section has been taken into account along with the findings of previous researchers in order to model the confinement effect of the concrete in hollow sections accurately.

To verify that the model was accurate, it was compared to previous experiments as well as the results of the current experiments discussed in Chapters 4 and 5. Due to the different experimentation types performed in previous literature and in this research, it was necessary to do both pushover analysis and beam loading analysis. The beam loading analysis was performed in order to model the experimentation presented in this research. Additionally, several different section types were modeled in order to better verify the model, including circular and square columns with two layers of transverse reinforcement.

3.3.1.1 Section modeling and material properties

To produce accurate results, the inputs must be as accurate as possible. The section geometry and material stress-strain behaviors are key inputs that govern the analysis results. Section geometry can typically be defined fairly accurately due to the figures and information presented by past researchers and also using the design information for the experiments presented in this research. Providing accurate material stress-strain behavior is somewhat more challenging, especially due to the limited information presented in past research. Reinforcing steel especially plays an important role in these types of tests because it directly controls the section capacity, and also the ductility if tension steel failure occurs first. In order to ensure the experiments conducted in this report could be modeled accurately, tension tests were performed on the reinforcing steel to obtain the actual stress-strain behavior.

As mentioned previously, the program is unable to model transverse reinforcement, and the confined concrete properties must be input directly. Mander's model was used to define the confined concrete properties, with some adjustments made depending on the section geometry and configuration. These adjustments were based on the literature review and the findings of the finite element analysis. Mander's model was then applied to the Concrete07 model (Chang & Mander, 1994) built into OpenSees by Waugh (2007). The Concrete07 model was used for all of the concrete, and the Steel02 (Filippou et al. 1983) model was used for all longitudinal reinforcing steel unless otherwise stated.

The section modeling method for hollow columns is discussed in this section. The modeling methods are discussed for hollow columns with both one and two layers of transverse reinforcement. Despite not being the focus of the research, the hollow columns with two layers of transverse reinforcement are discussed for comparison to the hollow columns with one layer of transverse reinforcement, and also due to the low amount of previous tests of hollow columns with one layer of transverse reinforcement. The modeling methods described in this section will be used in later sections to analyze and compare the response of previous experimental tests in order to verify the modeling and analysis methods. Four general modeling arrangements were assumed based on the different confinement configurations and are discussed below.

3.3.1.1.1 One layer of transverse reinforcement

As discussed in the literature review, Mander's model calculates the confined stress-strain behavior based on the confinement stresses (confining pressure) in the transverse directions for sections under pure axial load. For a solid circular column, the radial and circumferential stresses are approximately equal throughout the section. The same is true for the lateral stresses of a solid square column, which has the same amount of transverse reinforcement in each direction. When the circular or square column has a void in the center these stresses are no longer equal.

3.3.1.1.1.1 Hollow circular columns

In Section 3.2.6.4.1, the calculation of the radial and circumferential confining stresses for circular columns was discussed. As shown, the radial stress at the transverse reinforcement does not depend on the void dimension, but the circumferential stress does depend on this void dimension. The radial stress will be the same between a solid and hollow circular section at the transverse steel yield point, since the transverse reinforcement will generate the same radial stress at yield. However, in the case of a hollow section, the radial stress along the wall thickness follows a parabola distribution (as shown in Figure 3-13 for a two-thin-wall hollow section), which will decrease to approximately zero at the inside face since it is a free surface. This behavior has been demonstrated in the finite element analysis, and can be approximated as a linear decrease from the transverse reinforcement to the void. The circumferential stress is caused by the radial stress acting on the concrete. The section can be cut along the centerline and thought of as an arch with a distributed load at the top coming from the transverse reinforcement confining pressure. This load is then distributed to the base of the arch. In the case of a solid column it is distributed along the entire base, but with a hollow section, the load is distributed along the wall thickness, creating larger stresses. This concept is illustrated in Figure 3-38. The approximate stress distributions are illustrated in Figure 3-39.

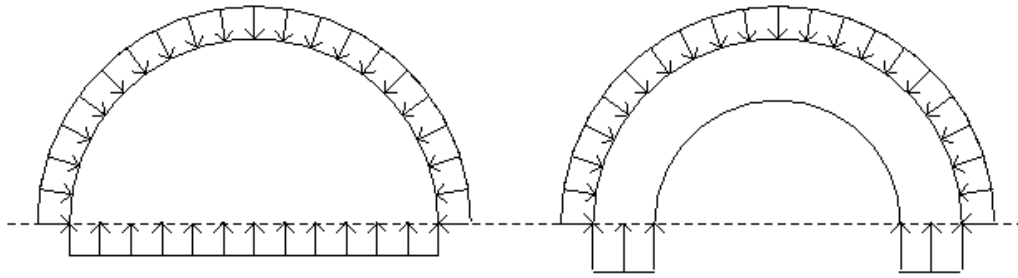


Figure 3-38: Circumferential stress distribution of solid and hollow circular columns

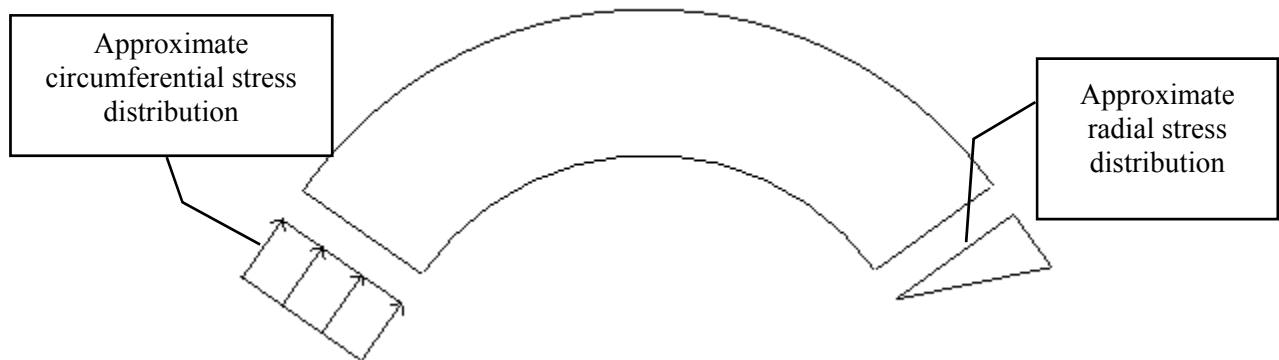


Figure 3-39: Approximated stress distributions in hollow circular sections with one layer of transverse reinforcement

Due to the fact that the radial stress decreases to approximately zero at the void, previous researchers assumed the concrete was only biaxially confined, therefore neglecting the radial stress and only taking into account the axial and circumferential stress. However, this is a very conservative assumption. Essentially, the radial stress will be similar to a solid section near the transverse reinforcement when the reinforcement yields, but decreasing to zero near the void. Additionally, the circumferential stress will be significantly higher for a hollow section, equating to an increase in circumferential stress of $\frac{d_s}{2t_s}$. The equations shown below illustrate this, based on the relationship for circumferential stress discussed in Section 3.2.6.4.1.

$$f_{cr} = \frac{2f_s A_s}{(d - d')s} \quad \text{(Equation 3-2)}$$

For a solid section, $d' = 0$:

$$f_{cr,solid} = \frac{2f_s A_s}{ds} \quad \text{(Equation 3-3)}$$

The circumferential stress of a hollow section relative to a solid section can then be found as:

$$\frac{f_{cr,hollow}}{f_{cr,solid}} = \frac{2f_s A_s}{(d-d')s} \times \frac{ds}{2f_s A_s} = \frac{d}{(d-d')} \quad \text{(Equation 3-4)}$$

This can be related to the wall thickness within the confinement instead of the difference in diameter:

$$2t = d - d' \quad \text{(Equation 3-5)}$$

Substituting this into the circumferential stress ratio between solid and hollow specimens gives:

$$\frac{f_{cr,hollow}}{f_{cr,solid}} = \frac{d}{2t} \quad \text{(Equation 3-6)}$$

This ratio indicates that a hollow column under axial compression will experience larger circumferential stress than that of a similar solid column. For example, a specimen with a diameter of confinement from center to center of 12 inches, and a wall thickness within the confinement of 2 inches, would experience $\frac{12}{2(2)}$ or 3 times the circumferential stress as a solid section with the same transverse reinforcement. The increase in stress indicates the concrete has high stress in the circumferential direction, but slightly lower stress in the radial direction. Near the inside face, the concrete is biaxially confined due to the high circumferential stress but lack of radial stress.

The conditions described hold true under pure axial compression. However, when subjected to flexure it becomes less clear how the stresses form. Only a portion of the transverse reinforcement will be restraining radial displacement, so only the compressed portion of the concrete will experience radial stress. This also means that the circumferential stress is likely not as high as under pure axial compression, since there is less overall radial stress when the specimen is under flexure. Therefore, it may not be accurate to account for large circumferential stresses in the concrete, since doing so may cause an overestimation of the confinement stresses.

An additional factor affecting the confinement of hollow columns is the increased deformability of the section. As discussed by Lignola et al. (2008) in the literature review, a hollow column requires less radial pressure to restrain displacement compared to a solid column. If solid and hollow columns with identical reinforcement are subjected to the same axial strain, the solid column will experience larger radial displacement, equating to larger hoop strain and larger radial stress. This idea is supported by the finite element analysis, which showed that the radial displacement for sections with identical reinforcement was higher for specimens with larger wall thickness at the same axial strains. This concept indicates that transverse reinforcement would not yield until higher axial strains when compared to a solid section with the same transverse reinforcement. The experimental testing performed by Hoshikuma and Priestley (2000) supports this claim, since their hollow test specimens showed that the transverse reinforcement had only reached 30 percent of the yield strain when the specimens failed due to the inside face crushing.

These observations have shown that for hollow columns, the concrete is well confined near the transverse reinforcement but not well confined near the inside face. Additionally, the axial strain at which yield of transverse reinforcement occurs is higher than that of a solid column. Essentially for the compression concrete, there are two controlling limits: failure of the confined concrete due to hoop fracture and failure of the concrete near the void. The location of the neutral axis, the transverse reinforcement quantity, and the concrete strength will control which occurs first. Since the radial stress changes over the wall thickness, it may be more accurate to divide the wall thickness into sections with different confined concrete properties to model the behavior. Ideally, a large number of sections would be used; however, the small increase in accuracy would not justify the significant increase in modeling and solution time, and it would not be feasible for design purposes. For this reason two sections have been used to approximate the radial stress distribution, which correspond to the controlling limits of the transverse reinforcement rupture and the inside face failure.

Figure 3-40 illustrates the two regions chosen. The thickness of each section corresponds to half the distance between the inside face and the center of the confinement reinforcement. The section near the inside face is conservatively modeled as unconfined concrete, neglecting the confinement contribution due to the circumferential stress as well as the small amount of radial stress near the inside face. The crushing of the inside wall has been shown to be brittle, so

providing a conservative estimate has been deemed by this research to be appropriate, especially since it is unclear if high circumferential stresses actually develop under flexure. For the concrete near the transverse reinforcement, the confined concrete properties have been estimated using Mander's model with an adjustment factor to account for the reduced radial stress due to the lower radial displacement of hollow columns. Instead of explicitly calculating the stresses in both directions (circumferential and transverse), it has been assumed that the circumferential stress is equivalent to the adjusted radial stress. This assumption has been made since it is unclear how much circumferential stress develops under flexure.

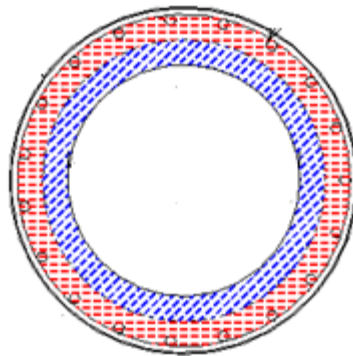


Figure 3-40: Regions for unconfined and confined concrete for circular hollow columns with one layer of transverse reinforcement

Based on the FEA, a simplified adjustment to Mander's model has been found for the outer layer modeled as confined concrete as described in Section 3.2.6.4.2. The analysis showed that Mander's model more closely matched the stress-strain from the finite element analysis when a reduction in radial stress was used. This reduction in radial stress has been taken into account by a hollow column confinement effectiveness factor, similar to the confinement effectiveness factor k_e used by Mander's model. The hollow column confinement effectiveness factor proposed, k_h , can be found for circular columns by the relationship below.

$$k_h = \frac{t}{D} + 0.45 \quad \text{(Equation 3-7)}$$

The calculation of the confined concrete properties in the layer of concrete near the transverse reinforcement is performed using Mander's model as if the column were solid. The factor adjusts

the calculated radial stress for a solid column with the same outside dimensions and reinforcement details to estimate what the radial stress would be for the hollow column. The only difference in the standard Mander's model procedure occurs when calculating the effective radial stress f_l' . The calculation of f_l' for hollow columns would be done as shown in the equation below:

$$f_l' = k_e k_h f_l \quad \text{(Equation 3-8)}$$

The confined concrete properties are then calculated in the usual manner using this adjusted effective radial stress. An example of this procedure is provided in Section 6.3.

3.3.1.1.1.2 *Hollow Rectangular Columns*

Similar to circular hollow columns, the lateral stress will be largest at the location of the transverse reinforcement and will decrease to zero at the inside face in a hollow rectangular column. The stress within the wall parallel to the transverse reinforcement will theoretically be higher for hollow rectangular sections than solid rectangular sections, due to the presence of the void. However, these relationships were described for pure axial compression, and it is unclear how well they describe the behavior when the columns are subjected to flexure. Additionally, it is not clear how much demand is actually applied to the transverse reinforcement due to the presence of the inner void. Other factors such as stress concentrations at corners or non-uniformity of stresses within the wall are not taken into account in the simple theory.

Due to the unknowns described for hollow rectangular columns with one layer of transverse reinforcement, additional finite element analysis was performed. It was found that the lateral stress near the transverse reinforcement for hollow square columns with one layer of transverse reinforcement was significantly reduced when compared to solid square columns with the same reinforcement details and overall dimensions. It was also found that the dimension of the void had little effect on this lateral stress. Based on this, a constant hollow column confinement effectiveness factor, k_h , of 0.28 was proposed for hollow square columns with one layer of transverse reinforcement. This adjustment factor would then be applied, as described for hollow circular sections, as an adjustment to the calculation of the effective lateral stress in a solid rectangular column for use in Mander's model. Mander's model would be used as if the column were solid, with the adjustment factor, k_h , of 0.28 applied when calculating the effective lateral

stress. This hollow column effectiveness factor is applied in addition to the confinement effectiveness factor, k_e , proposed by Mander et al. The value of k_e for rectangular sections is typically used as 0.75 as suggested by Priestley et al. (1996).

The section modeling method proposed for rectangular columns with one layer of transverse reinforcement is similar to that of circular columns with one layer of transverse reinforcement. Since the lateral stress decreases to zero at the void, the changing stress state is approximated by two different regions of concrete, as shown in Figure 3-41. The hashed area near the void is modeled as unconfined concrete, while the hashed area near the transverse reinforcement is modeled as confined concrete with the adjustment to Mander's model applied, as described.

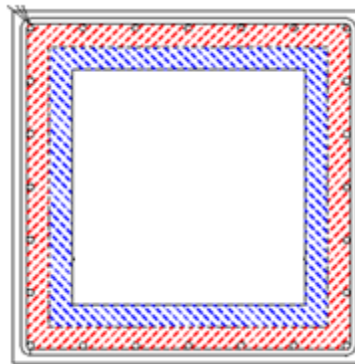


Figure 3-41: Regions for unconfined and confined concrete in rectangular hollow columns with one layer of transverse reinforcement

3.3.1.1.2 Two layers of transverse reinforcement

Although the focus of this research is on hollow columns with one layer of transverse reinforcement, a discussion of hollow columns with two layers of transverse reinforcement has been included to illustrate the differences between the confinement methods, as well as to provide further validation for fiber-based analysis. The more common confinement method for hollow columns is to provide two layers of transverse reinforcement, one near the outside face and one near the inside face. These layers are typically connected with cross ties, and this type of arrangement does not experience the problem of zero radial stress at the inside face like hollow columns with one layer of transverse reinforcement do. Both circular and rectangular columns

can be designed with this arrangement, and the calculation of confined concrete properties for these columns is described in this section.

3.3.1.1.2.1 Rectangular columns with two layers of transverse reinforcement

The confinement effect in solid rectangular hollow columns is calculated somewhat differently than that for circular columns, especially for rectangular solid columns with different amounts of transverse reinforcement in the x and y directions. Additional interlocking hoops are often provided in these columns, as well as hoops that are oriented at an angle as shown in Figure 3-42.

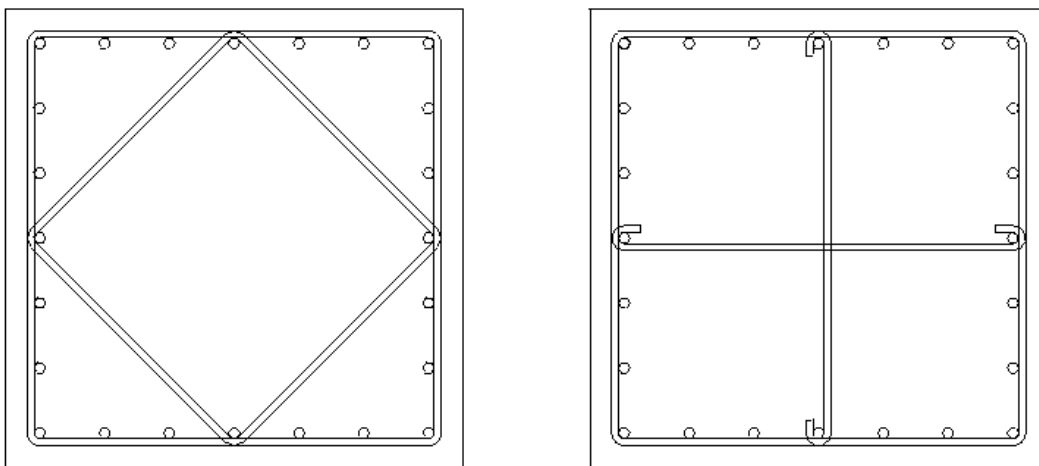


Figure 3-42: Possible transverse reinforcement arrangements in solid rectangular columns

When calculating the confined concrete properties for these columns using Mander's model, the procedure involves separating the amount of transverse reinforcement into x and y components. These components are then used to calculate transverse reinforcement ratios in each direction, and then the stresses in each transverse direction. Finally, the stresses are used with Figure 3-43, which was provided by Mander et al. to determine the confined concrete properties, where f'_{l1} and f'_{l2} are the lateral stresses in orthogonal directions.

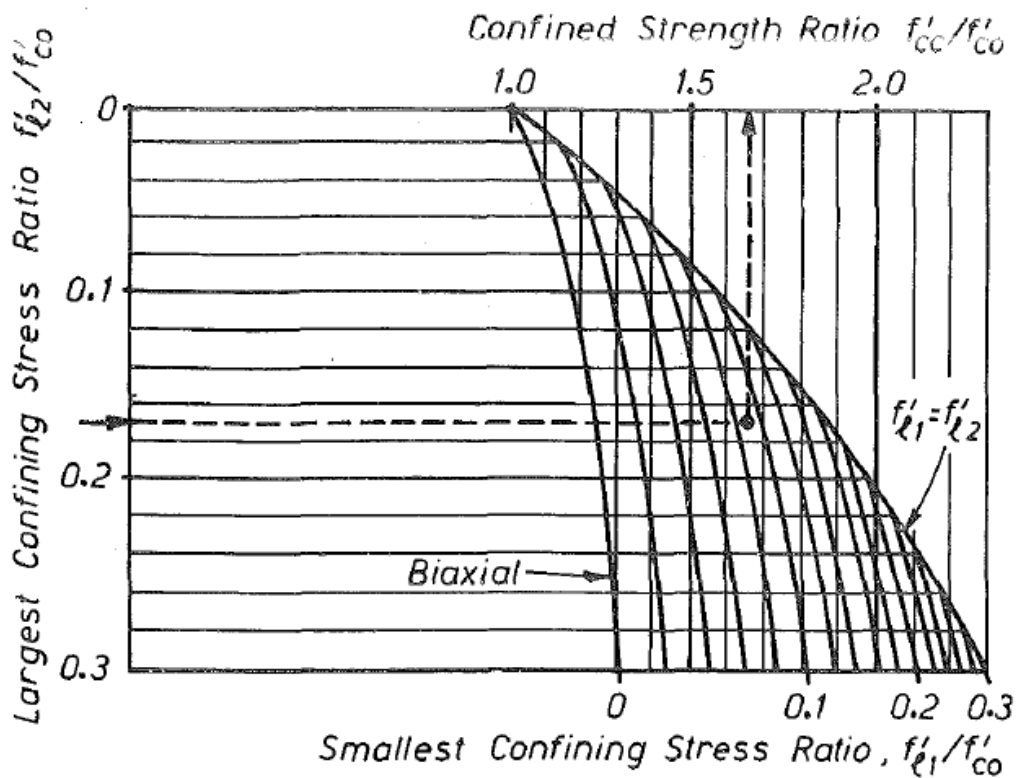


Figure 3-43: Confined concrete strength from lateral confining stress [Mander et al. (1988)]

For hollow rectangular sections, the provision of two layers of transverse reinforcement is often achieved by providing rectangular hoops or multiple ties with each wall. A configuration of rectangular hollow columns where the transverse reinforcement is provided by overlapping hoops is shown in Figure 3-44. When estimating the confined concrete properties for these arrangements, the columns can be thought of as four separate wall sections. Once this assumption has been made, the confined concrete properties can be estimated by treating each of these wall sections as a solid rectangular column, and calculating the confinement properties in each direction of this separate piece. See Figure 3-44 for an example of the separation of a hollow column with two layers of transverse reinforcement into individual wall sections.

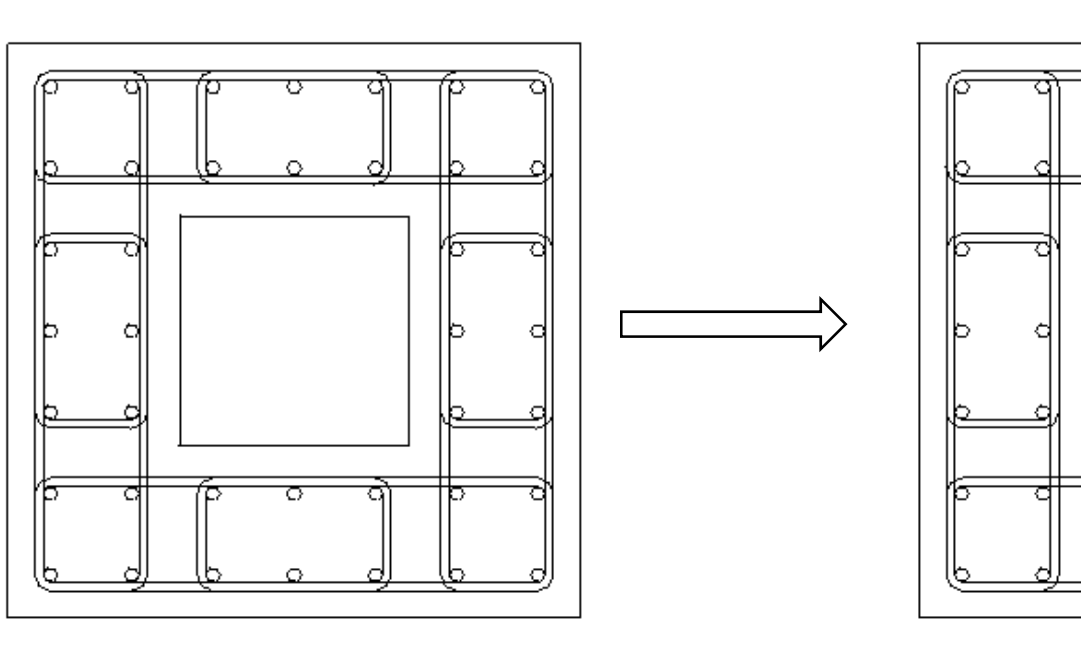


Figure 3-44: Hollow rectangular section confined with overlapping hoops and separation into individual wall section

3.3.1.1.2.2 *Circular columns with two layers of transverse reinforcement*

The calculation of confined concrete properties in circular hollow columns with two layers of steel is not as well understood as that of rectangular hollow columns. The finite element analysis has shown that the cross-ties between the inner and outer layer are essential to make the inner layer of confinement useful. These cross-ties have been assumed to transfer much of the demand to the outer layer of confinement. The finite element analysis suggests this is the case since two layers of steel without cross-ties experiences early failure due to the inner layer of confinement pulling through the inner cover.

Since the cross-ties seem to transfer the demand to the outer layer of confinement, it has been deemed appropriate to model the confined concrete by using the area of both the inner and outer confinement hoop when calculating the transverse reinforcement ratio. Unlike for hollow columns with one layer of transverse reinforcement, the transverse reinforcement ratio is taken to the net area of concrete. This method has been used since it is similar to the square hollow columns with two layers of transverse reinforcement, where the wall can be thought of as an

individual column. If you take a wall segment of a hollow circular column, it could similarly be thought of as an individual column of curved shape. The wall section is confined on both sides, so using the net area of concrete more accurately reflects the demands supplied to the transverse reinforcement.

3.3.1.2 Model verification

An analysis of previous test specimens was performed to verify that the suggested modeling methods can provide accurate results. Several previous experiments were selected in order to attempt to verify each type of arrangement (hollow sections with one layer of transverse reinforcement and hollow sections with two layers connected with effective cross-ties, both circular and square). Previous experiments were typically chosen for use if they experienced a flexural failure, since this would provide a more appropriate comparison to the model.

As discussed previously, providing accurate stress and strain behavior for the material models is very important to produce accurate results. Past researchers have often only reported tension steel yield stress and ultimate stress values without corresponding strain values, which cause difficulties in producing accurate analysis response in the nonlinear range. When using past research to check the accuracy of the analysis, the studies that provided more information about stress and strain of steel were used whenever possible.

3.3.1.2.1 Hollow circular columns with one layer of transverse reinforcement

Two specimens were tested by Hoshikuma and Priestley (2000), which were described previously in the literature review. A pushover analysis was performed for these specimens. The specimens were identical in section except for different amounts of longitudinal reinforcing steel. The sections can be seen below in Figure 3-45.

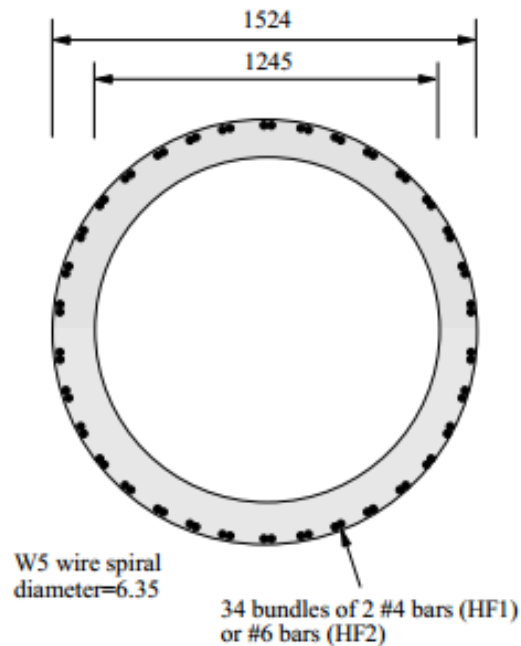


Figure 3-45: Cross-section dimensions (in mm) of the hollow column tested by Hoshikuma and Priestley (2000), (1mm = 0.0394 inch)

The specimens were cast as a hollow column with a foundation block at the base. A steel tube was attached to the top of the column to extend the column further, and the load was applied near the end of this steel tube. The steel tube was designed to remain in the elastic range during testing. The column was modeled with a nonlinear beam-column element, and the column to foundation interface was modeled using a section with a strain penetration model [i.e. using Bond_SP01 in OpenSees (Zhao & Sritharan, 2007)]. The base of the column below the strain penetration section was modeled as a fixed end. The loading steel tube was modeled using an elastic beam-column element. Two specimens were tested, with the same geometry and materials except for a differing amount of longitudinal steel. Sets of two bundled bars were used for longitudinal steel, and each of these was modeled as a single bar of equivalent area. Axial load was also applied identically to that applied in the experiment, with axial load of 654.9 kips being applied to specimen HF1 and axial load of 673.8 kips applied to HF2.

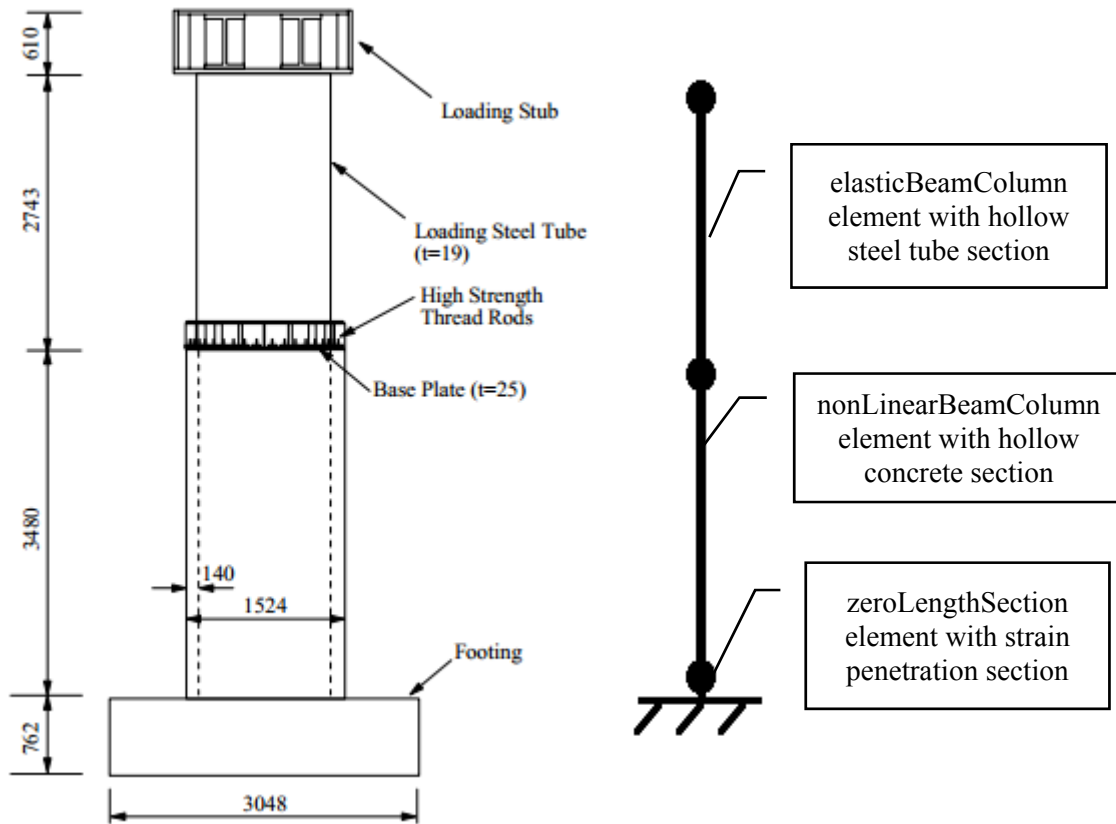


Figure 3-46: Test setup of Hoshikuma and Priestley (2000) and corresponding model configuration (Dimensions in mm), (1 mm = 0.0394 inch)

The section material models were defined, as described in Section 3.3.1.1.1.1, with two layers of concrete used to represent the inner unconfined layer and the outer confined layer. A pushover analysis was then performed for the modeled properties. The results of the analysis of the two test units can be seen in Figure 3-47. The experimental results are reported using a plot digitizer to extract the force-displacement envelope from the cyclic force-displacement presented in their research.

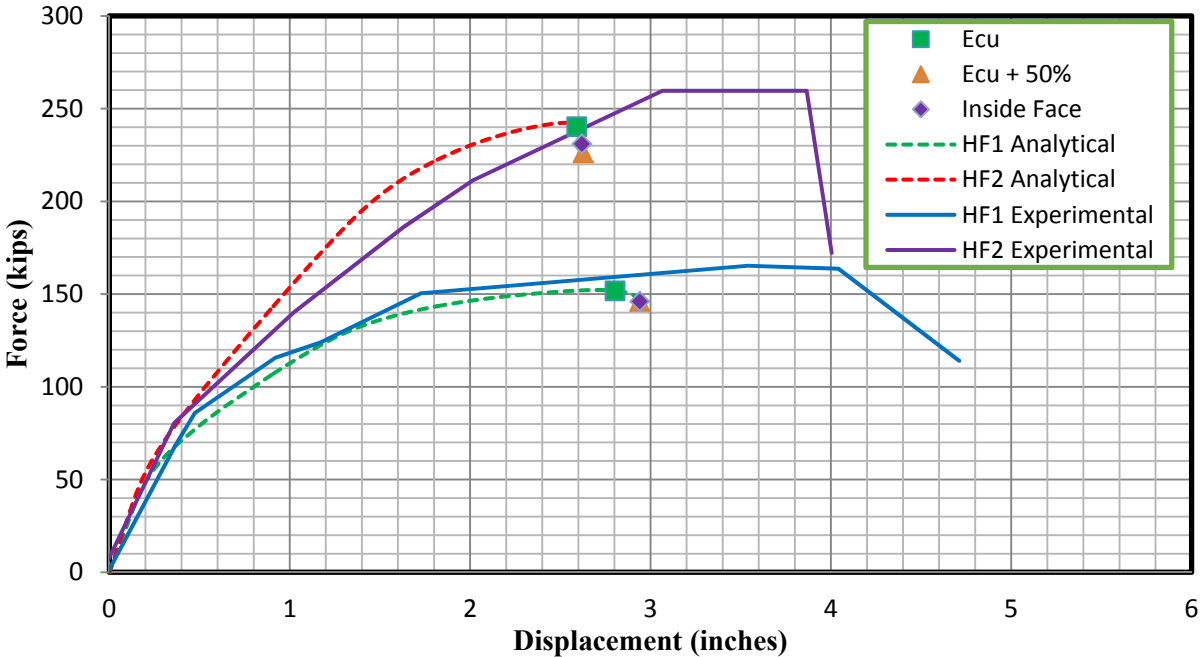


Figure 3-47: Comparison between analytical analysis and experimental results of Specimens HF1 and HF2 tested by Hoshikuma and Priestley (2000)

The analysis matches fairly well with the experimental results except for the early failure of the analytical columns. Shear was not accounted for in the analysis, and this may be contributing to the difference in the ultimate failure prediction. The predicted failure modes are plotted on the analysis as well. The actual specimens failed due to crushing of the concrete at the inside face. The analysis predicts that the confined concrete reaches the ultimate strain which is calculated by the following equation proposed by Priestley et al. (1996):

$$\epsilon_{cu} = 0.004 + \frac{1.4\rho_s f_{yh} \epsilon_{su}}{f'_{cc}} \quad \text{(Equation 3-9)}$$

Priestley et al. (1996) also state that this equation can often be conservative by at least 50 percent. For this reason, the ultimate strain of confined concrete predicted by this equation has been increased by 50 percent and has been considered as another possible failure point plotted in Figure 3-47 as well. The possible failure points predicted by the ultimate strain of confined concrete, and the ultimate strain of confined concrete increased by 50 percent, have been labeled in this and future plots as “Ecu” and “Ecu + 50%”, respectively.

The next failure mode predicted is the crushing of the inside face concrete, which agrees with the failure mode of the tested columns. Crushing the inside face concrete was considered to occur at a strain of 0.005 at the inside face, as suggested by Hoshikuma and Priestley (2000). The last point shown indicates the point where the ultimate confined concrete failure is considered, when increased by 50 percent to account for the conservatism of the ultimate estimate.

It is interesting to note that the equation proposed by Priestley et al. (1996) predicts failure of the confined concrete at approximately the same displacement as that of the prediction of the failure of the inside concrete face in Figure 3-47. Even when the prediction of failure of the confined concrete is increased by 50 percent, to account for conservatism in the estimate, this predicted failure still occurs at a similar displacement as that of the inside concrete face crushing. The experimental results of these tests showed that the confinement had only reached 30 percent of the yield strain when inside concrete face crushing occurred. This seems to indicate that estimates of the ultimate confined concrete strain are extremely conservative for hollow columns, due to the lower demand applied to the transverse steel by hollow columns.

3.3.1.2.2 Hollow square columns with one layer of transverse reinforcement

Several specimens were tested by Calvi et al. (2005), which were described previously in the literature review. The testing performed in the reported research is some of the only testing of hollow rectangular columns with one layer of transverse reinforcement available in the literature. Although this reported research focused on the shear response of the specimens, it has been used as an approximate verification of the analysis method due to the lack of previous testing of these columns.

Several different transverse reinforcement layouts were tested by Calvi et al. (2005), but the analysis was compared to the sections with one layer of transverse reinforcement, which had the dimensions and reinforcement configuration pictured in Figure 3-48. One of the tested specimens was chosen to be analyzed using the described analysis method. The specimen was labeled S250, and was subjected to 56.2 kips of axial load. The axial load was held constant throughout the testing. The research reported that the longitudinal and transverse reinforcement used in the specimen had yield stresses of 80 ksi, with ultimate stresses of approximately 97 ksi. A corresponding ultimate strain was not reported, so a fairly typical value of 0.08 was assumed. The concrete compressive strength was reported to be approximately 5 ksi. The test unit was

35.4 inches tall and cast on top of a foundation block. The specimen was tested under cyclic lateral loading at the top of the column with constant axial load applied.

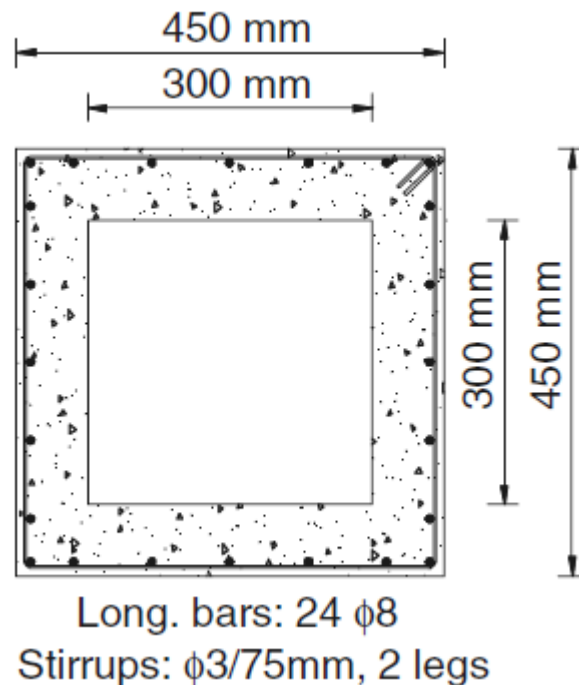


Figure 3-48: Cross-section dimensions and reinforcement layout of square hollow columns with one layer of transverse reinforcement tested by Calvi et al. (2005), (1 mm = 0.0394 inch)

The described section dimensions and properties were modeled using the procedure described in Section 3.3.1.1.1.2, including the use of two layers of concrete within the transverse reinforcement. The layer near the void was modeled as unconfined concrete, and the layer near the transverse reinforcement was modeled as confined concrete. The concrete properties for the layer of confined concrete were estimated using Mander's model, with the hollow column confinement effectiveness factor of 0.28 applied. Due to convergence issues for this specimen, the concrete was modeled using the Concrete02 model (Mohd Yassin, 1994) built into OpenSees. The analysis was then performed, and the resulting force-displacement response of the test unit and analysis are shown in Figure 3-49, along with several possible failure modes predicted by the analysis.

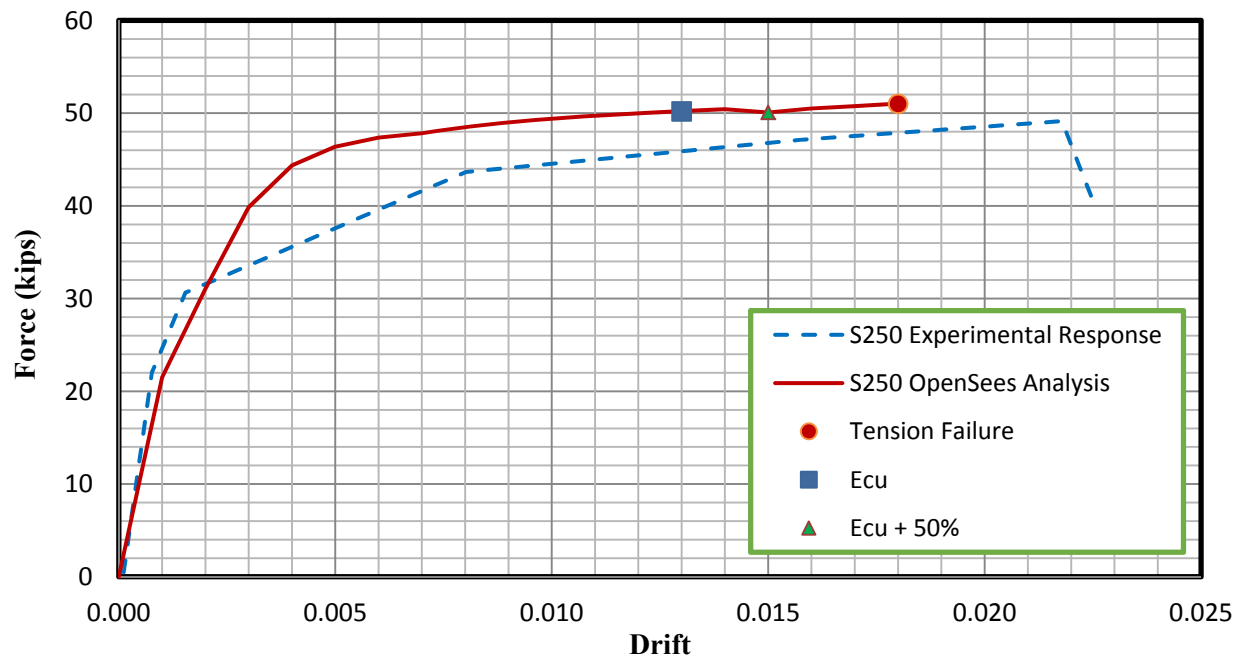


Figure 3-49: Force-displacement response comparisons between Test Unit S250 by Calvi et al. (2005) and analytical results

As shown, the analytical response agrees fairly well with the experimental response. The initial stiffness is captured closely, but the displacement of the test unit begins to increase more rapidly than the analytical displacement does. This rapid increase in displacement may be due to the contribution of shear deformation. Test unit S250 was designed and tested to fail in shear, and the shear failure caused the failure of the test unit. This also could be the reason that the experimental test unit experienced a larger ultimate displacement than what was predicted by the analysis, since the shear displacement would have been significant since the specimen failed in shear. It is also important to realize that the ultimate tensile strain of the longitudinal reinforcement was not reported, and a value of 0.08 was assumed. If the ultimate strain of the longitudinal reinforcement was actually higher than 0.08, this could also explain why the ultimate displacement of the test unit is higher than that predicted by the OpenSees analysis.

Also plotted on the figure is the failure point predicted by the ultimate concrete compressive strain, labeled Ecu, which was found using the equation given by Priestley et al. (1996). As

discussed previously, this equation is often conservative by 50 percent, so the failure point predicted by the ultimate concrete strain, increased by 50 percent, is plotted on the figure as well. As shown, even with the additional 50 percent, this estimate of the ultimate strain is very conservative for the hollow square column.

3.3.1.2.3 *Hollow circular columns with two layers of transverse reinforcement*

There are few previous tests performed on hollow circular columns with one layer of transverse reinforcement in the literature. Due to the limited previous testing information available, an analysis of sections with two layers of transverse reinforcement has been provided to further demonstrate the ability of the analysis to produce accurate results. An analysis of previous testing of hollow circular columns with two layers of transverse reinforcement by Yeh et al. (2001) has been performed. Three specimens were tested, and of those three only one specimen experienced flexural failure. This specimen was analyzed to further verify the analysis method as well as to determine the accuracy of the calculated confined concrete properties for this configuration. The modeling method for circular hollow columns with two layers of transverse steel which was discussed in the previous section was utilized for this column. The section layout can be seen in Figure 3-50.

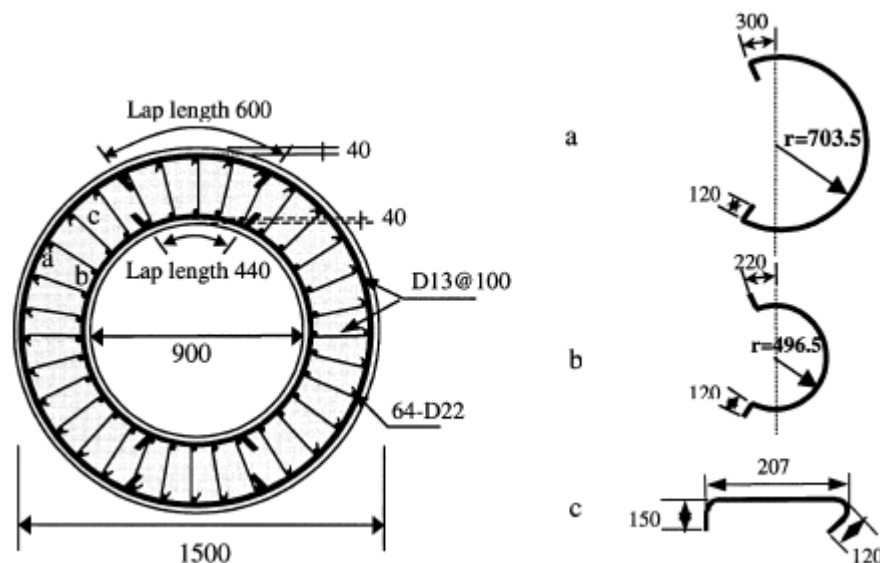


Figure 3-50: Cross-section dimensions and lateral reinforcement details of hollow columns tested by Yeh et al. (2001), (Dimensions in mm, 1mm = 0.0394 inch)

The specimen was tested and analyzed under an axial load of 809.3 kips. The analysis compared to the experimental results can be seen in Figure 3-51. As shown, the analysis is very close to the experimental specimen results. The experimental specimen failed due to rupture of the tensile steel. The predicted tensile steel failure strain of 0.15 is plotted on the analysis and corresponds well with the experimental failure point. Although the ultimate strain was not explicitly stated in the study, the strain of 0.15 corresponds well with the failure point for this test performed by Yeh et al. (2001) as well as the square column tests performed by Yeh et al. (2002), and it was assumed that this is approximately the steel failure strain. Additionally, the ultimate compression concrete strain as predicted by the equation given by Priestley et al. (1996) has been plotted as well as the ultimate concrete compression strain, with an additional 50 percent added due to the conservativeness of the estimate. This illustrates that the prediction of the ultimate compressive strain of the confined concrete is very conservative for hollow columns with two layers of transverse reinforcement.

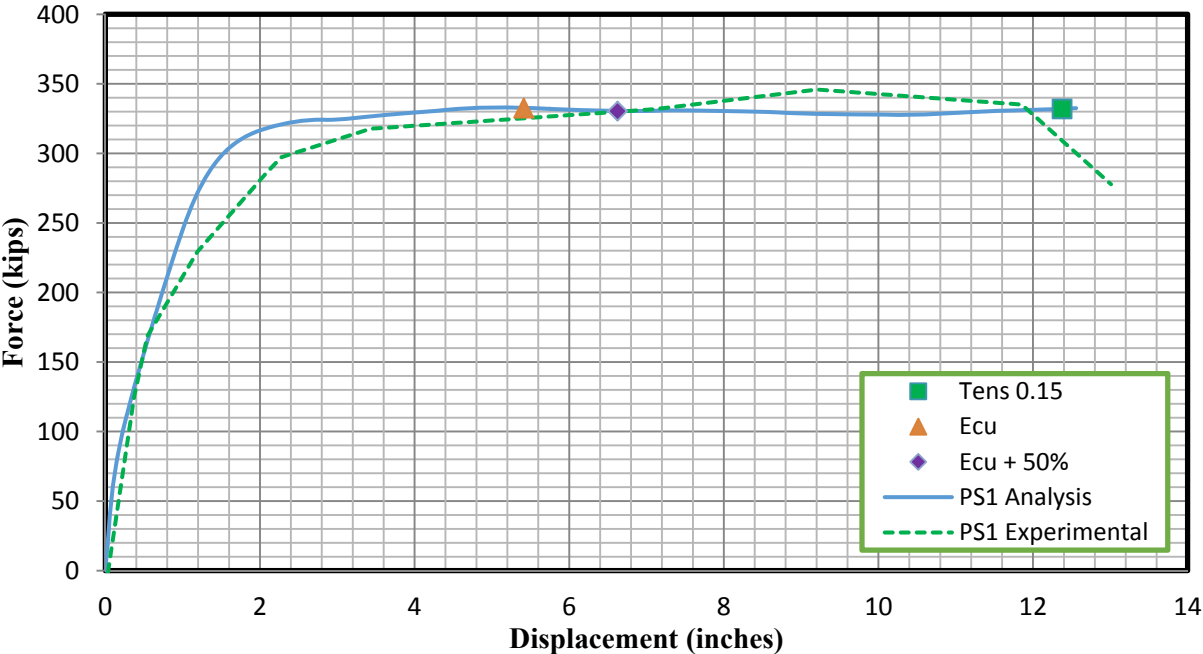


Figure 3-51: Comparison between analytical results and experimental results of Specimen PS1 tested by Yeh et al. (2001)

3.3.1.2.4 Hollow square columns with two layers of transverse reinforcement

Yeh et al. (2002) tested two square hollow columns, which contained two layers of transverse reinforcement and cross ties. The columns were connected to foundation blocks, and the cyclic loading was applied at the top of the column horizontally. The specimens had similar cross-section dimensions and the same longitudinal steel arrangement with different transverse reinforcement sizes and spacing. Different axial loads were applied to each column as well, with specimen PS1 having 301.2 kips of axial load applied, and specimen PI1 having 436.1 kips of axial load applied. These axial loads were included in the analysis. The section dimensions and reinforcement configuration of specimens PS1 and PI1 can be seen in Figure 3-52 and Figure 3-53, respectively.

The column was modeled as a nonlinear beam-column with a strain penetration section at the column-foundation interface. The base of the column was modeled as a fixed end. The concrete and steel properties were based on those reported in the research. The confined concrete was modeled using the previously described method for square columns with two layers of transverse reinforcement, involving treating each wall as a separate rectangular column. The pushover analysis was performed, and the results are shown in Figure 3-54, comparing the digitized force displacement envelope of the experiment to the pushover analysis. Several possible predicted ultimate points are also shown on the graph. The ultimate tension steel strain of 0.15 was not explicitly stated. The research paper reported that both specimens fail due to rupture of tension steel, and a tension steel strain of 0.15 corresponds fairly well with the failure points as well as the failure points of the circular specimen tested by Yeh et al. (2001).

As shown in Figure 3-54, the analysis corresponds fairly well to the test results, including the predicted failure region. The ultimate displacement of the test results is somewhat higher, and the initial stiffness is somewhat lower, but this may be because shear was not accounted for in the flexural analysis. As shown, the predicted ultimate compressive strains of concrete (ϵ_{cu} and $\epsilon_{cu} + 50\%$) are fairly conservative, since the ultimate strain, with an additional 50 percent added, is predicted to occur almost simultaneously with tensile rupture of longitudinal steel. The tests were controlled by tensile steel rupture without crushing of confined concrete.

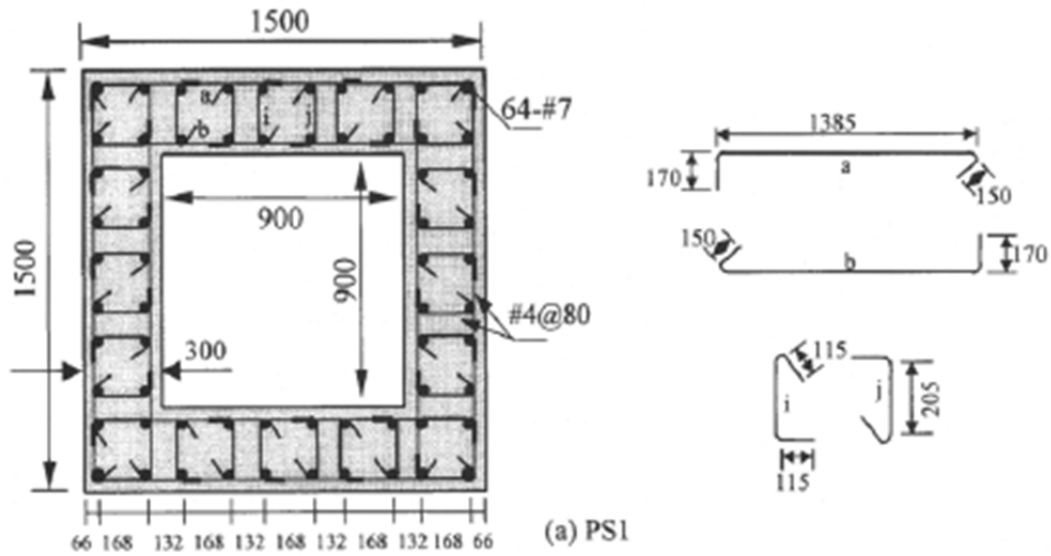


Figure 3-52: Cross-section dimensions of Specimen PS1 tested by Yeh et al. (2002)
 (Dimensions in mm), (1 mm = 0.0394 inch)

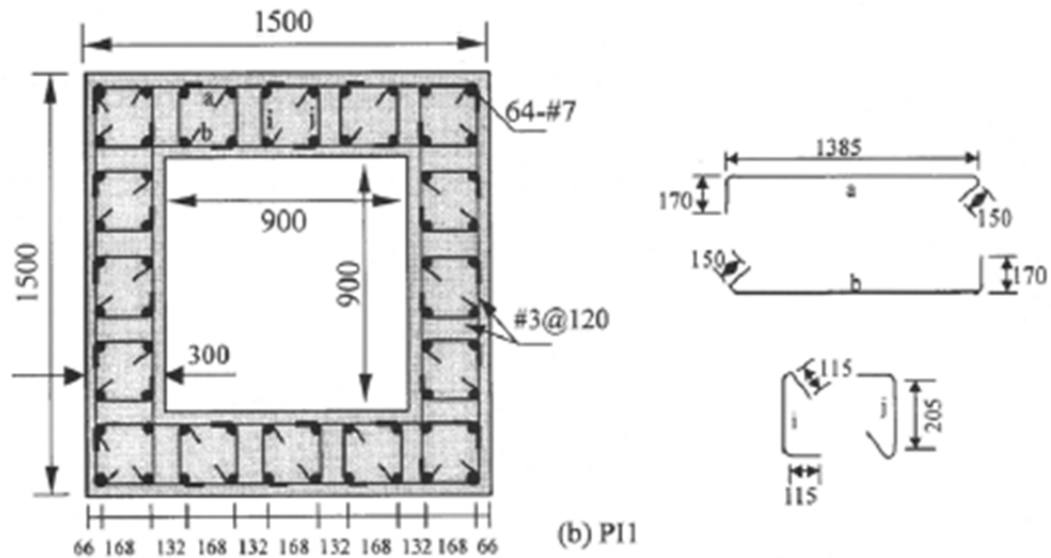


Figure 3-53: Cross-section dimensions of Specimen PI1 tested by Yeh et al. (2002)
 (Dimensions in mm), (1 mm = 0.0394 inch)

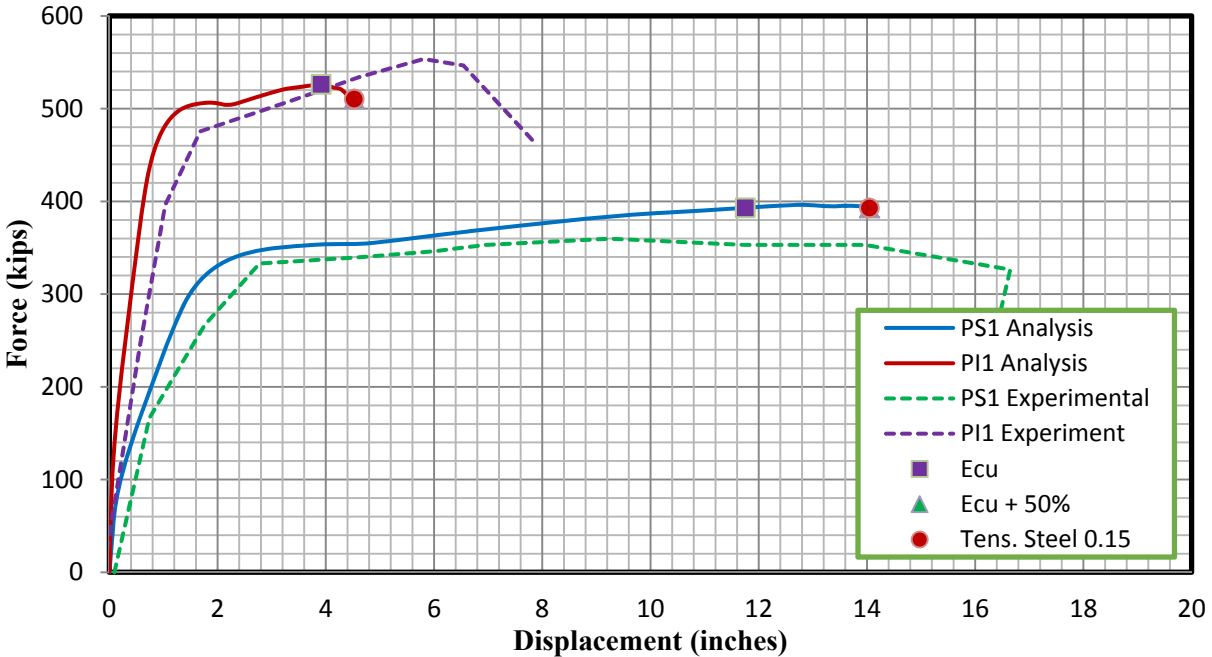


Figure 3-54: Comparison between analytical results and experimental results for hollow square specimens with two layers of transverse reinforcement by Yeh et al. (2002)

3.3.1.3 Applicability of model

The methods utilized for modeling the confined concrete properties have been developed based on methods used by previous researchers with some modifications to account for the void, which is present in hollow columns. The comparisons to previous experimental work illustrate that these methods are able to conservatively model confined concrete. When utilized in the OpenSees analysis, the material models have been able to predict the response of the specimens to a reasonable degree of accuracy.

Comparing the analysis results to the experimental results and to descriptions of the experimental behavior has shown that the analysis is also fairly capable of predicting the cause of failure and the ultimate force and displacement points. It can be seen that in many cases, the ultimate concrete compressive strain prediction provided by Priestley et al. (1996) is very conservative for hollow columns, even when increased by 50 percent. This discrepancy is likely due to the increased deformability of hollow columns, as discussed by Lignola et al. (2008). Since the hollow specimens require less pressure to restrain the radial displacement of the column, less

demand is supplied to the transverse reinforcement. This causes the transverse reinforcement to experience low strains, which means that the prediction of the ultimate compressive strain of confined concrete will be very conservative, since this prediction was based on hoop fracture in solid columns.

The prediction of crushing of the inside concrete face in hollow columns with one layer of transverse reinforcement has also been found to be conservative, as illustrated in the comparison to tests by Hoshikuma and Priestley (2000). The early prediction of the inside concrete face crushing may be caused by neglecting the influence of circumferential stress in the confined concrete model, as well as neglecting the small amount of radial stress near the inside concrete face. These stresses were conservatively neglected, but in reality the concrete strength near the inside face would likely have some increase in strength and ductility due to the confinement effect. An approach is discussed later in Section 5.6, which accounts for these stresses.

3.3.2 3D finite element analysis

Based on the confinement analysis under the concentric axial compression described previously, it was found that one layer of transverse reinforcement was sufficient to provide limited ductile behavior for hollow section with smaller wall thickness and the failure was primarily dominated by the inside concrete wall crushing; while two layers of transverse reinforcement connected with effective cross ties were required to achieve better confined concrete behavior for hollow section with larger wall thickness. For the hollow sections confined with two layers of transverse reinforcement and cross ties, the failure is typically characterized by the rupture of longitudinal reinforcing bars instead of inside concrete wall crushing. Therefore, such hollow columns usually propose a much more ductile behavior compared to those confined with a single layer of transverse reinforcement. In this section, hollow columns modeled with the same material properties as the confinement analyses were conducted under flexure loading, to represent the actual behavior experienced by the bridge columns and also to validate the findings derived from the confinement analysis.

Hollow sections with two different wall thicknesses (one inch and two inch) were analyzed under flexure loading. The load was applied the same way as the specimens tested in the structural lab, which will be described in detail in Chapter 4. Due to the double symmetry, only quarter of the

entire hollow columns were modeled to reduce the computational cost. The loading and boundary conditions are shown in Figure 3-55. The static general analyses were performed, which were divided into two steps: the axial load, simply supported boundary conditions and symmetric boundary conditions were applied in step 1; the lateral displacement (under displacement control) was applied in step 2, where the axial load and the boundary conditions were propagated from the step 1.

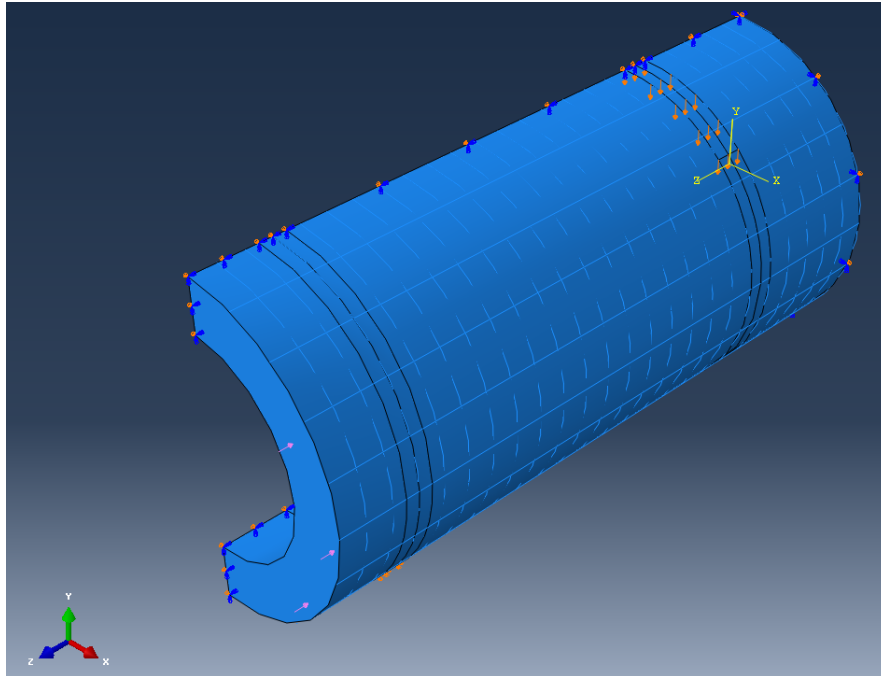
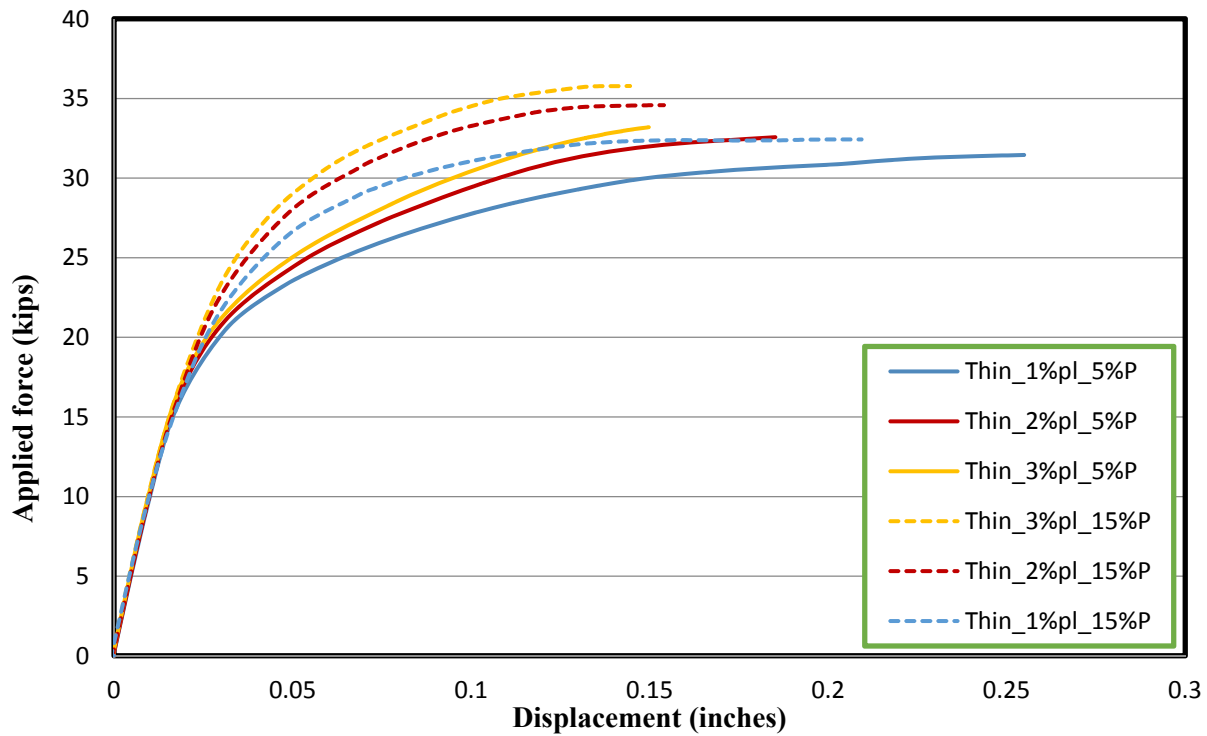


Figure 3-55: The loading and boundary conditions of the hollow columns modelled with a combined axial and flexure loadings

For the one-inch wall hollow columns, a single layer of transverse reinforcement was placed near the outside concrete wall face. Six such hollow columns were analyzed with 3 different longitudinal reinforcement ratios (1%, 2% and 3% based on the net concrete section) and two different axial load ratios (5% and 15% based on the net concrete section). Same volumetric ratio of transverse reinforcement ratio was applied for all the modelled one-inch wall hollow columns. The modelling matrix is presented in Table 3-11 and the derived force vs. displacement responses are shown in Figure 3-56. All the modelled specimens failed by inside concrete wall crushing.

Table 3-11: The modelling matrix for one-inch-wall hollow columns with a single layer of transverse reinforcement (1 inch = 25.4 mm, 1 kips = 4.45 KN)

Wall thickness-to-section diameter ratio	Longitudinal reinforcement ratio gross (net) (area of longitudinal reinforcement, in ²)	Axial load ratio gross (net) (axial load, kips)
0.83% (one-inch wall)	0.3% (1%) (0.017)	1.5% (5%) (7.8)
	0.6% (2%) (0.034)	1.5% (5%) (7.8)
	0.9% (3%) (0.051)	1.5% (5%) (7.8)
	0.3% (1%) (0.017)	4.5% (15%) (23.3)
	0.6% (2%) (0.034)	4.5% (15%) (23.3)
	0.9% (3%) (0.051)	4.5% (15%) (23.3)



* pl represents the longitudinal reinforcement ratio and P is the axial load ratio

Figure 3-56: Force - displacement response comparisons with different longitudinal reinforcement ratios and axial load ratios for one-inch-wall hollow columns with a single layer of transverse reinforcement

According to Figure 3-56, the hollow column with 1% of longitudinal reinforcement ratio and 5% axial load ratio based on net concrete area reaches the highest ductility, followed by the column with 2% of longitudinal reinforcement ratio. The hollow column with 3% of longitudinal reinforcement ratio experiences the lowest ductility. There is no significant difference in the ductility between the columns with 2% and 3% of longitudinal reinforcement ratio under the 15% axial load ratio. Both of these two columns experience a ductility which is much smaller than the column with 1% longitudinal reinforcement ratio. This set of analyses results were very comparable to the conclusions drawn by the previous researches (Zahn et al., 1990) that a relative ductile behavior could be expected from the thin-wall hollow bridge columns with a low longitudinal reinforcement ratio and a low axial load ratio.

For the two-inch-wall hollow columns, three types of confinement configurations were analyzed: one layer of transverse reinforcement placed at the outside concrete wall surface as well as two layers of transverse reinforcement placed at both the inside and the outside concrete wall surface with an inner to outer reinforcement ratio of 5:5 and 1:9. Adequate cross ties were provided to connect these two layers of transverse reinforcement effectively. The modelling matrix for the two-inch wall hollow columns is presented in Table 3-12 and the force vs. displacement response comparisons are shown in Figure 3-57. The two-inch wall hollow columns with one layer of transverse reinforcement failed by the inside concrete wall crushing, while the failure for the two-inch wall hollow columns confined with two layers of transverse reinforcement and cross ties was dominated by the rupture of longitudinal reinforcement. According to Figure 3-57, the hollow columns confined with two layers of transverse reinforcement connected with cross ties present significantly greater ductility compared to that with a single layer of transverse reinforcement. It indicates that two layers of transverse reinforcement connected with cross ties is an efficient configuration to confine the concrete for hollow columns with a relatively thick wall. In addition, an inner layer of longitudinal reinforcement was typically required for hollow columns confined with two layers of transverse reinforcement from the constructability point of view, which explained the greater ultimate capacity. Figure 3-58 shows the comparisons when same longitudinal reinforcement ratio was applied for better comparisons.

Table 3-12: The modelling matrix for the two-inch-wall hollow columns confined with three types of confinement configurations

Wall thickness-to-section diameter ratio	Confinement configurations	Proportion of inner to outer reinforcement amount
1.67% (two-inch wall)	One layer	-
	Two layers with cross ties	5:5
	Two layers with cross ties	1:9

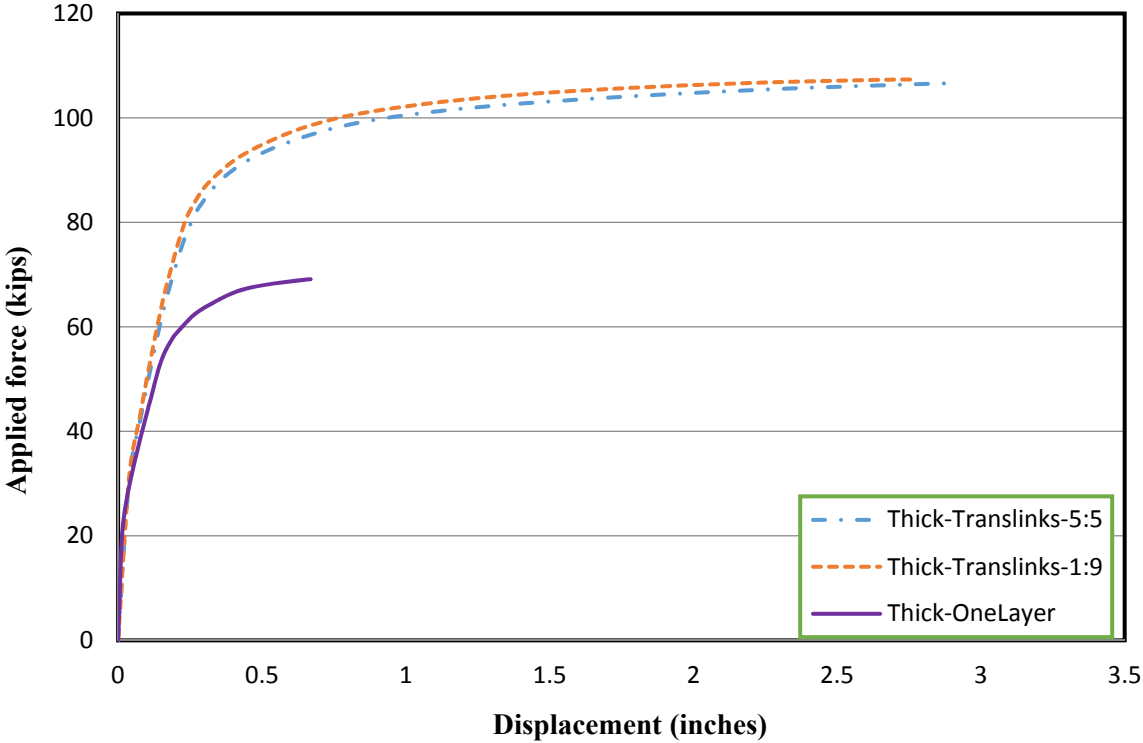


Figure 3-57: Force vs. displacement response comparisons for two-inch wall hollow columns with three different confinement configurations

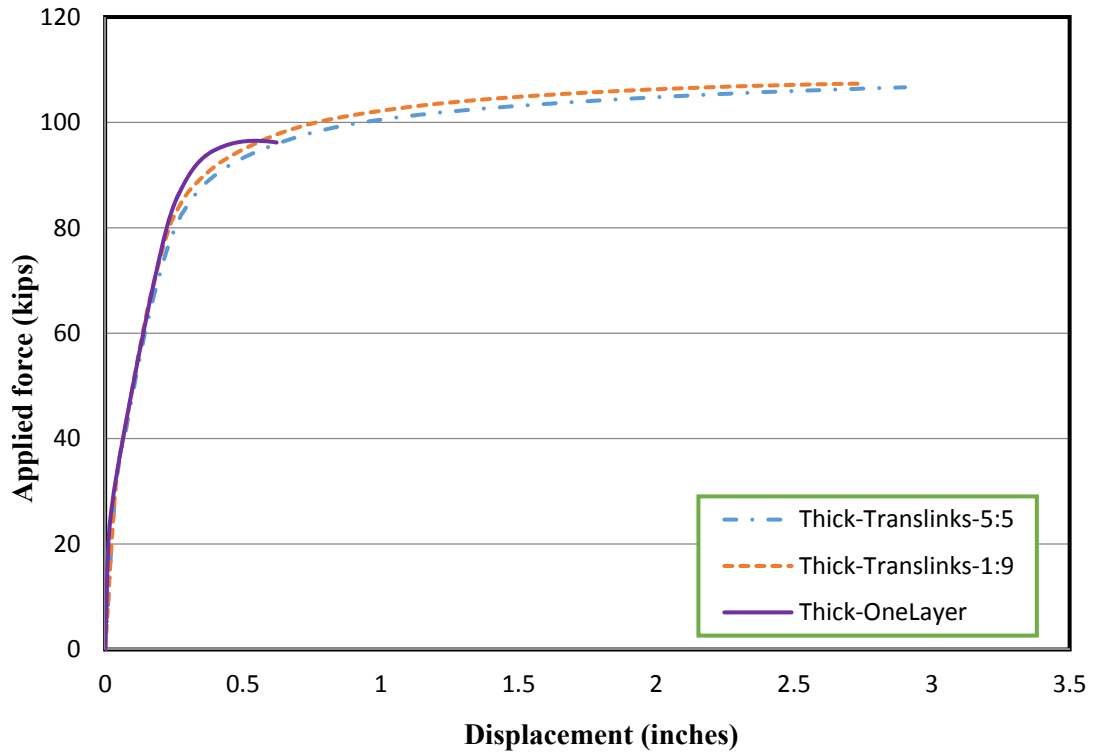


Figure 3-58: Force vs. displacement response comparisons for two-inch wall hollow columns with three different confinement configurations under the same longitudinal reinforcement ratio

CHAPTER 4 EXPERIMENTAL INVESTIGATION

4.1 Overview

Small-scale solid and hollow concrete columns were tested under various conditions in order to determine the accuracy of the analytical method for hollow columns with one layer of transverse reinforcement, described in Section 3.3.1.1.1. They were also tested to provide further information about the behavior of hollow columns. A total of 16 columns were tested, with eight circular and eight square cross sections. The specimens had similar reinforcement details, with the main test parameters being wall thickness and axial load ratio. A test frame was prepared in order to test the specimens under pure bending without the influence of shear in the critical region. Both monotonic and cyclic tests were performed.

4.2 Test specimen

Eight circular columns were tested. The columns were 48 inches tall with an outer diameter of 12 inches, representing a 6 foot diameter column at 1/6th scale. The smaller scale was selected in order to increase the number of test units. Although such a scale is typically avoided as it introduces challenges in finding suitable small diameter reinforcement and adds construction difficulties, it is expected that some large-scale tests will follow this study.

Two of the circular columns were solid sections, and six were hollow. Of the six hollow sections, two different wall thicknesses were used. Three specimens had a two-inch thick wall and the other three had a one-inch thick wall, corresponding to wall thickness to section diameter ratios of 0.17 and 0.08, respectively. The steel reinforcement in all eight columns was identical, with one layer of reinforcement placed near the outside concrete wall. The longitudinal reinforcement consisted of 20 #2 bars. The transverse reinforcement was provided by a continuous spiral of 0.208 inch diameter wire, spaced at 1.2 inches in the critical region. Outside of the critical region, the spiral spacing was shortened to one inch to ensure failure occurred near the critical region. These quantities of reinforcing steel correspond to gross reinforcement ratios (i.e, ratio to solid section, ignoring the void in the hollow section) of 0.87 percent for longitudinal steel and 0.97 percent for transverse steel. If calculated using the net section of present concrete for the one-inch thick specimens, the longitudinal reinforcement ratio would be 2.84 percent, and the transverse reinforcement ratio would be 3.5 percent. For the two-inch thick section using the net

section, the longitudinal reinforcement ratio would be 1.56 percent, and the transverse reinforcement ratio would be 1.8 percent. The amount of longitudinal reinforcement provided is somewhat low for bridge columns, but the gross section longitudinal reinforcement ratio is still greater than the minimum value of 0.5 percent recommended for circular columns by Priestley et al. (1996). This low amount of longitudinal reinforcement was provided since ductility would be reduced with more longitudinal reinforcing steel, because this would cause the neutral axis to move toward the void. An additional reason that a small amount of longitudinal reinforcement was provided was because of the limited space available due to the small wall thickness. The specimens were designed to have minimal cover concrete, resulting in a concrete cover of approximately 0.35 inches that was measured to the center of main longitudinal steel. This minimal amount of cover concrete resulted in narrow shrinkage cracks on the specimens prior to testing. The location of these cracks coincided with the transverse reinforcement, and the cracks occurred throughout the length of the specimens.

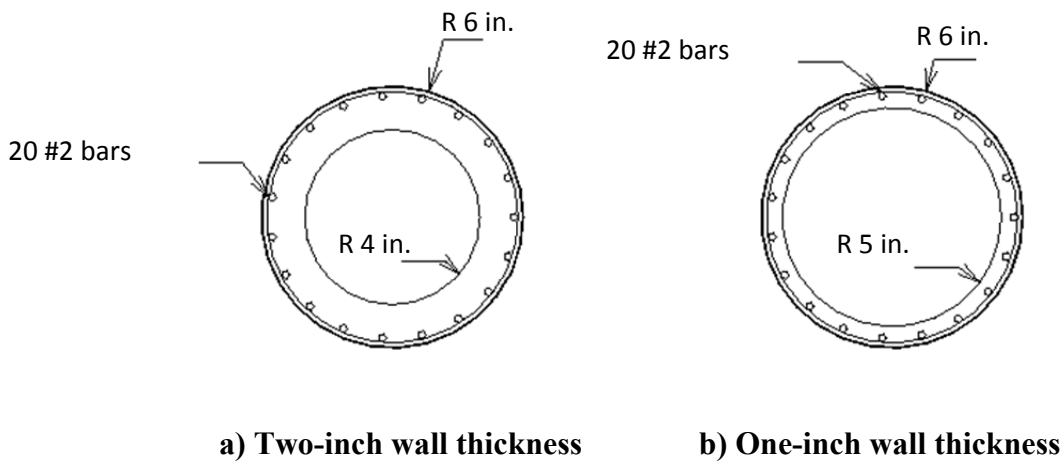


Figure 4-1: Cross-sections of circular hollow columns

Eight square columns were also tested, with only minor changes in the general details of the circular columns in order to provide similar reinforcement ratios to the circular sections. These columns were also 48 inches tall with 12 inch by 12 inch section dimensions. Of these eight columns, two were solid sections, three were hollow with a two-inch wall thickness, and three were hollow with a 1.25-inch wall thickness. The 1.25-inch wall thickness was provided instead

of the 1-inch wall thickness used for the circular sections in an effort to allow the concrete to fill the section more easily. The hollow columns with a 2-inch thick wall and a 1.25-inch thick wall had wall thickness to section diameter ratios of 0.17 and 0.1, respectively. Similarly to the circular sections, one layer of steel reinforcement was used near the outside concrete wall, except with 24 longitudinal #2 bars. The confinement was provided by a 0.208 inch diameter continuous square wire spiral, spaced at 1.2 inches in the critical region and 1 inch outside of the critical region. Using continuous square shaped spiral transverse reinforcement is uncommon in square columns, since it is not commonly manufactured, and individual hoops are typically used. However, due to the small section size of the specimens, this was the most readily available confinement configuration. The longitudinal and transverse reinforcement ratios to the gross section (ignoring the void for hollow sections) were 0.82 percent and 1.0 percent, respectively. If calculated using the net section of present concrete for the 1.25-inch thick specimens, the longitudinal reinforcement ratio would be 2.19 percent, and the transverse reinforcement ratio would be 2.89 percent. For the two-inch thick section using the net section the longitudinal reinforcement ratio would be 1.47 percent, and the transverse reinforcement ratio would be 1.84 percent. The amount of longitudinal reinforcement provided for the square columns is also fairly low, but the gross section longitudinal reinforcement ratio is still slightly over the minimum of 0.8 percent recommended for rectangular columns by Priestley et al. (1996). The square specimens also had minimal concrete cover, with a depth to the center of longitudinal reinforcing steel of 0.4 inches.

The test units have been given a naming system for easy referral. The first letter can be either S or H, indicating solid or hollow. If hollow, there will be a number immediately following the first letter representing the thickness of the wall. For example, a hollow specimen with a one-inch wall thickness would start with H1, while a solid specimen would just start with S. The second letter can either be C or S, for circular or square. The next character is a number indicating which test unit it is. Each type of specimen has an individual numbering system, so the second solid section would be labeled test unit 2 for solid sections, and the second hollow two-inch thick specimen would be labeled test unit 2 for hollow two-inch thick specimens. The last letter in the naming convention is either M or C for monotonic or cyclic loading. For example, of the three circular hollow one-inch thick specimens, the second one tested would have the designation H1C2-C if tested cyclically.

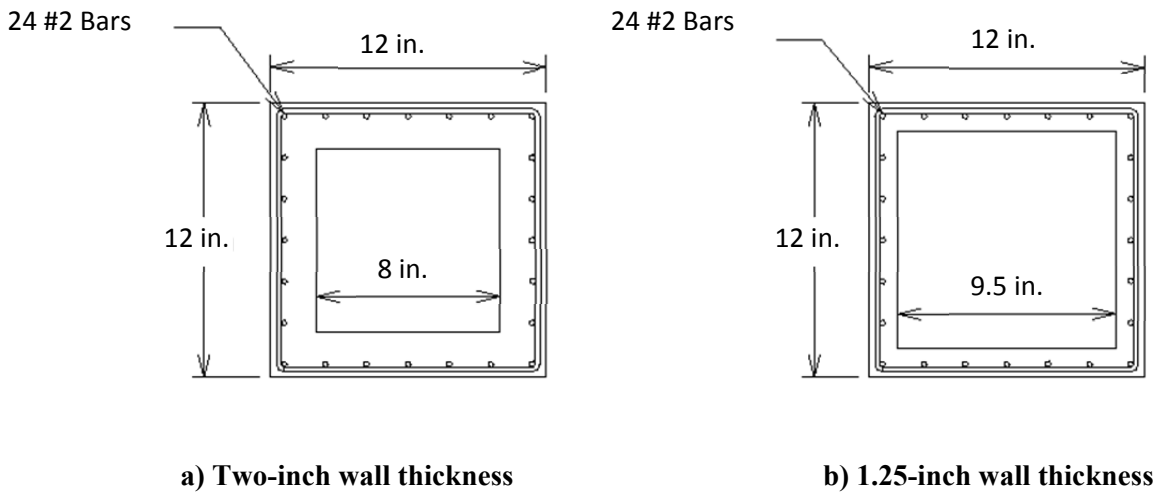


Figure 4-2: Cross-sections of square hollow columns

4.3 Material properties

The tables below summarize the steel and concrete properties for the test units. Table 4-1 shows the tested steel properties of the longitudinal and transverse reinforcement, while Table 4-2 gives the concrete strength on the day of testing for each unit. The steel used in the specimens for both longitudinal and transverse reinforcement had much higher yield strengths than typical reinforcing steel, as well as much lower ultimate strains. Though not expected, this seems to be true for the small diameter longitudinal reinforcement. This steel was used due to the limited options available for the small specimen size. At the time it was acquired, the ultimate tensile strain of the steel was expected to be significantly higher than what was found during material testing. The smaller steel ductility has an impact on the test results; however, the specimen behavior and the effects of using one layer of transverse reinforcement can still be studied effectively.

Table 4-1: Measured steel reinforcement properties

Steel	Diameter (inches)	Yield Stress (ksi)	Yield Strain (in/in)	Ultimate Stress (ksi)	Ultimate Strain (in/in)
Longitudinal	0.25	95	0.0033	100	0.02*
Transverse	0.208	95	0.0033	105	0.012*

*Significantly lower than expected

Table 4-2: Measured concrete strength on day of testing

Specimen	$f'c$ (psi)	$f'c$ of patched concrete (psi)	$f'c$ of grout (psi)
SC1-M	6309		
SC2-C	6248		
H1C1-M	5792	7000	7112
H1C2-C	6549	6738	
H1C3-C	6549	6738	
H2C1-M	6015		
H2C2-C	5677		
H2C3-C	5677		
SS1-M	7496		
SS2-C	7390		
H1.25S1-M	7573	7160	6016
H1.25S2-C	7283	7004	5603
H1.25S3-C	7283	7004	5603
H2S1-M	7573	7160	6016
H2S2-C	7594	7122	5557
H2S3-C	7594	7122	5557

4.3.1 Concrete quality

The small wall size of the hollow specimens presented a challenge when attempting to achieve good concrete fill in the specimens. The reinforcement cage further reduces the area which concrete can fill and restricts the ability to vibrate the concrete. For this reason, the concrete used was a self-consolidating concrete mix with a target strength of 5,000 psi. Aggregate size was limited to 3/8 inch in the concrete in an effort to achieve better fill between the reinforcement. These procedures helped to achieve good concrete fill for all solid sections as well as the circular two-inch thick specimens. However, this procedure did not help for the remainder of the specimens, which ended up needing some patches. The concrete and grout used for patching was intended to match as closely as possible to the initial mix, especially in strength and aggregate size. The patching was able to fill the voids which the initial concrete pour had left.

4.4 Test setup

A specialized loading frame was designed for the experiment in order to examine the effects of flexure independently, and the layout of this frame can be seen in Figure 4-3. Examining the effects of flexure independently was accomplished by placing the columns horizontally and loading them laterally at two points near the center of the column. This loading arrangement creates a constant moment region over the central portion of the columns, allowing the flexural effects to be examined with no shear present. The column supports were 42 inches apart, and the two lateral load points were applied 11 inches apart in each direction using an actuator for each direction. The actuators applied load to loading beams, which transferred the load to the two point loads. The point loads and support points were applied using one-inch thick curved steel plates for circular columns and 1.5 inch thick flat plates for square column. A layer of neoprene rubber was provided between the plates and the test specimens to help distribute the load more evenly. The lateral load applied by the bottom actuator was resisted by structural tube sections on top of the specimen and threaded rods which transferred the load to a bottom beam. The bottom beam was attached to the strong floor using structural tubes at each end and DYWIDAG bars. Lateral load applied by the top actuator was resisted by the beam assembly frame above the specimen, which was tied down to the strong floor by DYWIDAG bars, which ran through the square structural tube columns. The described setup can be seen in Figure 4-3. The various components are colored for better visualization, and some of the described components are labeled.

The axial load was applied through the use of two threaded rods connected by structural tube sections on either end to transfer the axial load to the column. Steel plates were used on either end to distribute the load. The columns were capped on each end with a layer of hydrostone to ensure even loading. A hydraulic actuator and load cell was used at one end between the structural tube and plate in order to apply the axial load, and was also used to keep the axial load constant throughout the testing, since the increasing specimen deformation would cause the axial load to increase. All specimens except for specimen SC1-M were held at constant axial load. The test frame setup is shown in Figure 4-3 through Figure 4-5.

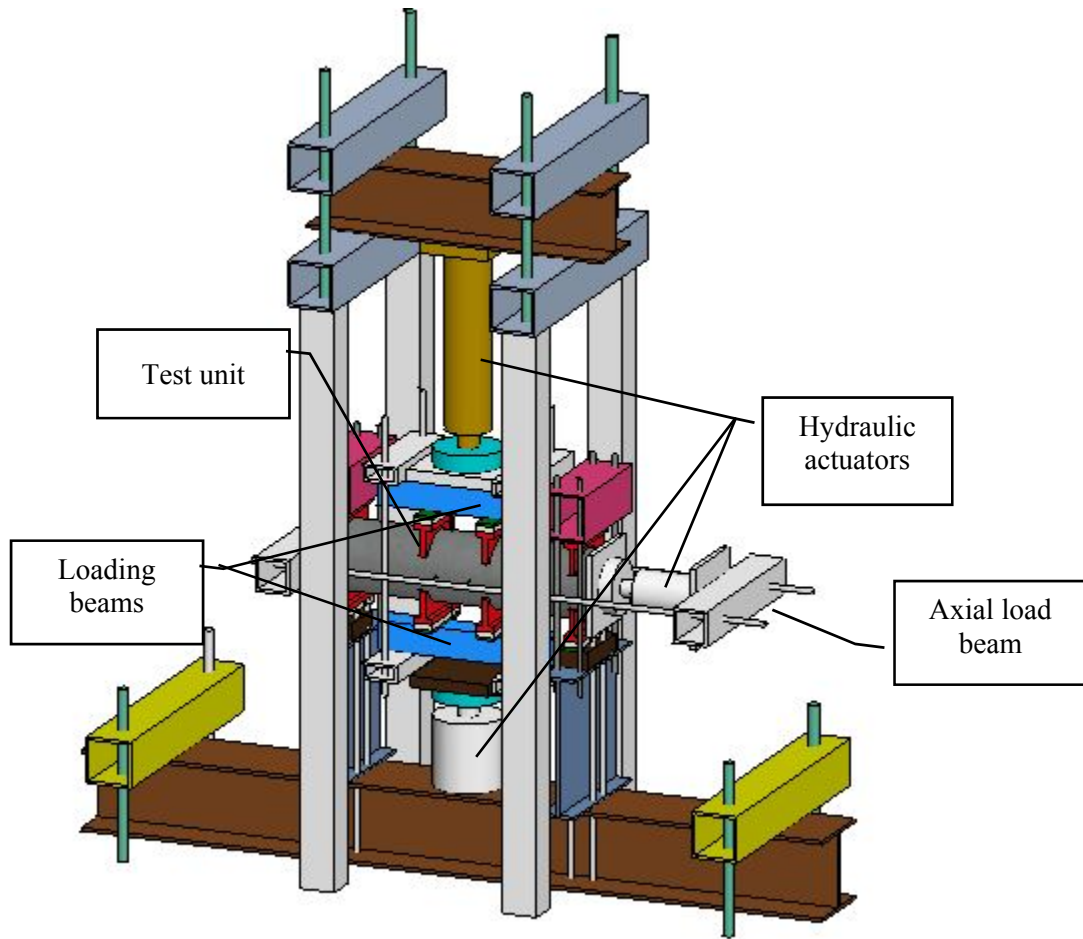


Figure 4-3: Overall test frame

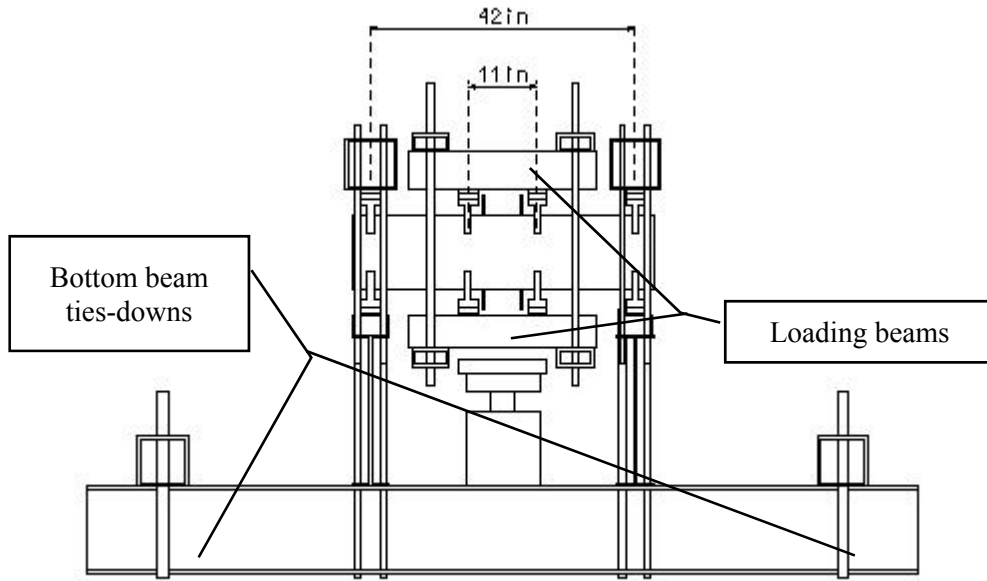


Figure 4-4: Frame cutaway showing test specimen setup



Figure 4-5: Picture of experimental testing setup

4.5 Test Instrumentation

Steel strain gauges were mounted to the longitudinal and hoop reinforcement, with 12 steel strain gauges being used on the circular specimens and 17 being used on the square specimens. The strain gauges are labeled according to the format SGLongL#H#. It can be SGLong or SGHoop, representing whether the gauge was on the longitudinal steel or the transverse steel. The term L# represents which longitudinal steel bar the gauge was located on or near, with the longitudinal bars being numbered around the circumference. Bar one was located at the extreme fiber of the section, which would experience the largest tension and compression strains under cyclic loading. For monotonic loading, bar one is always at the most extreme compression fiber. The term H# can either be H20 or H25, for which hoop the strain gauge was located on or near, counting up from the bottom. Figure 4-6 shows the location of the hoop sections and the spacing of the transverse reinforcement along the column height. For example, SGHoopL11H25 would be the gauge located on the hoop near longitudinal bar 11 at the bottom of the specimen, on the 25th hoop up counted upwards from the base.

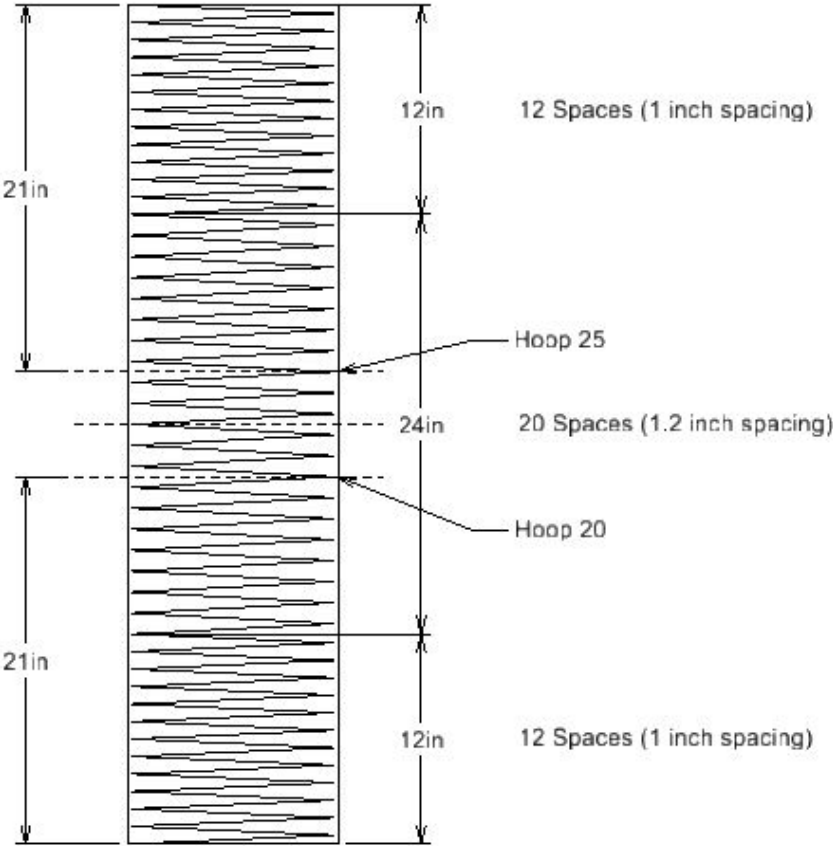


Figure 4-6: Transverse reinforcement spacing for both circular and square columns

The circular section has six strain gauges on the longitudinal steel and six on the hoop steel. The section labeled H20 is approximately 21 inches from the bottom of the specimen. Eight strain gauges are located near this hoop, consisting of four longitudinal and four hoop gauges. The section labeled H25 is approximately 27 inches from the bottom, and it has only four gauges, two longitudinal and two hoop gauges. Fewer gauges were used in this section because the response should ideally be symmetric. The square section has nine strain gauges on the longitudinal steel and eight strain gauges on the hoop steel. The section labeled H20 is approximately 21 inches from the bottom of the specimen and has 11 strain gauges, and the section labeled H25 is 27 inches from the bottom of the specimen and has six strain gauges. The circular strain gauge section layout is shown in Figure 4-7. The gauges not marked with an asterisk exist at both sections, H20 and H25, while the gauges which are marked with an asterisk only appear at section H20. The square strain gauge section layout is shown in Figure 4-8, and the same notation is used for the strain gauges in the square section.

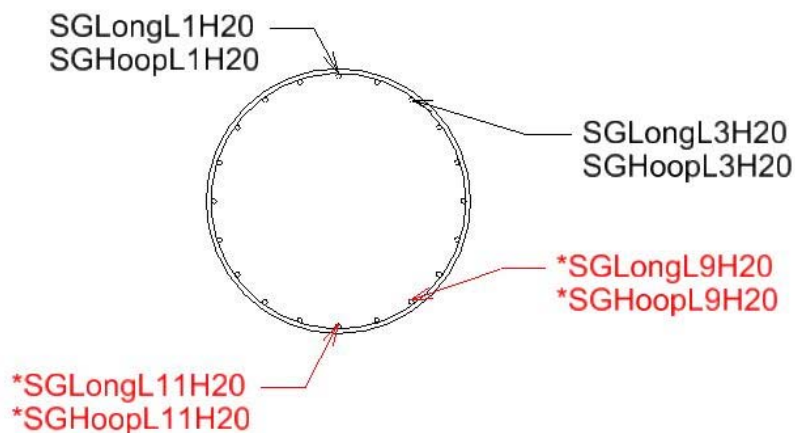


Figure 4-7: Strain gauge layout of circular section

In addition to the strain gauges, linear-variable-displacement-transducers (LVDTs) were used to measure both the column displacement as well as the curvature. Four LVDTs were attached at the center of the specimen, spaced at 90 degrees around the specimen circumference. These LVDTs spanned approximately six inches. These curvature LVDTs were anchored to the specimen using threaded rods which were either cast into the specimen or drilled into the

specimen. The threaded rods extended into the void of the hollow sections. The hollow circular sections had the threaded rods cast integrally with the section, while all other sections had holes drilled and threaded rods inserted and held in place using epoxy. In addition to the curvature LVDTs, three LVDTs were used to measure the specimen displacement. An LVDT was placed at each support, and an LVDT was placed at the center of the specimen. See Figure 4-9 for the layout of the LVDTs. One attached curvature LVDT is not shown in the figure and is attached to the side opposite of the side shown, similar to the other three attached LVDTs.

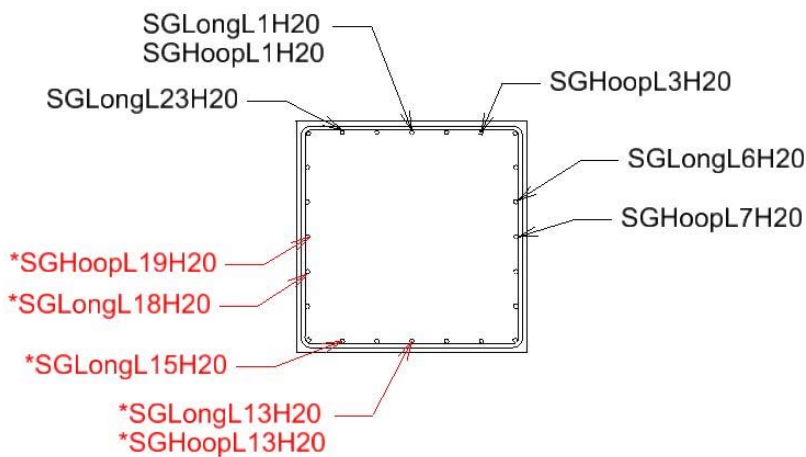


Figure 4-8: Strain gauge layout of square section

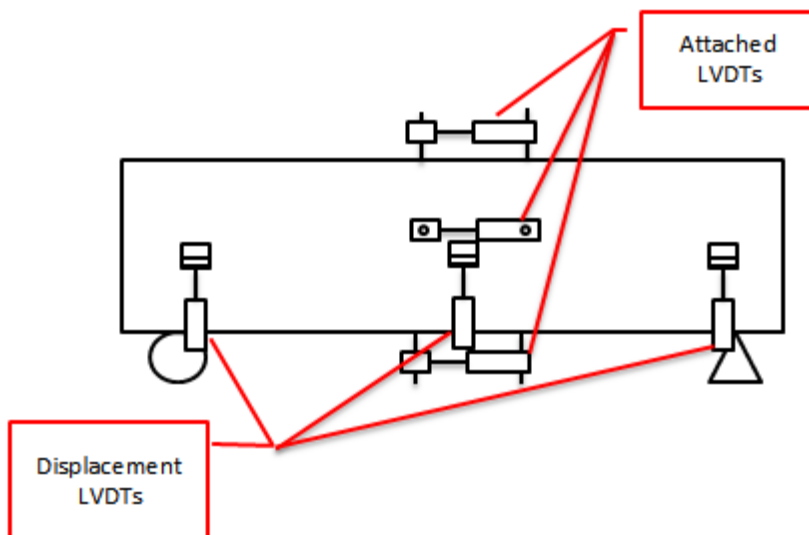


Figure 4-9: LVDT locations

In addition to the gauges and LVDTs, a 3D motion capture system was used to measure the displacement of points in space in real time. The Optotrak Certus Motion Capture System was used, which finds displacement of certain points using strobing LEDs. The LED arrangement consisted of 38 LEDs, and the general locations of these LEDs are shown in Figure 4-10, with each number representing an LED, according to the numbering scheme given to the LEDs. Several LEDs are not pictured, and these LEDs were either attached to the frame as a point of reference or were used as indicators. The system was set to output at five frames per second, and the outputs are given as the X, Y, and Z location of each LED, relative to a defined coordinate system. These coordinates were then used to calculate values such as displacement, axial strain, and shear contribution. LEDs 35 through 38 were used particularly for the shear displacement calculations, with LEDs 11, 12, 25, and 26 also used to check these shear calculations. LEDs 1, 2, 11, 12, and the central column of LEDs (vertically from 6 to 19) were used to calculate displacement values. The LEDs in the critical region (5 through 10 and 15 through 20) were also used to calculate axial strains.

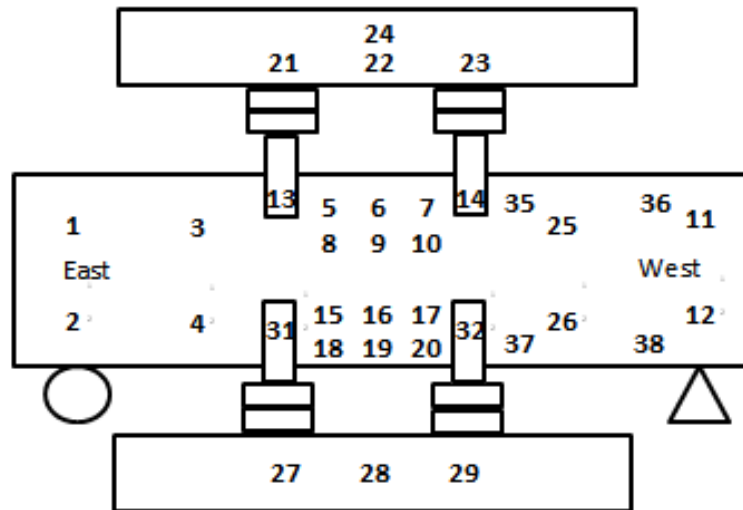


Figure 4-10: General LED layout

4.6 Loading protocol

The specimens were subjected to constant axial load and increasing flexural load until failure. The loading plan and amount of axial load for each specimen can be seen in Table 4-3 and Table 4-4. Axial load was applied for all specimens, and was held constant using a hydraulic actuator for all specimens except specimen SC1-M, which experienced increasing axial load due to flexure during the test. Flexural load was applied through the use of two manually controlled actuators. Increments in the force controlled range were applied under load control, with certain loads targeted, and the remainder of the test was performed under displacement control. The displacement control was performed by manually controlling the actuator and loading the test unit targeted displacements were achieved, which were monitored constantly throughout the test.

Table 4-3: Summary of the test of circular specimens

Circular					
	Thickness (inches)	Axial Load (kips)	Axial Load Ratio (ALR) (%)	ALR to Net Area (%)	Loading
SC1-M	Solid	22.6	3%	3%	Monotonic
SC2-C	Solid	45.2	6%	6%	Cyclic
H1C1-M	1	22.6	3%	10%	Monotonic
H1C2-C	1	22.6	3%	10%	Cyclic
H1C3-C	1	45.2	6%	20%	Cyclic
H2C1-M	2	22.6	3%	6%	Monotonic
H2C2-C	2	22.6	3%	6%	Cyclic
H2C3-C	2	45.2	6%	11%	Cyclic

Specimens loaded cyclically were subjected to four equal load increments in the linear range, with the fourth increment corresponding to the target first yield point found through OpenSees analysis of the test column. The increments in the force controlled range were load controlled. Each increment was one full cycle, with loads applied alternately in the lateral directions. The longitudinal steel strain was monitored during the linear loading, and the linear loading phase was stopped when yield strain was reached in the longitudinal steel, even if the target yield load was not attained. This point was then used to calculate the approximate ductility levels, and the loading then entered the nonlinear stage. In this stage, three cycles were performed at each

increment, with the increments occurring on ductility levels 1, 1.5, 2, 3, 4, etc. Increments in the force controlled range were labeled F1, -F1, and so on through -F4. Increments in the nonlinear range were labeled A, B, C and so on, with a number following each label, such as A1 or -A2, to represent which cycle was being applied at a certain displacement level and which direction the load was being applied. Increment A corresponded with theoretical ductility 1, B with ductility 1.5, C with ductility 2, and D with ductility 3, continuing in this pattern until failure. The loading history used for each specimen is shown in Figure 4-11. Specimens loaded monotonically were loaded in one direction until failure occurred. The loading was paused in the same increment levels as the cyclic specimens in order to observe and mark cracking.

Table 4-4: Summary of the test of square specimens

Square					
	Thickness (inches)	Axial Load (kips)	Axial Load Ratio (ALR) (%)	ALR to Net Area (%)	Loading
SS1-M	Solid	28.8	3%	3%	Monotonic
SS2-C	Solid	57.6	6%	6%	Cyclic
H1.25S1-M	1.25	28.8	3%	8%	Monotonic
H1.25S2-C	1.25	28.8	3%	8%	Cyclic
H1.25S3-C	1.25	57.6	6%	16%	Cyclic
H2S1-M	2	28.8	3%	6%	Monotonic
H2S2-C	2	28.8	3%	6%	Cyclic
H2S3-C	2	57.6	6%	11%	Cyclic

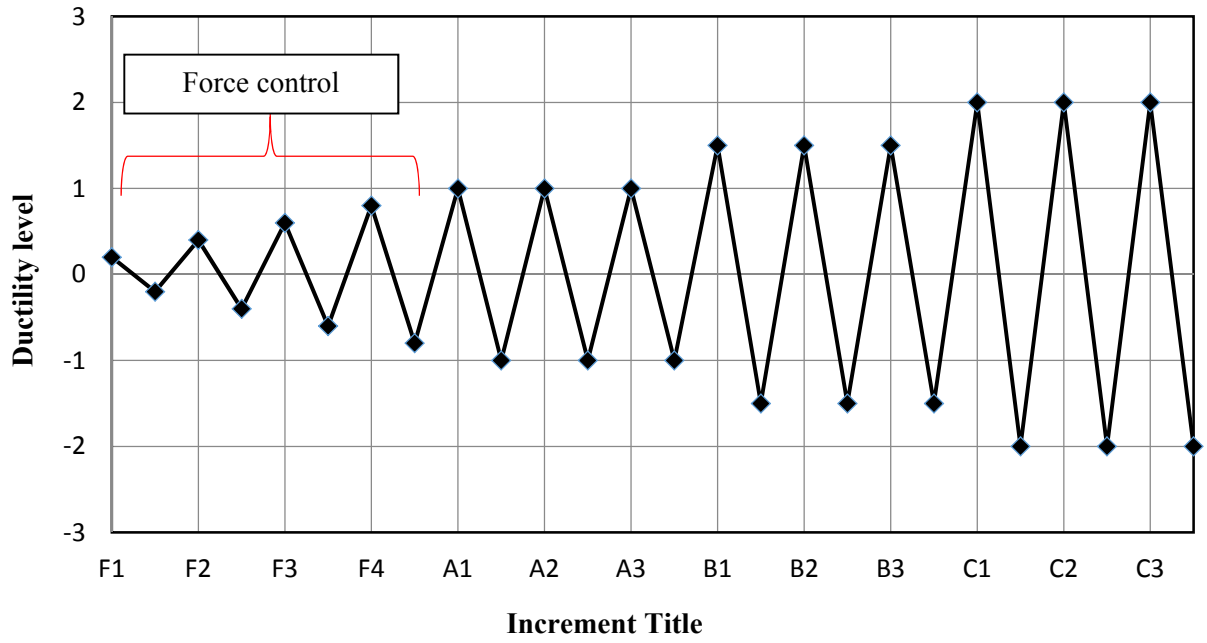


Figure 4-11: Loading history selected for testing

CHAPTER 5 EXPERIMENTAL AND ANALYTICAL RESULTS

5.1 Fiber-based modelling method

All test specimens were modeled using OpenSees (McKenna et al., 2000) to further determine the ability of the modeling method to accurately describe the response of the specimens. A general description of the analysis and modeling methodology is described in Section 3.3.1.1.1. The element geometry and loading used in this analysis are intended to model the actual testing setup as closely as possible. The element geometry is shown in Figure 5-1, with four force-based nonLinearBeamColumn elements that are capable of modeling nonlinear behavior. Forces were applied at the node locations (shown by arrows in the figure), with the axial load held constant and equal to the applied axial load in the test, and the lateral loads constantly increasing, to represent monotonic loading. Supports were modeled as a roller and pin, allowing axial deformation but restraining all other directional forces.

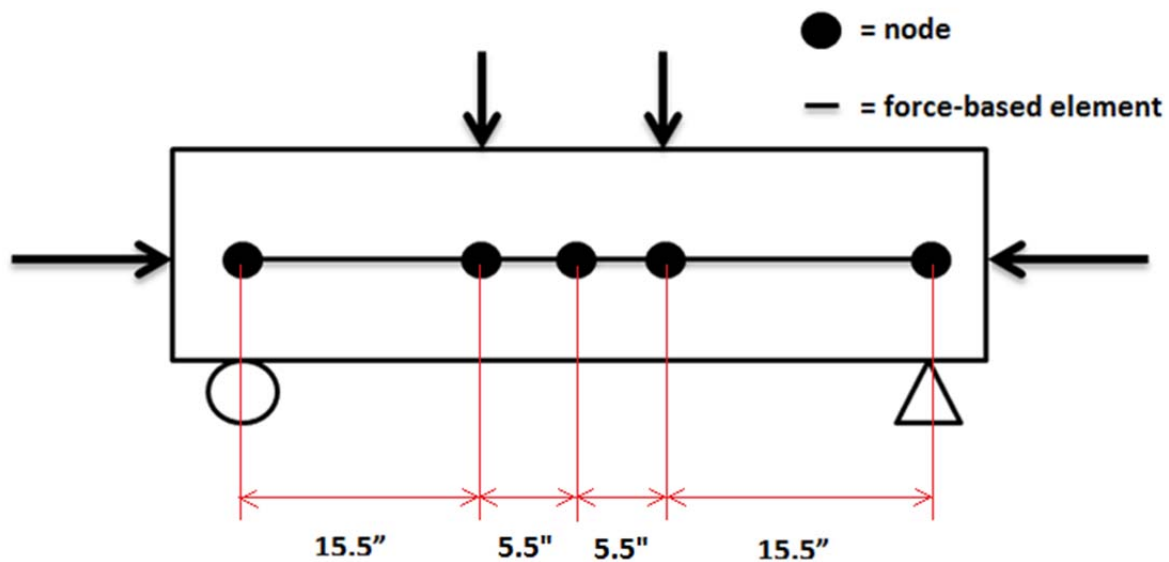


Figure 5-1: Schematic of the OpenSees model representing the test units

For all hollow specimens, two concrete types were considered, which were confined and unconfined concrete. The model by Mander et al. used to determine the confined concrete

behavior, and Concrete07 within OpenSees, was chosen to accurately represent this behavior. Unconfined concrete was provided for the concrete cover and also for the concrete at the inside face near the void if the column was hollow. Near the void the unconfined concrete was only provided half the distance to the location of the transverse reinforcement, with the other half being modeled as confined concrete for hollow columns, as discussed in Section 3.3.1.1.1. Solid columns were modeled as entirely confined concrete within the transverse reinforcement. For hollow columns, the confined concrete was modeled using the adjustment suggested to Mander's model, which was described in Section 3.3.1.1.1. The normal Mander's model procedure was used for solid columns. Longitudinal steel in all cases was modeled using the measured steel properties, and the Steel02 material model was used to apply these properties to the longitudinal reinforcement.

5.1.1 Hollow column section layout

The circular and square hollow columns were modeled using the procedure that was discussed and described in Section 3.3.1.1.1. Figure 5-2 and Figure 5-3 illustrate the general section geometry used, with the hashed areas showing the differentiation of confined and unconfined concrete within the transverse reinforcement. Solid columns had an identical steel layout corresponding to their shape, but the entire area within the transverse reinforcement was modeled as confined concrete. Although shown in the diagrams, transverse steel could not be modeled in OpenSees and the confined concrete properties were instead calculated and defined.

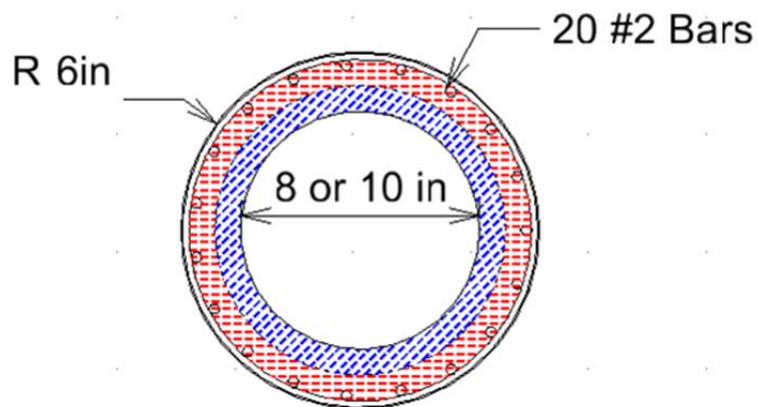


Figure 5-2: General section model for tested hollow circular specimens

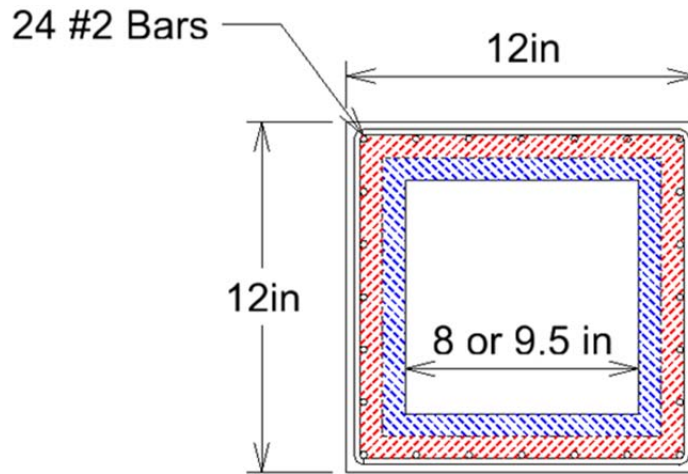


Figure 5-3: General section model for tested hollow square specimens

5.2 Finite element modelling method

5.2.1 Introduction

This section describes the details of the three-dimensional finite element model developed for the test specimens, which included both solid and hollow columns (one-inch wall and two-inch wall) confined with one layer of lateral reinforcement placed near the outside concrete wall surface. ABAQUS v6.12 was used for the analyses. Similar to the analytical analyses performed on the confinement effect, two elements types were primarily used in the development of the model: C3D8R and T3D2. The lateral reinforcement was 0.208 inches in diameter with 1 inch spacing along the entire height of the specimens. The longitudinal reinforcement was 0.25 inches in diameter and was uniformly distributed around the outer perimeter of the specimen. The bond between the reinforcement and surrounding concrete was modeled as an embedded region in ABAQUS, and the default values suggested by the software were used. The input material properties were defined based on the measured experimental properties, and the response was analyzed using the implicit static general solution.

5.2.2 Material model

5.2.2.1 Concrete

As discussed in Chapter 3 Section 2.2, the damaged plasticity model is the most accurate among the three concrete models available in ABAQUS, because it incorporated two damage variables, one for compression (compressive crushing) and one for tension (tensile cracking), to model the stiffness degradation during the inelastic action of concrete. The damage plasticity concrete model, with a concrete strength of 6500 psi (the measured concrete strength at the testing day), was used to model the concrete behavior in the plastic range. The elastic portion of the concrete curve was defined with the Young's Modulus and Poisson's Ratio. The concrete stress-strain behavior under uniaxial compression after elastic range was defined in terms of yield stress versus inelastic strain. This concrete material model could incorporate the confining effects of lateral reinforcement by defining the post-yielding response (yield stresses and inelastic strains) parallel to the Mander et al.'s model. Validation of this capacity was presented in Chapter 3, Section 2.5.1. Concrete behavior under uniaxial tension was assumed to be linear until forming the initial macroscopic cracks at the peak stress. A solid element (C3D8R), with eight nodes and three translational degrees of freedom at each node, was used to model the concrete elements. The input concrete properties are present in Appendix 8.3.

5.2.2.2 Steel reinforcement

Longitudinal and transverse steel reinforcement behavior were defined as a general elastic-plastic material model using a bilinear curve. The elastic portion of the steel response was defined by providing values for Young's modulus and Poisson's Ratio. For the post-yielding response, four points were defined to capture the actual behavior of reinforcing steel used in the test specimens, including yielding and rupture. A truss element, called T3D2, was assigned to the reinforcement elements. This element has two nodes with three translational degrees of freedom at each node. The Embedded Region option was used for connecting reinforcement elements to the surrounding concrete. This option could constrain translational degrees of freedom of the embedded element nodes (steel reinforcement) to the degrees of freedom of the set of surrounding element nodes called the host elements (concrete). The input steel properties are present in Appendix 8.3.

5.2.3 Boundary conditions

Due to double symmetry, only quarter of the entire section was modeled to reduce the computational costs. X and Z symmetric boundary conditions were applied in the plan normal to the x and z direction, respectively. The tested columns were simply supported at two ends with a 3 inches overhang length. In order to simulate the experimental tests realistically, the general analyses were divided into two steps as shown in Figure 5-4:

Step 1: Apply the x and z symmetric boundary conditions, simply support boundary condition, and the axial load.

Step 2: Apply the lateral load (under displacement control); the symmetric boundary conditions, simply support boundary condition and the axial load were propagated from the step 1.

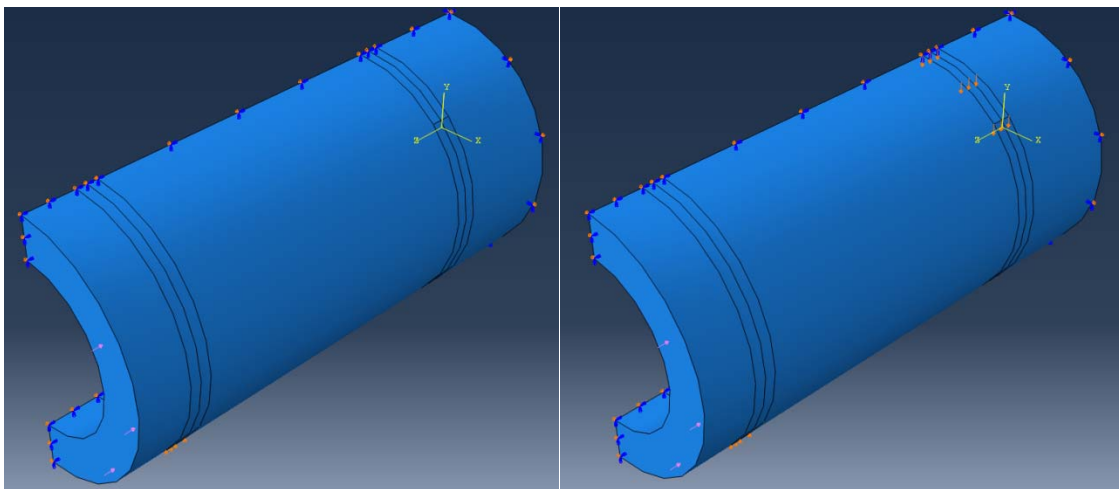


Figure 5-4: Analyses steps in ABAQUS

5.2.4 FEM results

The FEM results were discussed for the circular solid/hollow columns as well as the square solid/hollow columns in this section. The comparisons among the FEM results, the experimental results and the predictions based on the fiber-based analyses will be described in detail in section 5.3.

5.2.4.1 Circular columns

5.2.4.1.1 Solid columns

The failure of the solid circular columns was dominated by the rupture of longitudinal reinforcement at 0.02 in/in tensile strain. Figure 5-5 shows the behavior comparisons between the circular solid columns under 22.6 kips axial load and 45.2 kips axial load. According to this figure, the column unit under the higher axial load (45.2 kips axial load) reaches higher capacity. However, the displacements at the failure point (0.02 in/in tensile strain of longitudinal reinforcement) are around the same (0.48 inches) for both of these two specimens. When the longitudinal reinforcement arrived at 0.02 in/in tensile strain, the concrete compressive strain was 0.0054 in/in for the circular solid column under 22.6 kips axial load. This indicated that when the longitudinal reinforcement reached the ultimate strain, the concrete compressive strain was much smaller than the ultimate compression strain (0.015 in/in) as predicted based on Mander's model.

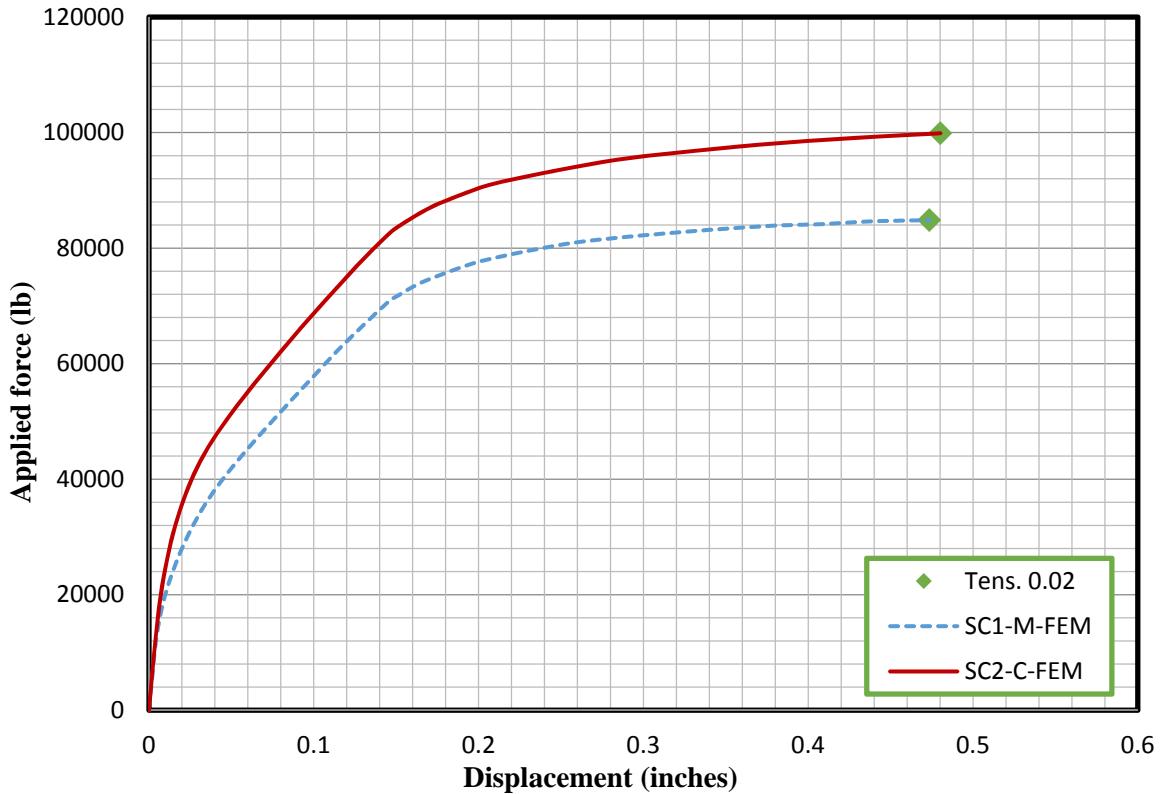


Figure 5-5: FEM results comparisons between circular solid columns under 22.6 kips axial load and 45.2 kips axial load

5.2.4.1.2 Two-inch wall hollow column

For the two-inch wall circular hollow columns, the failure was also dominated by the rupture of longitudinal reinforcement at 0.02 in/in strain. The inside concrete wall crushing (0.005 in/in) occurred after the rupture of longitudinal reinforcement. For the two-inch wall hollow column under 22.6 kips axial load, as the longitudinal reinforcement reached the ultimate tensile strain, the inside concrete wall strain was 0.003 in/in. For the two-inch wall hollow column under 45.2 kips axial load, as the longitudinal reinforcement reached the ultimate tensile strain, the inside concrete wall strain was 0.0046 in/in. Therefore, higher axial load was potentially detrimental for the hollow columns, since the inside concrete wall crushing occurred earlier for the hollow column under higher axial load than that under lower axial load. Figure 5-6 shows the FEM results comparisons between the two-inch wall circular hollow columns under 22.6 kips axial load and 45.2 kips axial load. The two-inch wall hollow column under higher axial load had a higher capacity, but the displacements at the failure point (0.02 in/in longitudinal reinforcement tensile strain) were around the same (0.58 in/in).

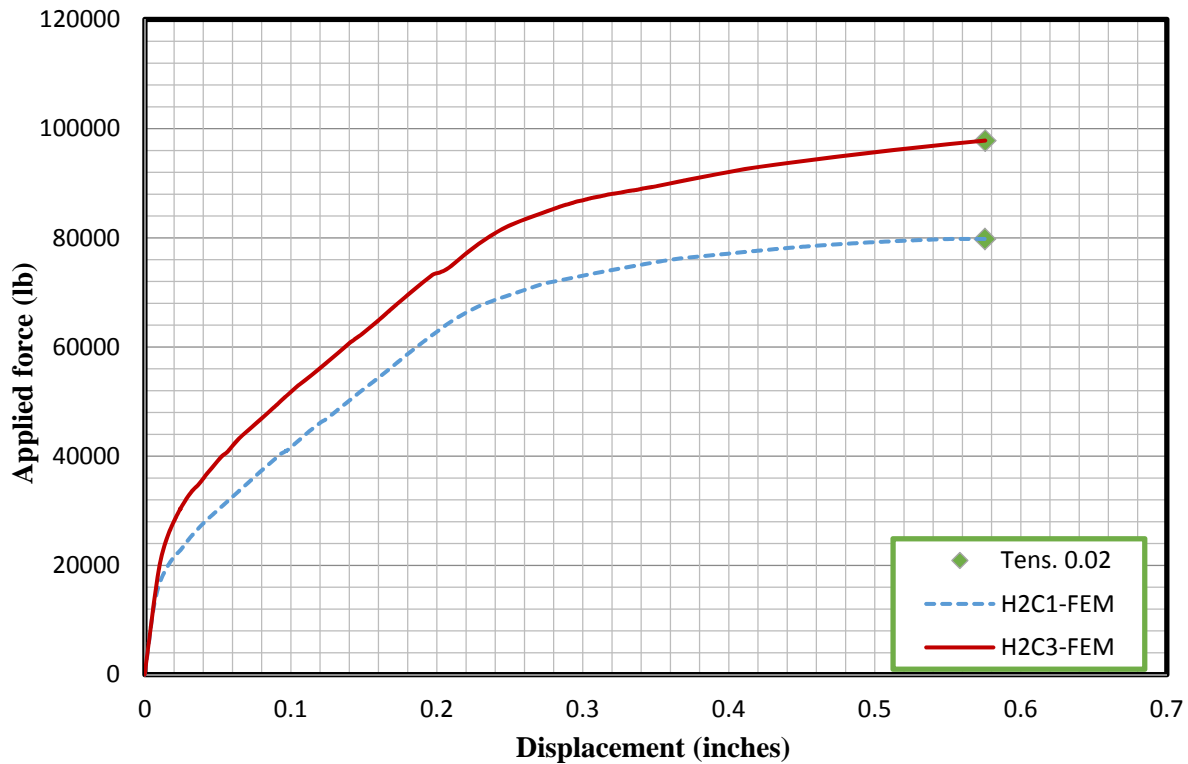


Figure 5-6: FEM results comparisons between two-inch wall circular hollow columns under 22.6 kips axial load and 45.2 kips axial load

5.2.4.1.3 One-inch wall hollow column

For the one-inch wall circular hollow columns, the failure was dominated by the inside face concrete crushing at 0.005 in/in. The one-inch hollow column under 45.2 kips axial load failed prior to that under 22.6 kips axial load (Figure 5-7). The inside concrete face crushing first occurred near the support as shown in Figure 5-8, which was different than the two-inch wall circular hollow column where the inside concrete face in the compression side experienced the largest compressive axial strains (Figure 5-9). The one-inch wall hollow column experienced local failure, which could be observed clearly in Figure 5-10, that the entire hollow column move downward instead of experiencing the curvature as the two-inch wall hollow column which is shown in Figure 5-11. One possible reason that caused this local failure may come from the significant reduced amount of materials for the one-inch hollow column. This would significantly reduce the structural stiffness and lead to local failure at the support.

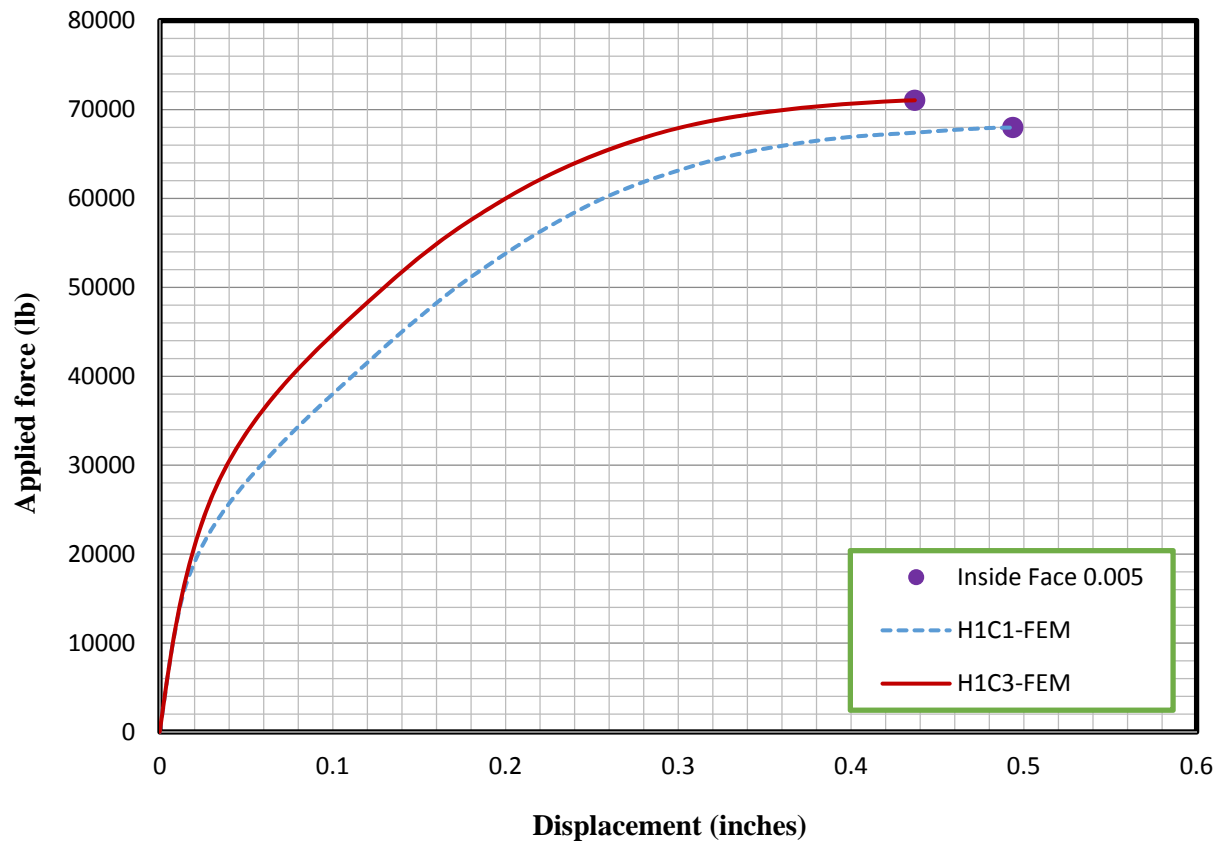


Figure 5-7: FEM results comparisons between one-inch wall circular hollow columns under 22.6 kips axial load and 45.2 kips axial load

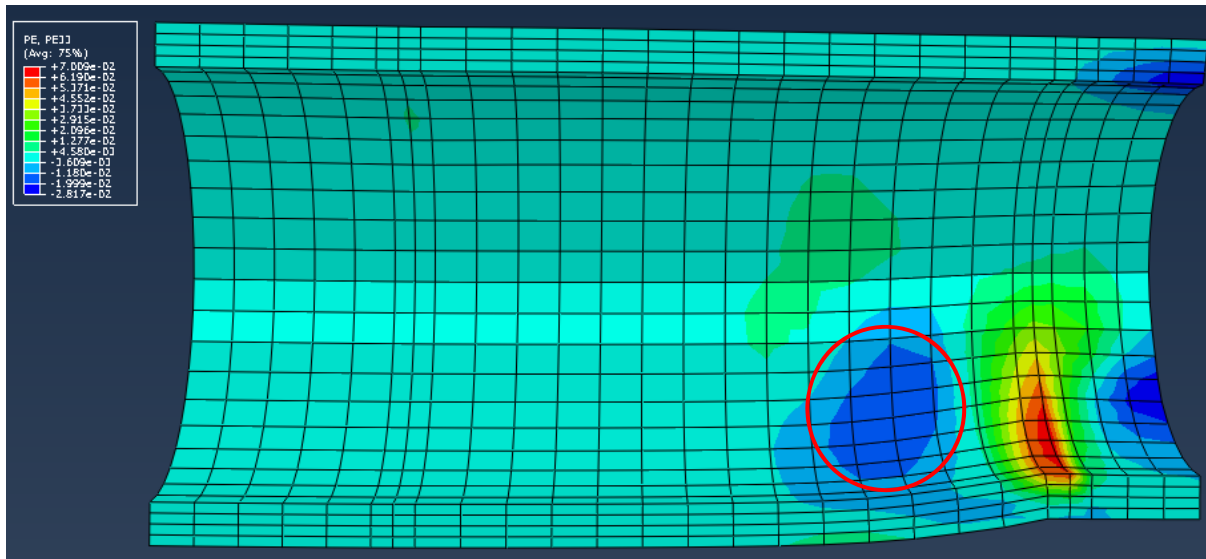


Figure 5-8: The axial compressive plastic concrete strain contour of one-inch wall circular hollow column under 45.2 kips axial load

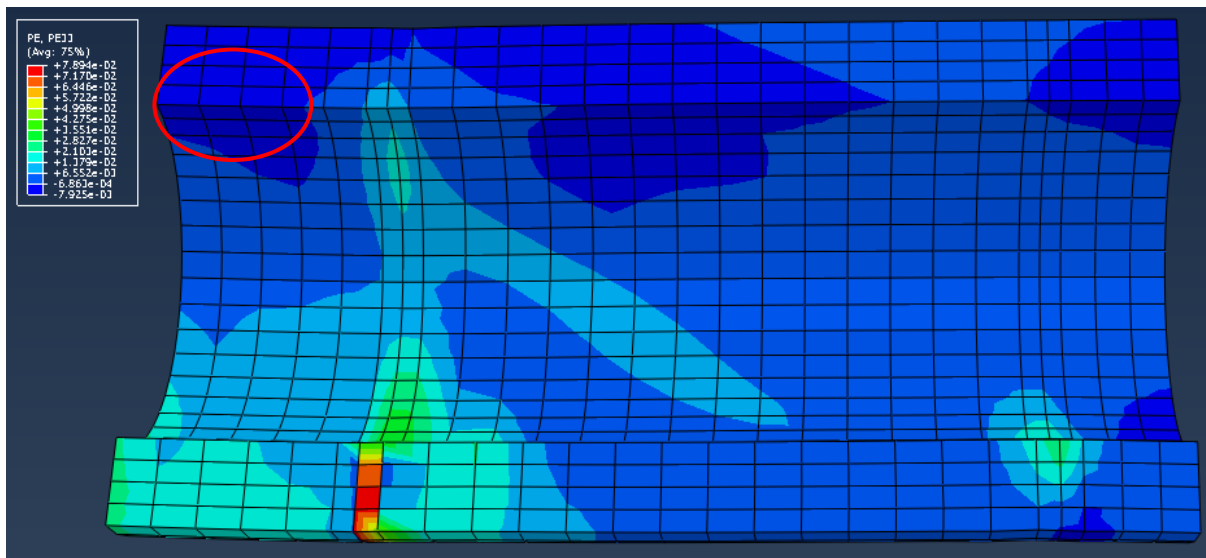


Figure 5-9: The axial compressive plastic concrete strain contour of two-inch wall circular hollow column under 45.2 kips axial load

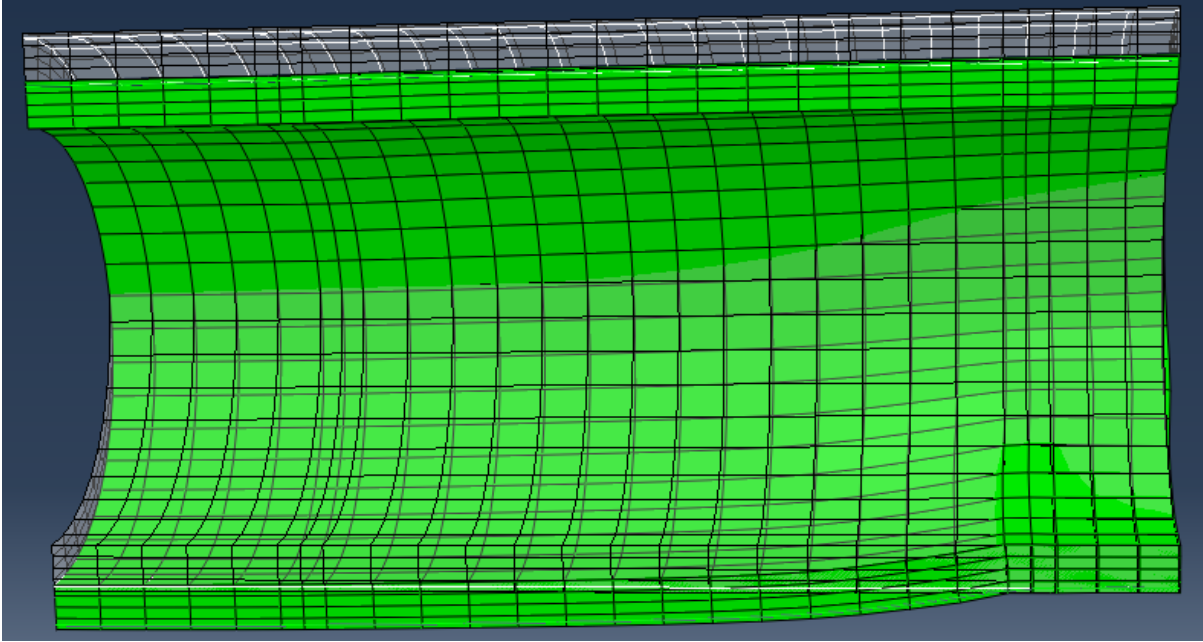


Figure 5-10: The deformed shape of one-inch wall circular hollow column under 45.2 kips axial load

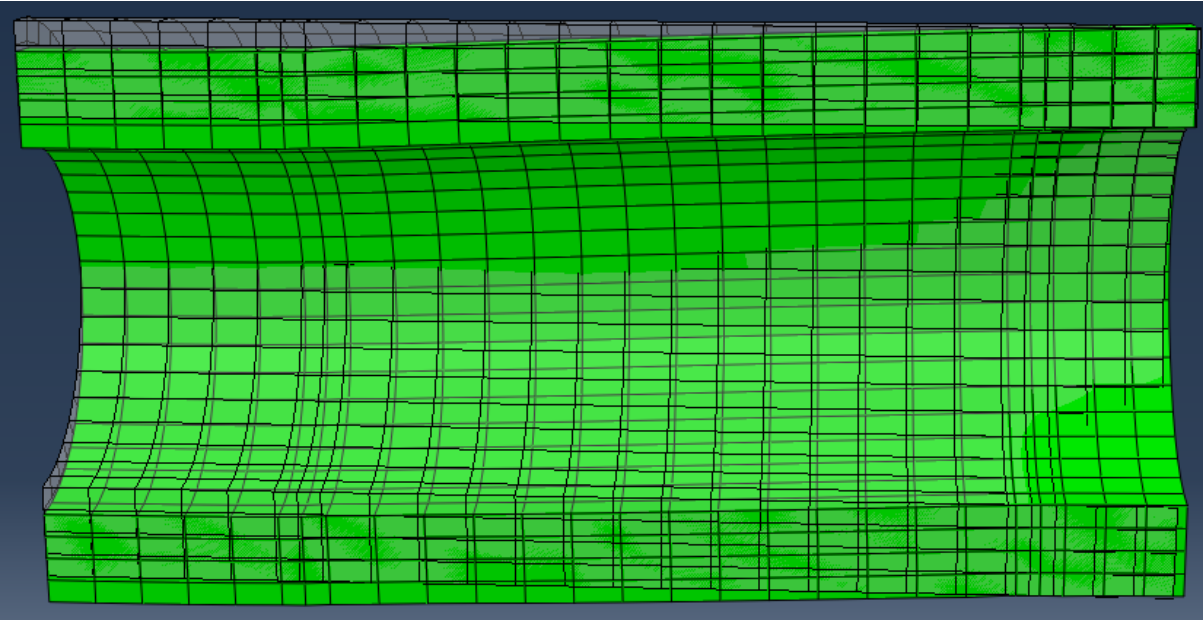


Figure 5-11: The deformed shape of two-inch wall circular hollow column under 45.2 kips axial load

5.2.4.2 Rectangular hollow columns

5.2.4.2.1 Solid column

The failure of the solid square columns was dominated by the rupture of longitudinal reinforcement at 0.02 in/in tensile strain. Figure 5-12 shows the comparisons between the square solid columns under 22.6 kips axial load and 45.2 kips axial load. According to this figure, the column under higher axial load (45.2 kips axial load) reaches higher capacity and higher ultimate displacement that is corresponding to the tensile failure of longitudinal reinforcement. When the longitudinal reinforcement arrived at 0.02 in/in tensile strain, the concrete compressive strain was 0.003 in/in for the square solid column under 28.8 kips axial load. This indicated that when the longitudinal reinforcement reached the ultimate strain, the concrete compressive strain was much smaller than the ultimate compression strain (0.026 in/in) as predicted based on Mander's model.

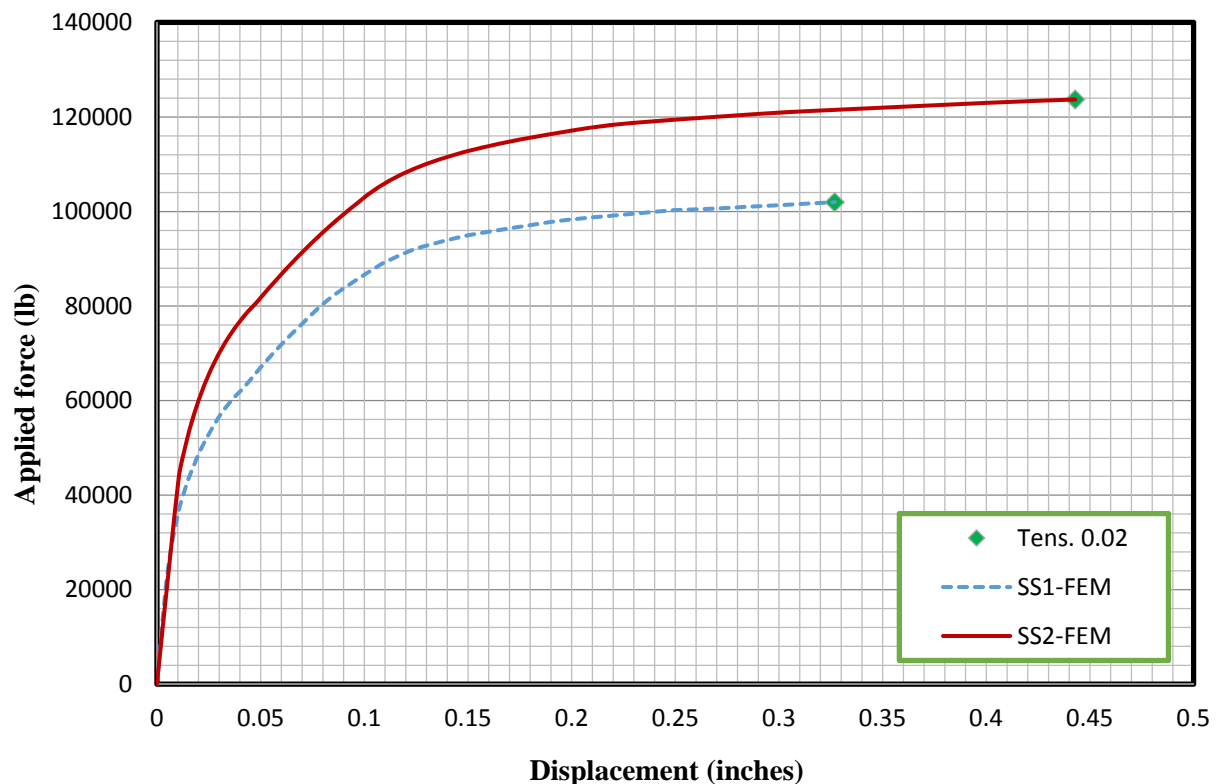


Figure 5-12: FEM results comparisons between square solid columns under 22.6 kips axial load and 45.2 kips axial load

5.2.4.2.2 Two-inch wall hollow column

For the two-inch wall square hollow columns, the analyses ran into convergence problems before failure occurred, although the stabilization option was incorporated into the analyses. The convergence problems may have come from the confinement effect for the two-inch wall square hollow section with a single layer of confinement reinforcement placed near the outside concrete wall, which required further investigations. Similar confinement analyses that have conducted for the circular hollow section described in Section 3.2, is expected for the square hollow section in future studies.

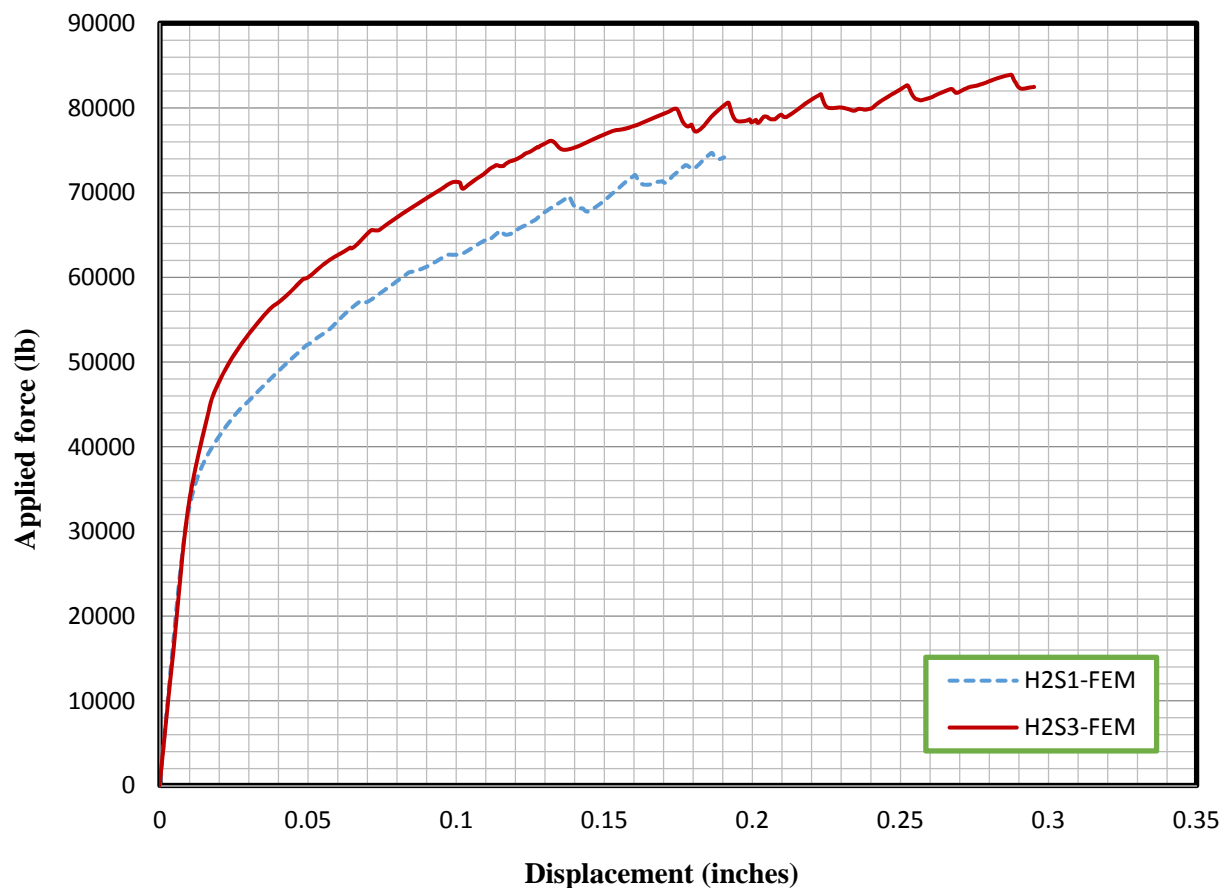


Figure 5-13: FEM results comparisons between two-inch wall square hollow columns under 22.6 kips axial load and 45.2 kips axial load

5.2.4.2.3 One-inch wall hollow column

Same as the two-inch wall square hollow columns, the stabilization option was also incorporated in the analyses for the one-inch square hollow columns in order to achieve better and easier

convergence. However, no failures were observed before the program could not converge any more.

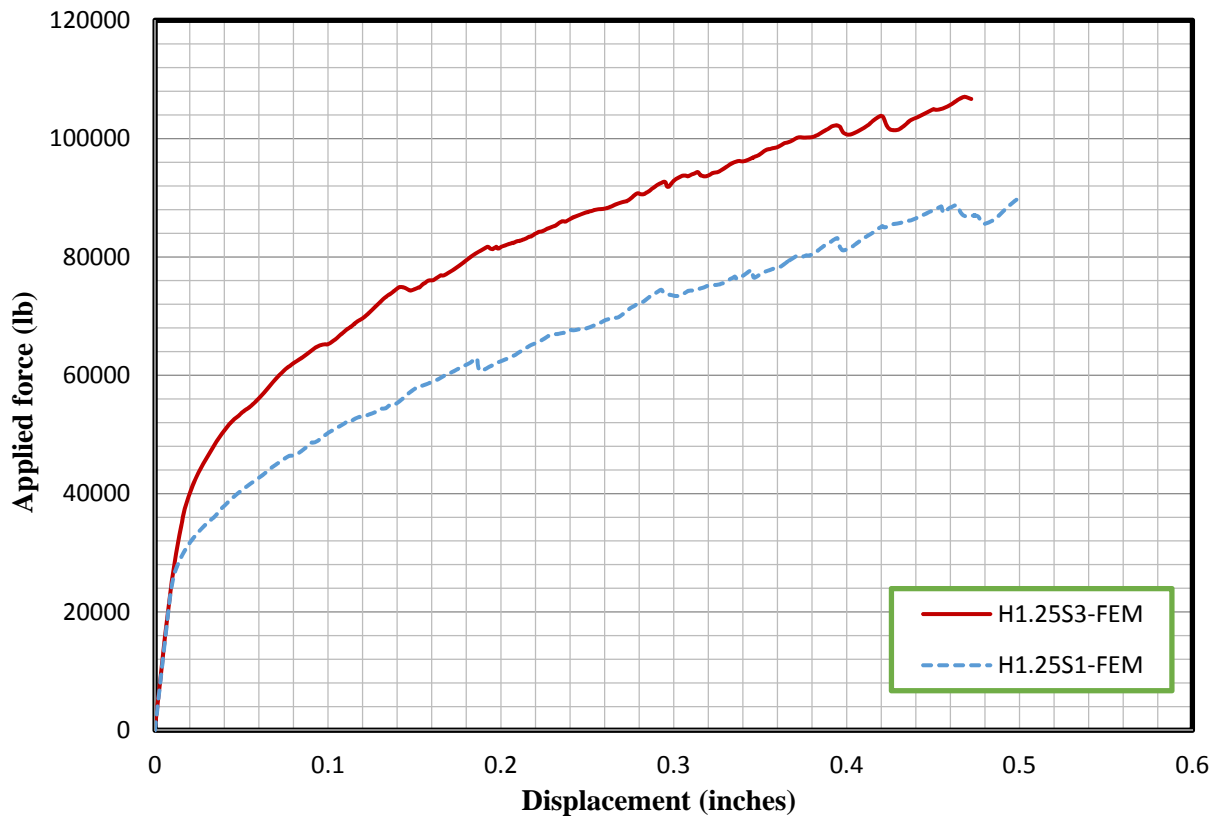


Figure 5-14: FEM results comparisons between one-inch wall square hollow columns under 22.6 kips axial load and 45.2 kips axial load

5.3 Comparisons between analyses results and experimental results

5.3.1 Circular section

The results of the circular tests are described in the following sections. The solid specimens and the two-inch thick specimens had satisfactory results, while the one-inch thick specimens experienced premature local and shear failures. These local and shear failures are suspected to be due to the small wall thickness combined with some of these areas needing concrete patching or due to poor consolidation within the small wall thickness. The solid and two-inch thick specimens had good concrete and did not require any patching, and thus the focus is placed more on these specimens.

5.3.1.1 Visual observations of circular specimens

SC1-M

Specimen SC1-M was loaded monotonically until failure. This specimen is the only specimen that was loaded using a SATEC uni-axial testing machine and therefore used a different setup than the other specimens. Additionally, the axial load was applied to this specimen through manual tightening of the nuts on each threaded rod through the end beams. The axial load was applied to all other specimens through the use of a hydraulic actuator. For this reason, the axial load for this specimen did not remain constant and crept up from 22.6 kips to approximately 40 kips by the end of the testing.

The load was applied monotonically, with pauses at predetermined points in order to inspect the critical region and mark cracks. Minor shear cracks first appeared in the linear moment region at approximately 36 kips of applied load, as well as minor flexural cracks in the constant moment region. The shear cracks gradually continued to increase in number and length throughout the testing, although they remained fairly small. Several flexural cracks appeared in the tension region, following the shrinkage cracks which were present after casting due to the small amount of concrete cover over the transverse reinforcement. These cracks continued to widen throughout the test. As the specimen failed, one of the flexural cracks widened a large amount and the specimen lost load capacity due to rupture of longitudinal reinforcement. The specimen failure occurred due to rupture of the longitudinal reinforcement, which was not unexpected due to the lower tensile ultimate strain of the reinforcement. The axial load was maintained throughout failure and did not drop. The cover concrete near the compression face crushed slightly after failure of the specimen occurred.

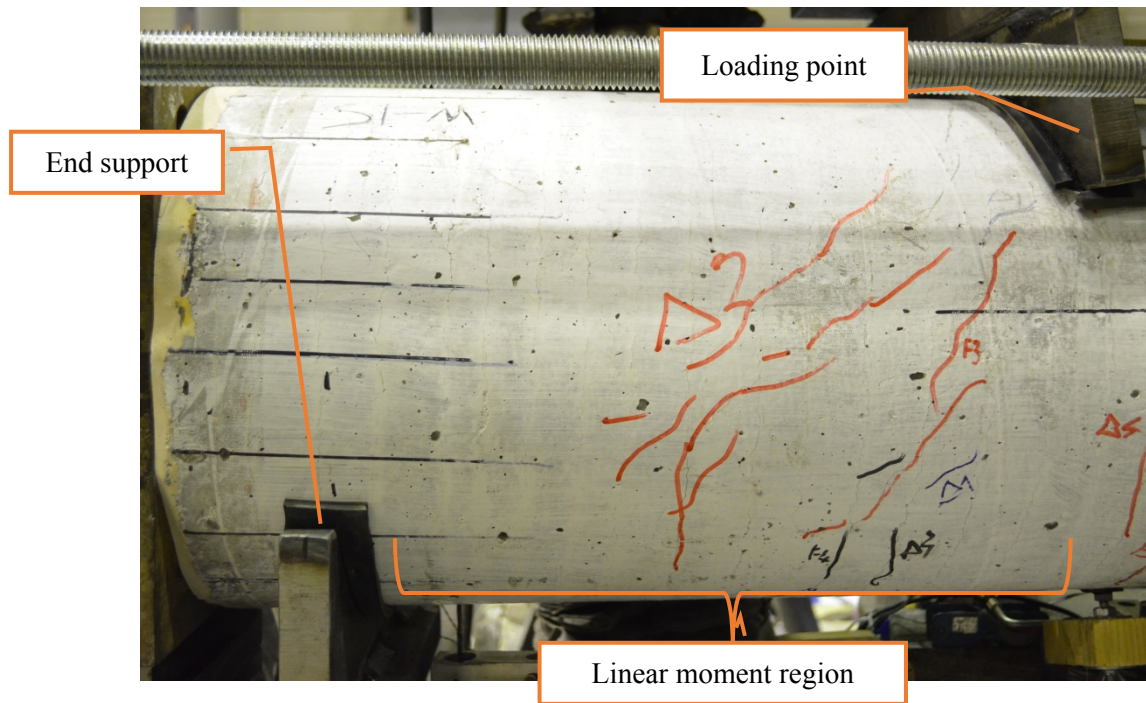


Figure 5-15: Specimen SC1-M shear cracking at peak displacement

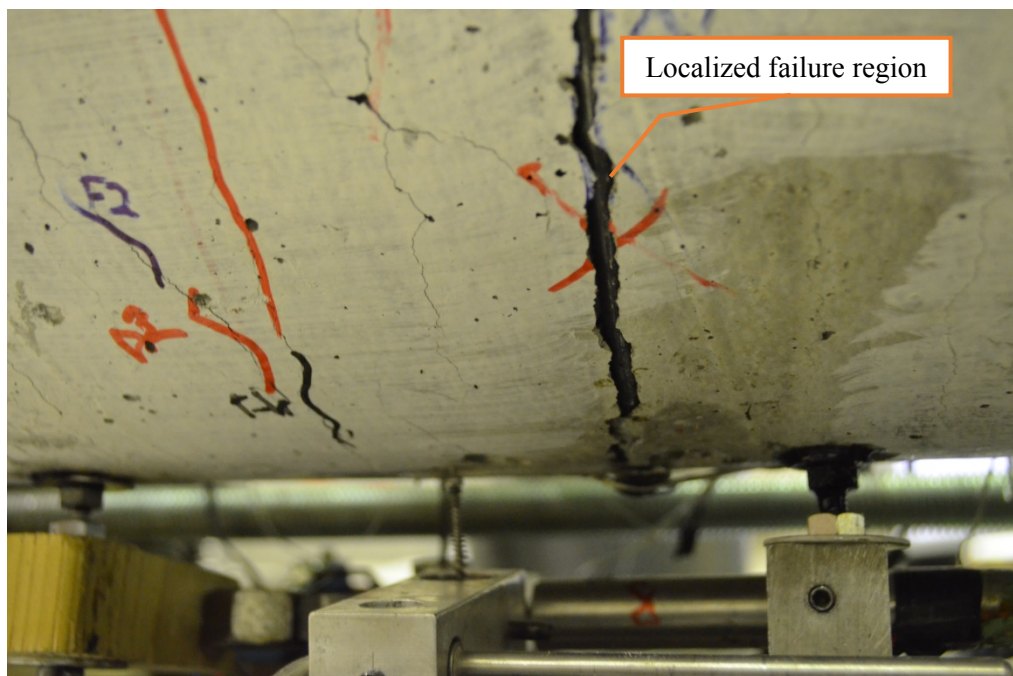


Figure 5-16: Large flexural crack in Specimen SC1-M at end of test

SC2-C

Specimen SC2-C was loaded cyclically using the frame, which was specifically designed for this testing. Three cycles were performed in the linear range in equal force increments until first yield of the longitudinal reinforcement was observed. After the first yield, three cycles were performed at increments based on ductility levels until specimen failure occurred. The specimen was tested under the target axial load of 45.2 kips, which was held constant during the test. Slight shear cracking in the linear moment region and flexural shrinkage crack widening in the constant moment region occurred near the first yield of the tension steel. More shear cracks appeared and flexural cracks continued to widen as the loading continued, and these crack patterns can be seen in Figure 5-17. The cover concrete crushed slightly during the second cycle near ductility level 1.5. During the cycles near displacement ductility level two, the cover concrete began spalling and flexural cracks grew much wider. During the first cycle to displacement ductility level three, the specimen failed due to tension steel rupture, and a large flexural crack opened up. This failure was not unexpected due to the low ultimate tensile strain of the longitudinal reinforcement.

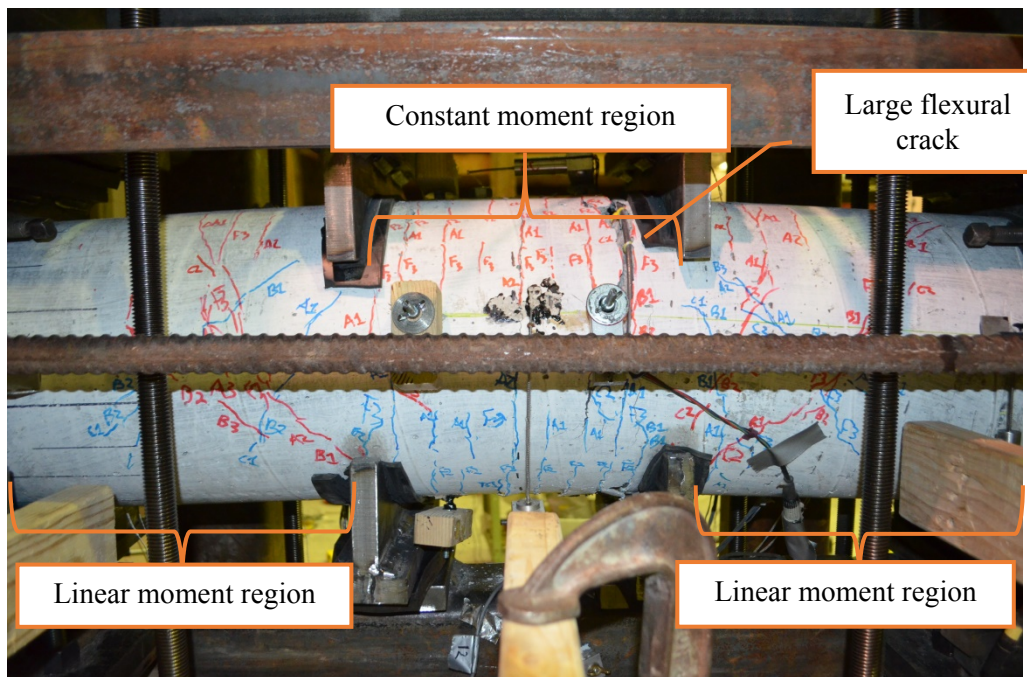


Figure 5-17: Specimen SC2-C after flexural failure

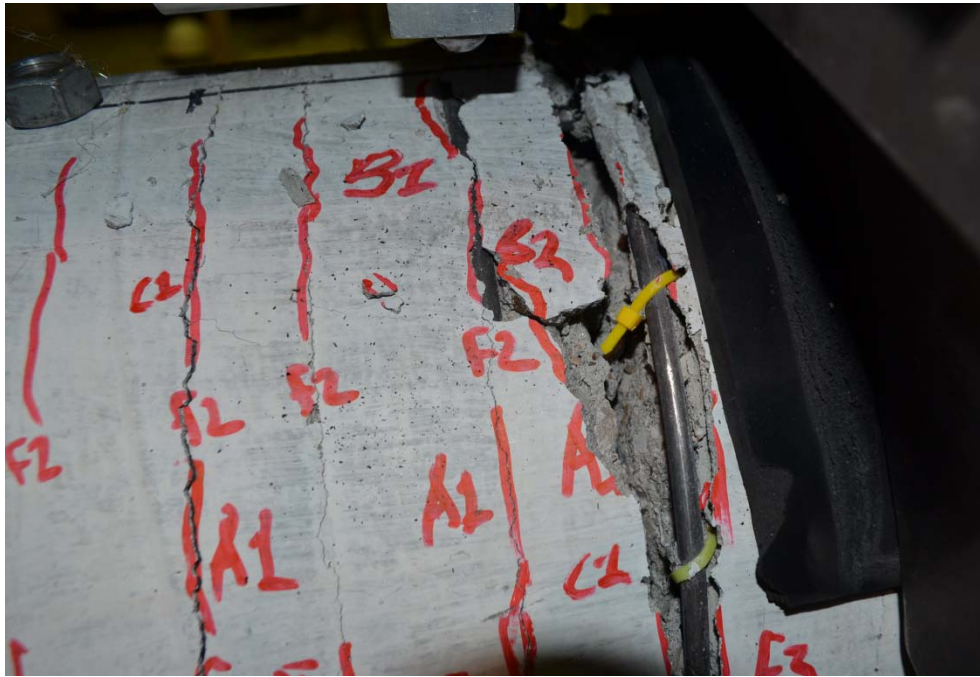


Figure 5-18: Close-up view of large flexural crack in Specimen SC2-C

H2C1-M

Specimen H2C1-M was tested monotonically until failure under the target axial load of 22.6 kips, which was held constant throughout the test. In the second increment in the force controlled cycles, shear cracks began to appear in the linear moment region, and flexural crack widening occurred in the constant moment region. The length and amount of small shear cracks continued to grow throughout the testing. The flexural cracks followed the shrinkage crack locations and continued to widen these cracks. The specimen failed on the push to displacement ductility three, and one of the flexural cracks widened significantly as the tension steel failed due to the low ultimate steel strain. Minor crushing of concrete cover was seen at the compression face after failure.

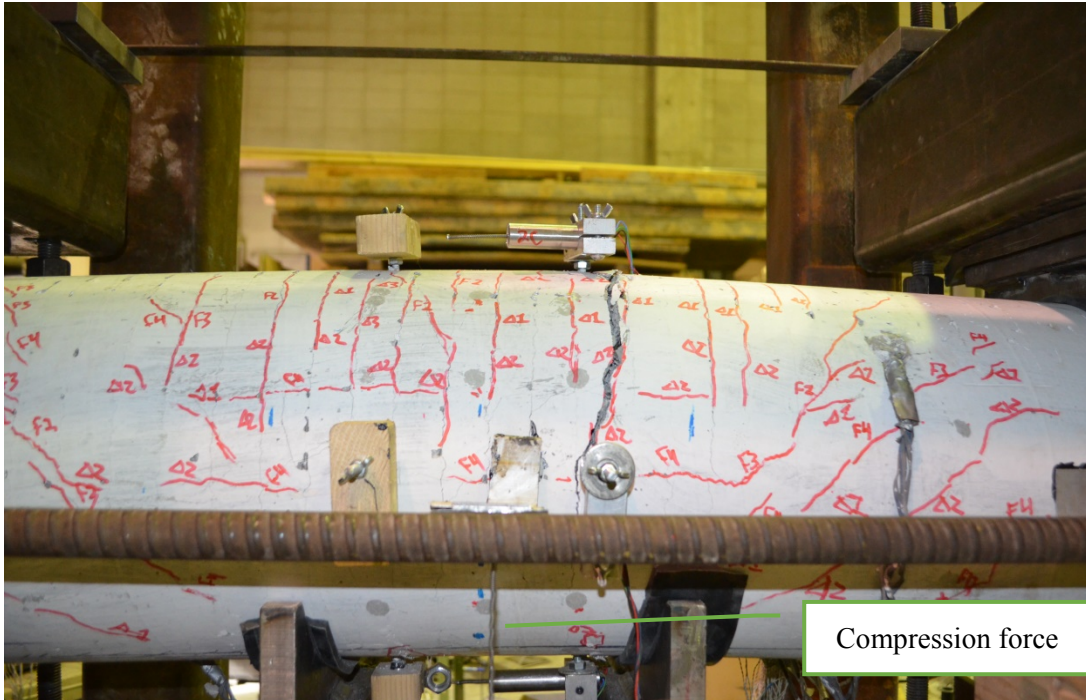


Figure 5-19 - Specimen H2C1-M after tension steel failure

The inside face concrete remained undamaged due to compression after the specimen failed. The inside face concrete before and after testing is shown in Figure 5-20. The images show the inside face concrete in the constant moment region at the extreme compression face.



a) Before testing

b) After specimen failure

Figure 5-20: Inside face at the compression face in the constant moment region of Specimen H2C1-M before and after testing

H2C2-C

Specimen H2C2-C was tested cyclically until failure under 22.6 kips axial load which was held constant throughout the test. Minor shear cracks began to appear in the second cycle in the linear range, as well as flexural widening of the shrinkage cracks. The amount and length of the shear cracks continued to increase, and the flexural cracks widened. Slight cover concrete crushing occurred in the first cycle at displacement ductility one. Tension steel rupture occurred on the first push to displacement ductility 1.5, and one of the flexural cracks widened significantly. The inside face extreme compression concrete did not experience damage for either loading direction.

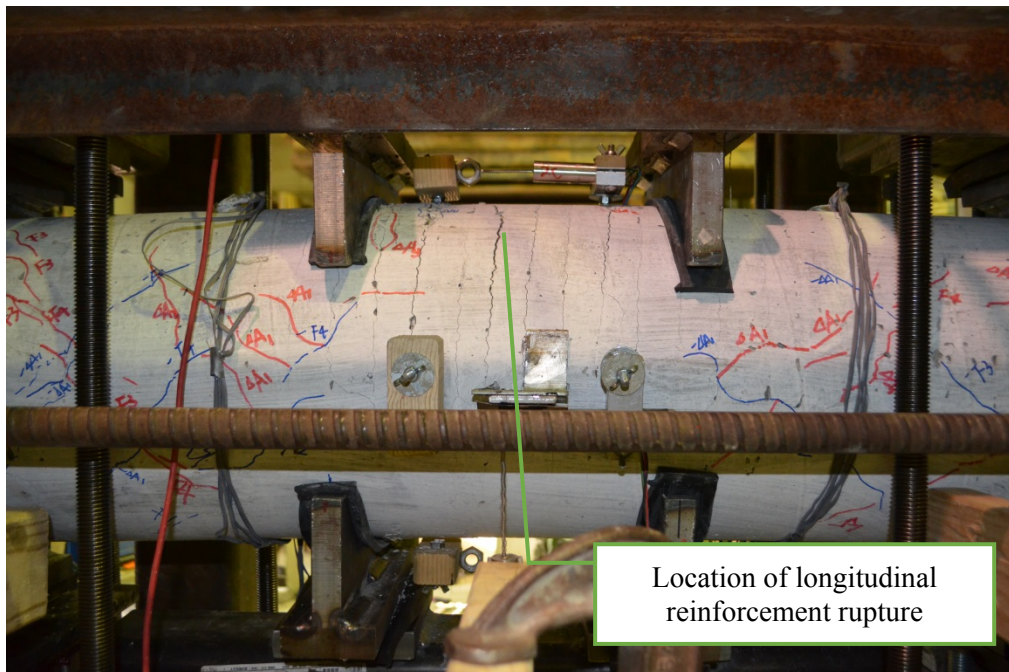


Figure 5-21: Specimen H2C2-C after failure

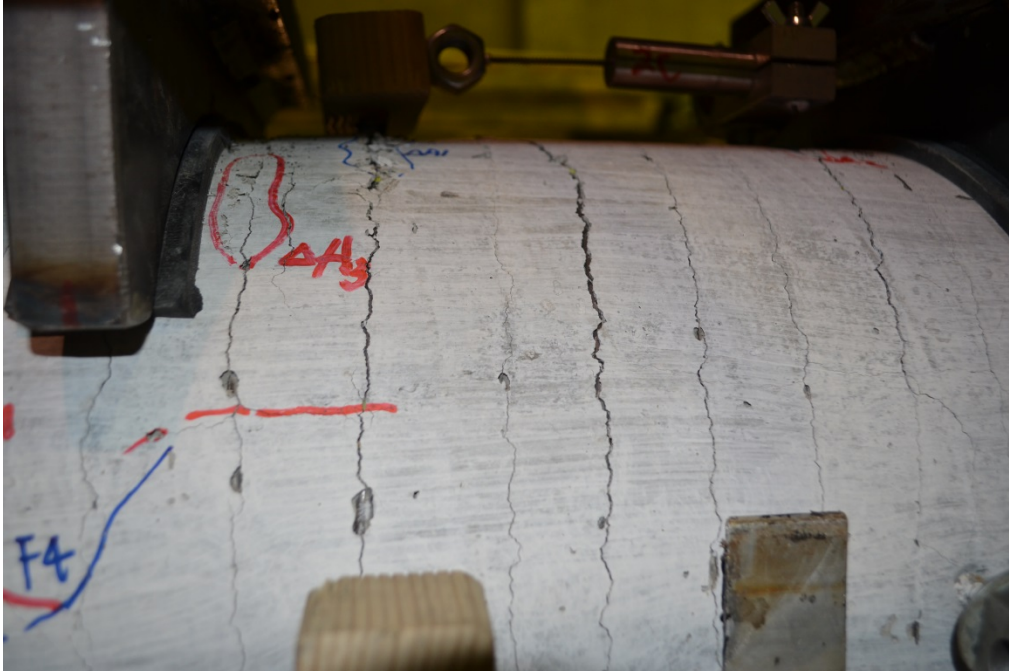


Figure 5-22: Close-up view of flexural cracks in Specimen H2C2-C after failure



Figure 5-23: Inside face of Specimen H2C2-C in constant moment region under compression

H2C3-C

Specimen H2C3-C was tested under lateral cyclic loading and subjected to the targeted axial load of 45.2 kips, which was held constant until the specimen failed. Minor shear cracking appeared in the linear moment region in the second cycle increment in the force controlled range. Shear cracking continued to increase as loading continued, and the shrinkage cracks began to widen under flexure in the constant moment region. Slight cover concrete crushing occurred in the first cycle at displacement ductility one. Some spalling of cover concrete occurred by the end of the third cycle at displacement ductility one. The specimen failed on the first push to displacement ductility 1.5 due to rupture of tension steel. The inside extreme compression face remained undamaged for both loading directions.

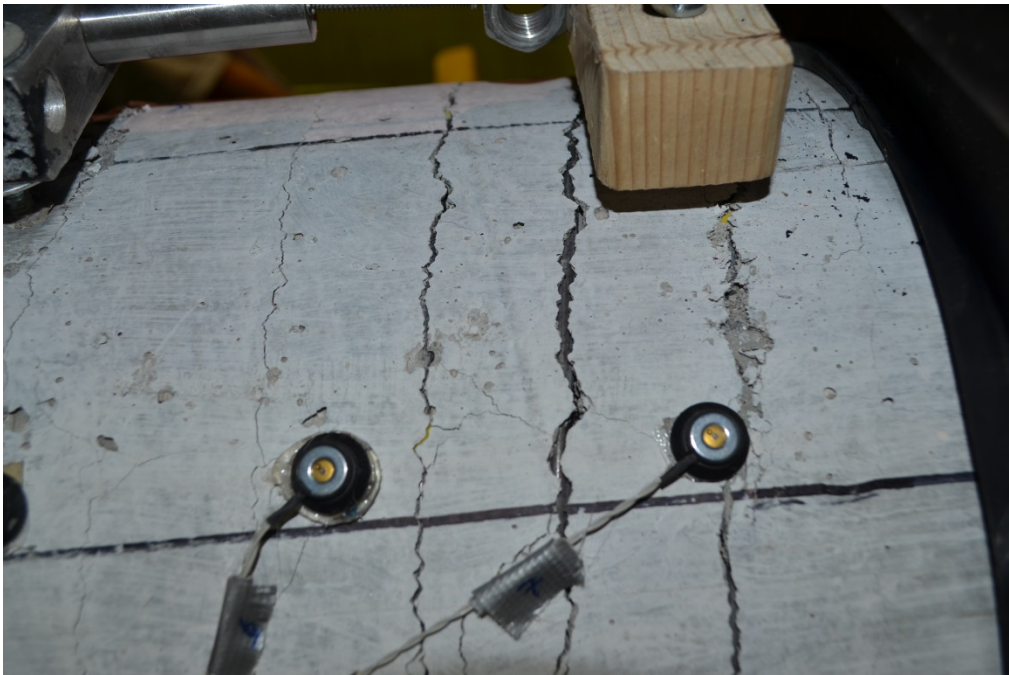


Figure 5-24: Close-up view of flexural cracks in Specimen H2C3-C after failure

H1C1-M

Specimen H1C1-M was tested monotonically under the target axial load of 22.6 kips which was held constant until the specimen failed. Shear cracking occurred in the linear moment region during the second push prior to first yield. Shear cracking continued to grow until failure, with

little flexural cracking visible in the constant moment region. On the way to the predicted first yield point, the specimen failed suddenly near one of the points of load application. There was some local failure near the loading plate which seems to have led into a shear failure at that location. The plate may have begun to punch through the wall, which weakened the specimen and contributed to a shear failure at that location. This punching is suspected to be a result of the very small wall thickness of the specimen. The inside compression face appeared undamaged before the sudden failure of the loading plate pushing through the wall.



Figure 5-25: Specimen H1C1-M shear/local failure at west point of load application

H1C2-C

Specimen H1C2-C was tested under lateral cyclic loading and subjected to the targeted axial load of 22.6 kips, which was held constant until failure. Four pieces of wood were added inside the specimen at the points where the load was applied as well as the supports in an effort to distribute the load more effectively and avoid local failure, as witnessed in H1C1-M. Some slight shear cracking appeared in the linear moment region in the second cycle before reaching the first yield strength. In the third cycle, there was some slight concrete crushing near the support. At the

first yield, there was a large amount of cover spalling in the linear moment region as well as a large number of shear cracks. In the second part of the first yield cycle, the specimen underwent a premature shear type failure, which can be seen in Figure 5-28. The inside face concrete in the constant moment region remained undamaged during the testing.



Figure 5-26: Specimen H1C2-C wooden braces located at load points and support to avoid punching failure



Figure 5-27: Specimen H1C2-C after shear failure



Figure 5-28: Specimen H1C2-C shear failure region

H1C3-C

Specimen H1C3-C was tested under lateral cyclic loading with the target axial load of 45.2 kips applied. Wooden braces were not placed inside this specimen at the loading and support locations because this specimen was tested prior to specimen H1C2-C, and it had not yet been made clear that punching failure could occur commonly for the small wall size. Some minor shear cracking began to appear in the linear moment region during the second cycle in the force-controlled range. On the second half of the second cycle, the specimen experienced a sudden local failure near one of the points of load application, as shown in Figure 5-29. This local failure again appeared to be caused by the loading plate punching through the thin wall of the specimen. There was no damage to the inside face compression concrete before this local failure occurred.

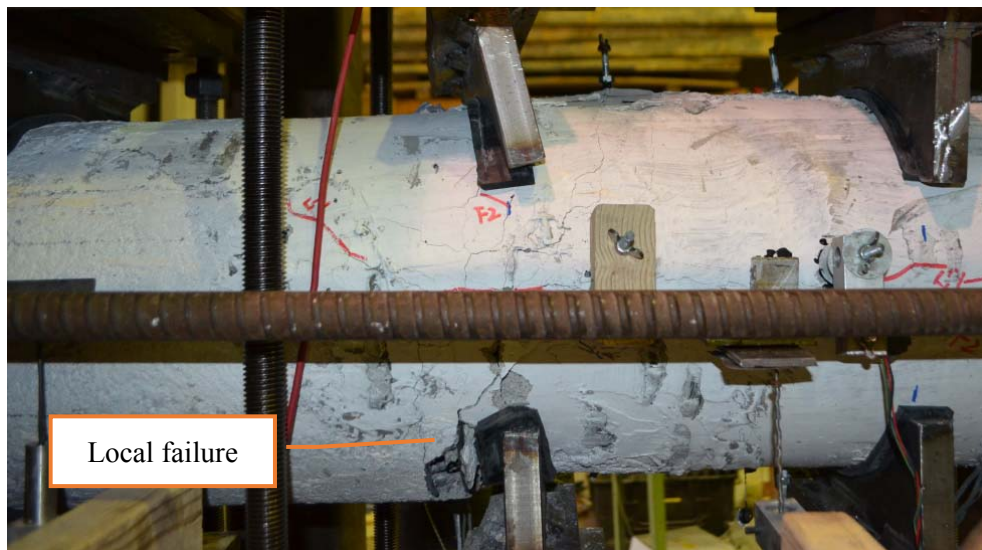


Figure 5-29: Specimen H1C3-C local failure near loading point



Figure 5-30: Close-up of local failure on LED side in Specimen H1C3-C after clearing damaged concrete

5.3.1.2 Circular section test results and comparison to analytical results

5.3.1.2.1 Overall force displacement response

Using the recorded values from the load cells and the measured displacements, the force-displacement response of each test unit was evaluated. The force-displacement response of each specimen can be seen in the figures below, as measured by the LEDs. The force reported is the lateral force supplied to the loading beam by the actuator. For the monotonic tests, only the overall envelop is shown. All of the LED data has been processed to remove outliers and noise. Additionally the force-displacement response of each specimen based on the finite element analyses is also included for comparisons. The experimental results and the finite element analyses shown in this portion include shear deformation as well.

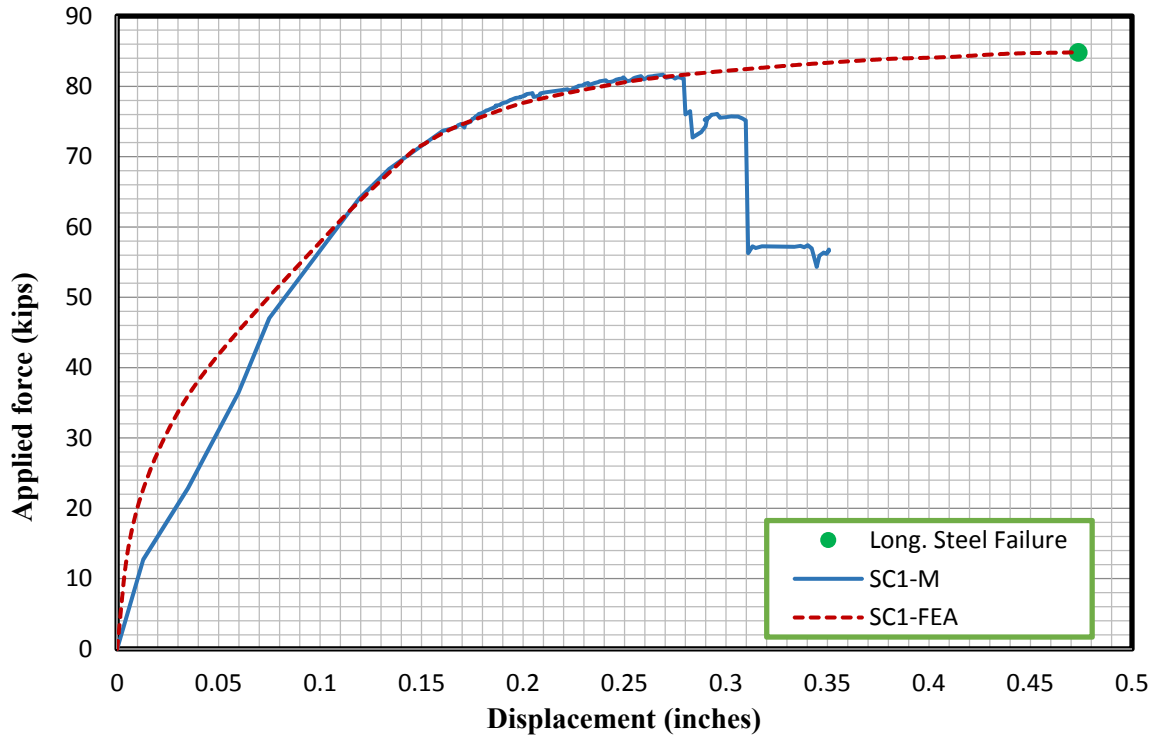


Figure 5-31: Force-displacement response of Test Unit SC1-M

Specimen SC1-M is the only specimen for which the axial load increased during testing as it was tested using a uniaxial machine. This specimen was tested without using a hydraulic actuator to control the axial load levels, so the lateral deformation during loading caused the axial load to increase. It started out at 22.6 kips of axial load, which corresponds to an axial load ratio of three percent, and had reached approximately 40 kips of axial load by the end of the testing, corresponding to an axial load ratio of 5.4 percent. This increase in axial load has been taken into account in OpenSees analysis comparisons, which are presented and discussed in later sections.

The large displacement imposed in Figure 5-35 occurred due to rupture of the longitudinal reinforcement, which resulted in a slight loss of strength capacity and a sudden deformation. As previously described in Section 4.6, the loading applied in the nonlinear region was done by manually targeting displacements. This meant that loss of strength was often associated with a significant increase in displacement as the pressure in the actuator balanced out.

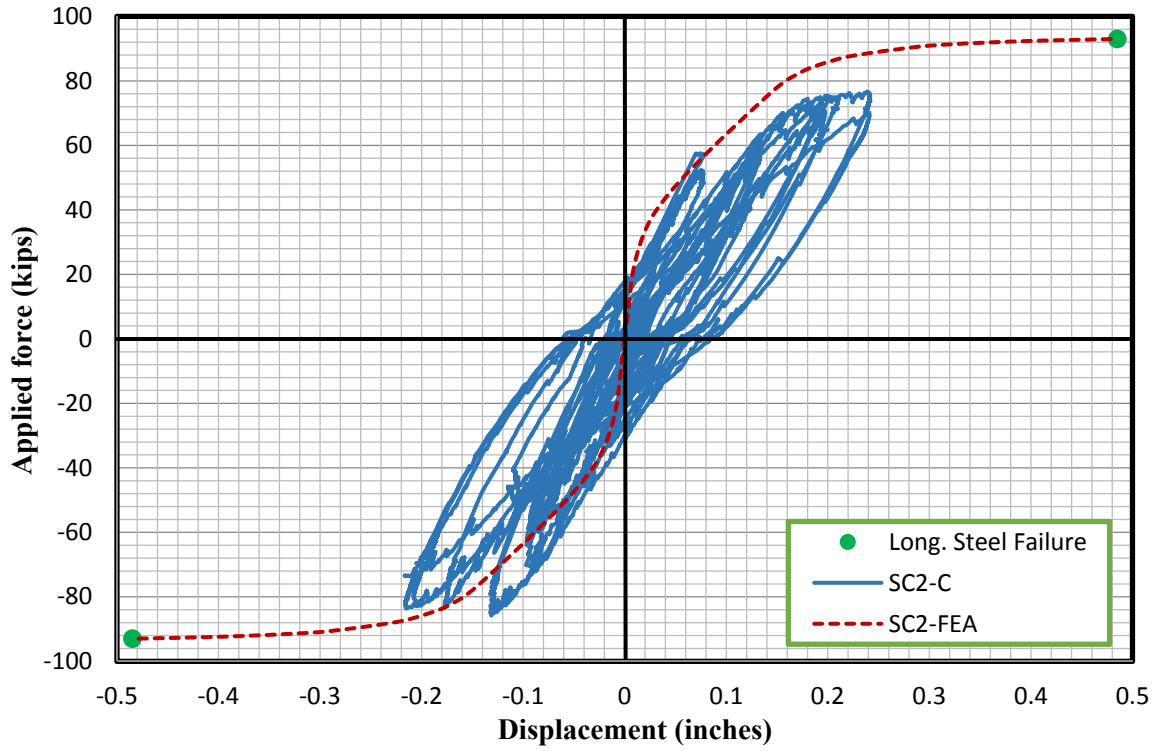


Figure 5-32: Force-displacement response of Test Unit SC2-C

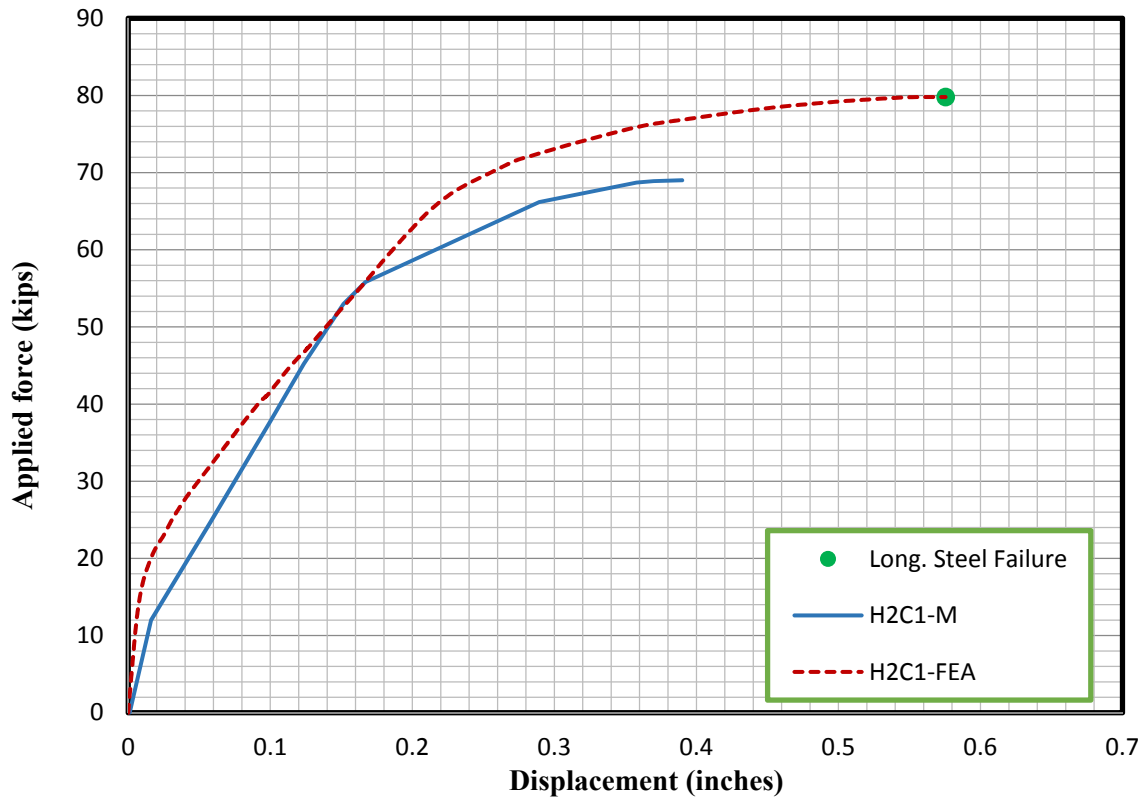


Figure 5-33: Force-displacement response of Test Unit H2C1-M

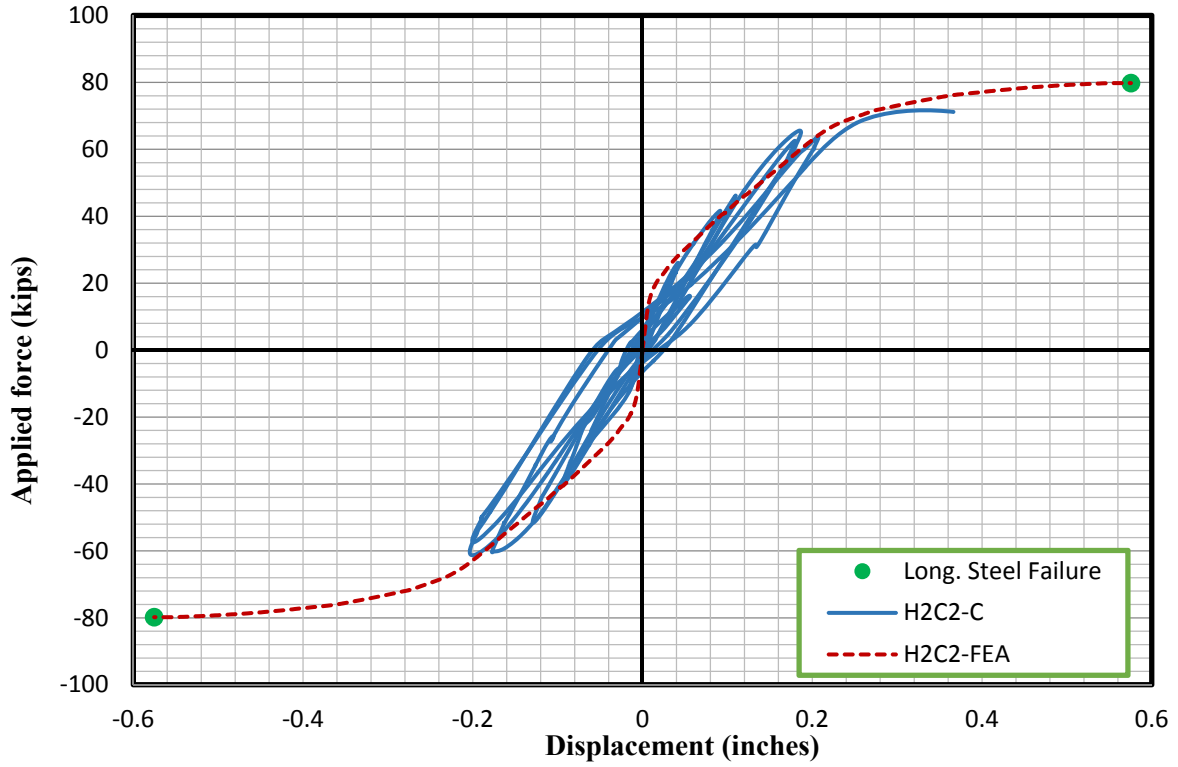


Figure 5-34: Force-displacement response of Test Unit H2C2-C

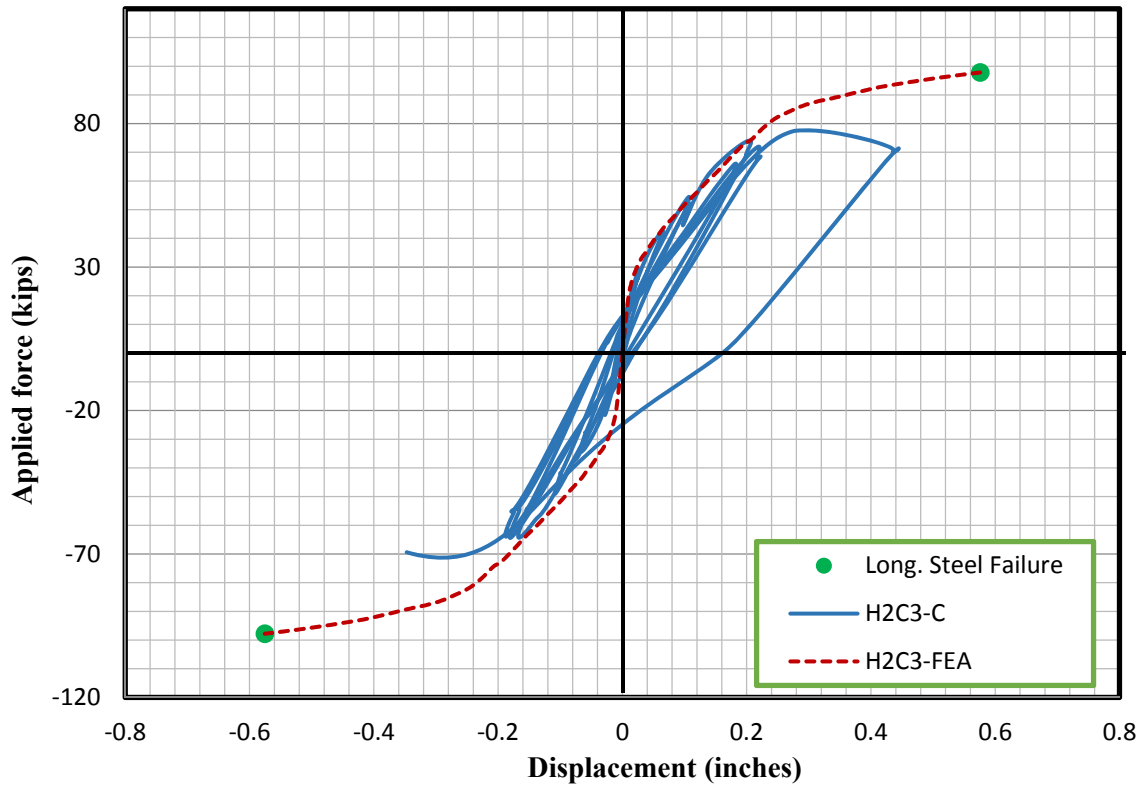


Figure 5-35: Force-displacement response of Test Unit H2C3-C

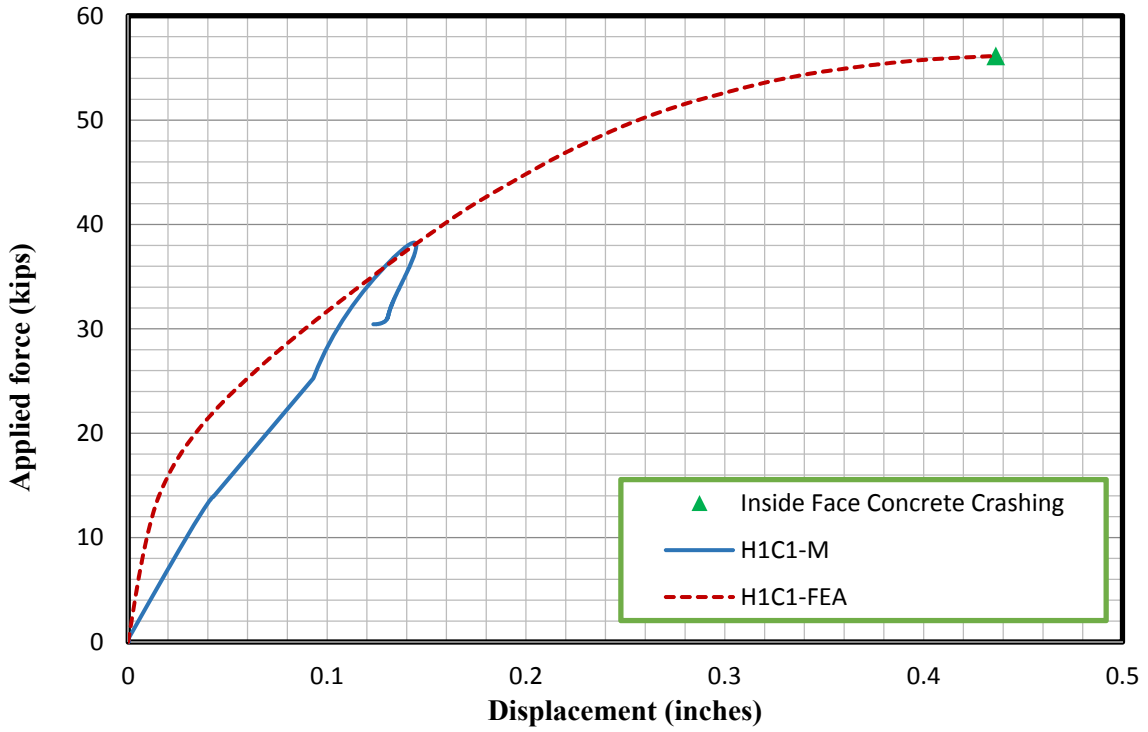


Figure 5-36: Force-displacement response of Test Unit H1C1-M

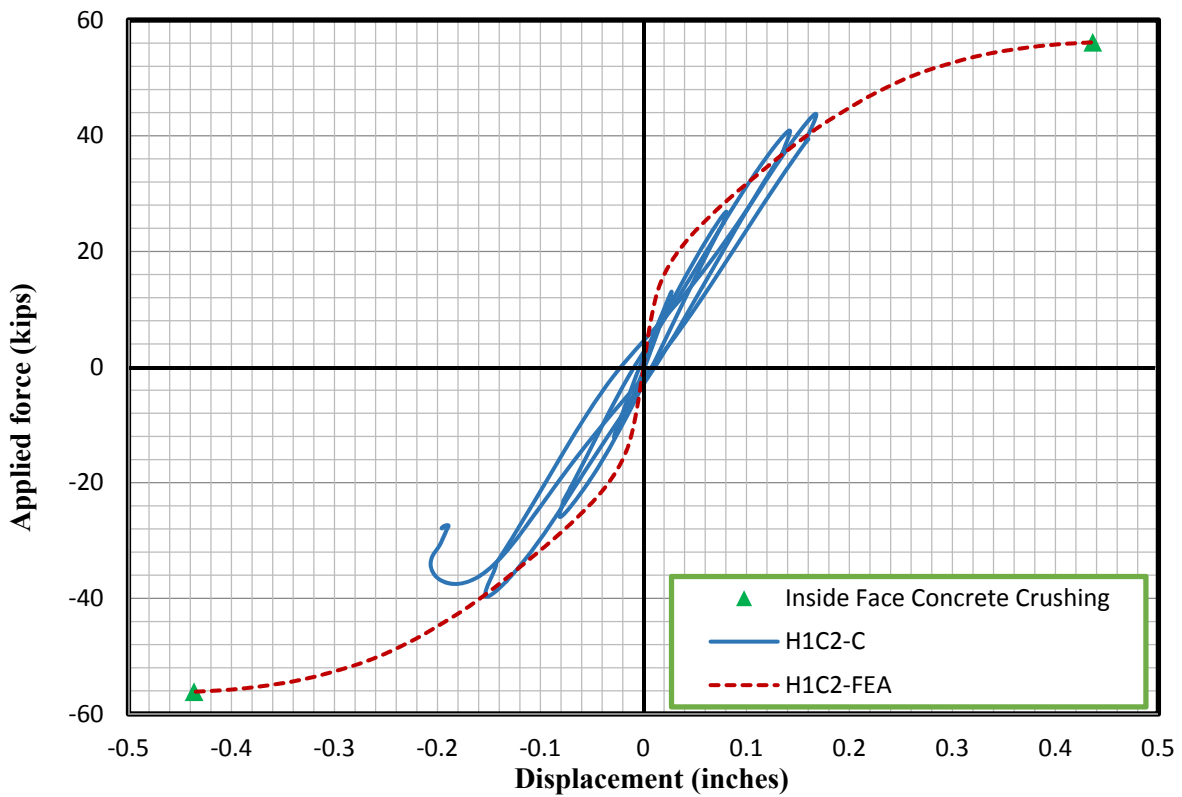


Figure 5-37: Force-displacement response of Test Unit H1C2-C

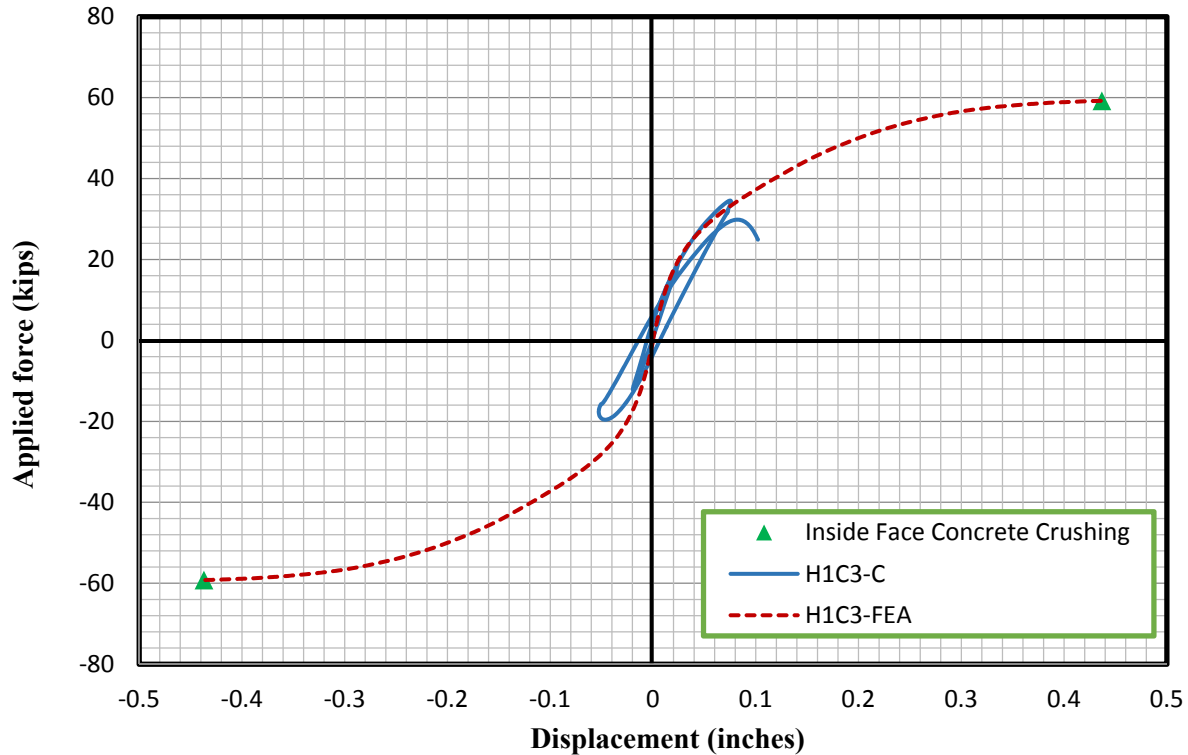


Figure 5-38: Force-displacement response of Test Unit H1C3-C

According to Figure 5-31 through Figure 5-38, the finite element model could relatively capture the experimental test responses satisfactorily, which indicated accepted accuracy for the FEM results, especially for the solid and two-inch wall hollow specimens. Lower stiffness of the test specimens in the initial loading stages compared to the FEM could be explained as the existence of the microscopic cracks in the test specimens due to shrinkage before testing. The tensile strength of the concrete could thus be ignored in the test specimens. However, zero concrete tensile stress was not allowable to achieve convergence in the FE analyses using the concrete damaged plasticity model. The 1.5 square root of f'_c was therefore assumed to be the concrete tensile strength to represent the material property as realistic as possible. This explained the initial greater stiffness of the force-displacement response of specimens based on the FE predictions. The displacement corresponding to the specimen's failure predicted by the FEM was also greater than that experienced by the test specimens. This could also be explained due to the greater concrete tensile strength input in the FEA.

For the one-inch hollow columns, the capacity and the ultimate displacement predicted based on the FE were both greater than those experienced by the test specimens. This was expected due to the premature failure or shear failure experienced by the test specimens, which was discussed in Section 5.3.1.1.

Figure 5-39 shows the force-displacement response comparisons for the solid, two-inch wall and one-inch wall hollow columns under 22.6 kips axial load. As shown, the solid column presents a higher capacity and higher stiffness compared to the hollow specimens. Although the capacity of the solid section was higher, this specimen also had an increasing axial load, which likely contributed to the lateral load capacity of the specimen. The two-inch wall hollow specimen experienced a larger ultimate displacement compared to the solid specimen, which was attributed to the greater shear deformation experienced in the hollow columns. The shear deformation experienced by the hollow specimens will be discussed in detail in the next section.

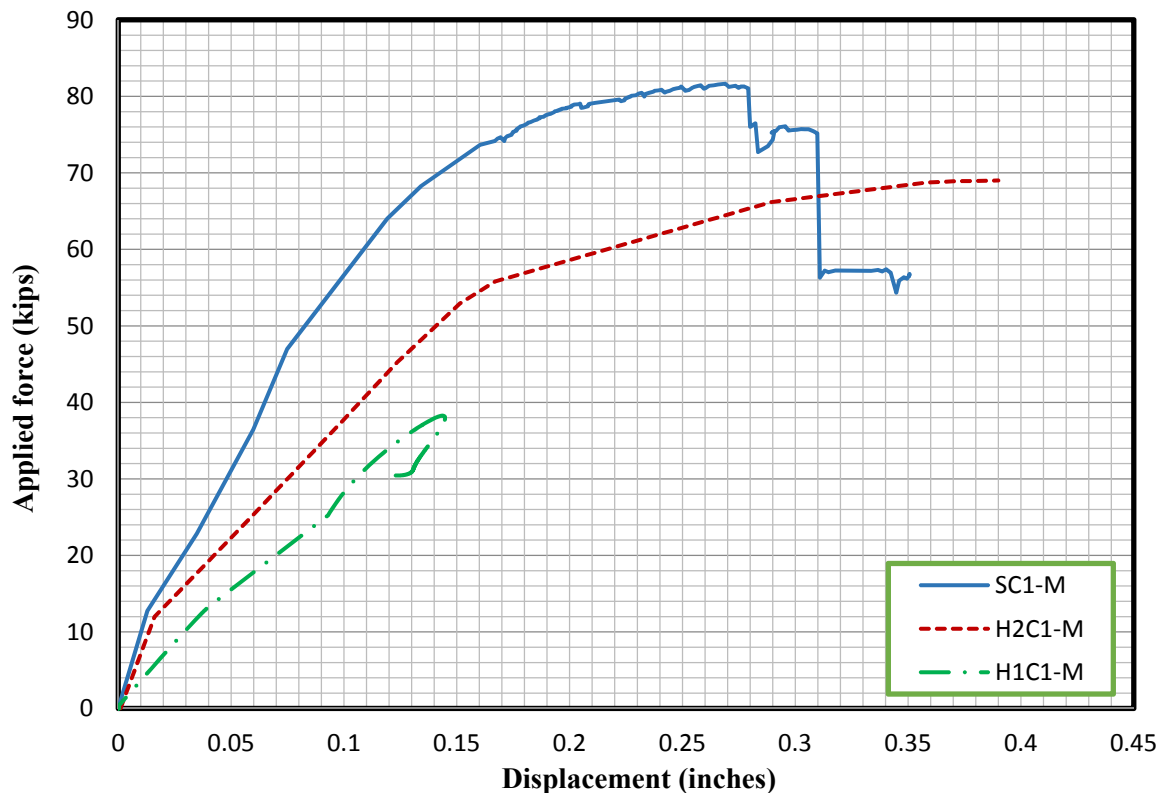


Figure 5-39: Force-displacement response comparisons for solid, two-inch wall, and one-inch wall hollow circular columns under 22.6 kips axial load

Figure 5-40 displays a comparison between monotonic and cyclic loading response. The specimens used for comparison are the hollow specimens with two-inch thick walls, both of which were subjected to 22.6 kips of axial load. As shown, there is little difference between the responses of the two units. Cyclic testing can often experience earlier failure due to material fatigue. However, the cyclic specimens in this experimentation were only subjected to a relatively small amount of cycles before longitudinal steel failure occurred, due to the small ultimate strain of the steel. For this reason, it is likely that not enough cycles were performed for material fatigue to have a significant effect, causing the response to be very similar between cyclic and monotonic testing.

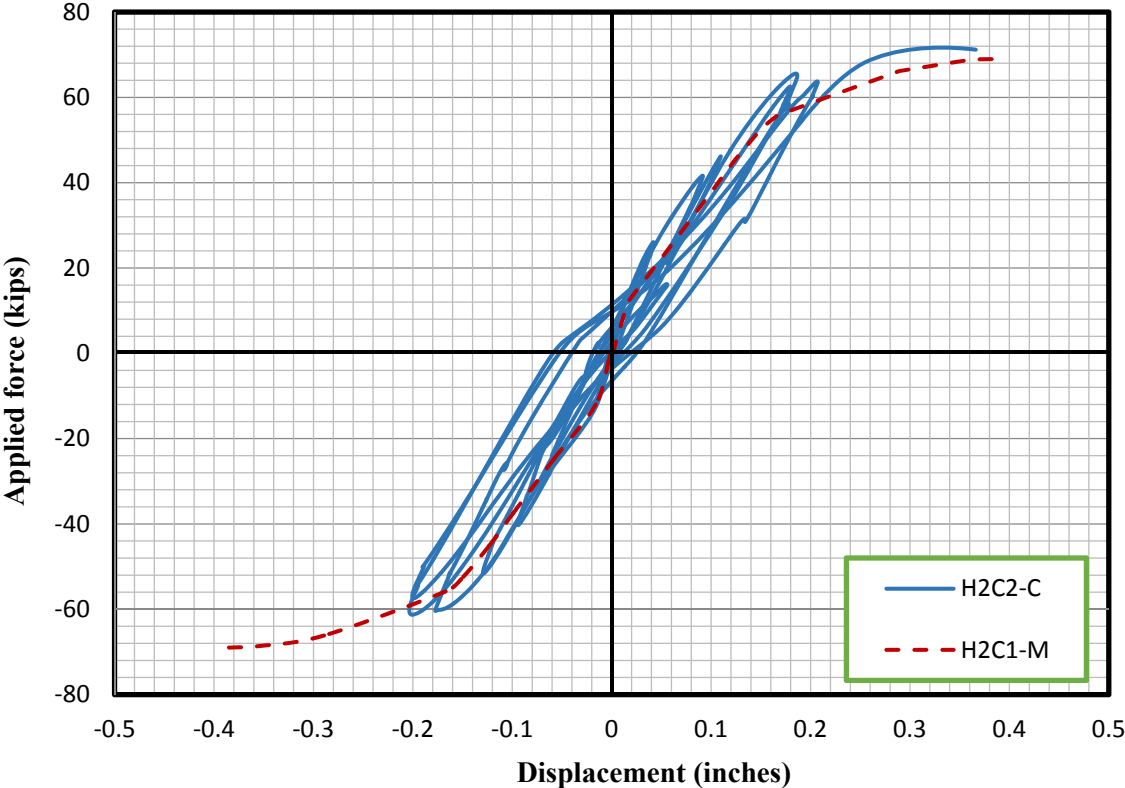


Figure 5-40: Force-displacement response comparisons of two-inch wall hollow columns under monotonic and cyclic loadings

5.3.1.2.2 Shear contribution

It became apparent when testing the hollow columns that the hollow columns experienced a larger percentage of shear displacement than the solid columns did. Typical analysis methods

used in design, as well as the OpenSees analysis used in this research, do not account for shear displacement, thus necessary to estimate the amount of shear displacement experienced by the columns. A method was utilized using a set of LEDs in the shear region to estimate the shear displacement. The method has been adopted, which was used previously by Sritharan (1998), and in this case a grid of LEDs was used to determine the various deformation components.

The shear contribution of the solid specimens was unable to be measured during testing since shear had not been identified as an issue and vision of key LEDs was blocked in many cases. However, the shear contribution of the hollow columns was able to be estimated well in most cases. The following plots show the shear displacement plotted against the applied load for all specimens as well as the force-displacement response of each specimen with shear included and with shear subtracted for comparison. For monotonic plots only, the envelope is shown for clarity.

The response shown in Figure 5-41 gives the overall force-displacement response as well as the force-displacement response with the shear deformation subtracted for specimen H2C1-M. The shear deformation is fairly significant for this specimen, and accounts for approximately 30 percent of the overall displacement of the specimen. The shear deformation is plotted against the applied load in Figure 5-42. As shown in the figure, the shear deformation increases linearly with increased loading in the measured portion of the specimen, indicating that shear capacity was not reached within the linear moment region of the specimen. This agrees with the observed test results which found some minor shear cracking in the linear moment region, and that the specimen ultimately failed due to flexure in the constant moment region.

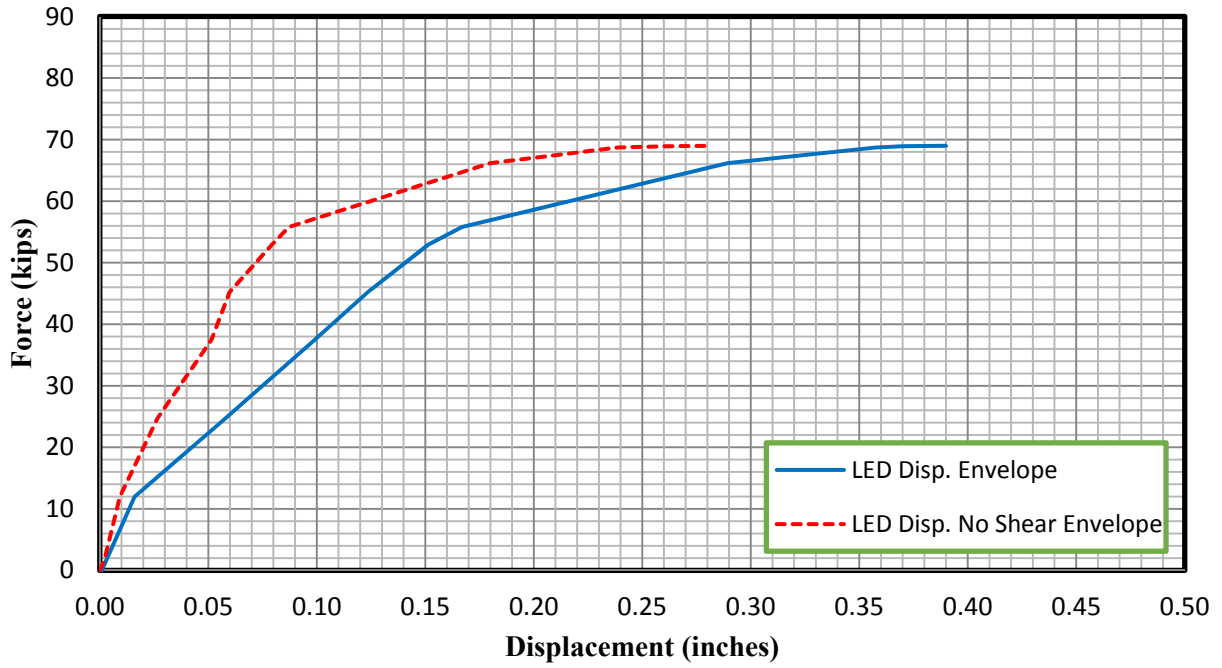


Figure 5-41: Force-displacement relationship of Specimen H2C1-M with and without shear deformation

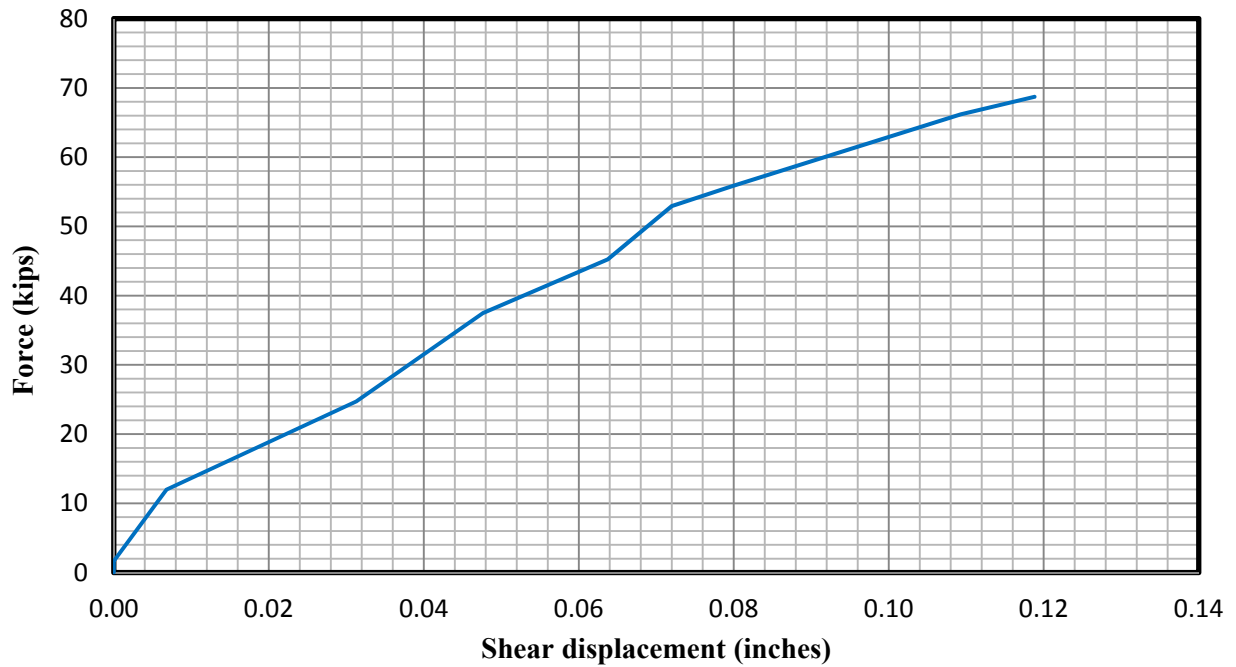


Figure 5-42: Force vs. shear displacement relationship of Specimen H2C1-M

The response with and without shear deformation for specimen H2C2-C is shown in Figure 5-43. Again, shear was fairly significant for this specimen, contributing 20 to 30 percent of the overall displacement, depending on which lateral loading direction was used. The difference in measured shear displacement in each loading direction may be due to local effects or possibly by some minor asymmetry in the column. The shear deformation is plotted against the applied load for this specimen in Figure 5-44. The shear deformation of this specimen also increases linearly as the applied load increases, as was the case for almost all of the specimens. For this reason the plots of shear deformation against the applied load are not shown for the remainder of the specimens. Specimen H1C3-C experienced some nonlinearity due to the local punching failure at one of the load application points. This point was near the linear moment region where the shear displacement was measured, which is why this local punching failure caused nonlinearity in the measured shear.

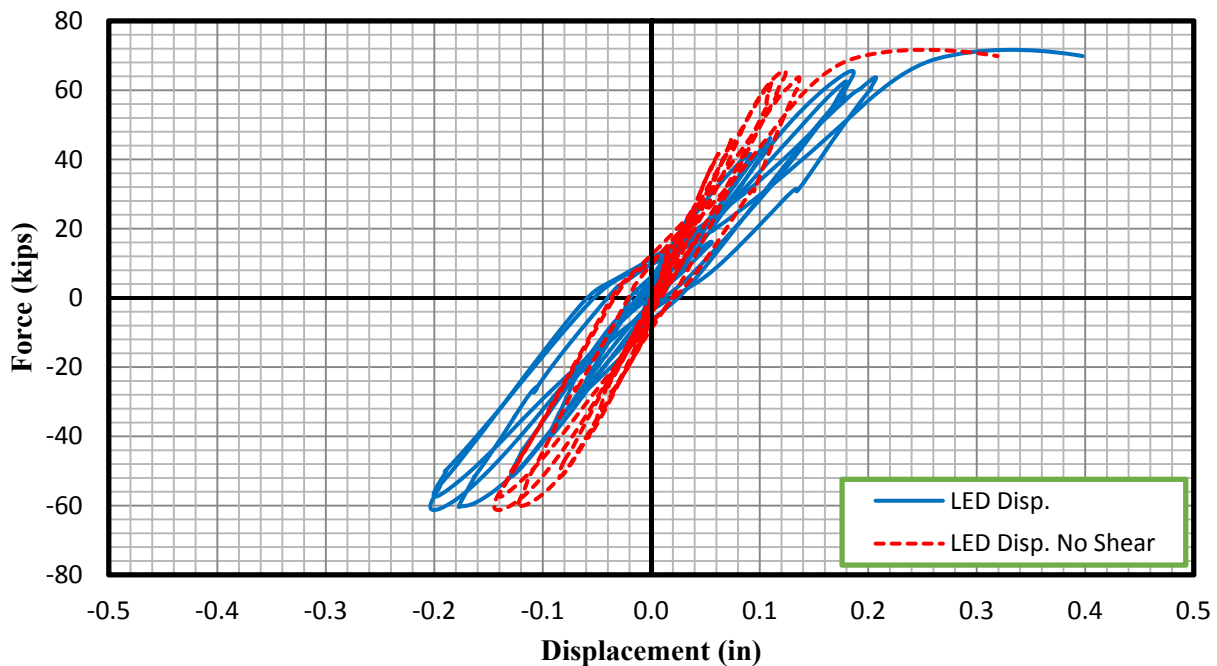


Figure 5-43: Force-displacement relationship of Specimen H2C2-C with and without shear deformation

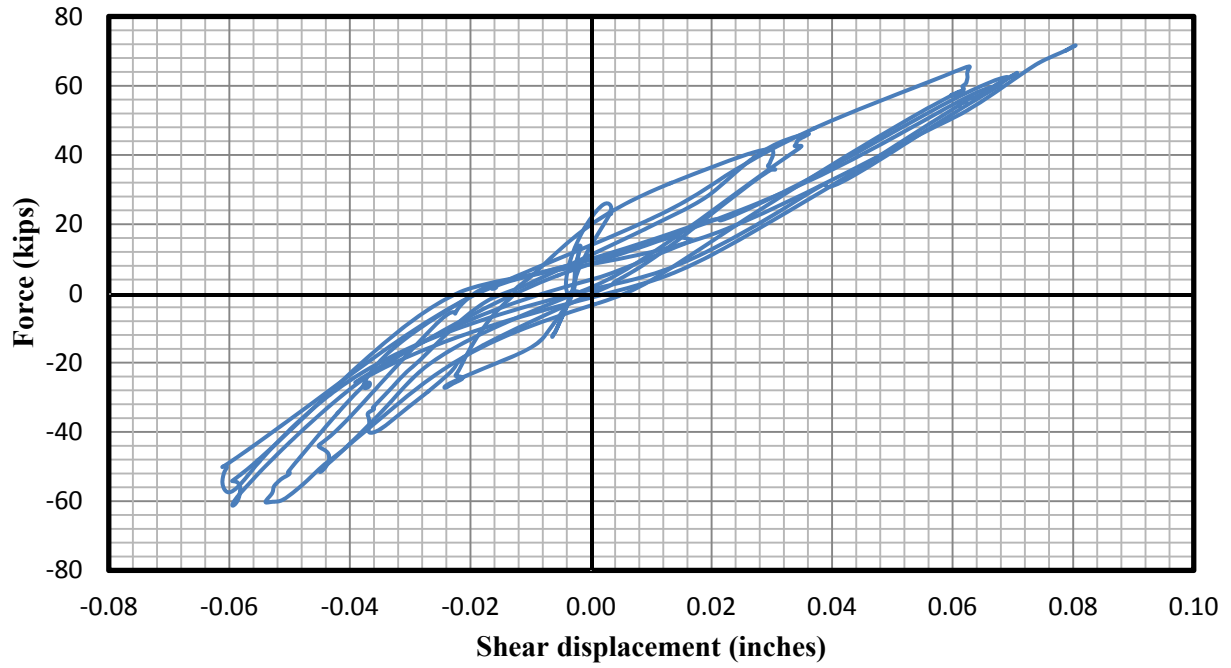


Figure 5-44: Force vs. shear displacement relationship of Specimen H2C2-C

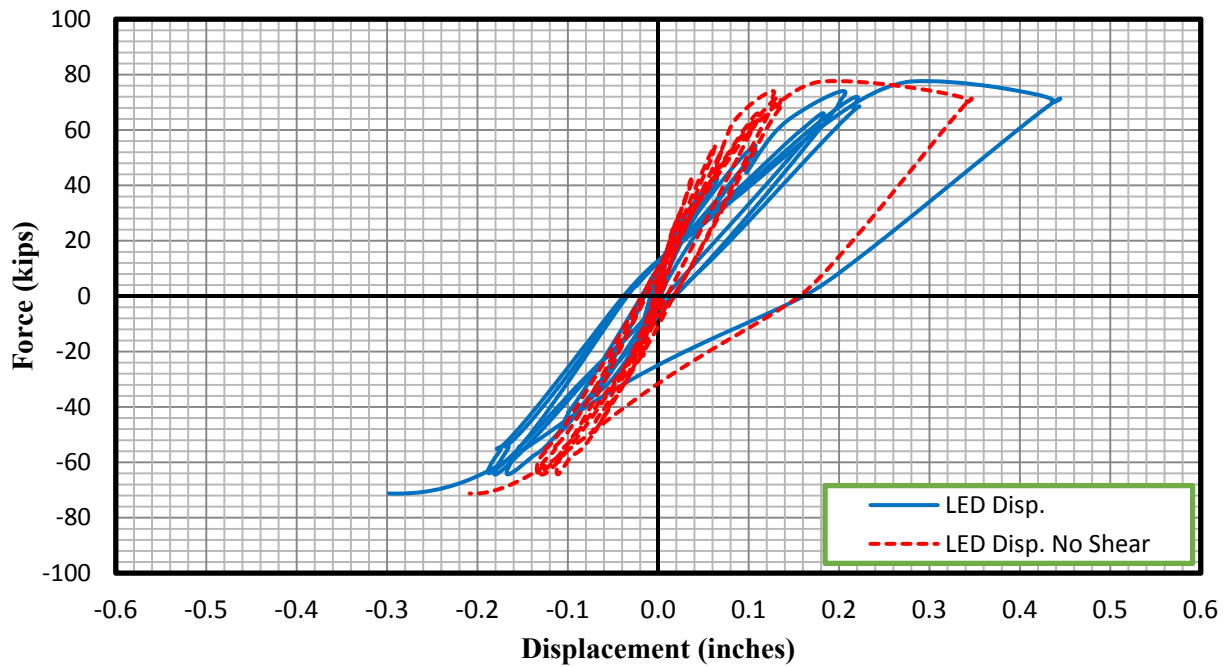


Figure 5-45: Force-displacement relationship of Specimen H2C3-C with and without shear deformation

Figure 5-46 through Figure 5-48 present the specimen force-displacement responses with and without shear for the one-inch thick specimens. It can be seen that for the one-inch thick specimens, the shear deformation is more significant than that of the two-inch thick specimens. For the one-inch thick specimens, the shear deformation typically accounted for between 40 and 60 percent of the overall displacement at the peak displacement.

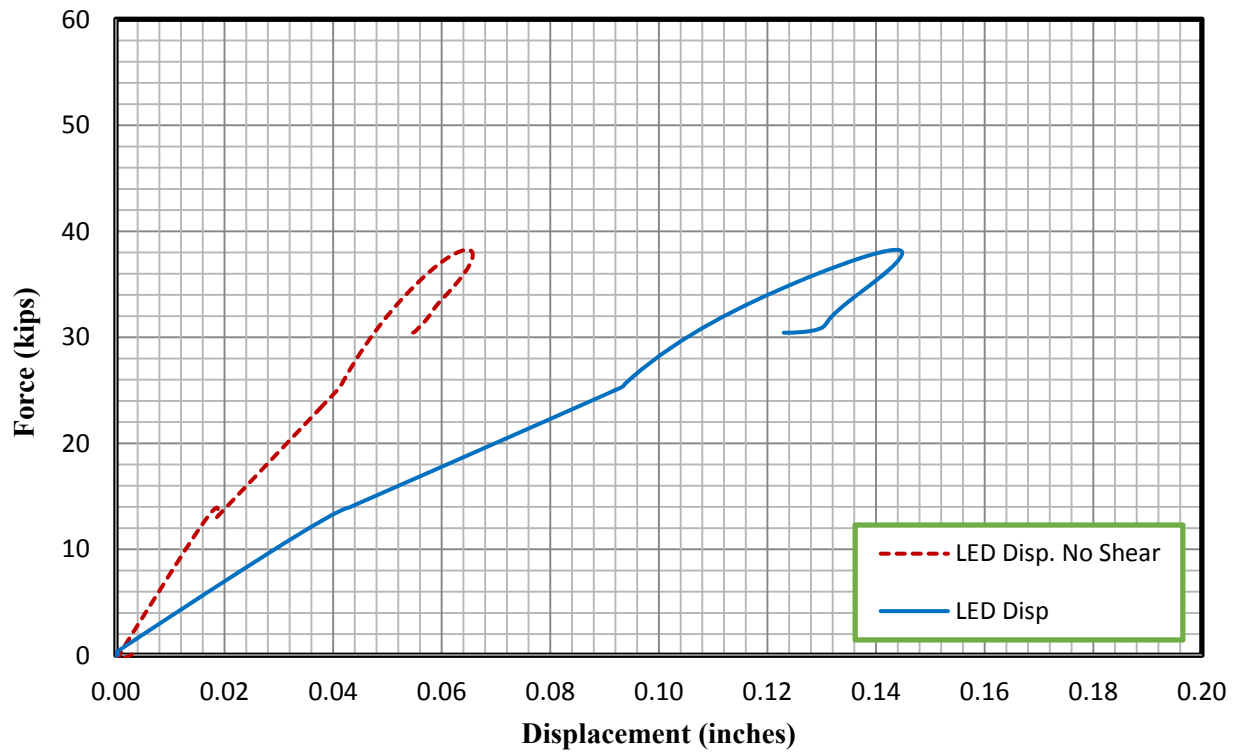


Figure 5-46: Force-displacement relationship of Specimen H1C1-M with and without shear deformation

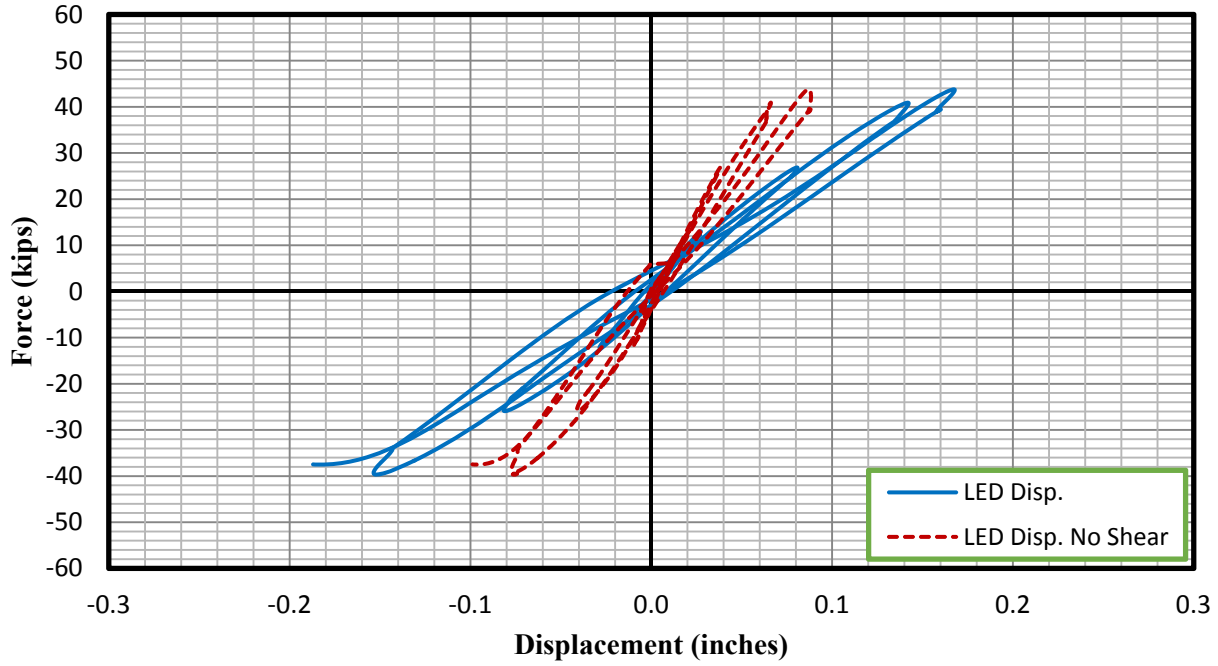


Figure 5-47: Force-displacement relationship of Specimen H1C2-C with and without shear deformation

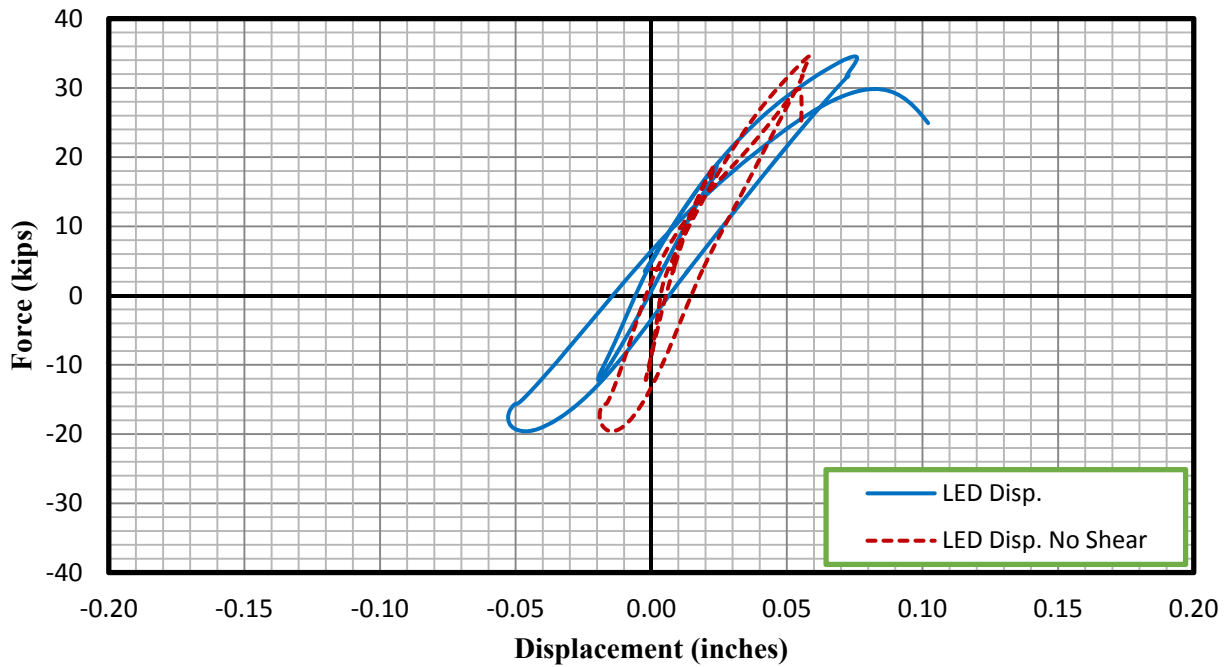


Figure 5-48: Force-displacement relationship of Specimen H1C3-C with and without shear deformation

5.3.1.2.3 Force-displacement response without shear

Due to the fact that the OpenSees method used in the research did not incorporate shear effects, the force-displacement response of the hollow test specimens with the shear component removed has been compared to the OpenSees analysis. For the solid sections, the shear component was not able to be measured during the testing, so the overall specimen displacement has been compared to the OpenSees analysis. An estimate of the shear component has also been provided for the solid columns using a model provided by Beyer et al. (2011), which was based on the curvature and geometry of the section. The model was developed for slender reinforced concrete walls, but has been applied to the current testing in order to provide an estimate of the shear contribution. The model has been shown in results for the solid section and has also been provided for the monotonically tested hollow section with a two-inch thick wall, in order to determine how applicable the model is to hollow columns. Additionally, the shear component was also removed from the finite element analysis and compared to the test results.

The force-displacement response of specimen SC1-M can be seen in Figure 5-49. As mentioned, the shear response of this specimen was not measured during testing, so the test results provided in the figure give the overall displacement of the specimen. The shear component of the response has also been estimated using the shear model mentioned in the previous paragraph (Beyer et al., 2011). This estimated shear component has been added to the flexural component provided by the OpenSees analysis and has been included in the figure. As shown, the analytical response including shear seems to match the test results more accurately than the flexural response from the OpenSees analysis alone, but also greatly overestimates the displacement at which longitudinal steel failure occurs.

It is also important to recall that specimen SC1-M experienced a steady increase in axial load throughout the test. The initial axial load was 22.6 kips, and the axial load had increased to 40 kips by the end of the test. This increase in axial load was accounted for in the OpenSees analysis to ensure the comparison would be accurate. The axial load during the testing with the approximated axial load used in the OpenSees analysis can be seen in Figure 5-50.

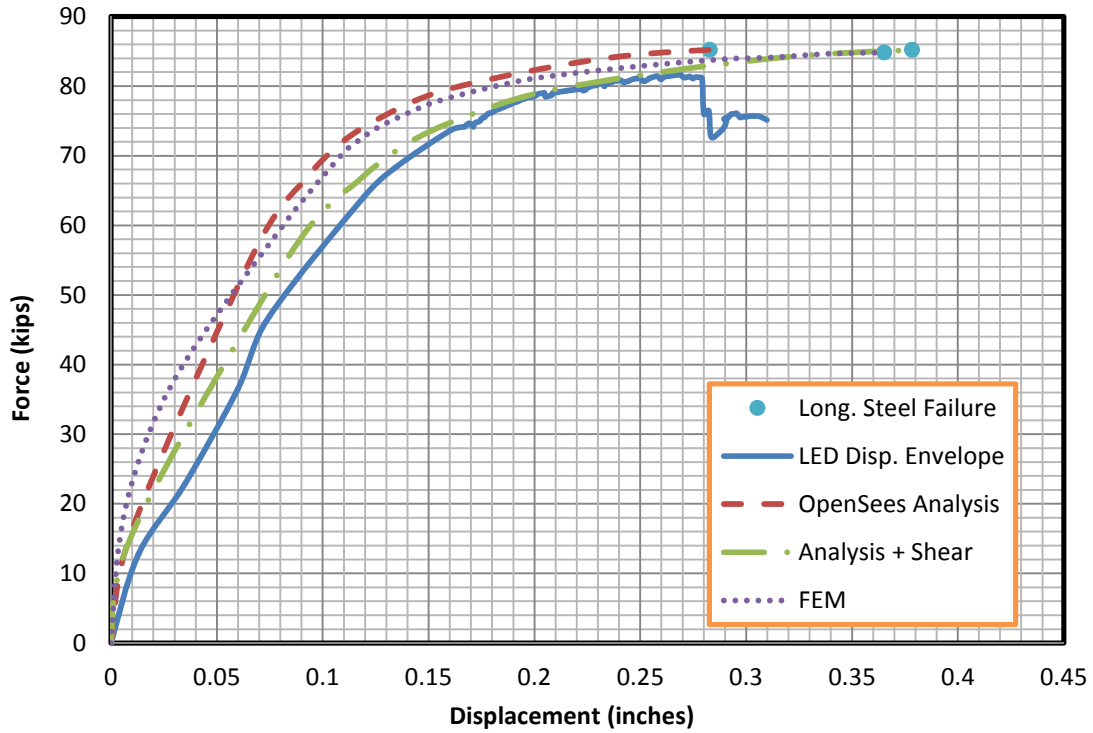


Figure 5-49: Measured force-displacement response of Specimen SC1-M compared to analytical envelope response

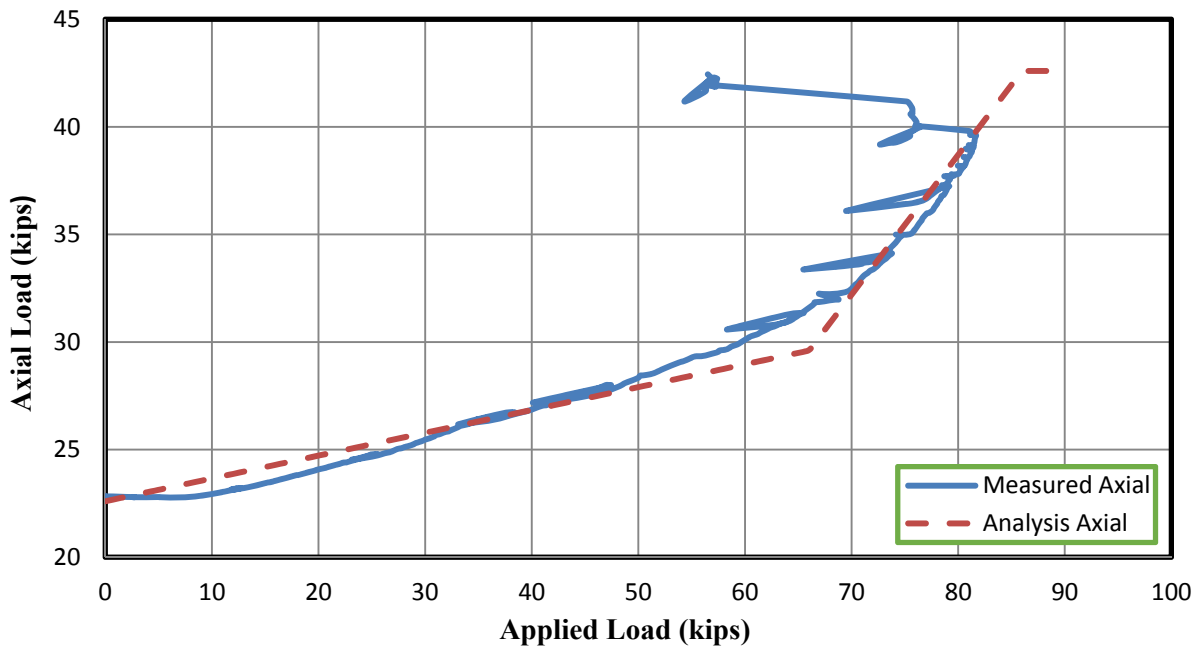


Figure 5-50: Experimental and analytical axial load vs. applied load relationship for the Specimen SC1-M

Figure 5-51 shows the results of specimen SC2-C plotted with the OpenSees analytical response and the FEA response. Similarly to the plot shown for specimen SC1-M, the estimated shear component has been added to the OpenSees flexural component and has been included in the figure. As noted for specimen SC1-M, the shear response for specimen SC2-C is fairly similar to the flexural response, although it provides a much higher estimate of the displacement at the longitudinal steel failure.

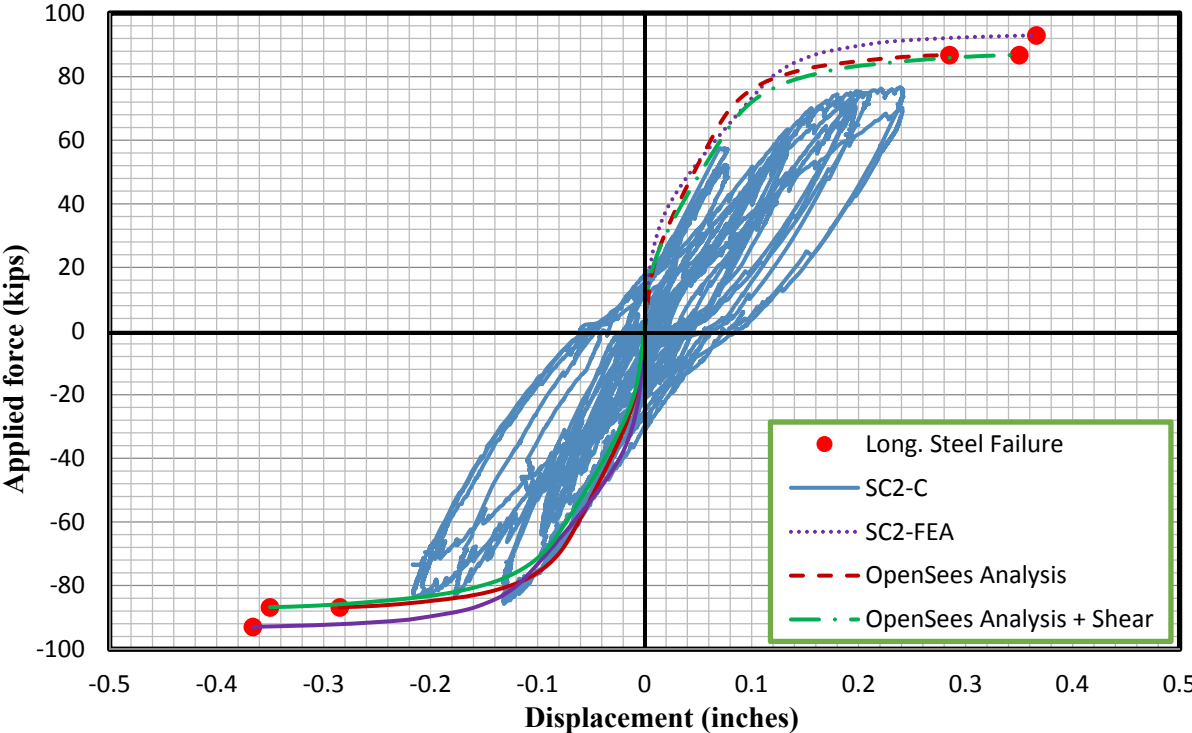


Figure 5-51 Measured force-displacement response of Specimen SC2-C compared to analytical envelope response

The experimental and analytical response of specimen H2C1-M, with the shear deformation removed, is shown in Figure 5-52 as well as the total experimental response, the OpenSees flexure response with the estimated shear component added, and the FEM results excluding the shear effects. In this case, the response with the OpenSees flexural and shear components combined significantly underestimates the overall measure response. This is most likely because the shear model was developed for shear walls and not for hollow columns. As mentioned in

Section 5.3.1.2.3, shear in hollow columns seems to be significantly higher than for solid columns, and current shear models have not taken this into account.

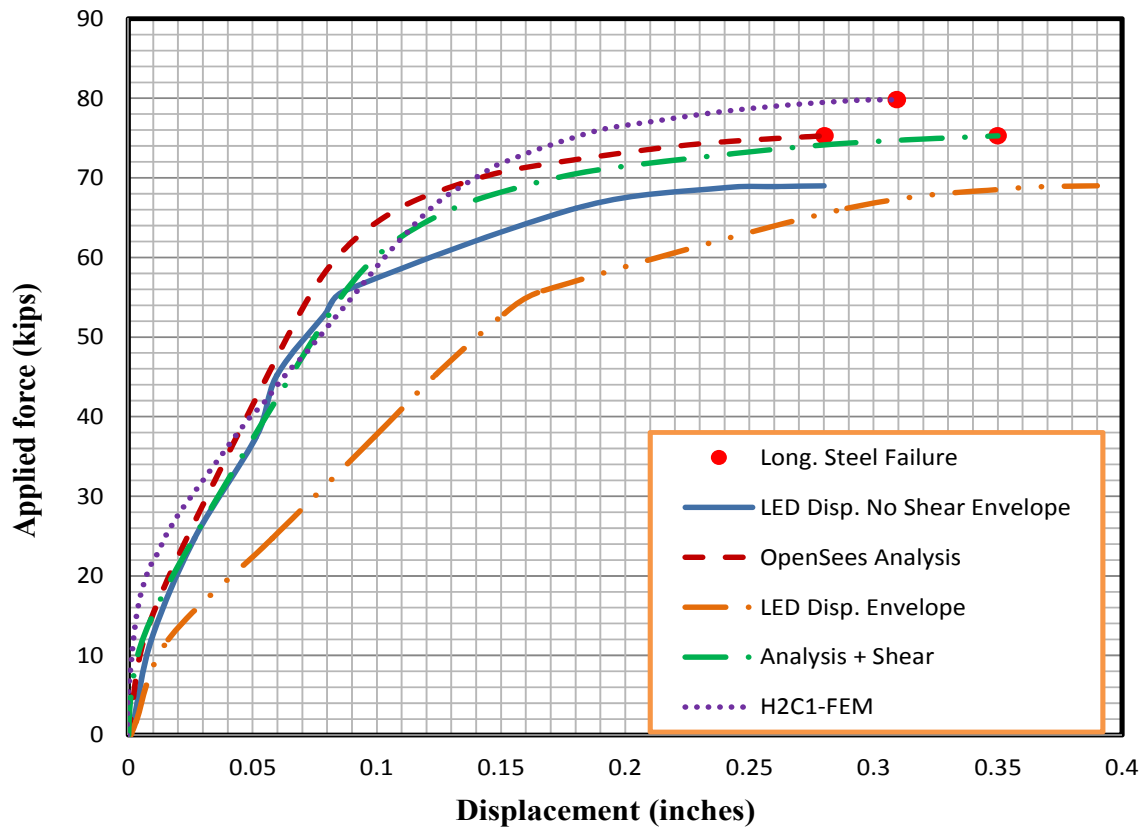


Figure 5-52: Measured force-displacement response of Specimen H2C1-M with shear deformation removed compared to analytical envelope response

The remainder of the force-displacement plots shown in this section have shear subtracted from the measured response and also show only the analytical flexural response as well as the FEM results excluding the shear effects for comparison. The expected failure mode, as determined from the analytical response, is also plotted in the figures. As shown, both the OpenSees analyses as well as the FE analyses results compares well to the measured experimental response without shear deformation for the solid specimens and for the two-inch thick specimens, including the failure mode and ultimate displacement at this failure point. For the one-inch thick specimens, the analytical response does not match the experimental response due to the early failure of the specimens caused by local and shear failures. The limitation of the wall thickness on the behavior of one-inch wall hollow columns was also validated by the FE analyses.

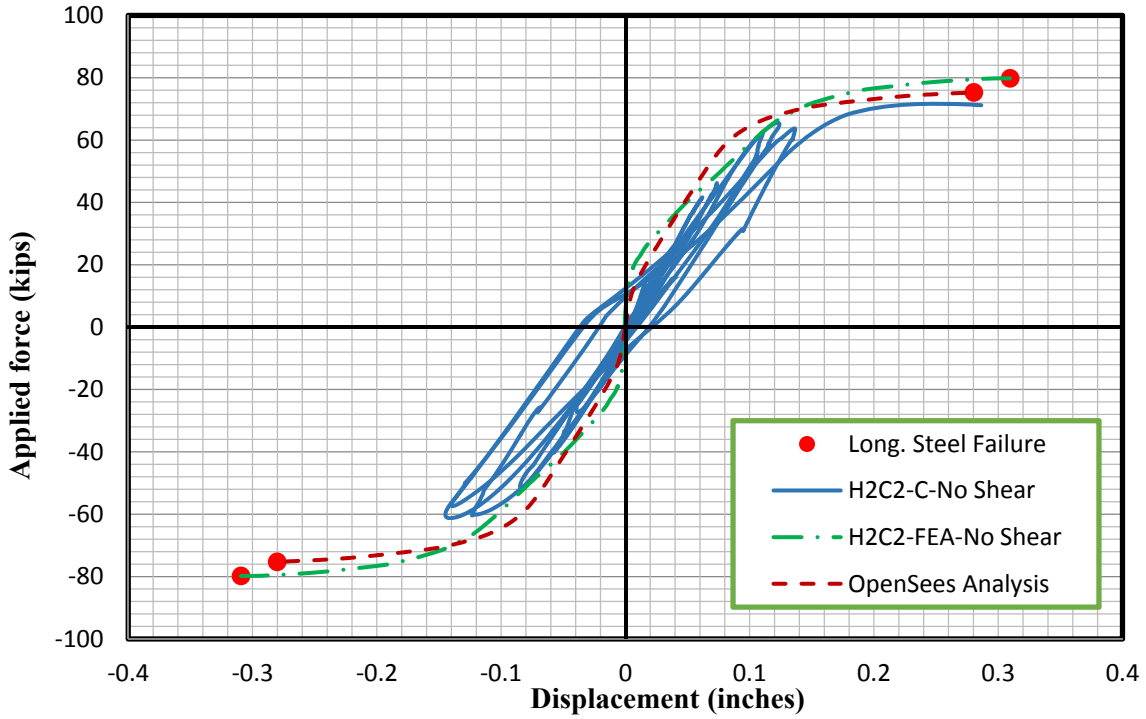


Figure 5-53: Measured force-displacement response of Specimen H2C2-C with shear deformation removed compared to analytical envelope response

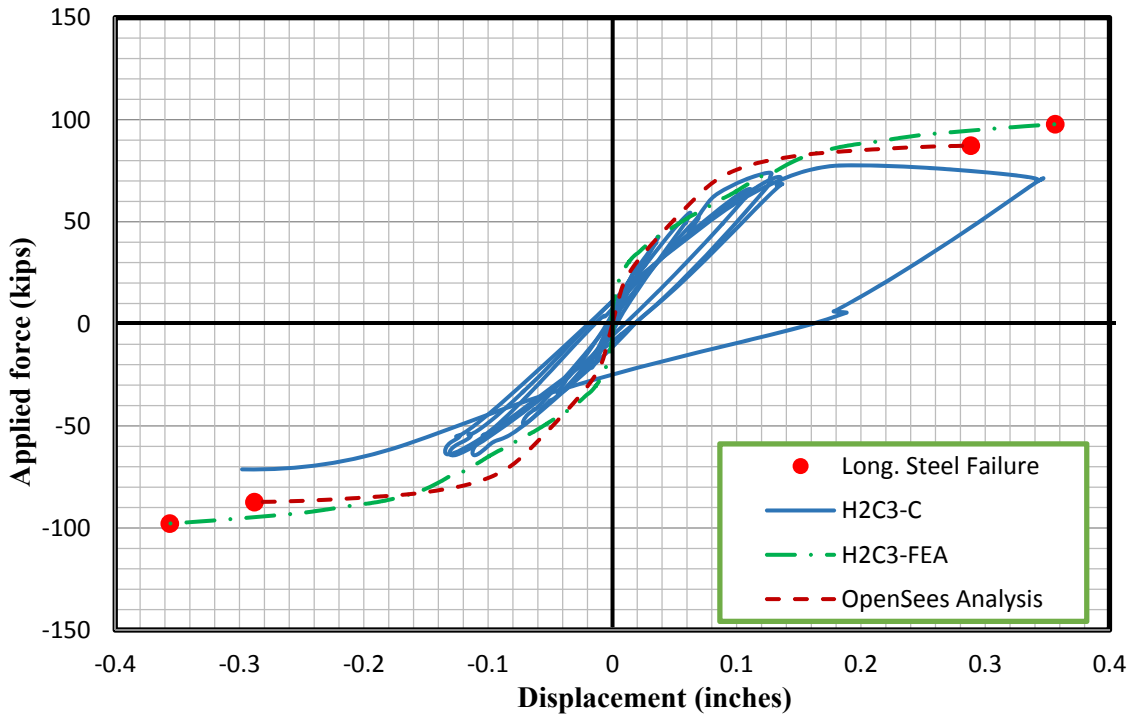


Figure 5-54: Measured force-displacement response of Specimen H2C3-C with shear deformation removed compared to analytical envelope response

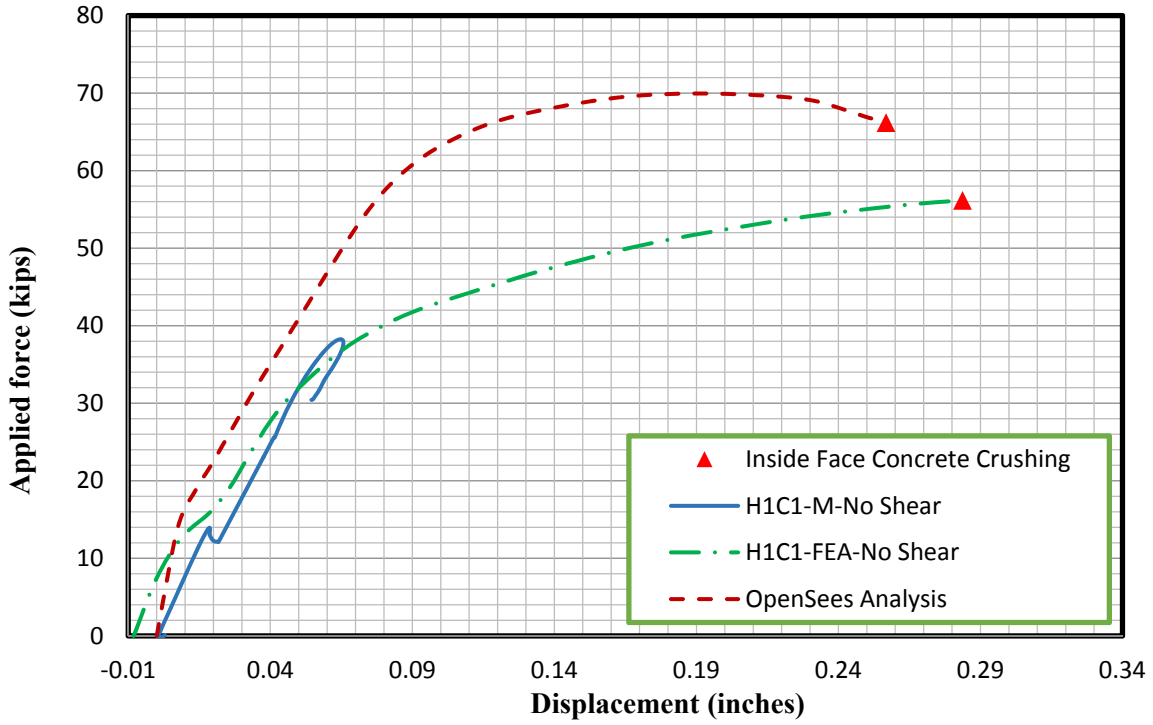


Figure 5-55: Measured force-displacement response of Specimen H1C1-M with shear deformation removed compared to analytical envelope response

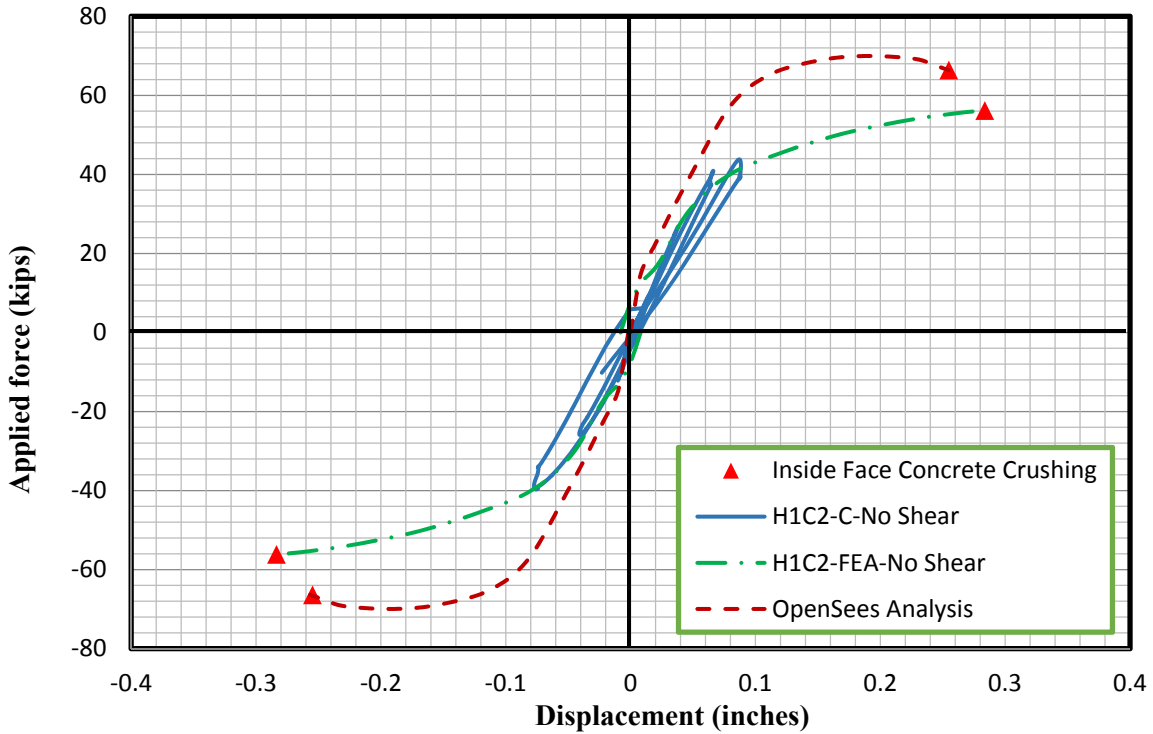


Figure 5-56: Measured force-displacement response of Specimen H1C2-C with shear deformation removed compared to analytical envelope response

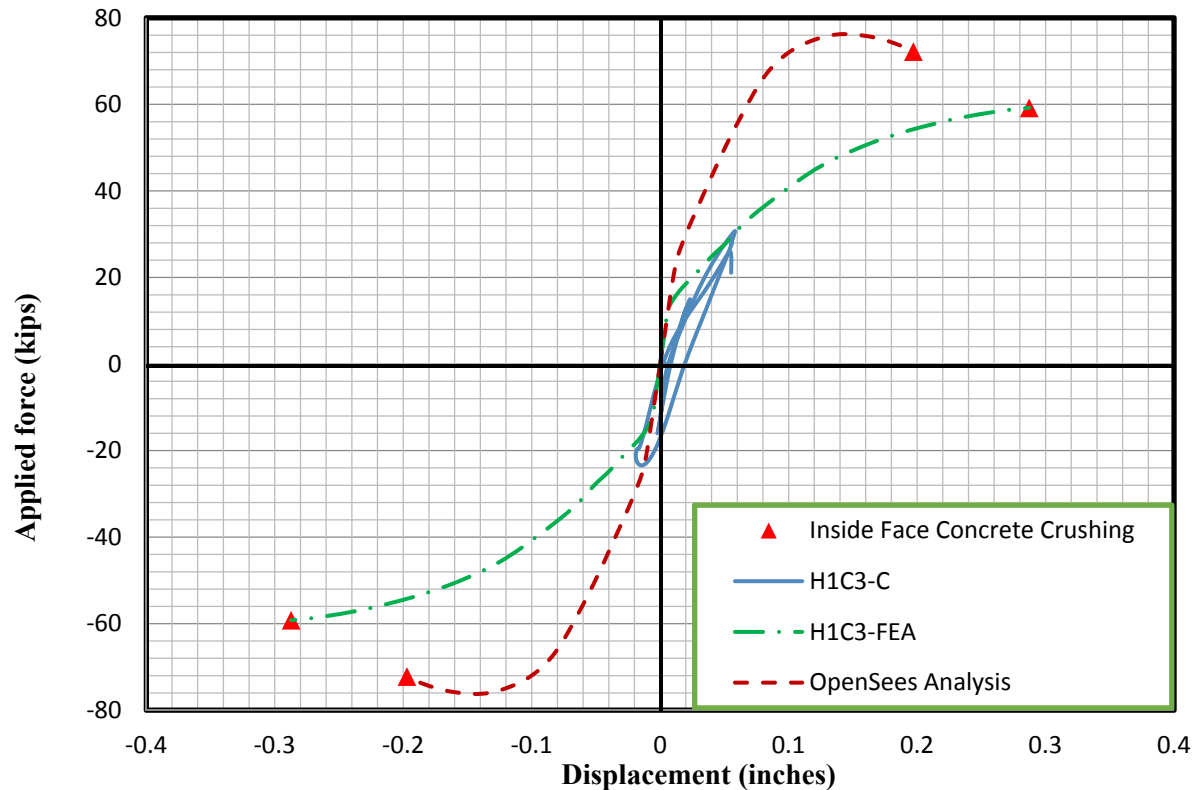


Figure 5-57: Measured force-displacement response of Specimen H1C3-C with shear deformation removed compared to analytical envelope response

5.3.1.2.4 Longitudinal bar strain

The longitudinal steel strain was measured during the testing, and plots of some of the measured strains compared to the applied load are shown in this section. The figures show longitudinal strains for the bars close to the extreme tension and compression edge in each section, which were measured by strain gauges attached to the longitudinal reinforcement. The strains presented are from the cyclic tests, and the figures are labeled as either near longitudinal bar 1 or longitudinal bar 11. The longitudinal steel strains provided by the OpenSees analysis are also shown in each of these plots to compare to the measured values. The analytical longitudinal steel strains are given at the extreme tension and compression reinforcing bars. The analytical steel strains are reported up until the predicted analytical failure occurs. For the solid and two-inch thick specimens, the analytical failure occurred due to tensile steel rupture. For the one-inch thick specimens, the predicted failure mode was crushing of the inside face concrete.

Only some of the measured strains have been presented, since in general the test results and comparison to analytical results are similar to what is shown in the figures below. The OpenSees analysis was in fairly good agreement with the measured steel strains for all of the solid specimens and two-inch thick hollow specimens.

The circular specimen strain gauge locations have been provided again in Figure 5-58 for quick reference. The gauges marked with an asterisk only appeared at one section in the specimen, while all other gauges were at both sections. A more in-depth discussion of strain gauge locations was provided in Section 4.5. The measured response compared to analytical response for certain longitudinal bars is provided in Figure 5-59 through Figure 5-63.

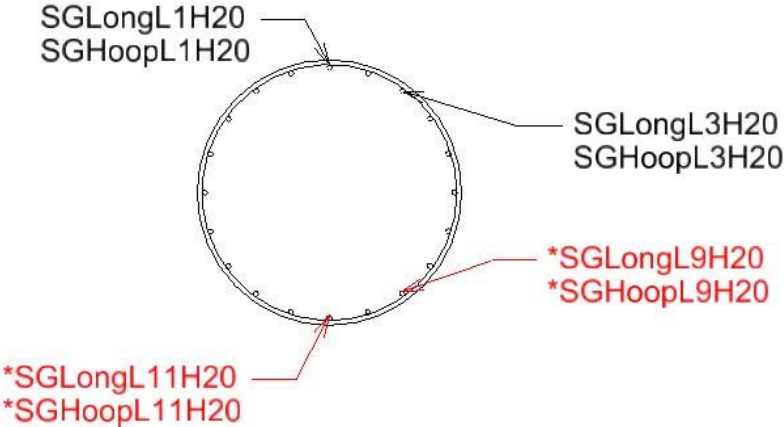


Figure 5-58: Circular section strain gauge locations

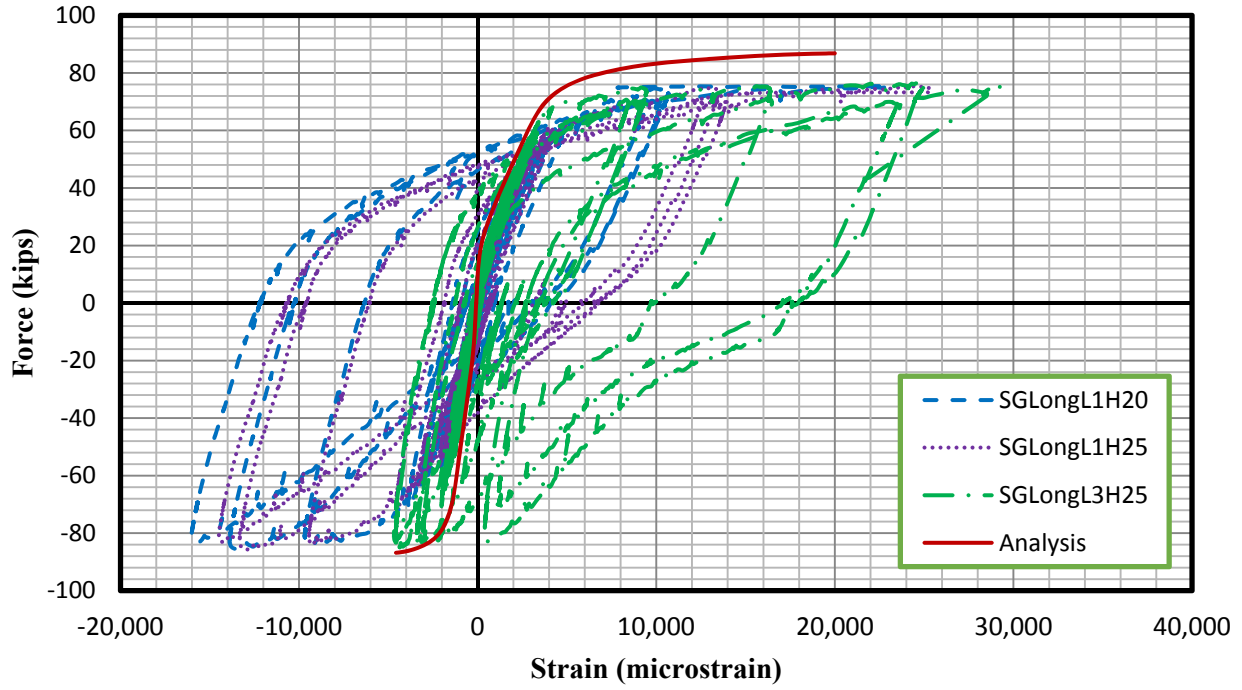


Figure 5-59: Specimen SC2-C longitudinal strain near longitudinal bar 1 vs. applied load

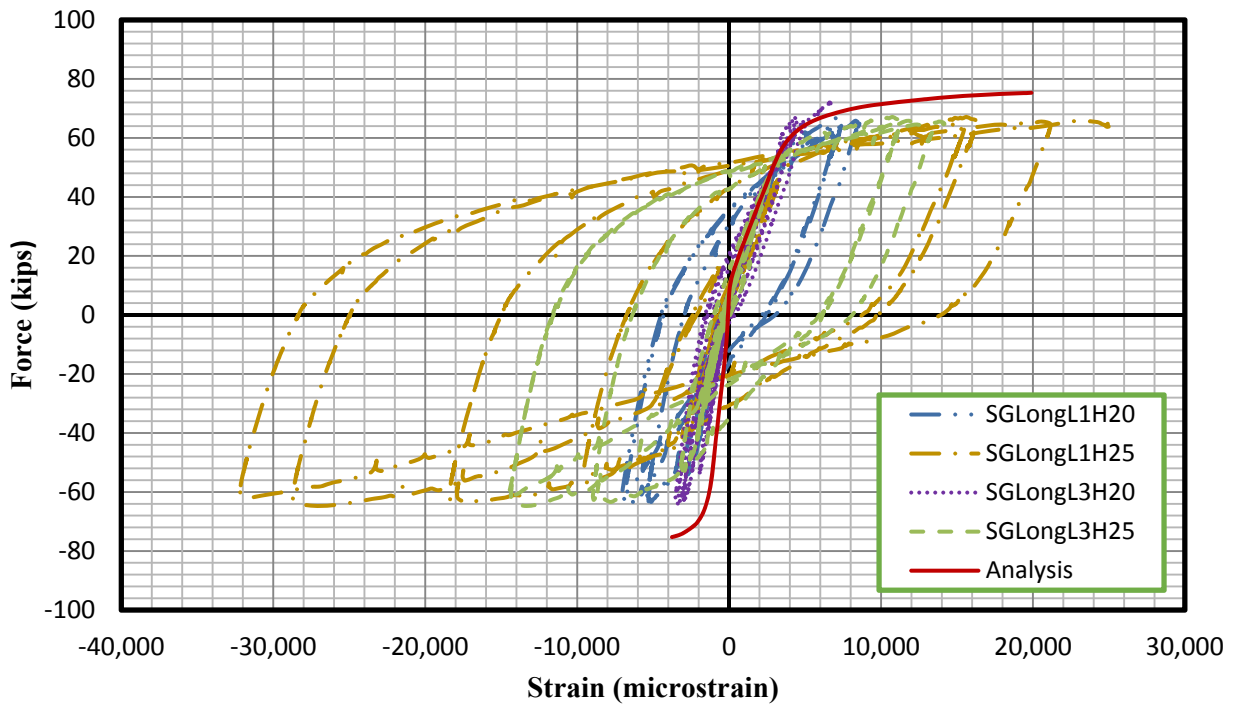


Figure 5-60: Specimen H2C2-C longitudinal strain near longitudinal bar 1 vs. applied load

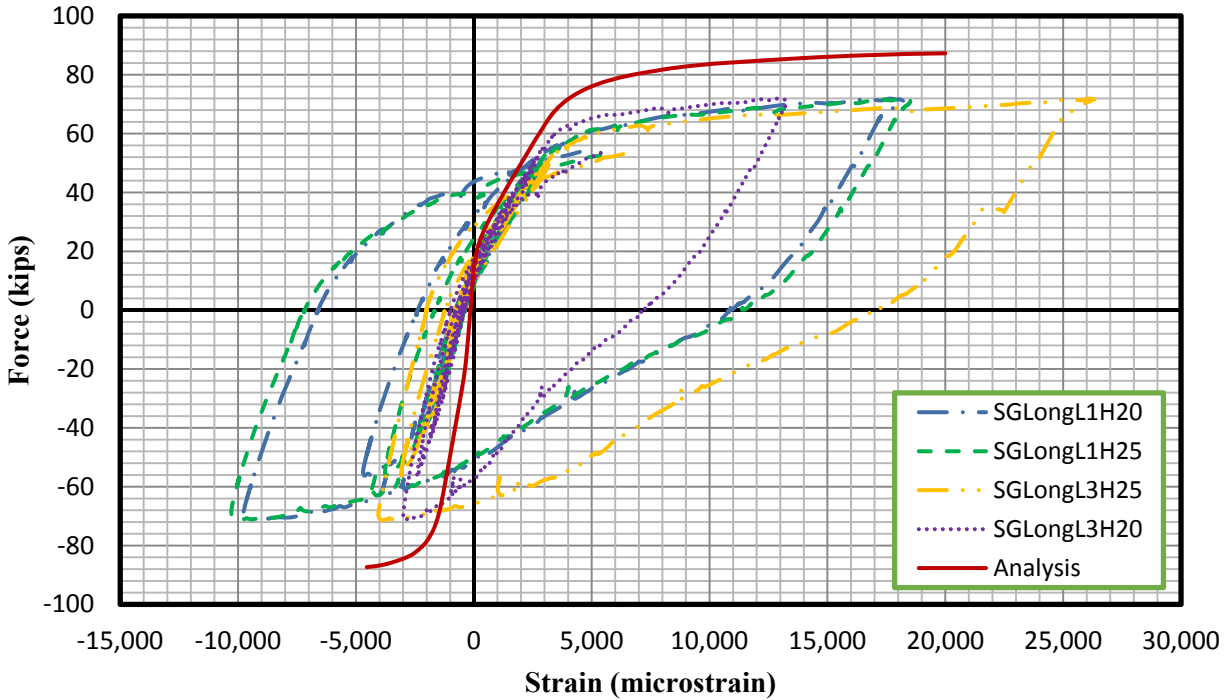


Figure 5-61: Specimen H2C3-C longitudinal strain near longitudinal bar 1 vs. applied load

The analytical longitudinal steel behavior in the plots for the one-inch thick specimens below shows the analytical steel behavior up to the point of specimen failure. These specimens were predicted to fail due to high inside face compression strain, and the analytical longitudinal steel has been plotted up until this predicted failure point. These one-inch thick specimens experienced early failure during the testing due to local and shear effects. The analysis only measured the flexural response, and thus the ultimate displacement and force predicted by the analysis are very different than what was seen during the testing. Despite this, the analysis was still able to agree with the measured strains in the linear range.

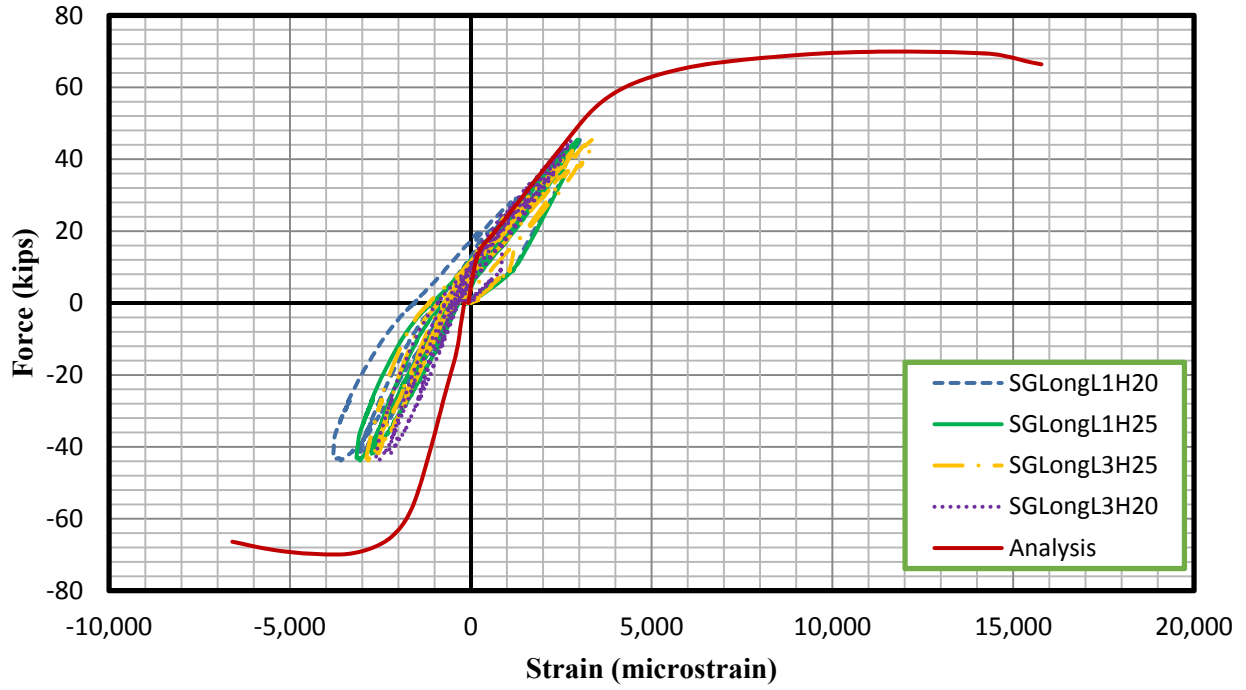


Figure 5-62: Specimen H1C2-C longitudinal strain near longitudinal bar 1 vs. applied load

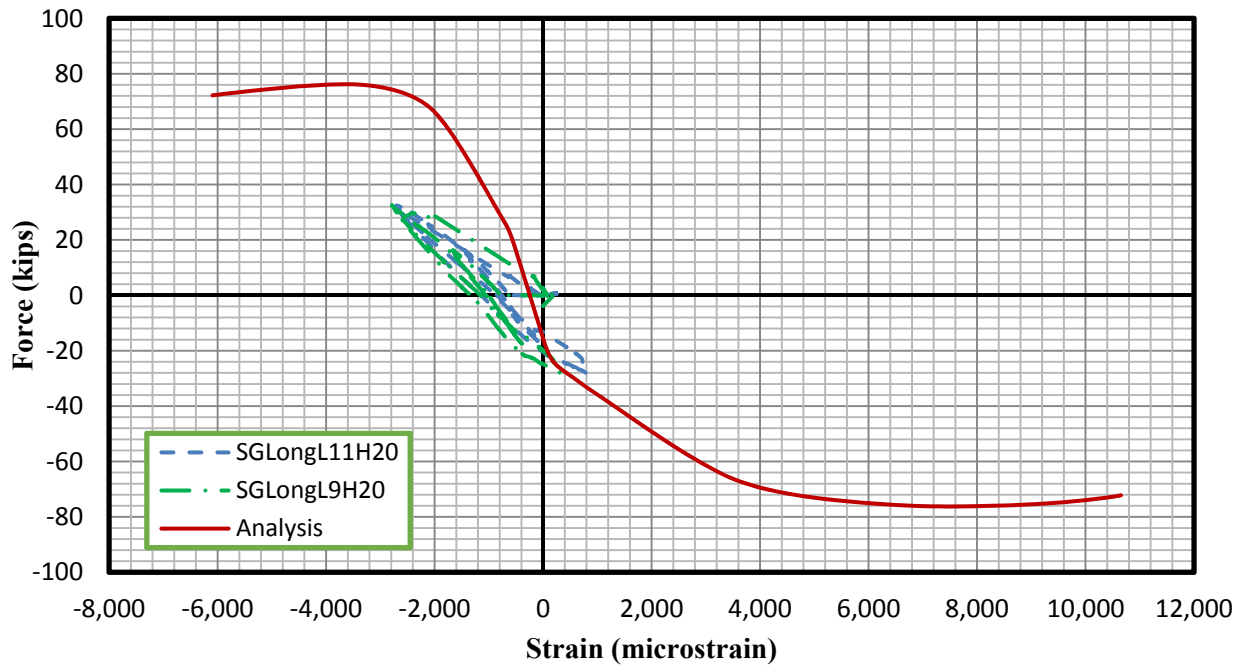


Figure 5-63: Specimen H1C3-C longitudinal strain near longitudinal bar 11 vs. applied load

As shown in Figure 5-59 through Figure 5-63 the analysis is able to match fairly closely to the actual measured values. The compressive strains measured by the strain gauges during testing appear very high in some cases. These high strains are likely caused by gauge errors, since these large compressive strains would have been visible due to increased damage to the concrete in the compressive region. Despite larger measured compressive strains, the measured tensile strains agree closely with the analytical tension steel strains. The next section presents the strains measured by LEDs attached to the concrete surface and compares them with analytical strains in order to provide additional verification of the analytical method, as well as to give another estimate of the extreme fiber compressive strains experienced by the test units.

5.3.1.2.5 Concrete strain

The concrete strains near to the top and bottom of the sections were found using the LED grid in the constant moment region. The location of the presented LEDs was fairly close to the extreme compression and tension faces, so the longitudinal reinforcement strains from the extreme tension and compression reinforcement found in the OpenSees analysis has been plotted for comparison. The tension and compression strains are presented in the same plot, as well as the analytical strains. The measured strains are labeled either “Strain57” representing the strain measured between LEDs 5 and 7, or “Strain1820” representing the strain measured between LEDs 18 and 20.

The layout of the LEDs used during testing is shown in Figure 5-64 for reference. The measured LED strains presented in this section were measured in the constant moment region. The strain gauge sets, which were used in the plots, are highlighted in the figure.

The measured and analytical strains are plotted against the applied lateral load for the solid and two-inch thick specimens in Figure 5-65 through Figure 5-67. The plots show good agreement between the measured and analytical strains. Additionally, the compressive strains measured by the LEDs are not as large as was shown by the strain gauges, and agree better with the visual results of the test specimens. The test specimens did not show signs of high compressive strains, since there was not a large amount of crushed concrete near the extreme compression region. Similar behavior and agreement was found for all circular solid and two-inch thick specimens, so only a few of the cyclic test results have been shown for brevity.

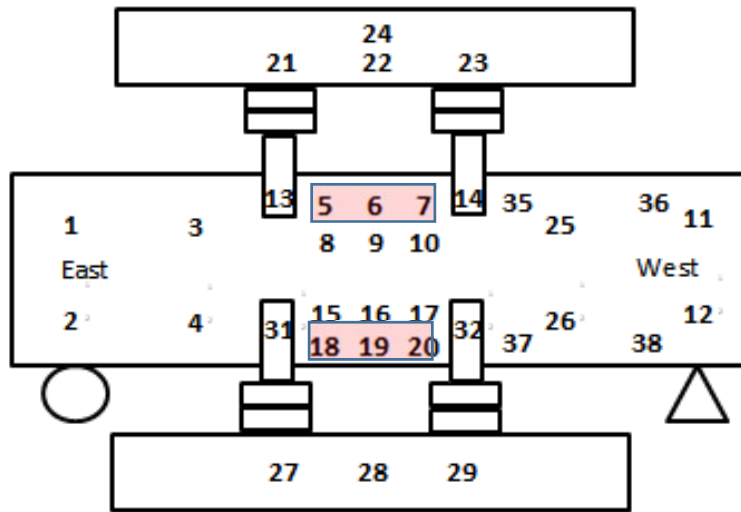


Figure 5-64: LED Layout with Highlighted Strain Locations

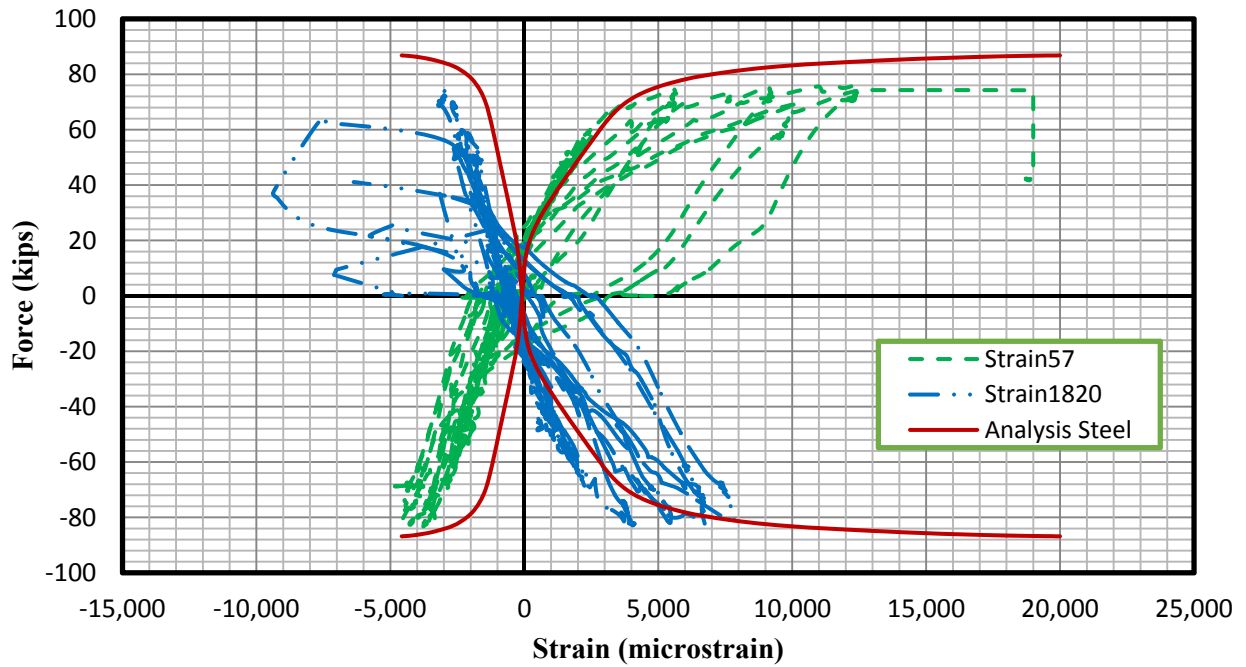


Figure 5-65: Attached LED concrete strain measured during testing and analytical steel strain vs. applied lateral load for Specimen SC2-C

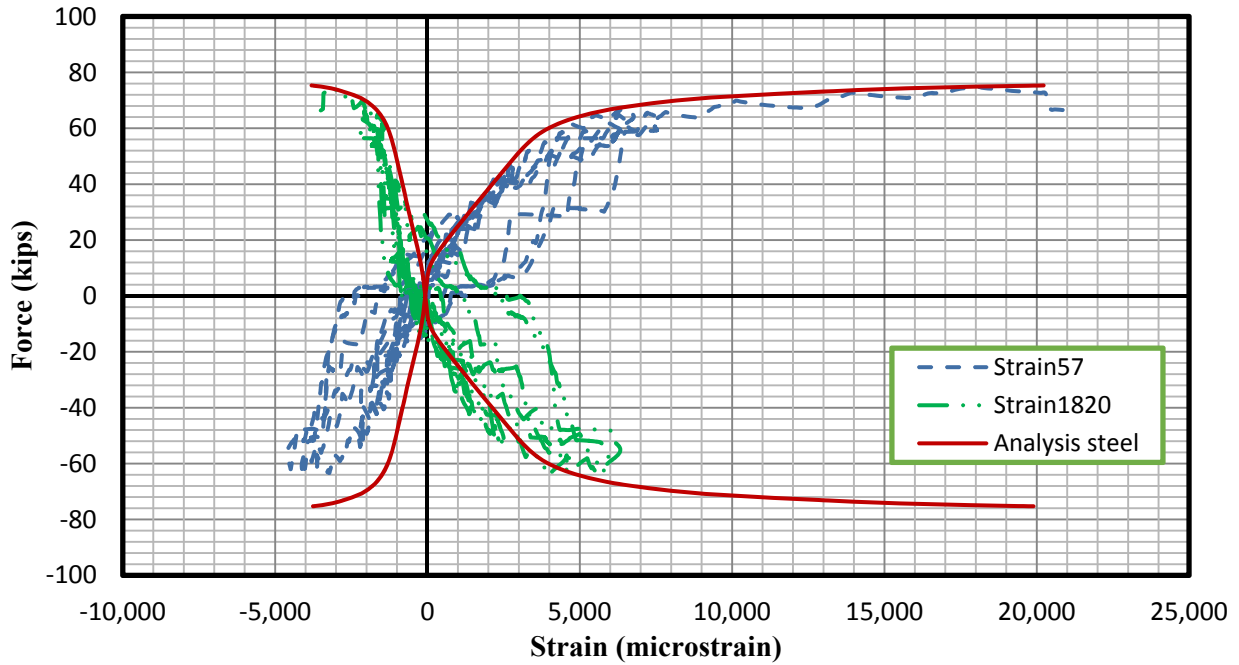


Figure 5-66: Attached LED concrete strain measured during testing and analytical steel strain vs. applied lateral load for Specimen H2C2-C

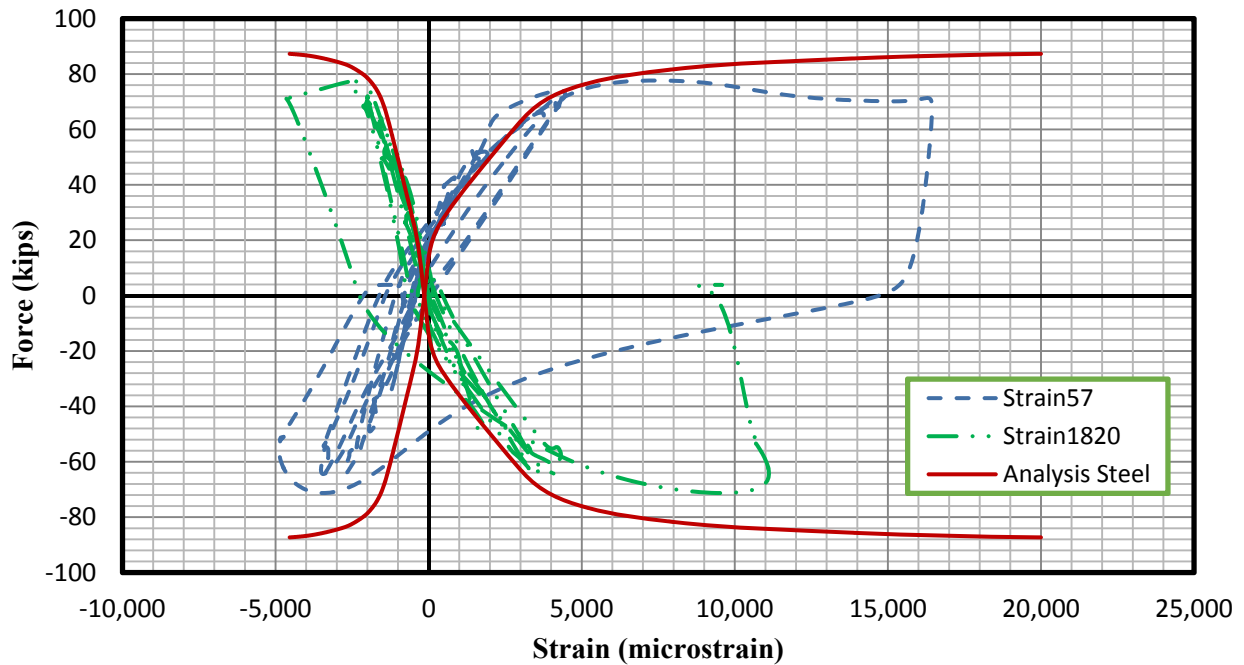


Figure 5-67: Attached LED concrete strain measured during testing and analytical steel strain vs. applied lateral load for Specimen H2C3-C

Figure 5-68 shows the LED strains attached to the concrete for one of the one-inch thick specimens. The analytical failure mode for these specimens was inside concrete face crushing, and thus the analytical tension steel strains are plotted up to the point of inside concrete face crushing. These specimens experienced early failure due to local and shear effects, which the analysis did not account for. For this reason the analysis results predicted much higher capacities and ultimate displacements than found through experimental testing. Despite the differences, the strains measured by the LEDs prior to failure still match closely with the strains at these force levels, which the analysis provides.

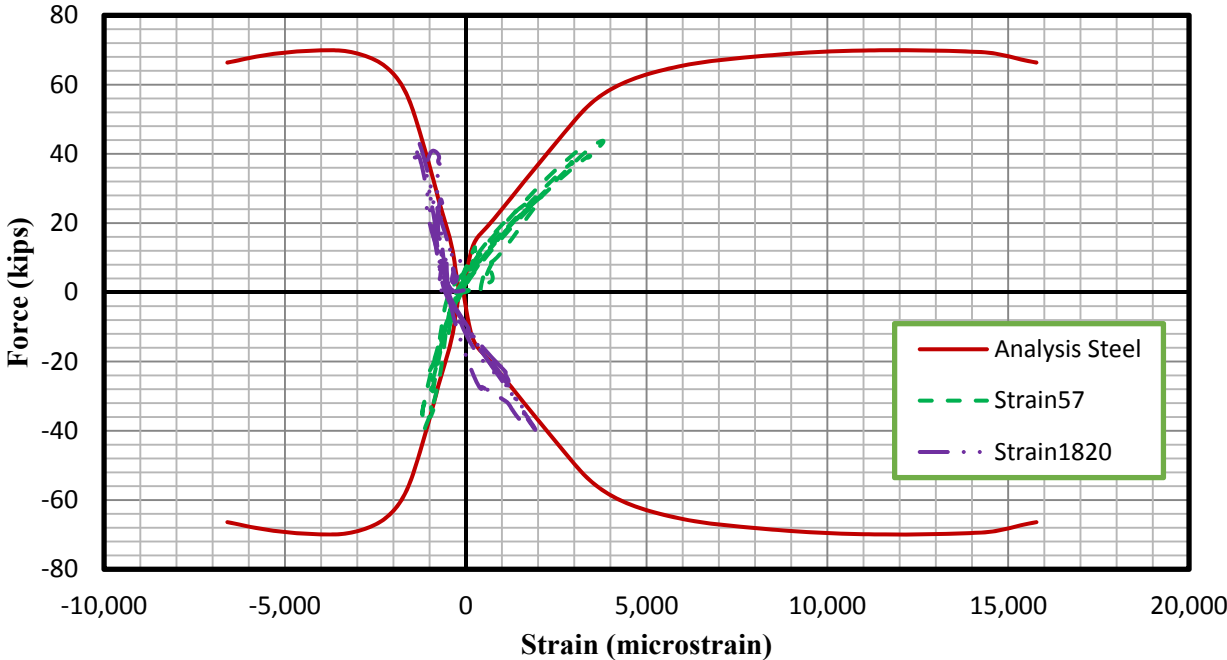


Figure 5-68: Attached LED concrete strain measured during testing and analytical strain vs. applied lateral load for Specimen H1C2-C

As shown in Figure 5-65 through Figure 5-68, the strains measured by the LEDs near the extreme tension and compression faces agree very closely with the extreme tension and compression analytical steel strains. The LED strains seem to provide a better estimate of the extreme fiber compression strain in the concrete when compared to the compression strains measured by strain gauges on the longitudinal reinforcement which were presented in the Section 5.3.1.2.4. The analytical strains match up well with the measured LED strains, even for the one inch thick specimens which experienced early failure.

5.3.1.2.6 Circular hoop strain

During the testing the strains were measured in the transverse reinforcement using strain gauges. These measured strains can provide information about the demand on the confinement, as well as providing an indication of if the transverse reinforcement was close to fracture. For the circular test specimens, the failures occurred due to longitudinal steel rupture at low steel strain for the solid and two-inch thick specimens and due to local failure for the one-inch thick specimens. These failures occurred at a fairly low ductility, which means that the confinement most likely was not subjected to high demand. This was found to be true based on the measured transverse steel strains, which at the most only reached close to 1500 microstrain prior to specimen failure out of all the specimens.

Specimen SC2-C experienced the highest transverse steel strain, which did not even reach the yield strain of the transverse reinforcement. For this specimen, a fairly clear pattern was noticed, where the transverse reinforcement reached higher tensile strains when that section was under compression, as would be expected. This pattern is illustrated in Figure 5-69 and Figure 5-70. The pattern is clearer in Figure 5-70, where the two gauges on the transverse reinforcement agree very closely.

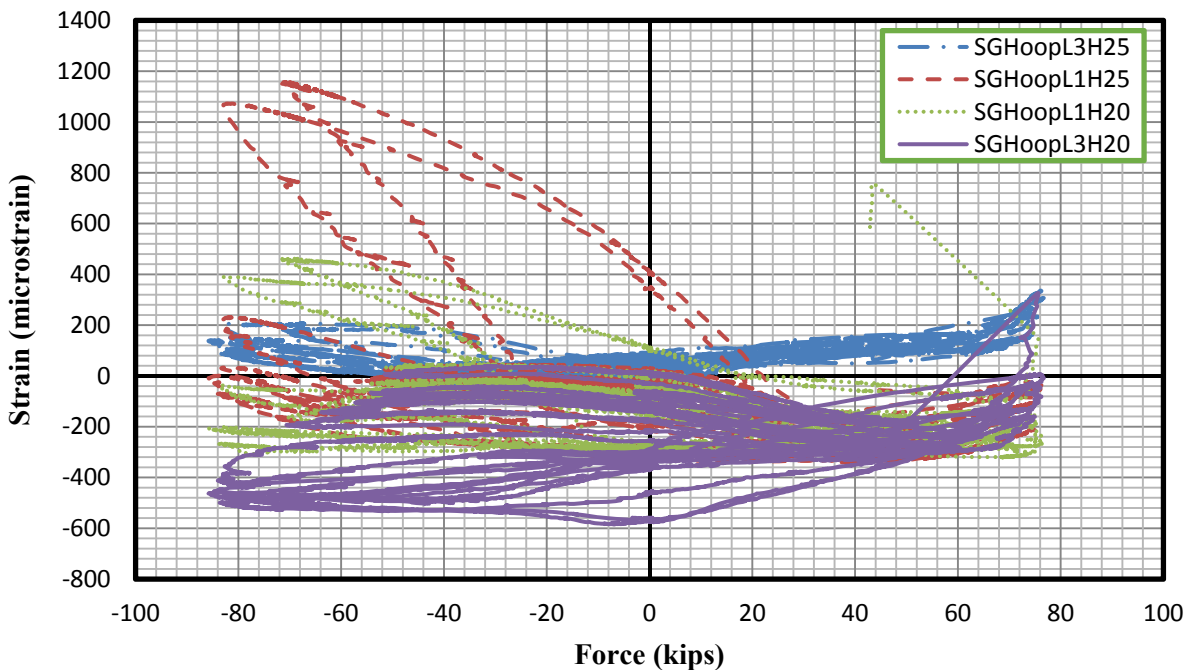


Figure 5-69: Hoop strains near longitudinal bar 1 vs. applied load in Specimen SC2-C

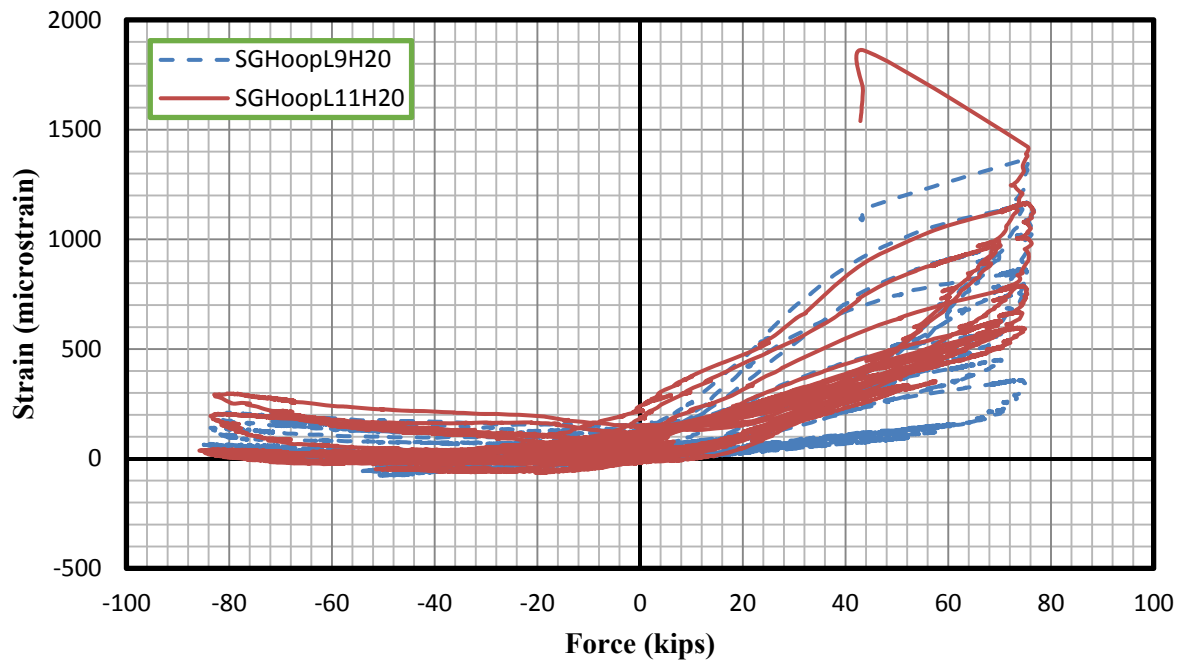


Figure 5-70: Hoop strains near longitudinal bar 11 vs. applied load for Specimen SC2-C

For the hollow sections, the pattern was typically much less clear, partly due to the fact that the transverse steel strains remained very low, usually under 1000 microstrain. These low strains for the hollow section illustrate that the failure of transverse reinforcement was not a concern, and that very little demand was induced in the transverse reinforcement. Even for specimen SC2-C which experienced higher transverse tensile strains, the transverse reinforcement did not yield, which showed that the specimen was confined adequately. This observation was consistent with the analytical findings based on the confinement analyses present in Section 3.2.6.

5.3.2 Square section

The results of the square column tests are described in the following sections. The solid test specimens had satisfactory results, while the hollow specimens experienced premature local and shear failures. These local and shear failures seem to have been caused by small wall thickness, poor quality concrete resulting from tight spacing in some areas although these regions were patched, and possibly inapplicability of shear design procedure developed for solid members to hollow concrete members.

5.3.2.1 Square section visual observations

SS1-M

Specimen SS1-M was loaded monotonically under 28.8 kips of axial load until failure. The loading was paused at predetermined targets to mark cracking. Flexural cracking began appearing at $0.75F_y$, where F_y is the force at first yield. Slight shear cracking began to occur when the specimen was pushed to the first yield point. Cracks continued to widen and the amount and length of the shear cracks gradually increased. The specimen failed due to tension steel rupture on the way to displacement ductility 3. Crushing of cover concrete at the compression face was observed after failure, especially at the specimen compression corners.

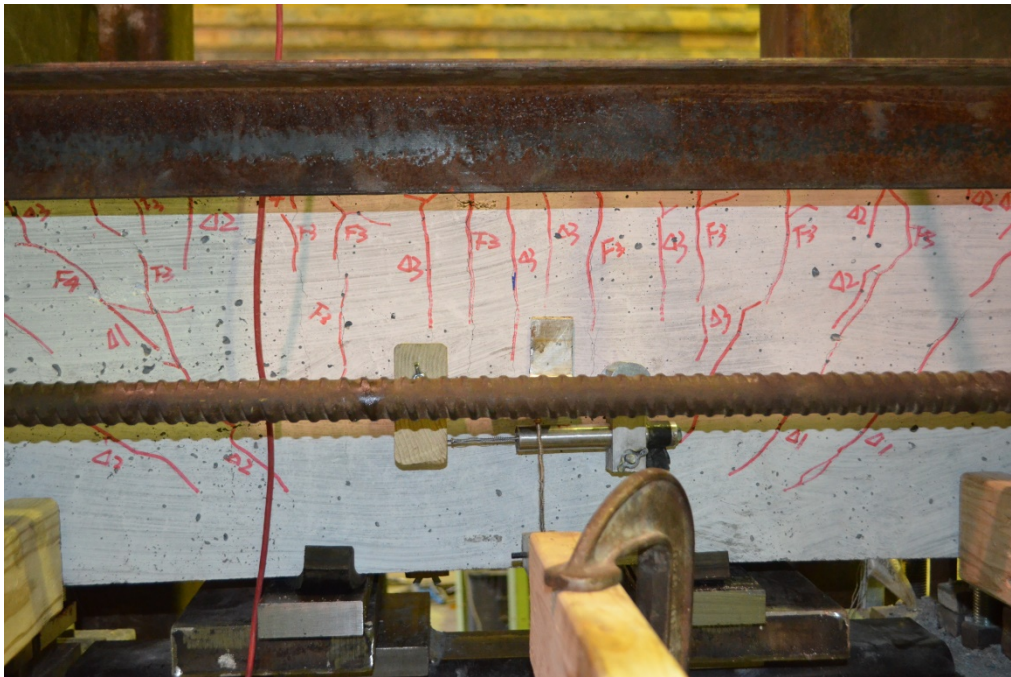


Figure 5-71: Specimen SS1-M prior to failure



Figure 5-72: Close-up view of large flexural crack after failure for Specimen SS1-M

SS2-C

Specimen SS2-C was loaded cyclically under 57.6 kips of axial load until failure. Slight flexural and shear cracks first appeared at $0.75F_y$, as observed for the monotonic loading case. The amount of flexural cracks gradually increased as loading continued, with the flexural crack spacing seeming to coincide with the transverse reinforcement spacing. The amount and length of shear cracks also gradually increased as loading continued. In the cycles near displacement ductility two, the cover concrete at the specimen corners under the central loading points began to crush slightly, most likely due to local stresses due to loading. The specimen failed during the first cycle at displacement ductility three due to tension steel reinforcement rupture, and a large flexural crack opened up. The cover concrete at the compression face was crushed after failure.

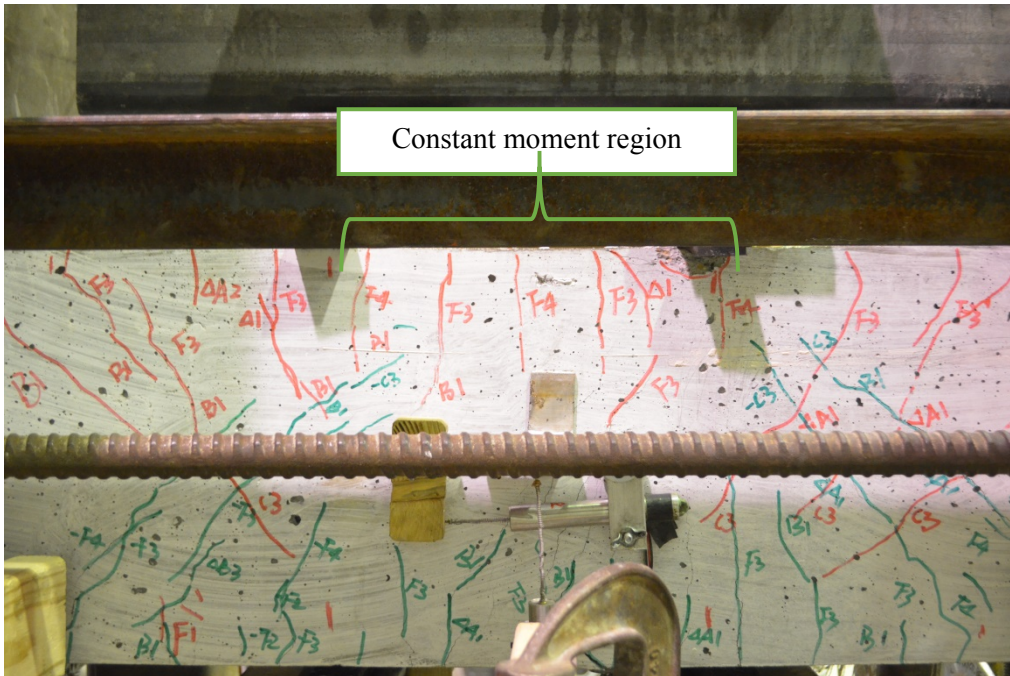


Figure 5-73: Crack pattern of Specimen SS2-C at displacement ductility three prior to failure



Figure 5-74: Large flexural crack in constant moment region of Specimen SS2-C after failure

The hollow square specimens presented in the remainder of this section experienced premature local and shear failure, as previously noted. The early failures may be due to the small wall thickness combined with local effects at the loading and support points. Additionally, these specimens had been patched to fix poor concrete fill, and the early failure seemed to coincide with patched locations, although it is unclear what the primary cause of failure may have been for these specimens.

H2S1-M

Specimen H2S1-M was loaded monotonically under 28.8 kips axial load until failure occurred. Minor shear cracks first appeared in the second increment in the linear moment region, followed by many small shear cracks appearing in the third increment. Flexural cracks began appearing in the constant moment region at F_y in the linear phase. As displacement ductility one was approached, some local concrete cover crushing appeared near the corners by the point of loading, followed by significant crushing as shown in Figure 5-75. After continuing loading, the specimen failed due to what appeared to be a combination of local failure at a point of load application and wall buckling occurring inward. The compression wall between the loading points appeared to fail with a section of the wall failing inward, causing the longitudinal reinforcing bars to buckle inward as well. Some longitudinal reinforcing bars on the side of the specimen near the compression face in the constant moment region were seen to be buckled shortly after failure as well, as shown in Figure 5-77. The amount of transverse reinforcement provided was above the minimums recommended in order to prevent longitudinal reinforcing bar buckling. It is likely that when the compression wall buckled inward the sudden loss of compression area resulted in high compressive stresses in the longitudinal reinforcement which may have caused the buckling to occur.

Flexural cracks could be seen to have widened presumably as a result of the observed failure. After removal of the load, it was seen that significant indentations in the concrete under the points of load application were visible. Photos of the inside face prior to failure shows some cracking before the inner compression wall suddenly failing inward.

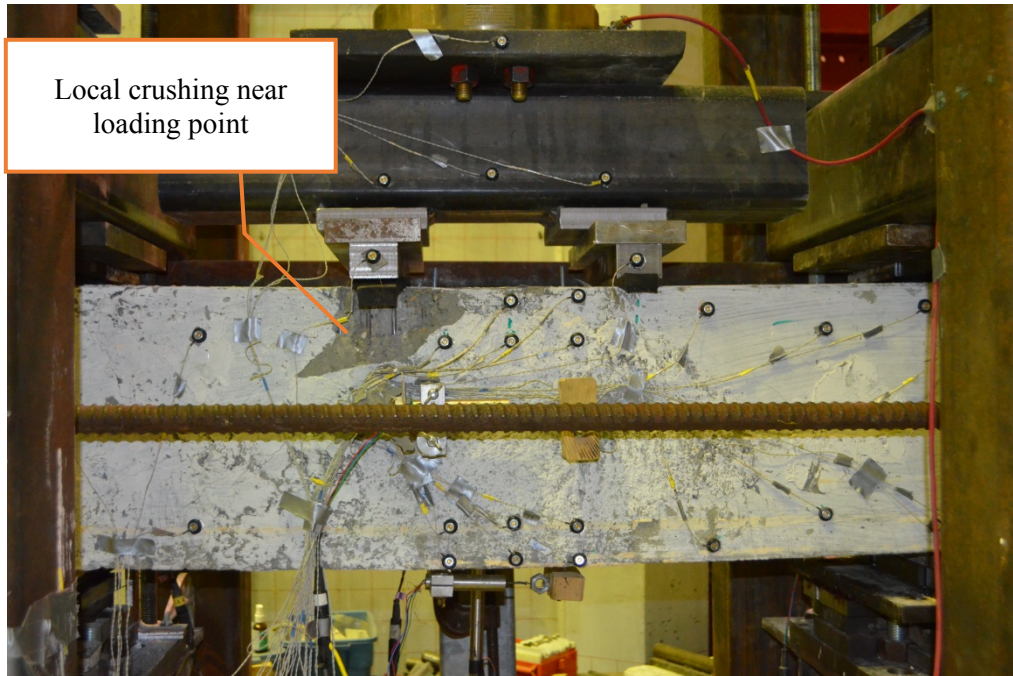


Figure 5-75: Local crushing and spalling of cover concrete in Specimen H2S1-M at displacement ductility one

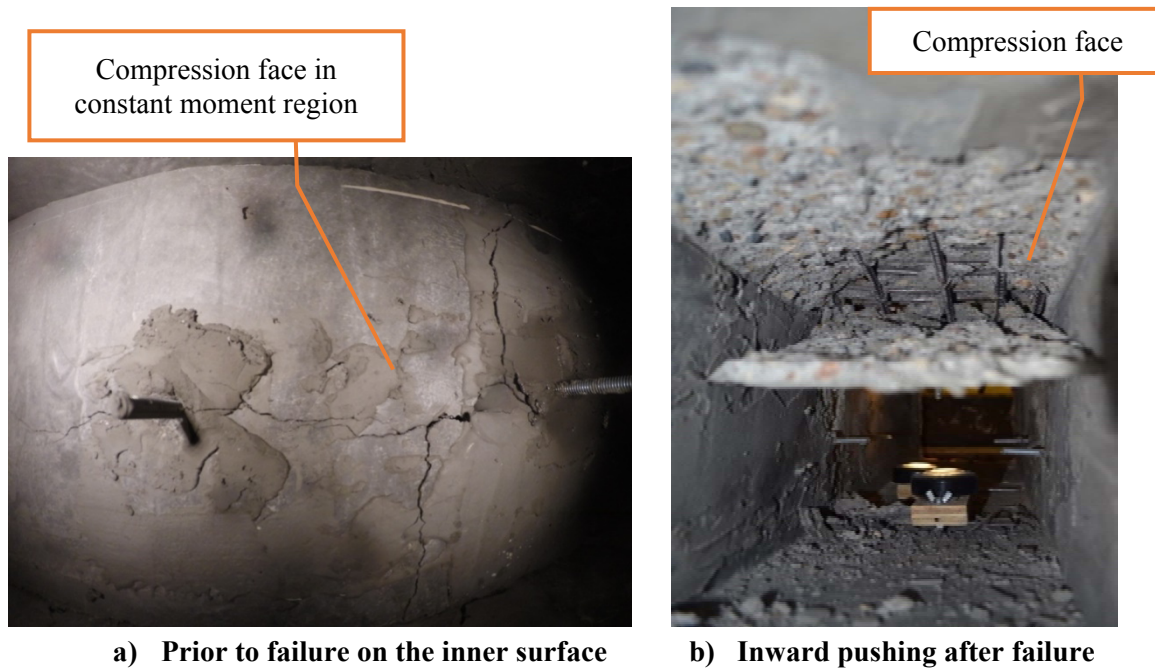


Figure 5-76: Compression face prior to failure and inward failure of the compression face concrete in the wall of Specimen H2S1-M



Figure 5-77: Longitudinal reinforcement buckling after failure in Specimen H2S1-M

H2S2-C

Specimen H2S2-C was tested cyclically under 28.8 kips of axial load until failure. After witnessing the local failure of specimen H2S1-M and following the experience from the hollow circular column testing, wooden support blocks were added inside the column at the support locations in an effort to brace this region and avoid local failure. Shear cracks first appeared in the linear moment regions at the cycle of $0.5F_y$, with more shear cracks appearing in the cycle at $0.75F_y$. Some concrete spalling in the linear moment region began appearing in this cycle as well. In the first part of the cycle at F_y , shear failure occurred with significant spalling of concrete in the linear moment region at one end of the specimen. On the front side, a large shear crack was visible, as shown in Figure 5-80. The inside face of the specimen in the central region experienced some cracking, but remained mainly undamaged.

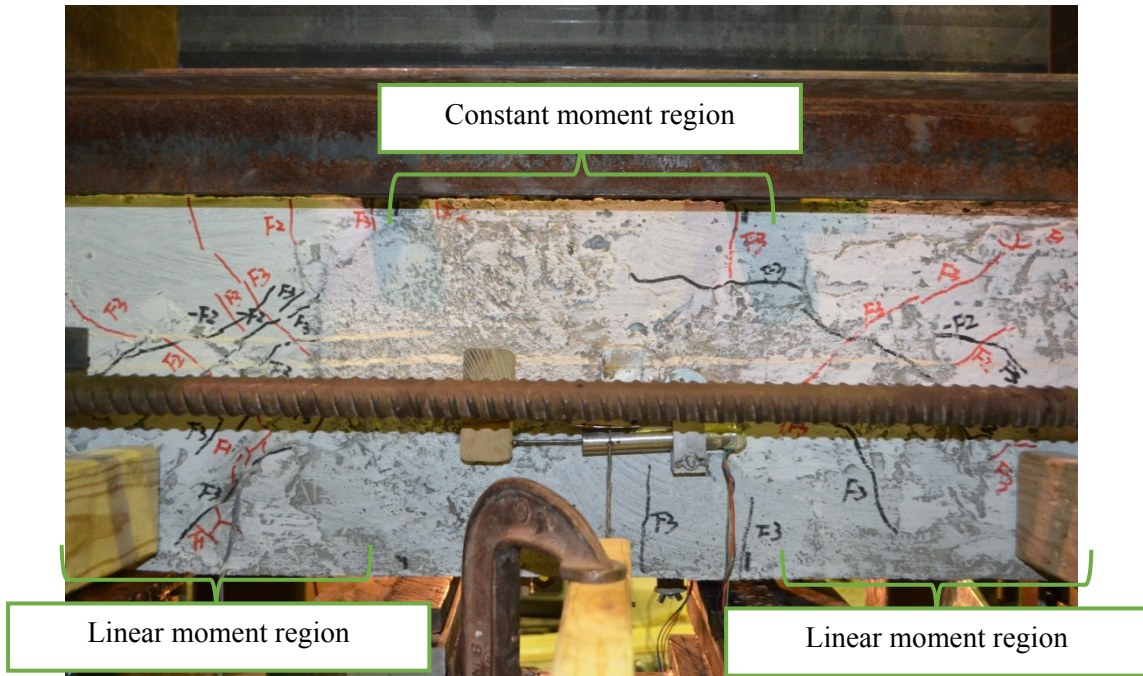


Figure 5-78: Crack pattern of Specimen H2S2-C in the cycle at $0.75F_y$



Figure 5-79: Shear failure in the linear moment region in Specimen H2S2-C



Figure 5-80: Large shear crack in the linear moment region on LED side of Specimen H2S2-C after failure

H2S3-C

Specimen H2S3-C was tested cyclically under 57.6 kips of axial load until failure. This specimen also contained wooden braces inside the column at the loading and support points in an effort to avoid local failure. Slight shear cracking appeared in the second cycle in the linear moment region with the number and length of the shear cracks increasing significantly into the cycles at $0.75F_y$ and F_y . Local cover concrete crushing began occurring at the loading points in the second cycle and continued to increase with some significant cover concrete spalling occurring in the cycle at $0.75F_y$. The specimen failed in the second part of the cycle at F_y , due to shear failure. The inside face experienced some slight cracking prior to failure but otherwise was mainly undamaged.

It was clear that shear effects were contributing significantly to the behavior of hollow columns. The measured displacements found during testing were much higher than anticipated based on the preliminary OpenSees analysis performed for these specimens. In order to quantify the effect of shear on the specimens, the shear component of the displacement needed to be estimated. A

measurement of the shear component of displacement was able to be taken by using a grid of LEDs, and the results of this investigation are further discussed in Section 5.3.2.2.2.

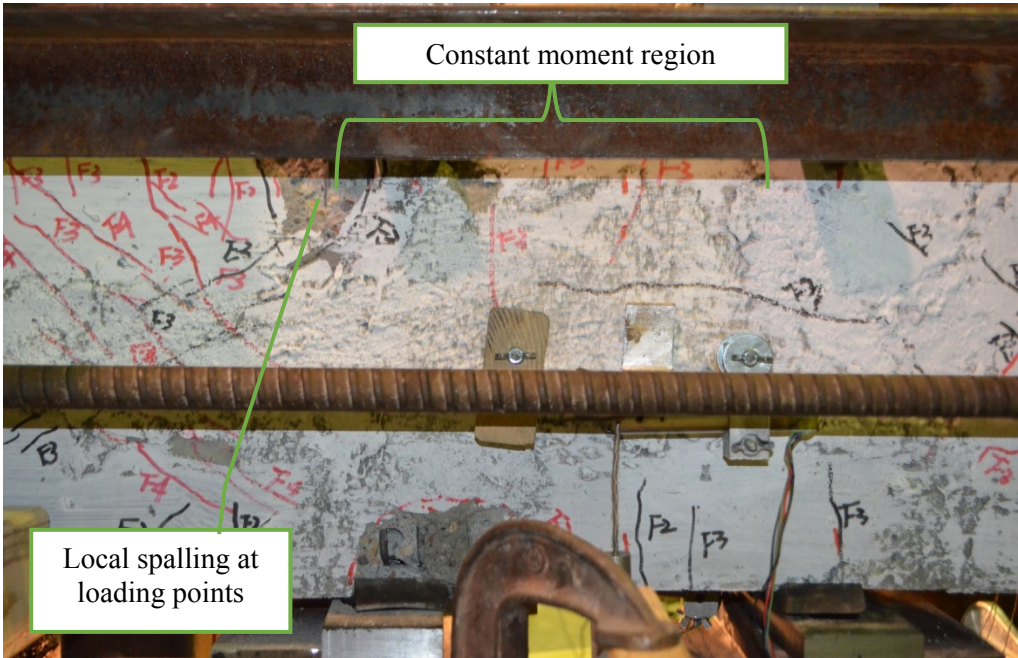


Figure 5-81: Local spalling and crack pattern in the first part of cycle at F_y in Specimen H2S3-C



Figure 5-82: Close-up view of local cover crushing at load point while unloaded prior to the second part of the cycle at F_y in Specimen H2S3-C

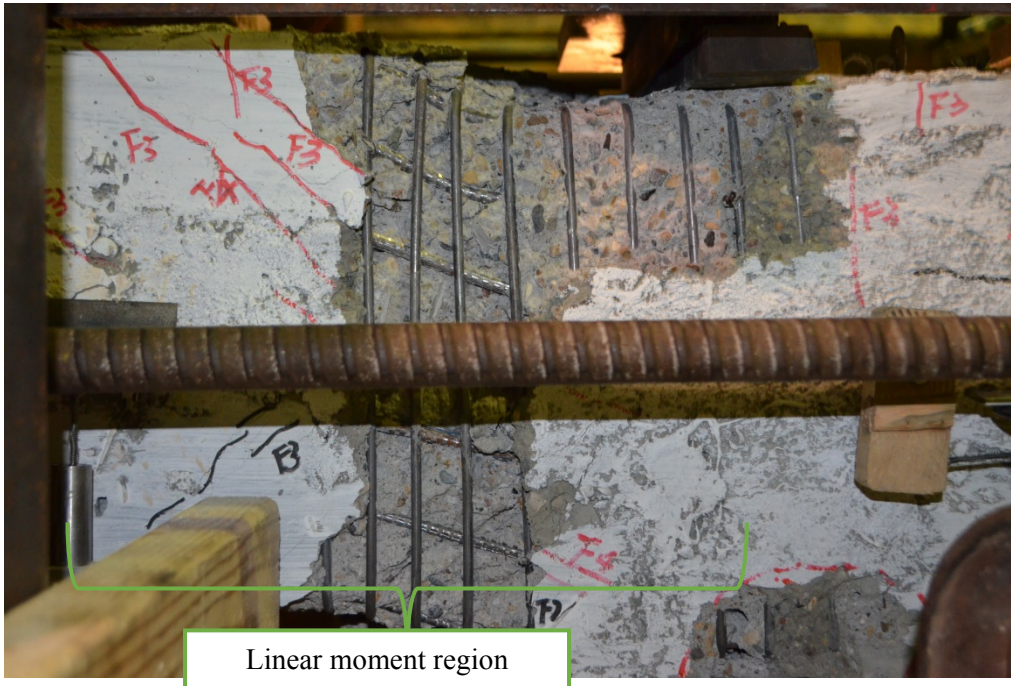


Figure 5-83: Shear failure in the linear moment region in Specimen H2S3-C

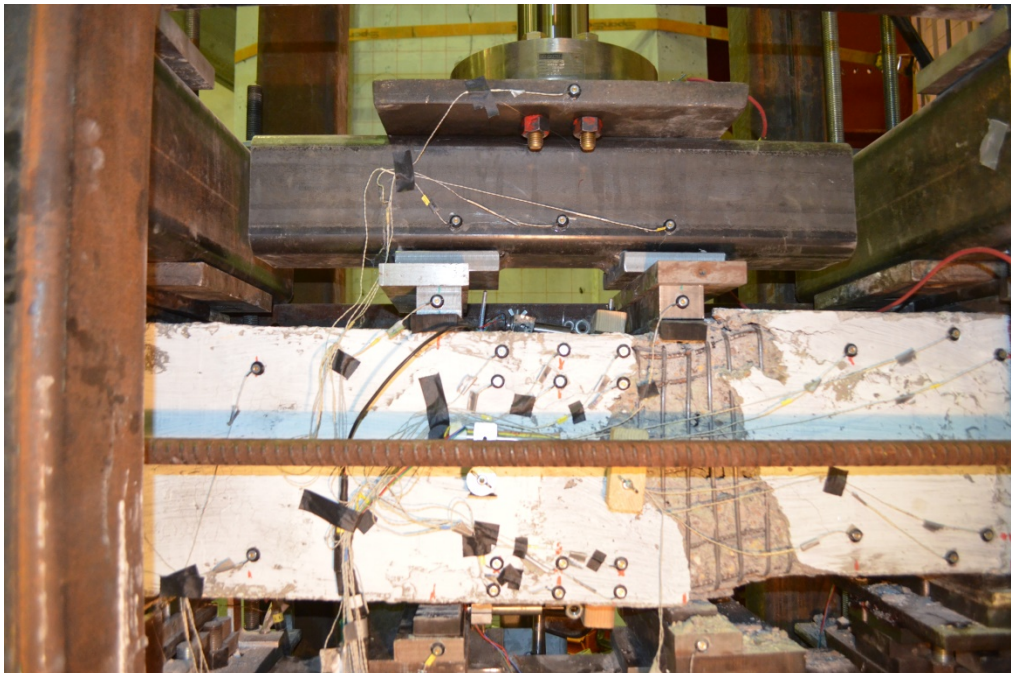


Figure 5-84: LED side after failure in Specimen H2S3-C

H1.25S1-M

Specimen H1.25S1-M was loaded monotonically under 28.8 kips of axial load. It also had wooden braces on the inside near the support and load locations in an effort to avoid local failure. The specimen experienced shear cracking in the linear moment region at $0.5F_y$. On the way to $0.75F_y$ the specimen experienced premature shear failure in the linear moment region at one end of the specimen. The shear failure was somewhat lopsided and a large damage region was visible on the backside of the specimen but not on the LED side. The inside compression face was mainly undamaged.



Figure 5-85: Shear failure in the linear moment region in Specimen H1.25S1-M



Figure 5-86: LED side of damaged linear moment region after failure in Specimen H1.25S1-M

H1.25S2-C

Specimen H1.25S2-C was tested cyclically under 28.8 kips axial load until failure and contained wooden braces at the loading and support points. In the cycle at $0.5F_y$, some slight shear cracks appeared in the linear moment region as well as some cover concrete spalling at one of the points of load application. In the second part of the cycle at $0.5F_y$, a local failure occurred at the support, as shown in Figure 5-87. The inside face compression concrete was not damaged during the testing.



Figure 5-87: Specimen H1.25S2-C support after failure

H1.25S3-C

Specimen H1.25S3-C was tested under 57.6 kips axial load until failure. This specimen also had wooden braces near the loading and support points. The specimen experienced premature failure in cycle at $0.5F_y$. The failure occurred near the support as shown in Figure 5-88 due to local crushing and loss of concrete. The concrete spalled off entirely from the wall on the side of the specimen near the end plate where the axial load is applied. The specimen quickly lost both lateral and axial load capacity after failure. No damage occurred to the inside compression face in the constant moment region of the column.

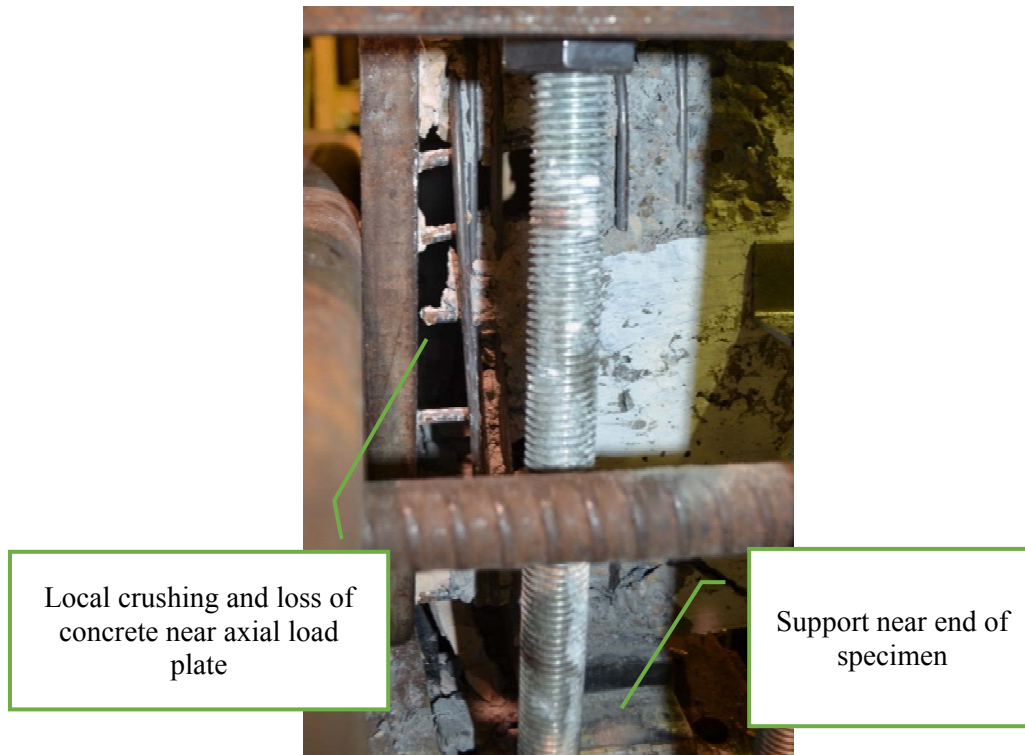


Figure 5-88: Specimen H1.25S3-C end support after failure

5.3.2.2 Square section test results and comparisons to analytical results

5.3.2.2.1 Overall force displacement response

The recorded values from the load cells and the measured displacements, has been used to determine the force-displacement response of each specimen. The force-displacement response of each test unit as well as that predicted based on the finite element analyses are shown in the figures below. Both the experimental responses and the finite element predictions shown in this section include the shear effects. The displacement response was found using the LEDs, and the data has been processed for to remove outliers and noise. For the monotonic tests, the envelope response has been provided to avoid noise and drops which occurred when the loading was paused for crack marking.

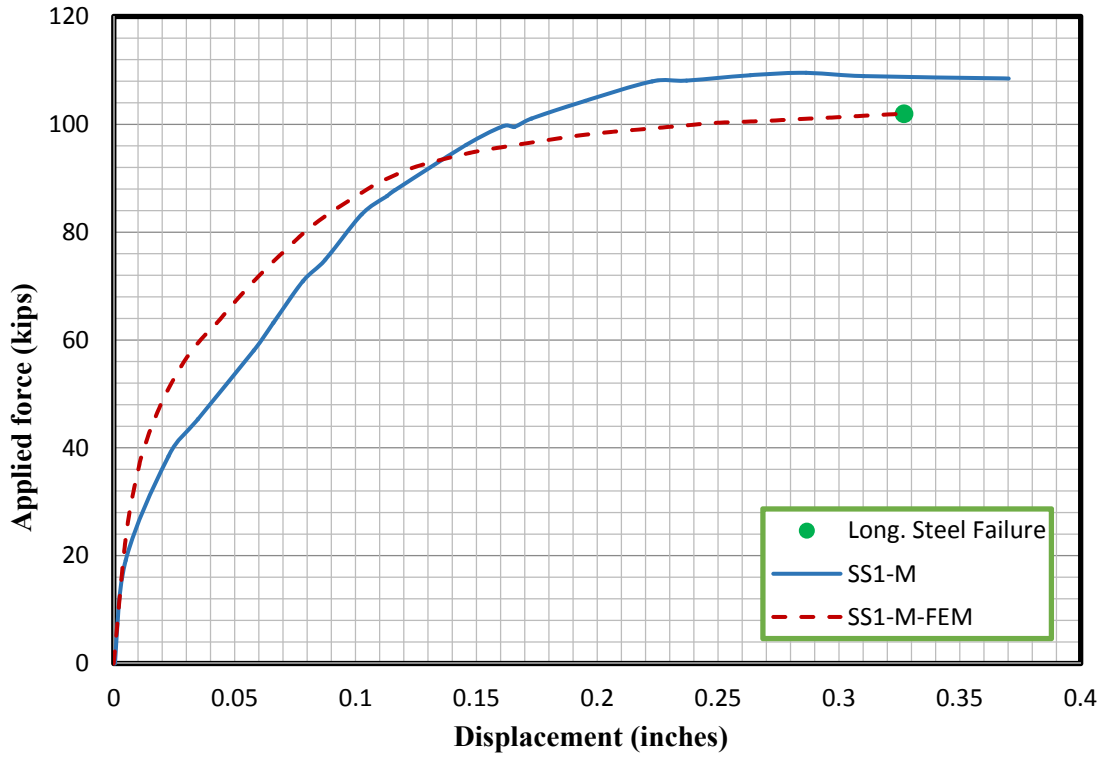


Figure 5-89: Force-displacement response of Test Unit SS1-M

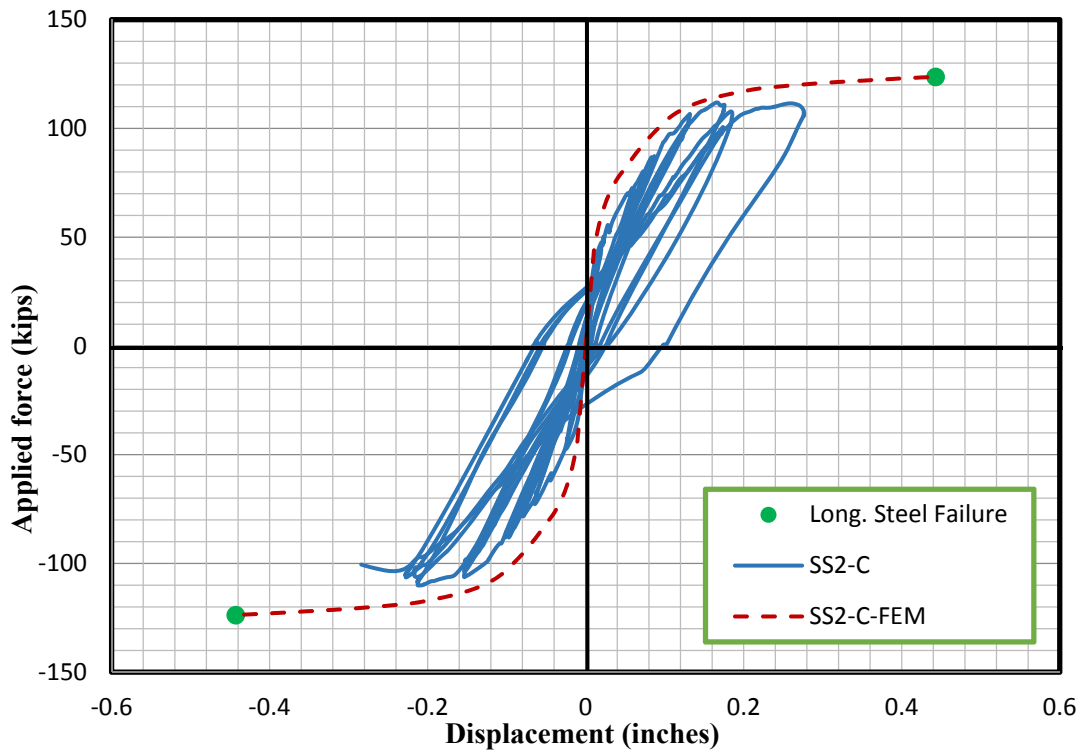


Figure 5-90: Force-displacement response of Test Unit SS2-C

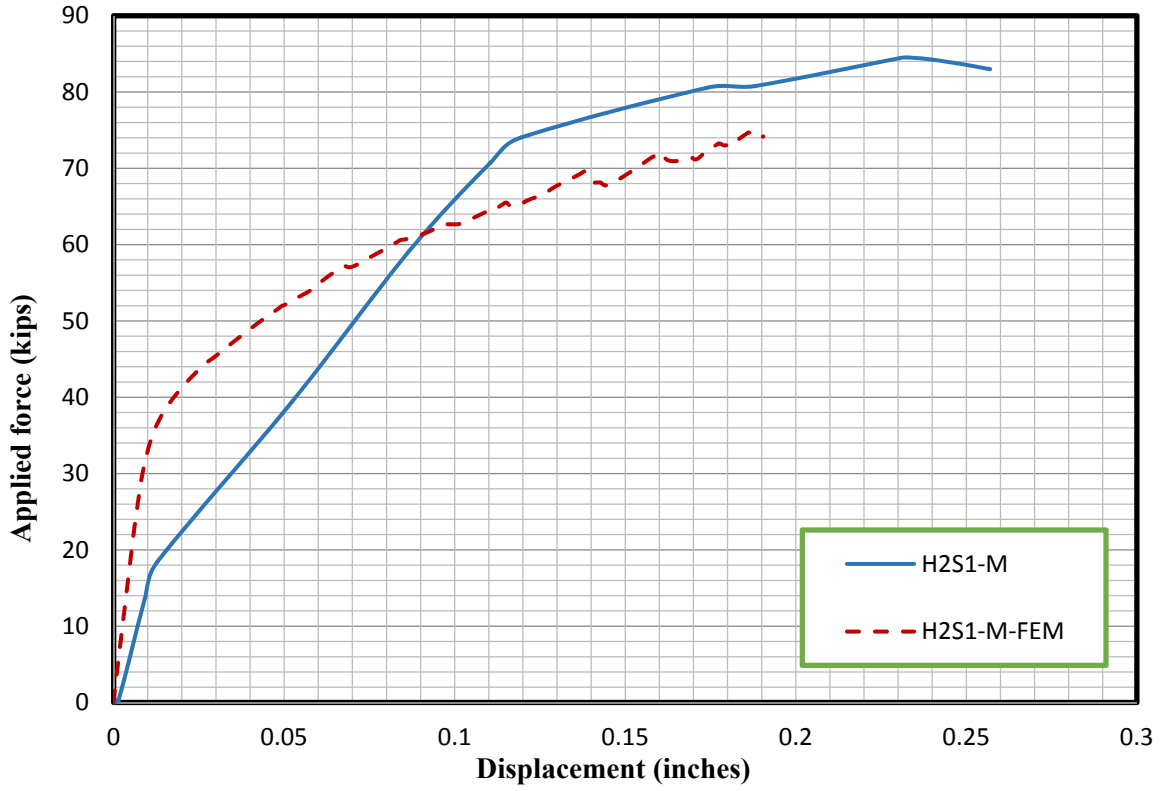


Figure 5-91: Force-displacement response of Test Unit H2S1-M

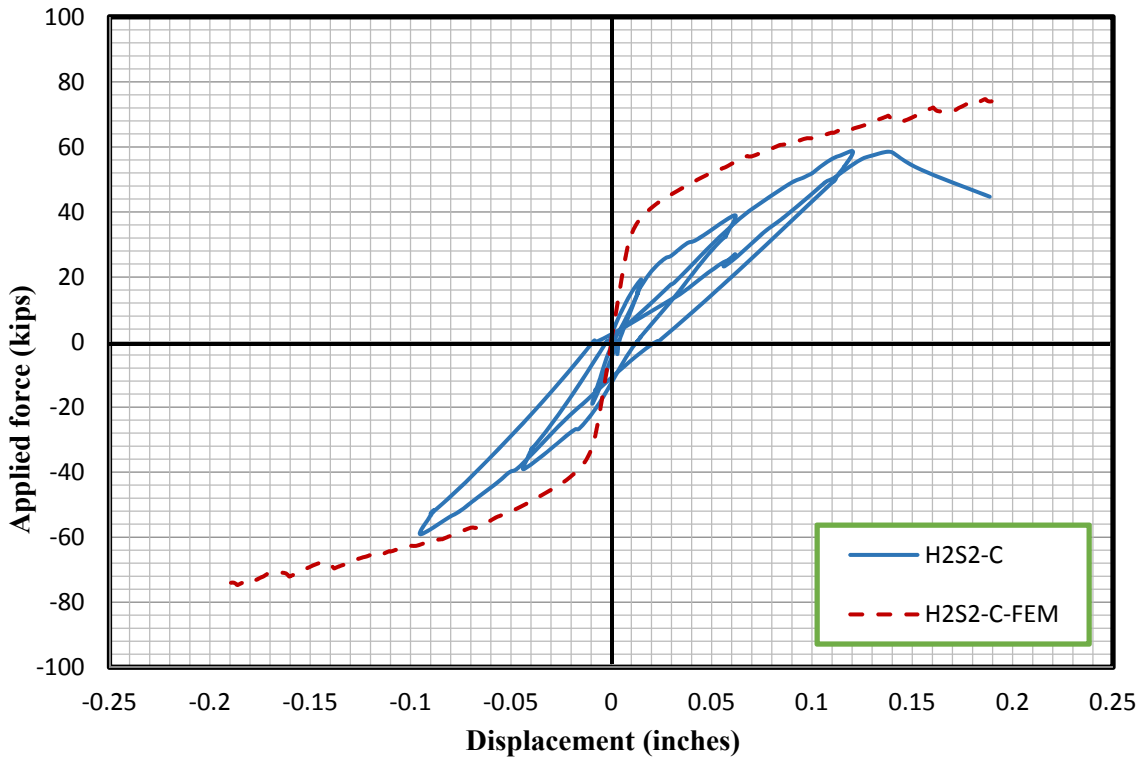


Figure 5-92: Force-displacement response of Test Unit H2S2-C

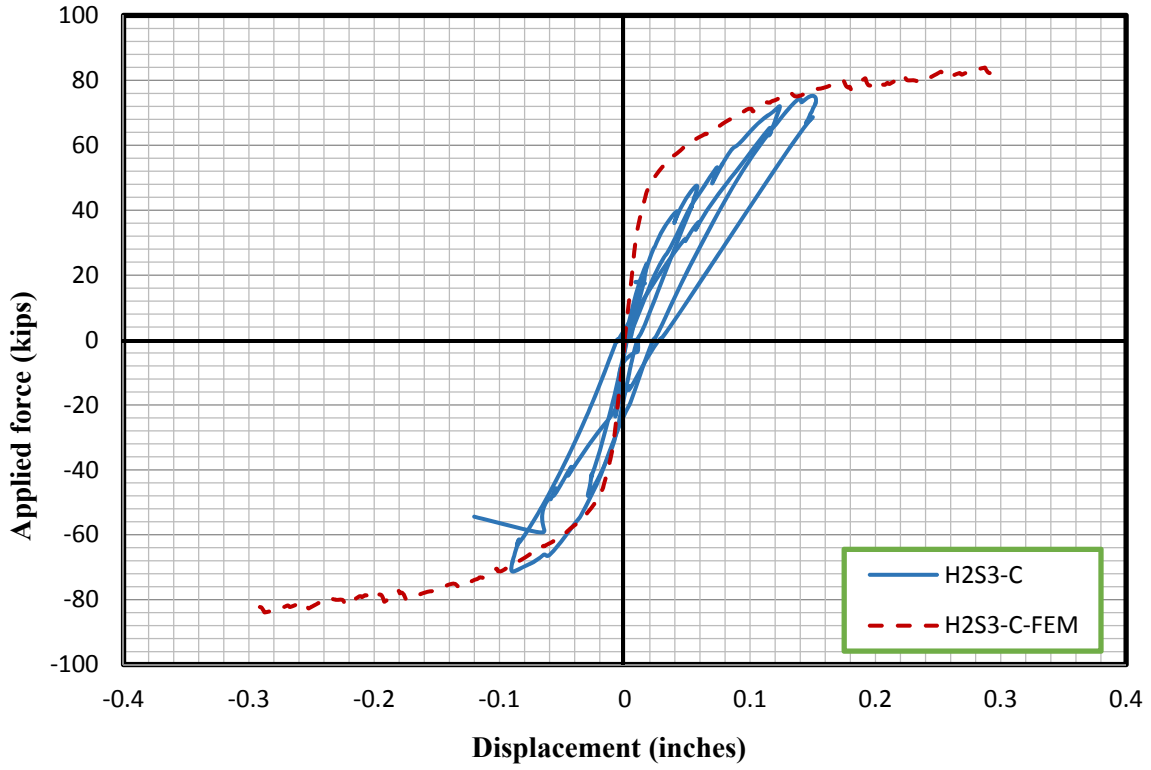


Figure 5-93: Force-displacement response of Test Unit H2S3-C

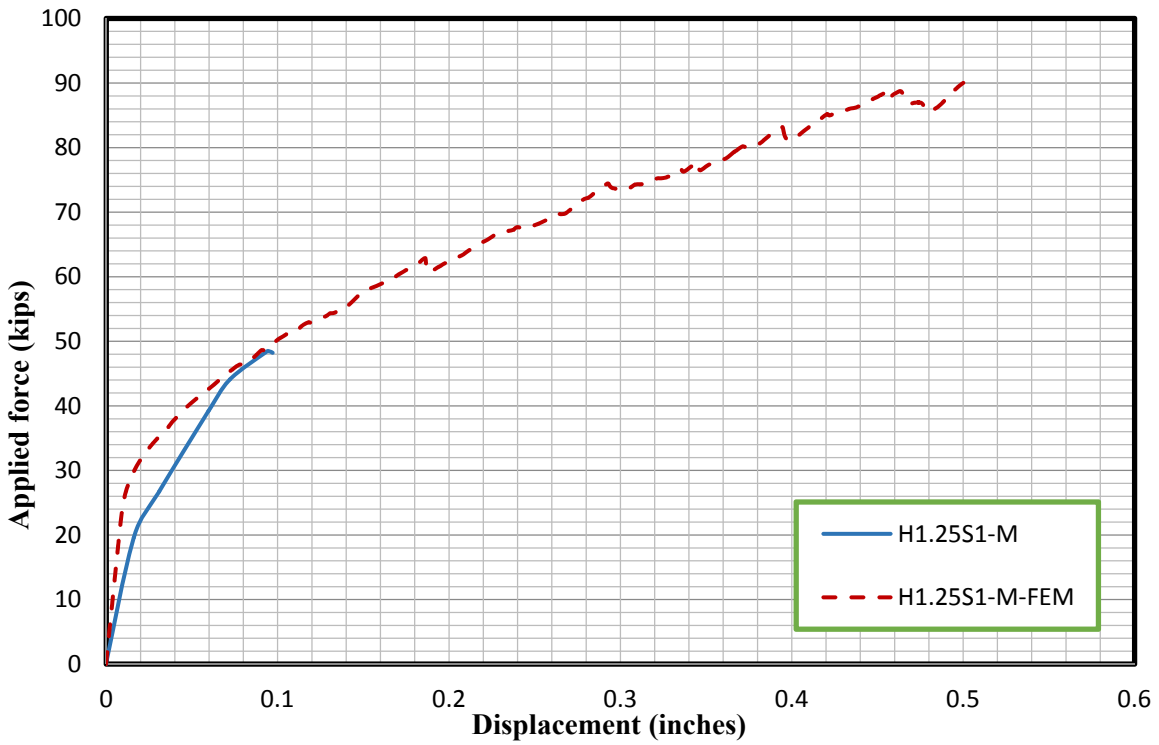


Figure 5-94: Force-displacement response of Test Unit H1.25S1-M

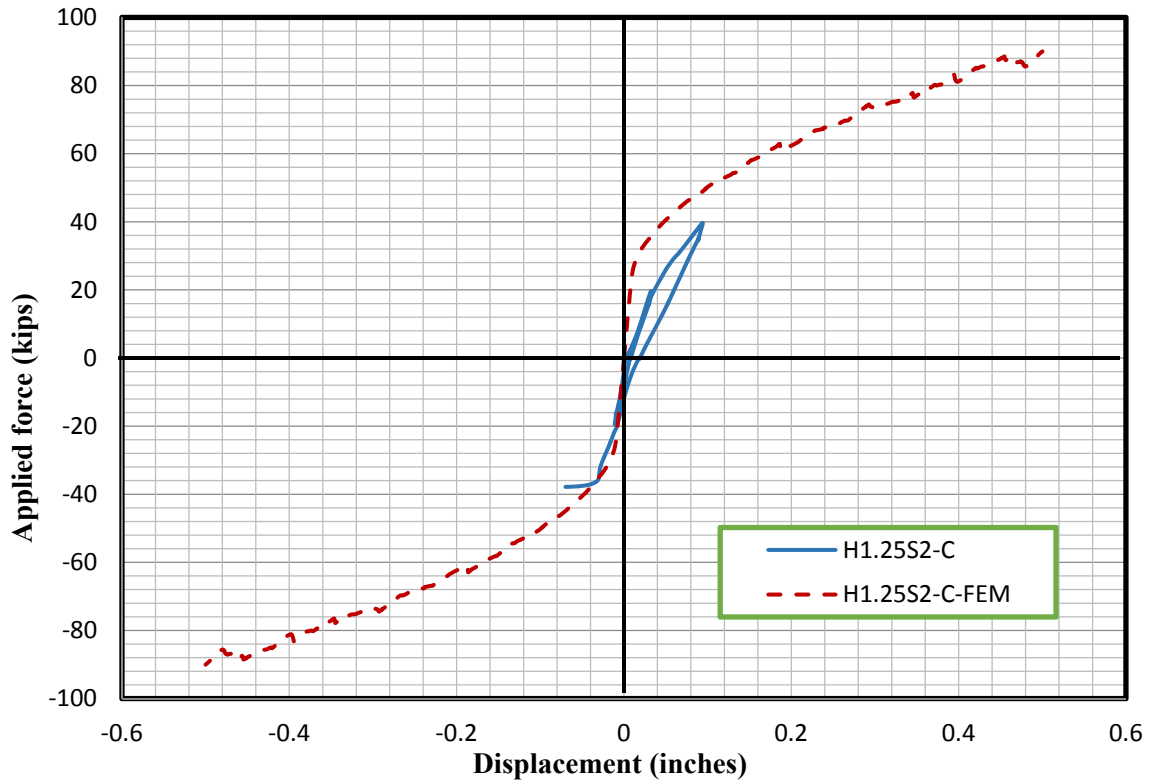


Figure 5-95: Force-displacement response of Test Unit H1.25S2-C

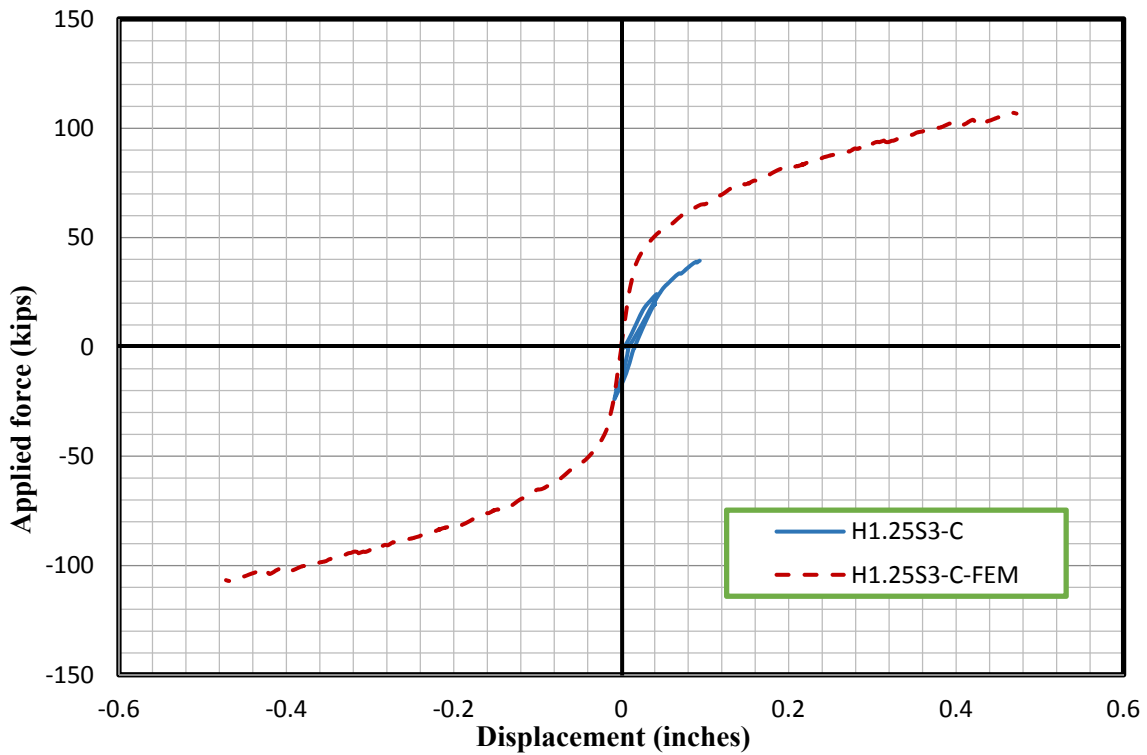


Figure 5-96: Force-displacement response of Test Unit H1.25S3-C

According to Figure 5-89 through Figure 5-96, the FE analyses could accurately capture the response of solid square sections. However, problems arose for the hollow square sections. As discussed in Section 5.2.4, the program could not get convergence even after the stabilization option was incorporated into the analyses for the hollow square sections. No failure was found from the FE analyses before the convergence problem occurred. The convergence problem may come from the confining effect for hollow square column with one layer of confinement reinforcement. The confinement reinforcement placed near the outside concrete wall may not confine the hollow section properly, due to the non-uniform confining pressure applied and the corner effect, especially for the larger wall thickness.

As shown in these figures, the initial stiffness of the hollow specimens based on the FE analyses results is significantly greater than that experienced by the test specimens. This may come from the $1.5\sqrt{f'c}$ of concrete tensile strength input in the ABAQUS. The second stiffness after the concrete cracking occurred is very comparable to that presented by the test specimens. This indicated that the FE analyses could capture the behavior of square hollow sections with moderate accuracy. However, the confinement effect for hollow square sections that had one layer of transverse reinforcement needs further investigation.

Figure 5-97 shows a comparison of the force-displacement response for the solid, two-inch, and 1.25-inch wall hollow columns under 28.8 kips axial load. As shown by the figure, the hollow columns experience larger displacements than the solid column. Additionally, it can be seen that the displacement seems to increase slightly for the thinner wall. The two hollow square specimens failed early due to local and shear effects, which is why their lateral load capacity is not as high as the solid column. The two hollow columns experienced similar stiffness early on, which is likely because there is not a very large difference in wall thickness between them.

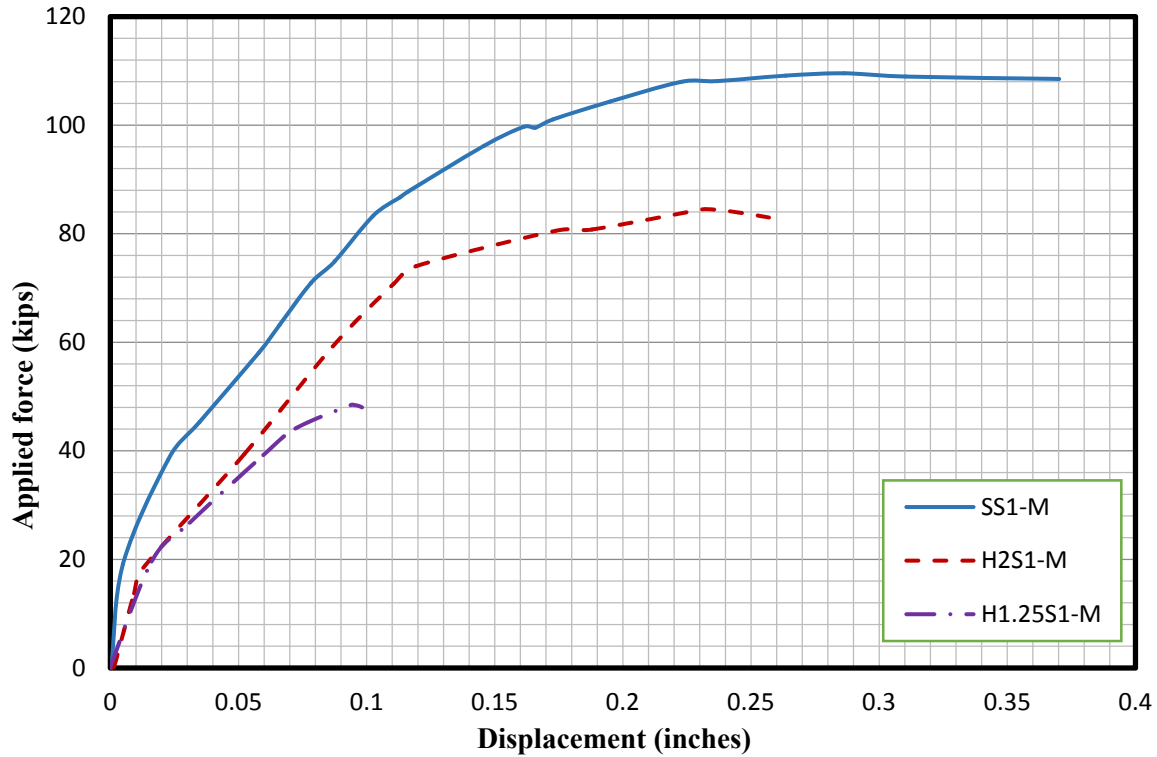


Figure 5-97: Force-displacement response comparisons for solid, two-inch wall, and 1.25-inch wall hollow columns under 22.6 kips axial load

5.3.2.2.2 Shear contribution

It became obvious during the testing that shear deformation was having a large effect on the test results for the hollow columns, which was evident in the fact that many of the square hollow columns failed in shear. The OpenSees analysis method used does not account for shear effects, and typical analysis methods used in design do not account for these effects either. Therefore, the shear contribution has been estimated in order to quantify the effect of shear on the square specimens and to provide a better comparison to the OpenSees analysis. The method has been adopted which was used previously by Sritharan (1998), and in this case, a grid of LEDs was used to determine the various deformation components. The following plots show the shear displacement plotted against the applied load for all specimens as well as the force-displacement response of each specimen with shear included and with shear subtracted for comparison. The LED data has been processed to remove noise and outliers, and the envelope has been provided for the specimens tested monotonically.

Figure 5-98 gives the overall force-displacement response as well as the force-displacement response with the shear deformation subtracted for specimen SS1-M. The shear deformation for this specimen accounts for approximately 25 percent of the overall force-displacement response.

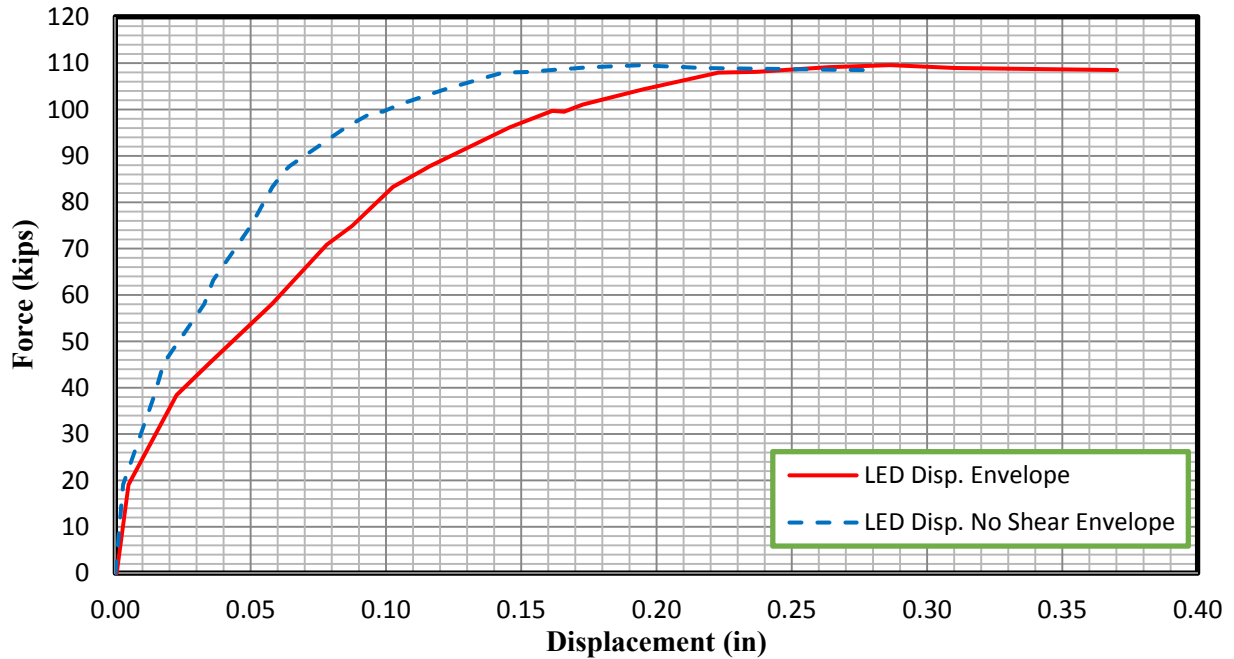


Figure 5-98: Force-displacement of Specimen SS1-M with and without shear deformation

Figure 5-99 gives the applied load plotted against the shear deformation for specimen SS1-M. As shown, the shear deformation maintains a mostly linear relationship with the applied load. The shear displacement response shown in the figure has been adjusted and zeroed. An initial negative shear displacement was measured before load was applied and during very early loading, so this initial shear displacement has been zeroed.

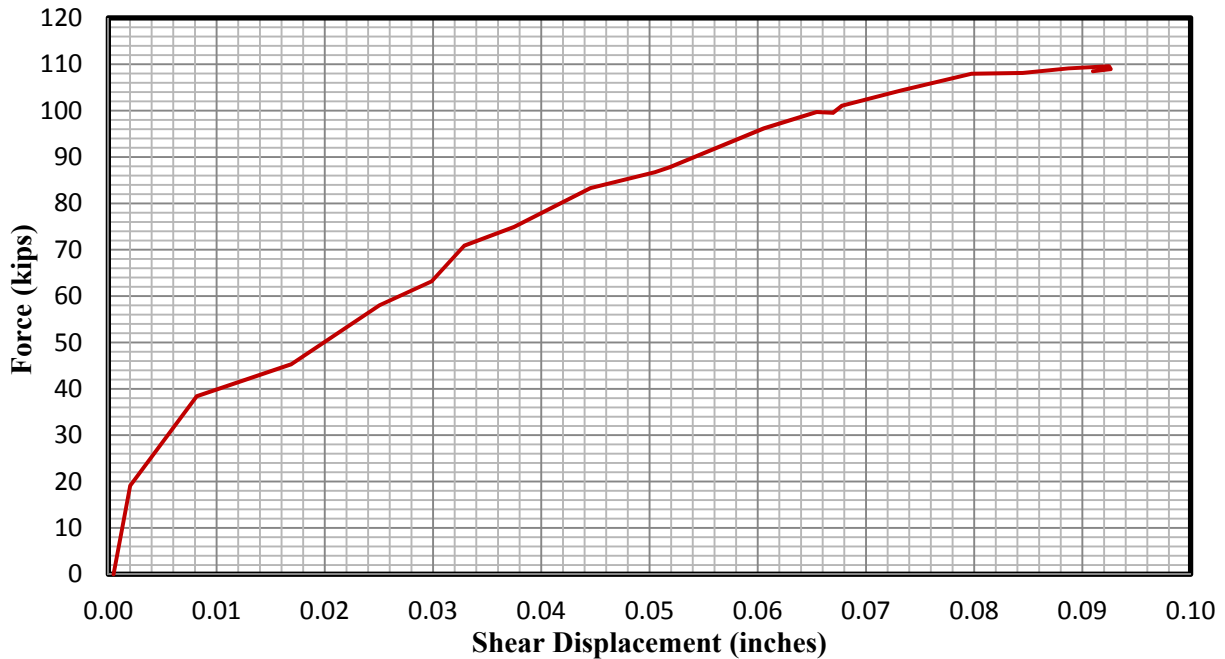


Figure 5-99: Force vs. shear displacement response for Specimen SS1-M

The force-displacement response of specimen SS2-C with and without the shear deformation can be seen in Figure 5-100. The shear component has a smaller contribution to the overall displacement for this specimen. The shear deformation is also somewhat uneven in each loading direction, with shear contributing approximately twenty percent of the overall displacement in the positive loading direction, but only eight percent in the negative loading direction. The shear deformation is plotted against the applied load for this specimen in Figure 5-101. As shown, in the positive loading direction, the shear response is very linear, while in the negative loading direction, there is very little shear deformation, and the shape does not coincide as well with linear behavior.

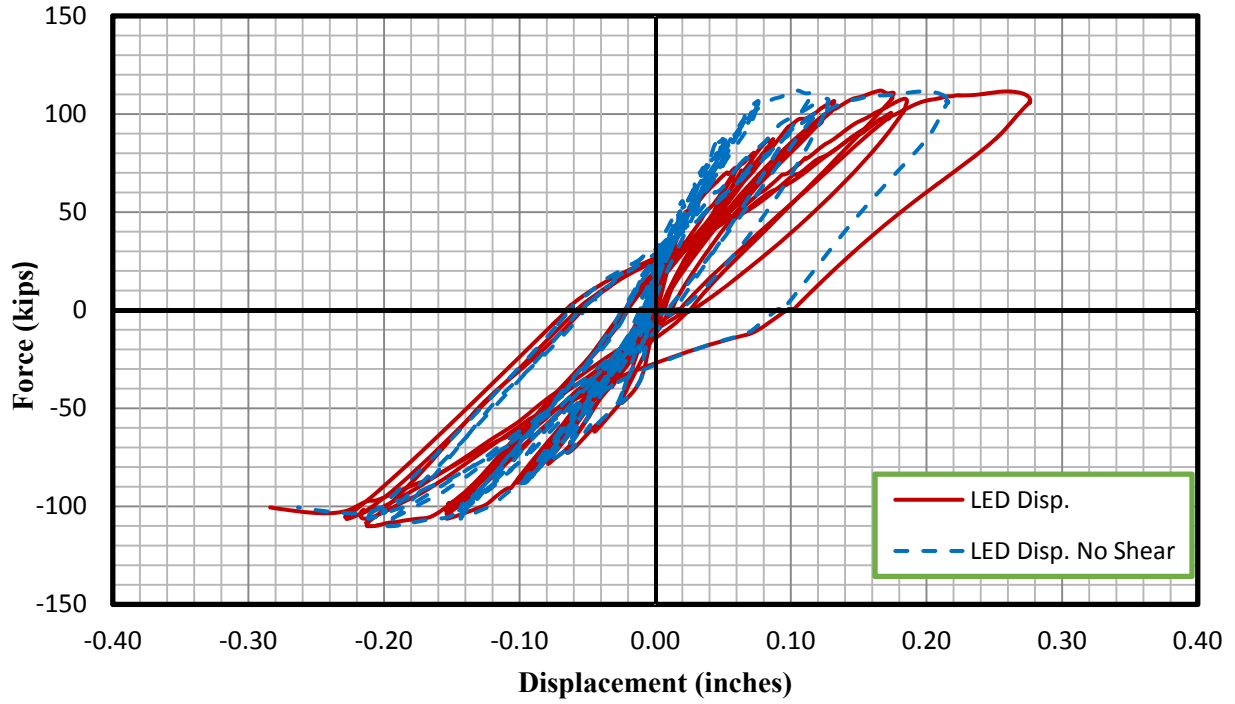


Figure 5-100: Force-displacement response of Specimen SS2-C with and without shear deformation

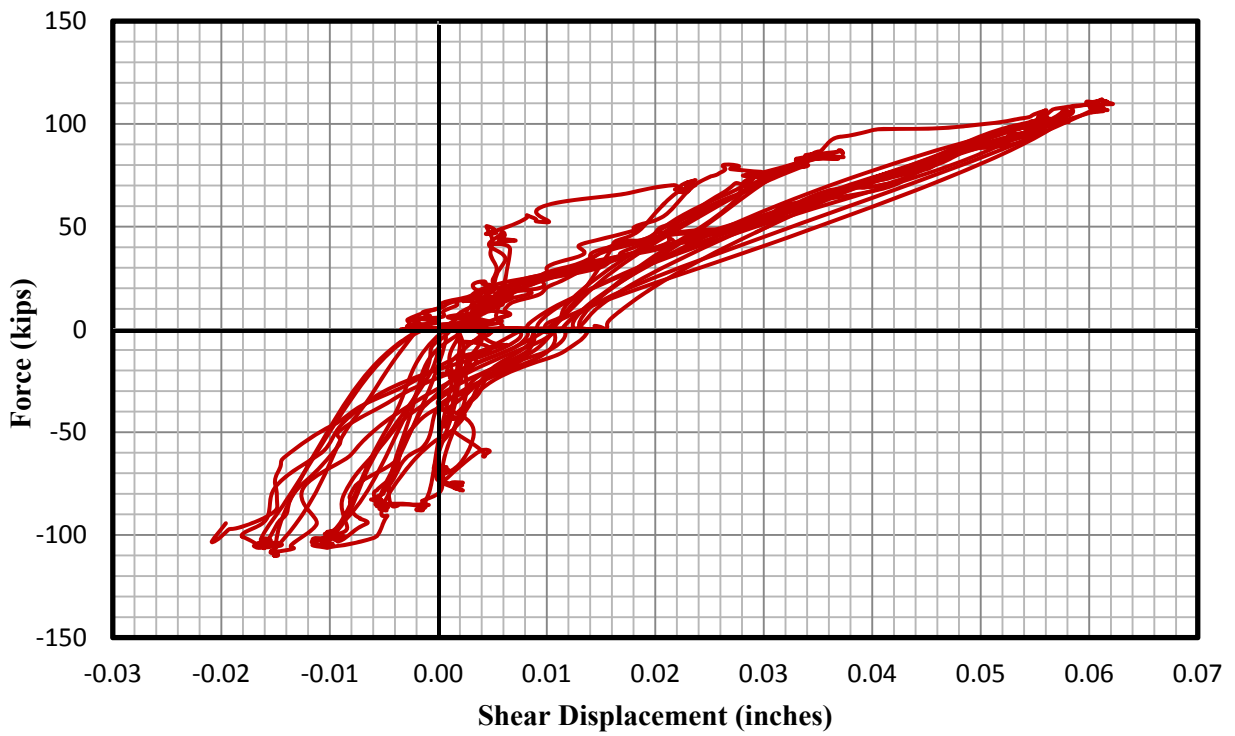


Figure 5-101: Force vs. shear displacement of Specimen SS2-C

The shear displacement measured for specimen H2S1-M accounts for approximately twenty percent of the overall displacement response, which is very similar to that of the solid sections. The force-displacement response with and without the shear deformation included can be seen in Figure 5-102, and the applied load is plotted against the shear deformation in Figure 5-103. The shear deformation response of this specimen is fairly linear as well. This specimen ultimately failed due to inward compression wall buckling and local effects at the load application points.

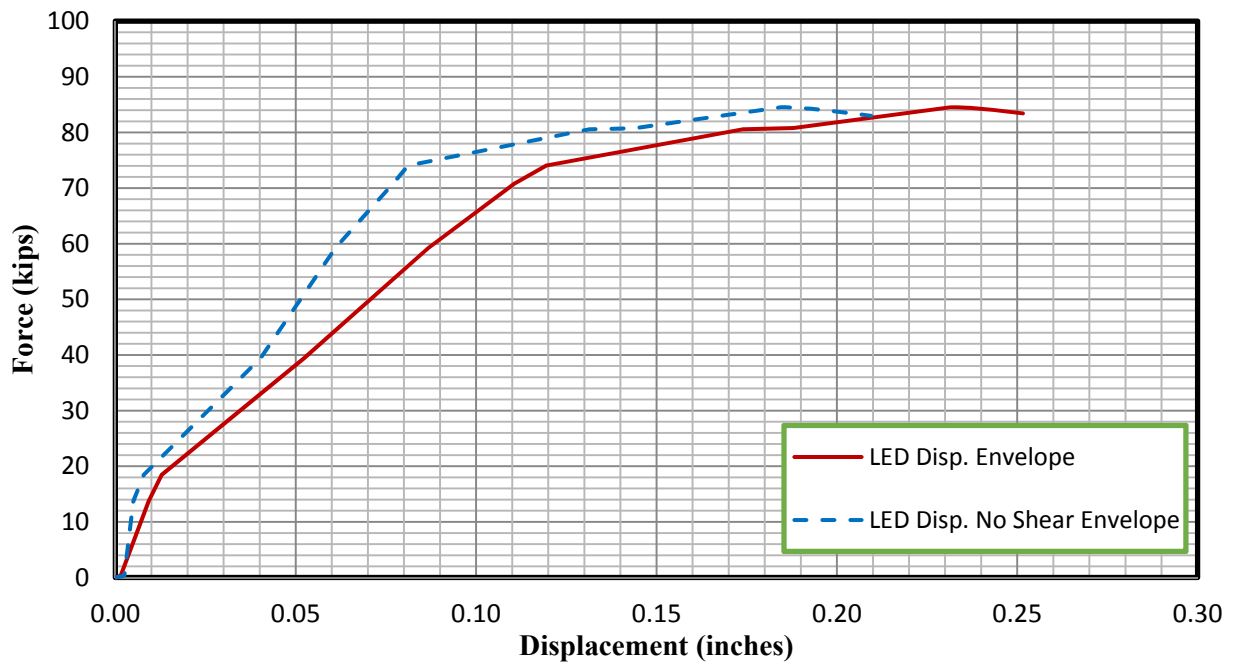


Figure 5-102: Force-displacement response of Specimen H2S1-M with and without shear deformation

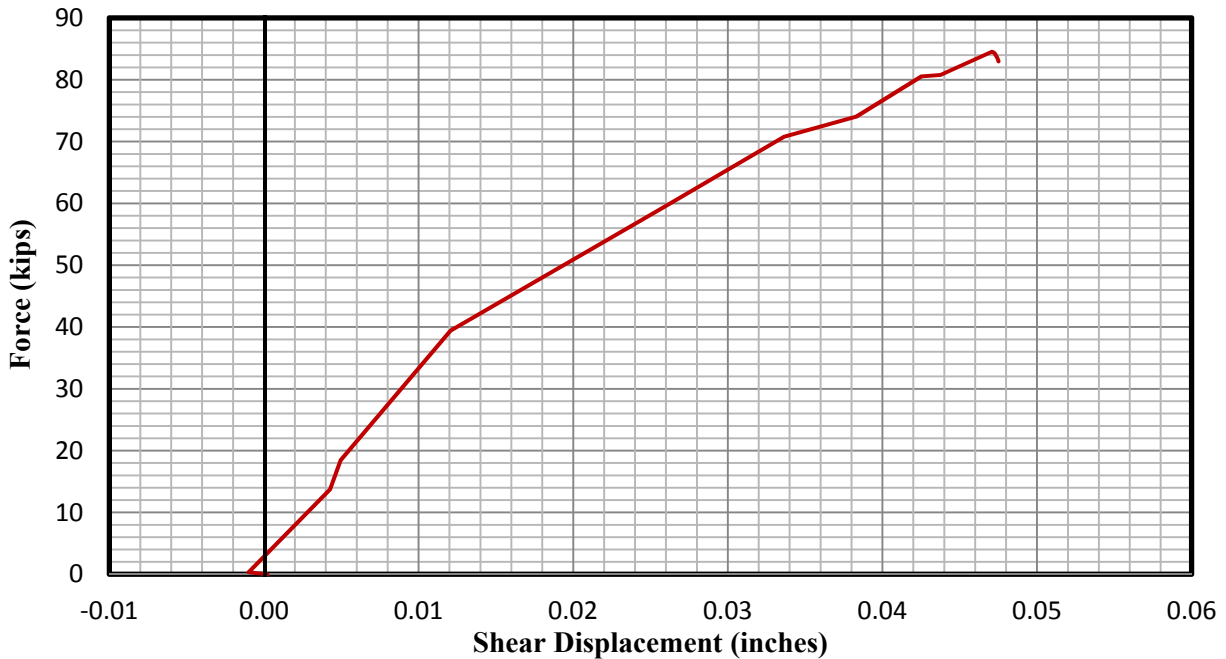


Figure 5-103: Force vs. shear displacement response of Specimen H2S1-M

The remainder of the specimens experienced premature failure caused by shear or by local effects at loading and support points. Despite some of these specimens failing in shear, the shear deformation at the failure point was not typically captured for the specimens, since the shear failure usually occurred outside the measured region. If the shear failure did occur in the measured region, the LEDs typically spalled off with the concrete in the region. Therefore the measured shear deformation maintains a fairly linear relationship with the applied load for all of the specimen, since the actual shear nonlinear deformation was unable to be captured. The force-displacement responses of these specimens with and without the shear deformation can be seen in Figure 5-104 through Figure 5-108.

Similarly to the circular hollow columns, it can be seen that for the square hollow columns, the shear deformation seems to increase with smaller wall thickness. For the two-inch thick specimens, the shear deformation seems to range from approximately twenty to thirty percent of the overall deformation, with contributions up to around fifty percent in the case of specimen H2S2-C. For the 1.25-inch wall specimens the shear deformation is more consistently around forty to fifty percent.

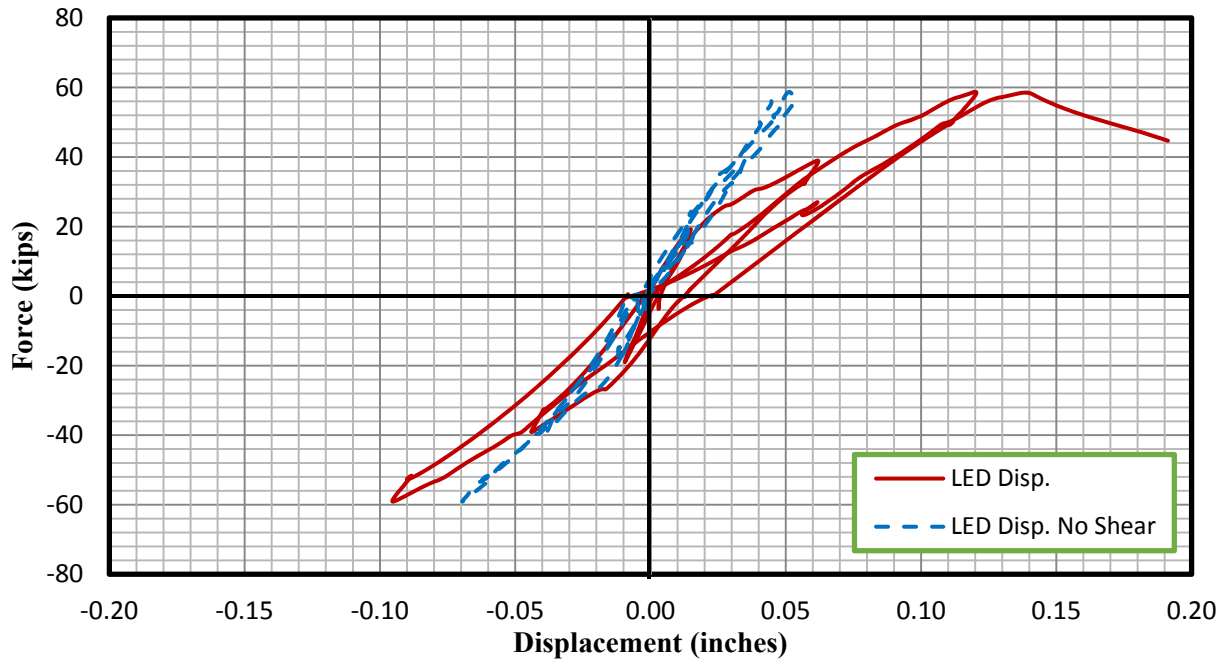


Figure 5-104: Force-displacement response of Specimen H2S2-C with and without shear deformation

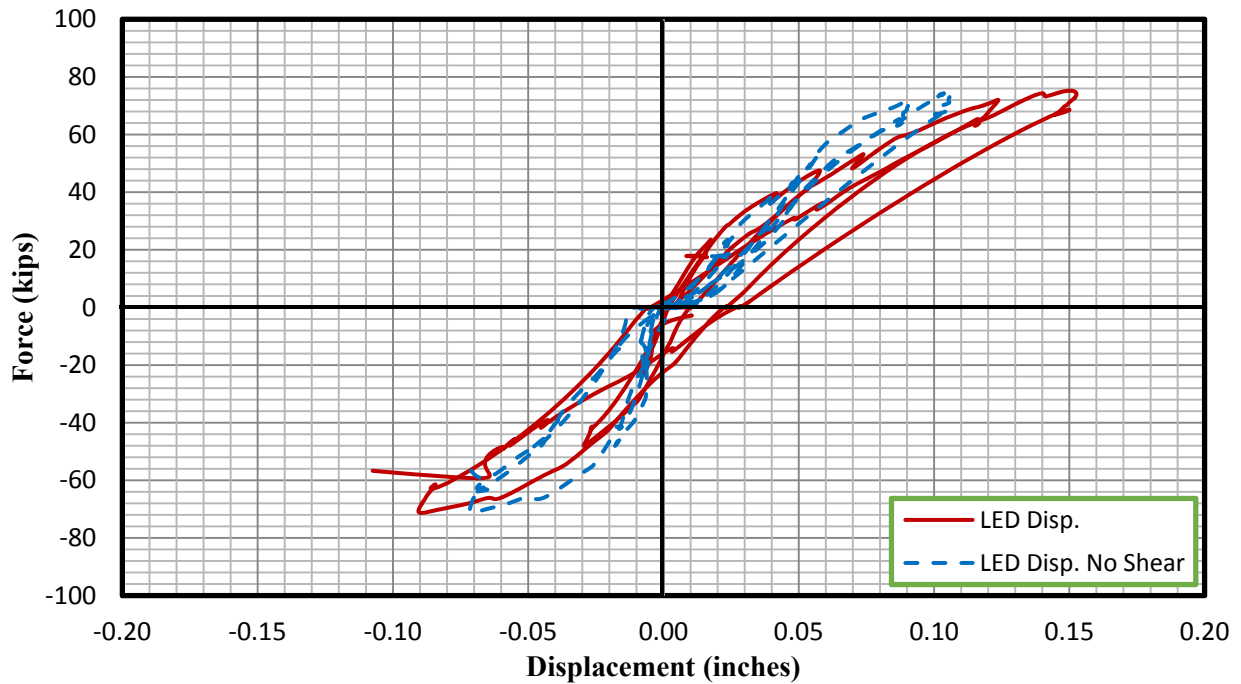


Figure 5-105: Force-displacement response of Specimen H2S3-C with and without shear deformation

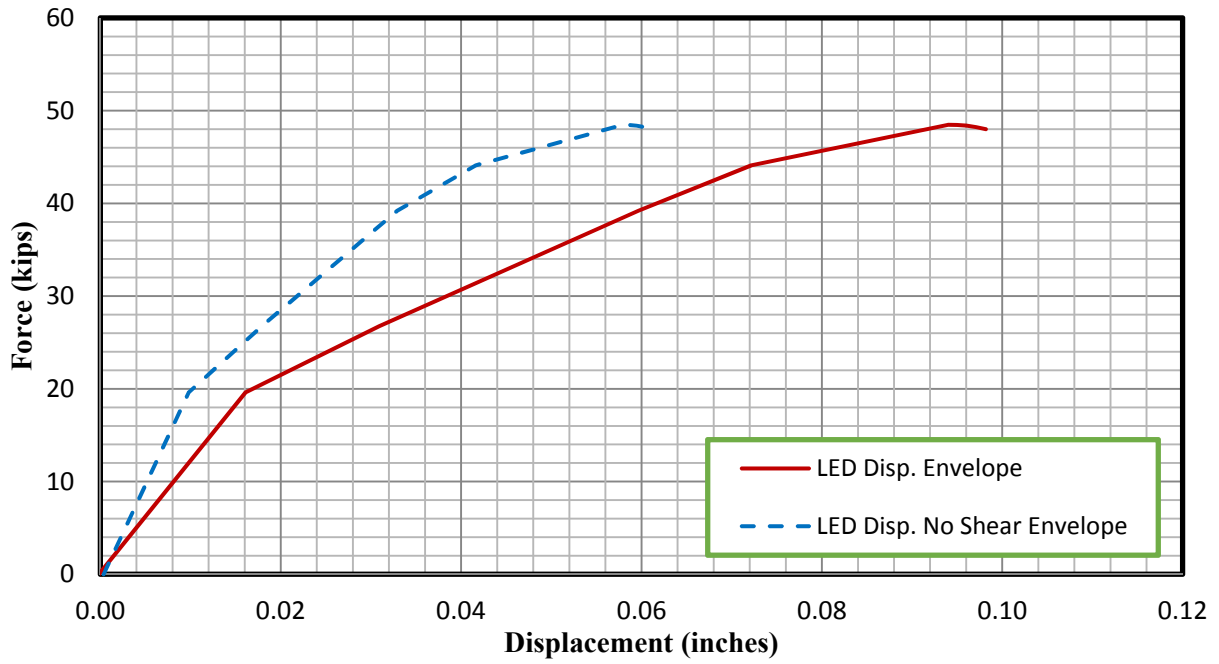


Figure 5-106: Force-displacement response of Specimen H1.25S1-M with and without shear deformation

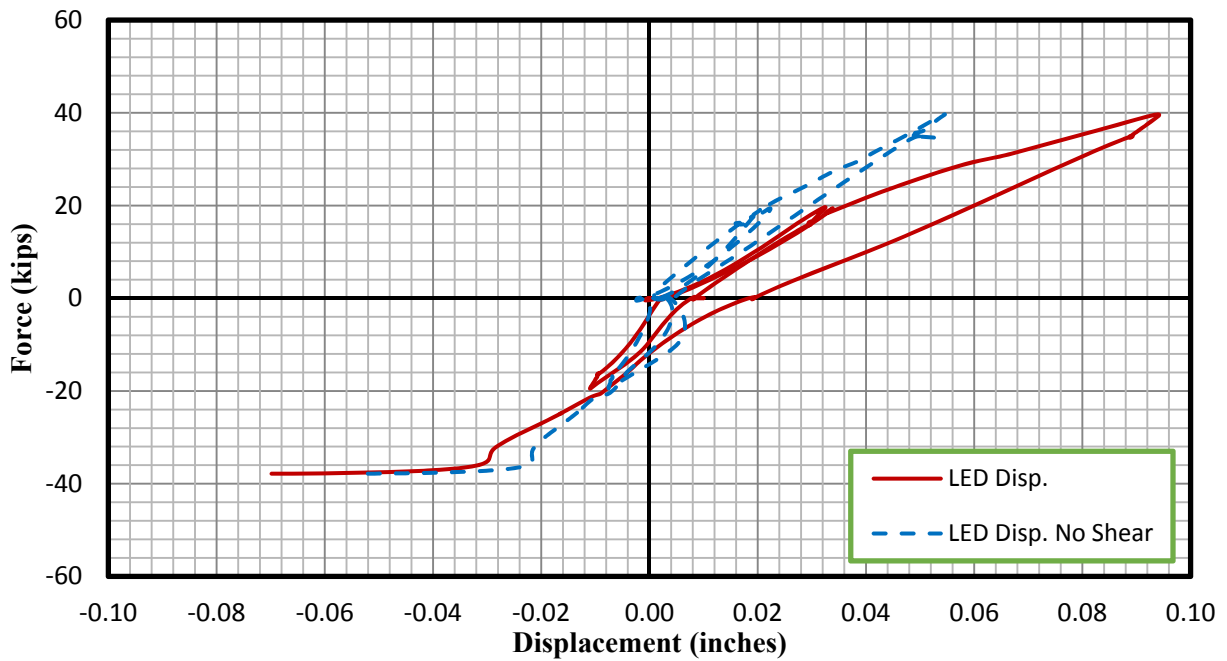


Figure 5-107: Force-displacement response of Specimen H1.25S2-C with and without shear deformation

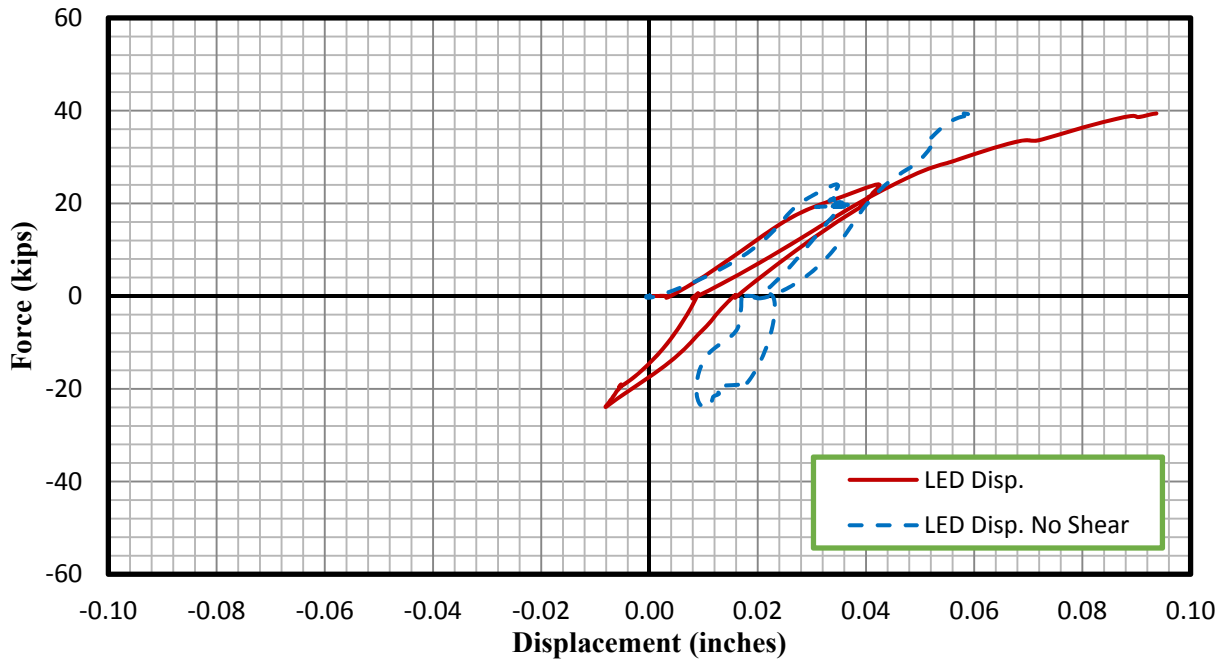


Figure 5-108: Force-Displacement of Specimen H1.25S3-C with and without Shear Deformation

The response with the shear deformation removed shown in Figure 5-108 for specimen H1.25S3-C indicates that when negative load was applied the specimen did not achieve negative displacement, and the displacement remained positive. This is most likely due to the early local and shear failure in this specimen, which may have caused nonlinear displacement in the specimen or possibly some local movement in the LEDs.

5.3.2.2.3 Force displacement response without shear

The figures below show the force-displacement response of each specimen with the shear deformation subtracted, as well as the OpenSees analysis force-displacement response and the finite element response of each specimen. The OpenSees response does not include shear effects, so it has been compared to the experimental results with the shear component subtracted. The shear deformation predicted by the FEA was also removed for comparisons. Included in the figures is the predicted failure mode based on the OpenSees response and the finite element analyses response. The predicted failure mode for all specimens was rupture of longitudinal reinforcement based on the OpenSees analyses. Due to the convergence problems associated

with the FEA for hollow square sections, no failure was found before the FE program stopped. Despite the early failure of the hollow specimens due to shear and local effects, it can be seen that the OpenSees analysis can often capture the initial stiffness of these specimens fairly accurately.

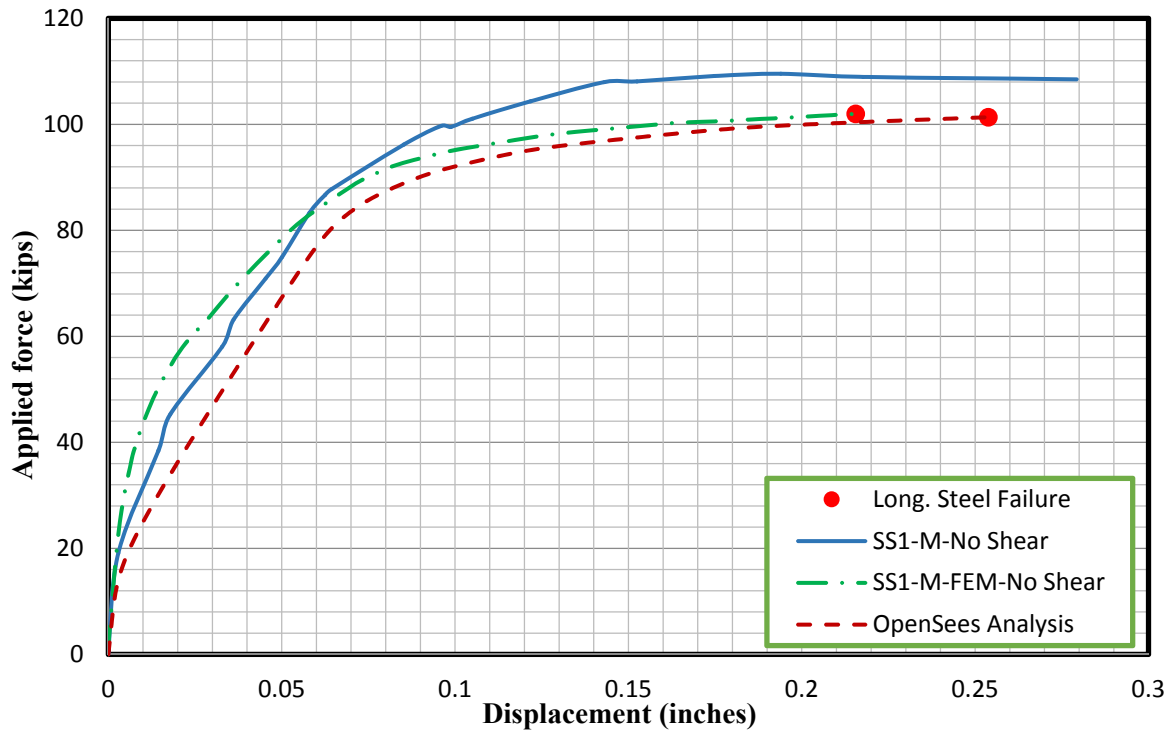


Figure 5-109: Measured force-displacement response of Specimen SS1-M with shear deformation removed compared to analytical envelope response

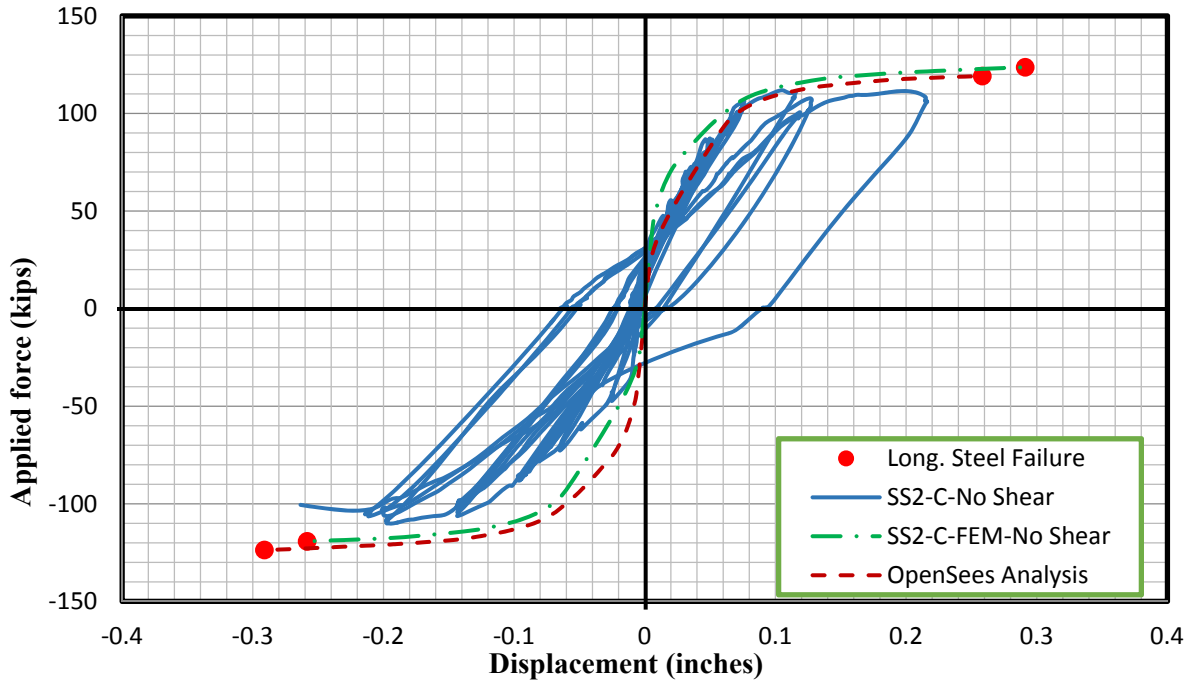


Figure 5-110: Measured force-displacement response of Specimen SS2-C with shear deformation removed compared to analytical envelope response

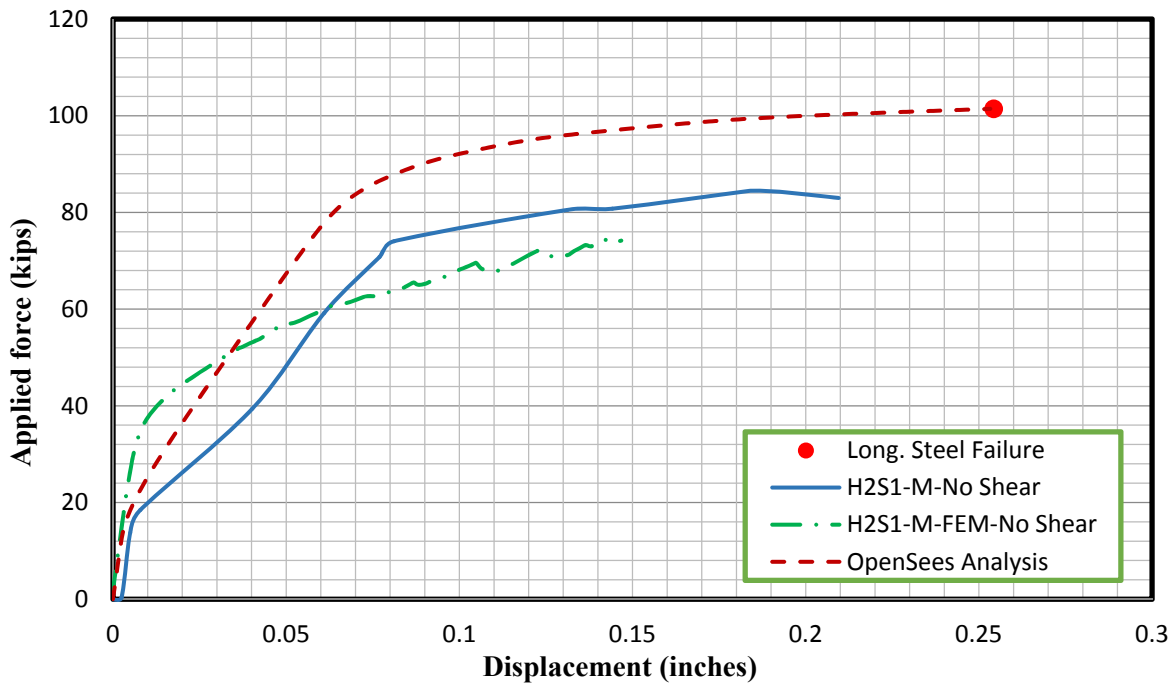


Figure 5-111: Measured force-displacement response of Specimen H2S1-M with shear deformation removed compared to analytical envelope response

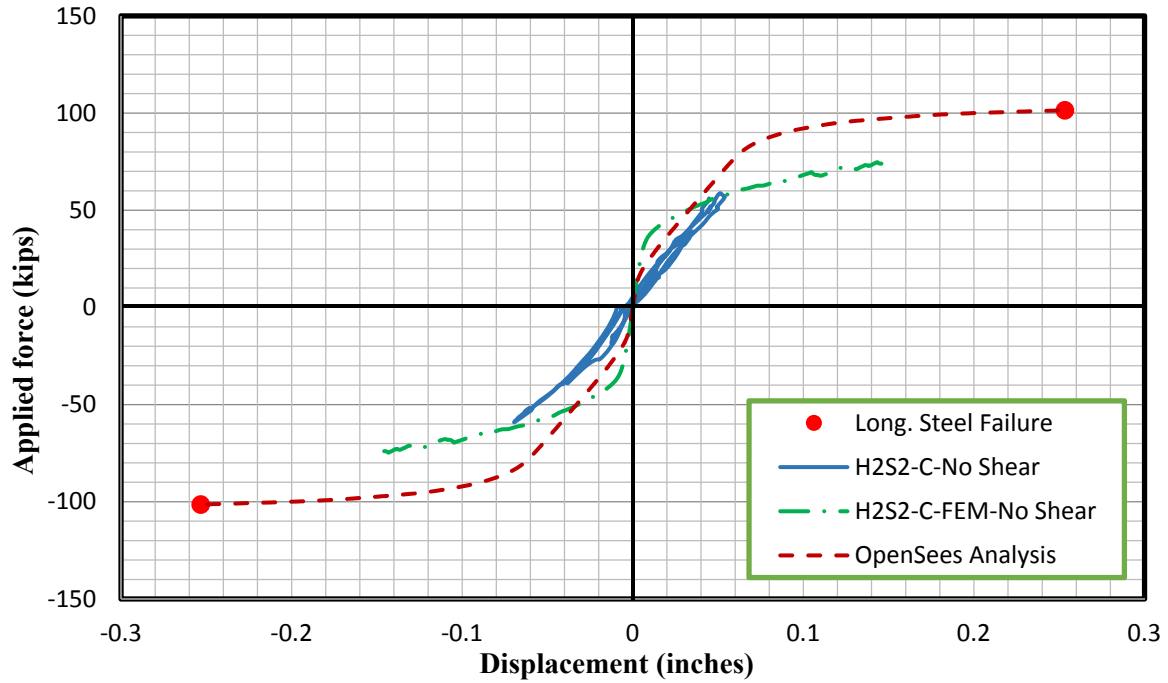


Figure 5-112: Measured force-displacement response of Specimen H2S2-C with shear deformation removed compared to analytical envelope response

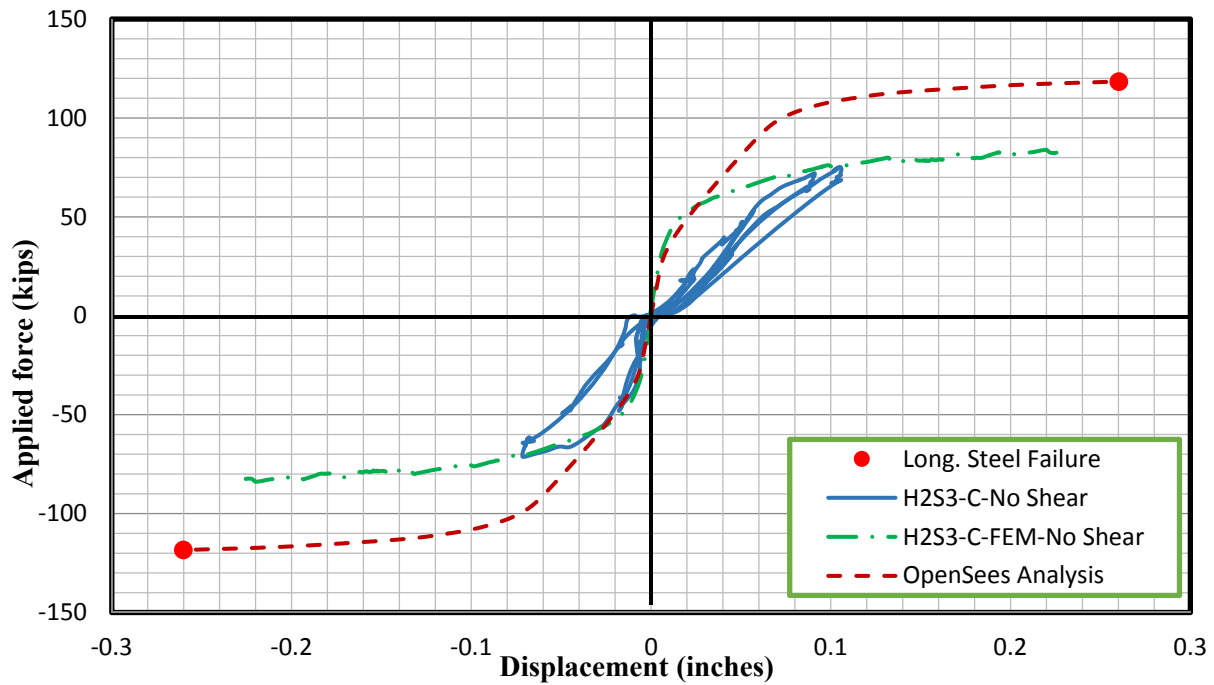


Figure 5-113: Measured force-displacement response of Specimen H2S3-C with shear deformation removed compared to analytical envelope response

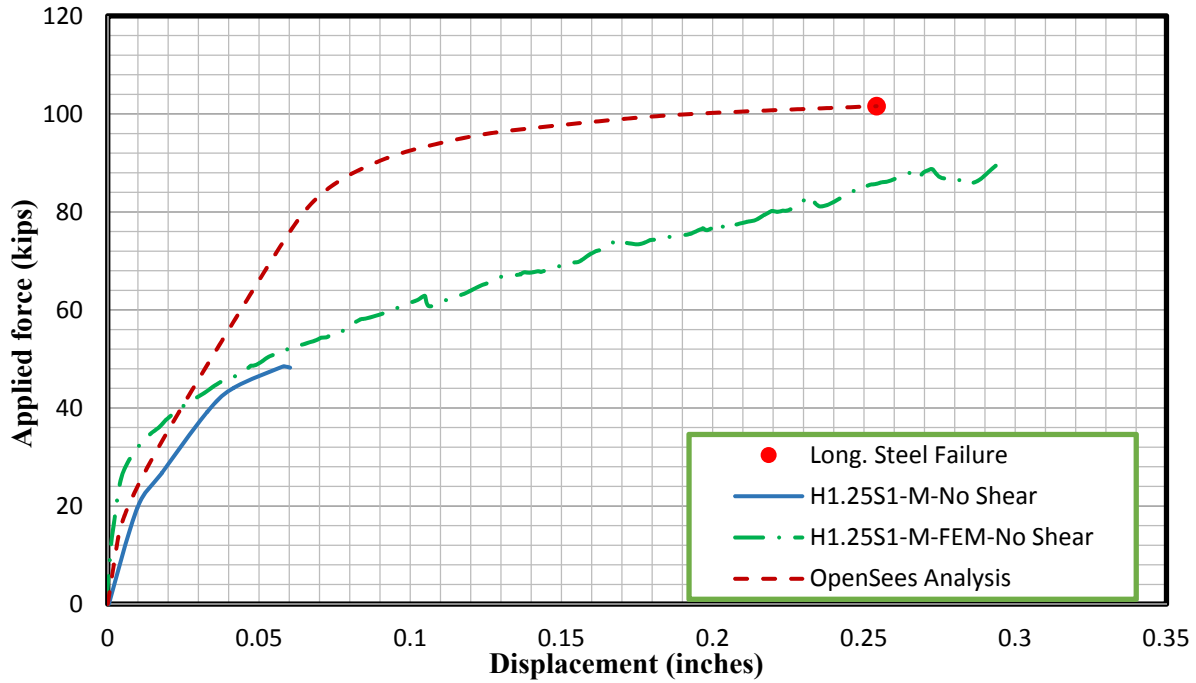


Figure 5-114: Measured force-displacement response of Specimen H1.25S1-M with shear deformation removed compared to analytical envelope response

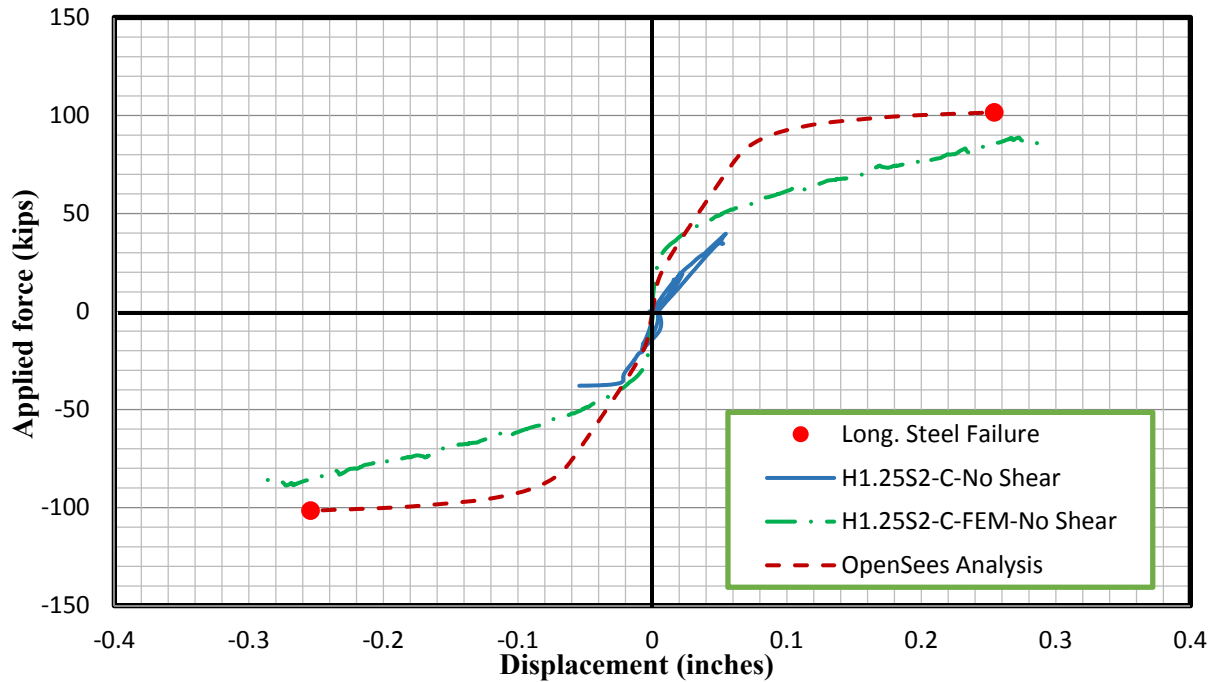


Figure 5-115: Measured force-displacement response of Specimen H1.25S2-C with shear deformation removed compared to analytical envelope response

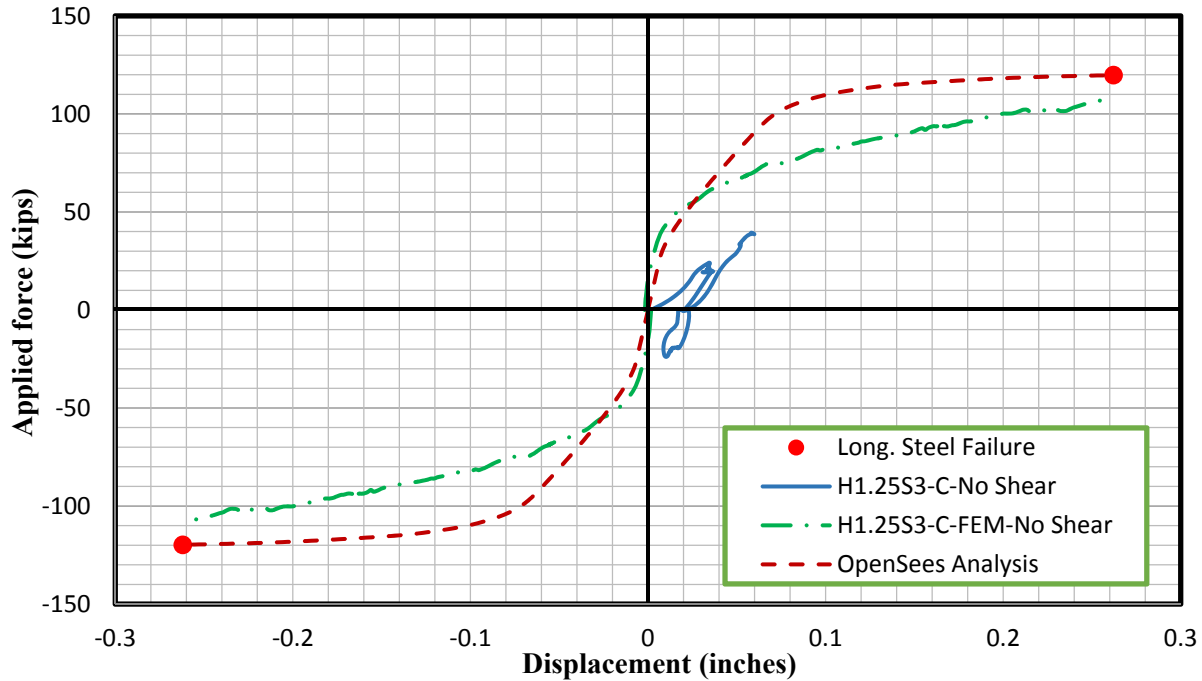


Figure 5-116: Measured force-displacement response of Specimen H1.25S3-C with shear deformation removed compared to analytical envelope response

5.3.2.2.4 Longitudinal bar strain

The following section shows the longitudinal bar strains of each specimen, measured by strain gauges attached to the bars. The longitudinal bar strain from the OpenSees analysis for each specimen is also shown for comparison. The analysis strains shown are from either the extreme tension or compression longitudinal steel bars. The measured and analytical strains are presented for the cyclically loaded specimens, with strains from one of the sides which experienced extreme tension and compression strains being shown. The figures are labeled as either near longitudinal bar 1 or longitudinal bar 12. The response from the OpenSees analysis is plotted up until the point where failure was predicted in the analysis. The predicted analytical failure mode was longitudinal steel rupture for all specimens.

Only some of the measured strains have been presented, since the comparisons are fairly similar for most specimens. The solid specimens show very good agreement to the analytical results, including the prediction of the ultimate failure mode. The hollow specimens agreed well with the predicted results for the most part in the force-control range of testing. However, the hollow

specimens experienced early failure due to local and shear effects, while the analysis indicated these specimens would experience failure due to longitudinal bar rupture at similar force levels as the solid specimens.

The square specimen strain gauge locations have been provided again in Figure 5-117 for quick reference. The gauges marked with an asterisk only appeared at one section in the specimen, while all other gauges were at both sections. See Section 4.5 for a more details of the strain gauge locations. The measured response compared to analytical response for certain longitudinal bars is provided in Figure 5-118 through Figure 5-122.

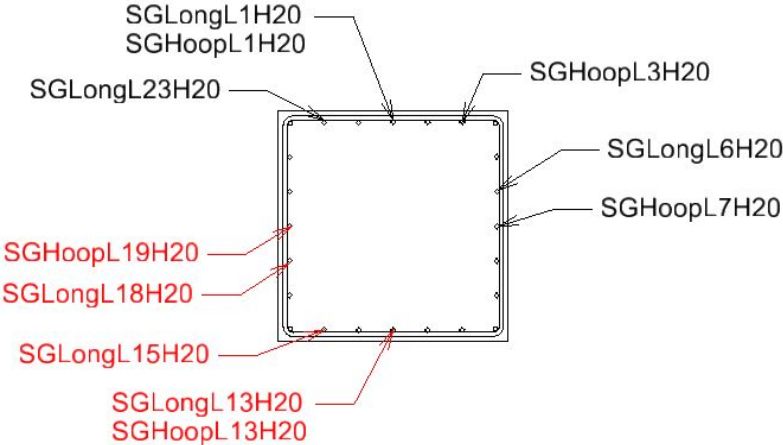


Figure 5-117: Square section strain gauge locations

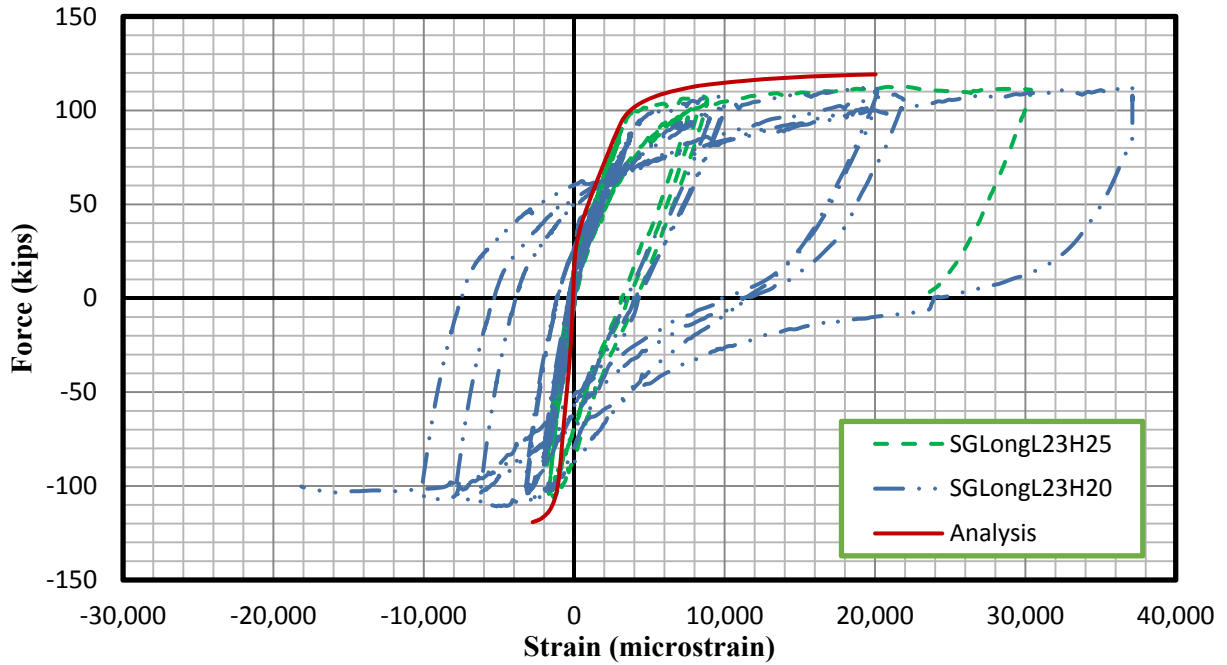


Figure 5-118: Longitudinal strain near longitudinal bar 1 vs. applied load of Specimen SS2-C

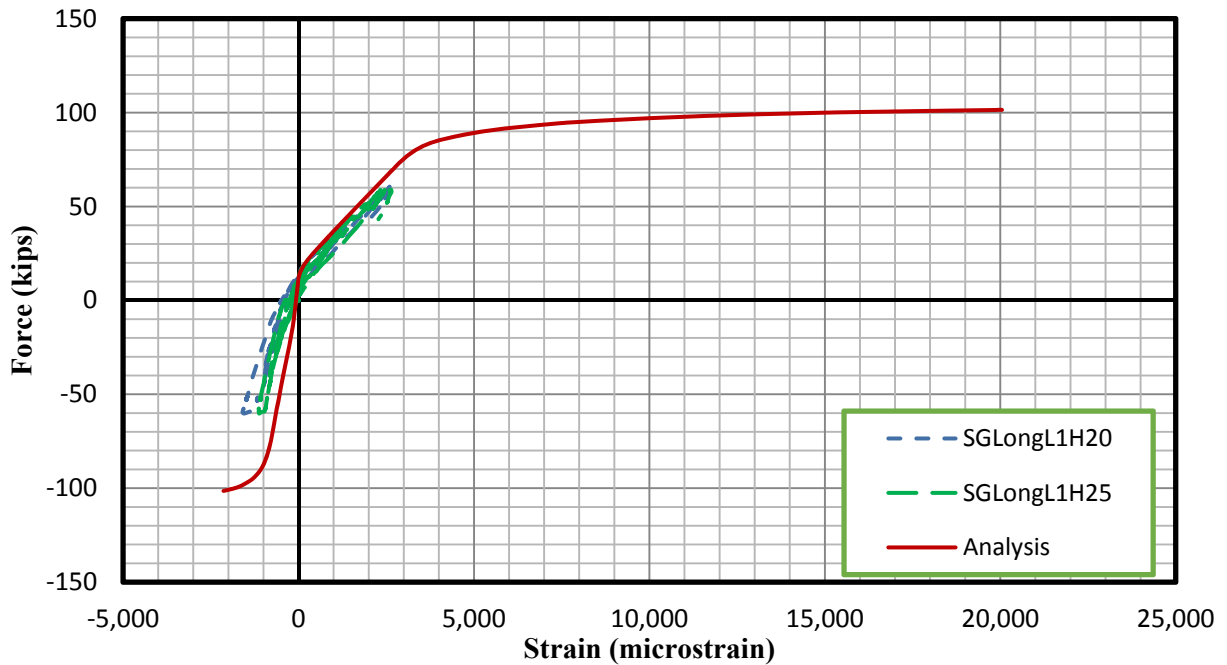


Figure 5-119: Longitudinal strain near longitudinal bar 1 vs. applied load of Specimen H2S2-C

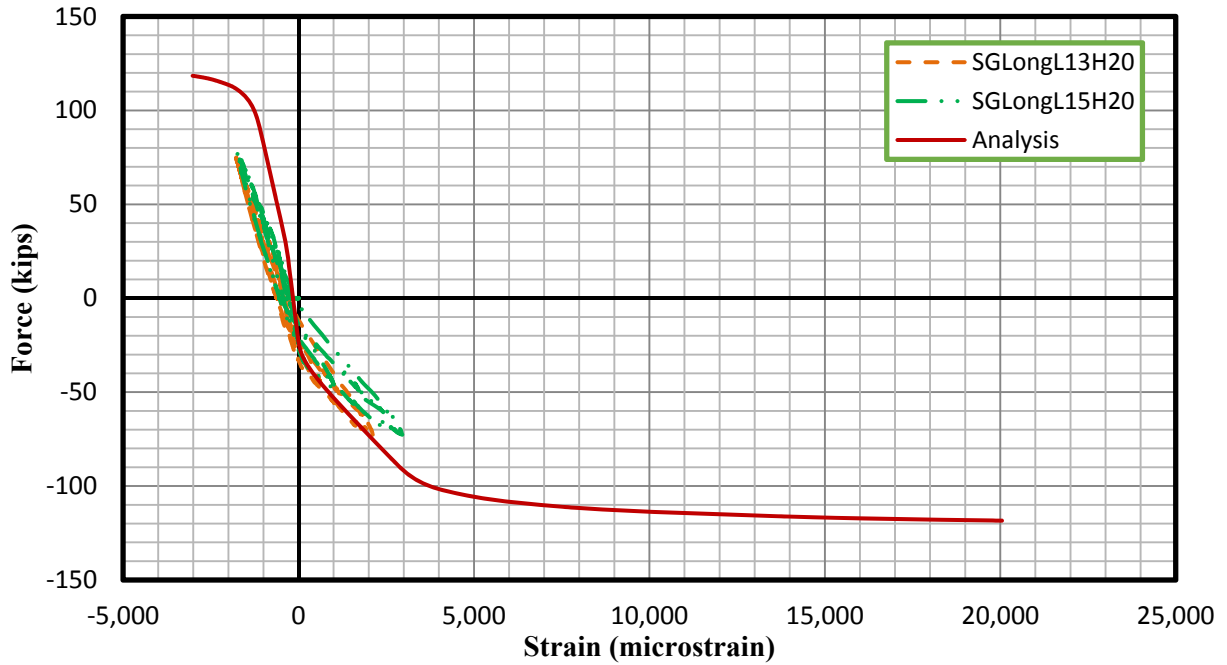


Figure 5-120: Longitudinal strain near longitudinal bar 12 vs. applied load of Specimen H2S3-C

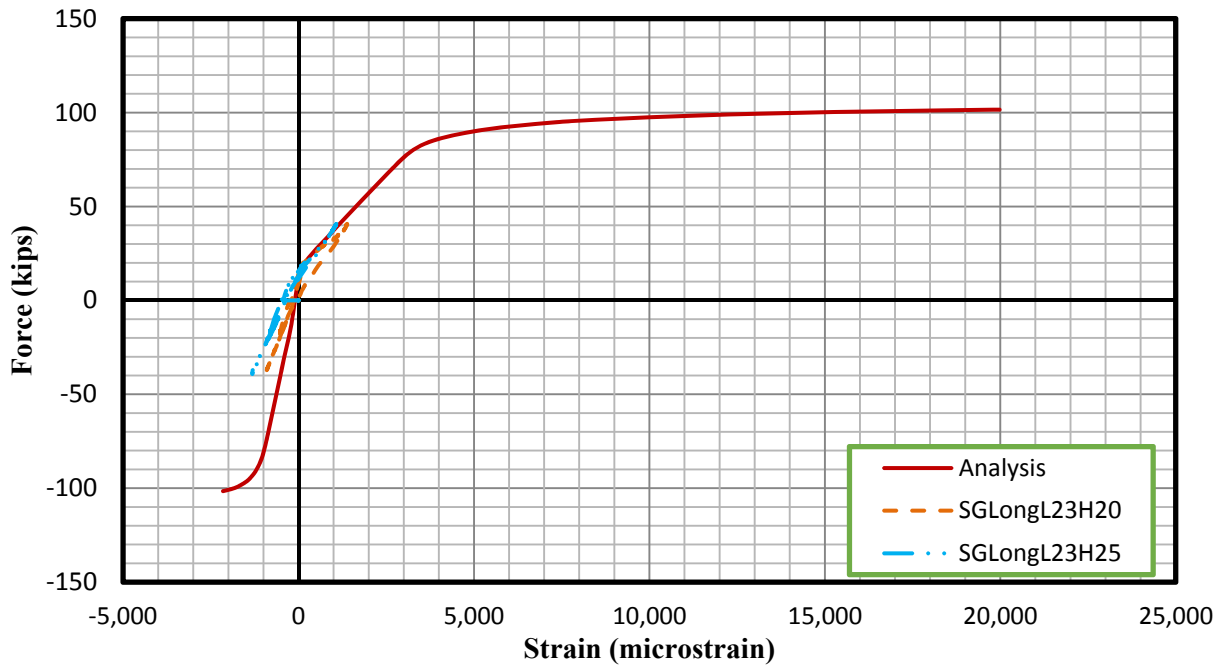


Figure 5-121: Longitudinal strain near longitudinal bar 1 vs. applied load of Specimen H1.25S2-C

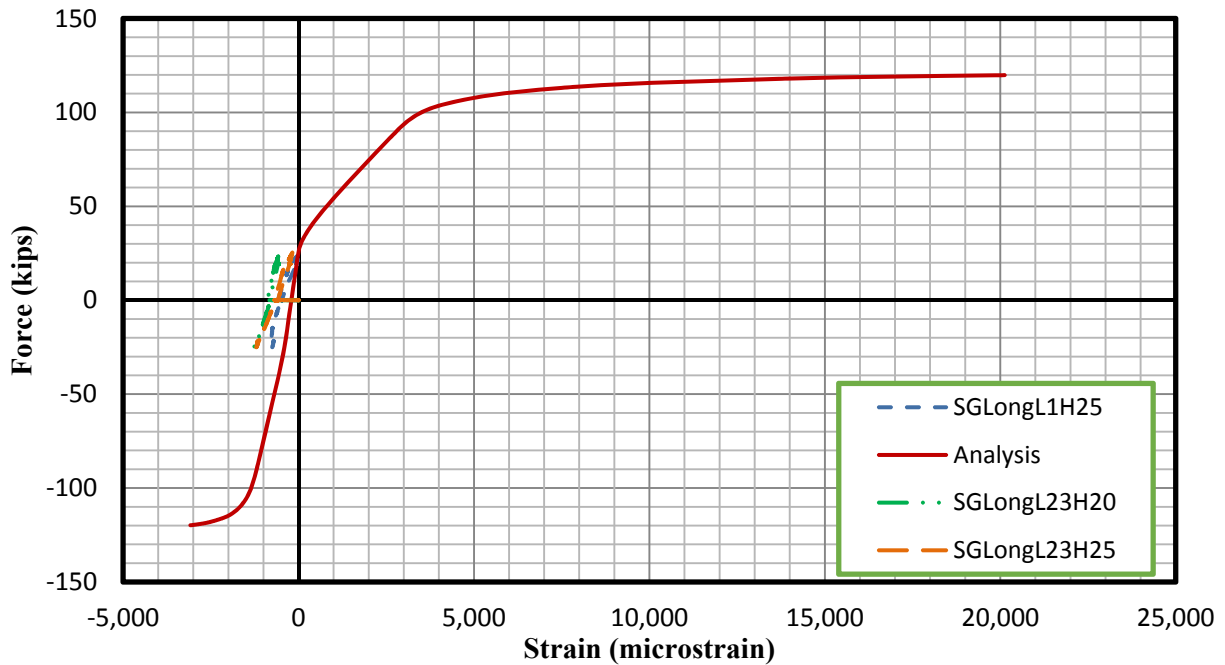


Figure 5-122: Longitudinal strain near longitudinal bar 1 vs. applied load of Specimen H1.25S3-C

As shown in the figures, the OpenSees analysis matches up fairly closely with the measured response from the strain gauges on the longitudinal reinforcement. Even for the hollow specimens for which early failure occurred, the analysis matches up well with the initial stiffness for most of these specimens. Similarly to the longitudinal strains for the hollow circular columns, the longitudinal strains in compression for these specimens can sometimes be fairly high. To verify these strains and provide a further comparison between the analytical and experimental results, the strains measured by the LEDs attached to the concrete are examined in the next section.

5.3.2.2.5 Concrete strain

The concrete strains near the extreme tension and compression fibers of the sections were found using the LED grid in the constant moment region. The location of the presented LEDs was fairly close to the extreme tension and compression fibers of the sections, so the longitudinal reinforcement strains from the extreme tension and compression reinforcement found in the OpenSees analysis has been plotted for comparison. The tension and compression strains are

presented in the same plot, as well as the analytical strains. The measured strains are labeled either “Strain57”, representing the strain measured between LEDs 5 and 7, or “Strain1820” representing the strain measured between LEDs 18 and 20. The measured LED strains have been processed to remove noise and outliers.

The layout of the LEDs used during testing is shown in Figure 5-123 for reference. The measured LED strains presented in this section were measured in the constant moment region. The strain gauge sets from which the strains were measured are highlighted in the figure.

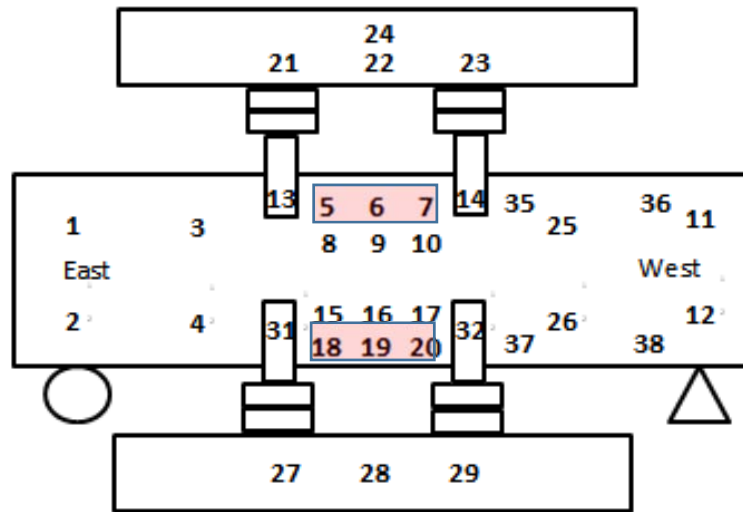


Figure 5-123: LED layout with highlighted strain locations

The measured and analytical strains are plotted against the applied lateral load for several of the specimens in Figure 5-124 through Figure 5-126. The plots show good agreement between the measured and analytical strains for most specimens. Additionally, the compressive strains measured by the LEDs are not as large as was shown by the strain gauges, and agree better with the visual results of the test specimens. The test specimens did not show signs of high compressive strains, since there was not a large amount of crushed concrete near the extreme compression region. The predicted failure mode for all of the specimens was longitudinal steel rupture. However, the hollow specimens failed early due to local and shear effects, and thus the

analytical results for these specimens predict larger loads at the ultimate failure. Despite this difference, the initial slope of the measured and analytical strains agrees well for most specimens, up until the point where the test specimens experienced early failure. The general comparison between experimental and analytical results is fairly similar for all specimens of the same wall thickness, and therefore only one of the cyclically loaded specimens for each wall thickness has been shown for brevity.

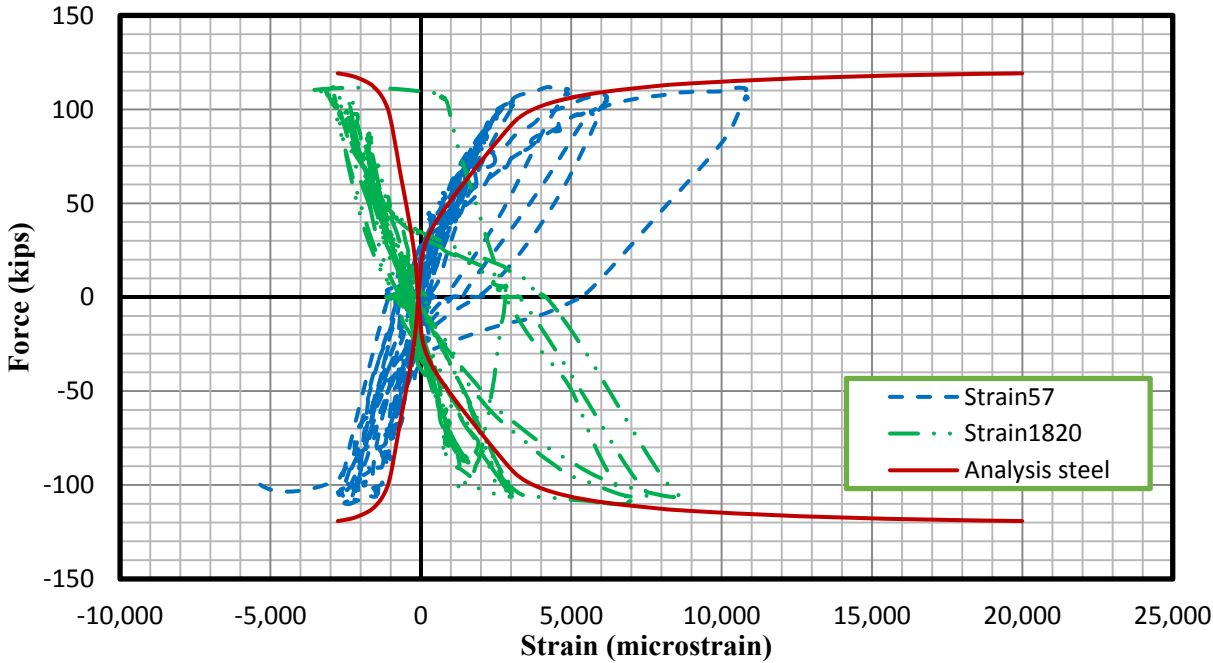


Figure 5-124: Attached LED concrete strain measured during testing and analytical steel strain vs. applied load for Specimen SS2-C

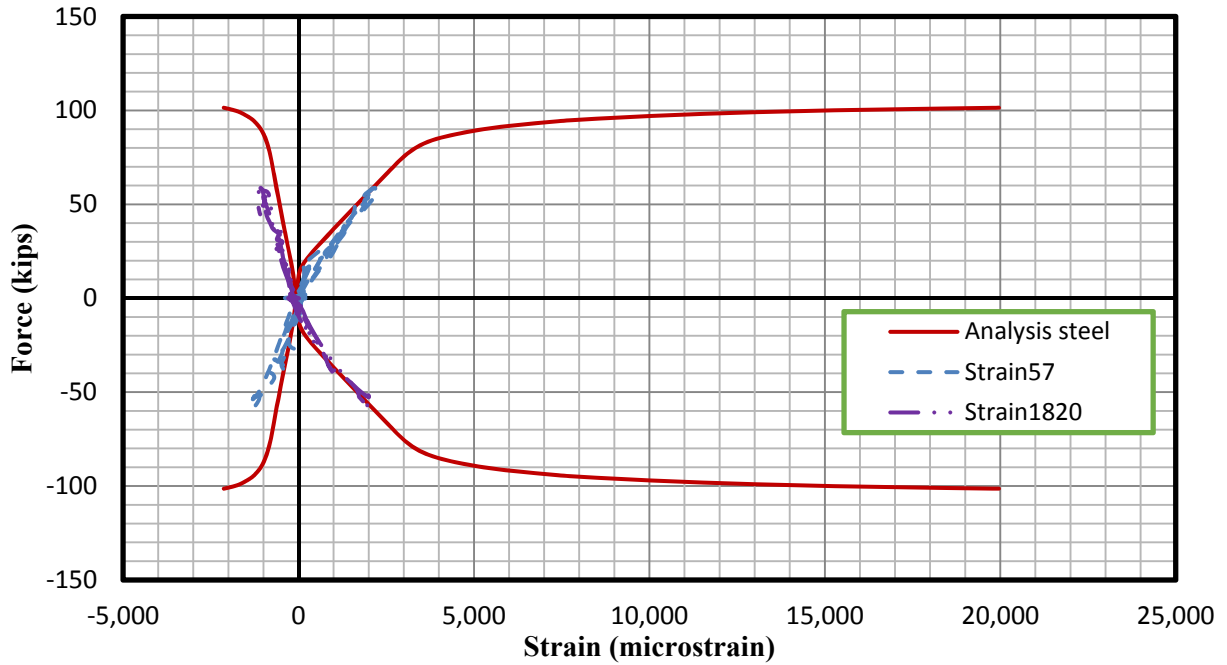


Figure 5-125: Attached LED concrete strain measured during testing and analytical steel strain vs. applied load for Specimen H2S2-C

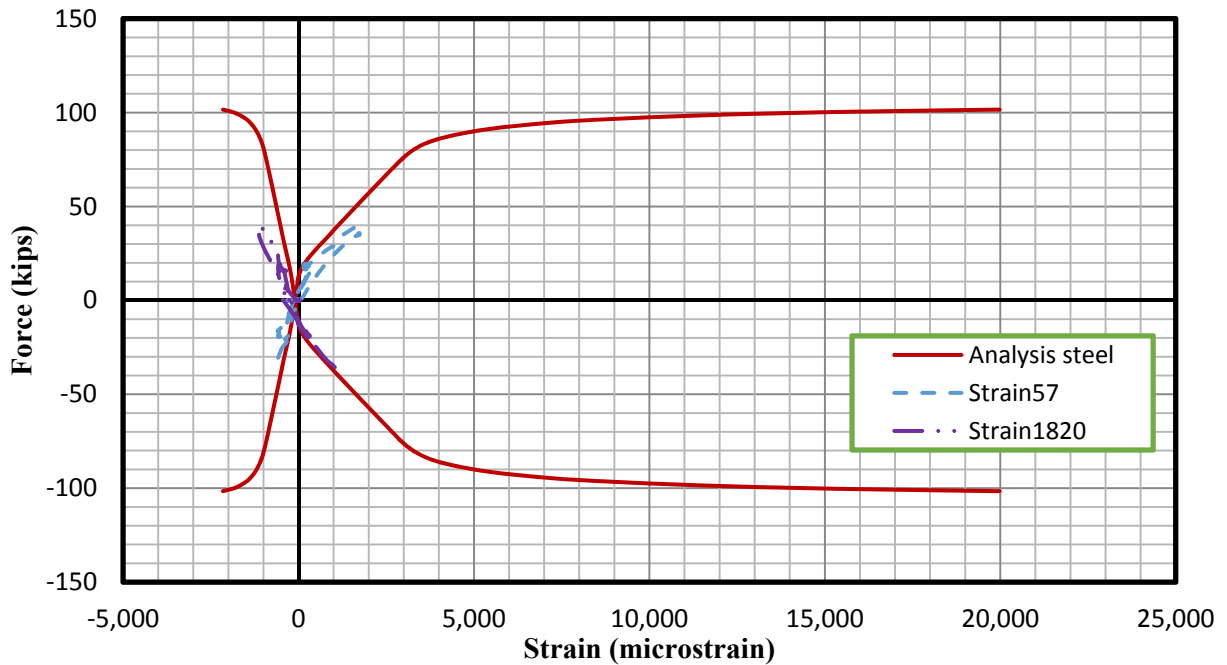


Figure 5-126: Attached LED concrete strain measured during testing and analytical steel strain vs. applied load for Specimen H1.25S2-C

5.3.2.2.6 Square hoop strain

The strains in the transverse reinforcement were measured within each wall for the square sections within the constant moment region. The measured strains can provide a good indication of how much demand is being applied to the transverse reinforcement. By examining the transverse strains for all of the specimens, it was found that the transverse reinforcement was subjected to low demand, with strains typically not reaching above 2000 microstrain. This indicates that the transverse reinforcement was adequate to prevent fracture of the transverse reinforcement and restrain radial displacement.

Figure 5-127 through Figure 5-129 below shows the strain measured in the transverse reinforcement during the testing of test unit SS2-C. Three plots are shown for the specimen, with each plot showing strain gauges near the extreme fiber tension or compression face, or on the side of the specimen. Theoretically, the transverse reinforcement would reach higher tensile strains when the section near the reinforcement is subjected to compression, since the transverse reinforcement must restrain the dilation of the concrete. Slight evidence of this pattern can be seen in Figure 5-127, where the transverse reinforcement strains become slightly higher when loading in the negative direction is applied, which would put compression on the section near longitudinal bar number one. However, the pattern is not very strong and the demand of the transverse reinforcement is very low. The plots for specimen SS2-C are shown as an example of the other specimens. The remainder of the specimens either had somewhat similar patterns or no patterns, with transverse steel strains not typically reaching higher than those shown for specimen SS2-C.

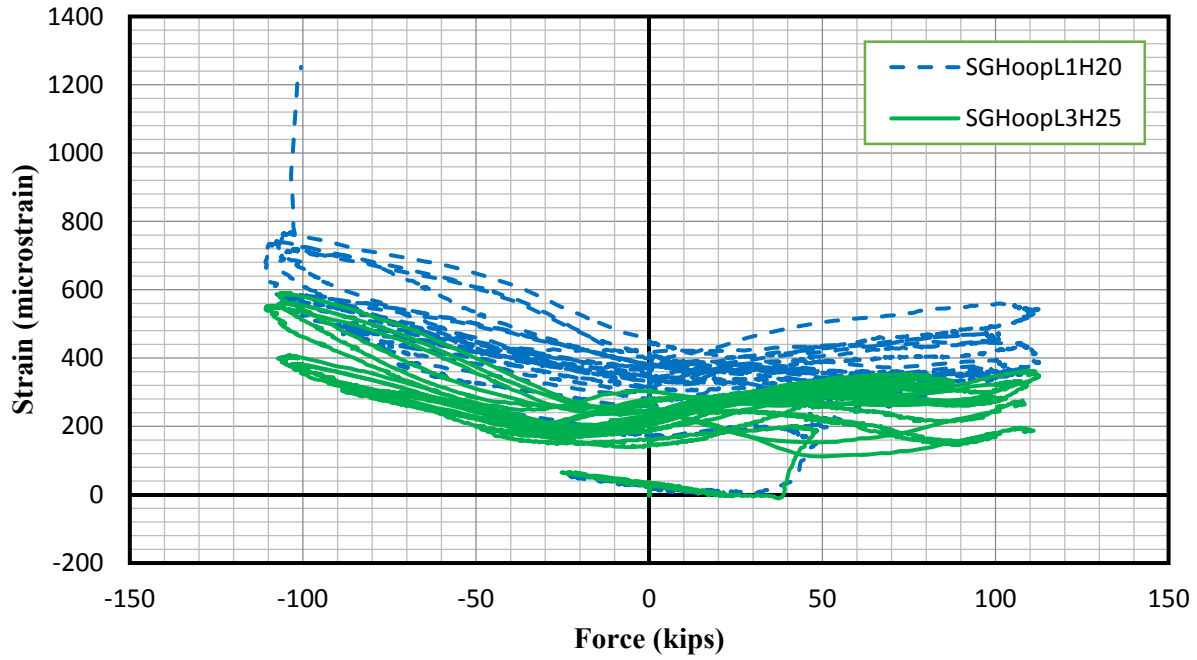


Figure 5-127: Hoop strain near longitudinal bar 1 vs. applied load for Specimen SS2-C

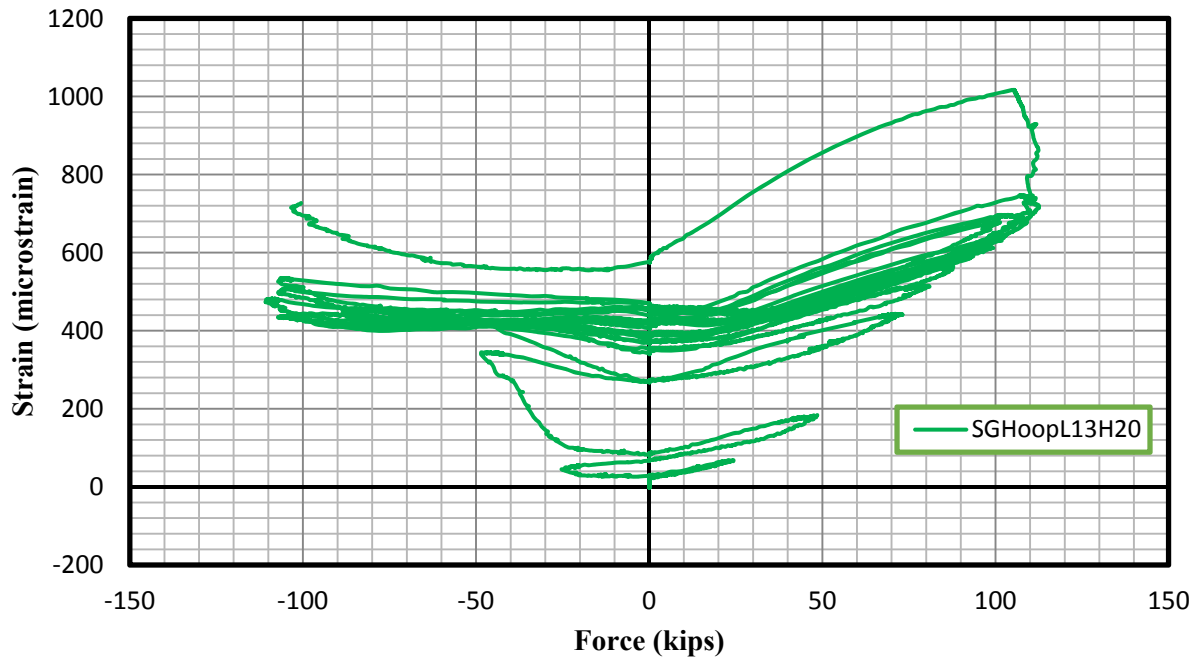


Figure 5-128: Hoop strain near longitudinal bar 12 vs. applied load for Specimen SS2-C

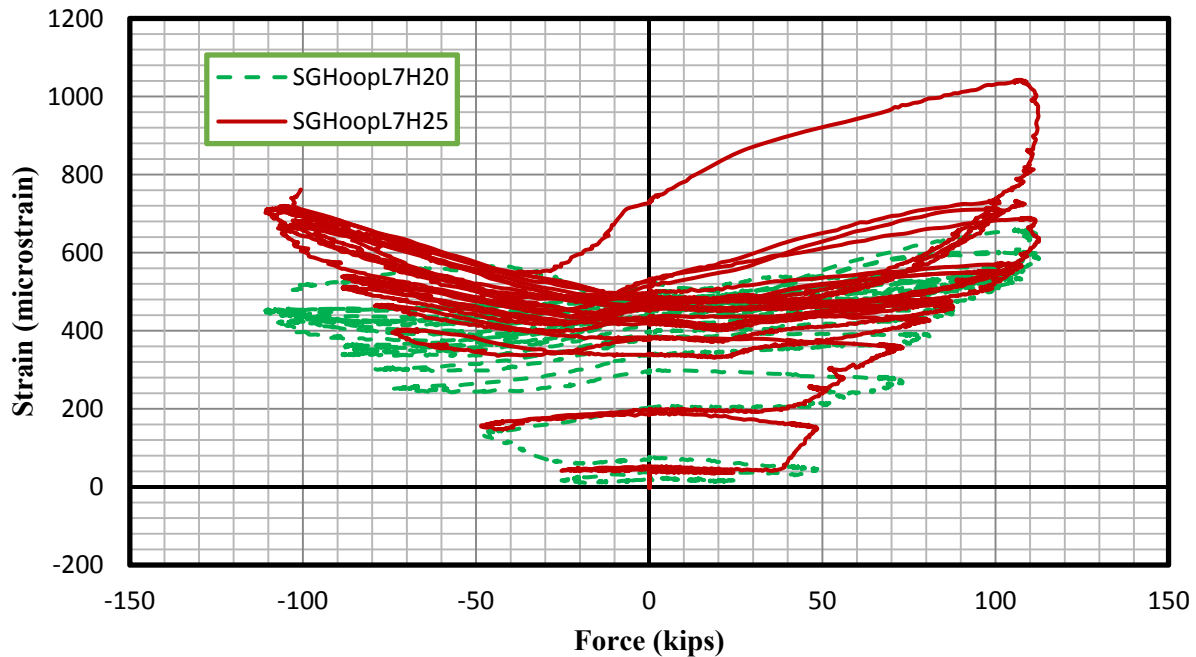


Figure 5-129: Hoop strain at side of section vs. applied load for Specimen SS2-C

5.4 Analytical accuracy

The experimental results and comparison to analytical results presented in Section 5.3 have shown that the analytical model is capable of representing the flexural response of hollow columns fairly accurately. However, to be sure that the test results and the analytical method agree, it is useful to show more detailed comparisons. This section provides comparisons of the strain profiles and the strain versus displacement responses for the specimen H2C1-M. This specimen was selected because it was hollow and loaded monotonically, which would allow for a more direct comparison to the analyses that were also performed monotonically. Specimen H2C1-M was found to show good response and did not experience early or local failure.

Figure 5-130 shows the measured and analytical strain values plotted against the displacements. As shown, the OpenSees analysis agreed very well with the concrete tension strain measured by the LEDs (labeled Strain57). However, there are some discrepancies for the FE analyses. As stated previously, due to the existence of shrinkage cracks in the test specimens before testing, the actual tensile strength of the concrete in the test specimens were around zero. However, zero concrete tensile stress was not allowable to achieve convergence in the FE analyses using the

concrete damaged plasticity model. The 1.5 square root of f'_c was therefore assumed to be the concrete tensile strength to represent the material property as realistic as possible. At the initial small displacement, the longitudinal reinforcement strain, as well as the tensile strain in concrete, was very comparable. This indicated that tensile concrete cracking was taking place. Once the displacement passed around 0.12 inches, the longitudinal reinforcement strain increased significantly and got pretty close to the measured values. The longitudinal steel strains measured on the most extreme tension bar were also plotted and agreed well with the analysis. These strains were only plotted to around 5,000 microstrain because after, they began to increase in strain rapidly, which may be due to damaged gauges. In the compression region, the two analysis methods agreed with each other, but the measured concrete compressive strains (labeled Strain1820 in the plot) were higher than those predicted by the analysis, which may be due to local effects.

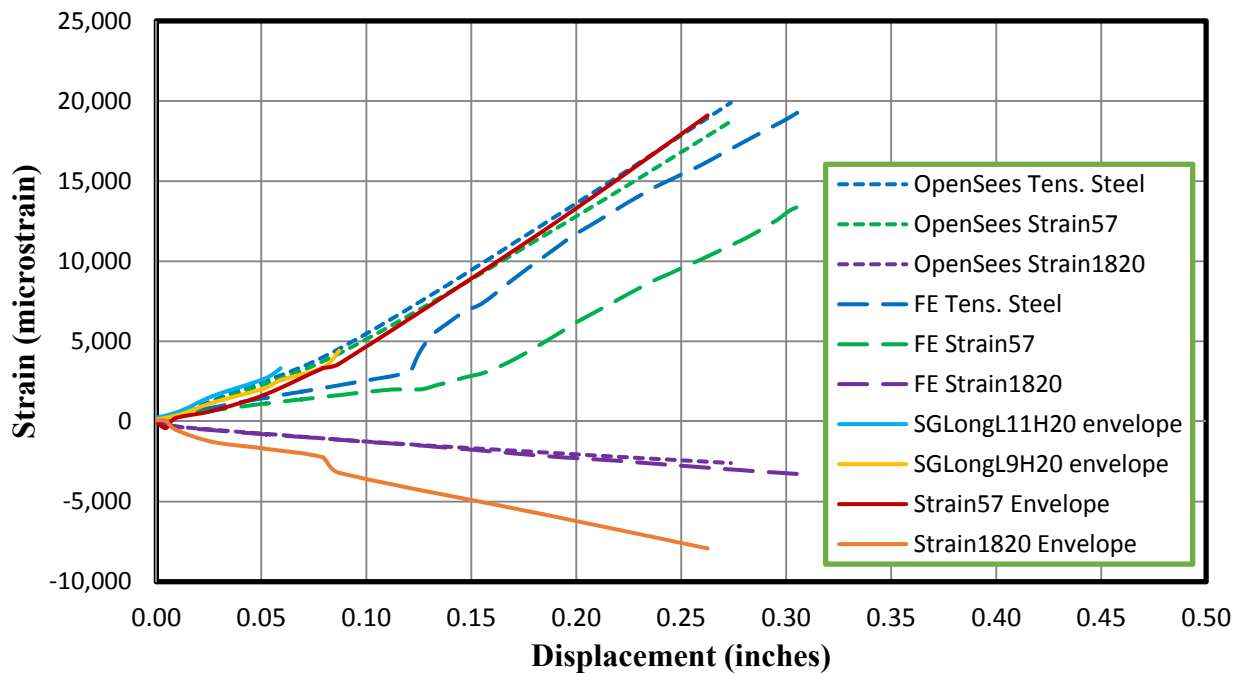


Figure 5-130: Measured and analytical strain vs. displacement relationship for Specimen H2C1-M

Additionally, several strain profiles are shown in Figure 5-131 through Figure 5-133, taken at different points in the testing. The points were chosen based on the measured tension strains of longitudinal reinforcement, and the analysis strain profiles were chosen based on the tension

steel strain corresponding to the measured point. In Figure 5-131, it can be seen that several points were plotted for the experimental results and analysis results at first yield. For the test results, the points are the measured tension steel strain and the four LED strains along the section in the constant moment region. The points on the analysis profiles correspond to tension steel strain, strain in concrete at the location of the most extreme tension LED set, strain at the inside compression face, and concrete compression strain at the point of the most extreme compression LEDs. The strain at the inside compression face as given by the analysis is at a similar depth to a set of LEDs, which were used to measure strains. As shown, the profile is fairly similar, with some small differences, especially at the compression face.

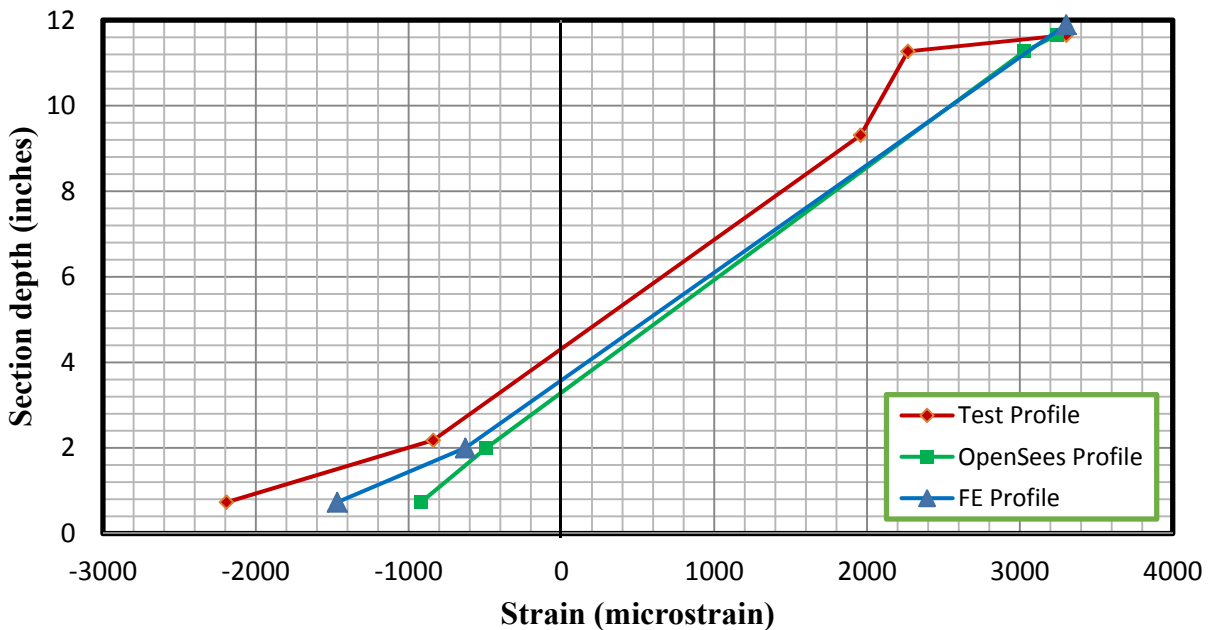


Figure 5-131: Strain profile at first yield (measured steel strain of 3300 microstrain) for Specimen H2C1-M

Another strain profile is shown in Figure 5-132. This strain profile was chosen because it was near to the last point in which the second LED row on the compression side was visible. The presence of this second LED row provides an additional data point, which gives a better idea of the strain profile, and this plot provides a good idea of the strain profile at higher extreme fiber strains. At this point, the specimen was well into the nonlinear range, as the tension strain was approximately 15,000 microstrain. The test profile is made up of the four LED strains measured

along the section. The tension steel strain is not shown due to the early increase in measured tension steel strains, which might be due to the gauges being damaged. The analysis profiles are made up of the same points, as described in the last plot. The most extreme compression strain measured by the LEDs is somewhat higher than the analyses, which might be due to some local effects that came from the low amount of cover concrete. This may also explain why the strain versus displacement plot in Figure 5-130 has higher measured compression strains than the analysis suggests it should have. The rest of the strain profile is fairly close to the analysis prediction.

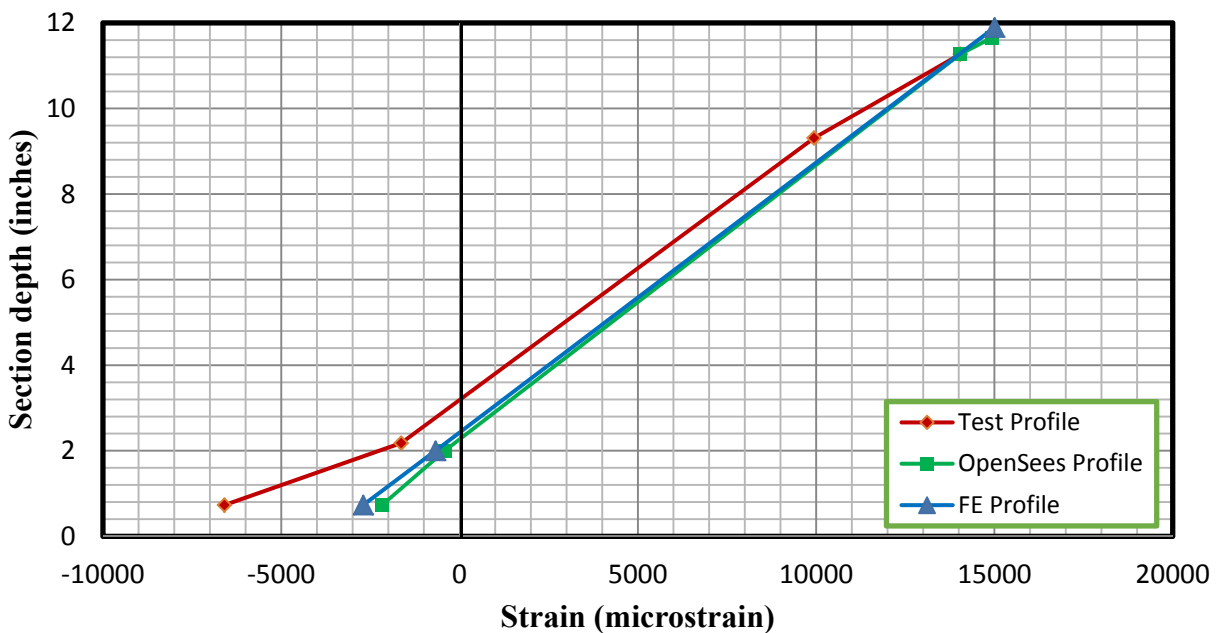


Figure 5-132: Strain profile between yield and ultimate for Specimen H2C1-M

Additionally, the strain profile near the ultimate point is shown in Figure 5-133. This point was chosen at an extreme tension steel strain of approximately 20,000 microstrain, and the analysis profiles were chosen based on this strain as well. In this case, the test profile was based on only three sets of LEDs, as the second row of LEDs on the compression side was not visible. Due to this, the test strain profile does not appear to match up with the analysis profiles as well, but this may be skewed due to higher measured compression strains at the extreme LED set, like those shown in Figure 5-132.

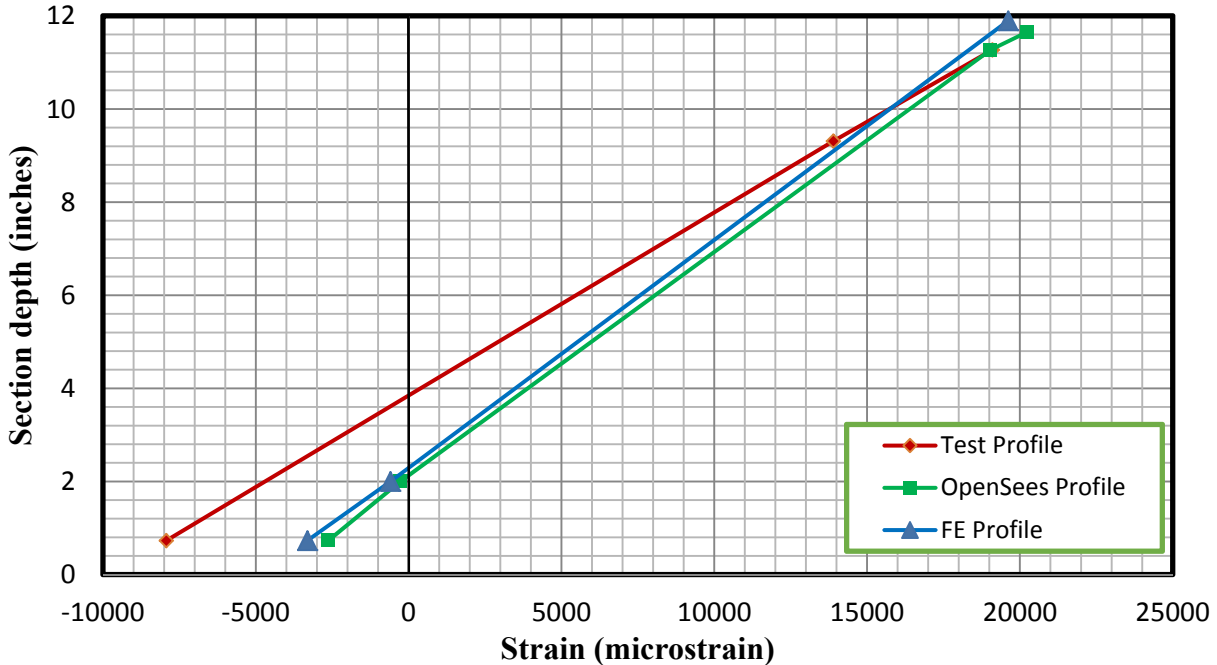


Figure 5-133: Strain profile at ultimate (tension strain 20,000 microstrain) for Specimen H2C1-M

The plots presented in this section indicate that the analysis methods are capable of modeling the flexural response of this specimen, including fairly accurate strain values and strain profiles. Combined with the remainder of the plots, which compare the other specimens to the analytical results, it indicates that the analysis methods can provide an accurate response for both solid and hollow columns.

5.5 Ideal specimens

The longitudinal reinforcing steel used in the test had an extremely low ductility as well as significantly high yield stress, as discussed in Section 4.3. The ultimate strain of longitudinal steel commonly used in bridges is typically around 0.08, while the longitudinal reinforcement used in this testing had an ultimate strain of only 0.02. Additionally, the longitudinal reinforcing steel had a yield stress of 95 ksi, significantly greater than typical longitudinal reinforcing steel which usually has a yield stress of approximately 60 ksi. These factors, especially the low ultimate strain, have caused the experimental test results to have a reduced ductility.

In order to understand how hollow columns may behave in actual bridges, an additional analysis of some of the test specimens has been performed. This additional analysis has been performed using material properties that are more typical of actual bridge columns, including longitudinal reinforcement with higher ductility. The extension of the analysis has been justified based on the comparisons to the actual tests presented in Section 5.3 and 5.4 as well as the comparisons to past research. As shown in the comparison to the experimental results, the hollow circular columns with a two-inch wall thickness experienced flexure failure and agreed well with the analytical model. The experimental results of the solid circular columns also compared well with the analytical model. The geometry of these specimens has been used for the analysis with realistic material properties, since the analysis of these specimens has shown good agreement with the experimental results.

The longitudinal and transverse reinforcement used in the extension of the analytical results has a yield strength of 60 ksi, with ultimate strain of 0.08, and ultimate strength of 90 ksi. The concrete strength is 4500 psi, which is a more common concrete strength. The dimensions and reinforcing steel amounts used for this analysis are the same as for the solid circular test specimens and the two-inch thick test specimens. Although the specimens showed good comparison to the OpenSees analysis, the confined concrete model was unable to be verified since the longitudinal reinforcement ruptured very early. However, the confined concrete model has been compared to test by Hoshikuma and Priestley (2000) and has been found to be fairly conservative, as shown in Section 3.3.1.2.1. Additionally, in Section 5.4, it was shown that the strain values and strain profiles from the analysis were comparable to the test results for the hollow specimen as well.

The solid and hollow specimens with realistic material properties were subjected to two different axial loads for the extended analysis. The force versus displacement responses of the analyses are shown in Figure 5-134 through Figure 5-137. The plots show the response as well as several possible failure points, with tension steel failure considered at a tension steel strain of 0.08 and inside face failure at a concrete compressive strain at the inside face of 0.005. The ultimate concrete compressive strain and the ultimate concrete compressive strain increased by 50 percent have also been shown in the figures. As discussed in previous sections, the ultimate compressive strain prediction has been shown to be very conservative for hollow columns. It is also important to note that the OpenSees model does not account for material failure. Despite the

force versus displacement response in the plots continuing on without a loss in load capacity after inside face or tension steel failure, in reality, the column would lose significantly capacity. Despite this, the plots have been continued to show when other failure modes may occur.

As shown in the figures, the two-inch wall hollow specimen loaded with 22.6 kips axial load is expected to fail by inside concrete face crushing, with a small reduction in ductility when compared to the solid specimen under 22.6 kips axial load. The solid specimen is predicted to fail due to longitudinal steel failure, since the ultimate concrete compressive strain prediction is often conservative by 50 percent and is therefore not considered to be the failure point. The two-inch thick hollow specimen under 45.2 kips axial load is expected to fail due to inside concrete face crushing at a much smaller ductility compared to the solid specimen under 45.2 kips axial load. The solid specimen is also expected to fail due to longitudinal tension failure due to the conservatism of the estimate of ultimate concrete strain. As shown, a fairly ductile response would be achieved by the hollow column under 22.6 kips axial load, while the hollow column under 45.2 kips of axial load has a more brittle response due to the larger axial load causing the neutral axis to develop further into the void.

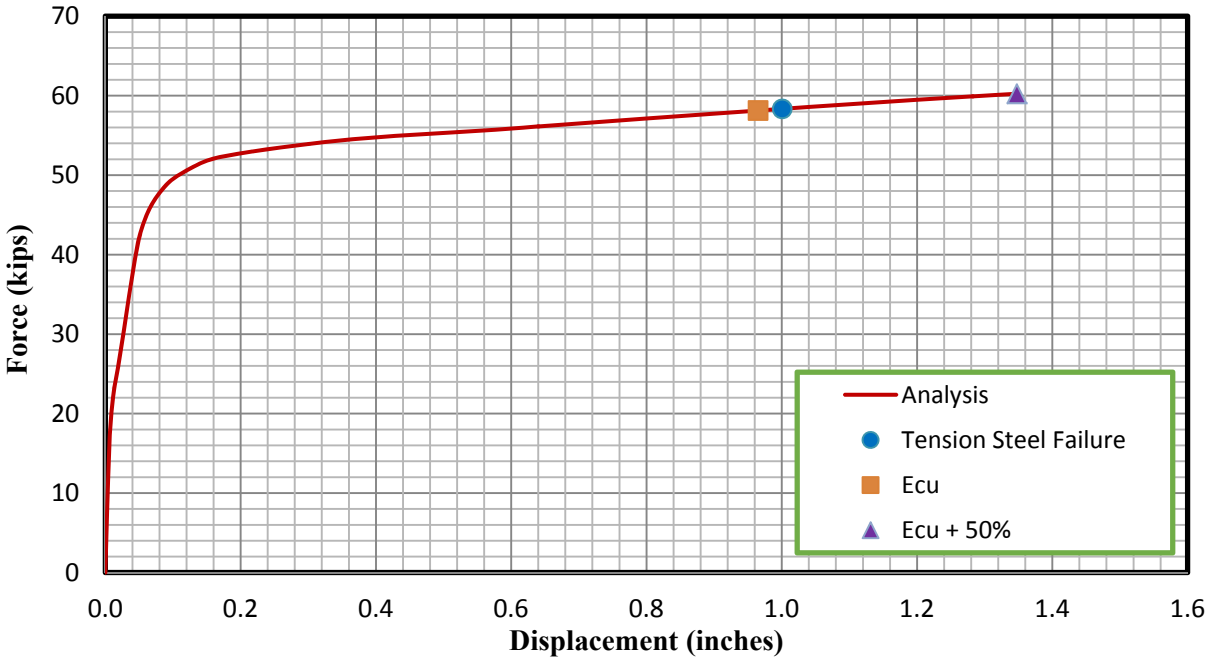


Figure 5-134: Analytical force vs. displacement response of ideal solid specimen under 22.6 kips axial load

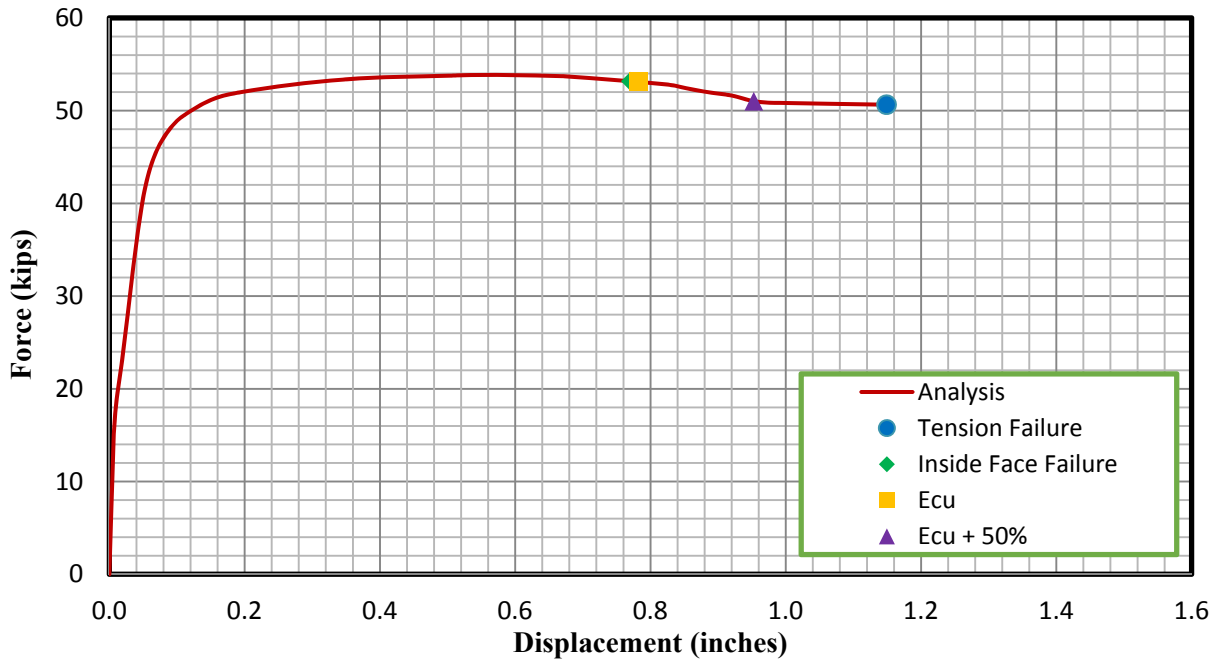


Figure 5-135: Analytical force vs. displacement response of ideal hollow two-inch thick specimen under 22.6 kips axial load

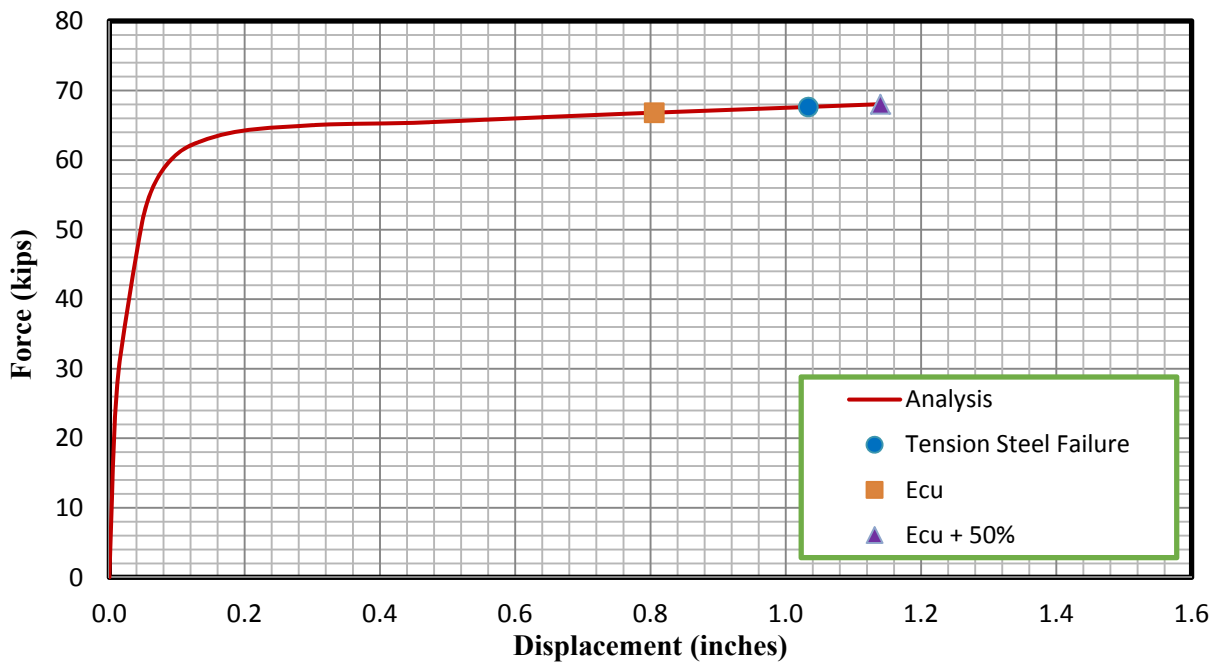


Figure 5-136: Analytical force vs. displacement response of ideal solid specimen under 45.2 kips axial load

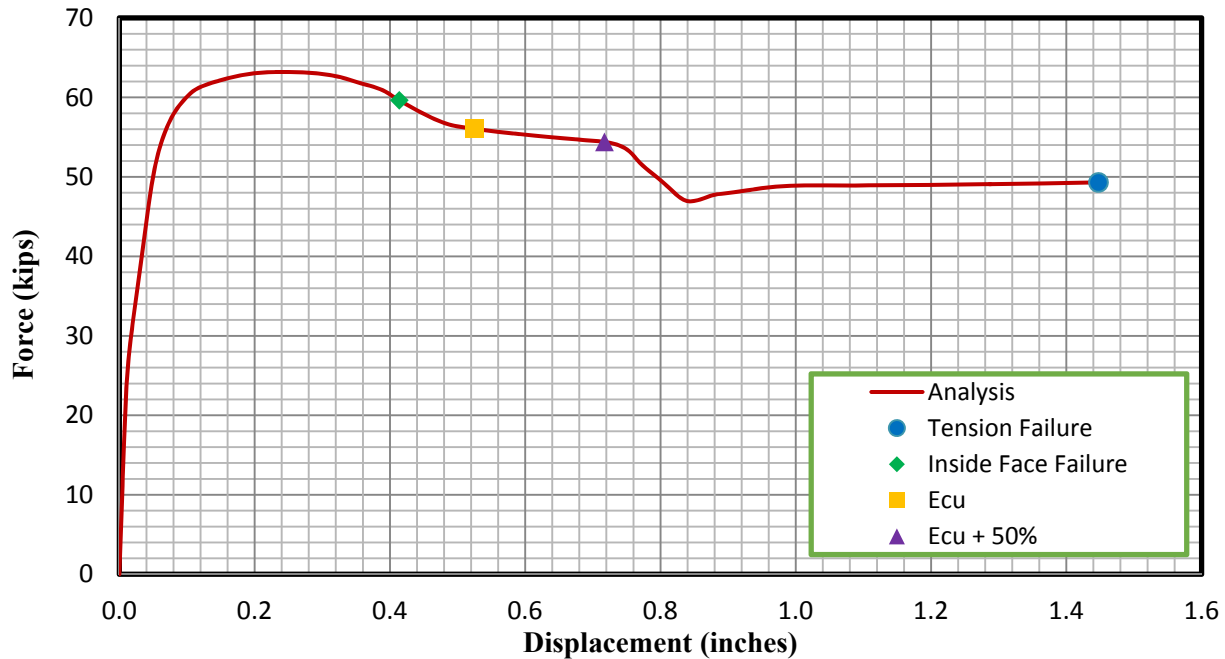


Figure 5-137: Analytical force vs. displacement response of ideal hollow two-inch thick specimen under 45.2 kips axial load

5.6 Alternative analysis method

The suggested analytical method for hollow concrete columns has been shown to provide a fairly satisfactory estimate of the response of hollow columns confined with a single layer of confinement reinforcement through comparison to the experimental results of previous researchers and the experimental results present in this study. However, it has been shown that the suggested analytical method can often be conservative by underestimating the ultimate displacement of the column. Therefore, it is worthwhile to investigate the suggested analytical method further, which was examined for circular hollow columns due to the availability experimental data at large lateral drifts.

Referring back to the confinement analysis results present in Section 3.2.6 (Figure 3-13 for the two-inch wall hollow section and Figure 3-17 for the one-inch wall hollow section), the inside concrete wall element (i.e., labelled as concrete layer 1) experiences small negative radial stress, which indicates that the inside concrete wall element experiences small positive confining pressure. In addition, the proposed adjustment factor, k_h , which accounts for the reduction of radial stress in hollow concrete columns, was based on the average radial stress throughout the

entire wall thickness. However, in the proposed analytical method for hollow concrete columns, the inside half wall thickness was assumed to be unconfined and the proposed adjustment factor (k_h) was applied to the concrete elements located near the transverse reinforcement only, which makes the proposed analytical model conservative. In addition, the influence of circumferential stress was ignored due to the lack of information about how much circumferential stress actually developed in the walls of hollow columns confined with a single layer of transverse reinforcement subjected to flexure. As discussed in Section 3.3.1, the circumferential stress was assumed to be equal to the modified radial stress. However, the circumferential stress in hollow columns is significantly greater than that in solid columns based on the recent finite element analysis performed on hollow concrete columns subjected to concentric axial compression and theoretical equilibrium equations as discussed in Section 3.2.6.4. Figure 5-138 plots the ratio between the circumferential stress in hollow columns and that in solid columns as a function of volumetric ratio of confinement reinforcement for different wall thickness. As shown, the circumferential stress in hollow columns is significantly higher compared to the solid columns and the ratio is in a range of two to seven depending on the wall thickness. Therefore, the effect of high circumferential stress in hollow columns should be taken into account when developing the confined concrete models for hollow columns.

The refined analysis method recommends taking the circumferential stress into account using weighted average method. By combining with different weight for radial stress and circumferential stress, it was found that a weight of 0.9 applied to the radial stress and a weight of 0.1 applied to the circumferential stress gives the best comparisons to the confined concrete strength in hollow columns derived from the finite element analysis as shown in Figure 5-139 for different volumetric ratio of confinement reinforcement.

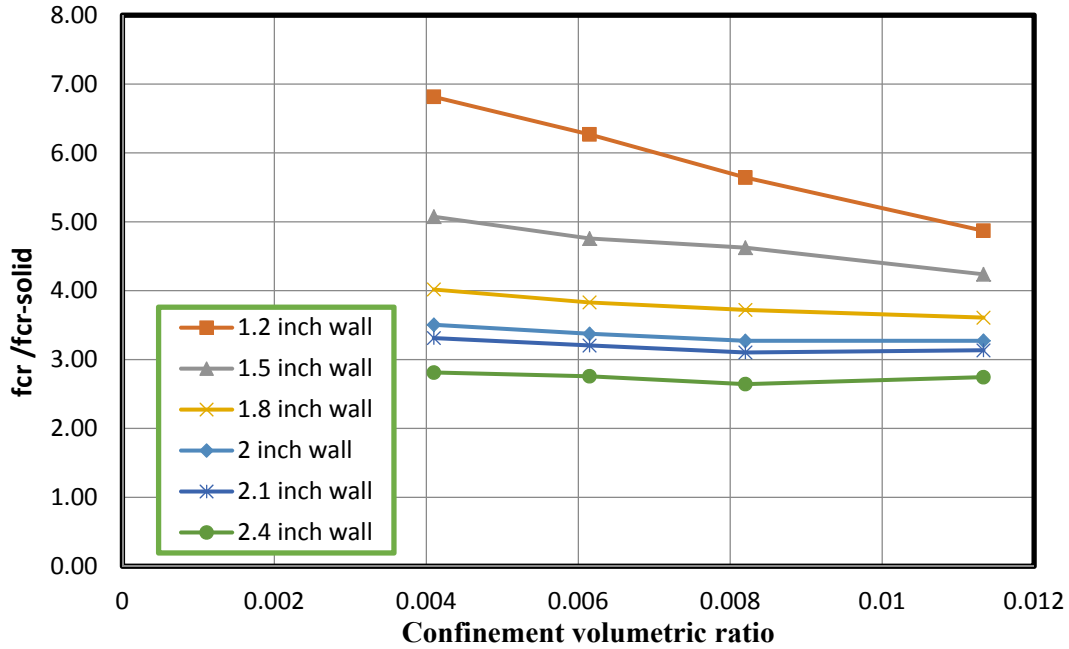


Figure 5-138: The ratio between the circumferential stress in hollow concrete columns and that in solid concrete columns against the confinement reinforcement volumetric ratio

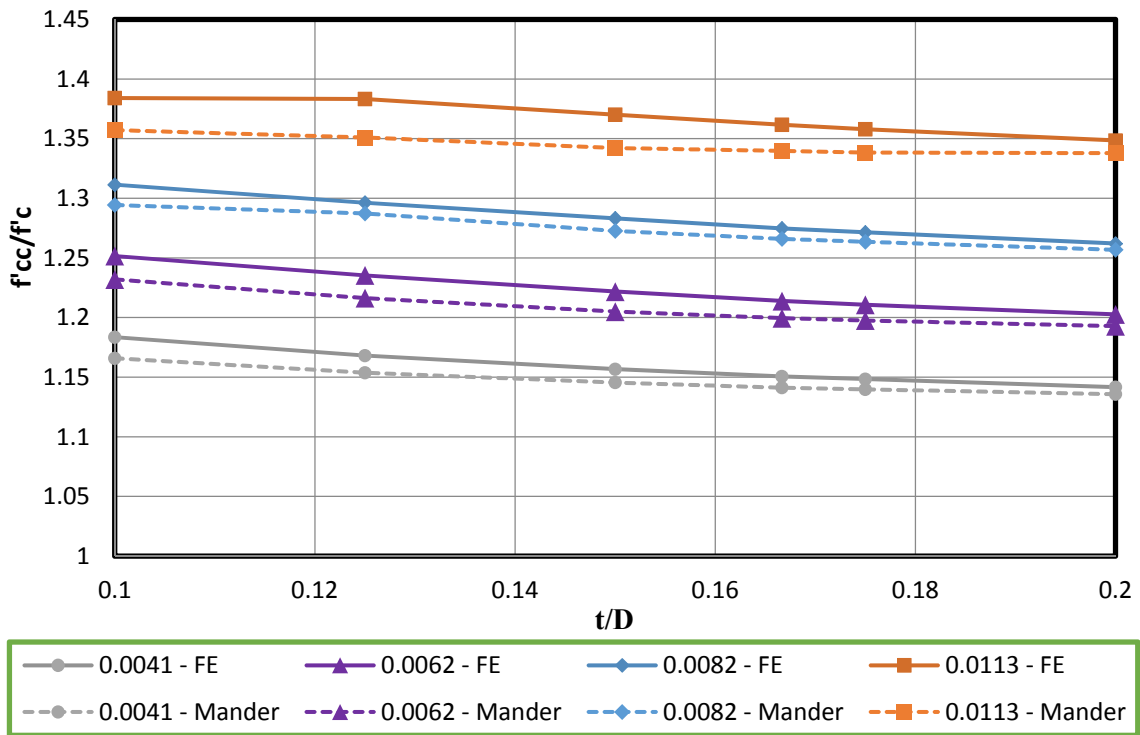


Figure 5-139: The confinement effectiveness coefficient comparisons between the refined analytical method and the finite element analysis

As discussed in Section 3.2.6.4, the transverse stresses in orthogonal directions are approximately equal to one another for a solid column. The refined analysis method applies a factor of $D/(2t)$, derived from the theoretical investigation presented in Section 3.2.6.4, to the transverse stress calculated for a solid section to determine the circumferential stress in a hollow section. The weighted average method is then used to calculate the average lateral stress in the wall of the hollow section. The original analysis method proposed in this report is summarized below, where $f_{rhollow}$ is the adjusted radial stress for a hollow column. The variable f_l is the lateral stress calculated for a solid column.

$$\text{Circular columns: } k_h = \frac{t}{D} + 0.45 \quad \text{Rectangular Columns: } k_h = 0.28$$

$$f_{rhollow} = k_h f_l \quad \text{(Equation 5-1)}$$

Equation 5-2 and Equation 5-3 summarize the modification to the analysis method, which includes the effect of circumferential stress. The effective lateral stress for a hollow column, $f'_{lhollow}$, is then calculated as previously described using the confinement effectiveness factor k_e , proposed by Mander et al. (1988). The confinement effectiveness factor is typically taken as 0.95 for circular columns and 0.75 for square or rectangular columns.

$$f_{crhollow} = \frac{D}{2t} f_l \quad \text{(Equation 5-2)}$$

$$f_{lhollow} = 0.9 f_{rhollow} + 0.1 f_{crhollow} \quad \text{(Equation 5-3)}$$

$$f'_{lhollow} = k_e f_{lhollow} \quad \text{(Equation 5-4)}$$

Using the method described above reduces the conservatism of the originally described method by taking the entire wall thickness within the transverse reinforcement as confined concrete. In addition, the effect of circumferential stress is also taken into account by using the weighted average method.

This refined analysis method has been compared to the experimental results by Hoshikuma and Priestley (2000), as well as the original analytical method, shown in Section 3.3.1.1.1. The original analytical method analyzed the section with the inside concrete near the void as

unconfined and without accounting for the circumferential stress effect, as described in Section 3.3.1.1.1. The refined analysis method uses the entire concrete wall within the transverse reinforcement as confined concrete, with the adjustment factor, k_h , used to calculate the radial stress from the stress calculated for a solid column as well as taking the effect of circumferential stress into account using the weighted average method as described above. The results of this comparison are shown in Figure 5-140. As shown in the figure, the refined analysis method provides a slightly less conservative estimate of the ultimate displacement when compared to the original analysis. As previously discussed, the ultimate concrete compressive strain estimates are very conservative for hollow sections, and inside compression face crushing has been considered as the ultimate failure mode for this analysis, which matches the results of the experimental analysis. The refined analysis method provides a response slightly closer to the experimental response, but is still fairly conservative.

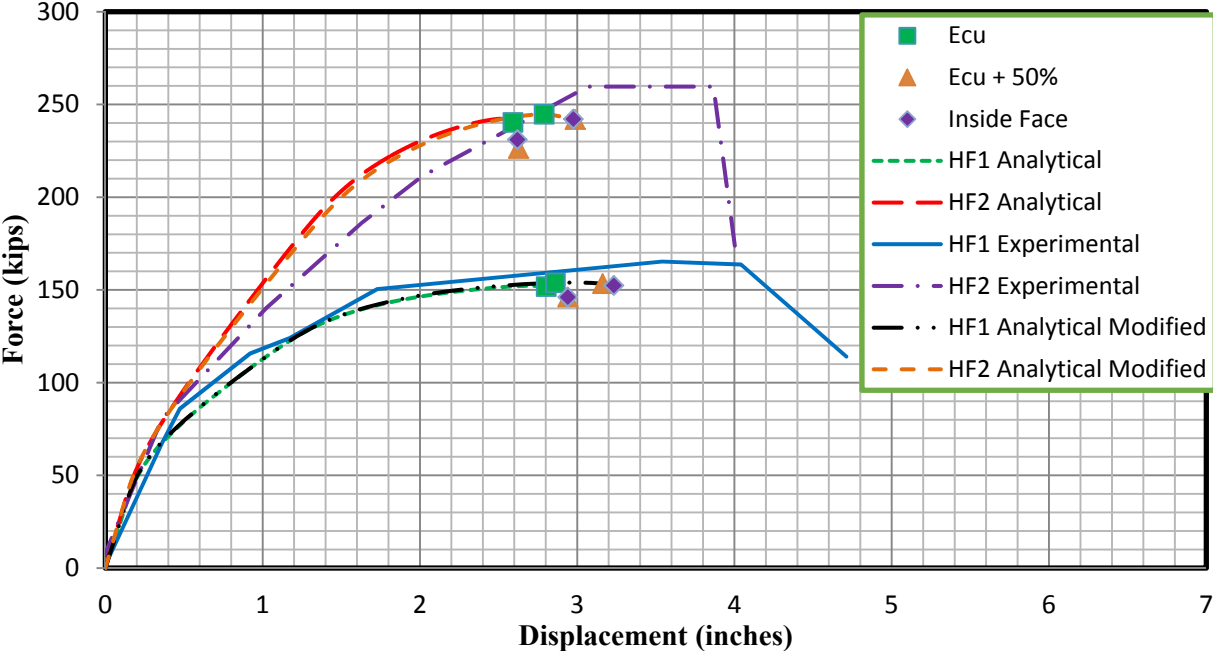


Figure 5-140: Comparison between original and refined analysis and experimental results of Specimens HF1 and HF2 tested by Hoshikuma and Priestley (2000)

The effect of using the refined analysis method depends on the section geometry and location of the neutral axis, since the analysis results will depend on the compressive strain applied to the concrete wall. To provide an example of the effect of the refined analysis method for a different

section, the analysis has been compared for the ideal specimens, which were analyzed and discussed in Section 5.5. The results of the comparison for the ideal specimen under 22.6 kips of axial load and 45.2 kips of axial load are shown in Figure 5-141 and Figure 5-142, respectively.

As shown in the figures, the refined analysis method seems to have a larger effect than what was found for the analysis of the experimental specimens tested by Hoshikuma and Priestley (2000). Additionally, the effect of the refined analysis method is more apparent for the ideal specimen subjected to 45.2 kips of axial load, since the original analysis indicates a much earlier failure. The refined analysis method shows that the ideal specimen subjected to 45.2 kips of axial load experiences early failure due to the crushing of the inside compression face, while the ideal specimen subjected to 22.6 kips of axial load was predicted by the refined analysis method to fail due to rupture of the longitudinal reinforcement.

It is important to note that although the analytical response has been continued past the initial predicted failure mode, the response beyond the inside compressive face failure prediction or tensile rupture prediction may be meaningless. The OpenSees analysis used in this research does not account for material failure. However, in reality, there would be a sudden loss of strength after the initial failure. As previously discussed, the confined concrete compressive failure has not been considered as a failure mode due to the conservative nature of the estimate but has been included for illustrative purposes. Despite the fact that the response after the initial failure may be meaningless, it has been included to show what the response might look like if the initial estimate were conservative and also to show how close the specimen was to reaching the other modes of failure.

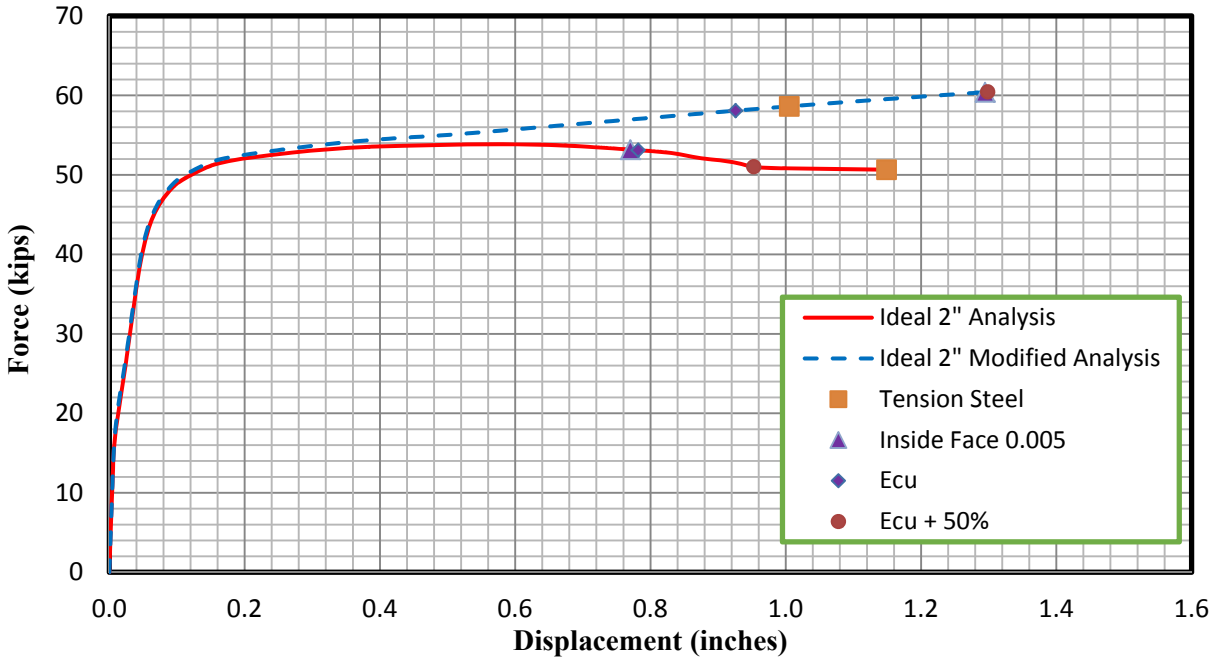


Figure 5-141: Comparison between original and refined analysis for ideal two-inch wall specimen under 22.6 kips axial load

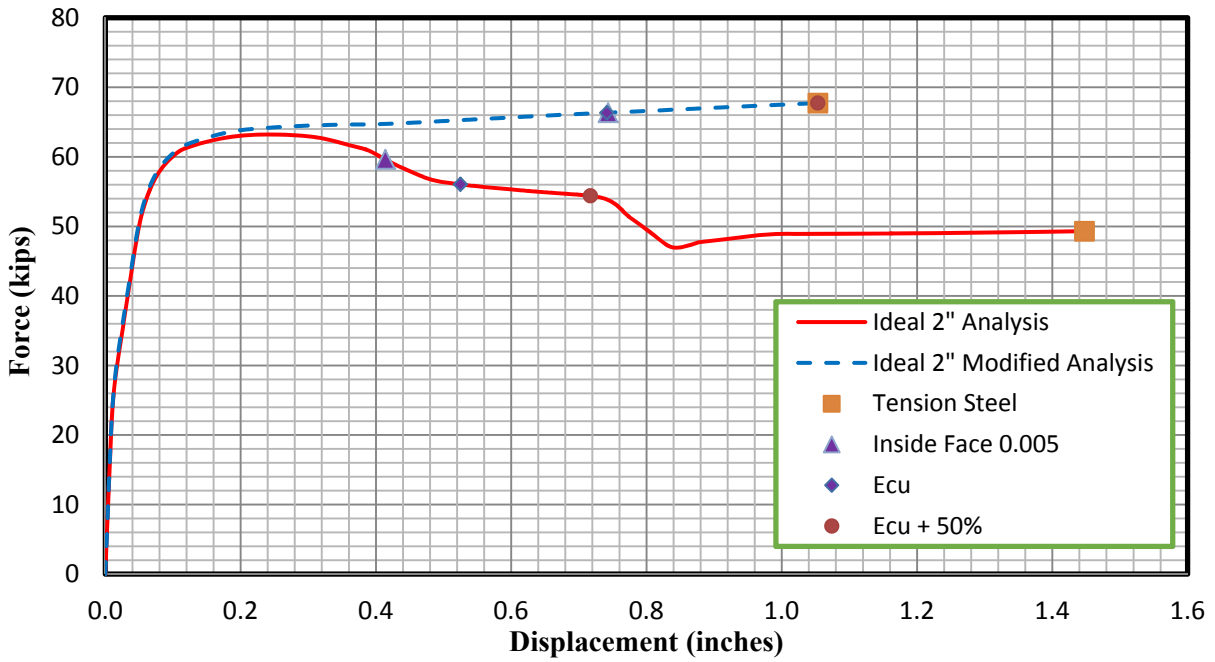


Figure 5-142: Comparison between original and refined analysis for ideal two-inch wall specimen under 45.2 kips axial load

The comparison of the refined and original response has shown that the method used for analysis can have some effect on the predicted response, with the amount of effect dependent upon the geometry of the section and the applied loading. Each method has shown to provide a conservative response when compared to the experimental results by Hoshikuma and Priestley (2000). It was shown that the analytical results did not change significantly when the refined analysis method was used for the comparison of specimens tested by Hoshikuma and Priestley (2000). However, the comparison to the ideal specimens under different axial loads has shown that using the refined analysis can have significant effect in certain cases. However, due to the limited available experimental research of hollow concrete columns confined with a single layer of transverse reinforcement and early failure of the specimens tested in this research, it is difficult to conclusively determine the accuracy of the refined analysis method unless further systematic tests are completed. With the lack of experimental verification, it would be safer to use the original analysis procedure in current design practice. However, it should be noted that the refined analysis method may be able to provide a more realistic response of hollow columns confined with a single layer of confinement reinforcement. In addition, both the refined and original suggested analysis methods were validated for circular sections only. For square sections, the analysis methods were solely based on the finite element analysis due to the lack of experimental data, which requires further investigations.

CHAPTER 6 CONCLUSIONS AND RECOMMENDATIONS

6.1 Conclusions

A systematic investigation into the confinement effects on hollow reinforced concrete columns in seismic regions has been presented in this report. This effort has focused on understanding the confinement effects at the section level, use of one versus two layers of confinement, their impact on column flexural response, theoretical characterization and experimental verification. The study led to more detailed understanding of how confined concrete columns behave under combined flexural and axial loads. Based on the completed work, this section presents the conclusions drawn from different parts of the study.

6.1.1 Confinement effect in hollow columns

The confinement effect in hollow concrete columns due to confinement configuration, wall thickness and confinement reinforcement amount were systematically investigated using the finite element modelling method. The confinement effect was primarily illustrated using key variables such as concrete dilation and confining pressure. Based on a detailed review of literature on large-scale hollow concrete columns tested under lateral loads and the confined concrete analyses conducted as part of this study, it was found that the hollow concrete columns confined with two layers of confinement reinforcement and cross ties are the most effective, but the required quantity near the inside concrete wall surface should be much smaller than that required near the outside concrete wall surface for circular hollow columns. Using this type of confinement configuration, the entire wall of hollow columns was confined effectively and a high ductility level (in a range of six to eight) would be expected, with the failure dominated by the longitudinal reinforcement rupture.

The hollow columns confined with a single layer of confinement reinforcement placed near the outside concrete face can produce satisfactory performance if the ductility demand was not very high (in a range of three to four), and the failure of such columns would be primarily dominated by the inside wall concrete crushing. In these columns, the inside concrete wall was relatively not confined, while the outside concrete wall experienced a smaller confining pressure coming from the outer layer of reinforcement compared to solid columns. This indicated that the

confinement effectiveness in hollow columns confined with a single layer of confinement reinforcement is not as well as that has been established for solid columns. Compared to circular hollow columns, the square hollow columns present further reduced confinement effectiveness. Therefore, the confined concrete models, developed and verified based on solid columns, needs to be modified appropriately to account for the reduction of confinement effectiveness in hollow columns. Suitable modifications have been proposed to a widely-used confined concrete model in current seismic design practice, for both circular and square hollow columns, which will be presented in Section 6.2.1.

6.1.2 Experimental study of hollow columns

The experimental study has demonstrated that hollow specimens with sufficient wall thickness can produce a dependable cyclic lateral response. The two-inch thick circular hollow specimens with a t/D ratio of 0.167 have demonstrated that providing one layer of reinforcing steel can be adequate as long as the neutral axis is in a favorable location. The neutral axis should be near to the wall so that the concrete compression strains at the inside wall are limited to avoid brittle failure. Providing a hollow column with a single layer of transverse reinforcement can produce good savings in cost due to the reduction of materials, such as concrete and reinforcing steel, as well as reducing the construction and labor costs and reducing the mass on supporting structures. Providing a single layer of transverse reinforcement where possible allows for better constructability and more room for concrete fill, as opposed to the typical hollow column design, which has an additional layer of inner reinforcement. Other findings of the experimental program are summarized below.

1. The two-inch thick circular specimens failed due to flexure and did not experience compressive damage on the inside face concrete. The specimen experienced flexural failure due to tensile steel rupture at a low ductility, but the lack of damage at the inside face suggests that the analytical does not overestimate the displacement at which the inside face fails.
2. The two-inch thick circular specimens experienced a similar capacity and ultimate displacement as the solid specimens. This further verifies that hollow columns with sufficient wall thickness and favorable neutral axis location can experience similar

capacity and response when compared to solid columns with the same outside diameter and reinforcement.

3. Shear displacement of hollow columns seems to be more significant than that of similar solid columns, and a trend has been shown with higher shear displacement for smaller wall thicknesses.
4. Local failure of hollow specimens was identified as an issue, which may be due to local forces applied to a small wall thickness, as well as the contribution of patches used to address poor concrete quality.

6.1.3 Analytical analyses of hollow columns

The finite element method was used to model both solid columns and hollow columns that had one layer of confinement reinforcement placed near the outside concrete face, with two different wall thicknesses, under combined axial and flexure load. The FEM results of hollow columns that had one layer of confinement reinforcement were also compared with the experimental results, which indicated satisfactory agreement, except for the square hollow columns. The FE analyses ran into convergence problems for the square hollow columns, although a stabilization option was incorporated into the analyses. The test specimens of square hollow columns also experienced premature local failure, which appeared to have stemmed from using a small wall thickness and poor effectiveness of the confinement reinforcement.

In addition to the FE analyses, an OpenSees fiber-based analysis was also used to model the response of the solid and hollow specimens. This type of analysis is comparable to the typical analytical methods used by engineers in the design of concrete bridge columns. Based on the finite element analysis results, an adjustment to Mander's model was implemented in the OpenSees analysis to more accurately reflect the stress state in hollow columns. The adjustment accounts for the reduced radial stress, which has been found to occur in hollow concrete columns, with zero radial stress at the inside face. The analysis was shown to be fairly accurate when compared to previous research, as well as to the tests performed in this study, when the effects of shear are not included. Based on these factors, the analysis was extended using more realistic material properties. It was demonstrated that satisfactory ductility can be achieved for hollow concrete columns with one layer of transverse reinforcement, although concrete crushing at the

inside face can be a limiting factor and should be considered in the design. The neutral axis location is critical to ensuring that inside concrete face crushing does not occur too early, and by designing the neutral axis to occur near the inside concrete face, this limits the compression strains in order to avoid early crushing.

The other compression limit state in hollow concrete columns is the crushing of confined concrete near the transverse reinforcement. The Mander's model was adjusted based on the finite element analysis and the test results. Several key findings were realized from this adjustment as well as from the results of experimental investigations by previous researchers.

1. Concrete near the transverse reinforcement in hollow columns experiences a lower radial stress (confining pressure) than do solid concrete columns with similar reinforcement at similar axial strains. This is likely due to the increased deformability of hollow columns, with the radial deformation requiring less confining pressure to contain, and with the ability of the concrete to move toward the void.
2. Concrete near the transverse reinforcement in hollow columns experiences a smaller strength increase, due to confinement reinforcement, than a similar solid column. The smaller radial confining stress likely contributes to this smaller increase in strength, as does the existence of the void.
3. Transverse reinforcement failure appears to be less of a concern for hollow columns than for solid columns, due to the increased deformability of the hollow columns. The radial displacement of a hollow column is easier to contain than that of a solid column, resulting in lower transverse reinforcement stresses. Previous research has demonstrated this low confinement demand, although further study is needed in order to quantify this behavior and provide a more accurate ultimate strain for confined concrete based on transverse reinforcement failure.

The analytical method discussed in this research, which is used to model the behavior of hollow columns confined with a single layer of confinement reinforcement, may be overly conservative due to the assumption that the concrete near the inside face is unconfined. In addition, the high circumferential stress developed in hollow columns was ignored. To address these concerns, a refined analysis approach, which uses the weighted average method to take the effect of circumferential stress into account, and suggests modelling the entire concrete wall within the

transverse reinforcement as confined concrete, was proposed. This refined analysis method was presented in Section 5.6 and was shown to provide a less conservative response when compared to the previous experimental results by Hoshikuma and Priestley (2000). However, due to the limited available experimental research of hollow concrete columns confined with a single layer of transverse reinforcement, it is difficult to conclusively determine the accuracy of the refined analysis method. Therefore, it would be safer to use the recommended analytical model in current design practice. However, in the analytical analysis of hollow concrete columns, the refined analysis method is able to provide a more realistic response.

6.2 Design recommendations

6.2.1 Applicability of Mander's model to hollow sections

Based on the comparison to previous test results, it has been shown that Mander's model can be applied to hollow columns with one layer of transverse reinforcement, as long as an adjustment to Mander's model is used along with adjusted modeling recommendations. The proposed adjustment is simple and easy to apply, and has been shown to be fairly conservative for circular columns when compared to experimentation by previous researchers. The proposed adjustment factor for circular columns is:

$$k_h = \frac{t}{D} + 0.45$$

And for square columns, the adjustment factor is:

$$k_h = 0.28$$

These adjustment factors were proposed based on the findings of the finite element analysis (Section 3.2.6.4.2), which found reduced radial stress near the transverse reinforcement for hollow columns. For circular columns, this reduction seemed to depend on the wall thickness ratio, and for square columns, the reduction seemed relatively constant. The adjustment factor for circular columns has been shown to be conservative, while the proposed adjustment for square columns has not been verified and requires further testing. An example which illustrates the use of the adjustment factor is provided in Section 6.3.

6.2.2 Design parameters

A more uniform definition of commonly used column design parameters has been suggested for hollow columns in order to facilitate a better comparison to solid columns. Parameters such as reinforcement ratios and axial load ratios are recommended to be reported using the gross section, as if the section was solid. This allows the engineer to compare the capabilities of solid and hollow columns more efficiently. This can be a source of confusion and error, so it is important to clearly state how the ratios were developed, regardless of whether the gross section or net section is used. Gross section ratios can provide easier comparisons to solid columns in order to determine whether a hollow or solid column may be preferable in certain design situations, while net section ratios (using only the area of present concrete for hollow columns) can be useful for determining how much of the concrete capacity is utilized by the axial load.

6.2.3 Confinement configurations applicability for different wall thicknesses

The effect of confinement configuration, wall thickness, and the proportion of the inner to outer layer of confinement reinforcement amount on the confined concrete behavior of circular hollow columns was investigated with the use of the finite element method in this report. Under the given volumetric ratio of transverse reinforcement, it was concluded that for a hollow section with a wall thickness-to-section diameter ratio smaller or equal to 0.125, one layer of confinement reinforcement placed near the outside concrete face would be adequate to provide limited ductile behavior, if the longitudinal reinforcement ratio and the axial load ratio were designed appropriately. In this case, providing two layers of reinforcement would not noticeably enhance the column behavior even if cross ties are used; however, it may cause problems due to reinforcement congestion. When using one layer of reinforcement, the crushing of the inside concrete wall would control the ultimate capacity and the ductility of such hollow sections. When small wall thickness was used, it was shown that these columns will be susceptible to local failure. In order to avoid such failure resulting from significantly reduced amount of materials, a minimum wall thickness-to-section diameter ratio of 0.1 is suggested in the design of thin-wall circular hollow columns. For a hollow section with a wall thickness-to-section diameter ratio greater than 0.125, two layers of confinement reinforcement connected with effective cross ties would provide better performance over using one layer of reinforcement, and the longitudinal

reinforcement rupture would control the ultimate capacity and the ductility of such hollow sections. However, due to the significant construction effort and cost associated with two layers of lateral reinforcement connected with cross ties, one layer of lateral reinforcement was also considered for larger wall hollow columns if the ductility demand was not very high. The behavior of such hollow columns would be satisfactory if the hollow columns are designed with the neutral axis located close to the concrete wall and away from the centroid of hollow columns. The modelled hollow columns were also analyzed subjected to a combination of axial and flexure loadings as would be the simulation case for a bridge column under lateral loading, such as that generated by an earthquake. The analyses results confirmed the finding from the concentric axial loading. Since the local failure took place for square columns with a t/D ratio of 0.167, further investigation is needed to establish the minimum wall thickness. However, design of these columns is not recommended with one layer of reinforcement due to the poor confinement effects.

6.2.4 Recommended hollow column design procedure with one layer of transverse reinforcement

Review of the design practices for hollow columns found that there are very few guidelines in existence and even fewer recommendations for design procedure. The test results presented in this report and in previous literature have suggested that solid and hollow columns with one layer of transverse reinforcement can have comparable capacity and ductility, as long as the hollow column is designed to ensure that the neutral axis is located near the inside wall to prevent large compression strains in the inside wall concrete. Based on recommendations by Hoshikuma and Priestley (2000), these inside face concrete strains should be limited to 0.005 for theoretical analysis, but they recommend a safe design limit of 0.0035.

The neutral axis location is thus very critical, and some iteration may be necessary in the design process in order to achieve a design with a safe neutral axis location and low inside face concrete compression strain. Inside face failure may still be the limiting factor in some cases, but with adequate neutral axis location, it can be made to occur at sufficient ductility. Due to the similarities between solid columns and hollow columns with the same details and well-designed neutral axis location, it has been found that the initial preliminary design and analysis can be performed as if the specimen were solid. A solid section can be initially assumed, and the

required diameter and amount of transverse reinforcement can be estimated in the usual fashion. Then, the neutral axis location of this preliminary solid column design can be calculated at the nominal moment capacity, which provides a good initial estimate of the neutral axis depth of the hollow column. Setting this neutral axis depth as the preliminary wall thickness then provides a good starting point for the hollow column design, which typically produces low concrete strains at the inside face concrete until a fairly ductile response is achieved. Then, further analysis and iteration of this section can be performed using the recommended adjustment to Mander's model. The wall thickness can then be increased or decreased as necessary. This relatively simple initial estimate of the required wall thickness can be a good indicator of whether a hollow column will be preferable to a solid column. If the required wall thickness is too large, it may be preferable to use a solid column. Alternatively, the wall thickness could be decreased further, and a second layer of transverse reinforcement near the inside face could be provided for increased ductility, with cross-ties connecting it to the outside layer of transverse reinforcement.

Other factors can be adjusted to enable a safe hollow column design, such as axial load ratio and longitudinal reinforcement amount. High axial load and high amount of longitudinal reinforcement cause the neutral axis to move more toward the center of the section, which can cause high axial strains at the inside wall of hollow columns. If the initial design indicates that inside concrete crushing may occur and the desired ductility may not be achieved, or that the required wall thickness may be too high, the amount of axial load or longitudinal reinforcement could be reduced, if possible, which could reduce the required thickness of the wall.

6.3 Design example

A demonstration of the suggested adjustment factor and methodology for hollow columns design is described in this section. An example of a simple bridge column design is presented, which illustrates the process of selecting the void dimension in a hollow column as well as adjusting Mander's model for the hollow column. The example makes some simplifying assumptions and shows the basic process suggested by this research without discussing detailing and other considerations such as shear design, which are outside the scope of this report.

The material properties were chosen to represent standard material properties used in typical columns. A clear concrete cover of two inches to the transverse reinforcement is typically required by codes and is used in this example.

Concrete:

Compressive strength of column at 28 days: $f'_c = 4.5 \text{ ksi}$

Reinforcing steel:

Yield strength $f_y = 66 \text{ ksi}$

Ultimate strength $f_u = 90 \text{ ksi}$

Ultimate strain $\varepsilon_u = 0.08 \text{ in/in}$

The example presents the design of a single column with dimensions intended to be fairly typical of those used in actual bridge columns in earthquake prone regions such as California. The column height is 20 feet and the initial column demands have been chosen as 650 kips of axial load and 220 kips of base shear. Based on this axial load, a diameter of 5 feet has been chosen to provide an axial load ratio of approximately 5 percent. The column has been initially designed identically to that of a solid column. The first step of the design process is to estimate the required amount of longitudinal reinforcement. This is typically done by utilizing provided column interaction charts to estimate the amount of longitudinal reinforcement necessary to achieve the required moment demand.

$$M_r = (\text{Base shear}) \cdot (\text{Column height}) = (220) \cdot (20 \cdot 12) = 52,800 \text{ k} \cdot \text{in}$$

Using this required moment demand an initial longitudinal reinforcement ratio of 0.0085 was chosen. The required area of longitudinal reinforcement was then calculated.

$$A_{l \text{ required}} = 0.0085 \cdot \frac{\pi}{4} \cdot 60^2 = 24.03 \text{ in.}^2$$

To meet this required demand 32 number 8 bars were chosen, which produces an actual area of longitudinal reinforcement of 25.3 in.² and an actual ρ_l of 0.0089. After determining the initial longitudinal reinforcement amount, the transverse reinforcement ratio could be calculated. The

following equation proposed by Priestley et al. (1996) was used to define the required amount of transverse reinforcement to achieve a ductile design.

$$\begin{aligned}\rho_s &\geq 0.16 \frac{f'_c}{f_y} \left(0.5 + \frac{1.25P}{f'_c A_g} \right) + 0.13(\rho_t - 0.01) \\ &= 0.16 \left(\frac{4.5}{66} \right) \left(0.5 + \frac{1.25(650)}{4.5 \left(\frac{\pi}{4} \cdot 60^2 \right)} \right) + 0.13(0.0089 - 0.01) = 0.006\end{aligned}$$

An initial transverse reinforcement spacing of 3.5 inches was then chosen, and the required diameter of transverse reinforcement was calculated as follows. Since the transverse reinforcement size is initially unknown, a D' of 56 inches is assumed, corresponding to the column diameter with the concrete clear cover subtracted.

$$\rho_s = \frac{4A_s}{D's} \rightarrow A_s = \frac{\rho_s D's}{4} \rightarrow A_s = \frac{0.006(56)(3.5)}{4} = 0.294 \text{ in.}^2$$

$$d_{transverse} = \sqrt{\frac{4}{\pi} (0.294)} = 0.61 \text{ inches}$$

Based on this required diameter of transverse reinforcement, a spiral composed of a number 5 bar spaced at 3.5 inches was chosen.

$$\rho_s = \frac{4(0.31)}{(54.6)(3.5)} = 0.0065$$

The actual transverse reinforcement ratio is 0.0065, which is greater than the requirement of 0.006. The next step of the design process is to perform a moment curvature analysis in order to ensure that the required moment capacity can be achieved and that adequate ductility can be provided. Mander's model is used with the calculated transverse reinforcement ratio in the usual manner in order to provide the confined concrete properties. The analysis was performed using OpenSees, and a nominal moment capacity of 55,056 k-in was found, which is greater than the required moment of 52,800 k-in, but which does not exceed the required moment by too much. Therefore this preliminary design is acceptable. If the required moment capacity was not met or if it was exceeded by too much, the amount of longitudinal reinforcement would be adjusted as well as the amount of transverse reinforcement if necessary. The analysis would be performed

again until a satisfactory amount of longitudinal and transverse reinforcement was found. For this example, 32 number 8 longitudinal bars with a transverse reinforcement spiral composed of a number 5 bar spaced at 3.5 inches is satisfactory.

Once the analysis has shown that a design meets required capacity, the analysis results can then be used to estimate the depth of the neutral axis at the nominal moment. For this example, the neutral axis depth, when the section reached nominal moment capacity, was approximately 11.7 inches. This neutral axis depth provides a good initial estimate of a wall thickness that can provide a fairly ductile response. A wall thickness of 13 inches was then chosen, which is fairly close to the neutral axis depth and which provides a $\frac{t}{D}$ ratio of 0.22. The next step is to calculate the confined concrete properties for this specimen using the adjustments proposed for hollow columns. Two layers of concrete were used, as previously described, with the half of the wall near the inside face modeled as unconfined concrete and the half near the transverse reinforcement modeled as confined concrete with the adjustment to Mander's model. The lateral reinforcement pressure was estimated as if the column was solid, and then the adjustment factor k_h for hollow columns was applied.

$$\rho_s = 0.0065, k_e = 0.95$$

$$f_l = \frac{1}{2} \rho_s f_{yh} = \frac{1}{2} (0.0065)(66) = 0.21 \text{ ksi}$$

For solid circular columns, a confinement effectiveness coefficient of 0.95 is typically assumed and would then be applied to this calculated lateral stress. The remainder of Mander's model would be performed as usual, including the calculation of the confined concrete peak strength and strain at peak strength. This procedure was performed for the initial analysis of this column as if it were solid as described above. However for hollow columns, it was shown in this report that less lateral stress is required to confine the hollow columns, so an adjustment factor was proposed. The adjustment factor, k_h , is applied as shown, in addition to k_e , which is still applied since it accounts for the arching effect between longitudinal and transverse reinforcement.

$$k_h = \frac{t}{D} + 0.45 = \frac{13}{60} + 0.45 = 0.67$$

$$f'_l = k_e k_h f_l = 0.95 \times 0.67 \times (0.21) = 0.13 \text{ ksi}$$

The confined concrete strength and peak strain is then calculated using the equations proposed by Mander et al. (1988). This assumes that the calculated lateral pressure is the same in both directions in the plane, which is likely a conservative assumption, since it has been demonstrated that circumferential stresses can be much higher in hollow columns.

$$\begin{aligned}
 f'_{cc} &= f'_c \left(-1.254 + 2.254 \sqrt{1 + \frac{7.94 f'_l}{f'_c}} - 2 \frac{f'_l}{f'_c} \right) \\
 &= 4.5 \left(-1.254 + 2.254 \sqrt{1 + \frac{7.94(0.13)}{4.5}} - 2 \frac{(0.13)}{(4.5)} \right) = 5.34 \text{ ksi} \\
 \epsilon_{cc} &= \epsilon_c \left[1 + 5 \left(\frac{f'_{cc}}{f'_c} - 1 \right) \right] = 0.002 \left[1 + 5 \left(\frac{5.34}{4.5} - 1 \right) \right] = 0.0039
 \end{aligned}$$

The resulting confined concrete strength is 5.34 ksi, and the strain at peak strength is 0.0039. For comparison, the confined concrete strength and peak strain for this column when calculated as solid was 5.74 ksi and 0.0048, respectively. Using the calculated design properties, a pushover analysis of the hollow column was then performed. Based on this analysis, the displacement ductility was determined to be 3.8. The controlling factor was the inside concrete face crushing, which was assumed to occur at a strain of 0.0035 and was recommended as a conservative design limit by Hoshikuma and Priestley (2000). For comparison, a pushover analysis of the same column as if it was solid was performed. The results of both analyses have been plotted in Figure 6-1, with several markers representing predicted failure points. The points labeled “Ecu” and “Ecu + 50%” represent the ultimate compression strain predicted by Priestley et al. (1996) and the ultimate compression strain with an additional 50 percent, respectively. The additional 50 percent point is added since it is known that the prediction of ultimate compression strain in the confined concrete can be significantly conservative. The tension failure is considered at strain in tensile steel of 0.08. The displacement ductility of the solid section is 5.4 if the ultimate point is considered at tension steel failure or 5.3 if the ultimate point is considered at the ultimate concrete compression strain plus 50 percent. When compared to the estimated displacement ductility of the hollow column of 3.8, it can be seen that the hollow column does experience a reduction in ductility due to the inside face crushing.

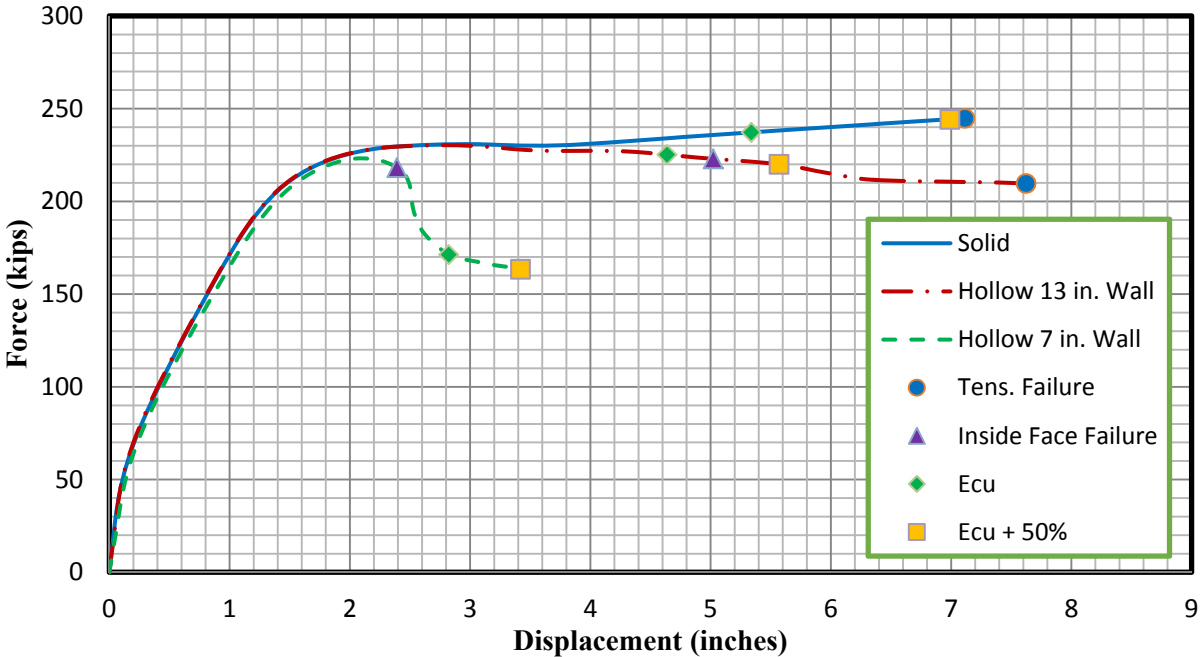


Figure 6-1: Pushover analysis of example column as hollow and solid

As shown in Figure 6-1, the columns have a similar response until close to the point where the hollow column inside face strain reaches 0.0035. The loss of capacity is due to the downward slope of the confined concrete at this point. This in turn causes the hollow column to rely more on the inside face concrete for strength and causes higher strains at the inside face, leading to inside concrete face crushing. For further comparison, an analysis of the same hollow column, except with a wall thickness of seven inches, has also been included in Figure 6-1. A wall thickness of seven inches corresponds to a wall thickness ratio of 0.12, and the k_h adjustment factor for this specimen would be 0.57. This wall thickness is much less than the neutral axis depth, and as a result, a brittle response is found. The ductility of the seven-inch thick specimen, when inside face failure is considered at a strain of 0.0035, was found to be 1.8.

This example illustrates that certain columns with limited axial load demand and lower amounts of longitudinal reinforcement can experience relatively ductile behavior, which may be satisfactory in many cases. The wall thickness ratio of 0.22, used in the example column, would correspond to a drop in mass and concrete material of 32 percent. Depending on the column demands and dimensions, even larger drops in material could be achieved while still providing

adequate ductility. It is important to note that the limiting inside face strain of 0.0035 was recommended by Hoshikuma and Priestley (2000) as a conservative design method and that actual ductility could be larger. For the 13-inch thick wall example, if inside face failure is considered as 0.005, this would correspond with a ductility of 4.1.

As described in the example, it is fairly simple to estimate the required wall thickness of the hollow column, which can help the designer to decide between using a solid or hollow column. If the design check shows that the wall thickness would be too large to have any advantages, two layers of transverse reinforcement could instead be provided to further reduce the wall thickness and help avoid inside concrete face failure.

Further example columns were analyzed in order to show a comparison of hollow and solid columns with different shapes and dimensions. The example columns were analyzed as solid, hollow with one layer of transverse reinforcement, and hollow with two layers of transverse reinforcement. The design of the columns followed the same procedure presented in detail in the example above. The solid specimens and hollow specimens with one layer of transverse reinforcement with the same outside diameter had the same amount of transverse reinforcement. The hollow specimen with two layers of transverse reinforcement of the same diameter had a second layer of reinforcement near the void. The same number of longitudinal bars was also provided near the outside of the specimen, in addition to more longitudinal steel in the layer near the void. Since this additional longitudinal reinforcement would result in a significantly larger flexural capacity, the diameter of the longitudinal reinforcement was reduced until a similar flexural capacity was achieved. The transverse reinforcement near the outside of the specimen was kept the same as the other specimens with the same diameter, but additional transverse reinforcement with the same diameter and spacing as the outside reinforcement was provided near the void, as well as cross ties to the outer reinforcement.

Table 6-1 provides a summary of the properties of each specimen that was analyzed. For the hollow specimens with one layer of transverse reinforcement, the concrete was modeled using the procedure described in Section 3.3.1.1.1, with the inside layer modeled as unconfined concrete and the layer near the transverse reinforcement modeled as confined concrete, with the adjustment factor for hollow columns applied. For the hollow specimens with two layers of transverse reinforcement the procedure described in Section 3.3.1.1.2 was used, with the

concrete between the layers of transverse reinforcement modeled as confined concrete. In Table 6-1, S, H1, and H2 represent whether the column was solid, hollow with one layer of transverse reinforcement, or hollow with two layers of transverse reinforcement, respectively.

Table 6-1: Properties of example columns

Diameter (in)	120	120	120	42	42	42	60	60	60
S, H1, H2	S	H1	H2	S	H1	H2	S	H1	H2
Void Diameter (in)	0	70	84	0	21	24	0	36	40
t/D	N/A	0.21	0.15	N/A	0.25	0.21	N/A	0.20	0.17
Concrete Strength (ksi)	4.5	4.5	4.5	4.5	4.5	4.5	4.5	4.5	4.5
Long. Steel Yield (ksi)	66	66	66	66	66	66	66	66	66
Long. Steel Ultimate (ksi)	90	90	90	90	90	90	90	90	90
Long. Steel Ult. Strain (in/in)	0.08	0.08	0.08	0.08	0.08	0.08	0.08	0.08	0.08
Long. Steel Diameter (in)	1.693	1.693	1.27	1	1	0.75	1.128	1.128	0.875
Number of Long. Bars (outside layer)	55	55	55	20	20	20	36	36	36
Number of Long. Bars (inside layer)	0	0	55	0	0	20	0	0	28
Transverse Steel Yield (ksi)	90	90	90	90	90	90	90	90	90
Transverse Steel Spacing (in)	3	3	3	4.5	4.5	4.5	3.5	3.5	3.5
Transverse Steel Diameter (in)	0.875	0.875	0.875	0.75	0.75	0.75	0.75	0.75	0.75
Axial Load (k)	5000	5000	5000	1500	1500	1500	800	800	800
Axial Load Ratio (gross section, %)	9.82	9.82	9.82	24.06	24.06	24.06	4.94	4.94	4.94
Axial Load Ratio (net section, %)	9.82	14.89	19.26	24.06	32.08	35.73	4.94	7.72	8.89
Column Height (ft)	20	20	20	15	15	15	20	20	20

The results of the analyses for the 10 foot diameter columns are presented in Figure 6-2. As shown, the solid specimen is predicted to experience transverse reinforcement failure near a displacement of 2.75 inches. However, since this estimate can often be conservative it may be more reasonable to assume failure occurs due to the rupture of longitudinal reinforcement. In comparison, the hollow specimen with one layer of transverse reinforcement is expected to experience early failure due to crushing of the inside concrete face at a strain of 0.0035. This early failure is likely due to the larger axial load ratio of 9.8 percent. A more ductile response could be achieved for this specimen if a smaller void was used, but this void dimension was chosen since the gain in efficiency diminishes as the size of the void decreases. The hollow

specimen with two layers of transverse reinforcement is shown to experience a more ductile response than the solid specimen, with rupture of the longitudinal reinforcement predicted to occur at a higher displacement. This larger displacement is achieved due to the greater compression in the concrete since the concrete area is reduced, consequently applying a larger compressive force in the longitudinal reinforcement and delaying the tensile rupture of the reinforcement. Since this specimen also has a large amount of transverse reinforcement compared to the net area of concrete, the ultimate confined concrete compressive strain does not occur until a displacement far beyond that of the rupture of the longitudinal reinforcement, and it has not been included in the figure for this reason. It is also important to note that several possible failure modes have been plotted in this figure and the examples following this figure, but in reality, after experiencing one of the failure modes a significant loss in strength is likely. The OpenSees analysis does not take material failure into account.

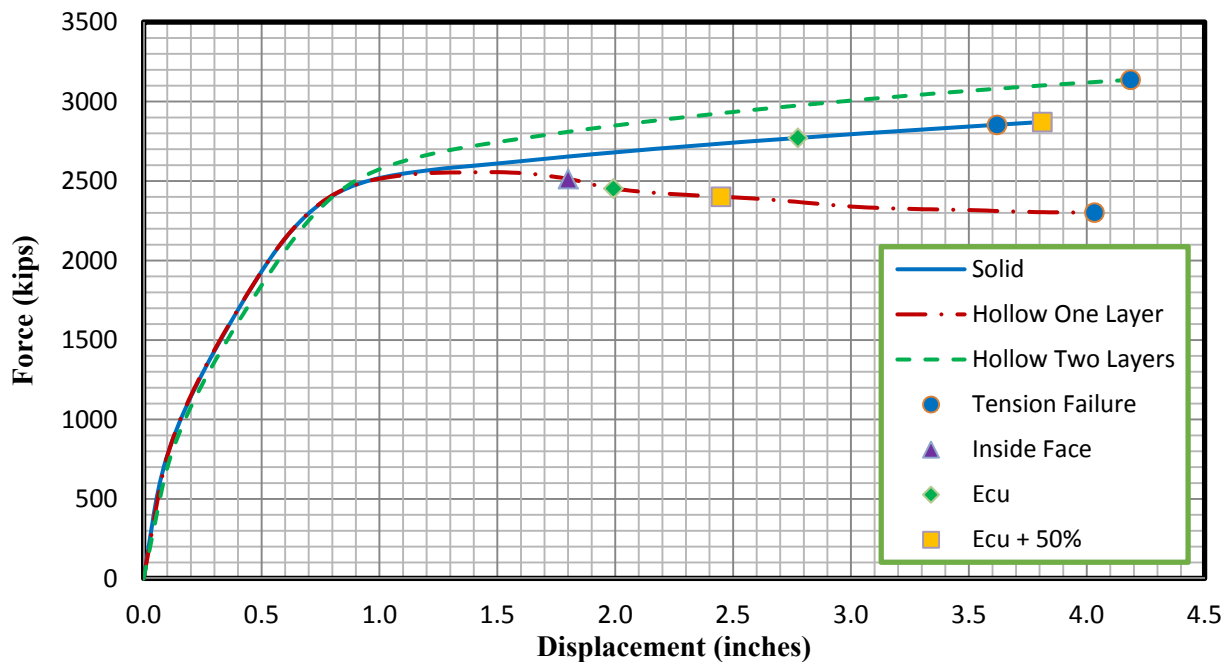


Figure 6-2: Pushover analysis of 10 foot diameter circular columns

The analytical results of the 3.5 foot diameter specimens are shown in Figure 6-3. As shown, the solid specimen experiences a ductile response and is expected to experience failure due to

rupture of transverse reinforcement. The hollow specimen with one layer of transverse reinforcement experiences a brittle response and early failure due to crushing of the inside face concrete. This early failure can be attributed to the high axial load, of approximately 24 percent to the gross section, that these columns were subjected to, causing the neutral axis to develop further into the void. The hollow specimen with two layers of confinement experiences a ductile response, and is expected to fail due to the rupture of the longitudinal reinforcement.

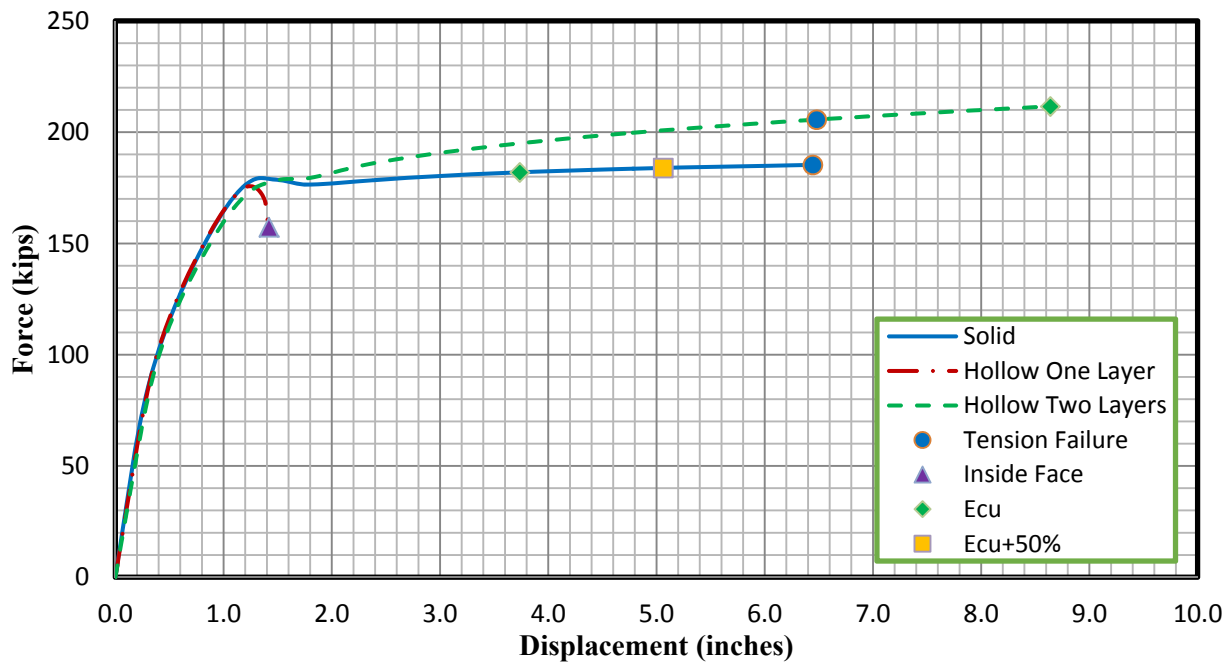


Figure 6-3: Pushover analysis of 3.5 foot diameter circular columns

The last set of example columns can be seen in Figure 6-4, consisting of square columns with an outside diameter of five feet. As shown, the solid column experiences a ductile response and is expected to fail due to rupture of the longitudinal reinforcement. Unlike the previous two sets of example columns, the hollow column with one layer of transverse reinforcement experiences a more ductile response, although ultimately failing due to crushing of the inside concrete face. The hollow column with one layer of transverse reinforcement experiences a more ductile response due to the lower axial load ratio combined with the fairly low longitudinal reinforcement ratio. The hollow specimen with two layers of transverse reinforcement again

experiences a ductile response and is expected to fail due to rupture of the longitudinal reinforcement.

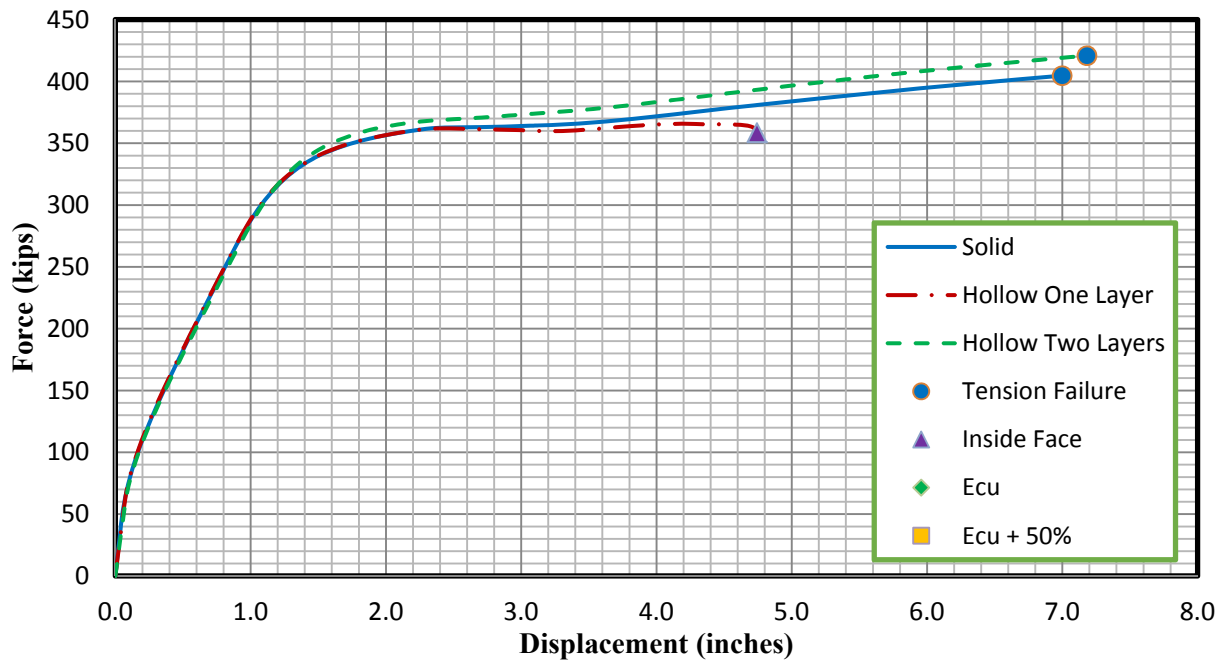


Figure 6-4: Pushover analysis of 5 foot diameter square columns

These examples have demonstrated that the response of hollow columns with one layer of transverse reinforcement is heavily dependent on the geometry and amount of axial load and longitudinal reinforcement. Additionally it has shown that hollow columns with two layers of transverse reinforcement are predicted by the analysis to experience a ductile response under a variety of geometric configurations and axial load ratios. The examples show that hollow columns can be suitable in many cases, and that whether one layer or two layers of transverse reinforcement is used will depend on the situation. Using only one layer of transverse reinforcement can meet ductility requirements if the neutral axis is not too far toward the center of the column, and also supplies the most economical construction in terms of mass and material. However, if the neutral axis occurs closer to the center of the column and higher ductility is required, two layers of transverse reinforcement may be ideal. A solid column could also prove to be the better choice if it is determined to be more economical. The ductility requirements of the column must be weighed with the economy and labor costs of each configuration.

6.4 Future research

The research performed has been able to provide recommendations for the design of hollow concrete columns with one layer of transverse reinforcement. Using the proposed analytical modeling method with an adjustment to Mander's model has been found to provide a fairly conservative estimate of the ultimate failure point for hollow circular columns. However, the proposed adjustment for square columns has been based solely off results of the finite element analysis, due to a lack of previous research and due to the early failure of square hollow specimens in this study. Although the finite element analysis has been shown to be comparable to actual test results, it is still recommended that further large-scale experimentation and research of square hollow columns with one layer of transverse reinforcement be performed.

Another area where future research is recommended is in the investigation of crushing of confined concrete near the transverse reinforcement in hollow columns. Transverse reinforcement failure is typically the limit for confined concrete crushing in solid columns, but no instances of transverse reinforcement failure have been reported in tests of hollow columns with one layer of transverse reinforcement. The increased deformability of hollow columns seems to make their radial displacement easier to contain, which could possibly allow a reduction in the amount of transverse reinforcement used for hollow columns. It would be beneficial to perform experimentation of hollow columns with one layer of transverse reinforcement and a reduced transverse reinforcement ratio. These tests should be designed in order to achieve transverse reinforcement failure to better quantify the concrete compression strain at which this failure mode occurs, as well as how much transverse reinforcement is necessary for hollow concrete columns.

Further research into the shear capacity and deformability of hollow columns is also recommended. The experimental program presented in this report demonstrated higher shear deformability of hollow columns, and the exact reason for this increase is not well known. It would be useful to be able to predict the shear deformation of hollow columns and to compare this deformation to similar solid columns.

REFERENCE

- AASHTO Guide Specifications for LRFD Seismic Bridge Design (2nd Edition) with 2012 and 2014 Interim Revisions. (2011; 2012; 2014). American Association of State Highway and Transportation Officials.
- Bousalem, B., & Chikh, N. (2007). Development of a confined model for rectangular ordinary reinforced concrete columns. *Materials and Structures*, 40(6), 605-613.
- Caltrans Seismic Design Criteria Version 1.7. (2013, April). Caltrans.
- Calvi, G. M., Pavese, A., Rasulo, A., & Bolognini, D. (2005). Experimental and Numerical Studies on the Seismic Response of R.C. Hollow Bridge Piers. *Bulletin of Earthquake Engineering*, 267-297.
- Chang, G., & Mander, J. (1994). *Seismic energy based fatigue damage analysis of bridge columns: part I - evaluation of seismic capacity*. NCEER.
- Filippou, F., Popov, E., & Bertero, V. (1983). *Effects of bond deterioration on hysteric behavior of reinforced concrete joints*. EERC.
- Hines, E. M., Seible, F., Priestley, M. (2002). *Seismic performance of hollow rectangular reinforced concrete piers with highly-confined boundary elements Phase I: Flexure tests Phase II: Shear tests*. Structural Systems Research Project, University of California, San Diego, Department of Structural Engineering, Report No. SSRP - 99/15
- Hoshikuma, J., Nagaya, K., & Taylor, A. (1997). Stress-strain model for confined reinforced concrete in bridge piers. *Journal of Structural Engineering*, 123(5), 624-633.
- Hoshikuma, J.-I., & Priestley, M. (2000). *Flexural behavior of circular hollow columns with a single layer of reinforcement under seismic loading*. Structural Systems Research Project, University of California, San Diego, Department of Structural Engineering. Report No. SSRP - 2000/13
- Kawashima, K. (1992, October). Dynamic Strength and Ductility of Hollow Circular Reinforced Concrete Bridge Pier. *Civil Engineering Journal*, 34(10), 34-39.
- Kent, D. C., & Park, R. (1971, July). Flexural Members with Confined Concrete. *Journal of the Structural Division*, 97(7), 1969-1990.
- Lee, J. a. (1998). Plastic-damage model for cyclic loading of concrete structures. *J. Eng. Mech. ASCE*, 124 (8) : 892-900.
- Lignola, G. P., Prota, A., Manfredi, G., & Cozenza, E. (2008). Unified theory for confinement of RC solid and hollow circular columns. *Composites: Part B*, 39, 1151-1160.
- Lubliner, J. O. (1989). A plastic -damage model for concrete. *Int. J. Solids Struct.*, 299-329.

- Mander, J., Priestley, M., & Park, R. (1988, August). Observed stress-strain behavior of confined concrete. *Journal of Structural Engineering*, 114(8), 1827-1849.
- Mander, J., Priestley, M., & Park, R. (1988). Theoretical stress-strain model for confined concrete. *Journal of Structural Engineering*, 1804-1826.
- Mo, Y., Wong, D., & Maekawa, K. (2003, June). Seismic Performance of Hollow Bridge Columns. *ACI Structural Journal*, 100(3), 337-348.
- Mohd Yassin, M. (1994). *Nonlinear Analysis of Prestressed Concrete Structures under Monotonic and Cycling Loads*. Berkeley: PhD dissertation, University of California.
- Papanikolaou, V. K., & Kappos, A. J. (2009, May). Numerical study of confinement effectiveness in solid and hollow reinforced concrete bridge piers: Methodology. *Computers & Structures*, 87, 1427-1439.
- Priestley, M., Seible, F., & Calvi, G. (1996). *Seismic Design and Retrofit of Bridges*. John Wiley & Sons, Inc.
- R. Snyder, J. V. (2011). *Seismic Performance of an I-Girder to Inverted-T Bent Cap Connection*. Sacramento: California Department of Transportation.
- Ranzo, G., & Priestley, M. (2001). *Seismic performance of circular hollow columns subjected to high shear*. Structural Systems Research Project, University of California, San Diego, Department of Structural Engineering. Report No. SSRP - 2001/01
- S Sritharan, M. N. (2000). Nonlinear finite element analyses of concrete bridge joint systems subjected to seismic actions. *Finite elements in Analysis and Design*, 215-233.
- Saatcioglu, M., & Razvi, S. (1992). Strength and ductility of confined concrete. *Journal of Structural Engineering*, 118(6), 1590-1607.
- Samani, A., & Attard, M. (2012). A stress-strain model for uniaxial and confined concrete under compression. *Engineering Structures*, 41, 335-349.
- Scott, B., Park, R., & Priestley, M. (1982). Stress-strain behavior of concrete confined by overlapping hoops at low and high strain rates. *ACI Journal Proceedings*, 79(1).
- Sheikh, Shamim; Uzumeri, Suzru; ASCE. (1980). Strength and ductility of tied concrete columns. *ASCE 15388 Proceeding*.
- Sritharan, A. S. (2014). *A Critical Review of Column Confinement Reinforcement Used in Current Seismic Bridge Design Practice*. Sacramento: California Department of Transportation.
- Sritharan, S. (1998). *Analysis of Concrete Bridge Joints Subjected to Seismic Actions*. San Diego: Doctoral Dissertation, University of California.
- Vallenas, J., Bertero, V. V., & Popov, E. P. (1977). Concrete confined by rectangular hoops and subjected to axial loads. *NASA STI/Recon Technical Report N 78*.

- Yeh, Y., Mo, Y., & Yang, C. (2001). Seismic performance of hollow circular bridge piers. *ACI Structural Journal*, 98(6).
- Yeh, Y.-K., Mo, Y., & Yang, C. (2002, March). Full-scale tests on rectangular hollow bridge piers. *Materials and Structures*, 35, 117-125.
- Zahn, F., Park, R., & Priestley, M. (1990, March-April). Flexural Strength and Ductility of Circular Hollow Reinforced Concrete Columns without Confinement on Inside Face. *ACI Structural Journal*, 87(2), 156-166.
- Zhao, J., & Sritharan, S. (2007). Modeling of strain penetration effects in fiber-based analysis of reinforced concrete structures. *ACI Structural Journal*, 133-141.

APPENDIX

Appendix A: Concentric Axial Load FEM Analysis Input Material Properties

Concrete

Elastic	
Young's Modulus	3823676
Poisson's Ratio	0.2

Plasticity			
Dilation Angle		32	
Eccentricity		0.1	
fb0/fc0		1.16	
K		0.666	
Viscosity Parameter		0	
Compressive Behavior			
0.177 dia. Confinement		0.125 dia. Confinement	
Yield Stress	Inelastic Strain	Yield Stress	Inelastic Strain
1600	0	1600	0
2400	0.000105	2400	0.000105
3245	0.00032	3245	0.00032
4500	0.000823	4500	0.000823
4550	0.00196	4550	0.00196
4470	0.0031	4350	0.0031
4250	0.0052	3980	0.0052
4000	0.0079	3550	0.0079
3600	0.0123	2900	0.0123
3000	0.0188	2300	0.0188
2500	0.0245	1900	0.0245
2000	0.0295	1600	0.0295
400	0.0495	400	0.0495

Tensile Behavior	
Yield Stress	Cracking Strain
530	0
450	0.008

Reinforcing Bar Steel

Elastic	
Young's Modulus	29000000
Poisson's Ratio	0.3

Plastic	
Yield Stress	Plastic Strain
60000	0
68000	0.02
90000	0.08
80000	0.25
1000	0.3

Appendix B: Model Validation – HF1 FEM Analysis Input Material Properties

Concrete

Elastic	
Young's Modulus	4500000
Poisson's Ratio	0.2

Plasticity			
Dilation Angle		45	
Eccentricity		0.1	
fb0/fc0		1.16	
K		0.666	
Viscosity Parameter		0	
Compressive Behavior			
35 mm confinement spacing		70 mm confinement spacing	
Yield Stress	Inelastic Strain	Yield Stress	Inelastic Strain
2500	0	3500	0
4000	0.000111111	4230	6.25E-005
5000	0.000388889	5500	0.000545
6500	0.0025	5792	0.001552
6450	0.0049	4500	0.004675
6000	0.0079	3600	0.0068
5000	0.0135	2700	0.009325
4200	0.0185	1800	0.01255
3500	0.0235	1000	0.01575
2800	0.0285	400	0.0184
400	0.0485		

Tensile Behavior	
Yield Stress	Cracking Strain
260	0
180	0.008

Longitudinal Reinforcing Steel

Elastic	
Young's Modulus	26825000
Poisson's Ratio	0.3

Plastic	
Yield Stress	Plastic Strain
61915	0
101500	0.1

Transverse Reinforcing Steel

Elastic	
Young's Modulus	25375000
Poisson's Ratio	0.3

Plastic	
Yield Stress	Plastic Strain
90625	0
118900	0.1

Appendix C: FEM Analyses of Test Hollow Columns Input Material Properties

Concrete

Elastic

Young's modulus	Poisson's Ratio
$57000 \sqrt{f'_c}$ (psi) = 4500000 psi	0.2

Post yielding

Plasticity	
Dilation Angle	32
Eccentricity	0.1
fb0/fc0	1.16
K	0.666
Viscosity Parameter	0
Compressive Behavior	
Yield Stress (psi)	Inelastic Strain (in/in)
2500	0
4000	0.0005
5000	0.0011
6500	0.0035
6450	0.0059
6000	0.0089
5000	0.0145
4200	0.0195
3500	0.0245
2800	0.0295
400	0.0495

Tensile Behavior	
240	0
160	0.008

Steel

Elastic

Young's modulus	Poisson's Ratio
29000000 (psi)	0.3

Post-yielding

Longitudinal steel

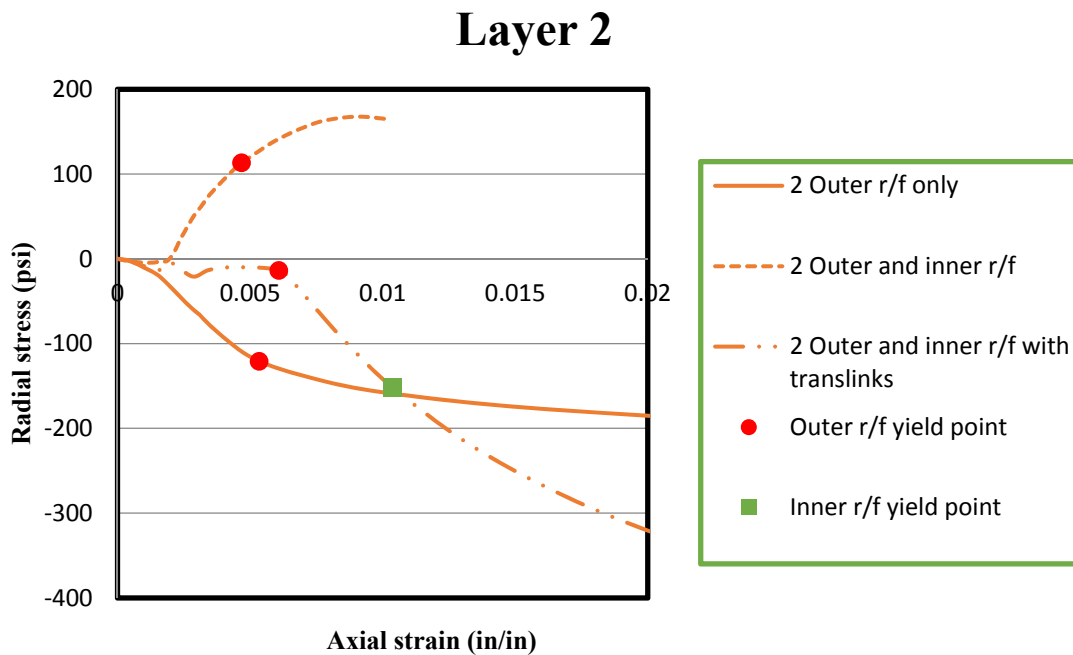
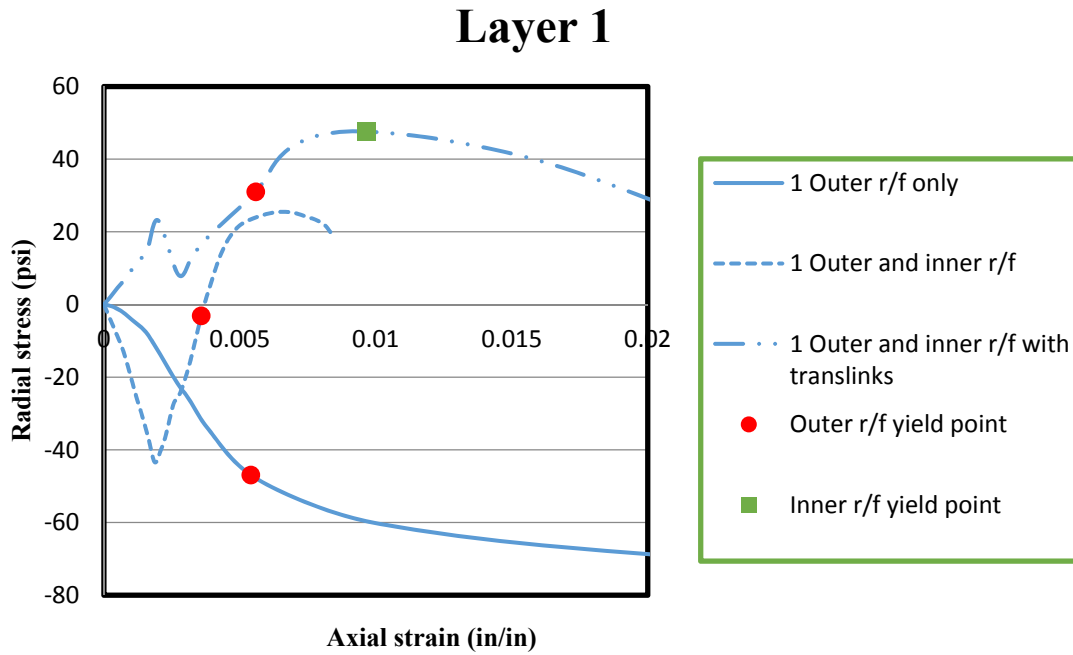
Yield Stress	Plastic Strain
90000	0
95000	0.003394138
98000	0.01662069
80000	0.12
1000	0.16

Lateral steel

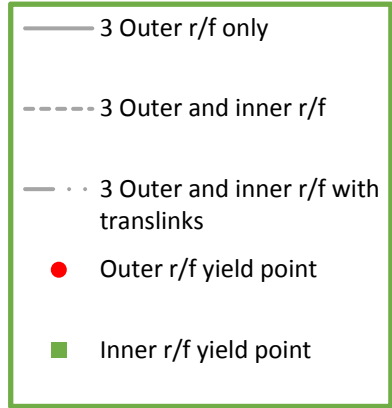
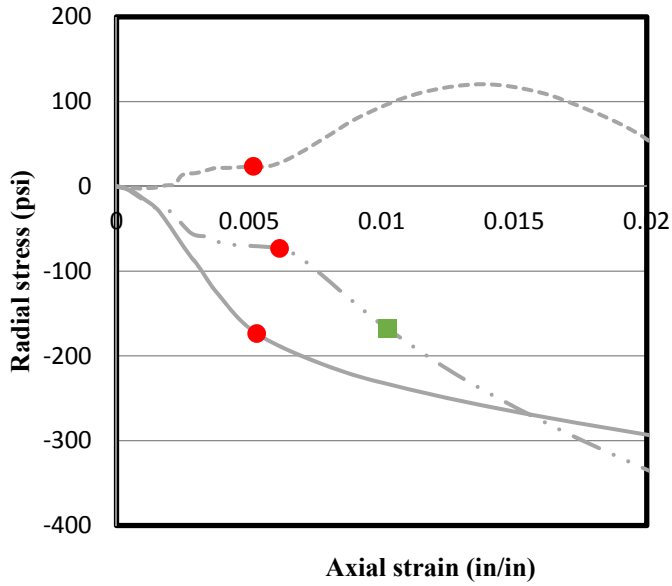
Yield Stress	Plastic Strain
95000	0
100000	0.008551724
80000	0.12
1000	0.14

Appendix D: Radial behavior of two-inch wall hollow section at given concrete layer

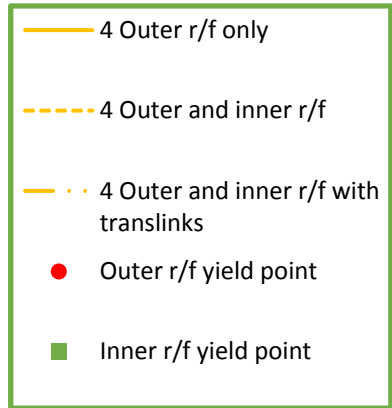
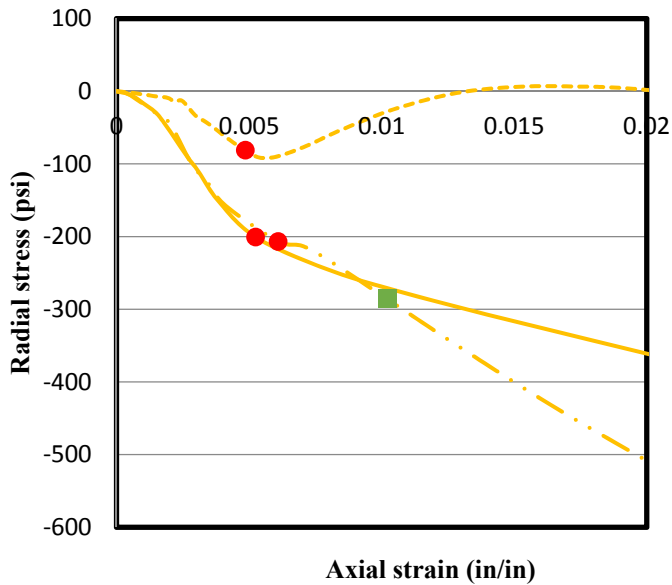
Appendix D presents the relationships between the radial concrete stress and the axial concrete strain with respect to each confinement configurations at given concrete layer of two-inch wall hollow section



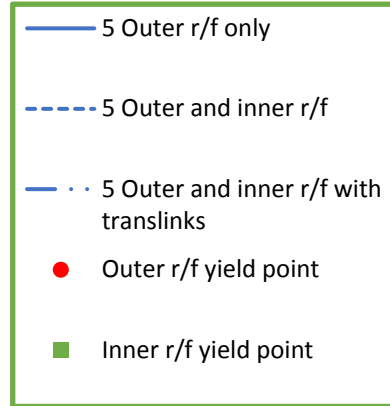
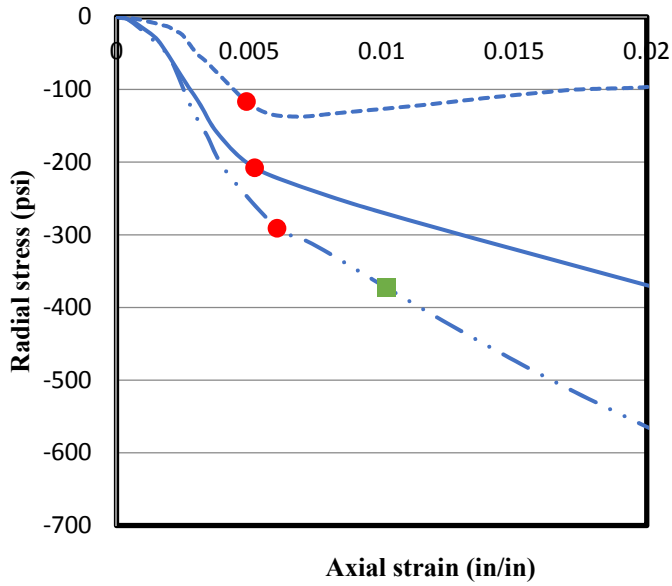
Layer 3



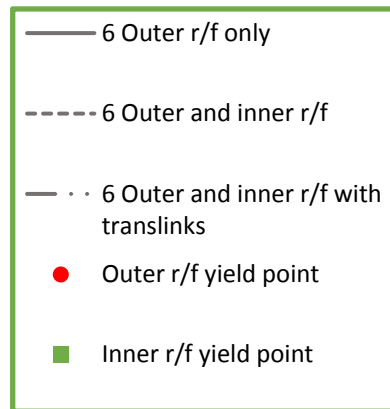
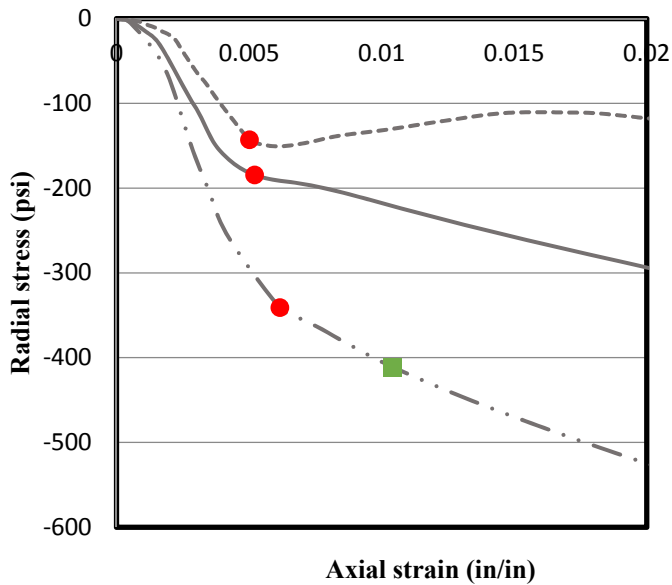
Layer 4



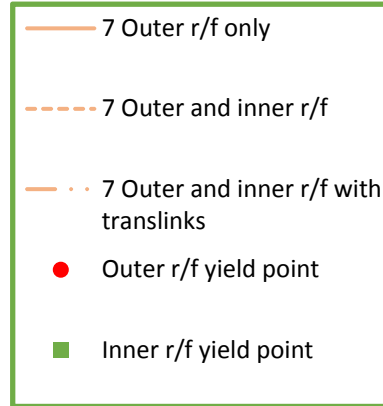
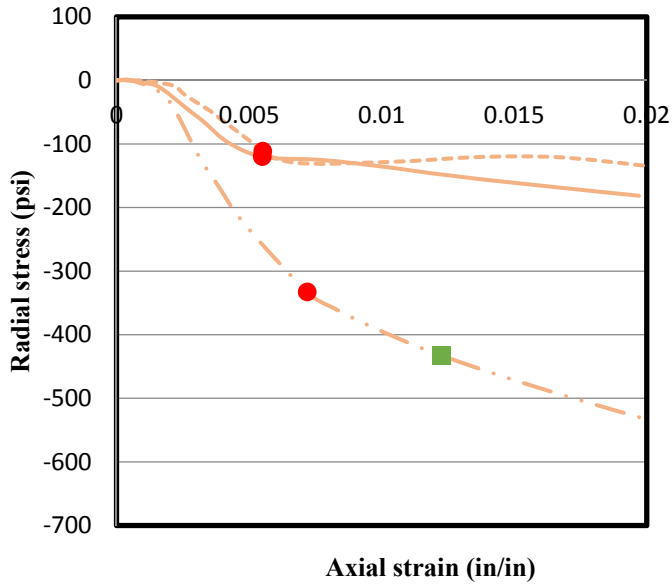
Layer 5



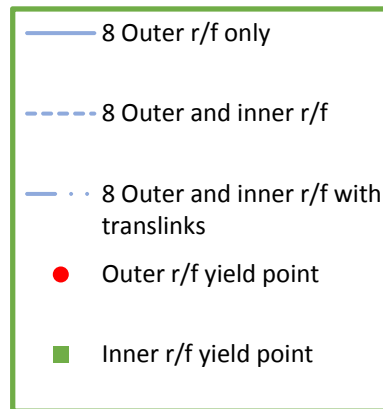
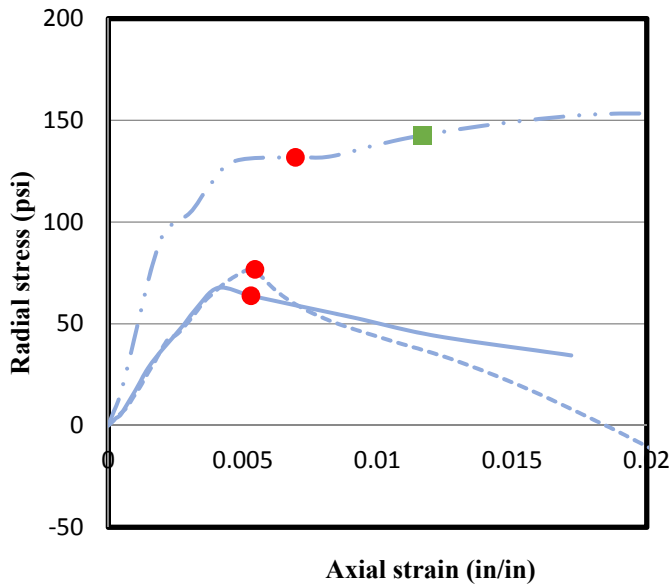
Layer 6



Layer 7



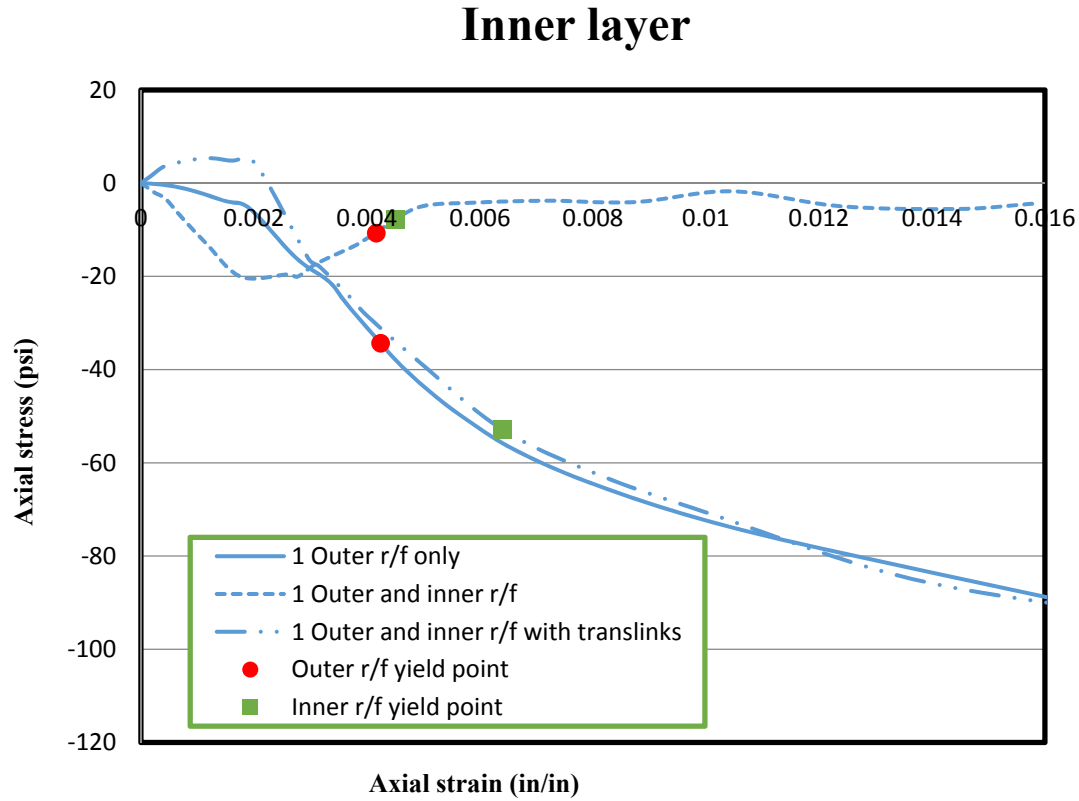
Layer 8



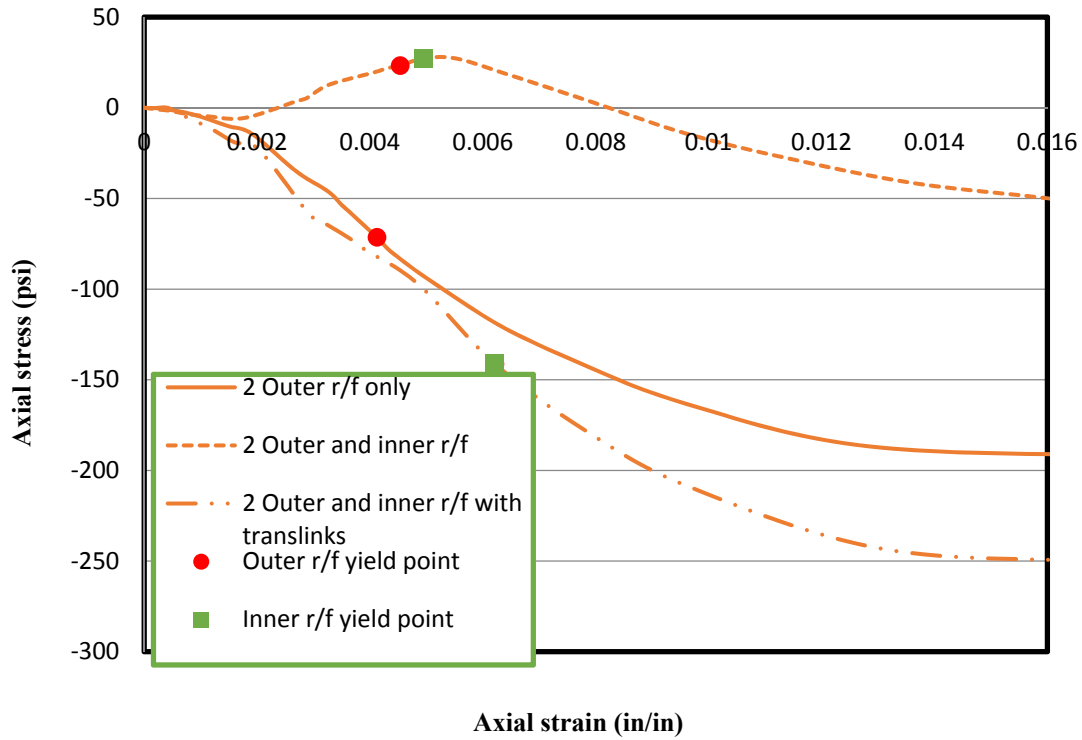
*r/f represents reinforcement

Appendix E: Radial behavior of one-inch wall hollow section at given concrete layer

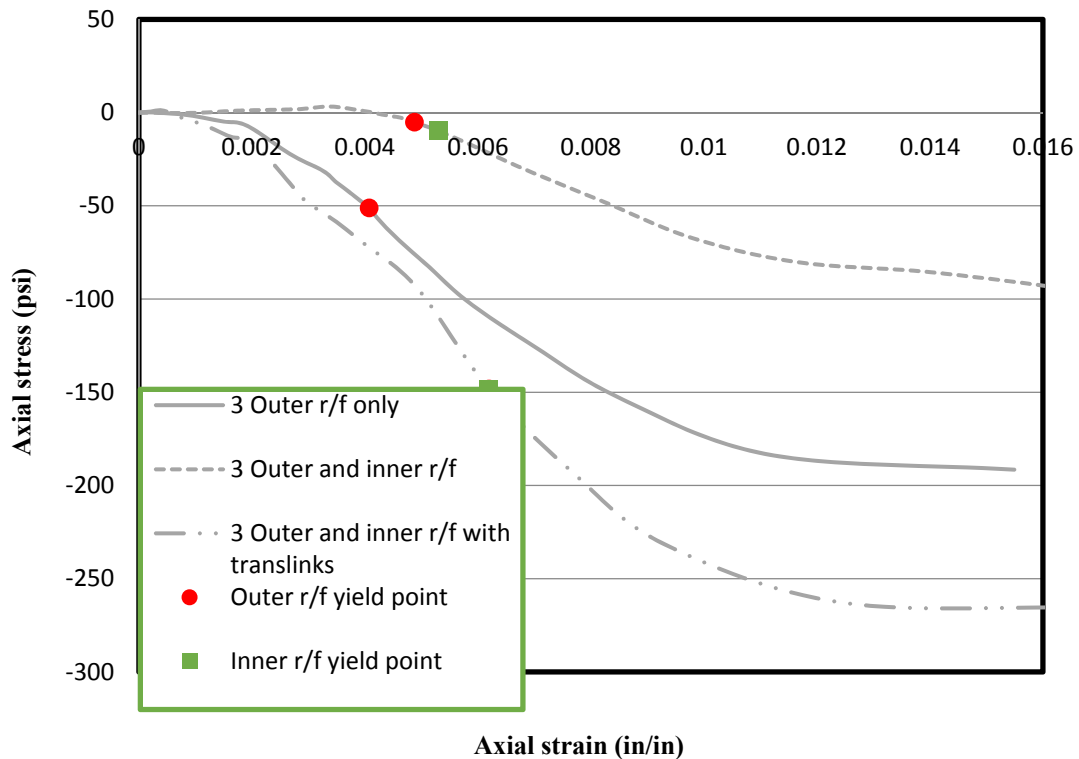
Appendix E presents the relationships between the radial concrete stress and the axial concrete strain with respect to each confinement configurations at given concrete layer of one-inch wall hollow section



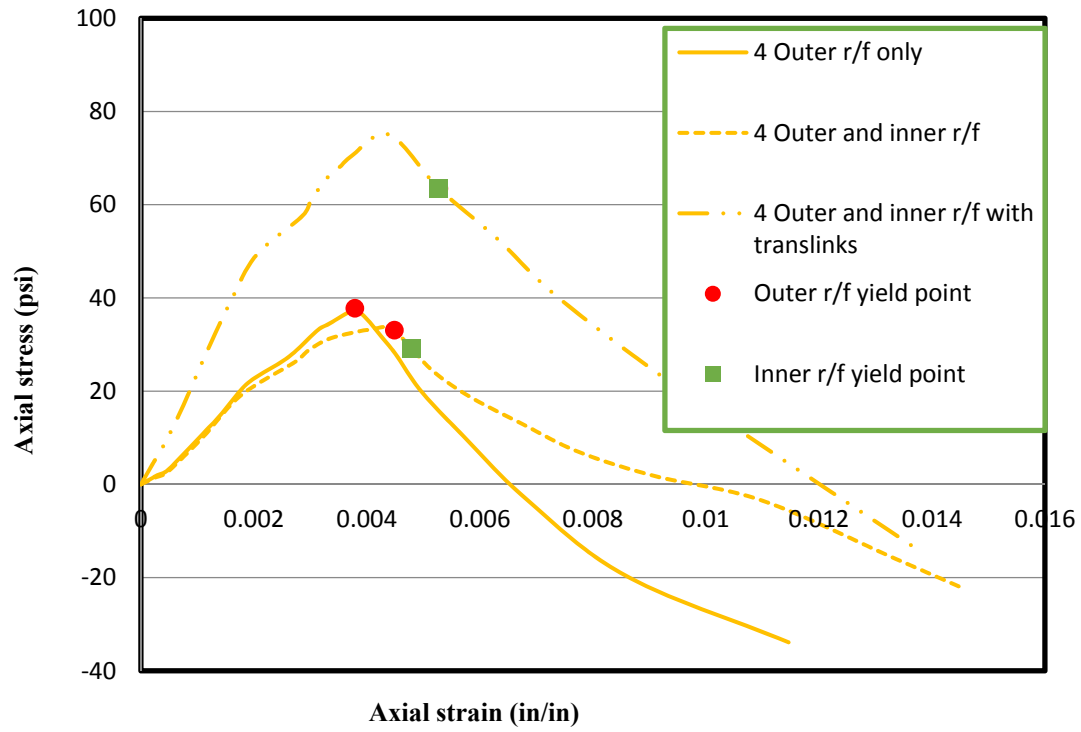
2rd layer from the inner layer



2rd layer from the outer layer



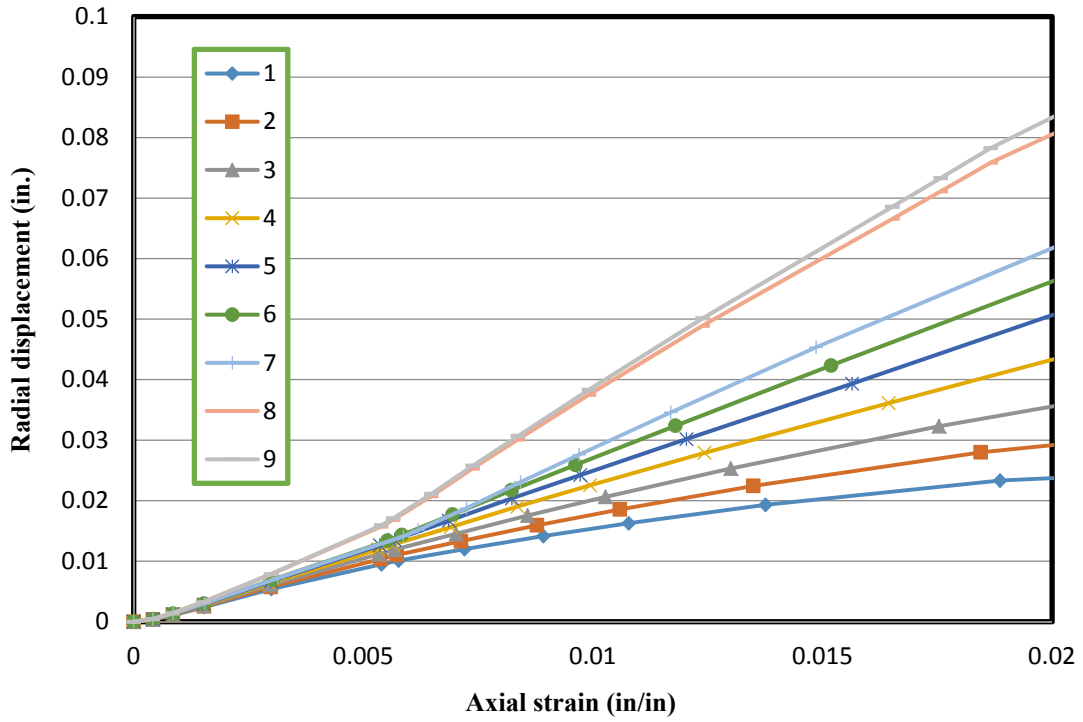
Outer layer



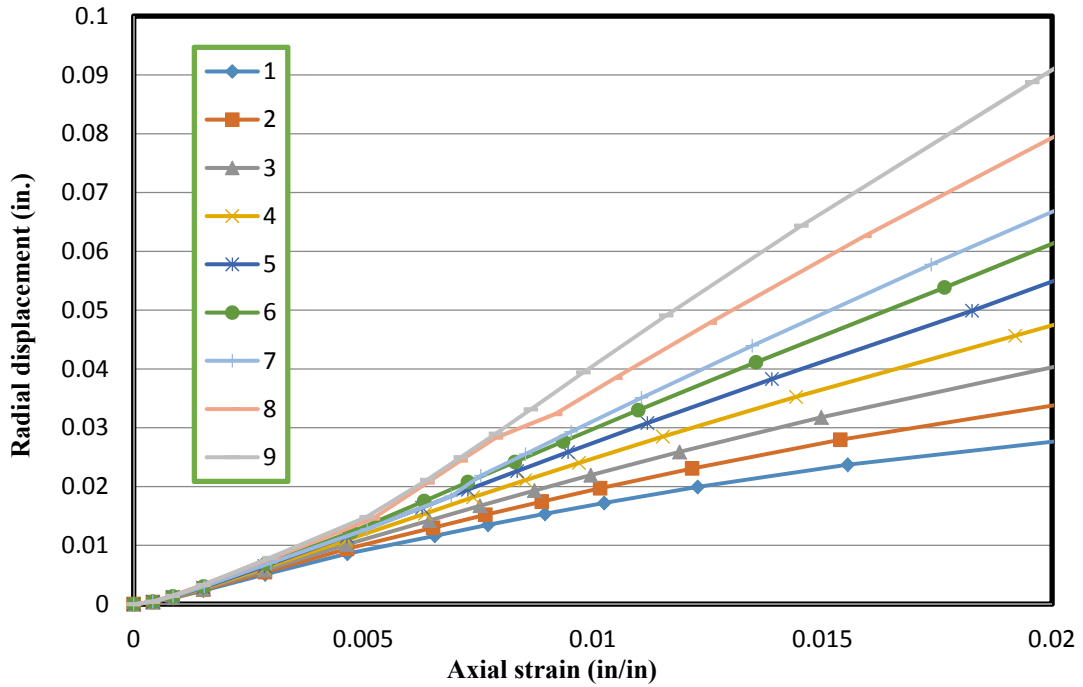
*r/f represents reinforcement

Appendix F: Concrete dilation

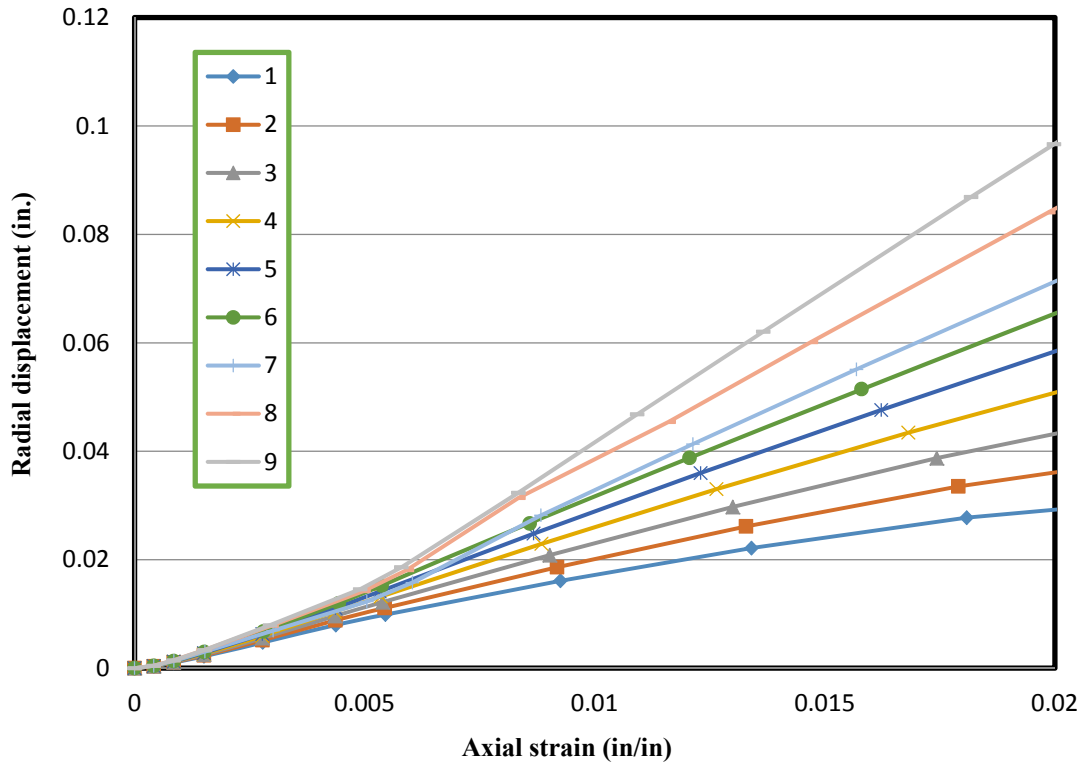
1. Circular sections



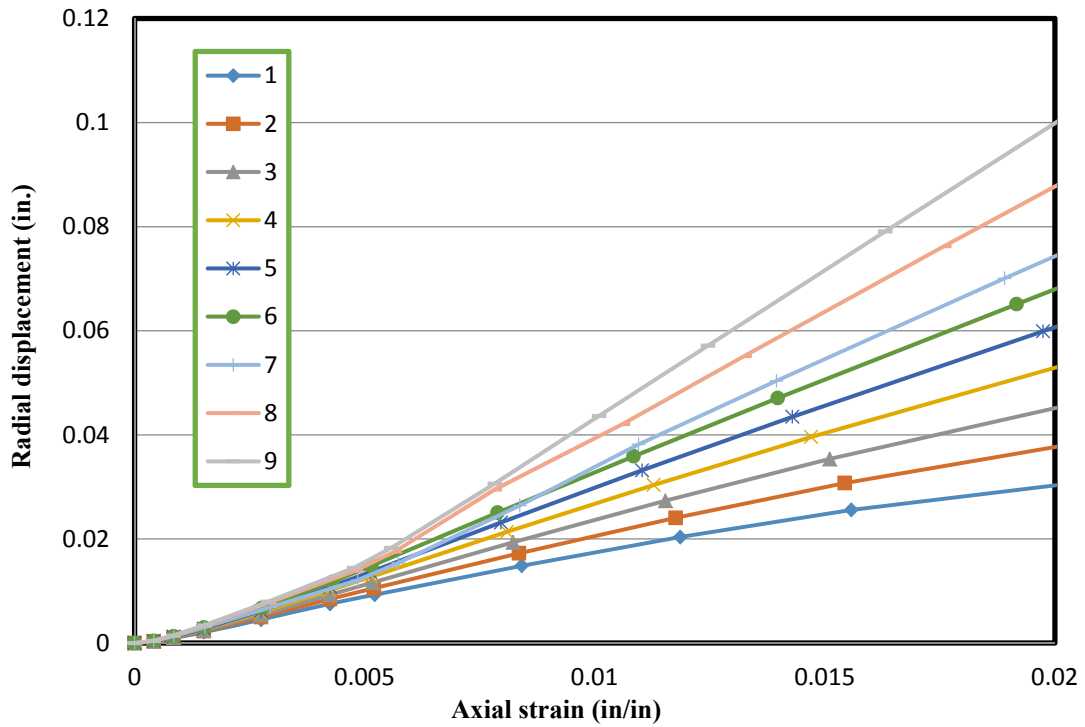
(a) 1.2 inches wall thickness



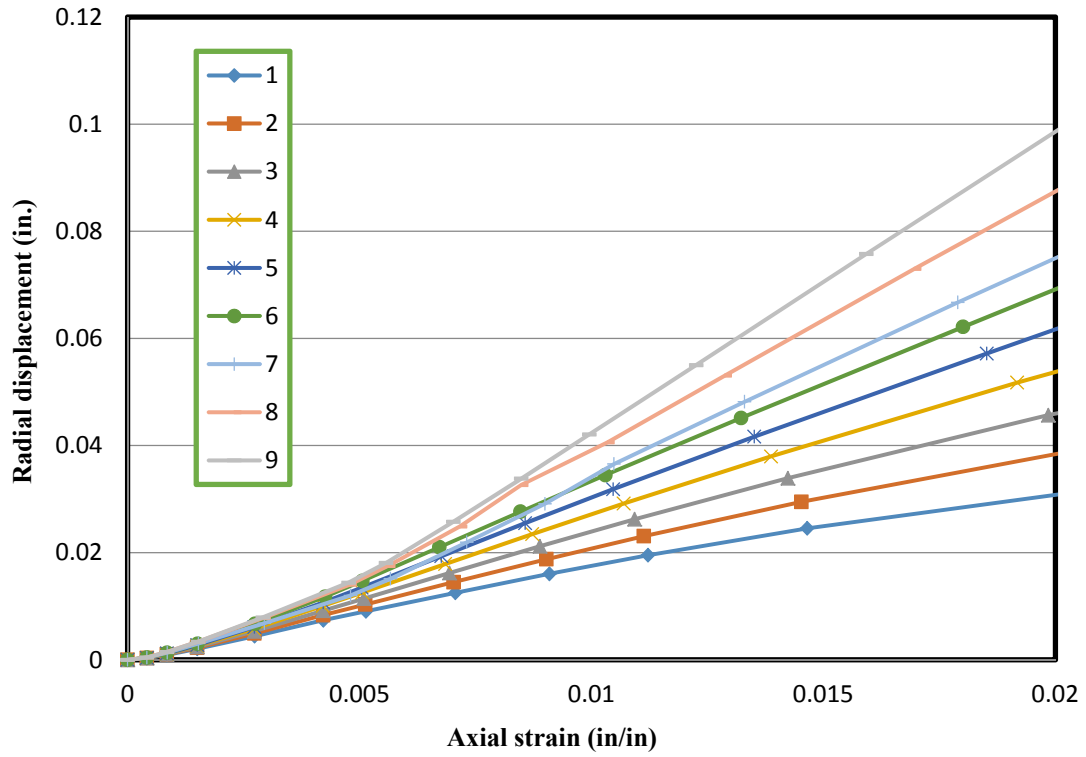
(b) 1.5 inches wall thickness



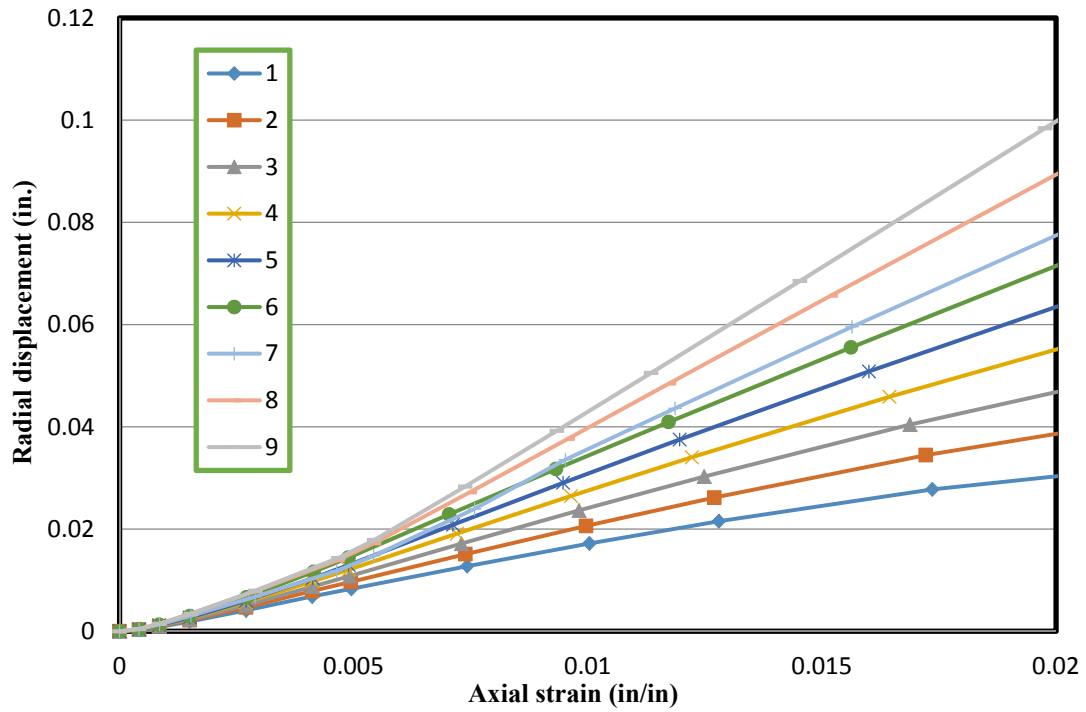
(c) 1.8 inches wall thickness



(d) 2 inches wall thickness

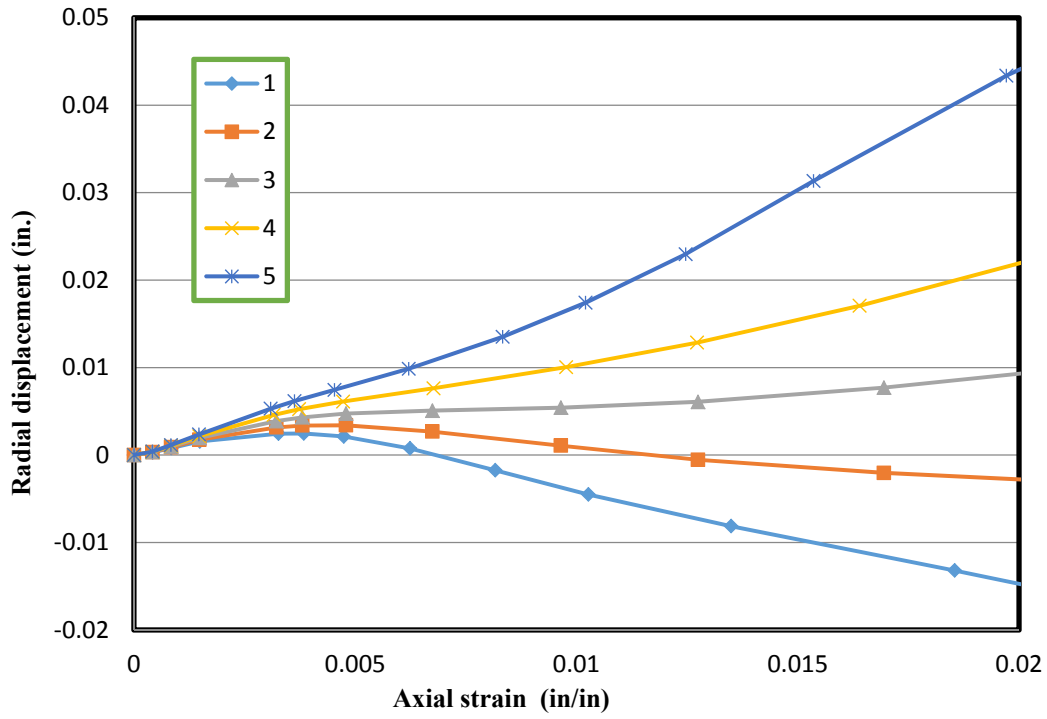


(e) 2.1 inches wall thickness

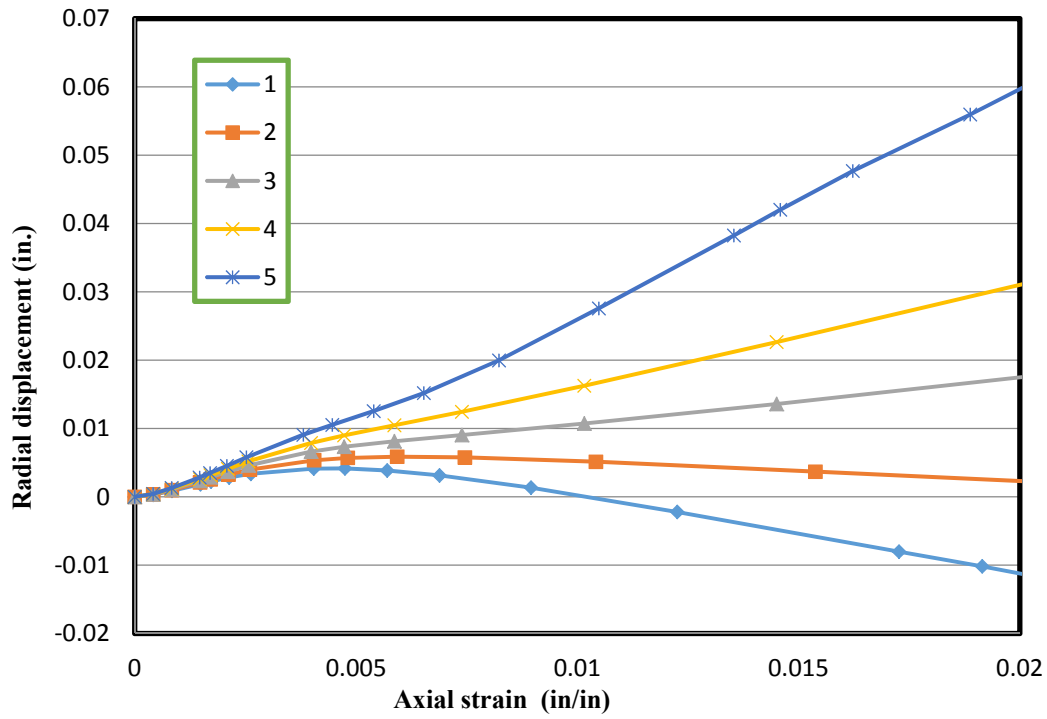


(f) 2.4 inches wall thickness

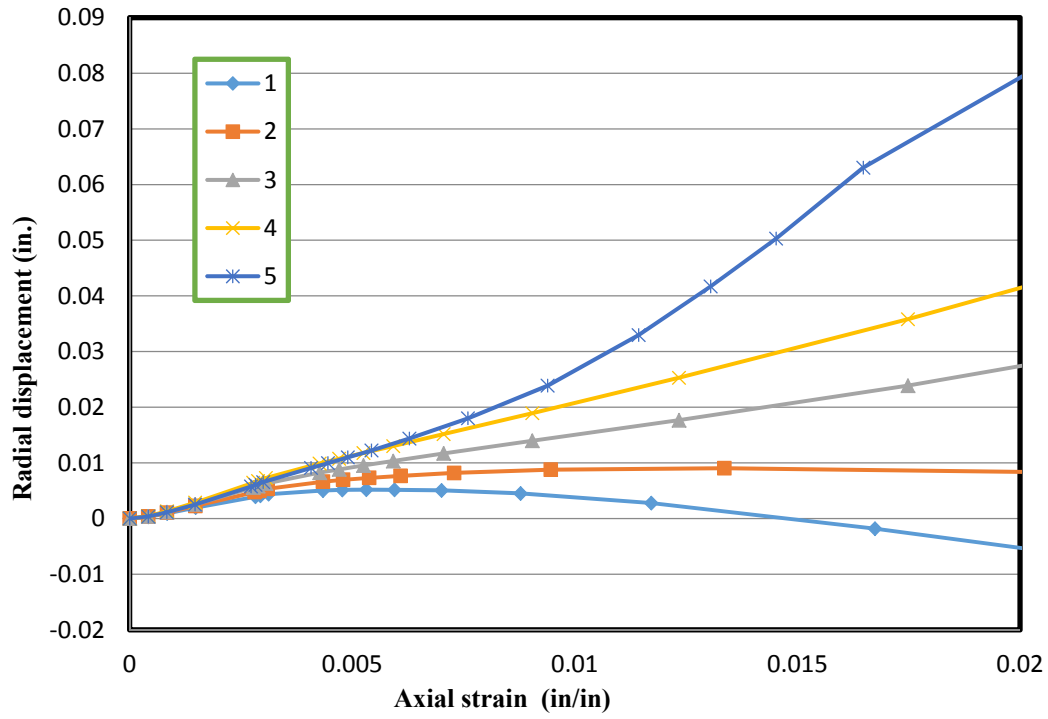
2. Square sections



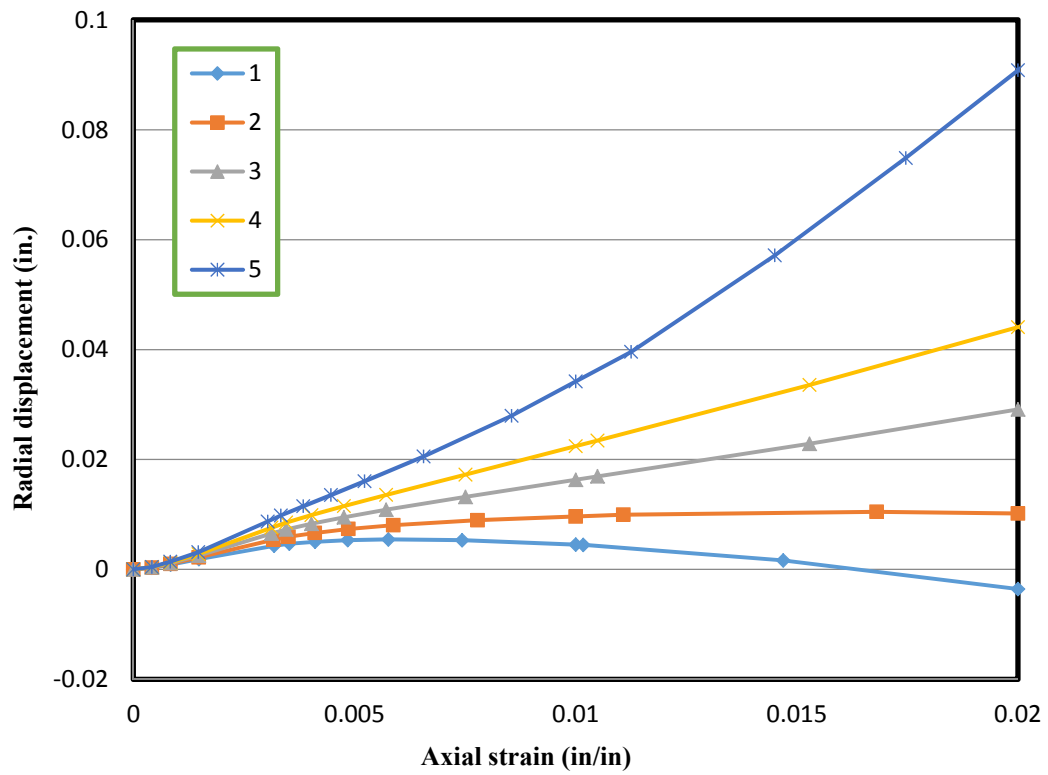
(a) 1.2 inch wall thickness



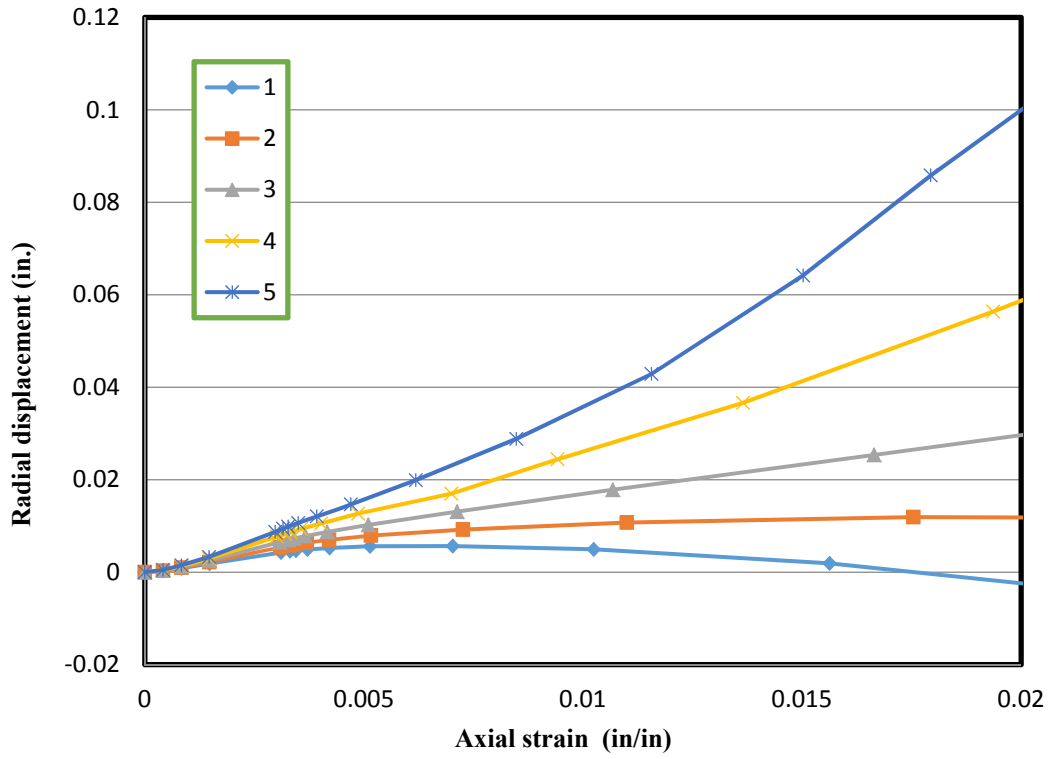
(b) 1.5 inch wall thickness



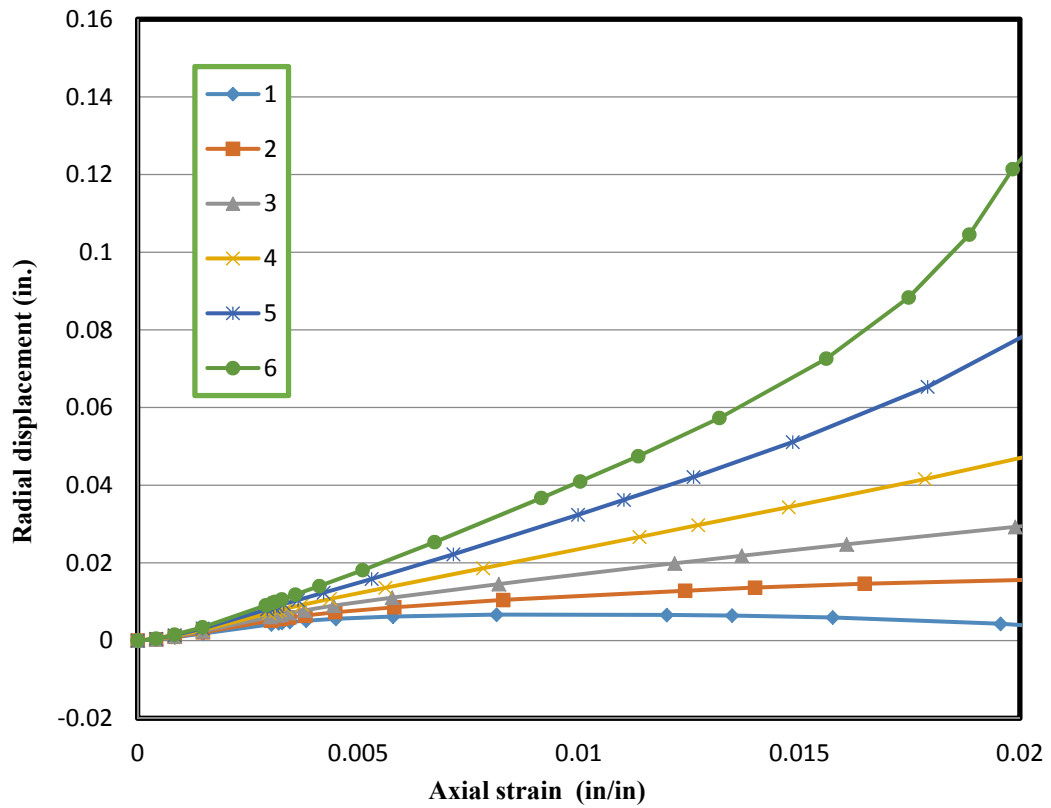
(c) 1.8 inch wall thickness



(d) 2 inch wall thickness



(e) 2.1 inch wall thickness



(f) 2.4 inch wall thickness

